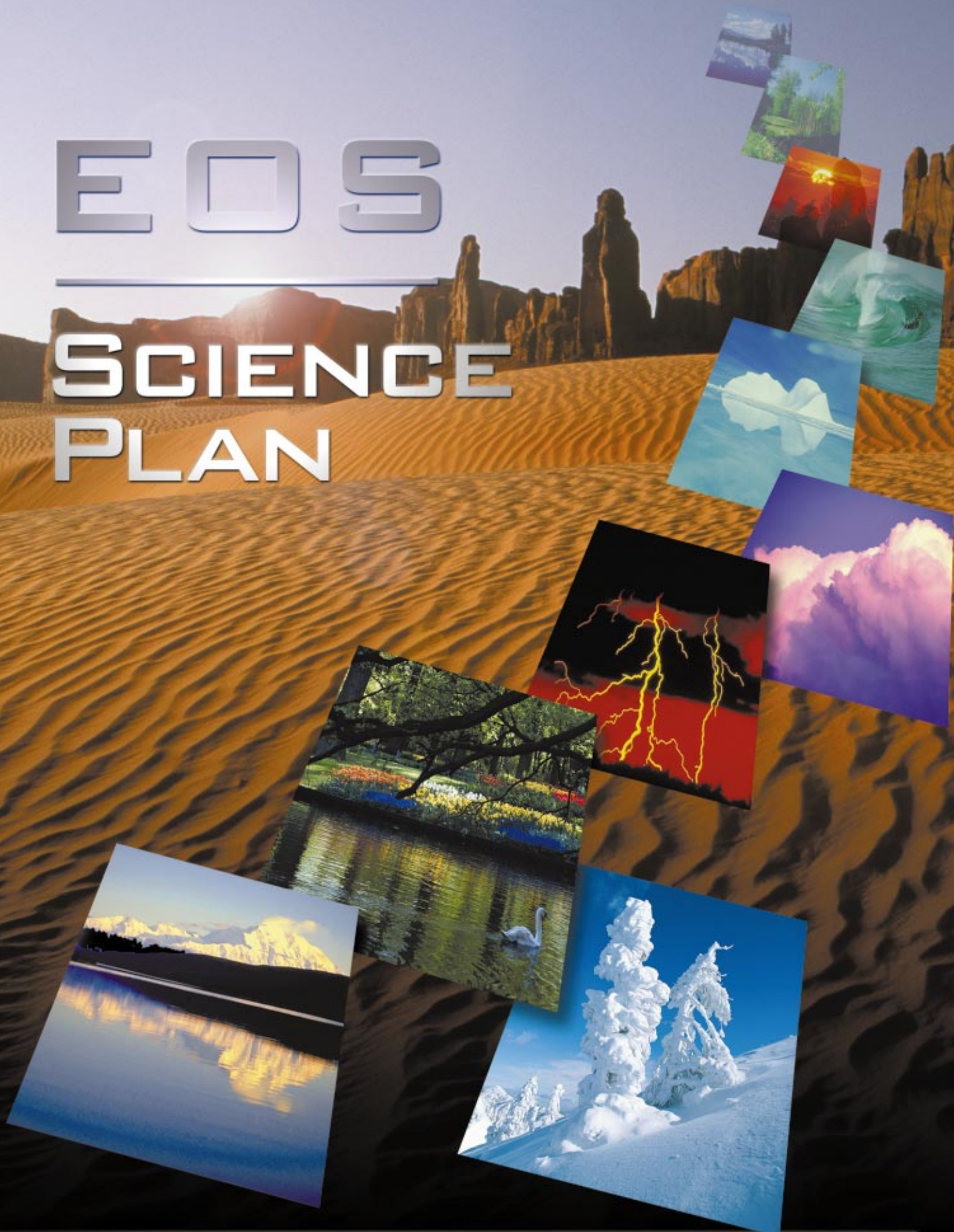


EOS

SCIENCE PLAN

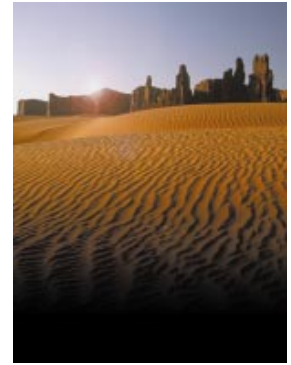


The State of Science in the EOS Program

EOS

SCIENCE
PLAN

The State of Science in the EOS Program



EDITOR Michael D. King
NASA/Goddard Space Flight Center

TECHNICAL EDITORS Reynold Greenstone
William Bandeen
Raytheon ITSS

DESIGN AND PRODUCTION Sterling Spangler
Raytheon ITSS



EOS

SCIENCE PLAN

The State of Science in the EOS Program



EOS SENIOR PROJECT SCIENTIST

Dr. Michael D. King
NASA/Goddard Space Flight Center
Code 900
Greenbelt, Maryland 20771
Phone: 301-614-5636
Fax: 301-614-5620
E-Mail: king@climate.gsfc.nasa.gov

FOR ADDITIONAL COPIES

Ms. Lee McGrier
NASA/Goddard Space Flight Center
Code 900
Greenbelt, Maryland 20771
Phone: 301-441-4259
E-Mail: lmcgrier@pop900.gsfc.nasa.gov

EOS HOMEPAGE

<http://eos.nasa.gov/>

TABLE OF CONTENTS

<i>Foreword</i>	1
<i>Preface</i>	3
<i>Chapter 1</i> Overview	5
<i>Chapter 2</i> Radiation, Clouds, Water Vapor, Precipitation, and Atmospheric Circulation	39
<i>Chapter 3</i> Ocean Circulation, Productivity, and Exchange with the Atmosphere	115
<i>Chapter 4</i> Atmospheric Chemistry and Greenhouse Gases	163
<i>Chapter 5</i> Land Ecosystems and Hydrology	197
<i>Chapter 6</i> Cryospheric Systems	261
<i>Chapter 7</i> Ozone and Stratospheric Chemistry	309
<i>Chapter 8</i> Volcanoes and Climate Effects of Aerosols	339
<i>Acronyms</i>	381
<i>Index</i>	387

Foreword

From the dawn of space exploration NASA has been in the forefront of providing the unique vantage point of space as an ideal setting for observing Earth as a whole system consisting of atmosphere, oceans, and continents capable of supporting life in our solar system. Today, NASA continues to sponsor research and development towards understanding the origins of life in the universe. The best proxy for this search and discover mission is life on Earth, and the NASA Earth Science Enterprise captures the spirit of exploration and focuses it back on our home planet. But this requires understanding Earth as an integrated system of atmosphere, land, oceans, and life, which has evolved in the past and will continue to evolve in the future. Building on our observations of the Earth since the earliest days of the space program—NASA built the first weather and land observing satellites—we are using orbiting spacecraft to bring congruency to multiple disciplines within Earth sciences through integrated observations, interdisciplinary scientific research and analysis, and modeling. This is the blueprint for the Earth Science Enterprise at NASA and its Earth Observing System (EOS) program.

The EOS program was established in 1991 as a U.S. Presidential initiative to provide in-depth scientific understanding about the functioning of Earth as a system. It was envisioned that such scientific knowledge would provide the foundation for understanding the natural and human-induced variations in Earth's climate system and also provide a sound basis for environmental policy decision making. Beyond scientific discovery and explorations, it was also envisioned that EOS would have practical societal benefits in the form of providing scientific knowledge toward the efficient production of food and fiber, management of fresh water resources, and improvement of air quality. Less than a decade later, EOS is now a reality and delivering on its promises. During the first phase of the EOS program NASA is funding the development and launch of 25 satellites, and a uniquely comprehensive Earth observations-related data and information system. Hundreds of Earth scientists and engineers are supported, and more than 350 students per year are pursuing graduate degrees in Earth science with NASA funding.

The EOS Science Plan is the product of several years of discussion and debate among the EOS investigators. The considerable time required to develop this document should be viewed as a major strength because of the deep-rooted commitments of the contributors to this document and their ability to deliver on their promise. The objective of this Plan is to convey how EOS investigators plan to utilize the space-based and in situ observations along with modeling and data analysis methods/techniques to address the EOS scientific and applications objectives. Therefore, the principal intended audience for this plan is the body of international Earth scientists and science program directors. Given the complexity of the task at hand and the level of details that had to be provided, the Plan became more than 350 pages long. A short version of the Plan has also been developed in the form of an Executive Summary. We believe that these two documents will be seen to be an effective means of communicating the scientific priorities of the EOS program and how NASA and EOS investigators plan to implement these priorities during the next 5-7 years.

As we move towards the next century the changing Earth's environment will be the focus of many agricultural, industrial, and societal concerns and policy decisions. NASA's Earth Science Enterprise is committed to timely provision of the scientific knowledge needed by world leaders to formulate sound and equitable environmental decisions.

Ghassem R. Asrar
Associate Administrator

Office of Earth Science
NASA Headquarters
Washington, D.C.

Preface

The EOS Science Plan was first proposed to the community of EOS investigators at a meeting of the EOS Investigators Working Group in the fall of 1994. As the concept of the Plan evolved, it was decided that the primary audience for the Plan would be the scientific community and not the general public. Thus, the audience not only includes members of the EOS scientific community, but also includes scientists in related fields who are not necessarily acquainted with the goals and philosophies of scientists in the EOS program.

Accordingly, readers will find a very thorough presentation of the state of the science being investigated by participants in the EOS program. They also will find discussions on how science investigations are being conducted both before and after launch of the EOS satellites. This review of the state of the science, along with its extensive documentation of scientific references, should be of value to both working scientists and to the graduate students who will take their place in the scientific endeavors of the next century.

Both the anticipated contributions of the EOS satellites to our knowledge of Earth science and the synergisms existing between the various instruments are discussed throughout the plan. Also described are the many theoretical studies [called Interdisciplinary Science (IDS) investigations] that draw upon the satellite observations, and the role of field investigations in both validating instrument observations and enhancing our understanding of Earth System processes.

The Plan consists of an overview chapter followed by seven topical science chapters that discuss, in considerable detail, all aspects of EOS science. The overview chapter was written by Eric Barron of The Pennsylvania State University and gives the background of concerns and recommendations that led to the formation of the EOS Program. Each of the topical science chapters has a lead author(s) who is an expert in the particular field and is a Principal Investigator on a related IDS team. Typically, lead authors were heading up EOS scientific working groups at the time they assumed responsibility for their respective chapters. Each lead author has drawn on a team of “contributing” authors who are named at the start of each chapter. The seven science topics addressed in the plan, with their corresponding chapter names and lead authors, are as follows:

2. Radiation, clouds, water vapor, precipitation, and atmospheric circulation
D. L. Hartmann – *University of Washington*
3. Ocean circulation, productivity, and exchange with the atmosphere
D. A. Rothrock – *University of Washington*
4. Atmospheric chemistry and greenhouse gases
D. Schimel – *National Center for Atmospheric Research*
5. Land ecosystems and hydrology
S. W. Running – *University of Montana*
G. J. Collatz – *Goddard Space Flight Center*
J. Washburne – *University of Arizona*
S. Sorooshian – *University of Arizona*

6. Cryospheric systems
 - B. E. Goodison – *Atmospheric Environment Service, Canada*
 - R. D. Brown – *Atmospheric Environment Service, Canada*
 - R. G. Crane – *Pennsylvania State University*
7. Ozone and stratospheric chemistry
 - M. R. Schoeberl – *Goddard Space Flight Center*
8. Volcanoes and climate effects of aerosol
 - D. L. Hartmann – *University of Washington*
 - P. Mouginiis-Mark – *University of Hawaii.*

Readers wishing to know more details about the IDS investigations or the planned EOS spacecraft missions and the instruments they will carry are advised to consult the 1998 edition of the Earth Science Enterprise/EOS Reference Handbook. The handbook also provides the names of all IDS Principal Investigators and Co-Investigators as well as the names of the EOS instrument team leaders, team members, Principal Investigators, and Co-Investigators. An excellent way to keep current with EOS developments is to consult the EOS Project Science Office website at <http://eos.nasa.gov/>.

It should be noted that EOS is a fluid program, with changes in long-term plans always a possibility due to new scientific developments or to budgetary considerations. Authors and editors have tried to keep abreast of changes in mission and instrument names, but some of the older terminology may not have been caught in every instance. For this we apologize.

Acknowledgments

Special thanks go to D. A. Rothrock, University of Washington, who provided the outline for all the topical science chapters, and thus, in a sense, gave the necessary impetus to the launching of this Plan. Much of the technical material in the Plan was provided not only by the listed lead authors and named contributors, but also by many other unnamed EOS scientists and engineers. R. Greenstone and W. R. Bandeen (both of Raytheon Corporation) provided technical editing throughout the lengthy process of assembling and refining in standard format the text and appendices of this Plan. Design and layout of the Plan were the work of Sterling Spangler (also of Raytheon Corporation).

Michael D. King
EOS Senior Project Scientist

January 1999

CHAPTER 1

Overview

LEAD AUTHOR E. J. Barron

CONTRIBUTING AUTHORS
D. L. Hartmann
M. D. King
D. S. Schimel
M. R. Schoeberl

CHAPTER 1 CONTENTS

1.1 Introduction	7
1.2 EOS science contributions	8
1.2.1 Radiation, clouds, water vapor, precipitation, and atmospheric circulation	8
1.2.1.1 Total solar irradiance	8
1.2.1.2 The role of radiation fluxes in the climate system	11
1.2.1.3 The role of convection and clouds in climate	12
1.2.1.4 Water vapor and climate	13
1.2.1.5 Precipitation	13
1.2.1.6 Atmospheric circulation, hydrologic processes, and climate	14
1.2.2 Ocean circulation, productivity, and exchange with the atmosphere	14
1.2.3 Atmospheric chemistry and greenhouse gases	15
1.2.4 Land ecosystems and hydrology	16
1.2.5 Cryospheric systems	17
1.2.6 Ozone and stratospheric chemistry	18
1.2.7 Volcanoes and climate effects of aerosols	19
1.2.8 National and international contributions to major field campaigns	20
1.3 Measurement strategy	21
1.3.1 Simultaneous observations	21
1.3.2 Overlap strategy	22
1.3.3 Diurnal sampling	23
1.3.4 Calibration requirements	23
1.3.5 Continuity	23
1.4 EOS contributions to national goals and needs	26
1.4.1 Atmospheric ozone and UV-B radiation	26
1.4.1.1 The national interest	26
1.4.1.2 National policy requirements	26
1.4.1.3 EOS policy-relevant contributions	26
1.4.2 Natural variability and enhanced climate prediction	28
1.4.2.1 The national interest	28
1.4.2.2 National policy requirements	28
1.4.2.3 EOS policy-relevant contributions	28
1.4.3 Long-term climate change including global warming	30
1.4.3.1 The national interest	30
1.4.3.2 National policy requirements	30
1.4.3.3 EOS policy-relevant contributions	30
1.4.4 Ecosystem change and biodiversity	33
1.4.4.1 The national interest	33
1.4.4.2 National policy requirements	33
1.4.4.3 EOS policy-relevant contributions	33
1.4.5 Human dimensions and economics	34
1.4.5.1 The national interest	34
1.4.5.2 National policy requirements	34
1.4.5.3 EOS policy-relevant contributions	34
1.5 Summary	36
Chapter 1 Index	37

1.1 Introduction

NASA's Earth Observing System (EOS) was designed to initiate a new era of integrated global observations intended to advance our understanding of the entire Earth system on a global scale through developing a deeper understanding of the components of that system, their interactions, and how the Earth is changing. EOS plays a critical role in addressing a key challenge—to develop the capability to predict the changes that will occur in the next decade to century, both naturally and in response to human activity.

The EOS program was founded in response to a compelling scientific vision driven by recognition of the societal importance of the natural variability on our planet and realization that humans are no longer passive participants in the evolution of the Earth system. In 1979, the World Climate Research Program (WCRP) initiated an international effort to understand the physical basis of climate in response to droughts and floods that revealed societal vulnerability to climate variability. In 1982, a NASA workshop led by Richard Goody described the need for a scientific program designed to “ensure continuing habitability” of our planet in the face of the expansion of the human population and its activities. Then in 1986, the International Geosphere-Biosphere Program (IGBP) was initiated with the objective “to describe and understand the interactive physical, chemical, and biological processes that regulate the Earth’s unique environment for life, the changes that are occurring in this system, and the manner in which they are influenced by human actions.”

A new view, based on an integrated programmatic framework, emerged as the central paradigm of both national and international programs. The foundation for this paradigm was a recognition that: 1) the Earth can be understood only as an integrated system; 2) each decade will likely bring a new specific environmental crisis for which the solutions must draw on years of accumulated understanding; and 3) science is a partner in decision-making, guided by the potential to benefit society and to enhance our economic security.

There is little doubt that an integrated Earth systems view would have eventually emerged as a product of the maturity of the Earth science disciplines and the powerful global and synoptic tools of study that have been developed over the last decades. However, a sense of urgency developed in direct response to the observations of ozone depletion over Antarctica, evidence of widespread tropical deforestation, and the record of increasing concentrations of carbon dioxide measured at Mauna Loa

observatory and the related climate model predictions of global warming.

The Earth System Sciences Committee commissioned by NASA (ESSC 1988) provided the intellectual framework for an integrated research approach designed to address these critical issues. The report called for sustained long-term measurements of global variables to record the vital signs of the Earth system and the observations required to provide a fundamental description of the Earth and its component parts. The report urged that, as part of an integrated research approach, these observations must be intimately coupled to focused process studies, the development of Earth system models, and an information system that ensures open access to consistent, long-term observations of the Earth system.

A consistent view is obtained from the broad suite of National Research Council (NRC) (1985; 1986; 1988; 1990; 1992) reports that also call for an observing strategy that strengthens the base of knowledge in all the sciences that deal with the Earth, quantifies the magnitude of the driving forces for global change, and monitors the state of the Earth system and its “vital” signs. These reports call for an observing strategy that focuses on the highest priority measurements needed for each of the major disciplines of the Earth sciences and on the importance of simultaneity, calibration, and continuity of measurements to establish how the Earth is changing, and to develop and validate global predictive models.

The role of satellite systems in developing this research strategy is unique because of the capability to provide a long-term, consistent, calibrated, global set of observations. NASA's EOS was designed specifically in response to the recommendations of the ESSC and the NRC, and was instituted as an integral element of the U.S. Global Change Research Program (USGCRP).

The U.S. Global Change Research Program outlined an accelerated, focused research strategy designed to reduce key scientific uncertainties and to develop more-reliable predictions. The research priorities of the USGCRP are based on a series of policy-relevant questions that reflect areas of substantial uncertainty (Table 1.1). The evolution of the USGCRP has continued to sharpen the set of questions as a result of discovery and debate. EOS objectives, and associated critical measurements, encompass many of the priorities outlined by the USGCRP and include contributions in seven disciplinary areas, each of which is the subject of a chapter in this Science Plan:

- Radiation, Clouds, Water Vapor, Precipitation, and Atmospheric Circulation;
- Ocean Circulation, Productivity, and Exchange with the Atmosphere;
- Atmospheric Chemistry and Greenhouse Gases;
- Land Ecosystems and Hydrology;
- Cryospheric Systems;
- Ozone and Stratospheric Chemistry; and
- Volcanoes and Climate Effects of Aerosols

The scientific challenges within each of these major research areas define an observation strategy in which simultaneity, calibration, and continuity are critical ingredients.

The evolution of the USGCRP has also resulted in a clearer call to address the implications of global change

through assessments of impacts, and a greater focus on the most policy-relevant themes. Four key USGCRP global change issues are: 1) seasonal-to-interannual climate variability, 2) climate change over decades to centuries, 3) changes in ozone, ultraviolet radiation, and atmospheric chemistry, and 4) changes in land cover and in terrestrial and aquatic systems. In addition to these areas of particular scientific and practical importance, USGCRP has defined an overarching objective (often referred to as “human dimensions”) to identify, understand, and analyze how human activities contribute to changes in natural systems, how the consequences of natural and human-induced change affect the health and well-being of humans and their institutions, and how humans could respond to problems associated with environmental change.

1.2 EOS science contributions

The EOS science contributions begin with a commitment to measuring 24 critical variables (Table 1.2). These 24 measurements are a foundation for a coordinated research program addressing the highest priority elements of the USGCRP.

1.2.1 *Radiation, clouds, water vapor, precipitation, and atmospheric circulation*

The temperature near the surface of the Earth is in thermodynamic equilibrium when the absorption of radiant energy from the sun is in approximate balance with the emission of radiant energy to space from the Earth. Thus, the energy output of the sun provides a critical control on the Earth’s climate. The amount of the solar energy that is absorbed by the Earth depends on Earth’s reflectivity, and the reflectivity is strongly dependent on the fractional coverage and optical properties of clouds in the atmosphere, the amount and optical properties of aerosol particles in the atmosphere, the atmospheric humidity, and the condition of the surface.

The surface temperature of the Earth depends not only on the absorbed solar radiation but also on the rate at which energy is re-radiated to space from the Earth. The rate of re-radiation is controlled by both the amount and the vertical distribution of not only the clouds and aerosol particles but also the atmospheric greenhouse gases in the atmosphere, of which the most important is water vapor. The water vapor distribution interacts strongly with convection in the atmosphere and the associated clouds,

precipitation, and large-scale circulations and also interacts strongly with the thermal structure of the atmosphere.

Understanding the interactions among the various elements mentioned above and incorporating this understanding into appropriate models constitutes a critical step in predicting future climate changes and their regional and global impacts. Likewise, improved understanding in these areas will help in the prediction of seasonal and interannual climate variability. Beyond the confines of the atmosphere there are also interactions with the oceans to be considered, and these are strongly modulated by clouds, water vapor, and large-scale circulations.

1.2.1.1 *Total Solar Irradiance (TSI)*

Long-term solar monitoring from space began with the Earth Radiation Budget (ERB) experiment in late 1978 and has continued into the present time frame with measurements from the Active Cavity Radiometer Irradiance Monitor II (ACRIM II) on NASA’s Upper Atmosphere Research Satellite (UARS). Consistent measurements by ACRIM instruments I and II have shown variations in TSI running from a low of about 1367 Wm^{-2} at a solar cycle minimum in 1986 to a high of about 1369 Wm^{-2} in 1992 at a solar cycle peak. Although these changes appear small, sustained changes in TSI of as little as a few tenths of one percent could be causal factors for significant climate change on time scales ranging from decades to centuries.

TABLE 1.1

What is the role of clouds in the Earth's radiation and heat budgets?
How do the oceans interact with the atmosphere in the storage, transport, and uptake of heat?
How will changes in climate affect temperature, precipitation, and soil moisture patterns, and the general distribution of water and ice on the land surface?
How can the reliability of global- and regional-scale climate predictions be improved?
What is the relative importance of the oceans and terrestrial biosphere as sinks for fossil fuel carbon dioxide, and how do they change with time?
What are the major sources responsible for the current increases in atmospheric nitrous oxide and methane?
What are the implications for stratospheric ozone, globally and in polar regions, of increased concentrations of chlorine and bromine?
What ecological systems are most sensitive to global change, and how can natural change in ecological systems be distinguished from change caused by other factors?
What are the likely rates of change in ecological systems due to global change, and will natural and managed systems be able to adapt?
How do ecological systems themselves contribute to processes of global change?
What are the natural ranges and rates of change in the climate and environmental systems?
How rapidly have ecosystems adapted to past abrupt transitions in climate?
Do past warm intervals in Earth history provide appropriate scenarios to test model predictions of future global warming?
What kinds of empirical data are needed to measure and understand human interactions in global change?
How and why do human beings and human systems influence physical and biological systems?
How do different coastal regions respond geologically and ecologically to higher sea level, and how can the contributions from changes in climate (e.g., glacier melting and ocean warming) be differentiated from those due to tectonic processes?
What are the magnitude, geographic location, and frequency of volcanic eruptions and their effect on climate?
How do permafrost regions of the Northern Hemisphere respond to climate warming?
What aspects of solar variability are influencing the stratospheric ozone layer?
What impacts do other inputs, e.g., particles, have on the upper atmosphere and how are they coupled to other atmospheric regions?
How does the sun's output vary and what is the impact on terrestrial climate?

Policy-relevant questions addressed by the USGCRP, including EOS.

TABLE 1.2

ATMOSPHERE	Cloud Properties <i>(amount, optical properties, height)</i>	MODIS, GLAS, AMSR-E, MISR, AIRS, ASTER, EOSP, SAGE III
	Radiative Energy Fluxes <i>(top of atmosphere, surface)</i>	CERES, ACRIM, TSIM, MODIS, AMSR-E, GLAS, MISR, AIRS, ASTER, SAGE III
	Precipitation	AMSR-E
	Tropospheric Chemistry <i>(ozone, precursor gases)</i>	TES, MOPITT, SAGE III, MLS, HIRDLS, LIS
	Stratospheric Chemistry <i>(ozone, ClO, BrO, OH, trace gases)</i>	MLS, HIRDLS, SAGE III, OMI, TES
	Aerosol Properties <i>(stratospheric, tropospheric)</i>	SAGE III, HIRDLS, MODIS, MISR, EOSP, OMI, GLAS
	Atmospheric Temperature	AIRS/AMSU, MLS, HIRDLS, TES, MODIS
	Atmospheric Humidity	AIRS/AMSU/HSB, MLS, SAGE III, HIRDLS, Poseidon 2/JMR, MODIS, TES
	Lightning <i>(events, area, flash structure)</i>	LIS
	SOLAR RADIATION	Total Solar Irradiance
Ultraviolet Spectral Irradiance		SOLSTICE
LAND	Land Cover & Land Use Change	ETM+, MODIS, ASTER, MISR
	Vegetation Dynamics	MODIS, MISR, ETM+, ASTER
	Surface Temperature	ASTER, MODIS, AIRS, ETM+
	Fire Occurrence <i>(extent, thermal anomalies)</i>	MODIS, ASTER, ETM+
	Volcanic Effects <i>(frequency of occurrence, thermal anomalies, impact)</i>	MODIS, ASTER, ETM+, MISR
	Surface Wetness	AMSR-E
OCEAN	Surface Temperature	MODIS, AIRS, AMSR-E
	Phytoplankton & Dissolved Organic Matter	MODIS
	Surface Wind Fields	SeaWinds, AMSR-E, Poseidon 2/JMR
	Ocean Surface Topography <i>(height, waves, sea level)</i>	Poseidon 2/JMR
CRYOSPHERE	Land Ice <i>(ice sheet topography, ice sheet volume change, glacier change)</i>	GLAS, ASTER, ETM+
	Sea Ice <i>(extent, concentration, motion, temperature)</i>	AMSR-E, Poseidon 2/JMR, MODIS, ETM+, ASTER
	Snow Cover <i>(extent, water equivalent)</i>	MODIS, AMSR-E, ASTER, ETM+

Key physical variables needed to advance understanding of the entire Earth system and the interactions among the components. The EOS instruments listed in bold font are primary sensors, bold italics represent secondary instruments, and roman fonts are contributing instruments for critical measurements.

NASA's EOS directly addresses this critical issue:

- EOS has the potential to determine TSI with 0.001% relative precision by using overlapping flights of the ACRIM instrument with 0.1% absolute accuracy. This precision is sufficient to detect climatically-significant changes.

1.2.1.2 *The role of radiation fluxes in the climate system*

The climate system is a heat engine that is driven by the spatial and temporal distribution of the entry and exit of broadband radiant energy. Radiation is the primary forcing element in climate change. Modern climate models have consistently indicated that CO₂ and other anthropogenic trace gases will change the vertical distribution of radiative fluxes in the atmospheric column so as to warm the troposphere and cool the stratosphere.

Radiation is important for climate feedback. Clouds are second only to greenhouse gases in terms of their effect on climate. However, there is great uncertainty about cloud radiative forcing and feedback, posing the most formidable obstacle to climate prediction by general circulation models (GCMs). We cannot reliably predict the climate response to a given radiative forcing because of the uncertainty in the cloud/climate feedback to changes in radiation at the Top of the Atmosphere (TOA). Estimating the radiative effects of clouds and retrieving cloud properties from space both require a detailed understanding of the scattering and absorption properties of clouds. The direct and indirect radiative effects of aerosols constitute the largest uncertainties in the anthropogenic radiative forcing of climate. Anthropogenic sulfate aerosols mostly scatter shortwave radiation and cool the climate. Smoke from biomass burning may have a global cooling effect of 0.2-2 Wm⁻². Although there have been fairly good simulations of transient temperature variations to the radiative forcing due to the aerosol plumes that resulted from the 1991 Mt. Pinatubo eruption, our knowledge of the global distribution of aerosols is inadequate to assess their role in future climate.

The surface of the Earth absorbs about twice as much solar radiation as does the atmosphere. The amount of solar radiation that is absorbed by the surface is modulated by a surface solar albedo that ranges from 0.06 for diffuse radiation striking the ocean to approximately 0.90 for some of the freshest snow. The Global Energy and Water Cycle Experiment (GEWEX) Surface Radiation Budget (SRB) Project has found that errors in both shortwave and longwave radiation measurements over snow and ice surfaces and for longwave radiation in persistently

cloudy regions are larger than those in other regions. Surface albedos and radiative fluxes over snow-free land are also not known to sufficient accuracy. Until surface albedo of all land surfaces is known to greater accuracy, it will not be possible to quantify adequately the radiative forcing to climate that is associated with changes in land use. Despite their importance, TOA shortwave and longwave radiative flux measurements currently available from the Earth Radiation Budget Experiment (ERBE) seem to have an error of about 5 Wm⁻², which presumably contributes to even larger errors in surface radiative fluxes. The surface energy budget also provides a key forcing to ocean circulation so that more-accurate information is needed in this aspect of radiation studies as well.

NASA's EOS directly addresses many of these critical issues:

- EOS will contribute to improved understanding of the effects of the atmospheric trace gases by producing more-accurate vertical profiles and time histories of water vapor and radiatively active gases and by validating the radiative transfer physics for both the natural and anthropogenic gases in the atmosphere.
- The EOS instrument Clouds and the Earth's Radiant Energy System (CERES), along with other EOS instruments such as the Multi-angle Imaging Spectroradiometer (MISR) and the Earth Observing Scanning Polarimeter (EOSP), is expected to provide significant advances in the estimate of radiative forcing by clouds. EOS will begin to resolve problems caused by cloud overlap and cloud geometrical thickness through use of both passive and active sensors.
- The long homogeneous record of clouds and radiation fluxes to be provided by EOS in the course of 15-to-18 years of observations will allow seasonal and interannual variability to be sampled adequately and will be used to understand connections within the climate system that only appear on longer time scales.
- EOS instruments MISR and EOSP will significantly advance our understanding of the distribution and radiative character of atmospheric aerosols.
- EOS will determine the surface albedo of all land surfaces to a greater accuracy, providing the possibility to better quantify the radiative forcing due to land use and land-cover changes.

- The retrieval of longwave radiation measurements will be improved by combining satellite measurements with data from ocean-based monitoring stations that would provide both SRB and cloud-base heights.

1.2.1.3 *The role of convection and clouds in climate*

Clouds not only affect the radiative energy fluxes in the atmosphere through scattering, absorption, and re-radiation, but vertical motions associated with them produce important convective transports of energy and moisture. Clouds produce a redistribution of energy between the surface and the atmosphere that may be larger than the net effect of clouds on the energy balance at the TOA. Convection associated with clouds also affects the exchange of heat between the surface and the atmosphere. The cloud type that appears to exert the greatest effect on climate sensitivity in state-of-the-art global GCMs is the tropical mesoscale anvil cloud that accompanies cumulus convection. The central question is how to represent such features as the detrainment of ice from cumulus updrafts into anvil clouds.

Scale is also a critical issue in understanding and predicting atmospheric circulation systems. Mesoscale models (MMs) have become powerful tools for understanding and forecasting regional atmospheric circulations, taking into account such features as severe midlatitude cyclones, hurricanes, orographically-forced flow, fronts, and thermally-forced flows such as land/sea breezes. Development and validation of these models and their parameterizations are important objectives in atmospheric sciences.

Radiative flux determinations are the highest priority measurements that are needed to understand the role of cloud feedback mechanisms in the climate system. At this time net radiative energy flux determinations at the TOA need to be supplemented by the more-difficult determinations of the net radiative energy flux at the Earth's surface. The vertical distribution of radiative cooling/heating inside the atmosphere is also very important. In order of priority are the TOA radiative flux, the surface radiative flux, and the radiative flux at the tropopause. In order to improve simulations of cloud forcing and its effect on climate sensitivity, more-detailed measurements of cloud properties are needed to provide understanding and model validation.

NASA's EOS directly addresses many of these critical issues:

- EOS observations will provide data for validation on three scales (global, regional, and cloud-resolving), and EOS interdisciplinary modeling investigations focus on a range of efforts that range from 100-year integrations (global), to 10-day integrations (regional), to 1-day (cloud resolving).
- The Lightning Imaging Sensor (LIS), whose lightning occurrence record will serve as an index of convection intensity, and AIRS, whose temperature and moisture profiles will yield estimates of convective available potential energy, will address key questions regarding cloud characteristics that are faced by climate modelers.
- Several EOS interdisciplinary investigations are pursuing improved understanding of cloud-climate feedbacks. The higher spatial resolution, availability of new cloud variables, and greater accuracy of EOS cloud observations will enable better validation of regional cloud simulations.
- TOA radiative flux measurements from space will enter their fourth generation with the CERES instruments on the Tropical Rainfall Measuring Mission (TRMM) and on the EOS AM-1 and PM-1 spacecraft. The most recent ERBE measurements provide the standard of comparison for global radiation data sets. The CERES measurement errors are expected to be a factor of 2-to-4 lower than the ERBE errors.
- In the EOS time frame, calculated shortwave surface flux accuracies should increase greatly as more-accurate cloud (Visible Infrared Scanner [VIRS], Moderate-Resolution Imaging Spectroradiometer [MODIS]), atmospheric (AIRS), and surface (MISR, MODIS) properties become available.
- In the EOS time frame, improved tropospheric water vapor determinations will help better determine downward longwave fluxes. The water vapor determinations will be available from the AIRS/Humidity Sounder from Brazil (HSB) instruments and, over land, from MODIS.
- Active systems such as the Geoscience Laser Altimeter System (GLAS) lidar from EOS and a proposed 94-GHz cloud radar may offer the best solution to the large uncertainty in the calculations of downward longwave flux at the surface due to uncertainties in cloud overlap.
- The EOS MODIS instrument has design capabilities specifically directed toward cloud-property determinations. Very-high-spatial-resolution measurements

from the EOS Advanced Spaceborne Thermal Emission and Reflection Radiometer (ASTER), multi-angle EOS MISR data, polarization of cloud particles determinations from EOS EOSP, all will contribute to the validation of the MODIS data. The final step in cloud remote sensing during the EOS era will be the combination of data from the passive sensors just cited with data from EOS GLAS (the active laser sensor) and the proposed cloud radar.

- Other cloud properties that will be the subject of investigation in the EOS era include cloud fraction, cloud visible optical depth and thermal infrared emittance, cloud particle size, cloud liquid/ice water path, and cloud mesoscale organization and structure. Improved spectral resolution (including solar, terrestrial infrared, and microwave coverage) and spatial resolution, multi-angle coverage, and the use of both passive and active sensors will lead to improvements in the determinations of these cloud properties.

1.2.1.4 Water vapor and climate

Most of the water in the atmosphere is in the form of vapor, and water vapor plays a critical role in many key processes in the hydrologic and energy cycles. Water vapor is the most important greenhouse gas, both in terms of its role in maintaining the current climate and in terms of its role in sensitivity through the water vapor feedback process. The abundance and vertical distribution of water vapor in the atmosphere interact very strongly with convection and cloudiness, thereby influencing the albedo of the planet as well as the infrared opacity of the atmosphere. Climate feedbacks are sensitive to the vertical distribution of both water vapor and temperature. In every respect, the water vapor data sets available to date are inadequate for climate studies. Radiosondes are limited in their geographic coverage, and satellite retrievals suffer from poor vertical resolution and accuracy.

NASA's EOS directly addresses many of these critical issues:

- Data from EOS instruments will improve the quality of global measurements of the water vapor distribution. In particular, the EOS instruments, AIRS, Advanced Microwave Sounding Unit (AMSU), and HSB, working in combination, will provide more-precise simultaneous measurements of temperature and humidity in the troposphere, with better vertical resolution than is currently available.

- EOS cloud and moisture measurements, when combined with wind estimates from data assimilation techniques and with in situ measurements from field programs, will provide a much better understanding of the mechanisms whereby the moisture balance of the troposphere is maintained.
- EOS data will play an important role in validating the new generation of climate models that account explicitly for cloud water and ice, their transport, and their evaporation to provide a source of water vapor in the free atmosphere.
- AIRS/AMSU/HSB, and the EOS instruments High-Resolution Dynamics Limb Sounder (HIRDLS) and Microwave Limb Sounder (MLS) will supply improved horizontal and vertical resolution temperature and moisture measurements. Also, the EOS Stratospheric Aerosol and Gas Experiment III (SAGE III) instrument will provide very accurate monitoring of water vapor trends in the stratosphere.

1.2.1.5 Precipitation

Rainfall plays a central role in governing the climate of the Earth. The latent heat release in convection is a major source of energy that drives the general circulation of the atmosphere. Much of the solar radiation absorbed by the Earth is used to evaporate water, which later condenses to release latent heat in the atmosphere during precipitation. Latent heat release in tropical convection forces atmospheric motions that disperse heat and moisture into the extratropics, diverting subtropical jet streams, and altering rainfall patterns in midlatitudes. Precipitation is also of critical importance to human systems and the distribution and character of life.

The distribution of precipitation is highly inhomogeneous in space and time. Because of the wide range of variability in both time (minutes to years) and space (less than a kilometer to thousands of kilometers) the long-term accurate mapping of global precipitation is a daunting task. Atmospheric models have been shown to be able to produce a global precipitation rate to within 10-20% of that observed, but they have many serious faults otherwise. They differ particularly in their ability to estimate regional and subcontinental rainfall variability, and they also underestimate the frequency of occurrence of the light-rain category. Satellite rainfall retrieval algorithms play a vital role in producing realistic global rainfall distributions because it is impossible to set up uniform networks of rain gauges over the entire globe.

NASA's Earth Science Enterprise directly addresses many of these critical issues:

- TRMM employs a suite of sensors including one microwave (TRMM Microwave Imager [TMI]), one visible (VIS)/infrared (IR) (VIRS), and one active precipitation radar (PR) with the objective of producing the best rainfall estimates from space, especially for the world's tropics and subtropics. Within the EOS measurement system, the key instruments for precipitation measurement are the Advanced Microwave Scanning Radiometer-EOS (AMSR-E) and HSB on the EOS PM-1 platform.

1.2.1.6 Atmospheric circulation, hydrologic processes, and climate

The presence of clouds, water vapor, and precipitation in the atmosphere significantly alters the Earth's radiation budget and causes differential heating between the tropics and the polar regions, between the oceans and the land, and between clear and cloudy regions. This differential heating is the main driver of the atmospheric large-scale circulation, and the essential component of the circulation is the wind. The consideration of the atmospheric wind circulation is indispensable in order to understand the role of the global hydrologic cycle, clouds, water, and precipitation on regional and global climate fluctuations.

While radiative forcings such as that due to doubling of CO₂ may be small, feedback processes in the climate system may amplify the initial response to the radiative forcing. Especially for climate changes on seasonal and interannual time scales, the large-scale circulation plays a fundamental role.

NASA's EOS makes a number of important contributions in addition to those described above:

- The EOS QuikSCAT, followed by the SeaWinds instrument on the Japanese Advanced Earth Observing System II (ADEOS II) spacecraft, will provide surface wind speed and direction over the oceans from scatterometry, and EOS passive microwave radiometry, using AMSR-E, will contribute to wind determinations over the ocean as well.

1.2.2 Ocean circulation, productivity, and exchange with the atmosphere

The oceans of the world play a key role in modulating climate. The ocean is a major agent in the equator-to-pole redistribution of heat. The positions of major current systems such as the Gulf Stream, the Kuroshio, and the Antarctic circumpolar current are major factors in gov-

erning temperature patterns and the transport of nutrients, chemicals, and biota. Models of ocean circulation are well-developed, although coupled models of ocean physics and biogeochemistry are in the initial stages of development.

The exchange of gases and, in particular, carbon dioxide, between air and sea is a crucial part of the climate perturbation equation and as such is a critical area of research for the EOS program (methyl bromide exchange is also of interest). Among questions that need to be resolved are: how do changes in surface forcing of heat, momentum, and nutrient fluxes affect carbon cycling in the upper oceans; what are the amounts of the fluxes of carbon dioxide, carbon monoxide, and dimethyl sulfide across the air-sea interface; and what are the factors affecting the productivity of the oceans. Global estimates of the mean and time-varying components of ocean photosynthetic carbon production and its relation to nutrient cycles differ widely and will not be resolved without sophisticated analyses and models involving both satellite and in situ data. Large uncertainties exist in the estimates of the carbon dioxide flux across the ocean-atmosphere interface. The oceans are a sink for carbon dioxide, and hence play a key role in moderating the effects of increased carbon dioxide on global warming.

The ability to forecast well in advance the timing and geographic extent of season-to-interannual climate anomalies is predicated on the thermal inertia of the climate system, which is based on the slow response to forcings of the oceans as compared to the more-rapid forcings of the atmosphere.

Air-sea momentum fluxes and near-surface winds modulate the coupling between the atmosphere and the ocean. Wind stress is the largest single source of momentum in the upper ocean, and air-sea momentum fluxes substantially influence large-scale upper-ocean circulation, smaller-scale mixing, and the detailed shape of the sea surface on all scales.

Decadal-to-centennial variations in the thermohaline circulation of the ocean depend on exchanges of heat and water with the atmosphere. Simple atmospheric boundary layer models can explain much of the observed pattern of sensible and latent heat fluxes over the global oceans. However, observations in the data-sparse areas of the southern and tropical oceans are insufficient to provide reliable estimates of the surface turbulent and radiative fluxes.

Freshwater forcing is an important aspect of the global water balance. Local freshwater at the ocean surface limits exchanges of heat and moisture with the atmosphere. In the atmosphere, fluxes of heat and moisture drive tropospheric vertical convection, horizontal

advection, and precipitation patterns. Notably, surface freshwater forcing is believed to play a primary role in setting the background state and timing of the El Niño Southern Oscillation (ENSO) phenomenon.

Major climate-related factors that contribute to sea-level rise are thermal expansion in the oceans as well as ablating mountain glaciers and polar ice sheets. Major uncertainties exist in the contributions of the Greenland and Antarctic ice sheets to recent changes in sea level as well as predicted future changes. Ocean tides cause a larger sea-level signal than temporal changes in ocean circulation and sea level so that an accurate tidal model is required to remove the tidal signal for studies of ocean circulation.

NASA's EOS directly addresses many of these critical issues:

- The EOS Jason-1 radar altimeter (Poseidon 2) will serve to determine multi-decadal global sea-level variations and their long-term trends; and the Advanced Microwave Scanning Radiometer-EOS Version (AMSR-E) and SeaWinds measurements will contribute wind-stress information as above.
- The EOS MODIS instrument will provide sea-surface temperature (SST) measurements, based on infrared emissions from the oceans, for cloud-free conditions to the level of a few tenths kelvin. EOS AMSR-E will provide SST measurements with an accuracy of 1-to-1.5 K in all weather conditions, providing substantial additional information on the role of the oceans in the Earth's heat and hydrologic cycles.
- The EOS MODIS instrument will also be key for the measurement of ocean color. These data will be used to estimate phytoplankton abundance and productivity, as well as the amount of dissolved organic material and suspended particulate material. MODIS will also measure sun-stimulated fluorescence from chlorophyll, which will greatly improve estimates of upper ocean productivity.
- Several EOS interdisciplinary science investigations (IDS) focus on the interactions between the atmosphere and ocean across the sea surface. EOS worldwide observations of ocean surface wind stress by the SeaWinds scatterometer instruments, with accuracies of 10-to-12% in speed, will be critical to achieving these objectives. In addition, the EOS AMSR-E passive microwave instrument will provide complementary continual observations of wind speeds and stress magnitudes over the oceans.
- IDS studies of the ocean's biological system and its interplay with the ocean circulation and the global carbon cycle will be the focus of several EOS science teams. Long-term, well-calibrated measurements of ocean color from the EOS MODIS sensors and from the NASA Sea-viewing Wide Field-of-View Sensor (SeaWiFS) are essential for these studies. These data will be combined with physical measurements (such as scatterometer winds and radar altimetry) in numerical models to study both open ocean and coastal ocean processes.

1.2.3 Atmospheric chemistry and greenhouse gases

The interaction of biological, geochemical, and photochemical processes, the so-called biogeochemical processes, affect the global carbon dioxide, carbon monoxide, methane, nitrous oxide, and ozone budgets. Six major factors drive global change, and therefore, EOS research.

First, changes of land cover/land use constitute one of the most potent forces affecting global greenhouse gases. Whereas fossil fuel burning and cement production add 5.5 Gt C/yr to the atmosphere, land-cover change adds another 1-2 Gt C/yr. Land-cover changes also affect nitrous oxide and nitric oxide emissions.

Second, interannual variability in climate has been shown to lead to substantial interannual variability in terrestrial ecology and atmospheric chemistry. Remote sensing from satellites is the best means for understanding the geographic distribution of climate anomalies and the spatial response of the oceans and land ecosystems.

Third, changes in global hydrology and patterns of soil moisture in wetlands strongly affect the methane budget. New improved regional and global data sets on wetland extent and seasonality are needed.

Fourth, the spatial distribution and budget of tropospheric ozone are caused by changing sources of precursors arising from fossil fuel burning, biomass burning, and, possibly, changing biogenic sources in soils and vegetation.

Fifth, the vertical distribution of tropospheric ozone influences the integrated radiative effect of ozone, and, hence, its effects on climate. The vertical profile will change as the geography of sources changes, as atmospheric convection and mixing change, and as further anthropogenic sources are introduced. Accurate predictive models will be extremely difficult to develop and evaluate without strong constraints from global observations.

Sixth, the processes that interact to control ocean carbon uptake are physical, chemical, and biological. The kinetics of carbon dioxide gas transfer across the ocean-

atmosphere interface is slow, on the order of a year, much slower than biological processes leading to carbon uptake. What determines the partitioning of anthropogenic carbon dioxide among the atmosphere, the oceans, and the terrestrial biosphere is still the subject of research.

NASA's EOS provides many key data products and analyses:

- EOS products will encompass many aspects of the carbon cycle, including provision of a global database of high-resolution analyses of land-cover change, estimates of the contribution of biomass burning to atmospheric CO₂, and trends in carbon fixation by terrestrial vegetation determined from observed changes in leaf-area index (LAI) and fraction of photosynthetically-active radiation.
- EOS will provide estimates of the extent and duration of inundation of wetlands and land cover, important elements in assessing methane production and oxidation.
- The EOS Tropospheric Emission Spectrometer (TES) will provide measurements related to nitrous and nitric oxide production and abundance.
- Ozone and related species will be monitored using EOS instruments, particularly those on the CHEM-1 mission. The Measurements of Pollution in the Troposphere (MOPITT) will make measurements of carbon monoxide and methane. MODIS observations of fire will lead to estimates of biomass burning contributions of hydrocarbons, methane, oxides of nitrogen, and nonmethane hydrocarbons to ozone production.

1.2.4 Land ecosystems and hydrology

Changes in land-surface processes and properties interact with, and cause changes in, both regional and global climate. The land-surface models that are utilized to assess these interactions generally contain formulations for surface radiation fluxes, turbulent and mass fluxes, liquid water fluxes, and control of water vapor and CO₂ fluxes by vegetation. However, these models still exhibit major differences in their predictions, and current models still do a poor job of representing water and energy exchanges between the land and the atmosphere that must be known in order to predict correctly the temporal and spatial fields of precipitation and surface radiation. Land-surface properties such as type of cover, LAI, roughness length, and albedo are essential variables to address these

limitations. Realistic representations of land-surface cover and moisture characteristics are likely to improve both climate and weather forecasting capabilities. There are also important questions regarding the interactions and feedbacks between the atmosphere and the surface in cases where the biosphere changes in response to elevated levels of atmospheric carbon dioxide.

Changing climate and land-surface characteristics may combine to change precipitation patterns, surface-water partitioning and storage, and river flows. Of further concern are the land processes that may alter water quality: erosion, sedimentation, and river biogeochemistry. One of the major objectives of research must be to improve hydrologic understanding at critical human scales. Thus key science issues for land-hydrology are to identify and quantify key hydrologic variables across a range of scales, and to develop or modify hydrologic process models to take advantage of operational and realistic data sources. The hydrologic variables that require more study include precipitation, runoff, evapotranspiration, near-surface soil moisture, infiltration and deep percolation, radiation, and near-surface meteorology. Information is also needed for the estimation of the land-surface water balance and the estimation of the possibilities for extreme hydrologic events such as severe storms, floods, and droughts. The role of river biogeochemistry in affecting water quality and the functioning of aquatic ecosystems must also be examined.

The primary concern regarding land-vegetation interactions is with how biome distribution is influenced by, and in turn influences, changes in land cover and climate. There are serious questions relating to how the regional distribution and magnitude of crop, range, and forest productivity will change with climate and land-use change.

NASA's EOS contributes substantially to addressing these issues:

- EOS vegetation measurements will range from interannual variability in spring phenology to seasonal changes in daily terrestrial surface CO₂ balance to annual and interannual changes in net primary production (NPP).
- Direct measurements from EOS will include aspects of land cover and land-cover change. Other biophysical variables such as LAI, fraction of photosynthetically-active radiation that is absorbed, albedo, and vegetation indices are derived from direct measurements. A key derived product is net primary production (NPP), and the EOS MODIS instrument

was specifically designed, in part, to calculate this parameter. MODIS will produce values of NPP on a weekly basis to be available globally at 1-km resolution.

- ASTER, operating in the visible, shortwave infrared, and thermal infrared, will provide surface reflectances and radiative (brightness) temperatures with 15-to-90-m resolution depending on wavelength. The thermal infrared radiances can be used to derive surface kinetic temperatures and spectral emissivities. The kinetic temperatures can then be used to determine sensible and latent heat fluxes and ground heat conduction. Still other parameters can be derived from the surface kinetic temperatures as well.
- The Enhanced Thematic Mapper+ (ETM+) on the Landsat 7 platform, operating in the visible, near and shortwave infrared, and thermal infrared, will be used primarily to characterize and monitor changes in land cover and land-surface processes. It will have a panchromatic band with 15-m resolution, and will have 30-m resolution in the visible and near-infrared channels, and 60-m resolution in the thermal infrared. The characteristics of ETM+ are such that it will provide data sufficiently consistent with previous Landsat data to meet requirements for global-change research.
- MISR, operating in the visible, and viewing the Earth at nine discrete angles, will provide measurements that lead to determination of surface albedo and vegetation canopy structural parameters, thereby leading to derivations of photosynthetically-active radiation and improved values of canopy photosynthesis and transpiration rates.
- MODIS, operating in the visible and infrared with spatial resolution from 250 m to 1 km at nadir, will be the primary sensor for providing data on terrestrial biospheric dynamics and vegetation process activity. Land products from MODIS include spectral albedo, land cover, spectral vegetation indices, snow and ice cover, surface temperature and fire, plus biophysical variables such as LAI and fraction of photosynthetically-active radiation.

1.2.5 Cryospheric Systems

The cryosphere is an integral part of the global climate system, with important linkages and feedbacks generated through its influence on surface energy and moisture fluxes, clouds, precipitation, hydrology, and atmospheric

and oceanic circulation. Because of the sensitivity of the cryosphere to temperature changes, accurate information on the rate and magnitude of changes in cryospheric elements (ice sheets, sea ice, snow cover, lake ice, permafrost) is essential. In particular, the potential for ice-sheet melting and associated sea-level rise under conditions of global warming is a central concern. High-latitude regions exhibit the greatest warming in response to higher levels of greenhouse gases in many GCM experiments. Unfortunately, climate models do not yet provide accurate meteorological simulations over the polar regions. Further, significant improvements in the representation of cryospheric processes and in understanding cryosphere-climate linkages and feedbacks are required to reduce uncertainties in the prediction of high-latitude climate change.

Realistic simulation of snow cover in climate models is essential for correct representation of the surface energy balance, as well as for understanding winter water storage and predicting year-round runoff. The lack of meteorological and snow-cover data to execute, calibrate, and validate snow-cover models is a major obstacle to improved simulations. Positive feedbacks involving sea ice and climate change have also been treated rather simply in global climate models although studies have shown that this important feedback is dependent on lead fraction, melt ponds, ice-thickness distribution, snow cover, and sea-ice extent. Glacier mass balance, and the potential for rapid ice-sheet thinning and sea-level rise, represents one of the most significant issues in assessing the impact of future climate change. Several issues limit our knowledge: large uncertainties in current ice-sheet mass balance estimates, questions of how climate change will be manifested and amplified in polar regions, the difficulty of predicting how atmospheric circulation and precipitation will change at high latitudes, uncertainties in the “fast physics” of ice flow, and questions concerning the characteristics of “triggers” for rapid change in ice flow (e.g., ice-shelf basal melting).

The major scientific challenges are: 1) to quantify the exchanges of freshwater between the hydrosphere and cryosphere, 2) to understand the role of such exchanges in climate variability and change, and 3) to improve the ability to simulate the important geophysical properties and processes controlling energy exchanges in the cryosphere. Long-term, consistent data sets are required to document changes in the cryosphere and to validate transient simulations using global climate models. Without a more thorough analysis of ice-sheet, snow-cover and sea-ice mass balance, it will be difficult to develop more-comprehensive models of the cryosphere.

NASA's EOS directly addresses many of these critical issues:

- MODIS will provide near-daily global coverage of snow-covered versus snow-free areas, and with MODIS' on-board visible/near-infrared calibrators, radiances of snow can be calculated. AMSR-E will provide a weekly snow extent product that will extend the long-term time series of passive microwave-derived snow extent started in 1978. The higher spatial resolution of AMSR-E compared to the Scanning Multispectral Microwave Radiometer (SMMR) and the Special Sensor Microwave/Imager (SSM/I) will improve the ability to map snow cover in forested regions. Combined, MODIS, AMSR-E, MISR, and ASTER will provide detailed, multi-sensor information on snow-cover extent, albedo, and surface temperature.
- EOS scientists are developing and validating algorithms that will use AMSR-E data to determine snow-water equivalent, an important parameter for weather forecasting and climate model validation.
- AMSR-E will provide data for deriving estimates of sea-ice concentration and sea-ice type, extending time series of ice extent in both polar regions and adding to the information on seasonal and interannual variability in the fraction of open water.
- ASTER and ETM+ provide the opportunity to monitor and detect changes in permafrost through measures of land cover, snow cover, snow depth, soil moisture, surface reflectance, surface temperature, and surface-displacement features.
- ASTER and ETM+ provide opportunities for increasing spatial and spectral resolution and repeat imaging capability of surface ice-sheet features.
- The Geoscience Laser Altimeter System (GLAS), by accurately measuring ice-sheet topography, will enable improved ice-flow models to be developed. With repeated measurements GLAS will reveal changes in surface elevation and hence mass balance of the ice sheets.

1.2.6 Ozone and Stratospheric Chemistry

Ozone influences climate. For instance, removal of ozone from the stratosphere causes cooling of the stratosphere and a small, but non-negligible, offset to the greenhouse

forcing from CO₂, N₂O, CH₄, and CFCs. The size of the radiative forcing due to stratospheric ozone loss is very sensitive to the profile of the ozone loss. Seasonal changes are determined by the winter-summer changes in the stratospheric circulation. Interannual changes are linked to the eleven-year solar cycle in ultraviolet (UV) input from the sun and to the amount of volcanic aerosols in the stratosphere. Superimposed on these variations are anthropogenic changes related to the release into the atmosphere of human-made chemicals containing chlorine.

The most significant departures from normal have been changes in Antarctic polar ozone, leading to the phenomenon known as the ozone hole. Not until 1996 had changes in Arctic polar ozone been detected that are comparable to the changes in the Antarctic polar ozone. In recent decades it has become clear that there are also significant decreases in stratospheric ozone in midlatitudes as well.

The basic outline of the chemical processes that control stratospheric ozone appears to have been established, and changes in stratospheric ozone distribution have been accounted for in terms of chemical processes, transport, interactions with aerosols and polar stratospheric clouds, and interactions with solar ultraviolet radiation and energetic particles. However, a number of issues remain. 2D ozone models are not able to provide accurate representations of the ozone trends that were observed in middle and high latitudes over the 1980-to-1990 time period, while the 3D models suffer from unrealistic temperature fields which, in turn, alter the photochemistry. Variability in ultraviolet radiation reaching the Earth leads to changes in global total ozone. Energetic particle flux variations from the sun may also drive natural ozone variations. Both natural changes and human-made changes must be understood and separated if we are to have a firm understanding of how stratospheric chemistry will evolve.

Required measurements must satisfy the need for meteorological information; the need for chemical information including both chemical and dynamical measurements in both the stratosphere and troposphere; the need for stratospheric aerosol and polar stratospheric cloud information; and the need for solar-ultraviolet flux determinations. In addition there must be a concerted effort at validating the satellite measurements.

NASA's EOS provides many key contributions:

- EOS limb sounders (MLS and HIRDLS) will greatly improve the accuracy, precision, and resolution of temperature measurements in the tropopause region. HIRDLS will provide higher horizontal resolution tem-

perature profiles than have been available heretofore. MLS will provide OH measurements that were not previously available.

- The SAGE III instrument will provide many advances including the first satellite measurements of the size distribution of polar stratospheric clouds.
- Fully interactive chemical dynamical models are being developed especially for interpretation of EOS data.
- Wind fields provided by the NASA/Goddard Space Flight Center (GSFC) Data Assimilation Office (DAO) are of sufficient quality to remove the dynamical uncertainty from tracer observations.

1.2.7 Volcanoes and climate effects of aerosols

Volcanic emissions can cause significant variations of climate on a variety of time scales—just one very large eruption can cause a measurable change in the Earth's weather with a time scale of a few years. Sulfur dioxide released from the magma may be oxidized to sulfuric acid aerosols in the stratosphere, where they may reside for a year or more, generally producing cooling at the Earth's surface. The amount of stratospheric aerosols and their effects on climate depend on the ability of the eruption to inject material into the stratosphere and on the sulfur content of the emissions. However, microphysical properties of the aerosol particles must be taken into account in reckoning whether their infrared absorptivity, which acts to warm the Earth, or their albedo effect, which acts to cool the Earth, will be dominant.

Stratospheric aerosols produced by volcanic eruptions can influence stratospheric chemistry both through chemical reactions that take place on the surface of the aerosols and through temperature changes induced by their presence in the stratosphere. The presence of volcanic aerosols in the stratosphere has recently been tied to depletion of stratospheric ozone in temperate latitudes. The concept is that sulfate aerosols serve as sites for heterogeneous chemical reactions which have the effect of destroying ozone.

Aerosols contributed by humans have been increasing, particularly those associated with SO₂ from combustion of fossil fuels and from biomass burning. The primary effect of these anthropogenic aerosols on the Earth's energy balance is a cooling of about -0.5 Wm⁻² compared to the forcing associated with the change in greenhouse gases during the industrial age of about +2 Wm⁻². Subsonic aircraft flying in the lower stratosphere

are also a source of aerosol particles. The direct radiative effects on climate of tropospheric aerosols are hard to assess because of the wide range of chemical compositions, time and spatial distributions, range of particle sizes and shapes, interactions with water vapor and clouds, and overall global variability that are dependent on both natural sources and human activities. Assessments of the indirect effects of tropospheric aerosols are even more difficult to make, yet they may be as significant as the direct effects.

Volcanoes pose significant hazards for people and property on the ground, and the major challenge to satellite-based observations of volcanic hazards is the development of techniques that can be used in a predictive manner to detect an evolving volcanic crisis and to provide timely information to the relevant authorities on the ground. The hazards associated with eruptions are diverse and numerous, and include the health hazards associated with low-altitude volcanic gases and loss of life and property by inundation by lava flows, pyroclastic flows, and mud flows. There is also an increasingly frequent potential for unexpected aircraft encounters with volcanic plumes or clouds, with the potential catastrophic loss of life due to a major air crash.

NASA's EOS directly addresses many of these critical issues:

- MODIS, MISR, ASTER, and ETM+ will be used to characterize the number, location, type, and duration of both lava-producing and explosive eruptions. Plume-top altitudes and topography provided by MODIS, ASTER, HIRDLS, and MISR will allow testing of physical models of plume rise and dispersal.
- Volcano topography will be derived from ASTER, Vegetation Canopy Lidar (VCL), and foreign-partner radars.
- Measurements of different aspects of sulfur dioxide abundance will be made by the Total Ozone Mapping Spectrometer (TOMS), the Ozone Monitoring Instrument (OMI), TES, MLS, and ASTER.
- Several EOS instruments, SAGE III, EOSP, MISR, OMI, GLAS, and HIRDLS, will monitor stratospheric and tropospheric aerosols. Continuous measurements made by MODIS, CERES, and SAGE III will provide an important record of the effects of volcanic aerosols on the Earth's radiation budget and on global vertical profiles of atmospheric temperature and com-

position. GLAS on the EOS ICESat-1 spacecraft and the Vegetation Canopy Lidar (VCL) will provide valuable information on the vertical and spatial extent of significant stratospheric and tropospheric aerosol layers.

- EOS measurements will also enable the first truly global inventory of volcanic eruptions, as well as the high-temporal-resolution study of surface flows and eruption plumes in the stratosphere. Through a combination of multiple EOS instrument measurements, volcano hazard mitigation will also be improved because of the dramatic increase in the quantitative measurement of lava temperatures, gas emissions, surface topography, eruption plume tracking, and ground deformation.

1.2.8 National and international contributions to major field campaigns

EOS observations and studies described above also support considerable surface observation efforts and major field campaigns. Examples of major programs include:

- FIRE (the First ISCCP Regional Experiment) is an ongoing multi-agency international program to support the development of improved cloud radiation parameterization schemes.
- GEWEX (Global Energy and Water Cycle Experiment) focuses on observing and modeling the hydrologic cycle and energy fluxes in the atmosphere, at the land surface, and in the upper layers of the oceans. GCIP (GEWEX Continental-Scale International Project) focuses on determination of the variability of the Earth's hydrological cycle and energy exchange budget over a continental scale.
- CLIVAR (for climate variability), a major project of the World Climate Research Program (WCRP), seeks to understand and predict climate variability on interannual-to-centennial time scales.
- GOALS (Global Ocean, Atmosphere, Land System), a major element of CLIVAR, directed to the study of seasonal-to-interannual variability.
- DEC-CEN (for decadal-to-century variability), a major element of CLIVAR, directed to the study of decadal-to-century time-scale natural variability and the role of human activities in modifying climate.
- JGOFS (Joint Global Ocean Flux Study), dedicated to satisfying critical elements of the IGBP, designed to study biogeochemical processes in the ocean and their role in climate change.
- GLOBEC (U.S. and International Global Ocean Ecosystem Dynamics program) with the goal of determining how marine animal populations respond to climate variability and long-term climate change.
- ARM (Atmospheric Radiation Measurement) Program, the largest contribution of the Department of Energy (DoE) to the USGCRP. It is a sophisticated measurement program using ground-based facilities as well as remotely-piloted aircraft to characterize the broadband and spectral components of both longwave and shortwave radiation reaching the Earth's surface, and to measure water vapor, temperature, and wind profiles throughout the lower atmosphere.
- BSRN (Baseline Surface Radiation Network), an international program of the WCRP designed to improve the accuracy and sampling rate of surface-measured shortwave and especially longwave radiative fluxes.
- ECLIPS (Experimental Cloud Lidar Pilot Study), will obtain observations of cloud-backscattering profiles from about 10 ground-based lidar sites around the world. It will provide cloud base altitudes for all cloud types including cirrus, and, in addition, will provide cloud top altitudes for optically-thin clouds.
- ACSYS (Arctic Climate System Study), a WCRP project aimed at improved understanding of the role of the Arctic in the climate system, and studying global climate change and variability in the Arctic.
- SHEBA (Surface Heat Budget of the Arctic Ocean), a multi-national project whose goals are to develop and test models of Arctic ocean-atmosphere interactions and to improve the interpretation of satellite remote-sensing data in the Arctic.
- BOREAS (Boreal Ecosystems Atmosphere Study), a large-scale international field experiment, with the objective of improving our understanding of the exchanges of radiative energy, heat, water, carbon dioxide, and trace gases between the boreal forest and the lower atmosphere.

1.3 Measurement strategy

EOS and follow-on missions serve a unique and valuable role in meeting global change objectives, including: repetitive, synoptic coverage of the Earth-atmosphere-ocean system; observations in spectral bands from the ultraviolet to the microwave, depending on application; problem-appropriate spatial resolution; and absolute radiometric calibration. No other current or planned remote-sensing system matches this combination of capabilities. In order to accomplish the measurement objectives of EOS, together with an awareness of multi-agency and multi-national satellite observing systems, EOS has developed a measurement strategy that includes:

- 1) Simultaneous observations with a group of sensors on the same platform (satellite) that, taken together, improve either the accuracy or the scientific content of observations in comparison with measurements from a single instrument. This strategy depends on a close coordination in space and time, and is generally easier, if not absolutely required, on a single satellite.
- 2) An overlap strategy such that sensors can be intercompared and intercalibrated in order to construct long-term climate records. This strategy depends on using similar or identical sensors in orbit at the same time, but not necessarily in the same orbit or observing the same locations at the same time.
- 3) A diurnal sampling strategy for rapidly varying systems or ones with significant temporal variation (most notably clouds) in which more than one satellite is in orbit at the same time (preferably one sun-synchronous and one precessing).
- 4) A calibration strategy required to perform intra-system and intersystem data comparisons for global change research and monitoring.
- 5) A data continuity strategy that does not mandate the cloning of the existing satellite systems but retains the scientifically essential capabilities of the EOS systems.

1.3.1 Simultaneous observations

Specific examples where simultaneous observations are vitally important to meeting the measurement objectives, or are necessary to have sufficient accuracy to enable health and property impacts to be accurately assessed are:

- 1) Cloud properties (amount, optical properties, height) derived from MODIS (or comparable well-calibrated multi-spectral imager) must be coincident in space and time with radiative energy fluxes (top of atmosphere, surface) derived from CERES. Due to the high temporal variability of cloud systems and the spatial variability of clouds at spatial resolutions as small as several hundred kilometers, it is necessary for a broadband sensor (like CERES) to be on the same platform or have simultaneity between three and six minutes with a multi-spectral visible-infrared imager (like MODIS).

If MODIS were to fail and CERES continue to operate, the radiation budget at the TOA (cloud radiative forcing) could still be derived, analogous to what was done with the Earth Radiation Budget Experiment (ERBE) between 1984 and 1989, but the cloud feedback could not. In this way, one could see what clouds en masse were doing to the Earth's atmosphere, but it would not be possible to determine whether the cloud forcing was due to changes in cloud type, vertical distribution, or amount.

If CERES were to fail but MODIS continue to operate, the cloud radiative and micro-physical properties (cloud phase, particle size, vertical distribution, etc.) could be determined, but not their radiative effect on climate either at the TOA or at the Earth's surface. The strategy that EOS has adopted to date is to baseline CERES and MODIS on the same platform (AM-1 and PM-1) to enable the enhanced science of cloud forcing and cloud feedback (response) to be performed.

- 2) Atmospheric temperature and humidity determinations require, at present, a combination of sensors. The EOS PM-1 satellite will include an advanced sounder system (AIRS, AMSU, and HSB). The three instruments together are necessary to obtain both temperature and moisture profiles in the Earth's atmosphere using both infrared and microwave sensors. The current National Oceanic and Atmospheric Administration (NOAA) operational sounding system (TIROS Operational Vertical Sounder [TOVS]) also includes a suite of three sensors measuring both infrared (High-Resolution Infrared Radiation Sounder [HIRS]) and microwave (AMSU, MHS) radiation. NOAA depends on this full system for weather forecasting and currently launches a replacement satellite if one of these sensors fails.

This is therefore, as currently implemented, a simultaneity requirement involving three sensors.

- 3) Ocean surface topography, as demonstrated on the Ocean Topography Experiment (TOPEX)/Poseidon and later this century on the joint U.S.-France Jason-1 satellite, involves a dual frequency altimeter, ranging system, and microwave radiometer. Once again, this suite of sensor capabilities can be flown together on a single satellite (as TOPEX/Poseidon and Jason-1) but a combination of 3 sensors is required to achieve an accuracy requirement of 3 cm at the ocean surface. The microwave radiometer is used to make water vapor (pathlength) corrections to the radar altimeter measurements, thereby improving their accuracy.

Other examples where simultaneity is desirable, but not absolutely required, or where the accuracy would be severely degraded without simultaneity, include:

- a) Tropospheric chemistry (precursors—the accuracy of methane (CH₄) and carbon monoxide (CO) measurements to be obtained from the Canadian-built MOPITT instrument, scheduled to be flown on EOS AM-1 in late 1998, is enormously enhanced by the ability to use MODIS to derive a cloud mask at a 1-km spatial resolution. Without the ability to have nearly simultaneous high-spatial-resolution measurements of cloud cover, the much coarser resolution MOPITT (22-km pixels) would have partially-filled fields of view that would contaminate the signal and degrade the accuracy of the CH₄ abundance and CO concentration determinations. It is not possible to quantitatively estimate the accuracy loss that would result without the presence of a high-resolution multispectral imager onboard the same spacecraft.
- b) Measurements of fire occurrence and volcanic effects over the land are aided by having a global surveyor with moderate-to-high spatial resolution (e.g., MODIS) that can determine the presence and location of fires, molten lava from volcanic eruptions, and burning oil wells, and then be used to schedule the acquisition of high spatial resolution, limited coverage sensors such as Landsat-7/ETM+ or AM-1/ASTER, each of which is able to obtain only about 100 scenes globally per day. This telescoping ability to find a hot thermal anomaly and subsequently to acquire high resolution imagery of the affected area, is exceedingly valuable. On the other hand, there is no requirement whatsoever that these measurements

be made simultaneously in space or time, only that both capabilities exist in orbit at the same time (different satellites and orbits permissible).

- c) Total solar irradiance (TSI) and ultraviolet spectral irradiance are complementary. When one sees a variation in the total irradiance from the sun, much of that variation occurs in the ultraviolet. Hence, monitoring both the spectral and total distribution of solar radiation is valuable, one for energy input to the climate system, and the other for its impact on the absorption within the atmosphere and subsequent role in ozone production. There is, however, no requirement that these measurements be made from the same satellite or in the same orbit, but that they be in orbit at the same time. If the Solar Stellar Irradiance Comparison Experiment (SOLSTICE) is lost, it has no impact on the total solar irradiance to be derived from ACRIM, for measurements from SOLSTICE are not required to interpret ACRIM observations.

1.3.2 *Overlap strategy*

The vast majority of EOS sensors, those that are used for long-term monitoring of climate parameters, require observations over a long period of time (e.g., 15+ years). This is generally beyond the scope of a single satellite/sensor system, thereby requiring multiple launches. The EOS observing strategy includes subsequent launches of similar sensors of potentially different optical and electronic design, and hence the long-term continuity of science results requires a minimum of a six-month period of overlap between subsequent launches of similar sensors. This overlap strategy assures an ability to intercompare the absolute calibration, performance, and idiosyncratic characteristics of subsequent observing systems.

In most cases, this observing strategy is highly desired in order to assure a long-term, high-quality, data set. For ACRIM measurements of TSI, however, it is an absolute requirement, since technology is beyond the capability of measuring absolute TSI to the required accuracy. Hence, in order to obtain a long-term data set over one or more solar cycles (11 years), it is necessary to have more than one TSI instrument, such as ACRIM, in orbit at the same time. Again, this does not require that they be on the same satellite or in the same orbit, but that a new satellite, with a replacement sensor, be launched before the failure of the replaced sensor.

1.3.3 Diurnal sampling

For ocean color and SST characterization, it is essential that well-calibrated data be available globally in order to quantify changes in the carbon uptake of the oceans during both El Niño and non-El Niño years. It is widely accepted by the Earth science community that uncertainties in cloud properties, especially their changes in response to a build up of carbon dioxide and other greenhouse gases in the Earth's atmosphere, are the largest source of uncertainty in current climate-model predictions of future climate response. Recent observations that the nighttime minimum temperature around the globe is increasing more rapidly than daytime maximum temperature seems to suggest changes are now occurring in global cloud cover, as other greenhouse gas explanations are unable to account for this behavior. A quantitative assessment of cloud properties (cloud droplet size, cloud height, etc.) requires a well-calibrated and continuous observing capability, coupled with advances in model development. Quantitative global observations are the greatest constraint on model parameterization and assumptions.

Unlike the ocean and atmosphere, the land surface is distinguished by high-spatial-frequency processes that require a high-spatial resolution to characterize. In particular, man-made changes (e.g., deforestation) are often initiated at scales requiring high resolution for early detection. The EOS satellites potentially offer the unique capability to seasonally monitor important small-scale processes on a global scale, viz, the inter- and intra-annual cycles of vegetation growth; deforestation; agricultural land use; erosion and other forms of land degradation; snow accumulation and melt and the associated freshwater reservoir replenishment; urbanization. The other systems affording global coverage do not provide the resolution to observe these processes in detail, and only the Landsat component of the EOS system provides a 20-year retrospective record of these processes.

To achieve a measurement strategy for highly-variable systems, most notably clouds and associated precipitation, EOS and partnering international space programs, include multiple satellites in orbit at one time or sometimes single spacecraft that are in mid-inclination and hence precessing orbits. An example of the latter is the TRMM satellite, launched in November 1997, that is in a 35°-inclination orbit covering primarily tropical latitudes. The orbit of this satellite precesses in time so that a single area on the Earth's surface is observed at different times of day on subsequent days. This diurnal sampling strategy is also important for severe weather, such as hurricanes, floods, lightning, and tornadoes, and is a primary focus of geosynchronous observing systems. The loss of

key observing capability or an entire satellite during the prime hurricane season in the fall has incalculable social costs.

1.3.4 Calibration requirements

Calibration is perhaps the most difficult EOS data continuity requirement to appreciate. The critical need to perform intra-system and intersystem data comparisons for global change research and monitoring justifies this requirement. In the future, EOS data will complement and add to the observations provided by systems of other agencies (e.g., NOAA, European Space Agency [ESA], National Space Development Agency of Japan [NASDA]) and will be compared to retrospective data acquired by earlier satellites, such as Landsat, the Earth Radiation Budget Satellite (ERBS), TOPEX/Poseidon, the Upper Atmosphere Research Satellite (UARS), the Solar Maximum Mission (SMM), and Nimbus-7. A lack of calibration would limit substantially the value of these comparisons. The situation is analogous to recording the height of a child with different sticks at different ages. If the different sticks are not calibrated in absolute units (e.g., in or cm), then we cannot infer the interannual growth rate of the child from stick-based measurements. Likewise, the reflected energy recorded by EOS sensors requires calibration in absolute units of energy. Otherwise, detecting and characterizing land-surface changes by comparing data from different sensors (e.g., MODIS to Landsat-7 data) becomes difficult, if not impossible. Similar examples can be found in such basic measurements as the energy output of the sun, Sea Surface Temperature (SST), total ozone content, energy balance of the Earth, ocean circulation, and global cloud cover.

Calibration will help prevent “apples-to-oranges” intercomparisons and analyses. Calibration will greatly enhance the role of EOS data to global-change research in the late 1990s and beyond. Without well-calibrated instruments it would not be possible to determine whether the ozone content of the Earth's atmosphere was decreasing over North America and Europe with any certainty, since it would also be possible that the satellite sensor had simply degraded. Without the ability to quantify such changes in the instrumentation, it would otherwise be impossible to ascribe changes to the global environment, whether due to humans or nature.

1.3.5 Continuity

The data continuity requirement does not mandate the cloning of the existing satellite systems. Only the scientifically essential capabilities of the EOS systems must be retained: i.e., the aforementioned repetitive, synoptic

coverage, spectral coverage, appropriate spatial resolution, and calibration. These capabilities should be achieved by the most cost-effective and reliable technological approach available. Further, data continuity must not serve as a constraint on scientific and technologic advancements at any given time (i.e., not frozen in 1970s technology). System advancements that advance the role of EOS and enhance the value of the data (e.g., the addition of certain spectral bands that facilitate atmospheric correction) should be fostered and encouraged. Data continuity is not an excuse for technologic and scientific stagnation. The requirement is set forth only to ensure that the unique and critical role of EOS, as afforded by its scientifically essential capabilities, continues into the late 1990s and beyond.

Specific examples where calibration, validation, and continuity are vitally important are:

- 1) Radar altimetry of the oceans from Jason-1 will be used to assess seasonal-to-interdecadal changes of the ocean circulation. At these time scales the ocean is thought to play a major role in climate change through the transport of heat and exchange of heat with the atmosphere. Radar altimetry is the only way to obtain global measurements of the upper-ocean circulation to determine how and where the heat is moved. This information is required to improve forecasts of seasonal-to-interdecadal climate change.
- 2) Jason-1, AM-1, and PM-1 measurements will provide crucial information for modeling the ocean ecosystems, since ocean ecosystems are strongly influenced by the advection of nutrients and plankton communities. Understanding how these ecosystems change on seasonal-to-interdecadal time scales is a goal of EOS and can only be done with continuous observations of the ocean circulation.
- 3) At time scales less than a century, the ocean circulation is primarily driven by the force of the wind stress on the ocean surface. The lack of long-term accurate observations of the wind stress at the ocean surface has been a primary deterrent to improved forecasts of ocean-atmosphere climate phenomena, such as the El Niño. EOS will address this issue by providing long-term observations of the global wind stress on the ocean surface with SeaWinds, to be flown on QuikSCAT and the Japanese ADEOS II spacecraft.
- 4) The direct observation of global sea-level rise on seasonal-to-interdecadal time scales is a goal of Jason-1. This unique parameter provides a means to monitor changes in the global climate, such as global warming or cooling, changes in the water cycle, or tectonic changes in the shape of the Earth's surface. This measurement requires accuracy of 1 part in 10^9 ; long-term calibration of the altimeter system is essential to sort out instrument drift from geophysical signal.
- 5) The observations of the ocean circulation provided by Jason-1 will be used in global ocean models through data assimilation to improve our ability to forecast climate change. Data assimilation improves a model forecast through the use of direct observations. Assimilation requires knowledge of both the uncertainty in the observations and the model physics. Calibration of Jason-1 instruments is essential to quantify the error budget of the altimeter system for model assimilation and prediction. The goals of Jason-1 cannot be achieved without careful calibration of the instrument throughout the lifetime of the mission.
- 6) Satellite altimetry provides the only means of measuring the global ocean in a synoptic fashion, in order to understand the physics of ocean circulation. Calibrated, long-term measurements of the ocean circulation are needed to develop and validate climate prediction models with practical benefits for society that could be measured in trillions of dollars over the next century.
- 7) Long-term observations of the ocean circulation from Jason-1 are crucial for understanding the seasonal, interannual, and decade-to-century fluctuations in ocean circulation that are both responsible for, and indicative of, climate change. Thus, both climate prediction and climate monitoring are at stake.
- 8) A long-term fluctuation in global heat transport, such as into the N. Atlantic via a conveyor-belt circulation, would manifest itself in subtle changes of the time-mean-height differences across the Gulf Stream and connecting currents, as well as in changes in the eddy variability along the entire path of the great conveyor. Model simulations combined with long-term ocean-height measurements could lead to an advanced warning of the regional aspects of global warming.
- 9) The primary purpose of the GLAS laser altimeter is to determine on-going changes in ice-sheet volume and interannual and decadal changes in ice elevations that may be caused by changes in melting and pre-

precipitation in polar regions. The data are needed to predict sea-level rise during the next century. About five years of GLAS observations are required to determine the present-day rate of ice growth or shrinkage. Longer-term observations are needed to determine how the melting and precipitation forcings are changing as climate warming occurs, in order to confirm or revise predictions.

- 10) Sea ice is a major variable affecting the predicted amplification of the greenhouse warming in polar regions and the moisture available for changes in snowfall and ice-sheet mass balance. While twenty years of satellite passive microwave observations of sea-ice area have demonstrated that significant decadal-scale changes occur regionally, the overall hemispheric and global changes have been small. Nevertheless, problems remain in producing a uniform time series due to changes in the sensors, inadequate calibrations, and data gaps. For example, a new data gap would be assured if recorders on the Defense Meteorological Satellite Program (DMSP) satellite carrying SSM/I were to fail. With the data sets available, it has been very difficult to assess whether the overall sea-ice changes observed during the last twenty years are associated with changes in polar climate or are instrumental. AMSR-E on EOS PM-1 will provide a well-calibrated long-term data set of sea-ice extent and open water within the ice pack, as well as snow cover on land and the extent and duration of snow melting.
- 11) Clouds and changes in cloud cover have an enormous impact on climate change, since the longwave greenhouse effect of clouds is approximately seven times larger than that of doubling carbon dioxide. Thus a small change in cloud-top altitude, cloud thickness, cloud-droplet size or phase, or extent, can have a dramatic impact on the nighttime minimum and daytime maximum temperature at the Earth's surface under changing climate forcing conditions. Hence, a long-term, well-calibrated multispectral data set (such as that to be provided by MODIS on EOS AM-1 and PM-1) is necessary to quantify cloud properties in the Earth's atmosphere. In addition, the radiation response at the TOA and at the surface, to be provided by CERES, are necessary to constrain climate models and hence improve our confidence in their predictions.
- 12) SST can be monitored from space provided the calibration of the thermal infrared channels is well determined and stable. Stability is necessary to be able to ascribe long-term changes to the ocean surface rather than to the instrument. Quantitative radiometry is also required to make atmospheric corrections, whereby the effects of the intervening atmosphere (aerosols, water vapor) are removed from the spacecraft signal to infer the color and hence chlorophyll content of the oceans.
- 13) Long-term ozone trends, and atmospheric constituent changes that lead to ozone loss, can most readily be monitored from space using well-calibrated sensors. TOMS ozone measurements over many years (and now to be supplemented by OMI on the Chemistry mission) have been extremely valuable for long-term ozone-trend measurements. In addition, SAGE II (and later SAGE III) has been really vital in quantifying ozone trends due to its self-calibrating capability. The MLS sensor on EOS Chemistry will continue very exciting results obtained from UARS that show a high correlation between enhanced chlorine monoxide (ClO) levels and reduced ozone in the Antarctic polar vortex. Of perhaps more relevance to the public at large is the very large signature of high ClO in the Northern latitudes over North America and Europe. Monitoring ozone degradation, and subsequent recovery (following implementation of the Montreal protocol) requires continued measurements of both ozone and chemical species that affect ozone concentration, using well-calibrated sensors.

1.4 EOS contributions to national goals and needs

The USGCRP is placing increased emphasis on policy relevance in defining the breadth and focus of the national research efforts. End-to-end assessments (from the human and natural forcing factors to the human mitigation and adaptation response) are key requirements for national policy development. This refocusing of the USGCRP is prompting an examination of existing programs to determine if they are sufficiently policy-relevant and if they are responsive to national needs. Consequently, the USGCRP office and leading global change agencies developed a preliminary set of questions and products to assess the policy relevance of major USGCRP efforts.

Much of the research underway and planned as part of NASA's EOS is directed toward the highest priority elements of the USGCRP. EOS directly addresses national policy requirements for atmospheric ozone, natural variability and enhanced climate prediction, and long-term climate change. EOS also provides fundamental measures related to ecosystem change and aids in biodiversity research. Much of EOS research is a prerequisite for significant elements of the human dimensions research plan.

1.4.1 Atmospheric ozone and UV-B radiation

1.4.1.1 The national interest

The development of the Antarctic ozone hole and the global depletion of stratospheric ozone is well documented from satellite (Nimbus 7 SBUV, TOMS, Meteor TOMS, ADEOS TOMS, and NOAA SBUV) and in situ measurements. Ozone is a primary shield from harmful ultraviolet radiation and is a significant element of the global energy balance. The depletion of stratospheric ozone has been tied to two major causes. First, ozone depletion is clearly associated with a six-fold increase in stratospheric chlorine above natural levels, in large part due to the human emission of industrial chemicals such as chlorofluorocarbons. Second, volcanic emission of sulfur dioxide can lead to ozone depletion and increased annual variability. For example, the eruption of Mt. Pinatubo is correlated with a 35% reduction in stratospheric ozone at low Northern Hemisphere latitudes. Three additional factors may influence ozone chemistry: 1) ozone depletion can be caused by other radical species that are products of industrial emissions, 2) global warming may be a significant factor in ozone depletion because greenhouse gas warming leads to stratospheric cooling, enhancing the formation of polar stratospheric clouds that in turn trigger ozone-destroying chemical reactions, and 3) the emissions

from high-altitude aircraft may also perturb stratospheric chemistry.

1.4.1.2 National policy requirements

The detection, causes, and impacts of significant changes in stratospheric ozone.

1.4.1.3 EOS policy-relevant contributions

EOS addresses the most important policy-relevant questions including the detection and prediction of ozone depletion, the isolation of human versus natural factors forcing changes in atmospheric ozone, the response of atmospheric ozone to human forcing, and an understanding of the uncertainties associated with ozone depletion and UV-B radiation.

1) What are the human and natural forcing agents in stratospheric ozone?

- HIRDLS, MLS, and SAGE III will monitor anthropogenic Cl and additional known threats from industrial chemicals including CFCs, other halogens (bromine-containing compounds), nitrogen compounds used both in agriculture and emitted directly by high-flying aircraft, and sulfur from stratospheric aircraft (leading to increased aerosols with resulting heterogeneous chemistry detrimental to ozone).
- The injected SO₂ from volcanic eruptions leads to more sulfate aerosols in the stratosphere, allowing enhanced heterogeneous chemistry (involving the industrial chlorine already in the stratosphere) detrimental to ozone. EOS will assess the role of volcanism in stratospheric chemistry through multiple measurements including: sulfate aerosols mapped and monitored by HIRDLS and SAGE III; total column abundance of aerosols measured with MODIS and MISR; volcanic gas (SO₂ and HCL) contributions measured with TES and MLS; and stratospheric sulfur dioxide monitored with TOMS and OMI. The chemical imprint of volcanoes will be directly tied to the latitude, season, and eruption characteristics of the volcanic eruptions.
- MOPITT will measure the concentration of CO, which is related to the tropospheric concentration of OH, and thus the indirect control of the amount of CH₄ and HCFCs that reach the stratosphere.
- AIRS and HIRDLS will provide an accurate record of natural temperature variations for the study of chemi-

- cal reactions. SAGE III and HIRDLS will measure polar stratospheric clouds and temperatures (e.g., stratospheric warmings). These measurements will provide an understanding of the role of natural temperature changes in producing ozone variability and the potential determination of the role of global warming.
- MLS will contribute measurements that are not degraded by clouds or volcanic aerosols, allowing critical observations of important extreme events such as volcanic eruptions and that can be made in the presence of polar stratospheric clouds.
 - The long-term measurements of ozone and other critical gases, temperatures, and aerosols provided by EOS and other sources is critical to separate natural variations and human-induced ozone depletion.
- 2) *What has been and will be the response of atmospheric ozone and UV-B radiation to human forcing?*
- HIRDLS and MLS data products make essential contributions to detecting ozone depletion agents including: ClO, BrO, OH, NO, NO₂ (chemical radicals); H₂O₅, ClONO₂, HCl, HNO₃ (chemical reservoirs); H₂O, N₂O, CH₄, F11, F12 (source gases); SO₂ (volcanic injections). These species define the chemical cycles that destroy ozone. The measurements will be continuously made from the upper troposphere through the mesosphere at high horizontal and vertical resolution. The instruments are sufficiently stable to detect 1% changes. Daily three-dimensional fields of all parameters are produced.
 - SAGE III and HIRDLS will measure stratospheric ozone, as well as NO₂, NO₃, OClO, H₂O, polar stratospheric clouds, temperature, and aerosols. EOS will provide 1-km vertical resolution, with excellent long-term precision, providing critical profile data needed to understand processes required to develop predictive models.
 - AIRS/AMSU will measure the vertical distribution of ozone in the troposphere and the stratosphere in five layers twice daily globally with an accuracy of 10% and will determine the total column with an accuracy of 3%, which can provide a backup for the TOMS and OMI instruments.
 - MODIS will measure total column ozone twice daily with 10-20% accuracy, which can provide backup for the more-accurate TOMS and OMI instruments.
 - EOS investigators will produce long-term calibrated data sets based on intercomparison studies including earlier Nimbus 7 SBUV, TOMS, Meteor TOMS, ADEOS TOMS, and NOAA SBUV/2 measurements. The ozone-mapping instruments on the European Remote-Sensing Satellite-2 (ERS-2) and the Environmental Satellite, ESA (ENVISAT) will provide additional calibrated data sets.
 - EOS global vertical sounding capability of the primary radicals, reservoirs, and source gases in the stratospheric chemical cycle and EOS aerosol measurements, in conjunction with existing capabilities with TOMS, provide considerable opportunity to develop predictive and diagnostic models for ozone depletion and UV-B radiation. EOS investigators will develop 3-dimensional chemical transport models of the stratosphere, in predictive and diagnostic modes, which can be utilized to calculate radical trace-gas concentrations, estimate ozone losses, and calculate the UV-B flux.
- 3) *What are the uncertainties and what is the potential for change?*
- EOS vertical profiles (MLS, HIRDLS and SAGE III) address major uncertainties in understanding stratospheric chemistry.
 - HIRDLS will provide daily measurements of the location and extent of polar stratospheric clouds on which chlorine is transformed into active forms.
 - Ozone decreases that may occur in response to the unprecedented high chlorine abundances expected during the next decade and to additional trace gases emitted by humans are not known. MLS and HIRDLS, by continuously monitoring the key radicals that destroy ozone, provide a capability for the earliest-possible detection of potential ozone depletion even by yet undiscovered processes for enhancing the role of human-produced chemical radicals.
 - EOS measurements, including stratospheric temperatures (AIRS, HIRDLS, MLS, and SAGE III) will increase our understanding of the potential ozone de-

crease in response to the stratospheric cooling caused by increasing atmospheric CO₂.

- EOS monitoring of clouds and the radiant energy budget will provide a diagnostic measure of the UV-B transmission that is cloud dependent. CERES, AIRS, MODIS, and MISR will produce cloud-forcing products and cloud-radiative properties useful for UV-B analysis.
- EOS will monitor volcanic eruptions and their impact as a major cause of natural variability in ozone chemistry and enhancement of the human forcing on ozone depletion.
- EOS will be able to contribute to the assessment of the impact of ozone depletion and associated increases in UV-B through comparisons with MODIS primary productivity measurements.

1.4.2 Natural variability and enhanced climate prediction

1.4.2.1 The national interest

The skillful prediction, months to years in advance, of precipitation and temperature can yield increased agricultural and forestry production and distribution, improved hydroelectric power planning and utilization, and more-effective responses to floods and droughts and better management planning. The goal is the utilization of short-term (seasonal and interannual) climate forecasting for social and economic benefit. Predictability has already been demonstrated for some aspects of the climate system, particularly for El Niño. Further, short-term climate forecasting, which requires a comprehensive knowledge of the atmospheric circulation and its interaction with the ocean and the land surface, contributes substantially to the predictions of long-term greenhouse warming. Short-term climate forecasts can be validated and verified and the economic benefits can be directly proven. Many of the challenges inherent to long-term prediction can be met on seasonal-to-interannual time scales. Finally, detection of long-term human-induced climate change requires an understanding of natural variability.

1.4.2.2 National policy requirements

- 1) Operational predictions one year ahead of interannual climate fluctuations.
- 2) Detection, causes, and impacts of natural decadal climate variations.

1.4.2.3 EOS policy-relevant contributions

EOS will help define the natural and human factors that influence seasonal-to-interannual climate. A significant fraction of natural climate variability is governed by modification of the atmosphere by global SST, by variations in land moisture, vegetation, and snow- and sea-ice cover globally. Additional variability is introduced from solar variability, longer-term anomalies, and volcanic eruptions. Human-induced modifications of atmospheric chemistry may alter the nature of seasonal-to-interannual variability. The EOS contributions to understanding climate variability will enhance the ability to predict climatic change and variability from seasons to decades in advance.

1) What are the natural and human factors that affect the seasonal-to-interannual climate and its anomalies?

- EOS investigators will contribute substantially to the understanding of ocean-atmosphere interactions. Investigators will be able to combine altimetry (TOPEX/Poseidon, ERS-1, ERS-2, Jason-1), scatterometry (NSCAT, SeaWinds), ocean color (MODIS, SeaWiFS), and SST measurements (MODIS, AIRS, AMSR-E), assimilate these observations into forecasting models and resolve major characteristics of the surface oceans responsible for natural variability. These observations, with the temperature and humidity measurements of AIRS/AMSU and the cloud-radiation budgets from CERES, will allow investigators to connect SST variations with the large-scale and mesoscale circulation and improve boundary layer models that describe air-sea interaction. Global assimilation schemes will provide operational products necessary for predictions of interannual fluctuations and will also contribute to our understanding of the coupled ocean-atmosphere interactions and the prediction of phenomena such as El Niño.
- EOS measurements of snow cover, sea ice, surface temperature, land cover, vegetation characteristics and related parameters (e.g., fraction of photosynthetically-absorbed radiation), surface albedo, atmospheric temperature and humidity and radiative fluxes (ASTER, MODIS, MISR, CERES, AIRS, AMSR-E) will be essential to initialize, validate, and verify climate models designed to assess the role of the land surface in governing seasonal-to-interannual variability at regional-to-global scales. EOS measurements will provide substantial improvements in comparison with existing capabilities (e.g., the Advanced Very High-Resolution Radiometer [AVHRR]). Measurements of

polar surface temperature, albedo, and sea-ice concentration will test climate model predictions of accelerated “greenhouse” warming in polar regions.

- EOS will be able to track and characterize emissions from volcanic eruptions that produce climatic variability on time scales of seasons to years. MISR and ASTER can track the height of plumes, MODIS and MISR the dispersal of the particulates, TOMS, OMI, TES, and MLS the dispersal of SO₂, and MISR, HIRDLS, and SAGE III the dispersal of stratospheric sulfate aerosols and the evolution of their vertical profiles. MODIS and MISR can provide a high-resolution view of the spatial distribution of stratospheric aerosols, and data from SAGE III, MODIS, and MISR can be used to monitor the evolution of the size of these aerosols.
 - EOS will be able to characterize the abundance and properties of natural and human-made tropospheric aerosols that may change the effect of greenhouse gases on climate. MODIS, MISR, and EOSP will detect regional and global changes of aerosol distribution and variability of their size. They will be able to track several sources of aerosol (e.g., MODIS observations of fires as a source of biomass burning aerosol). EOSP will also determine the aerosol refractive index, a measure of the aerosol composition. Wind-blown dust from arid regions will be monitored for major source regions. SAGE III will increase our understanding of aerosol loading and removal.
 - EOS (CERES, MODIS, AIRS, AMSR-E, and MISR) will provide a strong basis for monitoring variability in cloud properties (amount, type, liquid water content) which can both regulate climatic variability and define trends. Even 1-to-2% changes in cloud properties may be significant.
 - ACRIM will provide systematic monitoring of TSI variations, which are essential to separate anthropogenic forcing from natural variations.
 - SAGE III, HIRDLS, and MLS contribute observations to assess the interannual variability of radiatively-active gases (ozone, CH₄, F11, F12, nitrous oxides, water vapor) which may impact climate variability.
 - The ability of EOS to monitor land-surface energy and moisture fluxes (particularly soil moisture) using a new generation of spatially-distributed hydrologic models (based on MODIS, ASTER, AIRS, AMSR-E, and other satellite data) will help us to better understand land-atmosphere climate interactions.
 - EOS regional assessments provide baselines for determining changes in variability through monitoring of hydrologic parameters (precipitation, evaporation, water vapor, stream flows, glaciers, and snow cover) sensitive to climate change and through incorporation of historical observations.
- 2) *What is the ability to predict climatic anomalies a season in advance and what is the mechanism for verifying, distributing, and using these results? One-to-two years in advance?*
- EOS may not directly provide operational products that are predictions for a season or one-to-two years in advance; however, the entire suite of observations that define the characteristics of the surface (SSTs, land cover, (including snow), and sea ice) will provide important boundary conditions for predictions. The accuracy of these forecasts will likely depend on the accuracy with which we can measure the global state of the Earth system.
 - Global-scale, near-real-time documentation of anomalies in regional precipitation-evaporation, snow cover, sea ice, and cloud cover will be of major value in climate forecasting.
 - EOS will provide critical process information on air-sea interaction and cloud-climate interactions, which are major limitations in current climate forecasts and coupled atmosphere-ocean-land-ice climate models.
 - EOS observations from the full suite of surface and sounding sensors (particularly for temperature, humidity, clouds, and radiation) and 4-D assimilation efforts will contribute to forecast validation.
 - EOS monitoring of volcanic eruptions and their characteristics (aerosol loading and release of gases) will provide significant data for determination of climate anomalies.
 - MODIS, through its capability to monitor the extent and vigor of vegetation, will provide short-term predictive capability for drought monitoring in semi-arid environments.

- EOS altimeter and scatterometer measurements, coupled with in situ measurements from the World Ocean Circulation Experiment (WOCE) campaigns, will allow an improved understanding of the three-dimensional general ocean circulation and its influences on global change. These data and the associated understanding will aid the development of requisite models for making long-term predictions.

1.4.3 Long-term climate change including global warming

1.4.3.1 The national interest

Human activities are leading to changes in the land surface and the composition of the atmosphere with significant potential to cause decadal climate change. The alteration of the land surface modifies the energy-water-vegetation interaction at the land-atmosphere interface. Physically-based models indicate that changes in the surface energy and moisture budgets can have a significant impact on regional climates. Increases in carbon dioxide and other greenhouse gases influence the global energy budget promoting global warming and related climate changes. The detection of global warming is the subject of considerable debate, as the observing system in place over the last 100 years is inadequate to isolate long-term natural variability from human-induced change and lacks the capability to determine small changes in global temperature. Consequently, an assessment of global warming is dependent on the predictions of climate models. State-of-the-art general circulation models (GCMs) predict a global warming of between 1.5° and 4.5°C and substantial changes in precipitation and evaporation for a doubling of the atmospheric carbon dioxide concentration over its pre-industrial value. Improved estimates of mean sea-level change, on both local and global scales, as a means of detecting the consequences of greenhouse gas-induced global warming, is an important adjunct requirement. A climate change of this magnitude will have significant impact on energy utilization, agriculture (drought and floods), natural ecosystems, water resource availability, water quality, and potentially, sea level. However, the potential impact is very different for a 1.5°C warming as opposed to a 4.5°C warming. The magnitude and rate of global climate change control the potential impact on society.

1.4.3.2 National policy requirements

- 1) Plausible scenarios for regional climate and ecosystem change, suitable for impact analysis.

- 2) Improved estimates of the relative global-warming potential for various gases and aerosols, including their interactions and indirect effects of other chemical species.
- 3) Improved ability to determine the regional sources and sinks for atmospheric carbon dioxide, as part of the monitoring system for greenhouse-gas emissions-reduction agreement.
- 4) Reduction in the range of predictions of the rate and magnitude of global warming over the next century (through reductions in the uncertainties of cloud-climate interactions and ocean heat storage).
- 5) Predictions of anthropogenic interdecadal changes in regional climate, in the context of natural variability.
- 6) Detection, beyond reasonable doubt, of greenhouse-gas-induced global warming, and documentation of other climatically-significant changes in the global environment.
- 7) Improved understanding of the interactions of human societies with the global environment, enabling quantitative analyses of existing and anticipated patterns of change.

1.4.3.3 EOS policy-relevant contributions

The detection of climate change, the reduction in the uncertainty associated with climate change, the improvement of estimates of global warming potential and sources and sinks of greenhouse gases, and improved prediction of regional change, including natural variability, depend on: 1) an adequate monitoring capability, 2) improved knowledge of the forcing factors, 3) improved predictive capability to determine the response of the climate system, and 4) an assessment of the uncertainties. EOS contributes to each of these fundamental components required to serve national policy requirements. The synergy between many observations and many investigators will allow EOS to contribute to the understanding of the more-complex, yet essential, Earth processes, such as the hydrologic cycle.

- 1) *What are the human-induced and natural forcing changes in the global system and climate?*
 - MODIS, ASTER, and MISR will characterize changes in land-surface cover and surface vegetation, with the capability of providing long-term monitoring. EOS

- will provide surface fluxes of energy and carbon with unprecedented accuracy and spatial resolution. In conjunction with historical observations, the human alteration of the landscape can be mapped and utilized to determine the potential impact on climate.
- AIRS/AMSU/HSB will determine the three-dimensional structure of moisture in the troposphere and stratosphere and will measure the spectral changes in the longwave radiation going to space, which are needed to monitor the effects of trace gases on global warming.
 - EOS will assess the role of volcanism as a natural forcing factor in the global system. Sulfate aerosols will be mapped and monitored with SAGE III; total column abundance of aerosols will be measured with MODIS and MISR; volcanic gases can be measured with TES, OMI, and MLS. The role of volcanism versus human-induced aerosol loading can be deciphered based on the chemical imprint of volcanoes, monitoring of volcanic eruptions, and examining trends in aerosol loading.
 - MODIS, MISR, and EOSP will detect regional and global changes in tropospheric aerosols.
 - Jason-1 and other precursor altimeter missions will provide a well-calibrated long-term measurement of absolute sea level. The accurate monitoring and prediction of the mean sea level on a global basis provides a means of detecting the effects of greenhouse-gas-induced global warming. The accurate prediction of sea-level rise could have significant economic and societal impacts.
 - MOPITT and TES will measure CO and CH₄, and TES will measure H₂O, O₃, and N₂O, all of which are needed to begin to separate human and natural greenhouse forcing.
 - MODIS measures of biomass burning will contribute to knowledge of trace-gas emissions.
 - ACRIM will measure total solar irradiance, a fundamental measure of solar variability, which is needed to separate human and natural greenhouse forcing. SOLSTICE will measure the total variation of UV and its contribution to the natural variability of ozone.
 - EOS measures of ozone depletion will define the abundances and trends of this radiatively-important gas.
- EOS investigators will complete extensive model experimentation aimed at quantitative comparison of the different human-induced and natural forcing changes. These sensitivity experiments will be completed at both regional and global scales.
- 2) *What has been and will be the response of the climate system to human forcing?*
 - The response of the climate system will be defined by modeling efforts of EOS investigators based on a quantitative understanding of the natural and anthropogenic forcing from aerosols (MISR, SAGE III, EOSP, MODIS, HIRDLS), solar irradiance variations (ACRIM TSI), land-surface changes (MISR, MODIS, ASTER), and radiatively-important gases measured by EOS (H₂O, CH₄, O₃, CH₄, N₂O, F11, F12), and from other sources (CO₂). EOS provides an unprecedented opportunity to assess the response of the climate system based on the full spectrum of forcing factors.
 - The characterization of clouds (CERES, MODIS, ASTER, MISR, AIRS), the radiation balance (CERES), temperature and humidity (MODIS, AIRS/AMSU/HSB), winds (SeaWinds, Jason-1), and ice and snow cover (AMSR-E, MISR, MODIS) provide a unique capability to validate model predictions.
 - EOS will provide significant opportunities to document surface fluxes of energy and moisture over the land surface and the oceans, to document regional and global radiation budgets required to understand cloud-climate feedbacks, and to determine ocean heat transport. EOS will provide the first satellite-based opportunity to examine ice-sheet mass balance. These elements encompass major limitations in current climate models, and thus EOS will contribute substantially to the improved prediction of regional and global climate change in the next generation of climate models.
 - EOS investigators will utilize improved measurements of surface fluxes and clouds and radiation to develop high-resolution model predictions suitable for regional prediction of climate change.
 - 3) *How do human-induced changes compare to variations and changes in the natural system? Can these changes be detected and modeled?*
 - Natural variability of the climate system will be better defined through EOS observations of the temporal

and spatial variability of aerosols, vegetation, sea ice, snow cover, temperature, water vapor, ozone, and clouds. EOS will assess variability due to cloud interactions, vegetation and other surface changes, carbon/trace-gas perturbations, and the major climate forcing factors. MISR bi-directional reflectance measurements will distinguish between natural or human-induced land-surface cover and surface albedo variations, related to desertification, irrigation, deforestation, and urbanization. Characterization of aerosol characteristics (abundance, particle sizes, albedo, optical thickness) with MISR, MODIS, and EOSP, in conjunction with cloud measures, can be used to determine the indirect effect of aerosols as cloud-condensation nuclei to define the climate impact of aerosols, including their interactions. Measures of CO and CH₄ assist in the direct measurement of potential global warming.

- EOS 4-D assimilation models will provide a physically-consistent global measure of climate change.
 - EOS investigators will apply these satellite observations to assess the role of aerosol loading of the atmosphere in possible mitigation of global warming due to increased greenhouse-gas concentrations. The monitoring of aerosols, cloud properties, ozone, and water vapor will provide a basis for improved estimates of the relative global-warming potential of various gases and aerosols, including interactions and indirect effects.
 - The determination of the carbon balance of terrestrial ecosystems from satellites for different regions and resolutions will yield scenarios for fluxes under different climate conditions or land-management conditions. Terrestrial vegetation characteristics and ocean productivity measures will aid in the determination of regional sources and sinks for atmospheric CO₂, N₂O, and CH₄.
 - Multi-decadal regional historical studies will provide an important perspective on the impact of human-induced-versus-natural variations.
 - Improvements to climate models based on EOS observations and study will contribute to the development of more-realistic simulations of future climate. These model predictions can be verified by long-term observations or can provide estimates of the statistical likelihood of change.
 - Measurement of the major climate forcing factors by EOS is a prerequisite for detection of human-induced global change beyond reasonable doubt.
 - The long-term measurements of water vapor, atmospheric temperature, cloud properties, and SST (AIRS/AMSU/HSB, MODIS, CERES) are essential to detection of global change.
 - HIRDLS will measure stratospheric cooling, a major expected signal of greenhouse warming.
- 4) *What are the uncertainties and what is the potential for surprises, including sudden changes in the frequency and intensity of extreme events?*
- Uncertainties in cloud-climate feedbacks are regarded as one of the most important limitations of current models. The unparalleled measurements of clouds, cloud radiation, and water vapor will allow EOS investigators to incorporate much-improved parameterizations in climate models.
 - EOS observations of surface temperatures, atmospheric temperatures and moisture, surface characteristics, and winds will provide major opportunities to address the uncertainties associated with the fluxes of moisture and energy at the land-atmosphere and ocean-atmosphere interfaces and their parameterization in climate models.
 - Synergistic measurements of temperature and humidity with ocean altimetry and scatterometry will provide a unique opportunity to improve estimates of ocean heat transport, a major uncertainty in our knowledge of the climate system.
 - Current observations are inadequate to determine if the major ice sheets are growing or shrinking. The GLAS instrument will provide the first satellite-based opportunity to address this major uncertainty.
 - EOS monitoring of key climate quantities (e.g., SSTs, atmospheric temperature and moisture, clouds, radiation, and sea level) will be utilized to improve climate models and examine climate trends.
 - EOS plans to monitor the major climatic forcing factors (aerosols, radiatively active gases, solar irradiance, land cover change), which are critical to limiting the uncertainties in climate predictions.

- The location, duration, and type of activity associated with large volcanic eruptions, a major source of uncertainty, will be monitored by EOS.
- Models developed by EOS investigators provide one of the few opportunities to address the potential of changes in the frequency and magnitude of extreme events, and will also contribute to understanding of the frequency and intensity of other phenomena such as El Niño.
- Historical and pre-historical examinations of specific regions by EOS investigators will provide information on the frequency of extreme events and potential thresholds for their occurrence.

1.4.4 Ecosystem change and biodiversity

1.4.4.1 The national interest

The prevention of dramatic human-induced loss of species is a major responsibility, both from the view of species as natural resources and from our obligations for global stewardship. The loss of biodiversity will influence ecosystem function, including predation and dominance. Land use introduces patchiness or large-scale changes in habitats, modifying ecosystem function, including extinction, migration pathways, and survival. Land-use management may also be guided by the potential impact of utilization on carbon and nitrogen budgets. The record from Earth history indicates dramatic expansion and contraction of habitats in response to past global climate changes. Today, human activities play a considerable role in aiding or hindering habitat response to global change. Climate change will influence both the distribution of habitats and the patterns of land use. Changes in atmospheric chemistry will also influence ecosystem response. Ozone depletion and increased UV-B introduce the potential for ecosystem damage as well as human health issues. Sea-level increases in response to global warming will introduce considerable dislocations of estuaries, marshes, and near-shore ecosystems.

1.4.4.2 National policy requirements

The detection of significant changes in ecosystems and biodiversity, and determination of the response of ecosystems and biodiversity to the changes in atmospheric composition, UV-B, land use, climate, and sea level.

1.4.4.3 EOS Policy-Relevant Contributions

The EOS will specifically map changes in land-use patterns, vegetation type, and photosynthetic activity, which

will provide a foundation for ecosystem response models based on habitat scale and patchiness. EOS investigators will help produce better climate-change predictions which can be utilized to investigate ecosystem response in both terrestrial and oceanic realms. EOS models of carbon and nitrogen balance will aid in the assessment of the impact of land use and global-change-induced habitat changes. EOS instruments will provide the basis for detecting trends in ecosystems as a function of changes in atmospheric chemistry. EOS will also monitor volcanic eruptions as a natural disruptive force for ecosystems.

1) *What have been and will be the impacts of global change on terrestrial systems and their wildlife, including forests, grasslands, arid lands, the tropics, and high latitudes?*

- MODIS, ASTER, MISR and Landsat will map changes in land-cover patterns, including expansion and contraction of farmland, urban growth, deforestation, and forest regrowth. These changes in pattern can be related to land use or environmental change. EOS will provide essential databases on grasslands, tundra, forests, and tropical deforestation which will be a basis for ecosystem response studies.
- MODIS and MISR will produce measures of leaf area index (LAI) and the fraction of absorbed photosynthetically-active radiation, which can provide estimates of changes in net primary productivity.
- EOS instruments and models will be able to examine changes in carbon, NPP, and nitrogen balances and will be able to assess the impact of ecosystem disturbances on the carbon pool. EOS models will examine the potential of increased sequestration of CO₂ through forest management and practices.
- EOS will provide the basis to detect trends related to increased carbon dioxide and ozone depletion.
- EOS will produce climate predictions at global and regional scales in response to the full spectrum of climatic forcing factors (including land use) and will work to substantially improve climate models by addressing their major limitations with EOS observations. These predictions will be the basis to assess climate impacts on ecosystems, including potential biome shifts in response to global climate change.

- EOS investigators will use regional studies to examine past interdecadal variations in climate and biome distribution to analyze ecosystem response to climate change.
 - MODIS, ASTER, MISR, and Landsat will monitor the role of volcanism in ecosystem impact.
 - MODIS observation of fires adds an important capability to assess biomass burning, an agent of ecosystem change.
- 2) *What have been and will be the impacts of global change on coastal and marine ecosystems?*
- EOS investigators will develop biophysical models of the ocean circulation and productivity that can be utilized to examine the response to forcing factors such as changing wind stress, air/sea fluxes, and incident solar energy.
 - MODIS will examine coastal and marine ocean color, providing data on the impact of global change on ecosystems, and providing fundamental information on natural variability.
 - GLAS and Jason-1 will assess the mass balance of the ice sheets and mean sea-level change, providing key observations for potential impacts in coastal regions.
 - EOS observations in conjunction with models of the ocean circulation will examine the impact of wind forcing on coastal circulation, including the impact on fisheries.
- 3) *What have been and will be the impacts of global change on biodiversity?*
- Through maps of vegetation-cover change and habitat type and extent, EOS observations can be utilized to assess potential changes in biodiversity through the use of ecosystem models.
- 4) *What are the uncertainties and the potential for surprises and unexpected changes in the global ecosystem?*
- Through data-constrained simulation models of the carbon and nitrogen balance, EOS investigators will be able to examine the sensitivity of ecosystems to global change.

- EOS will provide extensive climate-model-sensitivity experiments for the full host of climate forcing factors at global-to-regional scales. These climate predictions are a prerequisite for assessing uncertainties and potential for surprises associated with ecosystem response to climate change.

1.4.5 Human dimensions and economics

1.4.5.1 The national interest

The potential magnitude of global change introduces the need to define strategies for mitigation or adaptation. The strategies for mitigation and adaptation may have widely different economic and societal impact involving health, standard of living, and quality of life. Knowledge of the rate and magnitude of global change and its impact at global and regional scales is essential to assess social and economic impact. Even moderate climate change may result in significant changes in the distribution and availability of critical resources such as water. We must be able to understand the nature of the human forcing of global change, particularly land and energy use. Human behavior, including valuation of the environment, issues of intergenerational equity, global-change decision making and the role of institutions become essential elements of assessing the human dimension of global change. Without these foundations, the strategies for mitigation or adaptation may be misguided, resulting in either inadequate or unnecessary policies.

1.4.5.2 National policy requirements

Definition of the interactions of global change with the major areas of societal activity and development of rational adaptation and mitigation strategies.

1.4.5.3 EOS policy-relevant contributions

EOS addresses natural hazards such as volcanism, but most importantly provides a realistic basis for understanding the potential rate and magnitude of global change. EOS studies will define the vulnerabilities of water resources, agriculture, and ecosystems to climate change. EOS will provide fundamental data sets on land-cover change, clearly addressing the need to understand one of the most significant human forcing factors of global change. EOS will also provide fundamental measures of sea-level change, a major factor in coastal regions.

1) What are the interactions with agriculture?

- MISR, ASTER, and MODIS will assess changes in land cover, surface albedo, biomass burning, and pro-

ductivity as a basis to assess human activity and to define the interactions between climate and agriculture.

- EOS temperature and humidity observations (AIRS/AMSU/HSB) and regional and global climate change predictions from EOS investigators will be the basis for determining potential changes in agricultural yields, agricultural management practices, and implications for land use.
 - The EOS focus on radiatively-important gases from agriculture may influence management practice.
 - A determination of the potential for volcanic eruptions may lead to agricultural risk evaluation.
- 2) *What are the interactions with freshwater resources?*
- EOS monitoring of snow cover and glaciers at a regional and hemispheric level (MODIS, AMSR-E) provides a basis for short-term assessment of a significant water-resource component. GLAS will measure global ice-sheet mass balance.
 - EOS climate predictions at global and regional scales will emphasize the water balance and its sensitivity to global change, meeting a major requirement to assess water-resource vulnerability to global change.
- 3) *What are the interactions in the coastal zone and marginal sea-ice zone, including fisheries?*
- High-resolution coastal-circulation studies, including biology, will provide important data on primary productivity, a key element in fisheries.
- 4) *What are the interactions with human health, including disease vectors, air quality, and UV-B radiation?*
- TES, MISR, ASTER, and MODIS will monitor volcanic gas hazards in association with major eruptions, which have the potential of human impact.
 - MLS, HIRDLS, and SAGE III will provide diagnostic information on ozone depletion by monitoring enhancements in precursor chemical radicals. This gives the capability for providing early warning potentials for increased UV-B.
 - TES and MOPITT will provide a large number of measurements (O_3 , CO, CH_4 , NO, NO_2 , and HNO_3) which will greatly aid our understanding of the chemistry of the troposphere.
- 5) *What are the interactions with land use, including soils and erosion?*
- EOS instruments will provide unprecedented measurements of the scale and magnitude of changes in land cover associated with land-use change.
- 6) *What are the interactions with business and commerce?*
- MODIS, ASTER, MISR, and Landsat will assess volcanic hazards, both on the ground and in the air, with implications for the destruction of regional commerce and disruption of aircraft flight patterns.
 - EOS predictions of climate change at global-to-regional scales will have substantial impacts on business and commerce through implications of climate change for agriculture and water-resource availability.
- 7) *What are the uncertainties and what is the potential for surprises?*
- Without a full examination of the potential impact of climate change and human-induced modifications to land cover, we will be unable to determine important potential societal impacts of global change.

1.5 Summary

NASA's EOS was designed to initiate a new era of integrated global observations intended to advance our understanding of the entire Earth System on a global scale through developing a deeper understanding of the components of that system, their interactions, and how the Earth is changing. The global homogeneous long-term measurements of the Earth system to be provided by EOS will result in enhanced assessment of global change and ultimately result in improved ability to predict seasonal and interannual climate variability. Through EOS we can expect significant enhancements in our ability to understand and predict global changes and their effects on human activities.

EOS will provide an unparalleled opportunity for long-term observation and monitoring of key variables such as total solar irradiance, radiative energy fluxes, cloud properties, aerosols, atmospheric chemistry, ice-sheet mass balance, land-surface characteristics, and precipitation. It will also provide improved understanding of the processes that relate different components of the Earth system. For example, EOS will address key priorities of

the USGCRP, such as the relationship between clouds and water vapor to global climate and their effects on climate sensitivity, while also providing a more-accurate treatment of clouds and water vapor and their radiative effects in global climate models. There will be better measurements of surface characteristics, energy fluxes, and precipitation, and consequent improved understanding of the processes that connect atmospheric and surface processes and hence more-accurate parameterizations in global-climate models. Improvements in observational knowledge and understanding of the processes that couple the atmosphere-land-vegetation systems and the atmosphere-ocean system will result in substantial improvements in our understanding and simulation of land surface and oceanic processes, and in the development of global climate models.

In this manner, EOS plays a critical role in addressing the key challenge—to develop the capability to predict the changes that will occur in the next decade to century, both naturally and in response to human activity.

Chapter 1 Index

- 24 key variables 10
 ACRIM 8, 11, 22
 ACSYS 20
 ADEOS 14, 24-27
 aerosols 19, 27, 29, 31
 agriculture 26, 30, 34-35
 aircraft exhaust 26
 AIRS/AMSU/HSB 12-13, 21, 26-29, 31-32, 35
 AMSR-E 14-15, 18, 28-29, 35
 ARM 20
 ASTER 10, 17-19, 22, 29-31
 atmospheric chemistry 15-16
 atmospheric circulation 14
 atmospheric temperature 21
 AVHRR 28
 biomass burning 11, 15-16, 19, 29, 31, 34
 BOREAS 20
 bromine 9
 BSRN 20
 calibration 7-8, 21-25
 carbon cycle 16
 carbon dioxide (CO₂) 7, 9, 11, 14-16, 18, 20, 23, 25, 28, 30-33
 carbon monoxide (CO) 14-16, 22, 26, 31-35
 CERES 11, 13, 19, 21, 25, 28-29, 31-32
 CHEM-1 16
 chemistry, stratospheric (see CHEM-1)
 chemistry, tropospheric 22
 chlorine 9, 18, 25-27
 climate change 30-33
 CLIVAR 20
 clouds 12, 21, 25
 coastal zone 35
 continuity 23-25
 convection 12-13
 cryosphere 17-18
 DAO 19
 DAS 79
 DEC-CEN 20
 diurnal sampling 21, 23
 DMSP 25
 DoE 20
 ECLIPS 20
 ecosystem 20, 26, 30, 33-34
 El Niño 15, 23-24, 28, 33
 ENSO 15
 EOS AM 12, 22, 25
 EOS PM 14
 EOSP 11, 13, 19, 29, 31-32
 ERB 8
 ERBE 11-12, 21
 ERS 27-28, 30
 ESA 23, 27
 ESSC 7
 ETM+ 17-19, 22
 field campaigns 20
 FIRE 20
 fires 22
 freshwater resources 35
 GCIP 20
 GEWEX 11, 20
 GLAS 12-13, 18-20, 24-25, 32-35
 GLOBEC 20
 GOALS 20
 greenhouse gases 15-16
 HIRDLS 13, 18-19, 26-27, 29, 31-32, 35
 HSB 12-14, 21, 31-32, 35
 human dimensions 7, 8, 26, 34-35
 human health 33, 35
 humidity 8, 12, 21
 hydrology 16-17
 ice sheets 15, 17-18, 32, 34
 IDS 15
 IGBP 7, 20
 infiltration and deep percolation 16
 interannual variability 11, 15-18, 20, 28-29
 Jason-1 15, 22, 24, 31, 34
 JGOFS 20
 LAI 16-17, 33
 lake ice 17
 land ecosystems 16-17, 30, 33-34
 land hydrology 16
 Landsat-7 23
 lightning 12, 23
 LIS 12
 measurement strategy 21-25
 methane (CH₄) 18, 22, 26-27, 29, 31-32, 35
 METEOR-3 26-27
 MHS 21
 MISR 11-13, 17-19, 26-35
 MLS 13, 18-19, 25-27, 29, 31, 35
 MMS 12
 modeling 12, 20, 24, 31
 MODIS 12, 15-19, 21-23, 25, 28-31
 MOPITT 16, 22, 26, 31, 35
 NASA 7, 15, 19
 NASDA 23
 natural variability 28-31
 nitric oxide (NO) 16
 nitrous oxide (N₂O) 9, 15-16, 29
 NOAA 21, 23, 26-27
 NPP 16-17, 33
 NRC 7
 NSCAT 28
 ocean circulation 14-15, 24
 ocean color 15, 23, 28, 34
 OMI 19, 25
 overlap strategy 21-22
 ozone 18-19, 25-28
 policy-relevant questions 9
 PR 14, 86, 207, 212, 18, 21
 precipitation 13-14
 QuikSCAT 14, 24
 radiation fluxes 11-12
 SAGE III 19, 26-27, 31
 sea ice 25
 sea level 24, 31
 SeaWiFs 15, 28
 SeaWinds 14-15, 24, 28, 31
 SHEBA 20
 SMM 23
 snow cover 17-18, 25-35
 SOLSTICE 22, 31
 SRB 11-12
 SSM/I 25
 SST 15, 23-25, 28, 32
 sulfate 11, 19, 26, 29, 31

sulfur 19, 26
sulfur dioxide (SO₂) 19, 26-29
TMI 14
TOA 11-12, 21, 25
TOMS 19, 25-27
TOPEX/Poseidon 22-23, 28
topography 22
TOVS 21
trace gases 11, 20, 27, 31
TRMM 12, 14, 23
TSI 8, 11, 22, 29, 31
USGCRP 7-9, 20, 26, 26
validation 12-13, 18, 24, 29
validation strategy 24
VCL 19-20
vegetation indices 16-17
VIS 14
volcanoes 18-20, 22, 26, 29, 31
water vapor 8, 11-16, 19-22, 25, 29, 32, 36
WCRP 20
wind 13-15, 19-24, 29, 34
WOCE 30

Radiation, Clouds, Water Vapor, Precipitation, and Atmospheric Circulation

LEAD AUTHOR D. L. Hartmann

CONTRIBUTING AUTHORS C. S. Bretherton
 T. P. Charlock
 M. D. Chou
 A. Del Genio
 R. E. Dickinson
 R. Fu
 R. A. Houze
 M. D. King
 K. M. Lau
 C. B. Leovy
 S. Sorooshian
 J. Washburne
 B. Wielicki
 R. C. Willson

CHAPTER 2 CONTENTS

2.1 Introduction	43
2.1.1 Role of radiation, clouds, atmospheric water, and precipitation in climate and global change	43
2.2 Major scientific issues	43
2.2.1 Total solar irradiance and the Earth's climate	43
2.2.1.1 Role of TSI in climate change	43
2.2.1.2 Space-based observations of TSI variability	43
2.2.1.3 Remaining uncertainties	45
2.2.1.3.1 Uncertainties resulting from measurement technology	45
2.2.1.3.2 Present and planned TSI monitoring	46
2.2.1.4 Needed observations and observational strategy	46
2.2.1.4.1 The “overlap” strategy with ambient temperature radiometers	46
2.2.2 Role of radiation fluxes in the climate system	47
2.2.2.1 Atmospheric and surface radiative fluxes and heating	48
2.2.2.2 Absorption, scattering, and emission by gases	49
2.2.2.3 Absorption, scattering, and emission from aerosols	50
2.2.2.4 Absorption, scattering, and emission from clouds	51
2.2.2.5 Absorption, scattering, and emission by the Earth's surface	52
2.2.2.6 Radiation in global climate models	55
2.2.3 Role of convection and clouds in climate	56
2.2.3.1 Cloud effects on the Earth's energy balance	56
2.2.3.2 Cloud effects on the surface energy balance	58
2.2.3.3 Observations of cloud properties	58
2.2.3.3.1 Surface observations	58
2.2.3.3.2 Satellite observations	59
2.2.3.4 Modeling of clouds in the climate system	59
2.2.3.4.1 Global climate models–cloud parameterization and role in sensitivity	60
2.2.3.4.2 Regional mesoscale modeling of clouds	62
2.2.3.4.3 Cloud-scale models	64
2.2.3.5 Observational strategy for radiative fluxes and cloud properties	65
2.2.3.5.1 TOA radiative fluxes	70
2.2.3.5.2 Surface radiative fluxes	70
2.2.3.5.3 Radiative fluxes within the atmosphere	71
2.2.3.5.4 Cloud properties	72
2.2.3.5.4.1 Cloud fraction	72
2.2.3.5.4.2 Cloud height	73
2.2.3.5.4.3 Cloud visible optical depth and thermal infrared emittance	74
2.2.3.5.4.4 Cloud particle size	75
2.2.3.5.4.5 Cloud liquid/ice water path	75
2.2.3.5.4.6 Cloud mesoscale organization and structure	76
2.2.4 Water vapor and climate	76
2.2.4.1 Water vapor feedback and climate sensitivity	77
2.2.4.2 Water vapor distribution and variability	78
2.2.4.3 Maintenance of the global water vapor distribution	78
2.2.4.3.1 Role of convection and clouds	78
2.2.4.3.2 Role of large-scale atmospheric motions	79
2.2.4.3.3 Role of surface temperature	80
2.2.4.4 Water vapor in global climate models	80
2.2.4.5 Needed observations of water vapor	81
2.2.4.5.1 Available climatologies	81
2.2.4.5.2 Needed improvements	82
2.2.5 Precipitation	82
2.2.5.1 Role and importance of precipitation	82
2.2.5.1.1 Role in climate system operation	83
2.2.5.1.2 Importance in global change scenarios	84

CHAPTER 2 CONTENTS (CONT.)

2.2.5.2	Spatial and temporal distribution of precipitation	85
2.2.5.3	Integration of ground data	86
2.2.5.4	Precipitation in climate models	86
2.2.5.5	Needed satellite measurements and algorithms	87
2.2.6	Atmospheric circulation, hydrologic processes, and climate	88
2.2.6.1	Hydrologic processes and the tropospheric circulation	88
2.2.6.2	Large-scale circulation and climate feedback processes	88
2.2.6.3	Need for satellite measurements of wind	89
2.2.7	Strategy for combining observations and modeling	89
2.3	Required satellite measurements and data sets	91
2.3.1	Summary of required satellite observations	91
2.3.1.1	Total solar irradiance	91
2.3.1.2	Radiative fluxes	91
2.3.1.2.1	TOA fluxes	92
2.3.1.2.2	Surface and internal atmospheric fluxes	93
2.3.1.3	Cloud properties	93
2.3.1.3.1	Cloud fractional area coverage	94
2.3.1.3.2	Cloud height	96
2.3.1.3.3	Cloud visible optical depth and infrared emissivity	97
2.3.1.3.4	Cloud particle size and phase	97
2.3.1.3.5	Cloud liquid/ice water path	97
2.3.1.3.6	Lightning	97
2.3.1.4	Atmospheric temperature profiles	97
2.3.1.5	Water vapor	99
2.3.1.6	Precipitation	99
2.3.1.7	Winds and circulation	99
2.3.2	Critical surface observations and field experiments	99
2.3.2.1	FIRE	100
2.3.2.2	GEWEX	101
2.3.2.3	Climate Variability (CLIVAR) Project	101
2.3.2.4	ARM	102
2.3.2.5	BSRN	102
2.3.2.6	ECLIPS	102
2.3.2.7	Ties to other research areas	102
2.3.2.7.1	Oceanic processes	102
2.3.2.7.2	Land processes	103
2.4	Summary of EOS contributions	103
2.4.1	Observation and monitoring of key climate variables	103
2.4.1.1	Total solar irradiance	103
2.4.1.2	Radiative energy fluxes—TOA, surface, atmospheric	104
2.4.1.3	Cloud properties	104
2.4.1.4	Precipitation	104
2.4.2	Understanding of the processes that relate clouds and water vapor to global climate and their effect on climate sensitivity	104
2.4.3	More-accurate treatment of cloud and water vapor and their radiative effects in global climate models	104
2.4.4	Better measurement of precipitation and understanding of the role of precipitation in connecting atmospheric and surface processes, and more-accurate modeling of precipitation in global climate models	105
2.4.5	Synergism with oceanic and land-surface processes	105
2.4.6	Enhanced assessment of global change: monitoring and trend detection	105
2.4.7	Improved predictions of future climates and the influence of climate change on humanity	106
	References	106
	Chapter 2 Index	113

2.1 Introduction

2.1.1 *Role of radiation, clouds, atmospheric water, and precipitation in climate and global change*

The temperature near the surface of the Earth is in thermodynamic equilibrium when the absorption of radiant energy from the sun is in approximate balance with the emission of radiant energy to space by the planet. Sources of heat that are internal to the Earth system are negligible in a global sense. The energy output of the sun is a critical control on the Earth's climate. The amount of available solar energy absorbed by the Earth depends on its reflectivity, which is strongly dependent on the fractional coverage and optical properties of clouds in the atmosphere, aerosol amount and properties, atmospheric humidity, and the condition of the surface. These properties in turn interact with the temperature distribution and circulation of the atmosphere. Surface ice cover is sensitive to the global mean temperature of the Earth, and cloud amount and properties may also change with the mean climate.

The surface temperature of the Earth depends not only on the absorbed solar radiation, but also on the relationship between the surface temperature and the rate at which energy is returned to space by the radiative emission of the Earth. This relationship is controlled by the amount and vertical distribution of greenhouse gases, clouds and aerosols, and their relationship with the temperature profile. The most important greenhouse gas is

water vapor, whose distribution is determined by a complex web of interactions within the climate system itself. The dependence of saturation vapor pressure of water on temperature provides one of the potentially most powerful positive feedback processes in the climate system. The water vapor distribution interacts strongly with convection and the associated clouds, precipitation, large-scale circulations, and the thermal structure of the atmosphere.

Understanding the interactions among radiative transfer, clouds, water vapor, and precipitation, and incorporating this understanding into appropriate models, constitutes a critical step in predicting future climate changes and their regional and global impacts. In addition, these processes are also important for seasonal and interannual variability. In particular, mechanical and thermodynamic interactions between the atmosphere and the ocean on these time scales are strongly modulated by clouds, water vapor, and large-scale circulations.

EOS will collect a set of global observations that bear directly on the radiative, cloud, and hydrologic processes in the Earth's atmosphere. Through instrument team investigations, interdisciplinary science investigations, and use by the wider scientific community, these observations will be translated into an improved understanding of these processes and into improvements in our models of climate (Hartmann 1994).

2.2 Major scientific issues

2.2.1 *Total solar irradiance (TSI) and the Earth's climate*

2.2.1.1 *Role of TSI in climate change*

Monitoring TSI, the energy from the sun that is available to be received at the average distance of the Earth from the sun, has been a goal of science for more than a century. At any time in the Earth's history the climate regime of the biosphere has been determined by the TSI, the atmospheric chemical composition, the distribution of oceans and land masses, and the circulations of the oceans and atmosphere that act in combination to determine the net retention of solar energy, its distribution within the climate system, and its ultimate return to space by radiative emission.

2.2.1.2 *Space-based observations of TSI variability*

The first long-term solar monitoring utilizing an Electrically Self-Calibrating Cavity (ESCC) sensor in space was the Earth Radiation Budget (ERB) experiment on the National Aeronautics and Space Administration (NASA) Nimbus 7 spacecraft. The ERB database, beginning in late 1978 and continuing to early 1993, is the longest currently available (Hickey et al. 1980; Hoyt et al. 1992). Unambiguous evidence of TSI variability was first detected in the highly precise results of the Active Cavity Radiometer Irradiance Monitor (ACRIM I) experiment on the NASA Solar Maximum Mission (SMM) in 1980 (Willson et al. 1981). The principal features of TSI variability have been identified in the ERB results as well. The mutually corroborative function of the ACRIM I and

ERB results has played an important role in verifying TSI variability on the solar activity cycle time scale.

A series of short-term TSI experiments have been flown on or deployed from the space shuttle to provide comparison experiments for satellite solar monitors. The Spacelab 1 and Atmospheric Laboratory for Applications and Science (ATLAS) flights between 1983 and 1993 employed two different TSI experiments, as has the shuttle-deployed and -retrieved European Retrievable Carrier (EURECA) platform that operated during 1992-1993 (Frohlich 1994; Crommelynck et al. 1994; Willson 1994). The shuttle ACRIM experiment has demonstrated a capability of sustaining flight-to-flight precision of the order of 100 parts-per-million (ppm). This precision is comparable to the accuracy achievable by radiometers operating at cryogenic temperatures, but significantly inferior to the precision accessible using an overlap strategy with “ambient temperature” satellite experiments (Willson 1995).

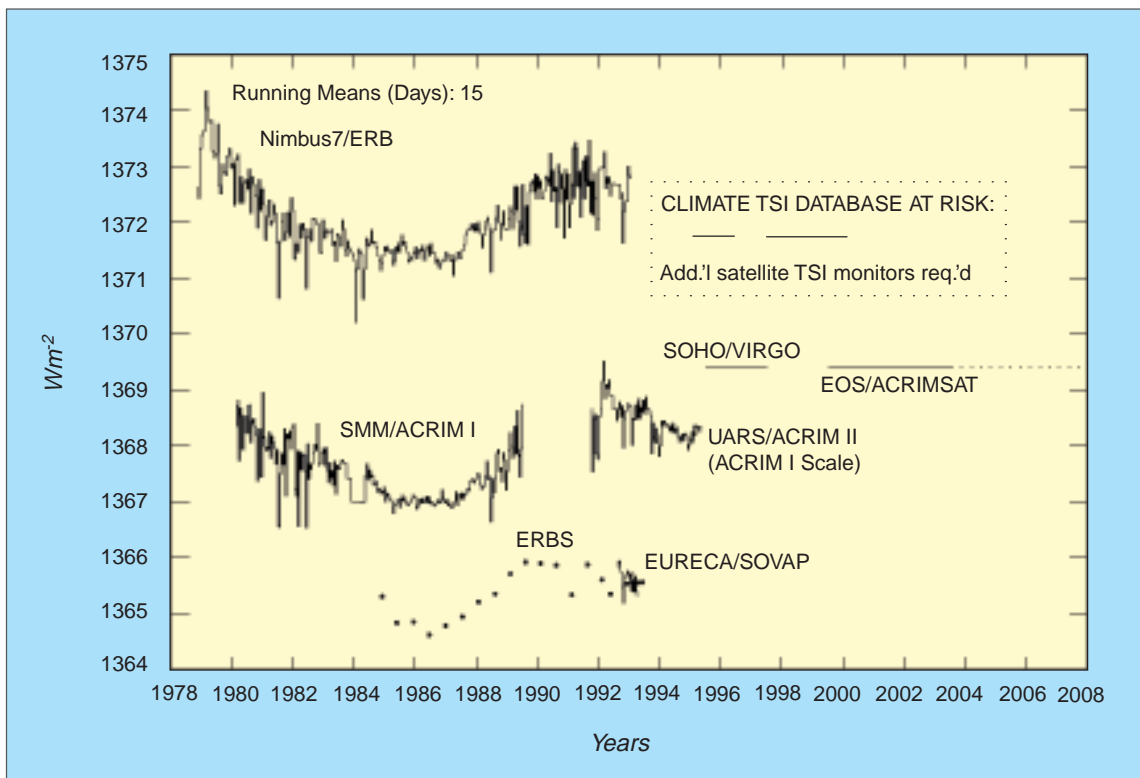
The results of modern TSI monitoring are shown in Figure 2.1. The Nimbus7/ERB, SMM/ACRIM I and Upper Atmosphere Research Satellite (UARS)/ACRIM

II experiments have documented the direct dependence of TSI on solar activity during solar cycles 21 and 22. Qualitatively similar results have been obtained with the Earth Radiation Budget Satellite (ERBS) solar monitor (Lee et al. 1995).

One of the most significant findings from the precision TSI database thus far is on solar cycle time scales: a direct correlation of luminosity and solar activity (Willson and Hudson 1986, 1988, 1991; Foukal and Lean 1988; Hoyt et al. 1992; Frohlich 1994). TSI showed a 0.1% peak-to-peak amplitude during solar cycle 21. The observed maximum of TSI at the maximum in solar activity agrees in sense with that predicted from the coincidence of the “Little Ice Age” climate anomaly and the “Maunder Minimum” of solar activity during the seventeenth and eighteenth centuries (Eddy 1977).

Solar cycle TSI variation is predicted with varying degrees of success by linear regression models using the precision TSI database and “proxies” of solar activity, such as the Zürich sunspot number, the 10.7-cm microwave flux, the He I 1083-nm full-disk equivalent width, and the “core-to-wing ratio” of the Mg II line at 280 nm. The

FIGURE 2.1



Record of total solar irradiance (TSI) monitoring from space. Includes data from Nimbus 7/ERB, Solar Maximum Mission, UARS/ACRIM, and ERBE solar monitor, plus some shuttle observations.

use of the He I model led to the initial realization of the primary role of faculae and the bright network in the solar cycle TSI variation (Foukal and Lean 1988, 1990; Livingston et al. 1988; Willson and Hudson 1988). The “proxy models” of TSI have been useful in providing qualitative explanations of solar phenomena, but in view of the fact that they are simple statistical constructs and not physical models, it is not surprising that significant differences are found between predictions of TSI and satellite observations.

An inverse relationship between sunspot area and total irradiance has been found on the solar rotational time scale (27 days) with deficits in total irradiance of up-to-0.3% (Willson et al. 1981, Willson 1982; Hudson and Willson 1982; Foukal and Lean 1988). There is growing evidence that most of the missing flux is balanced by excess facular radiation on the active region time scale (months) (Willson 1984; Foukal and Lean 1986).

On the shortest time scales, solar global oscillations of low degree have been detected in the ACRIM I total irradiance data, including pressure modes (time scales of minutes—the so-called 5-minute oscillations or “P-modes”) and possible gravity modes (time scales of hours to days). Interpretation of the 5-minute-oscillation results from the ACRIM I experiment has placed an upper limit on differential rotation of the outer solar atmosphere as a function of solar radius, and therefore on solar oblateness, providing support for the relativistic interpretation of the perihelion of Mercury observations (Woodard and Hudson 1983; Woodard 1984; Frohlich 1987; Woodard and Noyes 1985).

P-mode oscillations are constrained to the convection zone or just below, limiting the depth within the sun for which their analysis can provide new physical insight. Should gravity mode oscillations be verified in TSI data, their analysis would yield information on physical processes extending to the solar core.

TSI variations on time scales shorter than a year do not appear to be of direct climatological interest but contain information on solar variability that has provided new insight into the physics of the sun. Continuous TSI monitoring, particularly by satellites with a high solar-pointing duty cycle during each orbit can provide the observations that will facilitate future solar models that may predict TSI variability with sufficient precision to anticipate possible corresponding climate variations.

2.2.1.3 Remaining uncertainties

2.2.1.3.1 Uncertainties resulting from measurement technology

The “absolute” uncertainty of the *current generation* of TSI flight instruments, which operate at ambient temperatures, is about 1000 ppm in the laboratory and about two-to-three times larger in flight experiments (Willson 1973, 1979, 1982; Frohlich 1994). Ambient temperature TSI radiometry is a mature technology that has been thoroughly flight tested in various configurations on balloon, rocket, space shuttle, and satellite flight platforms (Willson 1973, 1979, 1982; Duncan et al. 1977; Hickey et al. 1988). The principal remaining sources of uncertainty for well-designed ambient temperature sensors are the determination of their aperture areas and the myriad of small, parasitic thermal interactions between the cavity detector and its surroundings.

The absolute uncertainty of a *new generation* of TSI sensors operating near the temperature of liquid Helium approaches 100 ppm in the laboratory environment—a 10-fold improvement relative to “ambient temperature” sensors. Cryogenic sensors face some daunting challenges in their transformation into space flight experiments, however. They must use small apertures (~0.3-cm diameter compared to 0.8 cm for “ambient temperature” radiometers) to minimize solar heating that would otherwise prevent their cryogenic coolers from reaching the required temperatures (< 20 K). The singular advantage of cryogenic sensors is that the parasitic thermal uncertainties are reduced to negligible levels. Aperture-area determination remains the most limiting source of uncertainty since their small apertures cannot be determined with the same accuracy as the larger ones employed in ambient temperature sensors.

Contamination is a major source of uncertainty in any TSI flight experiment, and it is of particular concern for cryogenic sensors. At low temperatures they would function as attractors for condensables and particulates. Accumulation of contaminants on the rims of their small apertures would cause larger errors than for ambient temperature instrumentation. A realistic expectation for their eventual in-flight performance would likely be in the several hundred ppm uncertainty range. Moreover, functional lifetime in orbit is a greater concern with cryogenic instruments.

2.2.1.3.2 Present and planned TSI monitoring

The impact of ambient temperature sensor “absolute” uncertainties on TSI monitoring can be seen in Figure 2.1. The highest (Nimbus7/ERB) and lowest (ERBS) lie at $\pm 0.25\%$ about the mean (1369 Wm^{-2}). This is within the expected uncertainty of these sensors’ “native” scales. Should the series of long-term TSI experiments be interrupted, the continuity of the long-term TSI database could not be re-established by deployment of another experiment with an uncertainty less than $\pm 0.25\%$. Since climate changes comparable to the “Little Ice Age” may involve TSI changes as small as 0.5% over 200+ years, the loss of contiguity in the satellite solar-monitoring experiments would render the database useless for climatology.

The ACRIM I experiment terminated with the re-entry of the SMM spacecraft in late 1989. The Nimbus7/ERB experiment ceased operations in early 1993. The precision TSI climate database is currently being sustained by two experiments: the UARS/ACRIM II launched in 1991 and the European Space Agency’s (ESA) Solar Heliospheric Observatory (SOHO)/Variability of solar Irradiance and Gravity Oscillations (VIRGO) launched in late 1995. The connection to the database compiled by the ERB and ACRIM I is conserved by the ACRIM II experiment. The ERBS TSI instrument is also contributing data, but it was launched in 1984 and is limited by aging spacecraft batteries.

The UARS has on-board resources and an orbit that could last to the year 2000. Problems with the batteries and solar panel drive systems raised some doubts about its life expectancy early in the mission but work-arounds appear to have stabilized the satellite. The SOHO/VIRGO experiment became fully operational in March 1996 and has a two-year minimum mission lifetime that could extend significantly by virtue of its Lagrangian point orbit. VIRGO has experienced some initial problems with its two TSI instruments, but appears to be capable of providing high-quality results using work-arounds.

The next planned TSI experiments are a series of ACRIMs designed to provide the database during the 15 years of the Earth Observation System (EOS) program. The first EOS/ACRIM will launch in 1999. The major concern in the effort to sustain the TSI database during the late 1990s is the possible cessation of UARS/ACRIM II and SOHO/VIRGO observations prior to the inception of EOS/ACRIM. Failure to overlap these experiments could result in a catastrophic loss of relative precision between the first 20 years of the long-term, precision TSI database and that to follow.

2.2.1.4 Needed observations and observational strategy

Sustained changes in TSI of as little as a few tenths of one percent per century could be causal factors for significant climate change on time scales ranging from decades to centuries (Lean et al. 1995). A precise, long-term record of solar luminosity variation is required to provide empirical evidence of the sun’s role in climate change and to separate its effect from other climate drivers. The same record, together with climate and other solar observations, will yield a valuable empirical record of TSI variability against which climate observations can be tested, and will also yield an improved understanding of the physics of the sun and the causes of luminosity variations. The record could also eventually lead to a predictive capability for solar-driven climate change.

The National Research Council (NRC) recently published its findings regarding research priorities for Solar Influences on Global Change, one of the seven science elements of the U.S. Global Change Research Program (USGCRP) (NRC 1994). Their recommendations include “monitoring total and spectral solar irradiance from an uninterrupted, overlapping series of spacecraft radiometers employing in-flight sensitivity tracking” as this element’s highest priority and most urgent activity.

Monitoring solar luminosity variability with maximum precision demands not only state-of-the-art technology but the use of an optimum research strategy. Following is an evaluation of approaches to sustain the precision TSI database with the requisite 10-ppm or smaller discontinuities between experiments.

2.2.1.4.1 The “overlap” strategy with ambient temperature radiometers

A relative precision smaller than 10 ppm should be readily achievable for the data of overlapped satellite solar monitors, assuming a sufficiency of overlapping comparisons and adequate degradation calibrations. The principal source of uncertainty for satellite experiments is degradation of their sensors by extended solar exposure during multi-year missions. The series of ACRIM experiments has employed a three-fold sensor redundancy and a phased operational modality that can calibrate such degradation with a residual uncertainty of less than 50 ppm per decade. Fully-implemented three-fold sensor redundancy is essential for adequate calibration of degradation in long-term satellite experiments.

The optimum overlap strategy is the intercomparison of successive, high-precision satellite solar-monitoring experiments at a precision level defined by their operation in the space-flight environment. A backup overlap

strategy would involve intercomparisons by a “third party” flight experiment, such as another satellite experiment or the shuttle-based TSI experiments that have made intercomparisons with two successive but non-overlapping satellite solar monitors.

The “overlap strategy” was to have begun with the in-flight comparison of the SMM/ACRIM I and UARS/ACRIM II experiments. Unfortunately, the SMM mission ended in late 1989, two years before the UARS could be launched. The relationship between the ACRIM I and ACRIM II experiments has instead been established using a “third party” overlap strategy based on the results of mutual comparisons of ACRIM I and ACRIM II with the less precise, but long-lived, Nimbus 7/ERB and ERBS experiments. The results are shown in Table 2.1. The ratio of ACRIM I to ACRIM II is 1.002069 with linear detrending of the slowly-degrading Nimbus7/ERB results. The Nimbus7/ERB experiment does not have a degradation calibration capability, and linear detrending can only approximate the effects of degradation on the comparison results. The uncertainties of the results in Table 2.1 therefore include some systematic errors and, as such, represent an upper limit for the backup overlap strategy. The statistical uncertainty of 10 ppm demonstrates the ability of the “overlap strategy” to produce high precision even when the comparison experiments are not optimized for the purpose.

The overlap strategy employing flight-tested ambient temperature TSI radiometers is the only approach currently available capable of sustaining the long-term climate TSI database with the precision required. A sensibly conservative overlap requires launch of an EOS/ACRIM experiment at the earliest possible time, now 1999, which will be in the eighth year of the UARS/ACRIM II experiment and near the end of SOHO/VIRGO’s third year.

The EOS/ACRIM experiment uses the ACRIM technology flown successfully on NASA’s SMM, UARS, Spacelab 1, and ATLAS missions. Two approaches to the EOS implementation of ACRIM observations appropri-

ate to the “mission-of-opportunity” status are under consideration. The basic philosophy of both is the use of inexpensive instrumentation made from commercial parts. The required five-year EOS data-segment lifetime reliability is achieved through the deployment of redundant instruments. The new, compact form of the ACRIM sensor assembly can be mated with small-satellite technology to construct a dedicated ACRIM satellite, or flown as secondary payloads on other satellites of opportunity using derated versions of compact, flight-proven gimbals for solar pointing.

The ACRIM implementation plan involves the initial launch of two ACRIM instruments as secondary payloads. Following intercomparisons on orbit, one will be used as the primary TSI monitor and the second held in reserve. Upon failure of the primary instrument, the reserve will assume that role, and another ACRIM will be deployed at the earliest opportunity to replace the reserve function. The first two ACRIMs can be on orbit within 24 months of project startup, enhancing the possibility of implementing the overlap strategy with the UARS/ACRIM II experiment during its extended mission and the SOHO/VIRGO experiment prior to the end of its two-year minimum mission. The series of ACRIMs proposed would provide overlapping satellite TSI observations throughout the EOS mission.

2.2.2 Role of radiation fluxes in the climate system

The climate system is a heat engine that is driven by the spatial and temporal displacement of the entry and exit of broadband radiant energy. A net flow of radiant energy at the top of the atmosphere enters the tropics and leaves at high latitudes. The resulting equator-to-pole heating gradient drives the circulations of the atmosphere and ocean. The largest fraction of radiant energy entering the climate system is absorbed at the surface in the form of solar radiation, but leaves from the atmosphere in the form of thermal infrared emission. This radiative heating below and cooling above drives the convective activity of the troposphere, resulting in abundant rainfall and cleansing

TABLE 2.1

<i>DATA</i>	<i>POLYNOMIAL FIT (DEGREE)</i>	<i>RATIO ACRIM I/ACRIM II</i>	<i>STANDARD ERROR (PPM)*</i>
Original Data	0	1.001890	13
Detrended Data	1	1.002069	10

* 1 sigma error

Ratio of SMM/ACRIM I and UARS/ACRIM II results constructed using mutual intercomparisons with the Nimbus7/ERB experiment. Demonstration of the backup capability of the overlap strategy for preserving the precision of the total solar irradiance database.

of the atmosphere. The general circulation and the hydrological cycle are maintained in their current states partly by the requirements of thermodynamic balance, whereby they transport and store heat, transporting energy from the point of absorption to the point of emission to space. The main processes for cycling energy by radiation, wind, and latent heating interact on a wide range of scales, from boundary-layer turbulence with scales of less than a meter to the large-scale components of atmospheric circulation with dimensions of 10^7 meters.

Radiation is the primary forcing of climate change; anthropogenic radiative forcing by changes in trace gases, aerosols, and surface optical properties is on the scale of decades; astronomical radiative forcing (Milankovitch orbital variations) is on the slower scale of the ice ages. Radiation is important for climate feedback. It is widely acknowledged that uncertainties in the radiative feedback to climate by clouds pose the most formidable obstacle to climate prediction by general circulation models (GCMs). The strong coupling of radiative and hydrological processes and the general importance of this coupling in environmental prediction has led to development of the complex Global Energy and Water Cycle Experiment (GEWEX) by the World Climate Research Program. The GEWEX Radiation Panel oversees a wide range of international activities involving satellite and surface measurements and modeling.

Pre-EOS satellite sensors have observed radiation in various narrow bands for remote-sensing applications and in the broadband shortwave (SW, solar wavelengths) and longwave (LW, thermal infrared) to monitor the Earth Radiation Budget (ERB) at the top of the atmosphere (TOA). The newer EOS sensors have more spectral coverage, a larger number of independent channels, and greater calibration accuracy. Further advances in our understanding of the role of radiative fluxes in climate can be expected from EOS implementation through:

- 1) simultaneous measurement of different quantities by multiple instruments to provide a more-complete picture of the Earth system and facilitate a more-comprehensive understanding;
- 2) synergistic integration of pairs of instruments to improve the accuracy of the retrieval for individual parameters;
- 3) commitment to a 15-year time series of observations, which is long enough to resolve some modes of natural interannual variability;
- 4) modeling and analysis within Interdisciplinary Science (IDS) investigations to provide scientific guidance for the prioritization of remote sensing, apply EOS satellite products to critical science questions, and apply ancillary data to improve the accuracy of EOS remote sensing and supply additional observables; and
- 5) a readily-accessible EOS Data and Information System (EOSDIS) for producing and distributing EOS data, precursor satellite data sets, and critical aircraft and in situ data.

2.2.2.1 Atmospheric and surface radiative fluxes and heating

Advances in thermodynamics, electromagnetic theory, and physical chemistry permitted Arrhenius (1896) to predict a global warming associated with increasing concentrations of CO_2 , because increased carbon dioxide would inhibit the upward radiative transfer of energy from the surface to space. Modern climate models have consistently indicated that CO_2 and other anthropogenic trace gases will change the vertical distribution of radiative fluxes in the atmospheric column so as to warm the troposphere and cool the stratosphere. These global model results are consistent with those of one-dimensional radiative-convective (RC) models, which demonstrate the large radiative forcing of the climate system by clouds and trace gases (Manabe and Wetherald 1967). Sellers (1969) and Budyko (1969) devised other simple climate models that focused on surface radiation and quantified a highly significant ice-albedo feedback mechanism. The potential significance of cloud-climate feedback was found to be very large in other low-order model studies (Paltridge 1980; Charlock 1981, 1982; Wang et al. 1981), and it remains such in state-of-the-art global climate models (GCMs) (e.g., Mitchell 1993a, b). The climate response to a given radiative forcing is still not reliably predictable because GCMs, which do not convincingly simulate clouds (Rossow et al. 1991) and their relation to TOA radiation (Barkstrom et al. 1989), are sensitive to uncertain radiative feedbacks, especially due to clouds (Cess et al. 1991). There have been fairly good simulations of transient temperature variations due to the radiative forcing of the 1991 Pinatubo volcanic eruption (Hansen et al. 1994) and even to the 1963 Agung eruption. However, see Hansen et al. (1978), and see also Chapter 8.

The simulation of the atmospheric circulation and climate requires an adequate vertical profile of diabatic heating (e.g., Hartmann et al. 1984), including radiation and latent heating. Surface fluxes are important for studies of ocean circulation and heat transport (e.g., Liu et al.

1994). Table 2.2 shows annually-averaged Earth Radiation Budget Experiment (ERBE) results (Harrison et al. 1990) for TOA SW and LW radiation and present estimates for surface radiation (Gupta et al. 1995) based on International Satellite Cloud Climatology Project (ISCCP) data. Confidence in the TOA results is tempered by the ~5 Wm⁻² discrepancy between the SW and LW results in Table 2.2; this may be due to ERBE angular modeling (Green and Hinton 1996). The surface radiative fluxes in Table 2.2 have errors that are probably larger than the errors at the TOA (see also Kiehl and Trenberth 1997).

2.2.2.2 Absorption, scattering, and emission by gases

Atmospheric gases have a greater effect on the climate than any other component of the Earth’s climate system. It is estimated that absorption of infrared radiation by atmospheric gases reduces the escaping longwave radiation by about 120 Wm⁻², whereas the reflection of solar radiation by clouds and the surface each return only about 50 Wm⁻² to space, when globally averaged. Emission and absorption of terrestrial thermal infrared energy by vibrational and rotational transitions in gases generate the so-called clear-sky greenhouse effect; H₂O, CO₂, and O₃ are the primary agents, with significant impact by CH₄, N₂O, and CFCs. In Figure 2.2, the calculated spectral distributions of downwelling longwave radiation for tropical and subarctic atmospheres under clear skies indicate two distinct wavelength regimes. At wavelengths less than 8 mm and greater than 12 mm, the atmosphere is opaque, mostly because of absorption by H₂O and CO₂; so that the downward longwave radiation follows the blackbody emission curve for a temperature close to that of the surface. Strongly-absorbed thermal wavelengths are useful for satellite sounding at altitudes well above the surface. Electronic transitions of gaseous molecules induce considerable absorption of the incoming solar energy, most of the atmospheric absorption in Table 2.2, for example. In Figure 2.3, the calculated spectral distribution of

downwelling solar radiation at the tropical surface under clear skies is shown for a solar zenith angle of 60°. Solar energy at wavelengths below 0.5 mm is strongly absorbed by O₃ and scattered by all molecules. The attenuation in Figure 2.3 between 0.5 and 0.8 mm is mostly due to scattering, though there is some absorption by O₂ and H₂O. Absorption by H₂O dominates the attenuation above 0.8 mm, and CO₂ also absorbs above 2.5 mm.

The two principal contributions that EOS can make in the area of absorption and emission by atmospheric gases are:

- 1) production of more-accurate vertical profiles and time histories of water vapor and other radiatively active gases; and
- 2) validation of the radiative transfer physics for natural and anthropogenic gases.

Because of the enormous importance of H₂O to both radiative and hydrological processes, it is retrieved by several EOS sensors, as described in Section 2.2.4.

The Measurements of Pollution in the Troposphere (MOPITT) instrument will provide CH₄ retrievals on EOS AM-1. This will be useful for careful budget studies of the radiative effect of anthropogenic trace gases. After 2000, retrievals of the radiatively significant species O₃, H₂O, CH₄, N₂O, and CFCs will be made by the High-Resolution Dynamics Limb Sounder (HIRDLS) in the upper troposphere and above; these are needed for studies of the secular trend in radiation near the tropopause and for the stratospheric radiation budget. The Microwave Limb Sounder (MLS) will also measure H₂O, O₃, and N₂O in the upper troposphere and is unique in providing data which are not degraded by cirrus. The Tropospheric Emission Spectrometer (TES) will cover most infrared active species from the surface to the lower stratosphere.

TABLE 2.2

SHORTWAVE		LONGWAVE		NET	
Incoming TOA Flux	341				
Absorbed TOA Flux	239	TOA OLR	235	Net TOA	+4*
Surface Insolation	184	Surface Downward	348		
Surface Absorbed	160	Surface Cooling	47	Net Surface	+113
Absorbed in Atmosphere	79	Atmosphere Cooling	188	Net Atmosphere	-109

* Net TOA radiation is a measure of ERBE estimate error, and is probably close to zero in reality.

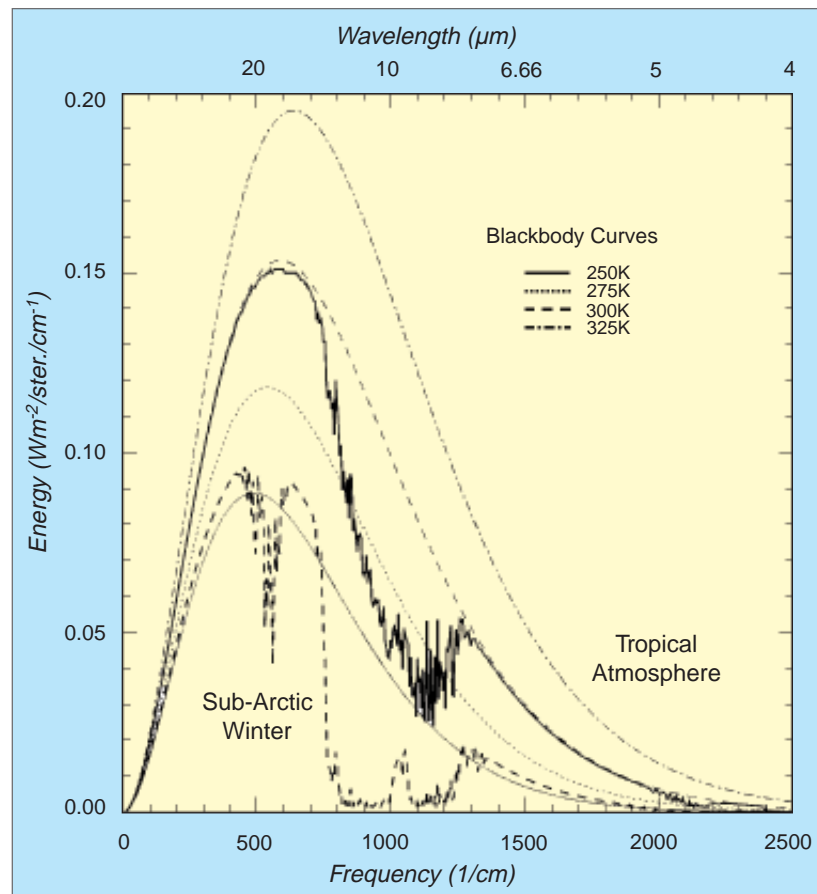
Radiation budget at surface and top of atmosphere (TOA) for February 1985 to January 1989. Units are Wm⁻². TOA values are ERBE estimates, and surface estimates are from surface radiation budget (SRB) calculations (Gupta et al. 1996). Atmospheric heating rates are calculated as residuals from the TOA and surface estimates.

The large spread of broadband radiative fluxes in the Intercomparison of Radiative Codes for Climate Models (ICRCCM) studies (e.g., Ellingson et al. 1991) clearly shows that the problem of calculating such fluxes for a given distribution of gases still exists. There are particular uncertainties in regard to the H₂O continuum. The Atmospheric Radiation Measurement (ARM) program is providing data for a continuation of ICRCCM at high spectral resolution. The Atmospheric Infrared Sounder (AIRS) and especially TES can make significant contributions to the extension of ICRCCM by issuing radiance data sets that can be used as a testbed for radiative transfer codes. The Clouds and the Earth's Radiant Energy System (CERES) will observe the net effect of all radiatively active constituents including gases at the TOA. CERES will also attempt retrievals of the radiation budget throughout the atmospheric column; this will constitute a time series of the greenhouse effect.

2.2.2.3 Absorption, scattering, and emission from aerosols

Aerosols have both direct and indirect radiative effects on the climate system; both effects constitute the largest uncertainties in the anthropogenic radiative forcing of climate. The direct effect is the scattering and absorption of solar energy by aerosols, which are composed mainly of insoluble dust, hydrocarbons, and hydrophilic particles. The direct optical effects are mainly due to aerosols with radii of a few tenths of a micrometer. The global aerosol optical thickness in the LW radiation is quite small, and aerosols usually make only a small contribution to the greenhouse effect. The direct radiative forcing of tropospheric aerosol is highly regional. Anthropogenic sulfate aerosols mostly scatter SW radiation and cool the climate; the global optical depth of sulfate aerosol is only roughly inferred from budgets of sulfur gases (e.g., Charlson et al. 1991). Soot from industrial areas can absorb strongly and induce heating; however, we lack both accurate budgets for the soot and reliable calculations for its small

FIGURE 2.2



Calculated spectral distributions of downwelling longwave radiation for tropical and subarctic atmospheres under clear skies. Blackbody curves for various temperatures are shown for reference.

optical impact (Penner et al. 1994). Natural and anthropogenic biomass burning produces huge quantities of smoke and may have a global cooling effect of 0.2 to 2 Wm⁻². The 1994 Intergovernmental Panel on Climate Change (IPCC) estimate of the direct radiative forcing of anthropogenic aerosols is small but uncertain. This uncertainty will remain large until: 1) a more-sophisticated surface-based network is in place to monitor the aerosol and radiative fluxes; and 2) EOS sensors like the Moderate Resolution Imaging Spectroradiometer (MODIS), the Multi-angle Imaging Spectroradiometer (MISR), the Earth Observing Scanning Polarimeter (EOSP), and CERES can be combined with outputs from such a network to produce more reliable estimates of the global amount and radiative forcing of aerosols.

Measurements of aerosols and their effects on the climate system are discussed more fully in Chapter 8 of this Plan, "Volcanoes and the Climate Effects of Aerosols."

2.2.2.4 Absorption, scattering, and emission from clouds

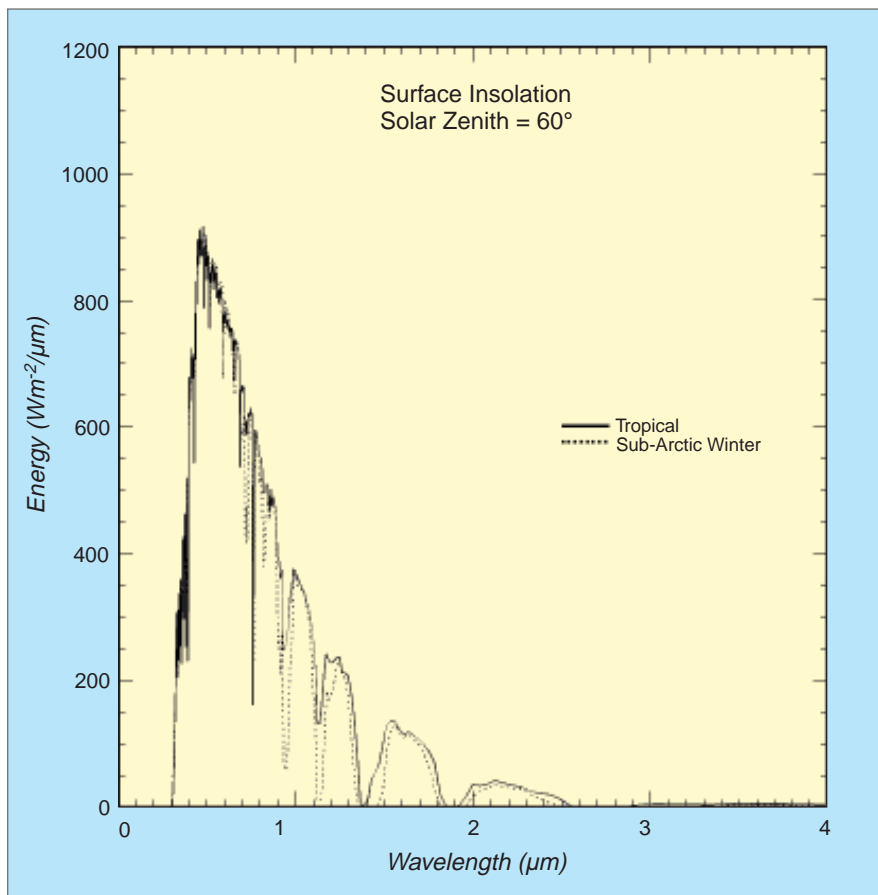
In terms of the radiative forcing of natural constituents, the effect of clouds on climate is second only to greenhouse gases, although it has been argued that the uncertainty in cloud radiative forcing and feedback is larger than that for greenhouse gases (Cess et al. 1991). The uncertainty posed by cloud-radiative feedback to climate has been widely recognized as a key problem in climate prediction. The cloud forcing to climate has been observed by ERBE (Ramanathan et al. 1989; Harrison et al. 1990) at the TOA. The ISCCP of the World Climate Research Program (WCRP) (Rossow and Schiffer 1991) has striven to provide estimates of cloud areas, cloud top heights, and cloud visible optical thickness based on an analysis of operational narrowband meteorological imagers. Estimating the radiative effects of clouds and retrieving cloud properties from space both require a detailed understanding of the scattering and absorption properties of clouds. Important problems remain in the directional scattering of solar radiation by realistic clouds, the radiative effects of the overlap of cloud fragments, and perhaps even in the basic absorption properties of cloudy atmospheres.

A debate on the net SW radiation absorbed by the atmosphere, perhaps founded on different interpretations of the few available in situ atmospheric radiation measurements, is in progress. Cess et al. (1996), Ramanathan et al. (1995), and Pilewskie and Valero (1995) contend that clouds increase the absorption of SW of the atmospheric column by 25-40 Wm^{-2} , resulting in a corresponding error in the present global SW budget of the atmosphere and surface. However, global surveys by Li et al. (1995) and Whitlock et al. (1995) imply that the SW budget of the atmosphere is correct to within 10-15 Wm^{-2} ; measurements by Hayasaka et al. (1995) and theoretical calculations by Chou et al. (1995) do not support the "anomalous" SW

absorption by clouds, either. EOS will have improved retrievals of radiatively active constituents (gases, aerosols, clouds, surfaces) and TOA fluxes, and it has excellent prospects for generating accurate fluxes of surface radiation and usable estimates for vertical profiles of radiation, particularly through combined use of satellite and in situ data.

The CERES record of radiation fluxes and cloud forcing will surpass ERBE in accuracy and in its ability to accurately estimate the radiative forcing by clouds. CERES will use multi-angle sampling for its broadband scanner and incorporate MODIS-based cloud and surface scene identifications for the development of angular distribution models. The development of such angular distribution models is needed to accurately measure the albedo of the planet. The solar radiance reflected from a particular region depends on the angle from which the region is viewed and the position of the sun. To estimate albedo, an angular distribution model is needed to relate measurements at particular angles to a total reflected short-

FIGURE 2.3



Calculated surface insolation as a function of wavelength under clear conditions for tropical and subarctic conditions.

wave flux integrated over all angles. The present ERBE record reveals a shortcoming in our understanding of directional reflection of solar radiation in that the estimated albedo shows a spurious dependence on satellite viewing angle. The directional aspects of cloud radiation will be investigated with MISR, which has a higher resolution than CERES. EOSP will also provide cloud optical thickness and phase. Cloud particle phase is important radiatively, for both remote sensing and for the energy budget, because liquid water and ice scatter radiation quite differently. MISR retrievals of the absorbing properties of aerosol will be needed as inputs to radiative transfer simulations of cloud SW absorption. An important aspect of EOS observations of clouds and radiation fluxes is the relatively long, homogenous, 15-18 year record that is its goal. Such a long homogenous record would allow seasonal and interannual variability to be adequately sampled and used to understand connections within the climate system that only appear on longer time scales, such as the El Niño-Southern Oscillation (ENSO) and decadal variabilities that are known to exist (e.g., Rasmusson and Wallace 1983; Deser and Blackmon 1993).

Landsat-based studies have shown that small-scale cloud structure causes systematic errors in the retrieval of cloud area with moderate-resolution instruments like Advanced Very High Resolution Radiometer (AVHRR), Visible and Infrared Scanner (VIRS), and even MODIS (Wielicki and Parker 1992). The same small-scale structure influences the broadband TOA albedo of cloudy regions (Cahalan et al. 1995). Plane parallel radiative transfer calculations with the “independent pixel” approximation show that when a homogeneous cloud field and an inhomogeneous cloud field present the same TOA albedo to space, the total atmospheric absorption for the inhomogeneous field is usually slightly larger. These problems will be addressed in detail with EOS AM-1 data, which will have the high-resolution Advanced Spaceborne Thermal Emission and Reflection Radiometer (ASTER), as well as MODIS, MISR, and CERES. The first-generation CERES IDS products will test the ability of plane parallel radiative transfer physics and MODIS cloud property retrievals to match the observed CERES instrument broadband TOA flux. The resolution of some discrepancies at TOA is expected to require advances in 3-D radiative transfer modeling and in the retrieval of cloud microphysical parameters as well as cloud geometry.

Cloud vertical structure poses another barrier to the attempt in EOS to retrieve the full vertical profile of radiation within the atmosphere. This is illustrated in Figure 2.4 where the cloud forcing to the global atmospheric LW cooling rate has been calculated with ISCCP cloud, temperature, and humidity data, and the Wang et al. (1991)

radiative transfer code. The mean LW cooling rate of the troposphere is roughly 2 K day^{-1} , and clouds obviously have an enormous impact in the LW, inducing more cooling in some regions and significant relative heating in others. In the left panel of Figure 2.4, it is assumed that the ISCCP clouds do not overlap. In the right panel of Figure 2.4, the cloud forcing difference for the randomly overlapped minus nonoverlapping clouds is shown; it is dramatic and spans roughly a full quarter of the cloud forcing range. Both random overlapping clouds and nonoverlapping clouds show the same picture to the operational LW radiometers used by ISCCP. EOS will begin to resolve the cloud overlap and cloud geometrical thickness dilemma by using combinations of passive sensors such as:

- MODIS and Advanced Microwave Scanning Radiometer (AMSR-E) sensors over ocean (e.g., MODIS will sense optically-thick ice clouds, while AMSR-E will detect underlying water clouds),
- MODIS and AIRS longwave sensors (e.g., for optically-thin cirrus over extensive low water clouds), and
- MISR multi-angle stereo views of broken and isolated cloud fields.

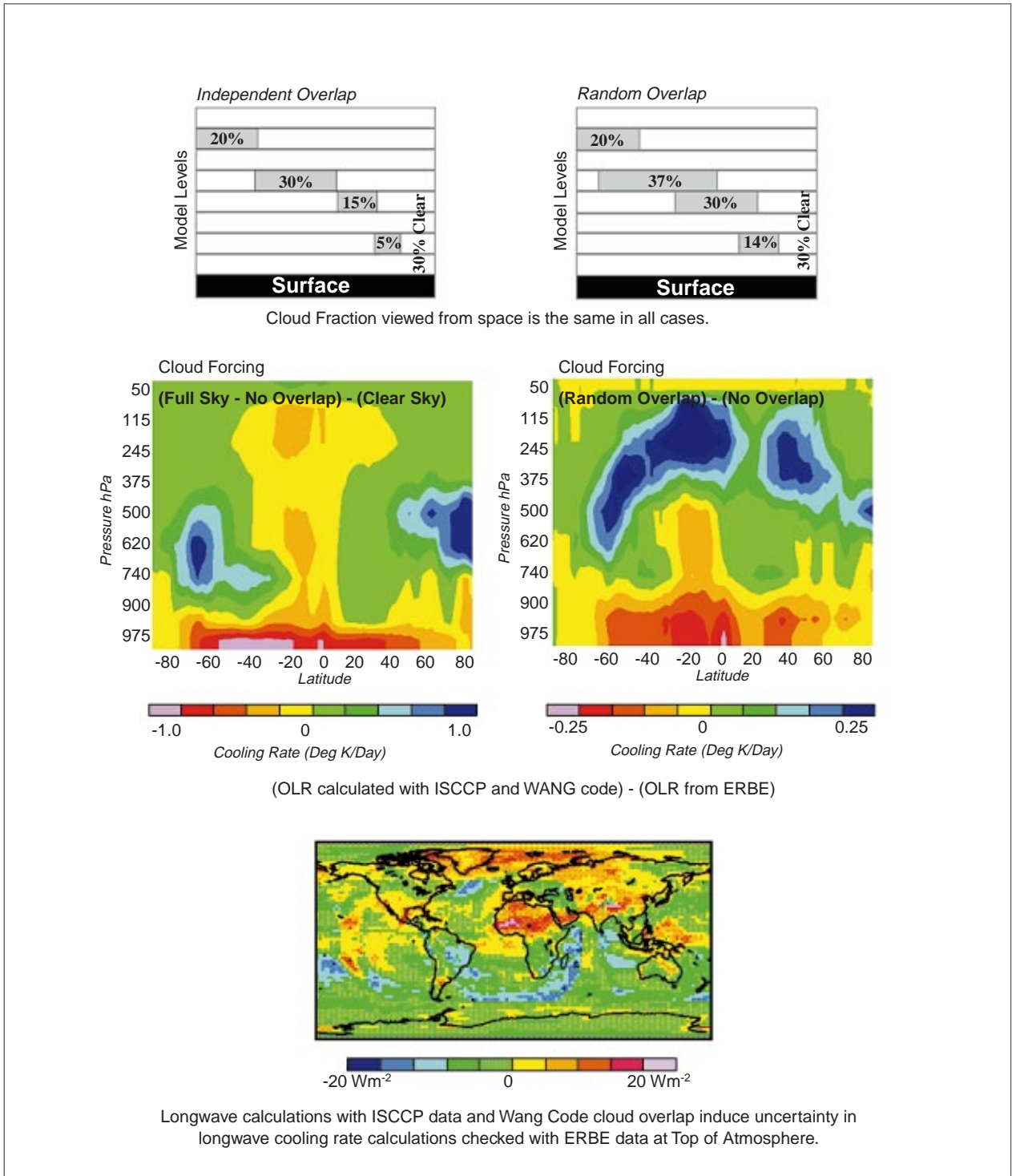
Active sensors have the best prospects for determining cloud geometry. Unfortunately, the sampling of the EOS Geoscience Laser Altimeter System (GLAS) lidar will be limited to nadir. GLAS can determine the geometrical thickness of optically thin clouds. The GLAS record of cloud top height will be a vital tool for evaluating the accuracy of cloud retrievals from passive sensors. A complete resolution of the problem posed by Figure 2.4 may require that a new type of instrument be flown on satellites, the Cloud Profiling Radar (CPR), which can detect the vertical distribution of cloud-size particles.

More-detailed plans for observing cloud properties are presented in Section 2.2.3.5.

2.2.2.5 Absorption, scattering, and emission by the Earth's surface

Table 2.2 shows that the surface absorbs about twice as much solar radiation as does the atmospheric column. Surface solar absorption is modulated by a surface solar albedo that ranges from 0.06 for diffuse radiation striking the ocean to approximately 0.90 for some of the freshest snow. Upward and downward LW fluxes at the surface are larger than any other radiative fluxes in the atmosphere, but their sum, the net LW flux, is generally not as large as surface SW net flux. Retrievals of surface fluxes by the

FIGURE 2.4



Effect of cloud overlap assumptions on longwave cooling in the atmosphere (Charlock and Rose 1994).

ongoing GEWEX Surface Radiation Budget (SRB) Project (Whitlock et al. 1995) are probably accurate to within 10-20 Wm^{-2} for a monthly average in the $280 \times 280\text{-km}^2$ equivalent-area grid boxes of ISCCP.

The SRB Project errors for SW and LW over snow and ice surfaces and for LW in persistently cloudy regions are larger than those in other regions. Both ERBE and ISCCP have difficulty distinguishing between low clouds and a snow-covered surface. Higher accuracy is needed from EOS to monitor secular trends in snow and ice albedo associated with global warming and to test this important feedback mechanism in GCMs; Groisman et al. (1994) describe a 10% decrease in the coverage of Northern Hemisphere seasonal snow during the past two decades. A similar problem is faced over sea ice; more-accurate surface radiation measurements are needed to develop models and monitor trends.

The surface albedo and radiative fluxes over snow-free land are not known to sufficient accuracy, either. Surface optical properties have been adequately determined with localized, in situ measurements in the First ISLSCP Field Experiment (FIFE) (e.g., Sellers and Hall 1992). The formation of the GEWEX Continental-Scale International Project (GCIP) is partly due to the fact that numerical weather prediction (NWP) is hampered by the limitations of parameterizations for surface hydrology, and one key to the improvement of the Soil-Vegetation-Atmosphere Transfer (SVAT) model or the Simple Biosphere (SiB) model systems is a more-accurate SRB. Over a typical land surface, the surface albedos retrieved by two satellite systems (using either different instruments or different algorithms) differ by a few percent. A change in land use or crop pattern would also induce a difference of a few percent; a change in regional climate can be forced by perturbing the surface albedo by the same magnitude. Until EOS determines the surface albedo of all land surfaces to greater accuracy, we cannot adequately quantify the radiative forcing to climate that is associated with changes in land use. The uncertainty to climate prediction posed by anthropogenic surface albedo forcing is anticipated to be regional. This problem will be best treated in tandem with the related issue of anthropogenic surface hydrological forcing (i.e., changes in evapotranspiration associated with land use; Shuttleworth and Dickinson 1989).

A more-accurate SRB is also needed for the development and validation of ocean modeling, wherein the surface energy budget is a key forcing to circulation (see also discussion in Chapter 3). The limiting factor on the SRB over the oceans provided by EOS will be due to downwelling LW over the extratropics, where downwelling LW from cloud bases is only slightly masked

by sub-cloud water vapor. The retrieval in EOS of downwelling LW over the oceans could be improved with a few ocean-based monitoring stations for SRB and cloud base height. If aerosol sun photometers were deployed at the same monitoring stations, EOS could validate retrievals of maritime aerosols. A satellite-based cloud radar would enable cloud base heights to be determined, which would greatly improve estimates of net longwave radiation at the surface.

The EOS AM-1 platform is well suited to provide a more-accurate SRB. The keys to implementation involve the deployment of field measurements before and after launch and integration of multiple EOS sensors. Present satellite-based retrievals of the SW SRB are limited by inadequacies in cloud screening (which will be handled by MODIS), quantification of aerosol optical properties (MODIS for scattering properties and MISR for absorbing and scattering properties), and specification of the directional characteristics of radiation throughout the spectrum (CERES and MISR). For monitoring secular trends, stable and broadband spectral coverage of an ERB sensor like CERES is essential. Climate is forced by broadband energy. Imager channels can be expected to change frequencies with time, so the monitoring of spectrally-dependent features like aerosol and surface scattering will not be fully consistent without an integration over the broadband. The retrieval of global land-surface radiation with MODIS, MISR, and CERES will be buttressed by ASTER, the space-borne "microscope," and by in situ monitoring of surface and atmospheric properties. ASTER will permit the reliable identification of a small subset of the global surface that is observed twice daily by MODIS and CERES at coarser resolution.

The surface information from the Pathfinder land program will prepare the research community to apply EOS data. (The EOS Program Office at NASA Headquarters has initiated the Pathfinder data set concept. Pathfinders provide access to large remote-sensing data sets applicable to global change research prior to the availability of data from the EOS satellites. Landsat data, held primarily by USGS/EDC, have been analyzed with support from NASA, EPA, and USGS.) The successful development of models for biospheric processes is dependent on an accurate specification of surface radiation parameters. Individually, the MODIS, MISR, CERES, and ASTER algorithms for surface remote sensing are on generally sound footing. The limited prelaunch exercises by each of the instrument teams have not, however, focused on the potential synergism of the instruments. A common focus of field programs on a very limited set of sites, preferably with continuous monitoring, would foster synergism. The same sites could serve for the validation

of EOS. The most obvious candidate is presently the ARM Southern Great Plains (SGP) site. Atmospheric measurement is thorough at the SGP site, especially during the ARM Intensive Observing Periods (IOPs), affording an excellent opportunity for space-based surface remote sensing. When the atmosphere is well characterized, it can be more reliably “subtracted.” The preparation and validation of EOS surface products would be advanced with in situ determinations of surface optical properties at the same sites. The in situ measurement of surface optical properties is the cornerstone of effective cooperation of EOS radiation programs with ARM and GCIP. Well-determined surface optics would provide a validation for the EOS remote sensing of the surface; the same surface optics provide ARM and GCIP with the means to “subtract” the surface and reliably specify the properties of the large fraction of the clouds that are optically thin. For the ASTER archive, a record at the ARM and the Baseline Surface Radiation Network (BSRN) sites is a must. A desert monitoring site is also suggested because of the unique optical properties of arid regions (i.e., nonblack surface LW emissivity); note the large discrepancy in Figure 2.4 between observed and calculated Outgoing Longwave Radiation (OLR) over the Sahara Desert, which is mostly cloudless.

2.2.2.6 Radiation in global climate models

The most general goal of the USGCRP is the development of global models for climate prediction. EOS will supply the global validation for the models, and theory indicates that radiation is the most critical component of the models and observations. The main radiative uncertainties are cloud feedback, water vapor feedback, direct and indirect forcing by anthropogenic aerosols, surface albedo feedback over land (snow and vegetation) and sea (sea ice), and anthropogenic surface albedo forcing (land use). Radiation and hydrology are closely linked through their shared dependence on water and energy cycles. Some of the main issues in the application of EOS to the task of improving the radiation in climate models can be highlighted by comparing a present model to satellite data. Focus will be placed on LW because it is less directional than SW and easier to both observe and calculate. In Figure 2.5, the OLR from the GEOS Data Assimilation System (Schubert et al. 1995; essentially a GCM run with analyzed meteorological data) is compared with ERBE data. The differences are huge, of opposite sign in the tropics and midlatitudes, and due mostly to cloud deficiencies. The right panel of Figure 2.5 compares a recalculation of OLR with the Wang et al. (1991) code using GEOS soundings but with observed ISCCP clouds.

While the OLR calculated with ISCCP is not perfect (note “rings” at the edge of coverage for the geostationary satellites used by ISCCP), the satellite clouds produce a more-accurate regional OLR than does the GCM. Many other models in the Atmospheric Model Intercomparison Project (AMIP) (Gates 1993) perform similarly to GEOS, when compared with satellite data. It should be noted that the GEOS fields of geopotential height, temperature, and wind compare very well with available observations. Therefore, a major challenge for EOS is to make models assimilate and predict cloud, water vapor, and radiation data as well as they currently do temperature, pressure, and wind data.

What about the modeled greenhouse effect inside the atmosphere? Figure 2.6 shows the difference between the LW heating rates in GEOS and those recalculated using the ISCCP clouds. To span the differences in the LW heating rate, scientists have been forced to use a span of 3.0 K day^{-1} (-1.5 to 1.5). In contrast, the mean LW heating rate (not shown) is approximately 2.0 K day^{-1} with a span of 4.0 K day^{-1} (-4 to 0). The probable error in the profile of the atmospheric greenhouse heating rates in the GCM has a span of 75% compared with the full range in the natural profile of the atmospheric greenhouse heating rates. GEOS does not use the Wang et al. (1991) code, but the differences due to the radiative transfer codes are fairly small. Most of the differences are due to clouds, and they greatly exceed estimates for error in the satellite clouds (i.e., nonoverlapping and randomly overlapping clouds in Figure 2.4).

There is clearly an important task in the application of EOS data to building better radiation simulations in climate models. In the comparison with the GEOS model and ERBE, better clouds are needed than in present models (Figure 2.5 and 2.6). Thought experiments (Figure 2.4) and comparisons with ERBE (the rings in the right panel of Figure 2.5) show that the clouds in present ISCCP observations need improvement, too. EOS PM-1 has a number of instruments to observe the state variables that generate clouds (AIRS, the Advanced Microwave Sounding Unit [AMSU], and the Humidity Sounder, Brazil [HSB]), cloud properties (MODIS and AMSR), and cloud-induced radiation (CERES). Implementing GCM radiation validation with EOS is straightforward: produce quality products from EOS AM-1 and EOS PM-1, get the data to the Distributed Active Archive Centers (DAACs), and have the IDS teams lead the way in utilizing the data in climate models. Fostering the development of better GCM parameterizations for radiation and cloudiness is an important mission of several EOS IDS investigations.

2.2.3 Role of convection and clouds in climate

Clouds have a strong effect on the radiative energy fluxes in the atmosphere. They scatter and absorb solar radiation, and absorb and emit terrestrial radiation, and these effects have a strong influence on the energy balances at the TOA, within the atmosphere, and at the surface. In addition, the vertical motions that are associated with clouds produce important convective transports of energy and moisture. The large-scale, mesoscale, and microscale interactions of clouds with the clear environment around them play a critical role in determining both the amount of water vapor that is retained in the clear atmosphere, and the amount of precipitation reaching the surface.

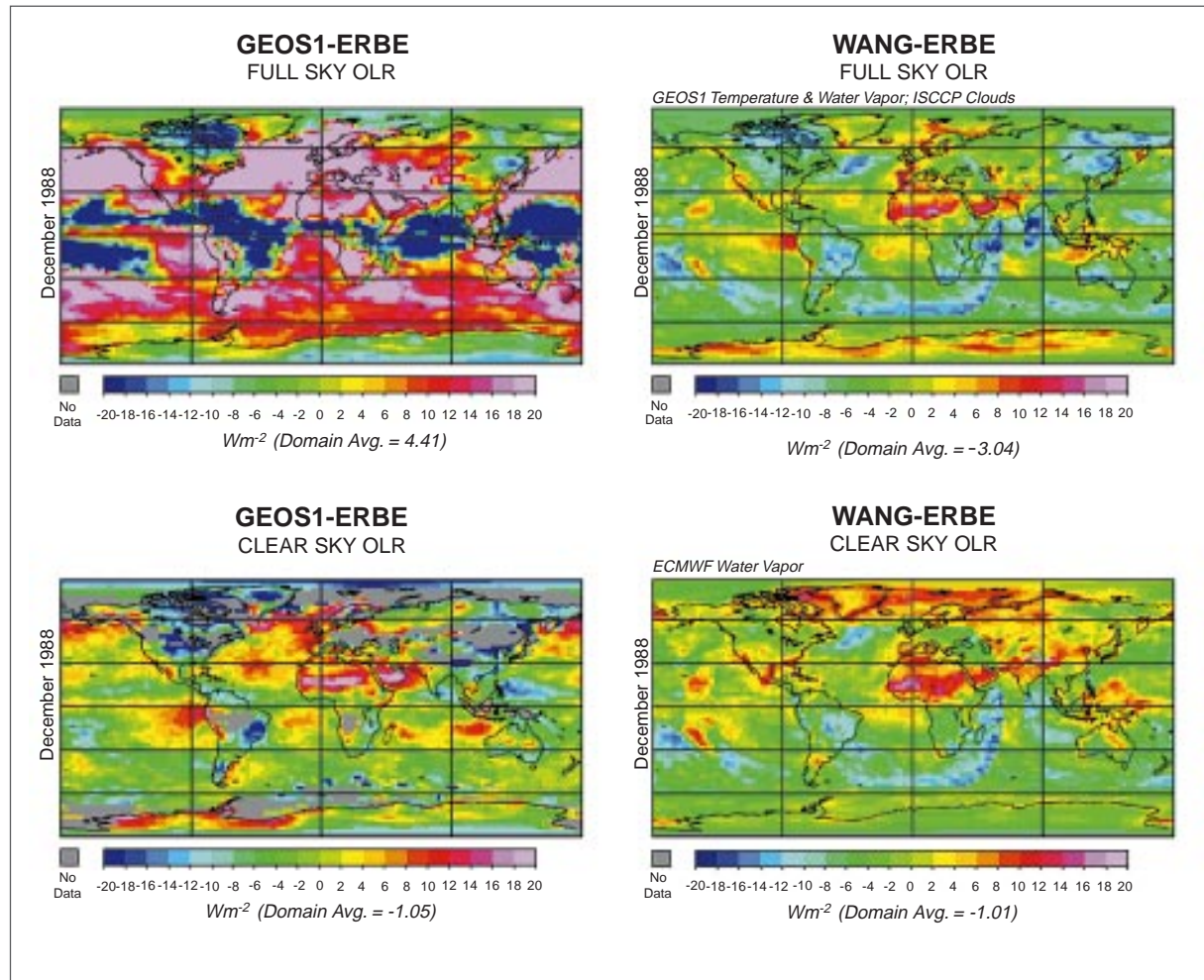
2.2.3.1 Cloud effects on the Earth's energy balance

The Earth's global radiation budget is illustrated in Figure 2.7 (pg. 59). Averaged over the globe and over a year,

about 340 Wm^{-2} of incident SW radiation is available from the sun. Of this, 30%, or about 100 Wm^{-2} , is reflected back to space, so that the climate system accepts 240 Wm^{-2} from the sun which, under equilibrium conditions, is equal to the LW emission to space by the climate system. The influence of clouds on the radiation balance of the Earth was estimated by ERBE (ERBE; Ramanathan et al. 1989; Harrison et al. 1990). These estimates revealed that if clouds were suddenly removed, and nothing else changed, the absorbed solar radiation would increase by about 50 Wm^{-2} and the emitted longwave radiation would increase by about 30 Wm^{-2} , yielding a net positive change in the energy balance of the Earth of about 20 Wm^{-2} (Table 2.3, pg. 59).

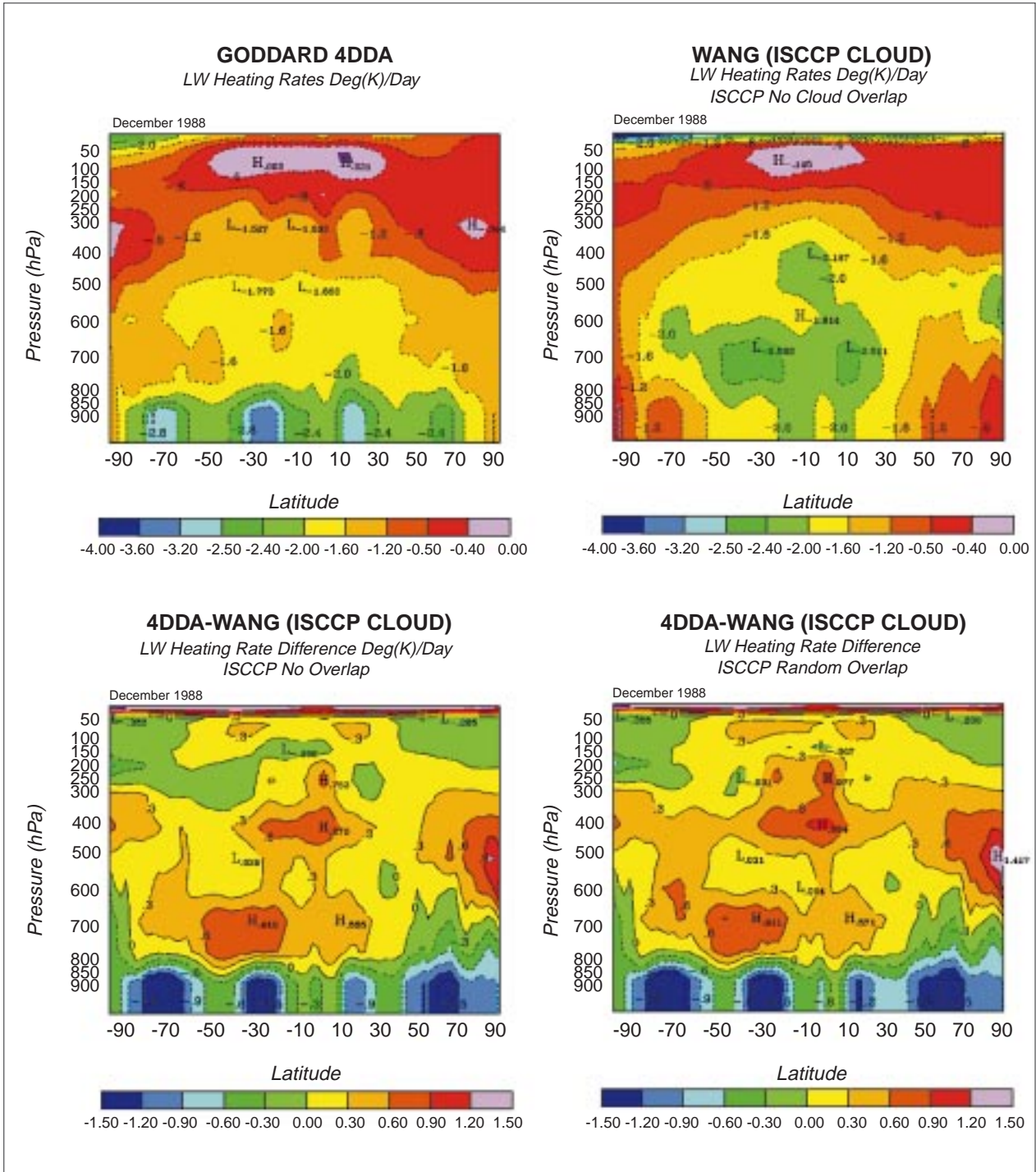
A convenient means of gauging the magnitude of a climate forcing such as that associated with the radiative effect of clouds is to compare it with the calculated

FIGURE 2.5



Comparison of outgoing longwave radiation in the GEOS data assimilation and in ERBE observations (Schubert et al. 1995; essentially a GCM run with analyzed meteorological data).

FIGURE 2.6



Comparison of longwave heating rates in the GEOS data assimilation product and estimates derived from ISCCP data (Charlock et al. 1994).

effect of a doubling of atmospheric CO₂. If the CO₂ concentration is instantaneously doubled, emission by the climate system is reduced by roughly 4 Wm⁻², or about 1.7% (Houghton et al. 1990), because of the increased greenhouse effect. This 4 Wm⁻² radiative imbalance would induce a time-dependent climate change, ultimately resulting in a new equilibrium climate. If it is simplistically assumed that climate change involves solely temperature changes, then the Earth would warm until radiative balance is achieved. That is, the LW emission must increase from 236 to 240 Wm⁻², which requires an increase in emission temperature of 1.2 K, or about 0.4% of its globally-averaged value of 288 K. Current GCMs produce a greater warming at the surface than this, but estimated warmings vary greatly from model to model, ranging from 1.7 to 5.4 K (Houghton et al. 1990). This disagreement stems from the different depictions of climate feedback mechanisms in GCMs that can either amplify or moderate the warming. For example, a warmer climate means a warmer troposphere that will contain more water vapor, which itself is a greenhouse gas. Thus water vapor provides a positive (amplifying) feedback mechanism. An intercomparison of 19 GCMs (Cess et al. 1990) showed the models to be in remarkable agreement regarding water-vapor feedback, though this does not guarantee that this assessment of the water-vapor feedback is correct (e.g., Lindzen 1990).

A common misconception is that because clouds cool the present climate, they will likewise act to moderate global warming. It is, however, the change in net cloud radiative forcing associated with a change in climate that governs cloud feedback. Cess et al. (1990) have shown that calculations of this cloud feedback vary widely from one global climate model to another, and that this feedback explains a substantial fraction of the variance in climate sensitivity in a sample of 19 global climate models.

2.2.3.2 *Cloud effects on the surface energy balance*

Since the clear atmosphere absorbs much of the same frequencies of solar radiation that are absorbed by clouds, the effect of clouds is a redistribution of solar heating in the atmosphere and, through the scattering of radiation by clouds, a reduction in absorbed solar radiation at the surface. Because the atmosphere is fairly opaque to terrestrial radiation, the reduction of emitted longwave radiation caused by clouds is felt mostly as reduced cooling of the atmosphere, except at high latitudes or altitudes where the water vapor content of the atmosphere is small. Therefore clouds represent a redistribution of energy between the surface and the atmosphere that may be larger

than the net effect of clouds on the energy balance measured at the top of the atmosphere. The convection with which clouds are associated is also of first-order importance in the exchange of heat between the surface and the atmosphere, so that more than radiation is involved in understanding the role of convection and clouds in the energy balance at the surface. The detailed physical and radiative properties of clouds are important, which in turn are related to the mechanisms that generate them and the environment in which they are found.

2.2.3.3 *Observations of cloud properties*

2.2.3.3.1 *Surface observations*

A nearly-global record of cloud observations by surface observers is available from surface weather observations (Warren et al. 1986, 1988). These data provide a longer record than that available from satellite observations, and also provide a wealth of information about the morphology of cloud systems observed over the Earth. The bottom-up view of surface observers is complementary to the top-down view from satellites. The cloud typing based on human visual observations of clouds provides valuable information on cloud genesis mechanisms and associated atmospheric structure. On the other hand, surface observations of clouds do not provide the quantitative information on radiative effects, drop size and phase, and cloud top structure that are recoverable from satellite-based observations.

Long records of surface observations of clouds show trends that may be related to corresponding decadal changes in sea surface temperature (SST). Long records of cloud observations can also be used in conjunction with upper-air observations from balloons to investigate the relationship of particular cloud types to atmospheric structure (e.g., Klein and Hartmann 1993b, Klein et al. 1995). Figure 2.8 (pg. 60) shows the trend in SST and low marine cloud amount for the period between 1952 and 1981 as determined from surface observations (Norris and Leovy 1994). Significant decadal trends over the oceans are observed in both SST and marine cloudiness. To evaluate the importance of such trends for climate requires detailed observations of cloud optical properties such as will be made available by EOS. To observe decadal changes such as these, an initial observing period of 15-18 years has been planned for EOS.

Observations of clouds by surface remote sensing and aircraft instrumentation are necessary to investigate mesoscale and microscale aspects of cloud development and interaction with the large-scale environment.

2.2.3.3.2 Satellite observations

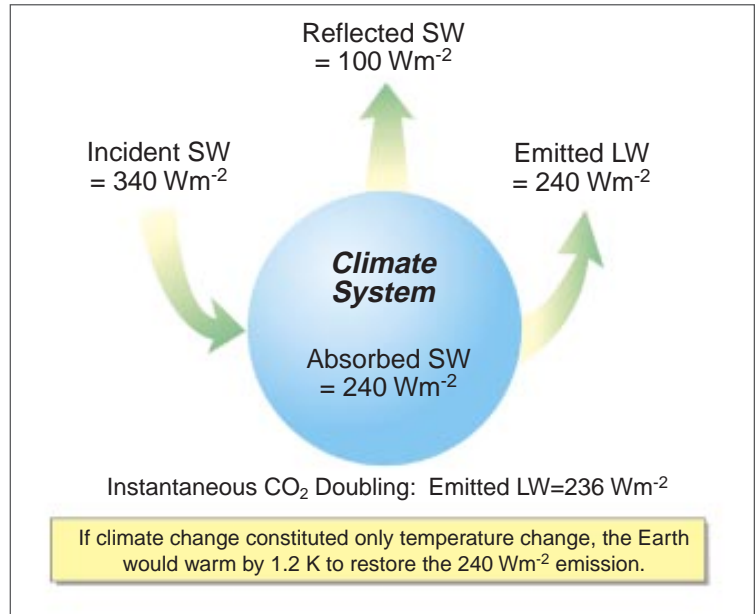
Satellites provide a means of developing global observations of cloud amounts and properties. The ISCCP attempts to take advantage of the visible and infrared information available from operational meteorological satellites to construct a climatology and time series of the abundance of clouds with optical depth and cloud top pressures paired into 35 categories, in three-hour intervals of time. These data are extremely valuable in characterizing global cloud coverage and type in a variety of other studies.

The greater spatial and spectral resolution from visible and infrared imagers that are part of the EOS program will allow clouds to be characterized from space more accurately and in greater detail. A key instrument in this regard is MODIS. MODIS offers spatial resolution as fine as 250 meters from some channels, which will reduce errors associated with partially-filled fields of view. MODIS will provide more-accurate, better-calibrated retrievals for cloud area, height, and optical thickness, and will further retrieve cloud particle size and phase, and estimate the cloud geometrical thickness (especially when combined with AMSR-E). MISR and EOSP will also contribute new information on cloud phase and particle size spectra. Distinguishing between cloud particle size and water amount contributions to cloud albedo is critical to monitoring and understanding key cloud forcing and feedback processes. The improvement in cloud sensing by EOS will be aided by the more-accurate EOS soundings of temperature and humidity from AIRS/AMSU/HSB.

2.2.3.4 Modeling of clouds in the climate system

The representation of clouds in climate models in a manner that accurately expresses their effect on climate and climate sensitivity is a critical goal of EOS. To this end

FIGURE 2.7



Schematic illustration of the Earth's radiative energy balance and how a doubling of atmospheric carbon dioxide would perturb that balance (Wielicki et al. 1995. Reproduced with permission from the American Meteorological Society).

EOS observations will be incorporated in the validation and testing of numerical models that simulate clouds. A substantial amount of work will be done within EOS IDS investigations, but the EOS data will be useful to the entire climate and cloud modeling community. Because of the large difference between the scales of individual cloud systems and the size of the Earth, cloud modeling is currently conducted on three scales. The first scale is that of the global climate model. While the whole planet is included, as it must be in a climate simulation and prediction, and the model may be integrated for 100 years or more, the grid points used to represent the climate are separated by a horizontal distance of about 100 km, and cloud processes must be represented implicitly through a so-called "parameterization." Cloud parameterizations in global models can be validated in two ways. In climate models the seasonal means and other statistics of cloud proper-

TABLE 2.3

	AVERAGE CONDITIONS	CLOUD-FREE CONDITIONS	CLOUD RADIATIVE FORCING
OLR	235	266	31
Absorbed Solar	239	288	-49
Net Radiation	4	22	-18

Global-annual-average conditions of top-of-atmosphere fluxes for average conditions, for clear-sky conditions, and cloud radiative forcing estimated from ERBE (Harrison et al. 1992). Units are Wm⁻².

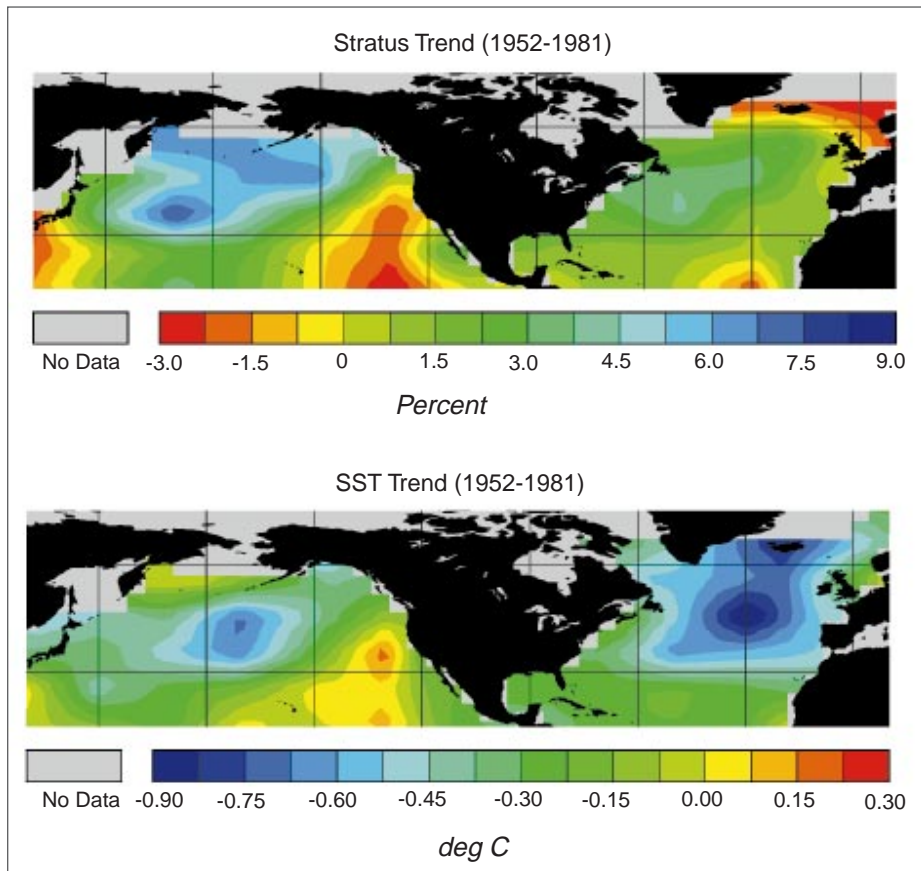
ties can be verified against similar statistics derived from observations. In weather forecast models, the day-to-day evolution of cloud properties can be verified against instantaneous observations. Both methods are useful and give different insights into the quality of the model simulation of clouds and water vapor. If a regional mesoscale model that represents only a part of the Earth is used, current computer technology will allow increasing the spatial resolution by a factor of 10 to about 10 km, but such models are normally run for no longer than a few weeks. A regional model can represent the mesoscale circulations that often develop in association with cloud systems, but the cloud-scale processes must still be parameterized. A cloud-resolving model requires a horizontal grid spacing of about 1 km or less, and only a small geographical region, perhaps incorporating only a single cloud, can be simulated with current computers. To make progress on the cloud problem, EOS investigations will pursue cloud modeling in each of these three categories: global, regional, and cloud-resolving models (Figure 2.9). EOS observations will provide data for validation on all of these horizontal scales, and for both instantaneous and

climatological comparisons. When EOS observations are coupled with in situ and ground-based observations and a rigorous program of numerical experimentation, the observations will offer the promise of a qualitative enhancement of our confidence in our ability to predict the role of clouds in global climate change, and thereby a refinement in our ability to predict future climate changes in response to natural and human influences. Numerical weather forecasting and seasonal and interannual forecasting will also benefit from this program of observation and research.

2.2.3.4.1 Global climate models—cloud parameterization and role in sensitivity

The history of prevailing opinion about the sensitivity of the Earth's climate to external perturbations roughly parallels that of developments in the parameterization of clouds in global climate models. The earliest GCMs assumed a fixed distribution of clouds and predicted modest equilibrium climate sensitivity. The advent of GCM cloud parameterizations resulted in generally higher estimates of sensitivity (Hansen et al. 1984; Washington and Meehl

FIGURE 2.8



Trends in SST and marine cloudiness (Adapted from Norris and Leovy 1994).

1984; Wetherald and Manabe 1986; Wilson and Mitchell 1987) for several reasons.

The most surprising result from these and later GCMs is the tendency of cloud cover to decrease with warming, especially low and middle clouds. To date, no theoretical basis for predicting the sign of cloud-cover feedback has emerged. This cloud-cover decrease, combined with the better-understood tendency of cloud height (and thus greenhouse effect) to increase with warming, caused the majority of GCMs from this period to predict net positive cloud feedback. Early parameterizations prescribed cloud optical properties, typically assuming decreasing albedo or optical thickness with increasing altitude. Increased cloud height then implies that column optical thickness decreases with warming, thus producing large positive cloud feedback.

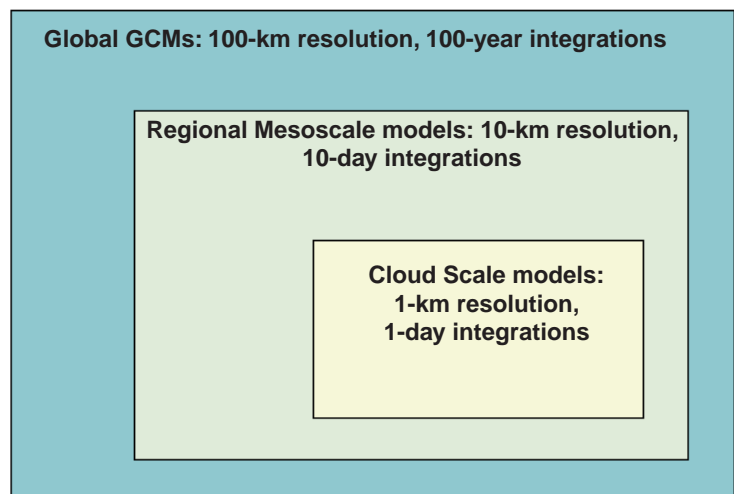
Radiative-convective models (Somerville and Remer 1984), based on observations of increasing cloud liquid water with temperature (Feigelson 1978), suggested that climate sensitivity might be halved if cloud optical thickness variations were taken into account. This has been incorporated diagnostically in some GCMs via a calculation of the adiabatic water content of a lifted cloud (Betts and Harshvardhan 1987) or the condensation required to remove supersaturation. An assumption about cloud particle effective radius is also needed. Since the albedo effect dominates the greenhouse effect of clouds globally, such models tend to produce negative cloud optics feedback and thus reduced sensitivity (cf., GCMs described in Appendices A and B of Cess et al. 1990).

The recent trend in GCMs has been to include cloud water as a prognostic variable, permitting fully interactive optical thickness calculations (Sundqvist 1978; Roeckner et al. 1987; Smith 1990; LeTreut and Li 1991; Tiedtke 1993; Fowler et al. 1996; Del Genio et al. 1996). This requires parameterization of a variety of poorly understood microphysical and small-scale dynamical processes (e.g., autoconversion, accretion, evaporation, Bergeron-Findeisen growth, cumulus detrainment, cloud top entrainment instability). Depending on how these details are represented, GCMs with prognostic parameterizations can produce either positive or negative cloud optics feedback. Uncertainties in the details of prognostic schemes, combined with the fact that some GCMs still prescribe optical properties or diagnose their temperature dependence, largely explain the persistent wide

range of GCM estimates of equilibrium climate sensitivity to a doubling of carbon dioxide (1.7-5.4 K). A critical goal of EOS is to incorporate more-detailed global observations of cloud liquid water and ice contents, cloud particle size, and the spatial and temporal distribution of cloud into a better understanding of how these properties depend on the climate, and to translate this into better models for climate predictions on a variety of time scales from weather forecasting to decadal climate change.

Climate sensitivity and cloud feedback depend on the nature of the climate change experiment that is performed. Prescribed uniform SST changes are a simple, inexpensive test of sensitivity (Cess et al. 1990). Recent intercomparisons of such experiments involving many GCMs indicate a significant convergence of results im-

FIGURE 2.9



Schematic diagram of the three types of models, including clouds.

plying small cloud feedback (Cess et al. 1996). But these simulations are not representative of an actual climate change, in which SST gradients can change because of regionally-varying climate forcing, changes in ocean circulation, etc. The same model can produce either small negative or large positive cloud feedbacks depending on the presence or absence of changes in SST gradients, because feedbacks are inherently regional and interactions with the dynamics affect climatic changes in cloud properties (Senior and Mitchell 1993; Del Genio et al. 1996).

Prognostic cloud parameterizations are of most interest to EOS, since they are laboratories for assessing which uncertain aspects of clouds should be focused on by future observational programs. Among the first-order questions faced by climate modelers are: What controls the detrainment of ice from cumulus updrafts into

mesoscale cirrus anvil clouds, and thus determines their shortwave reflectance? What causes the transition from nearly overcast marine stratus to scattered trade cumulus off the west coasts of continents in the subtropics, and is this indicative of a climate feedback mechanism? Why do satellite data suggest that low clouds generally get optically thinner with increasing temperature (Tselioudis et al. 1992)? Why do GCMs characteristically underpredict cloud forcing in the midlatitude storm tracks, thus compromising simulations of ocean heat transport (Gleckler et al. 1995)? What role do cloud interactions with sea ice play in determining the degree of polar amplification of climate warming? How large are the indirect effects of changes in tropospheric aerosols on cloud properties? How can small-scale cloud inhomogeneities be accounted for in relating grid-scale cloud water path to cloud albedo and emissivity? How can cloud cover be parameterized as a function of grid-scale climate parameters?

The cloud type that appears to exert the greatest effect on climate sensitivity in state-of-the-art GCMs is the tropical mesoscale anvil cloud that accompanies cumulus convection (Heymsfield and Donner 1990; Del Genio et al. 1996). The central question is how to represent the detrainment of ice from cumulus updrafts into anvil clouds. EOS observations can contribute to the answer in two ways:

- 1) By characterizing the microphysical and radiative properties of anvil clouds. CERES will provide the net radiative effect of anvils at the TOA. The liquid water path (LWP) of these clouds can be estimated by AMSR. Anvils are thought to be largely ice though, so microwave techniques for estimating ice water path from scattering at high frequencies must be pursued as a high priority by EOS. The scattering properties of ice clouds are not yet well defined; MISR will help constrain the phase function for anvil clouds while MODIS will estimate particle sizes and optical thicknesses. The same instruments will characterize these properties for the more ubiquitous and poorly understood thin cirrus that exist at all latitudes. Stratiform precipitation, the major water sink for anvils, will be measured by AMSR-E as well.
- 2) By relating anvil properties to convection strength. Direct measurements of vertical velocities are not possible, but the Lightning Imaging Sensor (LIS) lightning occurrence measurements will serve as an index of convection intensity, while AIRS temperature and moisture profiles will yield estimates of convective available potential energy.

Subtropical marine stratus and trade cumulus clouds are important to climate models not only as a source of cloud feedback but also as a key deficiency that causes climate drift in coupled ocean-atmosphere GCMs. A central question about these clouds is the reality of the ISCCP finding that the optical thickness of low clouds over ocean tends to decrease with temperature (Tselioudis et al. 1992). MODIS, with better than an order-of-magnitude higher resolution than ISCCP, should determine whether subpixel cloudiness variations contribute at all to this result. AMSR-E LWP data will provide corroborating information on larger spatial scales.

A related question for GCMs is how to translate grid-scale predicted cloud water content into cloud albedo, given small-scale inhomogeneities. The 250-m resolution of MODIS is sufficient to capture the most important scales of inhomogeneity (cf., Wielicki and Parker 1992), permitting optical thickness probability density functions to be characterized for different cloud types. This combined with MODIS particle-size estimates will help define parameterizations for albedo as a function of LWP.

Another particle-size issue is the poorly-defined indirect effects of aerosols on clouds, both the radiative effect of smaller droplets and the suppression of drizzle (Charlson et al. 1992). EOSP and MISR will define the tropospheric aerosol distribution, which can be combined with MODIS optical thickness and particle size to isolate the indirect radiative effect. In principle, AMSR can complement this by measuring drizzle rates for stratus, but current microwave algorithms are insensitive to light precipitation.

A key decision in GCMs is when to form liquid water vs. ice. Phase information is currently lacking on a global scale; field studies suggest that it is not simply temperature-dependent, but may be sensitive to cloud dynamics, age, etc. The altitude of transition from liquid to ice affects cloud feedback because of the different microphysical characteristics of liquid and ice (cf., Mitchell et al. 1989; Li and LeTreut 1992) and the unique physics of the mixed-phase region (Del Genio et al. 1996). EOSP is sensitive to cloud-top phase because of the different angular distributions of polarization of liquid and ice particles. MODIS can also discriminate phase via the different spectral dependences of liquid and ice absorption.

2.2.3.4.2 Regional mesoscale modeling of clouds

Many atmospheric circulations are organized on the mesoscale, which is defined as encompassing horizontal length scales of 20-200 km (Fujita 1984). An example of paramount importance for climate is mesoscale convective systems, which dominate weather over most of the

tropics and the summertime midwestern United States, throwing out cirrus anvils whose feedback on climate has been a subject of intense controversy (e.g., Ramanathan and Collins 1991; Wallace 1992; Fu et al. 1992; Hartmann and Michelsen 1993; Lau et al. 1994). Severe midlatitude cyclones, hurricanes, orographically-forced flow, fronts, and thermally-forced flows such as land/sea breezes are other examples of mesoscale organization. These circulations produce distinctive cloud features on the mesoscale. Ubiquitous cloud types such as boundary-layer stratocumulus and midlatitude cirrus clouds also show strong mesoscale patterning that affects the mean radiative impact of the cloud. Understanding the feedbacks between clouds, the associated mesoscale circulation patterns, and climate is a particularly challenging, important, and poorly-understood problem because of the range of length scales involved. Typically, processes inside the cloud involve circulations 1 km or less in size, and the mesoscale circulations evolve as part of atmospheric flow patterns thousands of kilometers across. Thus, our understanding of those aspects of the feedback between clouds and climate that are modulated by mesoscale processes is particularly rudimentary.

In the past decade, mesoscale models (MMs) have become a powerful tool for understanding and forecasting mesoscale atmospheric circulations. Examples of MMs widely used in this country include the National Center for Atmospheric Research (NCAR)/Pennsylvania State University (PSU) mesoscale model or MM5 (Grell et al. 1993) and the Colorado State University Regional Atmospheric Modeling System (RAMS). An MM is typically used to simulate a region 1000 km or more on a side with a horizontal resolution of 5–40 km and a vertical resolution of 1 km or less, and is typically used for time intervals of 24–72 hours. Usually, the boundary conditions for a simulation are taken from analyses generated by a larger-scale numerical model. Often, grid nesting is used to increase resolution in regions of particular interest or flow complexity. A mesoscale model typically includes a parameterization for cumulus convection. Other model physics may vary greatly in complexity depending on the model and the problem being investigated. For simulations of organized cumulus convection, models such as the MM5 and RAMS include cloud water and ice physics parameterizations similar to cumulus ensemble models (see below). A typical MM includes terrain-following coordinates and sophisticated land and ocean surface parameterizations. Recent MMs are nonhydrostatic and allow the user to embed a small region of particularly-fine mesh refinement as a cloud ensemble model.

Mesoscale models have very successfully simulated a variety of complex weather phenomena, including rapidly-deepening midlatitude cyclones, squall lines and their interaction with fronts, hurricanes, topographic damping, and trapped waves on inversions. Many of these phenomena depend on cloud processes, especially deep convection. The feedbacks can be quite subtle. Braun and Houze (1994) showed that improvements in the ice-physics parameterization of the MM5 made a substantial improvement to the longevity of a simulated squall line and completely changed its feedback on the large scale. Changes in the choice of cumulus parameterization can suppress the development of a hurricane. However, few studies have focused on applying MMs to the radiative impact of clouds or to the forecasting of cloud properties. In the coming decade, we foresee an exciting opportunity for using MMs to apply knowledge gained from small-scale models and observations of clouds to understand the climatically-important feedbacks between clouds and the larger-scale circulation systems in which they are embedded.

The increased use of MMs has particular promise in the following four areas:

1) *Tropical convection*

MMs have been successfully used to study severe midlatitude organized convection, which generally takes place in a highly conditionally-unstable environment in which a synoptic-scale weather system acts as a trigger to locally initiate convection. However, MMs have only just begun to be applied to the enormous regions of convection over the tropical west Pacific, over the ITCZs, and the monsoonal convection over the tropical land masses, even though this convection is predominantly organized on the mesoscale. Recent work done within an EOS IDS investigation has shown that the MM5 can simulate many important mesoscale features of tropical convection observed in the Tropical Ocean Global Atmosphere (TOGA)/Coupled Ocean-Atmosphere Response Experiment (COARE) experiment, such as the development of boundary-layer cold pools driven by convective downdrafts, the triggering of new convection at cold pool edges, and the degree of the localization of convection over the warmest water (Chen 1996). In the future, the optical properties of the modeled cirrus anvils will be compared with observations. MMs could be used in the future for climate-sensitivity studies, similar to cumulus ensemble models (CEMs) but using a larger domain, and for simulations of other parts of the tropics, such as the East Pacific and Central America, in which mesoscale

variability of convection can interact with mesoscale variability of surface characteristics and topography.

2) *Cirrus cloud evolution*

Cirrus cloud has a crucial radiative impact on the atmosphere, but it is perhaps the most difficult to model of all cloud types because it is very thin, its modeling is dependent on microphysical assumptions such as ice crystal size distribution, and because it is patchy, both due to the internal convective circulations that cause the cirrus fallstreaks often seen on a summer day (Houze 1993) and due to the large-scale circulations that maintain cirrus cloud. As part of NASA's First ISCCP Regional Experiment (FIRE) program, Cotton and coworkers (DeMott et al 1994; Harrington et al. 1995) have begun to forecast midlatitude cirrus cloud using the RAMS mesoscale model coupled to a sophisticated parameterization of cirrus microphysics, with moderate success. The evolution of tropical cirrus clouds, which start as anvils from Mesoscale Convective Systems (MCS), is of paramount importance to tropical-cloud climate interactions, but so far has not been investigated with an MM (DeMott et al. 1994; Harrington et al 1995).

3) *Midlatitude cyclonic cloud systems*

Persistent boundary-layer cloud over the summertime midlatitude oceans produces by far the strongest net cloud radiative forcing of any cloud type (e.g., Hartmann et al. 1992; Klein and Hartmann 1993b). However, both our observational and theoretical understanding of this cloud is rudimentary compared to subtropical stratocumulus cloud, which forms over cold upwelled water off the west coast of the major continents. The subtropical cloud forms in a relatively synoptically-steady regime of equatorward winds blowing from cold to warm water, in a region of strong mean subsidence. The midlatitude cloud forms in a much more synoptically-variable regime, making it much harder to interpret the observations. Mesoscale modeling of the boundary-layer evolution induced by passing synoptic-scale systems could help gain more insight into how this cloud is maintained.

4) *Boundary-layer fog and cloud prediction*

In coastal locations such as San Francisco or Los Angeles, the summertime weather is highly dependent on the inland penetration of air and cloud from the marine boundary layer. There is a strong diurnal cycle of cloud caused mainly by the strong daytime heating; the albedo of the cloud affects this heating cycle so that the clouds and circulations are strongly coupled. Ballard et al. (1991) used an MM for forecasting cloud and visibility on and near the coast of Scotland. A difficulty with such simula-

tions (and with mesoscale simulations of boundary-layer cloud in general) is the need to start with cloud in the initial conditions to achieve a realistic forecast, because cloud-topped boundary layers are typically strongly forced by cloud-top longwave radiative cooling (Lilly 1968). However, as representations of the interactions between boundary cloud, turbulence, and radiation in MMs improve, they should provide increased insight into both the weather and climate of coastal zones.

While mesoscale models have achieved popularity as a tool for understanding severe weather events, which often involve clouds and convection, their potential for understanding cloud-climate feedbacks still remains largely untapped. Aggressive pursuit of the above four areas should go a long way toward both using this potential and improving forecasts by better representation of cloud processes in mesoscale models. Such studies are being conducted with several EOS IDS investigations. The higher spatial resolution, new cloud variables, and greater accuracy of EOS cloud observations will enable better validation of regional cloud simulations.

2.2.3.4.3 Cloud-scale models

An important class of models that may emerge as a powerful tool for studies of the role of clouds on climate are the cloud-resolving models (also known as cumulus ensemble models [CEMs]). In CEMs cloud-scale dynamics are resolved based on nonhydrostatic governing equations. Subgrid-scale turbulence is included using higher-order closure schemes and latent heating is explicitly computed; therefore, no cumulus parameterization is required. In addition, the budgets of all three phases of water are explicitly computed by parameterized cloud microphysics. For example, the Goddard cumulus ensemble model (CEM) includes a parameterized Kessler-type-two-category scheme for cloud water and rain, and a three-category ice scheme for cloud ice, snow, and hail/graupel (cf., Tao and Soong 1986; Tao and Simpson 1993). The Goddard CEM also includes detailed shortwave and infrared radiation (cf., Chou 1991). CEMs have been used to study the mechanisms of cloud generation, microphysical processes in clouds, interactions and merging of cloud clusters, cloud-environment interactions and trace gas transport (Krueger 1988; Xu and Krueger 1991; Lipps and Hemler 1986). They have been used widely in simulations of convective processes in conjunction with major field experiments, i.e., PRE-STORM, EMEX, MONEX, TAMEX, and TOGA/COARE. Another very important application of CEMs is in the development of hybrid satellite retrieval algorithms for clouds, water vapor, precipitation, and related dynamical quantities such as the vertical profile of latent heating. For example, the Goddard

CEM is the centerpiece of the rainfall and latent heating profile retrieval algorithm for the Tropical Rainfall Measuring Mission (TRMM).

A typical CEM has a spatial resolution of 1-3 km and variable vertical resolution of 0.2-1 km, with finer resolution in the atmospheric boundary layer and coarser resolution in the upper troposphere or lower stratosphere above cloud top. Because of the large computational resources required, three-dimensional versions of CEMs are typically integrated for 24-36 hours over a domain of 500-km squares. For many applications, such as simulating line-type convection or organized mesoscale cloud clusters, two-dimensional versions of the CEMs with a larger domain are often used for economy of computation.

More recently, CEMs have been applied to the study of water and energy cycles within tropical clusters and climate cloud-radiative feedback processes (Lau et al. 1993; Held et al. 1993). Sui et al. (1993) used the Goddard cumulus ensemble model to study the water and energy cycles in tropical convection and their role in the climate system. They documented the importance of stratiform clouds in maintaining the moisture content of the tropical atmosphere. They found that the rate of conversion of ice-phase water into the vapor phase associated with the dissipation of upper-level cirrus clouds contributes to upper-tropospheric moisture about as much as moisture transport from deep convection. In the lower troposphere, the re-evaporation of rainwater and cloud water are the dominant sources of atmospheric moisture. These results will have important consequences regarding the role of stratiform clouds and water vapor in climate feedback processes. More recently, using cumulus ensemble models, Lau et al. (1994) have demonstrated that changes in cloudiness and related cloud radiative forcing are more sensitive to remote forcing due to the large-scale circulation than to the variation of local SST. CEMs have also been coupled to oceanic mixed-layer models to elucidate the mechanisms of diurnal variability of clouds and precipitation over the ocean.

Another potential application of CEMs in climate studies is the nesting of CEMs in MMs and in GCMs. One approach is to use the large-scale conditions generated by coarse resolution GCMs (typically $4^\circ \times 5^\circ$ or $2^\circ \times 2.5^\circ$ latitude-longitude) as a boundary condition to the CEMs. Alternatively, this may be achieved by double nesting between CEMs, MMs, and GCMs. Experimentation with one-way interaction, i.e., using larger models to force CEMs and MMs, has demonstrated some success in documenting the modification of regional convective processes due to climate changes such as deforestation. The nesting of models has the advantage of focusing computational resources only in the region of interest, thus saving un-

necessary calculation. However, the numerical treatment of interactions across the nesting boundaries can be a major problem. The challenge is to include the feedback from the cloud scale and mesoscale to the global-scale climate. Telescoping grids or polar rotations are viable alternatives, but these methods are only in early stages of development. Undoubtedly, the use of nested models will be important for understanding scale interaction between hydrologic systems and climate.

2.2.3.5 *Observational strategy for radiative fluxes and cloud properties*

Observations of net radiative energy fluxes at the top of the atmosphere have proven valuable in understanding the global energy balance, in determining horizontal energy transport by the ocean, and in defining the role of clouds in the energy balance of the Earth. Despite the scientific consensus that cloud-radiation effects strongly regulate ocean temperatures and climate, and despite the acknowledged inadequacy of current simulations of surface radiation by climate models, there currently is very little data on the global climatology of surface radiation fluxes. A global surface radiation climatology data set is a requirement for further advances in understanding the ocean-atmosphere interactions in the climate system, and for development and testing of more-realistic climate models. Efforts to produce such a climatology from satellite measurements are now underway (Li and Leighton 1993; Darnell et al. 1992; Gupta et al. 1992).

If the net radiative energy flux at the TOA is combined with the net radiative energy flux at the Earth's surface, the net atmospheric radiative cooling is obtained. The atmospheric radiative cooling is the net effect of infrared emission by the atmosphere, the absorption by the atmosphere of infrared radiation emitted by the Earth's surface, and the absorption by the atmosphere of solar radiation.

The vertical distribution of radiative cooling/heating inside the atmosphere is also very important. For example, simulations of the climatic effects of increasing carbon dioxide concentrations predict warming of the troposphere and cooling of the stratosphere (e.g., Cess et al. 1993), and there is some empirical evidence for such changes (Houghton et al. 1990). For this reason, measurements of the radiative energy flux at the tropopause are particularly important. Unfortunately, they are almost completely nonexistent. Additional resolution of the vertical structure of the radiative cooling would also be useful, particularly for the troposphere where cloud layers can produce very sharp local features.

In summary, following the TOA radiative flux, the next most valuable measurement would be of the surface

radiative flux, because of its importance for atmosphere-ocean and atmosphere-land interactions. After that, it would be best to obtain the radiative flux at the tropopause. Additional details of the radiative cooling profile within the troposphere would also be useful, but information at more than about 4-to-10 levels might be of marginal utility.

Radiative fluxes are the highest priority measurements necessary to understand the role of cloud feedback mechanisms in the climate system. Current global climate models cannot accurately model even the gross zonal mean seasonal changes in cloud radiative forcing, much less the desired regional effects. In order to improve simulations of cloud forcing and its effect on climate sensitivity, more-detailed measurements of cloud properties are needed to provide understanding and model validation. Wielicki et al. (1995) have suggested that measurements of the following cloud properties be developed to better understand cloud feedbacks and to validate their simulation in global climate models:

- *cloud LWP (or ice water path)*
- *cloud visible optical depth*
- *cloud particle size*
- *cloud particle phase/shape*
- *cloud fractional coverage*
- *cloud temperature/height*
- *cloud infrared emittance*

At least five of these cloud properties can vary independently (optical depth, size, phase, coverage, height). Since TOA SW and LW fluxes represent only two constraints, it must be concluded that GCM agreement with TOA SW and LW fluxes is a necessary, but not sufficient, condition to guarantee correct cloud physics and thereby correct cloud/climate feedback mechanisms.

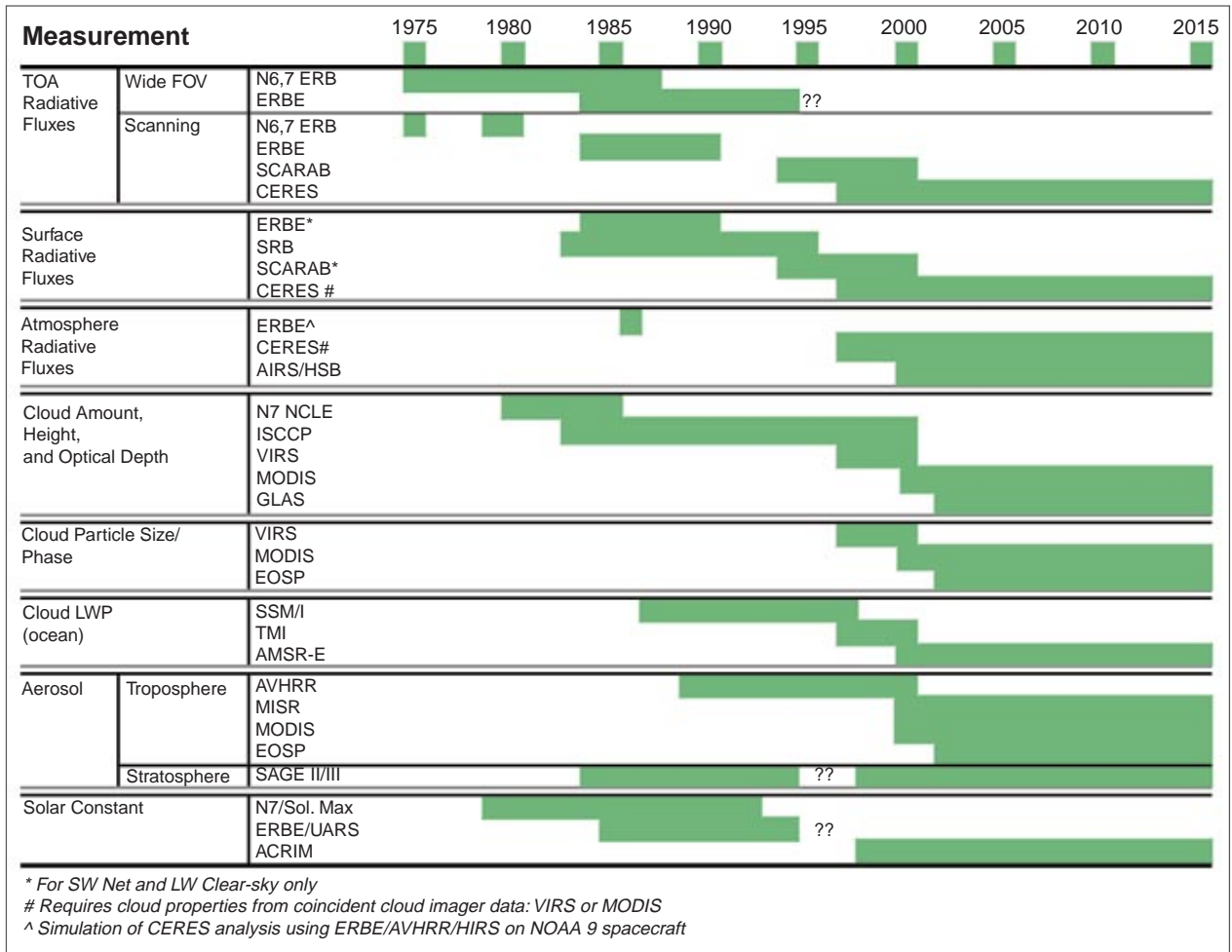
Figure 2.10 shows a timeline of satellite-based global radiation budget and cloud observations from 1975 to 2015. A major improvement in remote sensing capabilities began with the U.S./Japanese TRMM satellite in 1997 and continues with the NASA EOS AM-1 satellite as well as the ESA Environmental Satellite (ENVISAT) starting in 1998. An observational gap is already apparent for scanner-based radiation budget data from ERBE. Fortunately, the French/German/Russian Scanner for Radiation Budget (SCARAB) instrument was launched in December 1993 and should provide overlapping intercalibration with the ERBE nonscanners, which continue to operate. The first SCARAB instrument provided data for 1 year, and a second instrument will launch in 1997. EOS CERES (Wielicki et al. 1996) radiation budget measurements began with TRMM and continue with the EOS AM-1 and

PM-1 sun-synchronous orbits. The CERES measurements will improve the calibration, time sampling, and angular sampling over the earlier ERBE and SCARAB data sets. Cloud observations will be successively improved by VIRS in 1997, and later by MODIS, to be launched on the EOS AM-1 (1999) and PM-1 (2000) satellites. VIRS on TRMM adds improved calibration, spatial resolution (2 km IR), and cloud particle size information (1.6 μm channel) over the current AVHRR and geostationary cloud data sets, and will also provide diurnal sampling from its low-inclination orbit. MODIS adds improved detection of cirrus clouds (CO_2 slicing channels and 1.38- μm channel), improved resolution of boundary-layer cellular cloud fields (250-m-1-km spatial resolution), and improved cloud microphysics for both day and nighttime observations (1.6 and 2.1 μm , day, and 8.5 μm , night).

Table 2.4a summarizes the time and space sampling of the primary global and regional satellite observations for clouds and radiation in three time intervals: past/current, TRMM, and EOS. For the EOS-era observations, instruments are listed by spacecraft orbit. The first EOS AM-1 platform will be launched in 1999 in a sun-synchronous descending orbit at 10:30 a.m. The first EOS PM-1 platform will be launched in 2000 in a sun-synchronous ascending orbit at 1:30 p.m. These measurements are planned to provide a 15-year time series to allow studies of climate processes. The EOS orbits were chosen to optimize measurements of the diurnal cycle, surface land processes, and ocean biological processes. For the critical diurnal cycle of clouds and radiative fluxes, a third precessing orbit is provided by TRMM in 1997-2000, and potentially a TRMM follow-on mission beyond 2000. The ACRIM platform is planned for launch in 1999, the ICESat-1-GLAS platform in 2001, and the European Meteorological Operational Satellite (METOP) platform in 2002.

While Table 2.4a summarizes the major cloud and radiation satellite instruments, there are several instruments shown in Table 2.4b that provide critical supporting data. In general, these supporting instruments sacrifice time or space sampling capabilities in order to achieve additional special measurement capabilities. These capabilities can be used to test assumptions utilized in the global data sets. For example, pixel-beam filling issues and cloud inhomogeneity can be examined using the very-high-spatial-resolution Landsat-7 and ASTER data. Multiple-view-angle solar-reflectance data from Polarization and Directionality of the Earth's Reflectance (POLDER) and MISR can be used to test the assumptions of shortwave anisotropy and to examine non-plane-parallel radiative transfer effects of broken cloud fields. Medium Resolution Imaging Spectrometer

FIGURE 2.10



Timeline of the primary global and regional satellite observations for clouds and radiative properties (Wielicki et al. 1995, reproduced with permission from the American Meteorological Society).

(MERIS) and Global Imager (GLI) can provide an early independent method for the determination of daytime cloud height using oxygen A-band absorption of solar reflected radiation. Later observations by the GLAS lidar will provide a more-definitive test of cloud top height using active lidar for both day and night, and allowing better discrimination of multilayer cloud cases such as thin cirrus over low- or middle-level cloud. The Advanced Along Track Scanning Radiometer (AATSR) can test whether the determination of remotely-sensed cloud data is independent of viewing zenith angle. The EOSP measurements can provide an independent estimate of aerosols and cloud microphysics. While these tests do not replace the need for ground- and aircraft-based verification, they have the advantage of allowing tests over a complete range of global climate conditions. Field experiments give the most accurate and complete cloud and radiation data sets,

but for extremely limited time periods and climatic regions. Ultimately, the highest confidence is achieved only through a combination of field experiment data, special local high-resolution data, and global satellite data.

Improvements in global satellite observations of key climate parameters depend critically on two efforts. First, the derivation of advanced remote-sensing algorithms (often called inversion methods) is required to utilize the new measurements provided by EOS. Second, the new data must be rigorously validated against independent surface and aircraft in situ or remote-sensing observations. This section will summarize the state of the art in remote sensing of the key cloud and climate parameters discussed previously. This section will also identify problem areas critical to future advances in remote sensing, data analysis, and validation.

TABLE 2.4A

	<i>PAST AND CURRENT</i>	<i>TIME SPAN</i>	<i>CLOUD AND RADIATION</i>	<i>TIME SAMPLING (EQ. CROSSING, LT) OBSERVATIONS</i>	<i>MONTHLY AVERAGE GRID</i>	<i>NADIR FIELD OF VIEW (KM)</i>	<i>DATA SOURCE</i>
Pre-EOS	N7 ERB	1979-1990	SW, LW fluxes: top of atmosphere	1200	500 km	90; 1000	NSSDC
	N7 NCLE	1979-1990	Cloud amount, height	1200	500 km	8; 60	NSSDC
	HIRS	1989-1993	Cirrus height, emittance	0700, 1400	2.5°	20	NOAA
	ERBE	1984-1995+	SW, LW fluxes: top of atmosphere, cloud forcing	0700, 1400, Preprocessing	2.5°	40; 1000	LaRC V0 DAAC
	ISCCP	1983-1995+	Cloud amount, height, optical depth	Every 3 h	280 km	4-8	LaRC V0 DAAC
	SRB	1983-1995+	SW, LW fluxes: surface	Every 3 h	280 km	4-8	LaRC V0 DAAC
	SSM/I	1987-1995+	Cloud liquid water path (ocean only)	0630, 1630	1.0°	32-55	Wetnet
	SCARAB	1994-1997+	SW, LW fluxes: top of atmosphere	Preprocessing	2.5°	80	CNES/ France
TRMM (45°N-45°S)	CERES	1997-2000	SW, LW fluxes: top of atmosphere, surface,* in atmosphere*	Preprocessing	1.0°	10	LaRC V1 DAAC
	VIRS	1997-2000	Cloud amount, height, optical depth, particle size/phase	Preprocessing	1.0°	2	LaRC V1 DAAC
	TMI	1997-2000	Cloud liquid water path (ocean only)	Preprocessing	TBD	4.5-37	TBD

	<i>EOS (PLATFORM INSTRUMENT)</i>	<i>TIME SPAN</i>	<i>CLOUD AND RADIATION</i>	<i>TIME SAMPLING (EQ. CROSSING, LT) OBSERVATIONS</i>	<i>MONTHLY AVERAGE GRID</i>	<i>NADIR FIELD OF VIEW</i>	<i>DATA SOURCE</i>
EOS	AM-CERES	1999-2013	SW, LW fluxes: top of atmosphere, surface,* in atmosphere*	1030	1.0°	20	LaRC V1 DAAC
	AM-MODIS	1999-2013	Cloud amount, height, optical depth, particle size/phase	1030	5 km, 1.0°	0.25-1	GSFC, LaRC
	PM-CERES	2000-2015	SW,LW fluxes: top of atmosphere, surface,* in atmosphere*	1330	1.0°	20	LaRC V1 DAAC

TABLE 2.4A (CONT.)

EOS	<i>EOS (PLATFORM INSTRUMENT)</i>	<i>TIME SPAN</i>	<i>CLOUD AND RADIATION</i>	<i>TIME SAMPLING (EQ. CROSSING, LT) OBSERVATIONS</i>	<i>MONTHLY AVERAGE GRID</i>	<i>NADIR FIELD OF VIEW</i>	<i>DATA SOURCE</i>
	PM-MODIS	2000-2015	Cloud amount, height, optical depth, particle size/phase	1330	5 km, 1.0 °	0.25-1	GSFC, LaRC
	PM-AMSR#	2000-2015	Cloud liquid water path (ocean only)	1330-1030	TBD	10-20	TBD
	PM-AIRS/HSB	2000-2015	Temp/water vapor, cloud and surface emissivity	1330	TBD	15	JPL VI DAAC
	ACRIM	1999-2015	Solar constant	TBD	N/A	N/A	LaRC VI DAAC
	*Requires both CERES broadband scanner data and cloud imager data for within-atmosphere fluxes, and surface LW fluxes (cloudy). #Also planned for EUMETSAT METOP beginning in 2000 in a 1030 LT sun-synchronous orbit.						

Primary global and regional satellite observations of clouds and radiation in the pre-EOS and EOS era. Satellite data with 1/8 to 2-day coverage, and both day and night observations (Wielicki et al. 1995, used with permission from the American Meteorological Society).

TABLE 2.4B

<i>PLATFORM INSTRUMENT</i>	<i>TIME SPAN</i>	<i>CLOUD AND RADIATION OBSERVATIONS</i>	<i>SPECIAL CAPABILITIES</i>	<i>NADIR FIELD OF VIEW</i>	<i>SAMPLING LIMITATIONS</i>	<i>DATA SOURCE</i>
ADEOS 1: POLDER	1996-1999	Narrowband SW cloud anisotropy,	multiangle, polarization	day only, 50% duty	6 km	ESA
Landsat-7	1999-2002	Cloud properties at scales << 1 km	spatial resolution, calibration	1 per 16 days	15-120 m	EDC V1 DAAC
EOS AM: ASTER	1999-2003	Cloud properties at scales << 1 km	spatial, spectral resolution	1 per 48 days	15-90 m	EDC V1 DAAC
EOS AM: MISR	1999-2003	Aerosols, narrowband anisotropy, stereo cloud height	multiangle, calibration	1 per 9 days	200 m, 2 km	LaRC V1 DAAC
ENVISAT: AATSR	1998-2003	Dual-pathlength cloud properties	2-angle views	1 per 5 days	1 km	ESA
ENVISAT: MERIS	1998-2003	Oxygen A-band cloud height	oxygen A-band	day only	1 km	ESA
ADEOS II: AMSR	2000-2002	Cloud liquid water path	spatial resolution	oceans only	5-50 km	NASDA
ADEOS II: GLI	2000-2002	Cloud properties	oxygen A-band	no CO ₂ channels	250 m-1 km	NASDA
ICESat-1: GLAS	2001-2005	Lidar cloud and boundary layer height	active lidar	nadir only	70 m	GSFC V1 DAAC
EOS AM-2: EOSP	2003-2013	Aerosols, ice cloud microphysics	polarization, calibration	day only, large FOV	10 km	LaRC V1 DAAC

Supporting satellite observations of clouds and radiation in the EOS era. Satellite instruments with special capabilities but limited time sampling. Critical for global validation of primary data (Wielicki et al. 1995, used with permission from the American Meteorological Society).

2.2.3.5.1 TOA radiative fluxes

The measurement of TOA fluxes will enter its fourth generation with the CERES instruments on the TRMM (Simpson 1988) and EOS AM-1 and PM-1 spacecraft. The most recent ERBE measurements provide the standard of comparison for global radiation data sets. This success was gained through extensive pre-launch work with a science team to: a) oversee instrument design, development, and testing, b) design data products, and c) design analysis algorithms. A final key element was an integrated data management team to execute two versions of the data system before launch. This is the same overall strategy being used by the EOS project for the EOS data products.

Because there is no “ground truth” to test the accuracy of satellite TOA flux estimates, a comprehensive set of internal consistency checks is required to achieve high-quality data (Barkstrom et al. 1989). As a result of the extensive ERBE, Nimbus-3, and Nimbus-7 experience, there is a good understanding of the sources of error in determining TOA radiative fluxes.

In essence, the measurement of TOA fluxes is a 7-dimensional sampling problem: spectral (1), spatial (2), angular (3), and temporal (1). These sampling requirements lead to a measurement strategy with: a broadband instrument (spectral coverage) with crosstrack scanning (spatial coverage) plus a scanner that rotates in azimuth (angular sampling) and six observations per day from two sun-synchronous polar orbiters and one medium-inclination orbiter to sample diurnal variations (spatial, temporal, and angular sampling). Error estimates for such a sampling strategy are developed in Wielicki et al. (1995), and are much better than previously achieved. Overall, the CERES measurement errors are expected to be a factor of 2 to 4 lower than ERBE errors. The improvements are expected from three major sources:

- 1) Factor of 2 improvement in instrument calibration by using more-accurate ground and on-board calibration sources.
- 2) Factors of 2-4 improvement in angular sampling errors by the use of the rotating azimuth plane CERES scanner to fully sample angular space, combined with the use of advanced cloud imagers (VIRS, MODIS) to identify anisotropic targets as a function of cloud and surface properties.
- 3) Factor of 2-3 improvement in time-sampling errors by the use of a three-satellite sampling system and the use of improved shortwave models of the dependence

of scene albedo on varying solar zenith angles throughout the day.

2.2.3.5.2 Surface radiative fluxes

Global satellite estimates of radiative fluxes at the surface (up, down, and net) are now becoming available (Darnell et al. 1992; Li and Leighton 1993). In general, the intervening atmosphere complicates the measurement when compared to the more-straightforward derivation of TOA fluxes. A major advantage, however, is the ability to test satellite-based surface flux estimates directly against surface-based measurements such as those currently provided by the Global Energy Balance Archive (GEBA; Ohmura and Gilgen 1991; Li et al. 1995) and in the future by the BSRN (World Climate Research Program [WCRP] 1991) now being established around the globe. As a result of this ability, two independent approaches are desirable for determining surface radiative fluxes:

- 1) Calculation of surface fluxes using observed cloud and atmosphere parameters, with measured TOA broadband fluxes acting as a constraint on the radiative calculation.
- 2) Parameterized relationships between simultaneously-observed TOA fluxes (or radiances) and surface fluxes. Typically, the form of the parameterization is based on a radiative transfer model, but the final coefficients used are determined by comparisons against actual surface flux observations.

Work is progressing on both of these approaches.

Initial global surface radiation budget estimates of SW up, down, and net fluxes use ISCCP narrowband radiances, along with a narrowband-to-broadband transformation (Darnell et al. 1992; Pinker and Laszlo 1992). Verification against GEBA data and FIRE field experiment data indicates a monthly average of 2.5° regional mean insolation accuracies of about 20 Wm⁻² (1σ). While this is not as accurate as estimates of TOA fluxes using ERBE data, most of this discrepancy appears to be caused by spatial mismatching of the scales of observations of the satellite (250 km) and surface (30 km) observations, so that actual rms errors may be closer to 5-10 Wm⁻² (Li et al. 1995). In the time frame of the EOS observations, calculated SW surface flux accuracies should increase greatly as more-accurate cloud (VIRS, MODIS), atmospheric (AIRS), and surface properties (MISR, MODIS) become available, and as simultaneous

broadband measurements of TOA fluxes are available to constrain the model calculations, including implicit corrections for 3-D radiative transfer effects. The MISR measurements of bidirectional reflectance of vegetation canopies will provide improved separation of net surface SW flux into upwelling and downwelling components.

The second approach to SW flux estimation is to make use of a direct linear relationship between net SW flux at the top of the atmosphere and net SW flux at the surface (Cess et al. 1991; Li et al. 1993). This relationship is derived theoretically and verified against surface observations as a function of solar zenith angle. The rationale for this method (Davies et al. 1984) is that water vapor absorption and absorption by liquid water and ice occur in the same portion of the spectrum. To first order, then, placing a cloud in the atmosphere simply changes the vertical distribution of solar absorption, but not the total amount. The dependence of absorption on solar zenith angle can be understood as a change in path length. Because cloud particles reflect a significant amount of radiation even at absorbing wavelengths, however, and because reflection depends on particle size and shape, there are still questions about accuracy as a function of cloud type and height. The key to improvements in the empirical algorithm is to obtain more-extensive surface-observed net SW fluxes for validation as a function of varying cloud conditions and climate regimes. FIRE, the ARM program, and BSRN observations will be key to increasing the accuracy and confidence in this empirical approach.

The situation for LW surface fluxes is more complex and difficult, at least for the downward LW flux at the surface. Calibration of surface LW flux pyrgeometer measurements is still undergoing study, and downward flux radiative computations are dominated by low-level water vapor and cloud-base altitude (Gupta 1989; Gupta et al. 1992)—two of the more-difficult measurements to obtain from space. For clear-sky conditions, encouraging progress has been made in developing direct relationships between surface and TOA LW fluxes (Inamdar and Ramanathan 1994; Stephens et al. 1994). In the EOS time frame, improved lower-tropospheric water vapor will be available globally from the AIRS/HSB instruments and over land from MODIS (Kaufman and Gao 1992). Tests are under way using FIRE observations to examine methods to relate satellite measurements of cloud temperature and optical depth to estimated cloud geometrical thickness (Minnis et al. 1990, 1992). Recent sensitivity studies using ISCCP cloud data indicate that cloud overlap may in fact be the largest uncertainty for calculations of downward longwave flux at the surface (Charlock et al. 1994).

Methods to identify multiple cloud layers using satellite data have only recently begun, however, and a great deal of additional work is needed in this area. Two approaches appear promising. For optically-thin high clouds, infrared sounding channels can isolate the high cloud, while visible and infrared window channels are used for the low-level cloud (Baum et al. 1992). For optically-thick high clouds, a combination of optical measurements for the upper (ice) cloud and microwave measurements for the low (water) cloud may help define cloud overlap. In the long term, active systems such as the GLAS lidar for optically-thin cloud and a 94-GHz cloud radar for optically-thick cloud offer the best solution (WCRP 1994).

For surface LW emission, additional work is still required to improve models of land emissivity and directional thermal emission from vegetation canopies (Li and Becker 1993; Sellers and Hall 1992; Slingo and Webb 1992).

2.2.3.5.3 Radiative fluxes within the atmosphere

Determination of profiles of atmospheric radiative fluxes is necessary to estimate radiative heating rates within the atmosphere. Clearly, the most accurate measurement of radiative heating rate will be for the total atmospheric column. The total column heating rate can simply be determined from the difference between the TOA and surface radiative fluxes.

A second level of complexity is the determination of radiative heating rates within the atmosphere. Even for aircraft observations, this is an exceedingly difficult measurement, primarily because of the large spatial and temporal variability of cloud fields. Estimates from space will necessarily be a combination of observed atmospheric properties (temperature, water vapor, aerosols, clouds) used as input to radiative transfer calculations. One of the primary concerns is the accuracy of these radiative models, but an advantage available during the EOS period will be the use of broadband TOA flux observations to constrain the model solution. For example, if SW TOA fluxes calculated for a cloud field disagree with TOA measurements, then the satellite-derived cloud optical depth could be adjusted to get agreement. In this case, the error in both the satellite optical depth estimate and the radiative calculations could be caused by the use of a 1-D radiative transfer model for a 3-D cumulus cloud field. Since the TOA flux measurement can use CERES-measured anisotropic models appropriate for a 3-D cumulus cloud field, the TOA conversion of SW radiance to flux can in fact include the typical 3-D radiative properties of the cloud field, and thereby remove most of the bias in the radiative flux calculations of the effect of the cloud

within the atmosphere. The bias is removed by adjusting the cloud optical depth to one which would give a 1-D equivalent albedo. In this way, the radiative flux profile within the atmosphere will be consistent with TOA observations, and the cloud optical depth estimation can be corrected for first-order 3-D effects as well.

A second possible constraint on radiative fluxes within the atmosphere is the use of satellite-estimated surface radiative fluxes. If direct relationships between TOA and surface-observed radiative fluxes prove to be a more-accurate estimate of surface fluxes than radiative calculations using satellite-observed atmosphere and cloud properties, then the satellite-estimated surface flux estimates can be used as an additional constraint on the calculated radiative fluxes within the atmosphere. The use of the TOA and surface flux constraints would be weighted by the estimated accuracy of each radiative flux component. In this case, TOA fluxes would probably provide a stricter constraint than surface fluxes. Note that, if using radiative modeling proves more accurate in estimating surface radiative fluxes, then the only observational constraint is the TOA flux.

Even with TOA flux constraints, however, the ability to remotely sense cloud thickness, or cloud overlap, is subject to serious question. As a result, the initial strategy for EOS is to phase in progressively-more-advanced estimates of in-atmosphere radiative fluxes, as indicated in the following list:

- *At launch + 6 months:* TOA, surface, tropopause, 2-5 stratospheric levels
- *At launch + 24 months:* Add 500-hPa level
- *At launch + 36 months:* Add 4-12 tropospheric levels, as validation warrants

One of the elements for testing within-atmosphere flux calculations is likely to be the use of remotely-piloted aircraft currently under development, which are capable of gathering statistics over very long flight legs with accurately stacked flight tracks; ARM began test flights in spring 1994. The remote-sensing challenges for within-atmosphere fluxes are similar to those for downward LW flux at the surface: profiles of water vapor, cloud thickness, and cloud overlap.

2.2.3.5.4 Cloud properties

The remote sensing of cloud properties from space is complicated greatly by the rapid changes of clouds in both space and time. To further complicate matters, their radiative properties are a strong function of viewing angle and solar geometry. Where the remote sensing of TOA

fluxes was a 7-dimensional sampling problem, cloud properties add a vertical dimension for a total of 8.

Nevertheless, a great deal of progress has been made in recent years, especially through the work of ISCCP and FIRE. Overall lessons learned include:

- Cloud analysis can often be separated into cloud detection, followed by cloud property determination.
- Lack of accurate calibration of narrowband imaging radiometers remains a major stumbling block in climate work.
- No single cloud algorithm or portion of the spectrum (i.e., solar, infrared, microwave) can handle the diversity of cloud physical properties needed for the cloud/radiation problem.
- Significant improvements in cloud retrievals are still possible with current satellite data, including new estimates of cloud particle size.
- The next jump in quality should be provided by MODIS, the first instrument whose design specifically includes cloud property determination as a requirement.
- Validation of cloud physical properties requires not only tests against field observations, but also consistency between independent satellite methods. For example, very-high-spatial-resolution ASTER data are needed to answer questions about inadequate beam filling within the larger MODIS or VIRS pixels; multi-angle MISR data are needed to provide stereo cloud height confirmation, and confirmation of 3-D cloud radiative effects on retrieved cloud radiative properties; and EOSP measurements are needed to provide independent estimates using polarization of cloud particles, especially for ice particle clouds.
- The final step in cloud remote sensing will be the combination of passive and active remote sensors. EOS will begin this step with MODIS, AMSR-E, and GLAS (active lidar). Ultimately, a 94-GHz radar will also be required. It is clear that active remote sensors will require multiple spectral bands, just like the passive radiometers.

2.2.3.5.4.1 Cloud fraction

The problem of determining cloud fraction has typically been treated as either one of cloud detection (Rossow et

al. 1985) or energy balance (Coakley and Bretherton 1982; Minnis and Harrison 1984a-c; Stowe et al. 1988). Other methods include the use of spectral signatures or spatial textures (Stowe et al. 1991; Saunders and Kriebel 1988).

A cloud-detection method typically defines a threshold reflectance (solar wavelengths) or brightness temperature (thermal infrared) to distinguish between satellite measurement pixels containing clear-sky or cloudy-sky conditions. The major problem with this approach is how to handle partially cloud-filled pixels (i.e., the “beam-filling” problem).

An energy-balance cloud fraction measurement is based on the assumption that many, if not most, of the pixels may be partially cloud-filled. These methods use an estimate of a typical cloud reflectance (Minnis and Harrison 1984a-c; Stowe et al. 1988) or a typical cloud brightness temperature (Coakley and Bretherton 1982) to allow cloud fraction in each pixel to be linearly related to the reflectance or brightness temperature in each pixel.

Wielicki and Parker (1992) showed results of using 30-m-spatial-resolution Landsat data to test the performance of the ISCCP-determined cloud fraction on the spatial resolution of the data. Two things were found to occur. As expected, when the spatial resolution degrades, the beam-filling problem increases cloud fraction, especially for boundary-layer clouds. But unexpectedly, at full resolution, the ISCCP bispectral thresholds underestimate cloud fraction because they miss a significant amount of optically-thin cloud below the threshold. The net effect is a combination of a tendency to underestimate the optically-thin cloud and to overestimate the broken optically-thicker cloud. These results indicate that, for EOS, the 250-m channels on MODIS will greatly reduce the problem of beam-filling, but that further work will be required for the detection of optically-thin cloud.

Several advances in the EOS era that will give key improvements in cloud fraction measurements are:

- higher spatial resolution;
- additional near-infrared channels for thin cloud detection, especially the 1.38- μm channel added for detection of optically thin cirrus (Gao et al. 1992); and
- additional thermal infrared channels (3.7, 8.5, 13.3, 13.6, 13.9 μm) to allow improved detection of optically-thin cloud at night.

A second major concern is the variation of derived cloud fraction, as obtained by ISCCP and other studies as a function of viewing zenith angle (Minnis 1989). This

needs further study using multi-angle MISR and POLDER data for solar-channel cloud detection and the Along Track Scanning Radiometer-1 (ATSR-1) for the thermal infrared detection.

The third major concern is cloud detection in polar regions. In these regions, recourse is often made to a combination of spectral and textural measures to improve cloud detection (Ebert 1987; Welch et al. 1992; Yamanouchi et al. 1987).

2.2.3.5.4.2 Cloud height

The measurement of cloud height has typically been accomplished by one of three different methods:

- set measured brightness temperature equal to cloud top temperature assuming a black cloud (Stowe et al. 1988);
- use 15- μm infrared sounding channels to estimate the pressure level in the atmosphere at which the cloud is radiating (Smith and Woolf 1976; Chahine 1974); or
- use the solar reflectance measurement to estimate visible cloud optical depth (and thereby infer an infrared emittance) and then correct the estimate of cloud temperature if the cloud has emittance less than unity (Rossow et al. 1985).

Additionally, the spatial coherence method (Coakley and Bretherton 1982) has the ability to uniquely distinguish cloud fields with well-defined layers, as exhibited by small spatial variability in the cloud thermal infrared window emission. Several problems with these methods have recently been documented by FIRE:

- Even boundary-layer clouds are often nonblack (Wielicki and Parker 1992; Luo et al. 1994).
- Infrared sounder methods work well for upper-level clouds, but poorly for low-level clouds (Wielicki and Coakley 1981; Wylie and Menzel 1989).
- The ISCCP visible optical depth calculations have traditionally assumed water clouds, a poor assumption for cirrus (Minnis et al. 1990; Wielicki et al. 1990).
- In the presence of boundary-layer inversions over the ocean, conversion of cloud temperature to cloud height can cause large errors (Minnis et al. 1992).

These problems suggest that algorithms must be varied with varying cloud types. For boundary-layer stratus, spatial coherence will work best. For cirrus without lower-level cloud, the ISCCP method using hexagonal ice crystals (Minnis et al. 1990) is sufficient; for cirrus over low-level stratus, the infrared sounder methods work best. For large-scale storm systems, any of the methods should give accurate results.

The largest remaining problems are multi-level cloud situations (almost half of all cloud cases according to surface observations; Hahn et al. 1982; Tian and Curry 1989), and cumulus or altocumulus fields. Key improvements for these cases will come from the increased spectral resolution of MODIS as well as the increased spatial resolution to minimize beam-filling problems in interpreting thermal infrared channel observations. Recent studies have shown progress in cases of cirrus over stratus by using infrared sounder data to determine the upper cloud level, and multispectral thermal infrared window channel data using spatial coherence methods to determine the low cloud (Baum et al. 1994). Key validation data will come from surface lidar and radar, field experiments, and the spaceborne GLAS lidar and MISR stereo cloud-height capabilities. The most difficult area to validate will remain multi-level cloud, especially if both layers are optically thick in the visible and thermal infrared. In this case, the only validation tool will be the use of millimeter wavelength radar (WCRP 1994).

2.2.3.5.4.3 *Cloud visible optical depth and thermal infrared emittance*

The first global satellite estimates of visible cloud optical depth were provided recently by ISCCP. The methodology used was to calculate the expected visible reflectance for a water cloud of 10- μm spheres as a function of surface reflectance, solar zenith angle, and satellite viewing angle using a 1-D multiple scattering radiative transfer model (Rossow et al. 1991). A look-up table then converted reflectance into visible optical depth. The range of optical depths which can be measured is typically between about 0.5 and 100, limited by cloud detection limits on the lower end and lack of further sensitivity on the upper end. FIRE and other validation studies showed that there are three major difficulties with the present data:

- Most of the year-to-year variability in the ISCCP global cloud optical depth is caused by varying calibration of the visible radiometers (Klein and Hartmann 1993a). Improved calibration is critical.

- Nonspherical ice particle scattering differs greatly from the assumed 10- μm spheres, causing an overestimate of ice cloud optical depths (Minnis et al. 1990). The ISCCP data will soon be reprocessed using improved hexagonal crystal scattering for cold clouds (Takano and Liou 1989).
- The cloud-filled-pixel assumption causes substantial underestimates of cloud optical depth for cumulus fields, even when cloud amounts are correct or too small (Harshvardhan et al. 1994).

All of the above concerns should be greatly alleviated by the improved calibration and spatial resolution offered by the VIRS and MODIS instruments in the EOS era. An unresolved problem, however, is whether a 1-D radiative transfer model can be applied to inherently 3-D cloud structures such as cumulus. For boundary-layer clouds over ocean, new evidence implies that the relatively small aspect ratio (v/h) and optical depths of broken cloudiness cause errors due to the 1-D assumption being relatively small for domain-averaged values (Cahalan et al. 1994; Wielicki and Parker 1992; Duda and Stephens 1994). For cumuli over land, however, the larger aspect ratios and larger optical depths require re-examination of this result. In addition, initial observations of non-plane-parallel cirrus clouds during FIRE showed mixed results (Stackhouse and Stephens 1991). One of the key verifications of the importance of 3-D effects is the test for consistency in derived optical depth as a function of satellite viewing angle. POLDER and MISR data will provide key tests of this assumption on a global basis. Regional field experiment data will allow tests using in-cloud measurements combined with fully 3-D radiative transfer models. If 3-D effects are found to be critical, further studies of the remote sensing of cloud field horizontal structure will be required (e.g., Zhu et al. 1992). Continuing work will also be required to understand the effects of ice cloud particle shape and size on satellite-inferred optical depths.

Thermal infrared emittance is related to visible optical depth through cloud particle size and phase. For nighttime observations, estimates are typically made using either infrared sounder data (Smith and Woolf 1976; Chahine 1974) for upper-level clouds, or multiple thermal infrared window channels with varying response to cloud particle size (Luo et al. 1994) for lower-level clouds. Classically, the infrared sounder measurement is actually considered to be ϵA_c , or emittance times cloud fraction. Recent studies indicate, however, that for cirrus clouds, partially cloud-covered fields of view are not a problem for pixel sizes less than about 8 km (Wielicki and Parker

1992). In this case, the MODIS 1-km resolution infrared sounder channels should be able to unambiguously measure infrared cirrus emittance. Multispectral methods for low-cloud emittance need further validation by field experiments, although they appear promising.

2.2.3.5.4.4 *Cloud particle size*

A great deal of progress has been made recently in the remote sensing of cloud particle size. Two approaches have been examined initially; one using solar reflectance channels, and the other using thermal infrared channels. Both approaches make use of the large variation in the imaginary part of the refractive index for water and ice as a function of wavelength. For example, the imaginary part of the refractive index of water varies from about 10^{-8} at $0.6 \mu\text{m}$ to 10^{-4} at $1.6 \mu\text{m}$, 10^{-3} at $3.7 \mu\text{m}$, and 10^{-1} at $11 \mu\text{m}$. The origins of these approaches date back to Blau et al. (1966), Hansen and Pollack (1970), and Arking and Childs (1985).

Daytime methods use the visible channel to determine cloud optical depth, plus absorbing channels to estimate cloud particle size. In essence, the visible channel estimates the average number of scattering events per reflected photon, while the absorbing channel determines the absorption per scattering event, which is a function of particle size. The first global estimate of low-cloud water droplet size has recently been produced using the AVHRR 0.6-, 3.7-, and 11- μm channels (Han et al. 1994). In addition, aircraft radiometers and Landsat observations have been used in FIRE field experiments to show that for water clouds over ocean, the determination of effective droplet radius using visible, 1.6-, and 2.1- μm channels tracks changes measured by aircraft in situ data with possible offsets of about 30%. The discrepancy has recently been ascribed to either water vapor continuum absorption in the 1.6- and 2.1- μm region bands (Stephens and Tsay 1990; Nakajima et al. 1991), or to problems with the Forward Scattering Spectrometer Probe (FSSP) typically used to measure cloud droplet size distribution from aircraft. Further validation of the 3.7- μm methodology is required using aircraft observations. For both daytime methods, solutions become multivalued for very small particles (less than $5 \mu\text{m}$) and small optical depths (Nakajima and King 1990; Han et al. 1994). The primary uncertainties in these methodologies would appear to be inaccuracies in handling water vapor absorption in the window channels and in handling the horizontal and vertical inhomogeneities of clouds (Coakley and Davies 1986). The majority of work has been done for water clouds, but initial work on ice clouds has also begun (Wielicki et al. 1990; Stone et al. 1990). The major problem for ice clouds is the uncer-

tain scattering and absorption properties of nonspherical particles. Extensive further theoretical and observational work is needed for ice clouds. In particular, advances in aircraft probes are needed to routinely measure the number of small ice crystals and to measure the scattering phase functions of ice crystals.

Purely infrared methods to infer particle size have evolved more recently (Prabhakara et al. 1988; Ackerman et al. 1990; Luo et al. 1994). These methods rely on the variation in cloud emittance caused by varying particle size. Their primary advantage is the ability to provide night-time observations. Whereas the reflectance methods have greatest sensitivity to particle size at relatively-large optical depths, the thermal infrared methods are most sensitive for optically-thin clouds with optical depths of 1-2. Using the currently available 3.7-, 11-, and 12- μm data, the thermal infrared retrievals are limited, due to the strong ice and water absorption at these wavelengths, to an effective radius of about $30 \mu\text{m}$. Validation against field experiment data is just beginning for these new methods.

The increased number of spectral channels available on the VIRS and MODIS instruments will allow substantial improvements in cloud particle remote sensing. Key advances are the availability of global 1.6- and 2.1- μm channel data during the day and a new 8.5- μm infrared window channel at night. In the future over ocean regions, water cloud particle sizes should be verified independently by combining the microwave-measured LWP using TRMM Microwave Imager (TMI) data on TRMM and AMSR data on EOS PM-1 and METOP, and the VIRS- or MODIS-derived cloud optical depth using $r_e = 1.5LWP/\tau_c$ (Stephens 1978). A second independent verification can be obtained by using the polarization measurements of POLDER and EOSP, especially for nonspherical particles.

2.2.3.5.4.5 *Cloud liquid/ice water path*

Passive microwave radiometers on the Nimbus-7 Scanning Multifrequency Microwave Radiometer (SMMR) and the Defense Meteorological Satellite Program (DMSP) Special Sensor Microwave/Imager (SSM/I) platforms have demonstrated the ability to observe cloud LWP over ocean backgrounds (Greenwald et al. 1993). Over land, however, these methods are not applicable because of the large variability of surface emission at microwave frequencies. The primary difficulty in this measurement is caused by beam filling for the 10-30-km footprints typical of these measurements. For EOS, the AMSR-E field of view is about a factor of 2 smaller than is available with the current SSM/I data, thereby eliminating some of

the beam-filling concern. For applications where only a grid-box average LWP is required, beam filling is not a concern. Error analyses and verification against surface-based LWP measurements indicate instantaneous accuracies of about 25% for the current SSM/I instrument, with much smaller bias errors for monthly average data (Greenwald et al. 1993).

Over land, LWP estimates will have to be provided using VIRS or MODIS estimates of cloud optical depth and effective droplet radius, using the relation discussed in the previous section. Uncertainties will be larger than for ocean cases, but the magnitudes will require further analysis of FIRE and ASTEX data.

Currently, there is no method to infer ice water path (IWP) using passive microwave observations. Initial estimates of IWP for EOS will be obtained using VIRS- and MODIS-derived cloud optical depth and effective particle size. The key problem here will be lack of a good ground truth source for IWP and the greater uncertainties caused by nonspherical geometry for ice crystals. The nonspherical particles will cause increased errors in both optical depth (uncertain scattering phase function) and effective particle size (uncertain phase function and single scattering albedo), as discussed in previous sections. Much further work is needed in this area, both to provide improved new observational techniques and to gain improved information from current and planned observations. In this regard, the polarization information provided by POLDER or EOSP may provide key information for distinguishing ice particle habits. The most promising technique for remote sensing of IWP and particle size is the use of high-frequency passive microwave at 300-to-650 GHz (Evans and Stephens 1995a, b).

2.2.3.5.4.6 *Cloud mesoscale organization and structure*

The high cloudiness and precipitation in the tropics are dominated by mesoscale convective systems (MCS) (sometimes called “cloud clusters”). MCS occur in a highly-discrete intermittent manner. They have time and space scales much less than those of the large-scale circulation of the tropics. The mean cloudiness derived from satellite imagery, long-period rain accumulations at tropical locations, and the total latent heating of the tropical atmosphere are the net results of these sporadic and small-scale cloud phenomena.

The size spectrum of tropical MCS tends toward being lognormal. A small number of very large MCS account for a large portion of the total high cloudiness and rainfall. If an infrared temperature of 208 K is used to define “high cloud top,” then roughly one-fourth of the area covered by high cloud is accounted for by MCS in

the size ranges $< 7,000 \text{ km}^2$, $7,000\text{-}30,000 \text{ km}^2$, $30,000\text{-}90,000 \text{ km}^2$, and $>90,000 \text{ km}^2$ (Mapes and Houze 1993; Chen et al. 1995).

The cloud dynamical and microphysical processes within an MCS determine the amount of upper-level cloud and precipitation that are generated by the MCS. These processes vary across the size spectrum of MCS. The smallest MCS are dominated by convective processes. The larger develop broad regions of stratiform precipitation, and the large upper-level cloud shields delineating the large MCS are primarily associated with stratiform processes.

The convective and stratiform processes lead to different vertical profiles of latent heating, and they generate different types of ice particles in the upper-level cloud shields (Houze 1982, 1989, 1993). The large-scale tropical atmosphere responds differently to these different profiles of heating (Hartmann et al. 1984; Mapes and Houze 1995).

To understand the physical chain of events involved in the interaction of deep convective cloud systems and the large-scale circulation and climate over the tropical ocean, it is necessary to understand how the MCS in different parts of the size spectrum of the MCS contribute to the production of upper-level cloud and to latent heating. To do this, the individual MCS comprising the spectrum must be identified as must the regions of stratiform and convective precipitation within the MCS.

The EOS MODIS data (high-resolution infrared channel) can be used to identify the individual elements of the MCS spectrum by previously-developed methods (Williams and Houze 1987; Mapes and Houze 1993; Chen et al. 1996). The EOS AMSR-E data (especially the passive microwave channels at 90 and 36.5 GHz) will identify the precipitation within an MCS identified in the MODIS infrared (IR) data. This analysis will identify the regions where latent heat is being imparted to the atmosphere. The AMSR-E data will further indicate the locations of the convective and stratiform regions. This can be done approximately by using an appropriately-calibrated passive microwave threshold separating the higher-intensity convective rain from the lighter stratiform rain. The EOS data set will thus provide global analyses of the location and sizes of an individual MCS and how each member of the overall size spectrum of an MCS contributes to latent heating of the large-scale tropical atmosphere.

2.2.4 *Water vapor and climate*

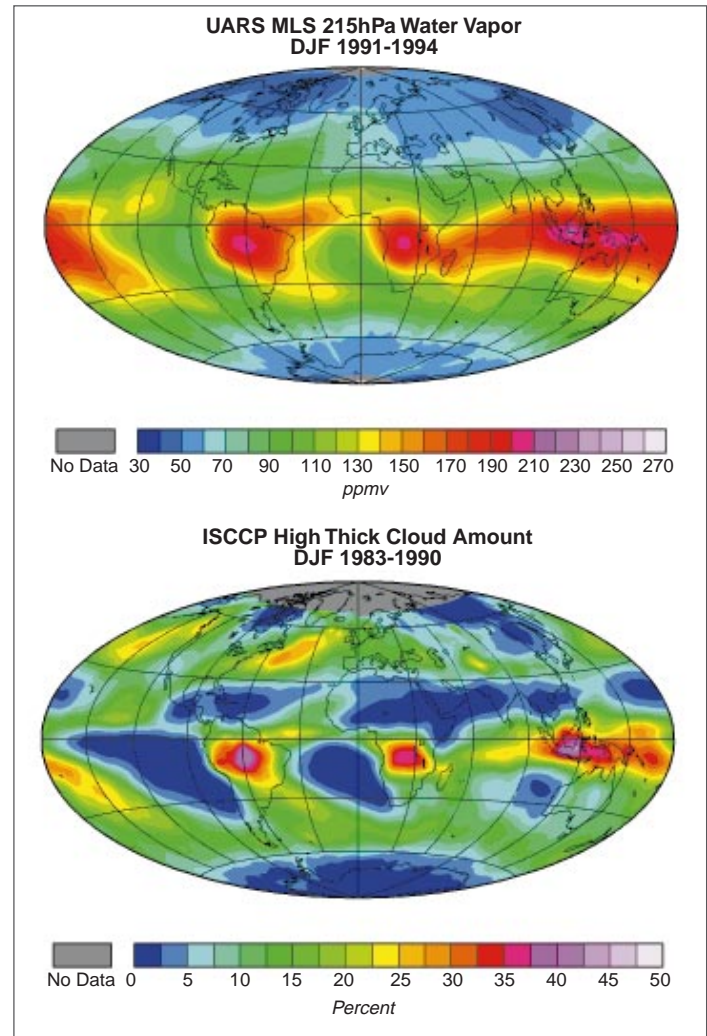
Most of the water in the atmosphere is in the form of vapor, and water vapor plays a critical role in many key processes in the hydrologic and energy cycles. Water va-

por is the most important greenhouse gas, both in terms of its role in maintaining the current climate and in terms of its role in sensitivity through the water vapor feedback process. The supply of moisture for precipitation and runoff in land areas is by lateral transport of water vapor in the atmosphere. River flow from land to ocean must be balanced by an equivalent transport of water vapor from ocean areas to land areas. The abundance and vertical distribution of water vapor in the atmosphere interact very strongly with convection and cloudiness, thereby influencing the albedo of the planet as well as the infrared opacity of the atmosphere.

2.2.4.1 Water vapor feedback and climate sensitivity

Because water vapor is the primary greenhouse gas in the Earth's atmosphere and the saturation vapor pressure increases exponentially with temperature, the abundance of water vapor in the atmosphere can provide a very strong positive feedback to climate change. The strong positive feedback associated with an assumption of fixed relative humidity was studied in early one-dimensional climate models (Manabe and Wetherald 1967), and its importance has been confirmed by succeeding observational (e.g., Raval and Ramanathan 1989) and modeling studies (e.g., Cess et al. 1990). The assumption of fixed relative humidity in climate sensitivity calculations has been challenged by Lindzen (1990), who called attention to the uncertainties associated with the detrainment of water from cumulus clouds and the associated distribution of water vapor in the middle and upper troposphere. He reasoned that warming in the equatorial region induces stronger and deeper cumulus convection, which would detrain at lower temperatures, and lead to drying in the upper troposphere. Betts (1990) argued that air in the convective regions detrains not only in the upper troposphere, but over a wide region between 150 and 550 mb where a significant fraction of the detrained water is in the form of ice from thick anvil ice clouds that dissipate and leave behind large amounts of water vapor, implying that a more-humid middle and upper troposphere could result from a warmer climate, i.e., a positive water vapor-temperature feedback.

FIGURE 2.11



Top panel shows the 215 hPa MLS water vapor climatology for December-February that uses measurements made from 1991-1993 binned into $4^\circ \times 4^\circ$ latitude/longitude boxes. The bottom panel shows the December-February 1983-1990 ISCCP fractional high thick (altitude above 440 hPa and visible optical depth greater than 9.38) cloud cover climatology map (Read et al.).

Water vapor abundance near the ocean surface is most closely linked to the saturation vapor pressure at the surface temperature, and in the upper troposphere is more strongly controlled by mesoscale and large-scale transport processes. The greenhouse effect is about equally sensitive to the relative humidity of the lower and upper troposphere. Climate models indicate that the net feedback is about equally sensitive to variations in the vertical structure of water vapor and temperature (Sinha 1995), and there may be some degree of cancellation between water vapor and lapse rate changes that occur in global climate models (Zhang et al. 1994). For the above rea-

sons it is critically important to understand the vertical distribution of water vapor in the atmosphere, its horizontal variation around the globe, and the processes that maintain this global water vapor distribution.

2.2.4.2 *Water vapor distribution and variability*

Until recently our knowledge of the global water vapor distribution derived primarily from global weather analyses based mostly on radiosonde observations. In the last few years these global analyses have begun to take better advantage of the water vapor information available from conventional polar-orbiting meteorological sounders. In addition, several attempts to make self-consistent water vapor data sets based on satellite sounding data have been initiated, including the TIROS Operational Vertical Sounder (TOVS) Pathfinder project under EOS. Other useful data sets include those derived from geosynchronous satellites that afford high temporal and spatial resolution to follow the influence of MCS on water vapor (Soden and Bretherton 1993; Udelhofen and Hartmann 1995), and high-vertical-resolution observations of water vapor in the upper troposphere from limb-scanning instruments such as the Stratospheric Aerosol and Gas Experiment (SAGE) (Rind et al. 1993) and MLS (Read et al. 1995). Wu et al. (1993) and Bates et al. (1996) also developed an intercalibrated satellite upper tropospheric water vapor data set using the High-Resolution Infrared Radiation Sounder (HIRS) on National Oceanic and Atmospheric Administration (NOAA) polar-orbiting satellites. Figure 2.11 (from Read et al. 1995) shows the strong association between humidity at 200 mb and deep convective cloudiness. These satellite observations provide homogeneous sampled observations of precipitable water and water vapor for the lower, middle, and upper troposphere and stratosphere. The typical accuracy is 20% for specific humidity and 10% for relative humidity. These accuracies are good enough to study the global water vapor climatology and seasonal variation, marginally good enough to study the large-scale features of interannual variation, but not adequate to study the long-term trends of water vapor and water-vapor processes.

Water vapor varies rather smoothly with longitude but decreases rapidly poleward. The annual mean value of the column-integrated water vapor, or total precipitable water, ranges by a factor of 10-20 from $\approx 50 \text{ kg m}^{-2}$ in the equatorial region to $< 5 \text{ kg m}^{-2}$ in the Arctic and to $< 2.5 \text{ kg m}^{-2}$ in the Antarctic (Peixoto and Oort 1992). Longitudinally, the total precipitable water varies by a factor of < 3 and is affected by land-ocean distribution and monsoon circulations. In the equatorial region, the most humid regions are located in the Congo basin, the

Brazilian basin, and the Indonesian region, where the trade winds bring in large amounts of water vapor to support strong convection. At higher latitudes, water vapor is generally more abundant over ocean than over land. Since most of the ocean is in the Southern Hemisphere, the longitudinal distribution of the total precipitable water is smoother in the Southern Hemisphere than in the Northern Hemisphere.

The specific humidity decreases nearly exponentially with height. This is because temperature decreases nearly linearly with height and saturation vapor pressure is an exponential function of temperature. The vertical distribution of specific humidity ranges over several orders of magnitude. More than 50% of the water vapor is contained in the region below the 850-mb level, while more than 90% is confined in the region below the 500-mb level (Peixoto and Oort 1992). The relative humidity also decreases with height. Minimum relative humidity is found in the subtropical regions and land-locked desert regions.

Data from EOS instruments will improve the quality of global measurements of the water vapor distribution. In particular, the combination of AIRS, AMSU, and HSB will provide more-precise simultaneous measurements of temperature and humidity in the troposphere, with better vertical resolution than is currently available. Vertical resolution is particularly important because climate feedbacks are sensitive to the vertical distribution of water vapor and temperature. Also, the vertical structure gives information about the mechanisms that maintain the water vapor distribution. Limb-scanning instruments such as MLS, SAGE III, and HIRDLS will measure the vertical water vapor profiles from middle troposphere to stratosphere with 200-km horizontal and 1-km vertical resolution. They will provide improved vertical resolution in the upper troposphere, and, because it is a microwave sensor, MLS will not be affected by the presence of cirrus clouds in this region. Together with more-accurate observations of thin cirrus clouds, these data can provide critical information on the effects of convection and cirrus clouds on upper-troposphere and lower-stratosphere water vapor.

2.2.4.3 *Maintenance of the global water vapor distribution*

2.2.4.3.1 *Role of convection and clouds*

The source of water vapor is evaporation from the surface. The climate system is in balance to first order, so that the globally-averaged precipitation rate is approximately equal to the evaporation rate. Precipitation occurs

primarily in association with convection and clouds, so that convection and clouds are the sink regions for water vapor in the atmosphere. If one thinks of the vertical distribution of water vapor, however, convection carries water from the lower to the upper troposphere, so that as far as the atmosphere above the planetary boundary layer is concerned, convection is a source of water vapor. This is especially true in the tropics, where large-scale motions mostly dry the troposphere by subsidence, and convection is the only major source of upper-tropospheric water vapor. The mechanisms whereby convection humidifies the upper troposphere have not been well quantified, and the changes in the relative efficiency of the drying and moistening mechanisms for the upper troposphere that would occur in association with a global climate warming are not known at all. These changes may have a profound effect on climate sensitivity and need to be understood.

EOS spaceborne measurements will provide accurate high-spatial-resolution measurements of water vapor and temperature profiles, together with cloud properties such as cloud-top height, visible optical depth, and mean cloud-particle radius. Instruments such as AIRS/AMSU/HSB, MODIS, MISR, EOSP, and GLAS may provide measurements of thin cirrus occurrence with very good height information for cirrus that are too thin to be detected by passive means. These data, combined with wind estimates from data assimilation and in situ measurements from carefully-designed field programs, will provide a much better understanding of the mechanisms whereby the moisture balance of the troposphere is maintained. With this information it will be possible to validate better physical parameterizations for the convective injection of moisture into the upper troposphere and gain more confidence in the simulation of water-vapor feedback in climate models. Investigations underway within the EOS IDS investigations are poised to take advantage of these new data and provide the diagnostic and modeling studies to translate them into improved climate predictions.

2.2.4.3.2 Role of large-scale atmospheric motions

Large-scale atmospheric motions also have a controlling effect on the distribution of water vapor in the atmosphere. In regions of mean descent the water vapor concentration is greatly suppressed. The effect is offset by lateral mixing by large-scale motions from regions where water vapor is injected into the troposphere (e.g., Peixoto and Oort 1992, Chapter 12). In the upper troposphere and lower stratosphere, some aspects of the distribution of water vapor can be understood by considering the important role

of mixing along isentropic surfaces (e.g., Kelly et al. 1991; Yang and Pierrehumbert 1994). Such mixing can play an important role in drying the troposphere because isentropic surfaces slope upward with latitude. Air is thus dehydrated by condensation and precipitation as it moves poleward and upward, and when it returns equatorward it provides a source of very dry air to lower latitudes and altitudes. Offsetting this drying action must be a cross-isentropic flow of water, either through diabatic advection or small-scale cross-isentropic transport of water, such as by penetrative convection.

The effect of large-scale motion on water vapor transport can be examined by studying the interannual changes of global water vapor distribution and transport using satellite observations and 4-D data assimilation. Interannual changes of deep convection in the equatorial Pacific associated with the ENSO dramatically alter the distribution of upper tropospheric moisture (Soden and Fu 1995; Bates et al. 1996) as well as global circulation patterns (e.g., Wallace and Gutzler 1981; Lau and Nath 1994). Since the influence of large changes in temperature and surface fluxes upon the moisture field is small compared to the seasonal changes, the impact of atmospheric motion on the water vapor field is more robust. The analysis of TOVS upper tropospheric relative humidity index and water vapor transport assimilated by the GEOS DAS suggests that the 1987 El Niño affected the tropics-extratropics water vapor transport and thus upper tropospheric humidity in the mid-latitudes (Fu and Soden 1996). Quantifying these changes can provide critical information to assess the effect of large-scale motion on water vapor transport and distribution, but is not possible with the accuracy of the current data sets. The EOS AIRS, AMSU, and HSB will provide specific humidity at 10% accuracy. With a more-accurate atmospheric heating field provided by CERES, MODIS, GLAS, and SAGE III, the assimilated wind fields by the GEOS DAS will be more reliable. Thus, the water vapor transport and distribution can be more-accurately estimated and the impact of large-scale motion on water vapor can be estimated quantitatively.

Measuring the effect of large-scale motions on the water vapor budget of the troposphere and lower stratosphere requires very accurate fields of winds, water vapor, and heating rate. These fields will be obtained through the assimilation of EOS radiances into dynamical models, followed by detailed diagnostic and sensitivity studies. Key EOS instruments include AIRS/AMSU/HSB for temperature and humidity profiles, and AMSR-E for precipitable water.

2.2.4.3.3 Role of surface temperature

The importance of surface temperature for the global distribution of water vapor can be easily appreciated from the high correlation between water vapor over the oceans and SST. The monthly mean precipitable water above the oceans can generally be prescribed from the SST (Stephens 1990). Location and season seem to have little effect on the relationship. This close relationship reflects the fact that SST, atmospheric circulation, and convective activities are highly interactive. Also, most of the total precipitable water is near the surface where it is highly influenced by the saturation vapor pressure associated with the SST.

A key consideration in global climate change research and forecasting is how the humidity distribution will respond to a climate forcing that increases the surface temperature. The first guess has traditionally been that the distribution of relative humidity will remain approximately fixed in some averaged climatological sense, so that increases in surface temperature will result in significant increases in the mixing ratio of water vapor in the atmosphere. These changes have consequences for the climate through the greenhouse effect of water vapor, and also for the hydrological cycle through the increased capability of the atmosphere to both provide moisture in regions of precipitation and also to carry it away from regions of new moisture deficit. The interactions among the water vapor distribution, surface temperature, and the hydrologic cycle over land and ocean are critically important, and the EOS observations and scientific investigations are directed toward a more-integrated understanding of these connections and their role in determining the future climate of the Earth. The combination of detailed information on clouds and more-accurate information on the vertical distribution of water vapor will be used by several EOS IDS investigations to better understand the processes that maintain water vapor in the atmosphere and the potential role of these processes in climate sensitivity and change.

2.2.4.4 Water vapor in global climate models

Global climate models contain an explicit atmospheric moisture balance equation, which includes evaporation from the surface, transport through the atmosphere, and precipitation. These models typically produce a strong water vapor feedback when they are forced with doubled carbon dioxide, or some other climate forcing, and this feedback contributes a significant part of the temperature increase (Hansen et al. 1984; Cess et al. 1990). Attempts are currently being made to include explicit cloud water and ice budgets as part of the climate modeling process,

and these interact very strongly with the water vapor distribution.

There are many reasons why simulations of water vapor in climate models are very difficult. The water vapor gradient is large, especially in the vertical where specific humidity varies by several orders of magnitude. To properly compute water vapor transport in the atmosphere requires high spatial resolution in both the horizontal and vertical directions. The spatial resolution of current GCMs is not sufficiently high, and many of the numerical schemes have difficulty conserving the water vapor field (Rasch and Williamson 1990). Parameterizations of sub-grid boundary-layer processes, convection, and soil moisture are difficult. The thick anvil clouds associated with deep cumulus towers contain a huge number of ice particles. These particles detrain away from the convection regions and are the main source of humidity in the middle and upper troposphere of the broad subtropical subsidence region (Sun and Lindzen 1993). Climate models are only beginning to explicitly account for cloud water and ice, their transport, and their evaporation to provide a source of water vapor in the free atmosphere. EOS data will play an important role in validating the new generation of climate models that explicitly include cloud water and ice, both in terms of the cloud simulation and the interaction of the cloud simulation with the water vapor budget.

Despite the difficulties encountered in computing water vapor transport, many climate models simulate the global water vapor field reasonably well. The most reliable element of the water vapor simulation is the total precipitable water. Comparisons of observations and 28 AMIP GCMs show that the models tend to underestimate precipitable water over Northern America, over the zonal band 35°N-50°N, and globally (Gaffen et al. 1995). The mean seasonal cycles are reasonably well simulated, but with a wide range among models. There is a clear tendency for the models to overestimate the poleward transport over much of the globe.

Due to the lack of a global data set, it is very difficult to validate the model simulations of the upper-tropospheric water vapor. Satellite-inferred humidity fields, such as those inferred from SAGE, TOVS, and the Geostationary Operational Environmental Satellite (GOES) radiance measurements, have been used to evaluate the validity of model simulations. There are a few studies addressing the field of relative humidity but none addressing specific humidity. Nevertheless, some GCMs are able to simulate either the seasonal variation of the upper-tropospheric relative humidity (Rind et al. 1991) or the large-scale pattern of the upper-tropospheric rela-

tive humidity as indicated by the brightness temperature in the water vapor absorption band (Salathé et al. 1995).

An important issue is the insertion of the H₂O information from the EOS sensors into research and operational NWP assimilation systems. Water vapor is important for the initialization of weather forecasts, and major centers are directly incorporating radiance information from sounding channels designed to detect the vertical distribution of water vapor in the atmosphere. A data assimilation product to be generated within the EOS program, GEOS-1, can be expected to apply the full complement of EOS H₂O sensors in determining the best water vapor fields. If operational weather prediction centers are given the applicable forward radiative transfer models to compute the observed radiances, given the humidity and temperature profiles, and are then supplied with the observed radiances within 2-3 hours after they are observed, they are likely to incorporate EOS data into their analysis/forecast cycle. This will benefit the forecasts issued and will also help in developing the optimal water vapor fields for use in research and monitoring. Radiation interacts with clouds at all scales.

2.2.4.5 *Needed observations of water vapor*

2.2.4.5.1 Available climatologies

A number of estimates of the climatological water vapor distribution are currently available. These come from operational analyses at the National Centers for Environmental Prediction (NCEP) (formerly the National Meteorological Center [NMC]) and the European Centre for Medium-Range Weather Forecasts (ECMWF), from special satellite data processing studies such as the TOVS Pathfinder, the GEWEX GVAP Project, and from attempts to provide high-spatial-and-temporal-resolution fields from geosynchronous satellites. All of these data sets suffer from one or more deficiencies that make them inadequate for detailed process studies, interannual variability studies, and long-term trends studies. Most are poorly calibrated or are based on an analysis system that changes with time. Most have rather poor vertical resolution, which makes it difficult to diagnose the processes that lead to the vertical distribution of water in the atmosphere.

Three-dimensional and time-continuous global water vapor data sets have been produced from four-dimensional data assimilations (Bengtsson and Shukla 1988; Kalnay and Jenne 1991; Schubert et al. 1995). Water vapor data from radiosonde and satellite measurements are integrated into global climate models. The assimilated field is thus consistent with measurements and modeled

physical processes. Its purpose is to provide research quality data sets suitable for climate studies.

Long-term radiosonde measurements of water vapor have been made routinely at selected locations over land. For temperatures below -40°C and relative humidities below 20%, radiosonde measurements are not accurate. Consequently, few radiosonde measurements are available in the upper troposphere (Peixoto and Oort 1983). The sensitivity of OLR to a given mass of water vapor peaks at the rather cold temperatures and low humidities of the upper troposphere, so that these observational problems are serious. The density of sounding is rather high in North America and Europe but not in other regions. Except for a few island stations, there are practically no upper-air soundings over the oceans. Compared to satellite-retrieved water vapor data, the radiosonde measurements have a high vertical resolution but usually are made only twice a day. Radiosonde measurements of water vapor suffer from various degrees of uncertainties. For the United States, radiosondes using the carbon hygrometer humidity sensor have problems that have been identified. Errors approaching 25% are reported (Wade 1994). Nevertheless, radiosounding of the water vapor in the middle and lower atmosphere is used for the validation of passive remote sensing of water vapor because of its availability and traditional acceptance as the standard of reliability. Validation in the upper troposphere, particularly in the tropics, is sorely lacking. Airborne measurements may make a significant contribution in this area in the near future. Humidity sounders may be placed on commercial aircraft, and additional flights of manned and unmanned research aircraft are needed.

The global distribution of water vapor is also derived from satellite measurements of radiances in the solar, thermal IR, and microwave spectral bands. Operational and research-mode water vapor profiles are derived from TOVS on NOAA satellites (Smith and Woolf 1976; Susskind et al. 1987). The total precipitable water (PW) over the oceans has been successfully retrieved from satellite microwave radiance measurements, such as SMMR and SSM/I (Prabhakara et al. 1985; Wentz 1994). Due to the high variability of land emissivity, microwave radiometry is not used to retrieve PW over land. It is generally believed that the accuracy of PW retrieval is better than 10%.

Water vapor in the stratosphere and the upper troposphere has been routinely retrieved from the SAGE II solar occultation instrument since 1985 (Rind et al. 1993). The SAGE II water vapor has a high vertical resolution of 1 km but a low horizontal resolution of several hundred kilometers. It also has a low sampling rate, with only

a few observations per month in equatorial regions, and it can only detect the humidity in regions that are cloud-free, so its sampling frequency in the upper troposphere is further reduced. The MLS gives a somewhat better spatial coverage in the upper troposphere because it is less sensitive to thin clouds (Read et al. 1995).

2.2.4.5.2 Needed improvements

In every respect, the available water vapor data sets are inadequate for climate studies. Radiosondes are limited to land areas with an uneven geographical distribution, and satellite retrievals suffer from poor vertical resolution and accuracy. It can be anticipated that global data sets with high spatial resolution (both horizontal and vertical) must come from satellite measurements. The areas that need the most improvement are:

- *Vertical resolution of water vapor, especially over oceans.* Most important convection and cloud processes are small scale (Starr and Melfi 1991). Information on high-vertical-resolution water vapor distribution is essential for understanding and parameterizing these processes. Current satellite-retrieval techniques cannot resolve water vapor distribution within a layer of $\approx 3\text{-}4$ km thick.
- *Upper-tropospheric specific humidity.* The outgoing longwave radiation and, hence, the greenhouse effect are sensitive to the specific humidity in the upper troposphere. Currently, the upper-tropospheric humidity cannot be obtained from radiosonde measurements. Current satellite retrievals of the upper-tropospheric humidity have either poor vertical resolution (HIRS and GOES/Meteosat), or low data sampling rate (SAGE II). A substantial improvement in vertical resolution, accuracy, and spatial sampling is expected from AIRS/AMSU/HSB on the EOS PM-1 satellite.
- *Water vapor content in the planetary boundary layer.* Convective activities depend critically on the properties of the planetary boundary layer. Due to the effect of surface temperature on the satellite-radiance measurement and the inherent low vertical resolution of the satellite water vapor retrievals, accurate retrievals of water vapor content in the planetary boundary layer are not currently available.
- *High-accuracy, high-vertical-resolution ground-based lidar measurements.* Developments of methodologies for retrieving water vapor from satellite-radiance measurements require high-accuracy and high-vertical-

resolution water vapor measurements for calibration and validation. Even radiosondes cannot provide such measurements, especially in the upper troposphere.

The EOS instruments, particularly AIRS/AMSU/HSB, seek to provide better vertical resolution and better calibration for tropospheric water vapor measurements. Improved horizontal- and vertical-resolution measurements in the stratosphere will be provided by HIRDLS and MLS. SAGE III will provide very accurate monitoring of water vapor trends in the stratosphere. High-vertical-resolution measurements in the upper troposphere in the presence of thin clouds will be provided by MLS. Assimilation of all of these data into a global analysis using a high-quality assimilation system will provide data sets necessary for studying and monitoring atmospheric water vapor.

2.2.5 Precipitation

2.2.5.1 Role and importance of precipitation

Rainfall is essential for the existence of the Earth's population. It determines the distribution of vegetation, food supply, and habitats of the diverse living species of plants and animals. Rainfall maintains life, but excessive as well as deficient rainfall may cause loss of life, property damage, and failure of crops, resulting in widespread socio-economic hardships. Tropical or midlatitude cyclones, thunderstorms, typhoons, or hurricanes that produce excessive rainfall become major natural disasters and afflict many nations. While flash floods can occur in a relatively short time, from a few hours to a few days, the effect of drought is often more widespread and lasts much longer and may produce even more-disastrous effects. During severe drought, crops fail and topsoils are blown away, often forcing massive migration, starvation, and death of people and animals. The severe drought of the Sahel in the 1980s, which lasted for close to a decade, is a grim example.

In addition to having a direct impact on human society, rainfall plays a central role in governing the climate of the Earth. The latent-heat release in convection is the main source of energy that drives the general circulation of the atmosphere, since much of the solar radiation absorbed by the Earth is used to evaporate water, which later condenses to release latent heat in the atmosphere during precipitation. It is responsible for many scales of tropical motions ranging from hurricanes, tropical cyclones, and monsoon depressions, to the much-larger-scale intraseasonal oscillation, Walker circulation, and Hadley circulation. Not only is tropical rainfall essential in main-

taining atmospheric motions in the tropics, it is known to have strong influence on weather and climate in the extratropics. Latent-heat release in tropical convection forces atmospheric motions that disperse heat and moisture into the extratropics, diverting subtropical jetstreams, and altering rainfall patterns in midlatitudes.

2.2.5.1.1 Role in climate system operation

From a climate system point of view, rainfall is a key agent that connects the Earth's oceans, atmosphere, land, and the biosphere through the global hydrologic cycle. Water vapor evaporated over the tropical and subtropical oceans is partially released locally in the form of rainfall in convection and partially transported away from the place of origin. The continental land surface receives its moisture supply via surface precipitation through a combination of local recycling processes and import of moisture from the adjacent oceans. The water received by the land is given up in part to the atmosphere by evaporation from the land surface or evapotranspiration from plants and trees. Except for a fraction of the water that is stored as underground water or as snow cover, most of the net fresh water input on the land surface is returned to the ocean through river run-off, thus completing the hydrologic cycle. The global precipitation rate determines the average "residence time" of water substance in the atmosphere, ocean, and land, which sets the internal clocks within these different components of the climate system. It is estimated that the replacement time scale (the reservoir size divided by the precipitation rate) is on the order of 10 days for the atmosphere (the fast component), 10^2 - 10^3 days for the land (the intermediate component), and 10^3 - 10^5 days for the upper ocean (the slow component). The Earth climate system evolves as a complex interplay among processes partaking in the fast, intermediate, and slow components giving rise to a myriad of fundamental climatic spatial and temporal time scales.

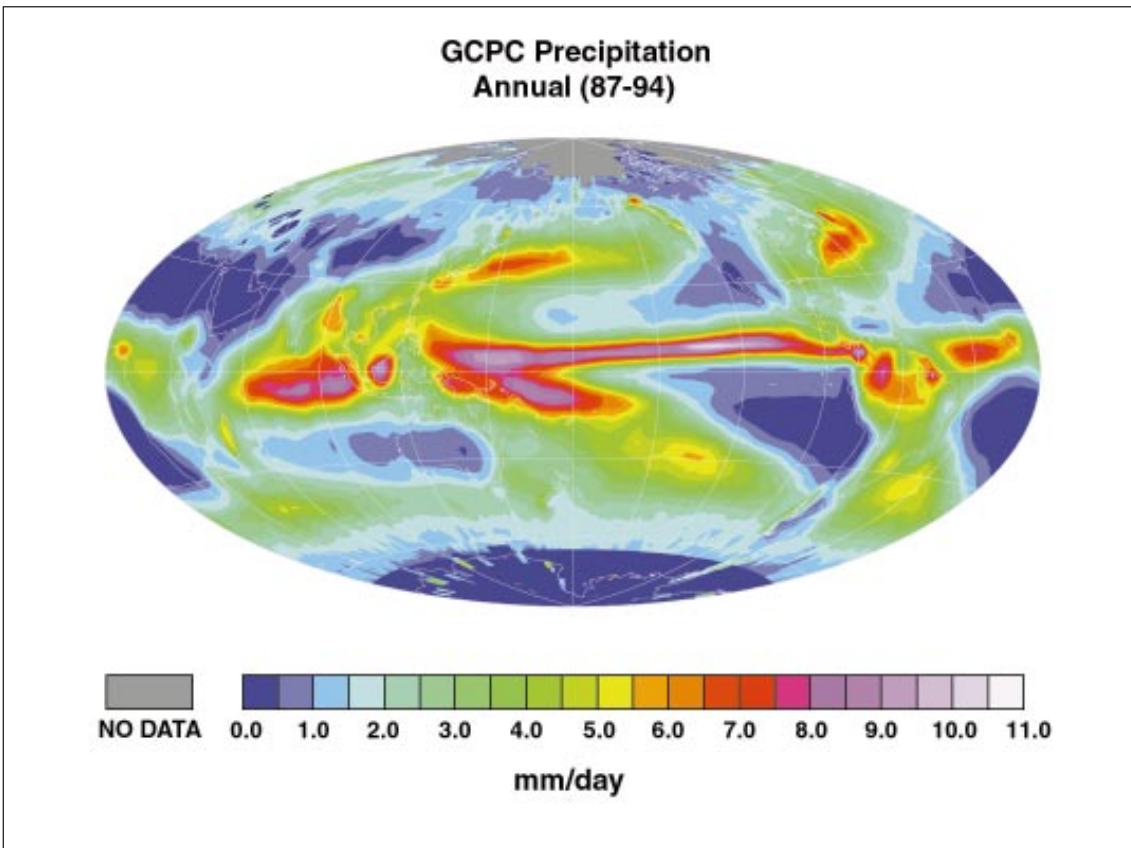
On the intermediate-to-slow time scale, clouds and water vapor are two of the most important factors that determine the Earth's climate, by virtue of their ability to reflect or absorb solar radiation and to re-emit longwave radiation. Both clouds and water vapor are intimately related to precipitation. Water vapor is transported from the surface to the upper troposphere by strong updrafts in moist convection, while cool, dry air is brought down by convectively induced downdrafts. The amount of water vapor that remains in the atmosphere and the amount of water substance in clouds in the atmosphere are therefore dependent on how much atmospheric water is depleted by precipitation. Measurements of precipitation are therefore central to a better understanding of the maintenance

of cloud populations. The interaction between the latent heating from precipitation and the radiation heating due to clouds and water sets up a large spatial gradient in total heating in the interior of the atmosphere and at the Earth's surface. This heating gradient is key to driving atmospheric large-scale mean motions in the tropics, such as the Walker and Hadley circulations, and the transient eddies in the extratropics. These motions produce the mean meridional transport of heat which is required to maintain the equilibrium equator-to-pole temperature difference of the present climate. It has been estimated that between the clear and cloudy region, such as the ITCZ and the subtropical subsidence region, the horizontal latent-heating gradient due to precipitation is about twice as large as the radiation heating set up by clouds and water vapor (Stephens and Webster 1984). While latent heating due to deep convection tends to be concentrated in the midtroposphere, cooling from cloud shielding of shortwave tends to occur most strongly at the surface. Consequently, the net heating gradient in the vertical is altered, leading to either enhanced stability (reduced precipitation) or reduced stability (increased precipitation).

Precipitation also plays an important role in the Earth's climate control through its influence on ocean temperature and circulation. Input of fresh water from precipitation on the ocean surface may alter the salinity and hence the density gradient in the ocean, resulting in alterations of ocean dynamics. Examples of regions where the precipitation-induced salinity changes may have an effect on ocean dynamics, which may have an impact on global climate, are the tropical western Pacific warm pool and the North Atlantic region. The former is the region for the TOGA COARE field experiment, which is aimed at providing a better understanding of the coupling between atmospheric hydrologic processes, in particular precipitation, and surface fluxes over the warm pool region (Webster and Lukas 1992). Fresh water input in the tropical western Pacific may have an influence on the timing and duration of major El Niño events. Similarly, the fresh water input at high latitudes may alter the large-scale ocean circulation and impact climate in the North Atlantic region (see discussion in Section 2.2.5.1.2).

Finally, it is common knowledge that precipitation is essential for the survival of the biosphere. Without precipitation, vegetation disappears and land turns into desert. Recent modeling studies have established that the land-surface vegetation may provide a positive feedback on rainfall through its ability to: (a) evapotranspire, (b) trap solar radiation within leaf organizations, (c) regulate evapotranspiration by stomatal control, and (d) modify (generally increase) the surface roughness on the scale of

FIGURE 2.12



Annual average (1987-1994) precipitation measurements from the Global Precipitation Climatology Project (GPCP).

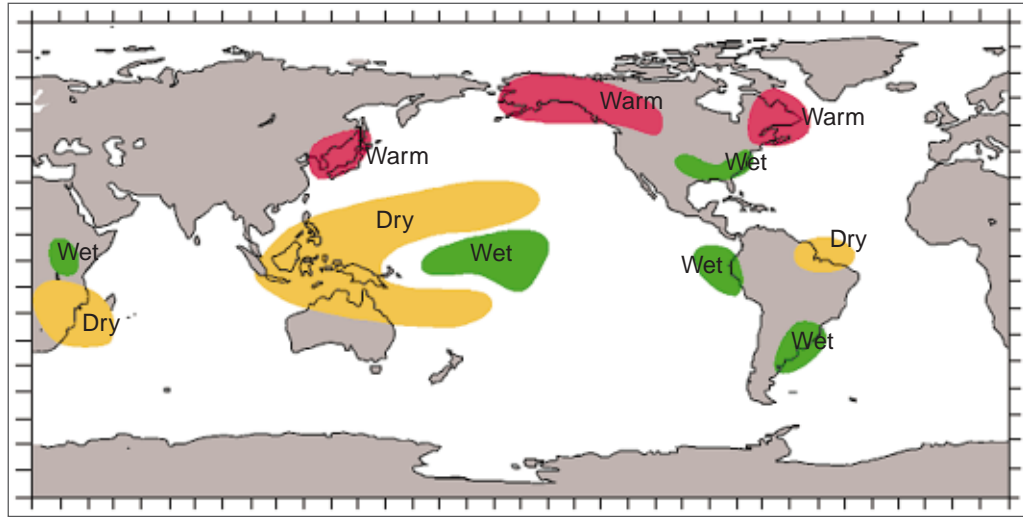
turbulent eddies. Model sensitivity studies have shown that the above biogeophysical effects, both individually and jointly, have produced increased rainfall over different regions of the world. Model experiments on deforestation areas such as the Amazon have shown a significant impact of precipitation on the regional scale. From a synthesis of modeling results of the last decade, it has been shown that the biosphere-atmosphere interactions play an important role in redistributing continental precipitation to fulfill the survival and growth requirements of different biomes: forests, pasture, agricultural lands, and deserts. However, studies of the scale dependence of the vegetation influence on global precipitation patterns are still rudimentary and have many uncertainties. For a better understanding of precipitation-biosphere interaction, improved representation of hydrologic processes, systematic investigations, and observational collaborations are essential.

2.2.5.1.2 Importance in global change scenarios

Because of the lack of long-term global data, the possible effects of global warming on precipitation rely mainly on

projections from climate models. Given the uncertainties of precipitation prediction in climate models (see Section 2.2.5.5), these projections should be considered extremely tentative. Based on the IPCC report (Houghton et al. 1996), the following scenarios for precipitation are possible due to global warming. Due to doubling of CO_2 , there will be an increase in global precipitation from 3-15%, mostly in the higher latitudes during the boreal winter. This increase is related to the dependence of saturation vapor pressure on temperature and to the poleward movement of the midlatitude oceanic storm tracks. In a warmed climate the drying season commences earlier and the soil moisture content in mid-to-late summer may be decreased. This warming and drying may be amplified through the summer by enhanced solar heating because of the drier surface and associated reduction in cloudiness. Climate models show reasonable agreement in terms of the occurrence of the summer land warming and drying in midlatitudes due to global warming. Changes in the monsoon circulation can also be expected. Model results from IPCC suggested that the East Asian monsoon may be strengthened because of the increased thermal

FIGURE 2.13



Summary of large-scale climate anomalies associated with the warm phase of the ENSO cycle during the Northern Hemisphere winter (Ropelewski and Halpert 1987, used with permission from the American Meteorological Society).

contrast between the Eurasian landmass and the tropical oceans, which are least sensitive to global warming (Held 1993).

The before-mentioned possible global change scenarios are for equilibrium climate, which may take hundreds of years to reach. The real impact of global change depends upon the way the Earth's climate evolves from the present to the future equilibrium climate. Hence the transient response to anthropogenic forcing over the next 50-to-100 years is most important. Here, the effect of the ocean is paramount, and changes of precipitation may play a critical role. Coupled models suggest that the increase in precipitation at high latitudes may result in a deceleration of the Atlantic oceanic meridional circulation, causing a reduction in the oceanic transport of heat from tropics to extratropics. This reduction in heat transport may lead to a delayed warming or even a temporarily cooler climate over the North Atlantic region as global warming progresses. A similar mechanism will cause a delayed warming in the southern oceanic regions (Held 1993; Manabe et al. 1991). Monitoring precipitation over the oceans will put us in a better position to detect the fingerprints of global warming and to develop sound policies for global change.

2.2.5.2 Spatial and temporal distribution of precipitation

The distribution of precipitation is highly inhomogeneous in space and time. The spatial and temporal scales range

from thundershowers that last from several minutes over a distance of less than a kilometer to displacements of major precipitation systems that cover distances of thousands of kilometers and last over several years. Because of the wide range of variability, the long-term, accurate mapping of global precipitation is a daunting task. To obtain a global rainfall map, land-based rain gauge, satellite-derived oceanic rainfall, and sometimes model-generated rainfalls are often blended in an optimal way to minimize the bias from each individual estimate. Figure 2.12 shows a typical annual distribution of rainfall from the Global Precipitation Climatology Project (GPCP) (Huffman et al. 1995). The major rainy zones include the eastern Pacific Intertropical Convergence Zone (ITCZ), the South Pacific Convergence Zone (SPCZ), the Asian monsoon, and the rainbelt over the Amazon and central Africa.

These rainfall patterns undergo large annual cycle variations (not shown). Most important, there is strong year-to-year variability in the precipitation pattern. Figure 2.13 shows the composite changes in precipitation patterns associated with an ENSO event including the timing of the extreme over different regions. Widespread drought conditions can be found over the maritime continent, northern and central Australia, northern India, northern Brazil, Central America, and southeast Africa. Flood conditions are found over the equatorial central Pacific, the west coast and southeast coasts of South America, and the southeast and southwest United States.

In the tropics, the precipitation pattern shifts are very robust and are directly related to the changes in tropical SST due to ENSO. In the extratropics, the changes in precipitation result from alteration of the subtropical jetstreams and wintertime storm tracks, and have much larger variability. There are also other observed trends and large interannual and possibly interdecadal changes in precipitation that are not related to ENSO. An example is the dramatic and prolonged decrease in rainfall in the Sahel region from the early 1970s to the late 1980s. There are speculations that desertification induced by overgrazing may have been responsible for the prolonged drought (Charney 1975). Another plausible explanation is that the observed precipitation “trend” is a part of the natural decadal or bidecadal oscillation in SST in the coupled ocean-atmosphere system. At present, there is no generally-accepted explanation for the occurrence of such a prolonged drought, much less a method to predict its occurrence.

2.2.5.3 Integration of ground data

Surface observations of precipitation play an important role in the validation and calibration of remote sensing and model-based estimates of large-scale precipitation patterns. Rainfall measurements from rain gauge networks have been traditionally regarded as the “ground truth” of precipitation. Recently, ground-based radar data have also been used to improve sparse rain gauge-derived precipitation data. However, it should be mentioned that, for both oceans and remote areas of the globe, precipitation is poorly observed and almost no ground data are available for these locations.

In order to serve the needs of climate study, great efforts have been made to collect ground precipitation data over the globe. In the United States, the National Climatic Data Center (NCDC) routinely archives hourly and 15-minute precipitation data from over 5,000 stations nationwide. Legates and Willmott (1990) published a mean seasonal variability in gauge-corrected global precipitation. Recently, Legates has created a global-mean monthly precipitation archive based on surface and ship observations. In addition, the database of the Global Historical Climatology Network (GHCN) contains monthly total precipitation from 7533 stations throughout the world. Both of these databases are now accessible through EOSDIS. The GPCP seeks to construct an optimal global data set from microwave, IR, and in situ data. A global, two-year, 2.5-degree data set for 1987-1988 is currently available (<http://orbit-net.nesdis.noaa.gov/gpcp/>).

The Next Generation Weather Radar (NEXRAD) program of the United States has made great efforts to develop, procure, and deploy an advanced Weather Sur-

veillance Radar-1988 Doppler (WSR-88D) system that will replace the current meteorological radar system. The first WSR-88D system was installed near Oklahoma City, Oklahoma, in 1990. When the last installation is completed during 1996, a NEXRAD network consisting of at least 136 operational WSR-88D systems will cover most of the contiguous United States and provide quality high-resolution, real-time-processed precipitation data. Weather radar systems have been developed in Europe (European Communities COST-73 Weather Radar Network), Japan (the Japanese Weather Radar Network), Australia, and many other countries; however, there is no worldwide radar database yet.

Because rain gauge observations are point values, it is necessary to apply interpolations, such as distance weighting and Kriging, to render the spatial distribution of precipitation. However, highly-inhomogeneous characteristics of precipitation distribution (described in Section 2.2.5.2) require an unmanageably high-density gauge network. On the other hand, because radar images provide the high-resolution, real-time precipitation distribution, compositing techniques have been developed that use high-quality gauge measurements within the radar image to calibrate the precipitation quantity. These composite gauge-radar data are considered more reliable for climate studies. Climate statistics also offer alternative means to integrate precipitation.

2.2.5.4 Precipitation in climate models

Because precipitation is a noisy field, it is one of the most difficult hydrologic parameters for which to validate simulations. At present the reliability of precipitation estimates in climate models is not very high. Yet it should be noted that uncertainties in global rainfall estimation, especially over the oceans, are as large if not larger than those among climate models. Recently, an intercomparison study of precipitation processes in over 30 state-of-the-art global-climate models has been carried out under the AMIP. The result of AMIP should provide a snapshot of the current capability of global-climate models in precipitation simulation. The following is a summary of the results for the AMIP global-climate models (Lau et al. 1995).

- Most models are able to produce a global precipitation rate to within 10-20% of the observed, which is comparable to the standard deviation among “observations.”
- Most models show a conservation of water substance, to within 5-10%. Because of the possible large errors in regional water balance associated with a 5% error in global water balance, it is not clear that climate

models with that level of deficiency can be tolerated for global-change regional precipitation assessment. Models that have Evaporation-Precipitation (E-P) imbalance over 10% are clearly not suited for long-term climate water resource assessments.

- While most models can simulate the annual cycle reasonably well, compared with the observations in a region with strong annual cycles, models generally have problems in simulating the annual cycle in a region of strong dynamical control, i.e., $P-E > 0$.
- Models differ substantially in regional- and subcontinental-scale rainfall variability. Model rainfall estimates disagree most in the eastern Pacific ITCZ, the South and Southeast Asian monsoon, and the Mexican region. All models underestimate the northward advance and the intensity of the East Asian summer rainbelt. The extratropical wintertime rain belts are also underestimated in most models.
- All models underestimate the frequency of occurrence of the light-rain category ($< 1 \text{ mm day}^{-1}$). This may be related to the poor treatment of shallow clouds and stratocumulus in all climate models.
- Over 90% of the models show enhanced skill in prediction of precipitation pattern changes due to SST-anomaly forcing from the ENSO. However, all models show no skill in extratropical interannual rainfall prediction.
- More than 30% of the models seem to have unrealistically strong land-lock convection and excessive rainfall over steep terrain. These may be due to the deficiency in the vertical coordinates over steep terrain. Spurious, small-scale rainfall, likely due to truncations and other basic numerical problems, is still present in a number of the climate models.

Given the above assessment, it is clear that climate models still have a long way to go before their precipitation projections for climate change can be trusted with any reasonable level of reliability.

2.2.5.5 Needed satellite measurements and algorithms

To better understand the role of precipitation in driving the Earth's climate and to validate global climate models, quantitative information regarding the global distribution of precipitation is essential. For understanding the physics of precipitation processes and its interaction with land surfaces, daily sampling over the globe and sampling at

shorter time intervals over selected target regions are both desirable. Because it is impossible to set up uniform networks of rain gauges over the entire globe, satellite rainfall retrieval algorithms will play a vital role in producing realistic global rainfall distributions. The synergistic use of remote-sensing, ground-based, and model-based rainfall information is of paramount importance.

Satellite retrieval of rainfall has a heritage beginning with the passive microwave measurements made by the Electrically Scanning Microwave Radiometer (ESMR) on board Nimbus-5, SMMR on Nimbus-7, and SSM/I on the Defense Department satellites and the Microwave Sounding Unit (MSU) on NOAA polar-orbiting satellites. In addition, AVHRR on NOAA operational satellites and similar IR sensors on geostationary weather satellites, GOES and the Japanese Geostationary Meteorological Satellite (GMS), have provided extremely useful estimates of rainfall. Both the microwave and the IR measurements have their inherent drawbacks. For example, microwave measurements are reliable over the oceans but not over land because of the large variation of background emissivity over land. IR measurements rely on relationships between cloud top temperature and rainfall, which may vary greatly in different rainfall regimes and are indirect at best. TRMM employs a suite of sensors including one passive TMI, one VIS/IR scanner (VIRS), and one active precipitation radar (PR), and aims at producing the best rainfall estimation from space, which is based on algorithms that combine measurements from all the sensors.

Within the EOS measurement system, the key instruments for precipitation measurement are the AMSR-E and the HSB on the EOS PM-1 platform. While there may be an inherent sampling problem with precipitation measurements based on a single satellite, because of the strong diurnal cycle in rainfall, it is expected to be eased by coordinated measurements by microwave and IR sensors flown by Europe and Japan. It is important that different equator crossing times are maintained for these different satellites, so that different parts of the diurnal cycle can be sampled. It is expected that knowledge gained from TRMM will be used for guidance to improve the rainfall estimates from combined satellites and sensors. The use of hybrid algorithms, which combine IR and microwave information, will be pursued. While TRMM is uniquely equipped to make measurements of precipitation over the tropical regions, through a combination of passive and active microwave instruments, it falls short of providing global coverage. Hence, the TRMM capability should be extended to higher latitudes with AMSR-class passive microwave sensors from sun-synchronous polar orbits with morning and afternoon crossing times. The Advanced Earth Observing Satellite II (ADEOS-II) and METOP mis-

sions will carry AMSR and the Multi-frequency Imaging Microwave Radiometer (MIMR), respectively. Both missions are suitable for sampling precipitation at high latitudes; however, they will both be in midmorning orbits. The SSM/I and SSM/IS passive microwave radiometers on the DMSP series can provide precipitation measurements, but these have less precision and coarser spatial resolution than those from either AMSR or MIMR. Moreover, the DMSP measurements continue to be at dawn and dusk, which limits their utility for capturing the diurnal dynamics of precipitation processes. There is a need for sampling precipitation globally in an early afternoon crossing orbit to complement the morning measurements from the ESA and the National Space Development Agency of Japan (NASDA) platforms. AMSR-E on the EOS PM-1 satellite is intended to achieve this objective. Without AMSR-E or a similar passive microwave imager, a significant portion of the science supported by the EOS PM-1 mission will be seriously compromised. Without an AMSR or MIMR, placement of a modified TMI would at least accomplish the desired diurnal sampling, although not at the desired spatial resolution.

2.2.6 Atmospheric circulation, hydrologic processes, and climate

2.2.6.1 Hydrologic processes and the tropospheric circulation

As discussed in the previous chapters, hydrologic processes due to clouds, water vapor, and precipitation are critically important in determining the Earth's climate. The presence of these hydrologic parameters in the atmosphere significantly alters the Earth's radiation budget, in particular in generating differential heating between the tropics and the polar regions, between the ocean and the land, and between clear and cloudy regions. This differential heating is the main driver of the atmospheric large-scale circulation. The essential component of the circulation is wind.

The continuity equation of water vapor for the atmospheric branch of the hydrologic cycle can be written in the following form:

$$\frac{\partial W_a}{\partial \tau} = \nabla \cdot \sum \langle q \vec{V}_a \rangle = E - P$$

This equation shows the linking among the total atmospheric columnar water vapor, W_a , the divergence of vertically-integrated moisture by wind $\nabla \cdot \sum \langle q \vec{V}_a \rangle$, evaporation E , and precipitation P . It is clear from this equation that moisture transport plays an important role

in determining the amount and the distribution of water vapor in the atmosphere. The dynamics of atmospheric motions also determine the amount and types of clouds in the atmosphere. The rising motions in the tropics and the subsidence in the subtropics associated with the Hadley circulation are closely linked to the meridional distribution of E-P. Climatologically, the subtropics is a source of atmospheric moisture (E-P>0) and the equatorial and midlatitude regions are sinks (E-P<0). Within the tropics, the eastern Pacific is a source and western Pacific a sink of atmospheric moisture, connected via the Walker circulation. On a more-regional scale, the land regions of the Asian monsoon act as a sink, and the adjacent oceans are sources of moisture during the boreal summer monsoon (Lau et al. 1995). The annual reversal of the surface wind and associated low-level moisture convergence play an important role in determining the distribution of precipitation and evaporation over the monsoon region.

In addition, many weather and climate anomalies in the extratropics have been attributed to climate anomalies in the tropics, e.g., the Pacific-North American teleconnection pattern (Horel and Wallace 1981; Wallace and Gutzler 1981). This kind of remote response to local forcing is effected by transport and energy dispersion via the atmospheric circulation. Hence consideration of the atmospheric wind circulation is indispensable in order to understand the role of the global hydrologic cycle, clouds, water, and precipitation on regional and global climate fluctuations.

2.2.6.2 Large-scale circulation and climate feedback processes

For long-term climate changes resulting from natural and anthropogenic causes, knowledge of the changes in the radiative forcing of the planet is of foremost importance. It is now recognized that, while the radiative forcings such as that due to doubling of CO₂ may be small, feedback processes in the climate system may amplify the initial response to the radiative forcing, thus making it more detectable. These feedback processes involve the interaction of clouds, radiation, and dynamics and in many cases, especially for seasonal-to-interannual time scales, the large-scale circulation plays a fundamental role. To fully understand climate feedback mechanisms, it is important to keep in mind that physical processes from cloud-scale radiation to global circulation interactions are taking place simultaneously at all time scales. In the recent debate regarding the thermostat mechanisms for tropical SST (Ramanathan and Collins 1991), many authors (Fu et al. 1992; Hartmann and Michelsen 1993; Lau et al. 1994; and others) have pointed to the importance of the large-scale circulation vs. that due to local feedback as the

fundamental mechanism for regulating tropical SST. Pierrehumbert (1994) argued that radiative cooling from the dry atmosphere of the subsiding branch of the large-scale circulation may be needed to balance the heat accumulated by the warm tropical ocean. Bony et al. (1995) have shown that the sensitivity of the greenhouse effect to SST is much larger for seasonal and interannual variations compared to climate-change estimates. It is quite obvious that for seasonal-to-interannual changes, it is the change in large-scale circulation, not local cloud-radiative processes, that is causing the large sensitivity. This is confirmed by the recent work of Lau et al. (1997), which shows that the sensitivity of outgoing longwave radiation to SST is reduced by a factor of three when the effect of the large-scale divergence is removed. Thus it is extremely important to consider the contribution of the large-scale circulation when using seasonal and interannual variability as surrogates for climate change.

Atmospheric transport of energy and water by large-scale motions may also play a critical role in determining the amount of polar amplification associated with climate change. Atmospheric motions carry more than half of the poleward transport of energy at most latitudes, and all of the transport into polar latitudes.

2.2.6.3 *Need for satellite measurements of wind*

EOS will provide some very important measurements of surface wind speed and direction over the oceans from scatterometry (NASA SeaWinds scatterometer on QuikSCAT and also on ADEOS II) and passive microwave remote sensing. These data will be particularly critical for estimating air-sea exchanges of heat, momentum, and moisture.

For a proper description of the global tropospheric circulation useful for climate studies, a global wind measurement accuracy of 2-3 m s⁻¹ with a horizontal resolution of 100 km and a vertical resolution of about 1 km in the vertical, preferably higher resolution (0.5 km) in the planetary boundary layer, with a temporal coverage of 6 hours is required (Baker et al. 1995). The current global radiosonde network for tropospheric wind measurements is grossly inadequate to provide this coverage, especially over the tropical and southern oceans and for the remote continental and desert regions. Yet these regions, such as the central equatorial Pacific, the Indian Ocean, and the midcontinental desert region, are the most important climatic regions because they encompass the sources and sinks of atmospheric heat and moisture, where potential and kinetic energy are exchanged through the large-scale circulation. The network of radiosonde wind observations is not expected to be significantly upgraded in the next several decades because of the budget constraints of world

governments. Currently, a reliable mapping of the global wind distribution has relied mainly on four-dimensional data assimilation systems. However, in the absence of real data input over large regions, 4DDA data are mostly model climatologies. That is why the largest differences between wind products for the major 4DDA systems, e.g., ECMWF and NMC (Trenberth and Olsen 1988) are found over the southern oceans. Similarly, observation system simulation experiments with lidar winds are found to have the largest impact over the tropical and southern oceans (Baker et al. 1995). In the current EOS payloads for AM-1 and PM-1, there is no consideration for tropospheric wind-measuring instruments. In the new EOS/ESE era, we should seriously consider a satellite wind-measurement system, such as a lidar, which depends on aerosol backscatter, to provide uniform, global, and continuous wind coverage. These satellite winds will then be assimilated into state-of-the-art 4DDA systems to provide a global wind measuring system in the troposphere. Improved tropospheric wind measurements will also allow trajectory computations for atmospheric chemical species that will have an impact on global change.

2.2.7 *Strategy for combining observations and modeling*

To solve many of the scientific problems described in preceding sections requires a thoughtful and careful integration of improved observations with improved theory and models. Figure 2.14 illustrates a strategy for combining EOS global satellite observations with critical modeling and correlative observational efforts. None of these efforts alone can provide a high degree of confidence in climate predictions, such as those used to study global-warming scenarios. At the largest time and space scales, climate models must be tested against global satellite observations of temperature, humidity, precipitation, clouds, radiation, and large-scale wind fields. Current global models do not perform adequately on this test, diminishing our confidence in their predictions. Direct tuning of climate models to satellite observations must be avoided, however, as it invalidates the independence of the data, and provides no new or improved physics to the model. Instead, cloud-scale and regional-scale models with more-advanced cloud physics and radiation physics must be tested against both field experiment data and satellite data. Once the models pass these tests, they can be reduced to simpler forms for inclusion in global climate models. In addition, field experiment and surface data must be used to verify the accuracy of the global satellite remote-sensing observations, and provide additional information not accessible from space.

Confidence in climate predictions will require, as a minimum, the achievement of four basic elements:

- detailed dynamical, physical, and radiative cloud models verified against field and laboratory experiments for a wide range of cloud types and conditions;
- successful construction of simplified climate model parameterizations derived from more-detailed models and theories and validated against observations;
- availability and verification of the accuracy of global satellite observations of key variables; and
- agreement of climate models with satellite observations on a range of space and time scales (global, synoptic, regional, yearly, seasonal, monthly, and diurnal).

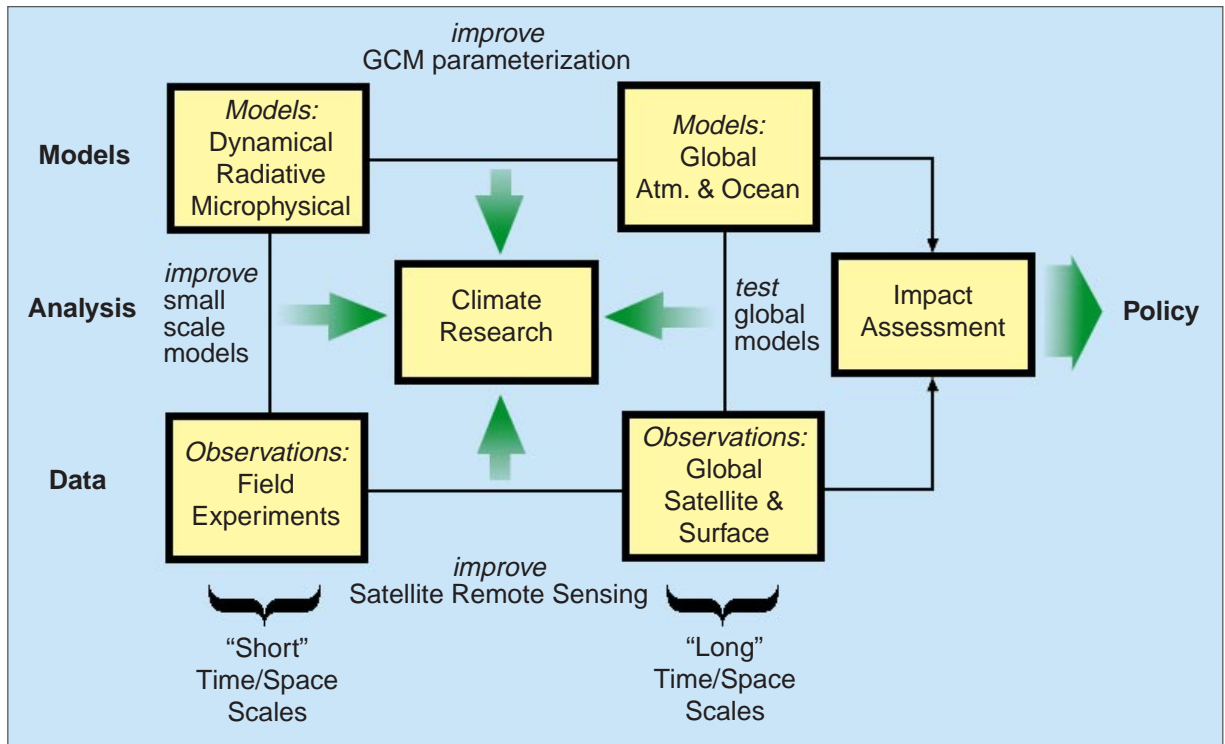
In fact, this process is iterative, and all four tasks should be pursued simultaneously.

Satellite data useful for climate studies have historically been collected by both operational satellite systems (NOAA, Department of Defense [DoD]) as well

as NASA research satellites. Some operational systems such as GOES and AVHRR are designed for an operational weather forecasting mission and therefore lack the high-quality calibration required for climate research instruments such as ERBE and SAGE II (McCormick et al. 1992). This accurate and stable calibration is critical to providing climate data that will improve GCMs as well as monitor climate change. An advantage of the operational systems, however, is a well-developed and stable data-processing and distribution system, as well as the commitment to long-term data collection that results in climate records with long time coverage and minimal data gaps. A critical problem for national and international efforts in remote sensing of climate is to bring together high calibration and characterization of remote-sensing instruments with a commitment to collect homogeneous measurements over a long period of time.

EOS will attempt to describe the radiative effects of clouds on fluxes at the large scale for climate monitoring and for validation of GCMs, mesoscale models, and cloud-scale models. A profitable interaction between EOS and the new generation of models will be fostered by the participation of EOS teams in small-scale, intensive measurement programs such as ARM and the GEWEX-WCRP

FIGURE 2.14



Observational strategy for the determination of the role of clouds and radiation in climate. Confidence in climate model predictions of global warming requires iterative improvements in global climate modeling, global satellite observations, and cloud/regional-scale modeling of cloud dynamical and radiative processes (Wielicki et al. 1995, used with permission from the American Meteorological Society).

TABLE 2.5

PARAMETER NAME	UNITS	ACCURACY ABS::REL	TEMPORAL RESOLUTION	COMMENTS
Irradiance, Solar, Total	Wm ⁻²	0.1% :: 0.001%	1/(2 min)	ACRIM

Total solar irradiance

BSRN. ARM and the BSRN function continuously and can provide much data to EOS researchers, in some cases at no cost. Through GCIP, the ARM Southern Great Plains (SGP) site is already targeted for the validation of operational tools such as the NMC Eta mesoscale model. A surface-based CPR will soon be deployed at the ARM SGP site. The same sites can be used as a focal point for the development and validation of EOS remote sensing.

Concentration on a limited number of well-instrumented sites will foster interactions even within EOS. Strong interaction between detailed surface-based observations and high-quality global remote sensing by EOS is critical to gaining increased understanding of the radiative effects of clouds and the proper simulation of cloud effects in climate models.

2.3 Required satellite measurements and data sets

2.3.1 Summary of required satellite observations

We present here an abbreviated description of some key EOS observations related to radiation, clouds, water vapor, precipitation, and atmospheric circulation. More-complete descriptions of the EOS instruments and detailed descriptions of data products can be found in the EOS Data Products Catalog.

2.3.1.1 Total solar irradiance

The total solar irradiance at the Earth is about 1370 Wm⁻² and was observed to vary peak to peak by about 1.5 Wm⁻² or 0.1% during solar cycle 21. If this amount of total solar irradiance change were applied continuously to a relatively sensitive climate model [$\Delta T = 1.0 \text{ K}/(\text{Wm}^{-2})$], a surface temperature response of about 0.26 K would be induced. This temperature change is small compared to those that might result from a doubling of CO₂, but it is significant compared to the estimated 0.5 K warming during the last century, and would be significant in the problem of early detection and assessment of global climate change. By using overlapping flights of ACRIM instruments (0.1% absolute accuracy), it is believed that a relative precision of 0.001% can be achieved. This relative precision would be sufficient to detect any climatically-significant changes in total solar irradiance on time scales of up to a century (see Table 2.5).

2.3.1.2 Radiative fluxes

All of the energy exchange between the Earth and space is achieved by radiative transfer, as is much of the impor-

tant energy exchange within the climate system. To provide points of reference for required accuracies, consider that observed changes in climate forcing associated with total-solar-irradiance changes are about 0.25 Wm⁻², and the expected climate forcing from doubling CO₂ is about 4 Wm⁻². Variations of radiative fluxes within the climate system that are associated with season, location, weather, or natural interannual variability are much larger, often on the order of 100 Wm⁻². While it seems beyond current capability to measure the small changes in fluxes within the climate system that are directly associated with total solar irradiance or atmospheric CO₂ variability, useful measurements can be made of the magnitude and variability of radiative fluxes in the climate system, and these can be used to both understand climate and validate climate models. Current climate models appear to be in error by tens of Wm⁻², so that an achievable accuracy of 5 Wm⁻² is very useful, despite being larger than the expected climate forcings.

In planning to make observations of radiative fluxes within the climate system it is helpful to consider the general requirements for resolution of the frequency spectrum, spatial resolution, temporal resolution, and calibration. To accurately estimate the total radiative energy flux, the measurements must span the range of frequencies that contribute significantly to the flux. In instruments such as CERES, which are specifically designed to measure total solar or longwave energy flux, a thermal detector is used. In order to understand what causes a change in radiative flux it is useful to separate contributions from

different wavelength intervals that respond differently to changes in temperature, clouds, aerosols, water vapor, or other greenhouse gases. MODIS provides both high spectral and spatial resolution.

In order to measure the gross energy balance of the Earth, global coverage is required; global coverage is achievable from a single polar-orbiting satellite. In order to measure fluxes in the atmosphere and at the surface, and to evaluate the role of clouds in the radiation balance, it is necessary to have sufficient spatial resolution in the basic observations to have a high probability of obtaining measurements for which the instrument field of view contains no clouds. A reasonable frequency of such clear scenes is obtained for pixels of about 25 km across, though much higher spatial resolution can be required for other purposes such as cloud detection. For example, to adequately reduce the effect of partially-filled pixels on the determination of cloud properties, it has been estimated from Landsat data that the size of pixels should be no larger than 250 m. This resolution has been provided for two of the channels on MODIS.

In addition to wavelength dependencies, the dependence of outgoing radiance on satellite viewing angle can be used to retrieve physical properties such as aerosol abundance or type. In many retrieval problems using solar radiation, knowledge of the bidirectional reflectance distribution function (BRDF: the dependence of the radiance on the solar and satellite viewing angles at the point of interest for a particular scene type) is critically important. MISR, which can view a pixel as small as 275 m in 4 frequencies from 9 angles during a single overpass, was designed to provide accurate BRDFs and exploit the potential of angular sampling for remote sensing. CERES has been provided with two scanning instruments on early platforms so that the angular and diurnal sampling errors can be minimized. One scanner is intended to operate in the cross-track direction to provide global coverage, while the other rotates in azimuth to provide better angular sampling.

Temporal sampling is also an issue. Radiation fluxes respond strongly to changes in clouds, humidity, and temperature, which evolve on time scales of hours. It is not possible to follow these high-frequency developments from polar-orbiting satellites, although the aggregate effect of these phenomena can be captured in spatial and temporal averages of data from polar-orbiting satellites. An important systematic variability of radiative fluxes occurs on the diurnal time scale. At most points on the globe a strong 24-hour rhythm in insolation drives corresponding variations in clouds, temperature, and radiative fluxes. The diurnal variation is important because it represents a known forcing which can be used as a probe

to understand the response of certain facets of the climate system. It is also important to remove any systematic effects of the diurnal cycle on our sampling of radiative fluxes and clouds. For this reason, it is necessary to fly radiation and cloud instruments in at least two sun-synchronous orbits simultaneously, usually an AM (~10:30) and PM (~13:30) equator crossing time, plus either one precessing orbit or a third sun-synchronous orbit. Current planning is for TRMM and TRMM follow-on to provide the precessing orbit to complement the two EOS sun-synchronous orbits. This provides observations of most points at six local times each day, sampling which is sufficient to resolve the diurnal cycle and to reduce monthly mean time sampling errors to values similar to errors expected for calibration and angular sampling (Wielicki et al. 1996). An important complement to these global diurnal-resolving radiation measurements will be the planned launch of a Geostationary Earth Radiation Budget (GERB) broadband radiometer on the Meteosat Second Generation (MSG) spacecraft scheduled for launch in 2000.

2.3.1.2.1 TOA fluxes

Fluxes of solar and longwave radiation at the TOA are the energy exchange of the Earth with space. These fluxes are modulated by clouds, temperature, humidity, aerosols, and greenhouse gases, and the relationship between these fluxes and the surface temperature is a fundamental measure of climate sensitivity. The natural variability of TOA fluxes on decadal time scales can be observed with highly-calibrated instruments in properly maintained orbits (e.g., Cess 1990). With a combination of highly-accurate broadband radiance measurements from CERES and higher-spatial and spectral-resolution radiances from cloud imagers (VIRS on TRMM, MODIS on EOS AM-1 and PM-1), each flown in two sun-synchronous orbits with different equator crossing times (CERES, MODIS), as well as a precessing orbit (CERES, VIRS), it will be possible to provide TOA flux measurements with an estimated absolute accuracy of 2.5 Wm^{-2} for LW and 5 Wm^{-2} for SW. These absolute accuracies are specified as the absolute error of a large ensemble of instantaneous observations with a mean emitted TOA LW flux of 240 Wm^{-2} and a mean reflected SW flux of 300 Wm^{-2} , typical of the EOS AM-1 or EOS PM-1 orbit solar illumination conditions. Instantaneous relative errors (1 standard deviation) for the same ensemble of instantaneous observations are expected to be about 5 Wm^{-2} for LW and about 15 Wm^{-2} for SW TOA fluxes for CERES pixels of about 20 km in diameter (see Table 2.6). These instantaneous satellite swath data will be useful for many scientific investigations.

For global-scale diagnostic studies and model validation, spatially-gridded and time-averaged data will more commonly be used. Spatial gridding will start at $1^\circ \times 1^\circ$ latitude-longitude resolution and be nest-able to coarser grids. Two important products for use in analysis and model validation are planned. Global synoptic maps at three-hour intervals are planned for use in validating weather prediction models. Daily and monthly mean maps also will be generated and made available for modeling and diagnostic studies. For monthly averages it is planned to also produce mean monthly diurnal variations of flux quantities at three-hourly intervals and also to use scene identification information to produce separate clear-sky and total-sky fluxes, so that the role of clouds in modifying these fluxes is isolated. Because averaging reduces random errors associated with sampling and inversion, the expected accuracies of the monthly-mean, spatially-averaged data are greater than those of corresponding instantaneous observations. The error estimates assume a three-satellite system (see Table 2.7).

2.3.1.2 Surface and internal atmospheric fluxes

Using measurements of temperature, water vapor, and clouds from EOS instruments as input to a model calculation, and constraining these models further with TOA flux measurements, it is possible to produce estimates of radiative fluxes at the surface and at several levels within the atmosphere, for example, at 500 mb and at the tropopause. A similar suite of instantaneous, synoptic, and diurnally- and monthly-averaged products is planned. The accuracies of the surface and internal atmospheric radiative fluxes that will be achieved are less certain than for fluxes at the TOA, since more modeling is required and the experience base with this type of flux estimate is less developed than for the TOA problem.

2.3.1.3 Cloud properties

Because of the critical importance of cloud properties to many of the outstanding global climate questions (Section 2.4), and because of the extreme difficulty in deriving accurate cloud data, cloud properties are derived by many

TABLE 2.6

PARAMETER NAME	UNITS	ACCURACY ABS::REL	TEMPORAL RESOLUTION	HORIZONTAL RESOL::COVER	COMMENTS
Radiative Fluxes, SW, TOA	Wm ⁻²	15 Wm ⁻² :: 15 Wm ⁻²	100 Hz	20 km :: G	CERES/MODIS
Radiative Fluxes, LW, TOA	Wm ⁻²	5 Wm ⁻² :: 5 Wm ⁻²	100 Hz	20 km :: G	CERES/MODIS

Top-of-atmosphere radiative fluxes: Instantaneous pixels

TABLE 2.7

PARAMETER NAME	UNITS	ACCURACY ABS::REL	TEMPORAL RESOLUTION	HORIZONTAL RESOL::COVER	COMMENTS
Radiative Flux, LW, Statistics, TOA, Clear_sky and Total_sky	Wm ⁻²	TBD	1/(3hr) [avg]	1.0° × 1.0° :: G	Synoptic OLR at 3-hour intervals
Radiative Flux, SW, Statistics, TOA, Clear_sky and Total_sky	Wm ⁻²	TBD	1/(3hr) [avg]	1.0° × 1.0° :: G	Synoptic solar radiation at 3-hour intervals
Radiative Flux, LW, Statistics, TOA, Clear_sky, Total_sky, Monthly_Avg	Wm ⁻²	3 Wm ⁻² :: 2 Wm ⁻²	1/mon	1.0° × 1.0° :: G	Monthly averages of longwave radiation
Radiative Flux, SW, Statistics, TOA, Clear_sky, Total_sky, Monthly_Avg	Wm ⁻²	4 Wm ⁻² :: 3 Wm ⁻²	1/mon	1.0° × 1.0° :: G	Monthly averages of shortwave radiation

Top-of-atmosphere radiative fluxes: Gridded data

of the EOS instruments. Clouds affect almost all of the EOS observations, and, as a result, the different measurement strategies used by each instrument provide fundamentally different information on cloud properties:

- **MODIS:** Provides high-spatial-resolution, global, cloud-property measurements. This instrument represents a major improvement in global cloud measurements for a wide range of cloud properties. MODIS is the prime instrument for EOS cloud-property measurements. Roughly 12 cloud spectral channels, 0.25- to 1-km fields of view.
- **ASTER:** Extremely high-spatial-resolution regional data used to verify the effect of sub-pixel cloud variability on MODIS global cloud retrievals. Eight cloud spectral channels, 15-m-to-90-m spatial resolution for selected 60-km regions.
- **MISR:** Multi-angle views (9 along-track views from nadir to 70° fore and aft) with high spatial resolution (275 m to 1.1 km) in 4 solar spectral channels. Used for narrowband cloud anisotropy measurements as well as stereo cloud heights for broken cloud fields. Especially useful for studies of the anisotropy of non-plane-parallel broken cloud fields, and non-spherical ice particles (Kahn et al. 1996).
- **AIRS:** High-spectral-resolution but coarse-spatial-resolution infrared data used to measure the spectral variation of cloud emittance and confirm the interpretation of cloud particle phase and size determined using higher-spatial-resolution but coarser-spectral-resolution MODIS data. Up to 2300 spectral channels in a 14-km field of view.
- **EOSP:** Unique solar-reflected radiation polarization measurements at coarse spatial resolution (10 km). Useful at small optical depths and for cloud particle size and phase estimation. EOSP and MISR are the instruments most likely to have information on ice crystal shape.
- **GLAS:** Active lidar useful for remotely sensing cloud height and base of optically-thin clouds. Only nadir viewing. Offers the most accurate cloud screening and cloud-height checks of MODIS global cloud retrievals.
- **SAGE III, HIRDLS:** Height measurement and detection of extremely thin cloud in the upper troposphere or stratosphere (i.e., polar stratospheric clouds and thin

cirrus). Spatial resolution is very coarse (200 km) but these instruments give unique measurements of sub-visible clouds.

- **CERES:** Broadband, highly-calibrated coarse-spatial-resolution radiation-budget measurements. CERES data are used to constrain cloud-property retrievals in the CERES data products by providing a broadband TOA flux constraint. The objective of CERES cloud products for matched CERES/MODIS and CERES/VIRS fields of view is a radiatively consistent set of cloud and radiation data.
- **VIRS:** Provides an advance over current AVHRR for TRMM cloud measurements with 5 spectral channels, a 2-km nadir field of view, and on-board solar calibration. Data will be analyzed as part of CERES cloud/radiation data products.

Tables 2.8-2.17 summarize accuracies and space/time characteristics of the key cloud data products planned for EOS. The tables are presented individually for each major cloud property. Since accurate tools to objectively validate global cloud measurements have only recently become available, all estimates of global cloud property accuracies are very preliminary. The combination of multiple EOS sensors and new ground-based and aircraft-based instrumentation will provide a great improvement in the knowledge of the accuracy of cloud property measurements and their dependence on cloud type and climate region. As a minimum, accuracies will differ for clouds over ocean and land, for optically-thick versus thin clouds, and for low versus high clouds. The validation of these cloud properties will be a major effort within EOS and will require both dedicated field campaigns (e.g., FIRE) as well as long-term surface site data (e.g., ARM).

2.3.1.3.1 Cloud fractional area coverage

The fractional-area coverage of clouds over the globe should be monitored with the precision necessary to measure changes of a few percent in $2.5^\circ \times 2.5^\circ$ regions over a period of decades.

Our ability to measure the global distribution of tropospheric clouds from space will be greatly enhanced by MODIS, because of enhanced spatial resolution (250 m, 1 km) in the traditional visible and thermal infrared spectral channels, because of new spectral channels which will enhance the detection, cloud height, and particle size determination of thin cloud (1.38, 8.5, 13.3, 13.6, and 13.9 μm), and, finally, because of its greatly improved solar calibration using both on-board sources and lunar stabil-

TABLE 2.8

PARAMETER NAME	ACCURACY ABS::REL	TEMPORAL RESOLUTION	HORIZONTAL RESOL::COVER	VERTICAL RESOL::COVER	COMMENTS
MODIS Cloud Cover	0.05 :: 0.05	2/day [d,n]	5 km :: G	N/A :: Cloud	
MISR Cloud Fraction, Altitude-Binned (Nadir)	TBD :: TBD	1/(2-9 day) [d]	17.6 km :: G	4 km :: Atmos	

Cloud fractional area coverage

TABLE 2.9

PARAMETER NAME	ACCURACY ABS::REL	TEMPORAL RESOLUTION	HORIZONTAL RESOL::COVER	VERTICAL RESOL::COVER	COMMENTS
MODIS Cloud Height, Top	50 hPa :: 50 hPa	2/day	0.5° :: G	N/A :: Cloud	
AIRS Cloud Height, Top	0.5 km :: 0.25 km	2/day [d,n]	50x50 km :: G	N/A :: Cloud	
GLAS Cloud Height, Top	:: 75m	25 ms	70 km ::	75 m ::	
EOSP Cloud Pressure, Top	30 hPa :: 30 hPa	1/day [d]	40 km :: G	30 hPa :: Cloud_top	
HIRDLS Cloud Height, Top	0.4 km :: 0.4 km	2/day [d,n]	400x400 km :: G	0.4 km :: Trop	
SAGE-III Cloud Height, Top	0.2 km :: 5%	1/(2 min), 30/day	<2°x<1° :: G	0.5 km :: Strat/Trop	

Cloud height

TABLE 2.10

PARAMETER NAME	ACCURACY ABS::REL	TEMPORAL RESOLUTION	HORIZONTAL RESOL::COVER	VERTICAL RESOL::COVER	COMMENTS
MODIS Cloud Optical Depth	10% :: 20%	1/day [d]	5 km :: G	N/A :: Cloud	
MODIS Cloud Emissivity, Top	::	2/day	0.5° :: G	N/A :: Cloud	
AIRS Cloud Emissivity, IR Spectral (3-14 μm)	0.05 :: 0.025	2/day [d,n]	50x50 km :: G	N/A :: Cloud	
EOSP Cloud Optical Thickness	20% :: 10%	1/day [d]	40 km :: G	Column :: Cloud	
GLAS Thin Cloud /Aerosol Optical Depth	20% ::	1/(2-16 day)	2-100 km :: G	N/A :: Atmos	For thin clouds only

Cloud optical depth and IR emissivity

TABLE 2.11

PARAMETER NAME	UNITS	ACCURACY ABS::REL	TEMPORAL RESOLUTION	HORIZONTAL RESOL::COVER	VERTICAL RESOL::COVER	COMMENTS
MODIS Cloud Particle Phase	water/ice	90% Conf :: 90% Conf	2/day [d,n]	5 km :: G	N/A :: Cloud	
MODIS Cloud Particle Size (Effective Radius)	μm	0.4 :: 2.0	1/day [d]	5 km :: G	N/A :: Cloud	
EOSP Cloud Particle Phase	water/ice	:: 95% Corr	1/day [d]	100 km :: G	N/A :: Cloud_top	
EOSP Cloud Particle Size	μm	25% :: 25%	1/day [d]	100 km :: G	N/A :: Cloud_top	

Cloud particle size and phase

TABLE 2.12

<i>PARAMETER NAME</i>	<i>ACCURACY Abs::REL</i>	<i>TEMPORAL RESOLUTION</i>	<i>HORIZONTAL RESOL::COVER</i>	<i>VERTICAL RESOL::COVER</i>	<i>COMMENTS</i>
AMSR-E Cloud Liquid_Water Content	3 mg cm ⁻²		14 km :: Ocean	N/A :: Trop	Pixel-scale observations
AMSR-E Cloud Liquid_Water Content	1 mg cm ⁻²	1/day	1.0° ::	N/A :: Trop	Spatial averages for daily maps

Cloud liquid water path

ity checks. Multi-angle observations in shortwave channels from MISR will provide improved angular directional models for use in cloud detection. ASTER will provide data to verify the effect of beam filling on MODIS cloud detection, especially for small cumulus clouds over land.

2.3.1.3.2 Cloud height

In order to understand the role of clouds in the longwave radiation balance and to monitor interannual variability in the distribution of cloud top height, it is desirable to obtain cloud top height measurements with an accuracy of about 0.3 km for monthly means. This gives an uncertainty in the cloud top temperature for tropospheric clouds of about 2 K, and an uncertainty in blackbody emission of about 3 Wm⁻² for low clouds in the tropics, and less for colder clouds. The spatial resolution of the basic measurements should be close to 250 m, in order to avoid errors associated with partially-filled scenes.

A variety of instruments will give information on cloud top heights or pressures. The best combination of

spatial resolution and global coverage will be provided by MODIS, but other instruments will provide cloud height data based on other techniques, which will add value to the cloud top height data set. AIRS cloud data sets can be determined in conjunction with high-quality determinations of the temperature and humidity fields. GLAS will provide very precise and sensitive data on cloud top from lidar measurements, but only along the satellite ground track. These data will be very useful for validating other methods of cloud height determination and also for detecting cloud tops in polar darkness and above snow where other methods may have large uncertainties. EOSP makes use of polarization information, which other instruments do not. HIRDLS, MLS, and SAGE III use limb measurements of the atmospheric emissivity in different wavelength regions and can give information on thin clouds in the stratosphere and upper troposphere.

TABLE 2.13

<i>PARAMETER NAME</i>	<i>ACCURACY Abs::REL</i>	<i>TEMPORAL RESOLUTION</i>	<i>HORIZONTAL RESOL::COVER</i>	<i>VERTICAL RESOL::COVER</i>	<i>COMMENTS</i>
AIRS/AMSU Temperature Profile	1.0 K :: 0.4 K	2/day [d,n]	50 × 50 km :: G	1 km :: Atmos	
MODIS Temperature Profile	0.5 K :: 0.5 K	2/day	5 km :: G (clear)	:: Atmos (20 levels)	
HIRDLS Temperature Profile	1 K < 50 km; 2 K > 50 km :: 0.3 K < 50 km; 1 K > 50 km	2/day [d,n]	400 × 400 km :: G	1 km :: 5-130 km	
MLS Temperature Profile	<2 K :: 0.2-1 K	2/day [d,n]	1.3° × 2.5° :: 82°N-82°S	2 km :: 5-80 km	
SAGE-III Temperature Profile (O ₂ Conc.), Solar	2 K :: 2K	1/(2 min), 30/day	<2° × <1° :: G	1 km :: 6-70 km	
TES Temperature Profile	2 K :: 0.2 K	1 (4-day survey) /mon	53 × 169 km :: G	4-6 km :: 0-33 km	

Atmospheric temperature profile

2.3.1.3.3 Cloud visible optical depth and infrared emissivity

Cloud visible optical depth is an integrated measure of the reflecting power of a cloud at visible wavelengths, which accounts for reflection by both liquid water and ice. The relationship between visible optical depth and reflected solar radiation depends on the solar zenith angle, the albedo of the underlying surface, and a number of variables of lesser importance. Radiative fluxes are most sensitive to changes in cloud optical depth when the optical depth is relatively small where the most precision in measurement is therefore required. Global remote measurements of cloud optical depth should have a detection threshold of 0.05 and an accuracy of about 20%.

2.3.1.3.4 Cloud particle size and phase

Cloud particle size has importance for the formation of clouds and precipitation, and also for the radiative effects of clouds. For water clouds the optical depth is approximately proportional to LWP divided by cloud particle radius, so percentage errors in LWP and cloud radius are about equally important for deducing the relationship between cloud substance and cloud optical depth. For a fixed LWP, the albedo of a water cloud varies by about 0.2 as the effective droplet radius is changed from 5 μm to 25 μm . If the insolation is 400 Wm^{-2} , then an albedo accuracy of about 0.01 is required to give an accuracy in absorbed solar radiation of 5 Wm^{-2} . In order to obtain this accuracy in computing albedo from observations of LWP and effective radius, the effective radius should be known to an accuracy of 1.25 μm . It is anticipated that the effective radius of clouds may be obtainable with this accuracy from MODIS, MISR, and EOSP measurements. These instruments may also be used to distinguish ice clouds from water clouds with a certainty of 95%.

2.3.1.3.5 Cloud liquid/ice water path

Cloud liquid/ice amounts can be inferred from visible optical depth using a model, if the effective particle radius and phase are known. Observations of LWP over water surfaces can be obtained in a different way, from microwave measurements (e.g., MIMR or AMSR). Albedo increases most rapidly with liquid water content when the liquid water content is small; albedo becomes only weakly sensitive to liquid water amount changes when the liquid water amount is large. From the perspective of its effect on planetary albedo then, precision in the measurement of relatively small values of liquid water below about 5 mg cm^{-2} is required. A precision of about one part in fifty within this range, or 0.1 mg cm^{-2} is necessary to give the required accuracy of 5 Wm^{-2} for fluxes

of solar radiation. This accuracy in LWP is much higher than that offered by the methods available for inferring it.

2.3.1.3.6 Lightning

Lightning flashes associated with electrical discharges in clouds can be detected from space. These observations provide a global survey of thunderstorm occurrence and cloud electrification processes. LIS will detect such occurrences with a relatively inexpensive instrument on TRMM and succeeding satellites. LIS will provide a wide variety of data on the number, location, and intensity of lightning flashes as observed by a spaceborne camera.

2.3.1.4 Atmospheric temperature profiles

In order that temperature profile measurements from satellites can provide a significant benefit to current weather forecasting efforts, it has been determined that profiles with an accuracy of 1 K for vertical scales on the order of 1 km are required. In addition, horizontal spatial resolution of 50 km or less is desirable to better define the positions of fronts and other thermal features. The AIRS instrument was designed with these requirements in mind. High spatial resolution and scanning capability are required so that the effects of clouds on the infrared radiances used for sounding can be minimized. The addition of AMSU microwave channels improves the capability of the AIRS instrument to provide accurate temperature profiles under partly cloudy conditions.

MODIS provides a backup temperature profile retrieval capability about equal to that of current operational instruments. Other instruments provide measurements of temperature with lower horizontal resolution either by limb-viewing in the stratosphere (HIRDLS, MLS, SAGE III) or as a required adjunct to retrievals of atmospheric chemical constituents (TES).

Most modern data assimilation systems for use in numerical weather prediction assimilate radiances from satellite temperature sounders rather than inverted temperatures. This is because the inversion process is underdetermined for the high vertical resolution used in weather prediction models, so that the inversion is often an optimal modification of an a priori profile. The model forecasts often contain realistic temperature variations of small vertical scale that cannot be resolved with nadir sounding channels, and the assimilation of remote sounding data should not corrupt this information. It is better to modify the model temperature profile optimally to conform to the radiances, than to make the model temperatures conform to an inverted temperature profile based on some other a priori temperature profile. This process can be incorporated into the data assimilation system with all

TABLE 2.14

PARAMETER NAME	UNITS	ACCURACY ABS::REL	TEMPORAL RESOLUTION	HORIZONTAL RESOL::COVER	COMMENTS
AIRS Level-1B Radiance	Wm^{-2} $\text{sr}^{-1} \mu\text{m}^{-1}$	0.2° NEdT :: 0.2° NEdT	2/day [d,n]	15 × 15 km :: G	
AMSU Level-1B Radiance	K	0.2° NEdT :: 0.2° NEdT	2/day [d,n]	15 × 15 km :: G	
HSB Level-1B Radiance	K	0.2° NEdT :: 0.2° NEdT	2/day [d,n]	15 × 15 km :: G	

Radiances for temperature profiling

TABLE 2.15

PARAMETER NAME	ACCURACY ABS::REL	TEMPORAL RESOLUTION	HORIZONTAL RESOL::COVER	VERTICAL RESOL::COVER	COMMENTS
AIRS/AMSU/HSB Humidity Profile g/kg	10% (goal) :: 5%	2/day [d,n]	50 × 50 km :: G	2 km :: Atmos	
AIRS/AMSU/HSB Precipitable Water (mm)	5% :: 3%	2/day [d,n]	50 × 50 km :: G	N/A :: Atmos	
AMSR-E Precipitable Water (g/cm ²)	0.2 g cm ⁻² ::		14 km :: Ocean	Column :: Trop	MIMR also planned for METOP-1.
AMSR-E Precipitable Water - gridded	<0.1 g cm ⁻² ::	1/day	1.0° ::	Column :: Trop	MIMR also planned for METOP-1.
HIRDLS H ₂ O Concentration	5-10% :: 1-10%	2/day [d,n]	400 × 400 km :: G	1 km :: 5-70 km (given accuracies for 7-70 km)	
HIRDLS H ₂ O Concentration - gridded	5-10% :: 1-10%	2/day [d,n]	4° × 4° :: G	1 km :: 5-70 km	
MLS H ₂ O Concentration	<5% :: 1-10%	2/day [d,n]	1.3° × 2.5° :: 82°N-82°S	2 km :: 5-80 km	
MODIS Water Vapor Profile	5-50 % :: 6-50 %	2/day	5 km :: G (clear)	:: Atmos (15 levels)	
SAGE-III H ₂ O Conc & Mixing Ratio, Solar	10% :: 15%	1/(2 min), 30/day	<2° × <1° :: G	1 km :: 3-50 km	
SAGE-III H ₂ O Conc & Mixing Ratio, Lunar	10% :: 15%	1/(2 min), 30/day	<2° × <1° :: G	1 km :: 3-50 km	
TES H ₂ O/HDO Mixing Ratio	:: 0.5-50 ppmv	1 (4-day survey) /mon	53 × 169 km :: G	2-6 km :: 0-33 km	

Water vapor profiles and precipitable water vapor column

other data types if a forward radiative transfer model for the sounding channels is available. For these reasons radiances for the frequency intervals required for sounding temperature and humidity must be made available to operational weather prediction centers within two-to-three hours of collection, so that they may be assimilated and contribute to timely forecasts. For the desired precision of 1 K in temperature sounding, these radiances must have an accuracy corresponding to 0.2 K noise equivalent temperature difference. AMSU and HSB provide microwave radiances that improve soundings of temperature and humidity in the presence of clouds.

2.3.1.5 Water vapor

Water vapor measurements in the atmosphere are critically important for many purposes. Water vapor mass mixing ratios vary from about 20 g/kg in the tropical boundary layer to less than 1 g/kg in the Arctic winter. Humidities vary between about 10% and 100% of the saturation value for a particular location. Water vapor decreases upward because of the decrease of temperature with altitude and reaches values around 2 ppm near the tropical tropopause. From the perspective of its effect on the energy balance of the Earth, about the same fractional precision at all levels of the atmosphere is required because a molecule of water at the tropopause is much more effective in reducing emitted energy than a molecule of water vapor in the tropical boundary layer. This precision is required for layers of about equal thickness in height at all levels. An accuracy of 5-10% is very useful. Such accuracy is difficult to achieve at all levels with a single instrument. AIRS/AMSU/HSB provide good spatial resolution and adequate vertical resolution in the lower troposphere, while limb-viewing instruments such as SAGE III, HIRDLS, and MLS provide good vertical resolution and precision in the upper troposphere and lower stratosphere. Profiles of somewhat less accuracy and resolution can also be obtained from IR channels on MODIS, when AIRS/AMSU/HSB are not available.

2.3.1.6 Precipitation

Measurement of precipitation by passive remote sensing from space is a developing science. Requirements for spatial and temporal resolution and accuracy vary widely depending on the application. For global-scale studies and climate model validation, averages over 100-km \times 100-km regions with accuracies of 10% would be extremely useful. The primary technology for estimating precipitation globally during the EOS period will be passive remote sensing from microwave imagers such as MIMR and AMSR-E, which have comparable capabilities. The ac-

curacies for these measurements will likely be less than required, but will represent an improvement over current estimates. In the tropical regions precipitation estimates will also be available from the precipitation radar on TRMM.

2.3.1.7 Winds and circulation

Direct wind measurements with an accuracy of 10% for wind speed and a 20° random error would be very useful. Such measurements for near-surface winds over the ocean are attainable with scatterometers such as SeaWinds. Wind speed estimates with comparable accuracy are also available from passive microwave radiometers, and the along-track data from the Dual-Frequency radar Altimeter (DFA). Sea-surface wind velocity measurements are very useful for calculating air-sea exchange of heat, momentum, and moisture between the ocean and the atmosphere, and are also useful in validating surface wind simulations in climate models and numerical weather prediction models.

No direct measurements of wind speed in the free troposphere or in the boundary layer over land will be included in the planned phases of EOS. Wind vectors in the free troposphere will be derived indirectly by assimilating data into a global model. Direct measurement of tropospheric winds with lidar would be very useful for both weather forecasting and climate modeling, but this capability was eliminated from the EOS program for cost reasons. New technologies that would make direct wind measurements economically and reliably from space should be pursued.

2.3.2 Critical surface observations and field experiments

A vital component of any Earth observing system aimed at obtaining long-term global observations of multiple components of the Earth-atmosphere-ocean system is a well-coordinated ground-based monitoring network together with periodic field experiments. The importance of this part of any integrated global climate observing system cannot be underestimated. This component is vital for the purposes of: 1) assessing the accuracy of satellite-derived geophysical parameters, such as aerosol optical thickness, surface radiation budget components, cloud top altitude, sea surface temperature, total ozone content, etc.; 2) evaluating the precision and accuracy of the satellite sensor calibration through intercomparison of satellite measurements with calculations based on radiative transfer computations using surface and aircraft measurements of atmospheric composition; and 3) providing enhanced information on the characteristics of

TABLE 2.16

<i>PARAMETER NAME</i>	<i>ACCURACY Abs::REL</i>	<i>TEMPORAL RESOLUTION</i>	<i>HORIZONTAL RESOL::COVER</i>	<i>VERTICAL RESOL::COVER</i>	<i>COMMENTS</i>
AMSR-E Precipitation (Land)	100% ::		6 km :: Land		MIMR also planned for METOP-1.
AMSR-E Precipitation (Ocean, 2 layers)	50% ::		14 km :: Ocean		MIMR also planned for METOP-1.
AMSR-E Precipitation (Land) mapped	20% ::	1/day	1.0° ::		MIMR also planned for METOP-1.
AMSR-E Precipitation (Ocean) mapped	10% ::	1/day	1.0° ::		MIMR also planned for METOP-1.

Precipitation

TABLE 2.17

<i>PARAMETER NAME</i>	<i>UNITS</i>	<i>ACCURACY Abs::REL</i>	<i>TEMPORAL RESOLUTION</i>	<i>HORIZONTAL RESOL::COVER</i>	<i>COMMENTS</i>
SeaWinds Wind Vectors, Near_Surface	m s ⁻¹ ,dg	> of 2 m s ⁻¹ or 10% rms (speed); 20° rms (direction) ::	90% of oceans every 2 days	50 km :: Ocean (1600 km swaths)	
AMSR Wind Speed, Sea_sfc	m s ⁻¹	1.5 m s ⁻¹ ::		14, 25 km :: Ocean	MIMR also planned for METOP-1.
AMSR-E Wind Speed, Sea_sfc-averaged	m s ⁻¹	<0.5 m s ⁻¹ ::	1/day	1.0° ::	MIMR also planned for METOP-1.
Radar Altimeter Wind Speed, Along-track	m s ⁻¹	2 m s ⁻¹ ::		7 km :: Ocean	

Wind speed and direction near the ocean surface

surface and atmospheric constituents assumed in the remote-sensing retrievals using satellite observations. Space, surface, and aircraft approaches are all required to observe the range of critical physical processes that occur from the microscale (e.g., microphysical properties of clouds) to the macroscale (e.g., basin-wide SST variations associated with El Niño). To this end, many surface observational networks and airborne field experiments have been established. Highlighted below is a selection of these extremely important programs, emphasizing their role in improving the understanding of the role of clouds and radiation in climate.

2.3.2.1 FIRE

FIRE is an ongoing multi-agency, international program to support the development of improved cloud radiation parameterization schemes for use in climate models, to provide an assessment of the accuracy of ISCCP-derived

cloud products, and to test and develop new remote-sensing methods for future spaceborne missions and to assess their accuracy through intercomparisons with in situ microphysical measurements. FIRE has been conducted in two phases, the first from 1985-1990 and the second from 1991-1995, and has thus far concentrated on two cloud types: marine stratocumulus and cirrus.

Marine stratocumulus clouds exert a large influence on the radiation balance of the Earth-atmosphere-ocean system through their large areal extent, temporal persistence, and high reflectivity to solar radiation. Cirrus clouds, on the other hand, exert their greatest radiative influence on the Earth's climate through their effects on longwave radiation emitted to space. Both of these cloud types are spatially and temporally persistent in the Earth's atmosphere, and both create difficulty in the remote sensing of cloud properties from spaceborne sensors. As a direct consequence of the need to determine

the optical and microphysical properties of clouds from present and future spaceborne systems, such as MODIS, a need arose to conduct intensive field observations (IFOs) of marine stratocumulus and cirrus clouds. These two field campaigns, conducted as major components of FIRE (Cox et al. 1987), have focused exclusively on these two cloud types. Largely as a result of these four field experiments (conducted in 1986 and 1987; repeated and enhanced in 1991 and 1992), the radiative and microphysical properties of these cloud systems have been more extensively studied than others.

In all of these intensive field campaigns, emphasis has been placed on coordination between aircraft-, spacecraft-, and ground-based observing systems, and has led to a number of important insights. For marine stratocumulus clouds, outstanding problems include the discrepancy between observations and theory of the absorption of solar radiation by clouds, the discrepancy between remote sensing and in situ estimates of the effective droplet radius derived from spectral reflectance measurements, and the variability and spatial structure of stratocumulus clouds derived both from reflection and transmission measurements. For cirrus clouds, the thermal emission characteristics of these clouds suggest that the effective radius of ice crystals is much smaller than previously believed and, in addition, the thermal emittance of cirrus clouds is generally less than theoretically predicted for a given value of the visible albedo. These important results, described in detail by King (1993), lead immediately to the conclusion that carefully planned airborne field campaigns, together with coincident ground-based observations, are essential for assessing the accuracy and validity of satellite-derived geophysical cloud properties. Plans are currently being developed for FIRE phase III, which will likely include campaigns in complex environments such as Arctic stratus clouds overlying sea ice, a regime for which remote sensing of cloud properties from space is especially difficult.

2.3.2.2 GEWEX

GEWEX is an international program of the WCRP that focuses on observing and modeling the hydrologic cycle and energy fluxes in the atmosphere, at the land surface, and in the upper layers of the oceans. This enormous program plans to compare results from ongoing process studies aimed at improving the parameterization of clouds, radiation, and surface processes with coincident satellite observations and modeling studies (Chahine 1992). As such, it has a considerable validation component that will prove a valuable source of data to assess the accuracy of satellite retrieval schemes such as the remote sensing of

atmospheric temperature and moisture profiles, vertically integrated water vapor (precipitable water), cloud base altitude, surface longwave flux, and cloud optical and microphysical properties. Since passive satellite observations are especially sensitive to cloud top properties, a valuable role of GEWEX is assessing the longwave radiation flux reaching the Earth's surface under cloudy conditions in both a dry and humid environment. Here again a combination of surface observations, temperature and moisture soundings, focused airborne observations, and modeling studies will provide an opportunity to assess the accuracy of satellite-derived geophysical properties and to translate the results of process studies to the global scale.

The GEWEX program will focus on five main components of the hydrologic cycle: clouds and radiation, atmospheric moisture, precipitation, ocean fluxes, and land surface processes. Since current satellite-derived moisture data are accurate to ~10-20% over the oceans and 20-30% over the land, since water vapor is the most important greenhouse gas, and since clouds and their radiative properties play a major role in cloud feedback processes, process studies such as GEWEX are vital to enhancing the value of the spaceborne observations to be provided as part of the Earth Science Enterprise (ESE) program (TRMM, EOS AM-1, EOS PM-1). Over the oceans, two current experiments are providing valuable data on ocean fluxes, including cloud radiative properties, TOGA and the World Ocean Circulation Experiment (WOCE). In late 1992 and early 1993 COARE was conducted in the western tropical Pacific as part of the TOGA program, and this large multinational and multiagency program obtained numerous data sets on cloud radiative and microphysical properties as well as passive and active microwave measurements of precipitation patterns. This valuable data set will provide much needed information that will enable algorithms to be tested and evaluated for both the EOS (MODIS, GLAS, AMSR) and TRMM programs.

2.3.2.3 Climate Variability (CLIVAR) Project

The CLIVAR Project of the WCRP (WCRP 1995) seeks to understand and predict climate variability on interannual-to-centennial time scales. It is initially organized into three component programs. CLIVAR-Global Ocean Atmosphere Land System (GOALS) will study seasonal-to-interannual variability and prediction, CLIVAR-DecCen will study decadal-to-centennial variability and predictability, and CLIVAR-ACC will study modeling and detection of anthropogenic climate change. The science goals of EOS intersect strongly with the goals

of CLIVAR in the areas of radiation, clouds, water vapor, precipitation, and atmospheric circulation, as well as in other areas.

2.3.2.4 ARM

The ARM Program (Stokes and Schwartz 1994) is a research program of the U. S. Department of Energy (DoE) and is the largest component of DoE's contribution to the USGCRP. This program is aimed at assessing the radiative properties of the atmosphere under both clear and cloudy conditions, and thus consists of a sophisticated measurement program from ground-based facilities as well as from remotely-piloted aircraft. ARM is therefore complementary to NASA's Earth Science Enterprise in that it provides an intensive ground-based component that emphasizes process studies focused on two related scientific issues in the development of models to assess human impact on climate: 1) radiative energy transport and 2) cloud formation, maintenance, and dissipation.

The measurement program will focus on Cloud and Radiation Testbed (CART) sites consisting of facilities at three key locales around the world: 1) the SGP of the U. S., 2) the western tropical Pacific, and 3) the north slope of Alaska. Each of these sites will characterize the broadband and spectral components of both longwave and shortwave radiation reaching the Earth's surface, as well as measure the water vapor, temperature, and wind profiles throughout the lower atmosphere. These measurements will aid both in improving parameterization of the radiative properties of the atmosphere for use in GCMs and as ground and airborne calibration/validation sites for EOS sensors such as CERES, MODIS, AIRS, MISR, and EOSP. All three of these distinct climatological regimes will be well characterized by the time of the launch of the first EOS AM-1 platform in 1998, and can thus be used as prime locations for intercomparisons of clear sky, aerosol, and cloud properties (including cloud base altitude). Finally, in addition to the CART sites, the ARM program has an aggressive modeling component, including radiative transfer, cloud formation, and data assimilation.

2.3.2.5 BSRN

The BSRN (WCRP 1991) is an international program of the WCRP designed to improve the accuracy and sampling rate of surface-measured shortwave and, especially, longwave radiative fluxes. Data collection has recently begun at a few sites, and should increase to about 30 sites within the next few years. A key element of these data is the provision of downward longwave flux at the surface at all BSRN stations, since most observational records at the surface cover shortwave fluxes only. The recom-

mended BSRN instrument complement includes: shortwave total, direct, and diffuse downward fluxes, longwave downward fluxes, and synoptic and upper-air observations. Expanded measurements at some sites will include lidar for cloud base altitude and direct solar spectral irradiance at specified wavelengths for aerosol optical properties. These data will provide a critical database for validation of satellite-inferred downward shortwave and longwave radiative fluxes and for monitoring long-term trends.

2.3.2.6 ECLIPS

Another key international experiment is the Experimental Cloud Lidar Pilot Study (ECLIPS) (Platt et al. 1994). ECLIPS is designed to obtain observations of cloud backscattering profiles (including cloud base altitude and cloud top altitude for optically-thin cloud) from about 10 participating ground-based lidar sites around the world. About half of these sites provide lidar depolarization measurements to distinguish water and ice clouds, and several use uplooking 11- μm radiometers to provide improved estimates of cloud optical depth. The ECLIPS lidar systems have derived nearly continuous cloud observations for two experiment months, and conducted a third experiment in conjunction with Lidar In-space Technology Experiment (LITE), a lidar system successfully flown on space shuttle Discovery in September 1994 (STS-64). These lidar systems provide a unique and objective data set for cloud base altitude for all cloud types, including cirrus. For cloud base altitudes below 4 km, the NOAA ceilometer database will also be a critical data source.

2.3.2.7 Ties to other research areas

2.3.2.7.1 Oceanic processes

The storage and transport of heat by the ocean are strongly affected by surface forcing of momentum, heat, and moisture through interaction with the atmosphere. The surface thermal forcing of the ocean is composed of radiative (shortwave and longwave) and turbulent (sensible and latent) heat fluxes. The most viable method of monitoring these fluxes over adequate temporal and spatial scales is by spaceborne sensors. Scatterometry and passive microwave imaging can give surface wind stress over the ocean, which is key to momentum, heat, and moisture exchange rates.

The relative accuracy of surface solar irradiance derived from satellite data has been found to be sufficient in monitoring the seasonal cycle over most of the ocean and the interannual anomalies over the tropical oceans. The surface flux derived from satellite data has been used to study the evolution of major climate signals, such as

the ENSO (e.g., Liu and Gautier 1990; Chertock et al. 1991). It has also been used to examine the feedback of cloud and atmospheric circulation on SST changes over the global ocean (Liu et al. 1994). Cloud and moisture feedbacks are important for the seasonal-to-interannual predictability associated with ENSO.

The surface heat flux could be integrated to give the mean meridional heat transport by the ocean. In the past, only meteorological reports from volunteer ships were used (Tally 1984), but satellite data have the potential of providing better coverage. To adequately resolve the meridional heat transport, an absolute accuracy of better than 10 Wm^{-2} in the total heat flux is required (WCRP 1982). While surface shortwave radiation estimates from satellite data approach this accuracy, the estimation of other components needs improvement. Such improvement is expected in the next decade with the launching of advanced sensors for surface wind and atmospheric temperature and humidity soundings.

The radiation that penetrates the ocean surface, particularly within the photosynthetically-active range (0.4–0.7 μm), is important to ocean biological productivity and the distribution of chemical species in the ocean (Platt et al. 1988). The monitoring of ocean surface solar irradiance, together with observations from future ocean color sensors, will also advance our understanding of the biogeochemical cycle in the ocean.

2.3.2.7.2 Land processes

Clearly radiation, clouds, water vapor, and precipitation interact strongly with land surface processes. Information on all components of the surface radiation budget is vital for land surface studies, covering the gamut from land surface climatology to ecology. Precipitation and

evaporation control the availability of surface moisture for plants, animals, and people. Large-scale circulations provide a supply of moisture to the land and exchange other gaseous compounds of importance between land areas and the rest of the globe.

It is clear that currently the surface radiation balance is not modeled well in climate or numerical weather prediction models (Nobre et al. 1991; Shuttleworth and Dickinson 1989). It is also clear that realistic changes in land surface albedo, brought about by land use change, could have a large influence on continental climatologies (Nobre et al. 1991; Lean and Warrilow 1989). Lastly, increasing evidence of the linkages between a region's cloud climatology and its surface hydrometeorology is being seen. The role of vertical water recycling in Amazonia in maintaining the "protective" cloud layer over the region is just beginning to be understood. A detailed, reliable global data set on the surface radiation budget and surface albedo is urgently needed if the models are to be improved.

Global carbon cycle (fast component): Global photosynthesis and fast cycle respiration are closely tied to the energy and water cycles, and so in large part they depend on the terms discussed above. In addition, the incoming flux of photosynthetically-active radiation (0.4–0.7 μm) is a critical forcing of photosynthesis (Sellers and Schimel 1993).

Ecology and global carbon cycle (slow component): The biogeography of the world's vegetation is closely coupled to the physical climate system. Key drivers are water availability and temperature that determine the rate of soil respiration and litter turnover. These factors are in turn linked to the surface radiation climatology, precipitation, and evaporation.

2.4 Summary of EOS contributions

2.4.1 Observation and monitoring of key climate variables

2.4.1.1 Total solar irradiance

The EOS/ACRIM experiment was selected to provide the total solar irradiance database during the EOS mission. The ACRIM measurement approach, capable of providing the maximum precision for the long-term TSI database with current measurement technology, employs an "overlap strategy" in which successive ambient temperature TSI satellite experiments are compared in flight, transferring their operational precision to the database. ACRIM

flight instrumentation has demonstrated a capability of providing annual precision smaller than 10 ppm of the TSI.

A successful deployment of ACRIM using the mission overlap strategy will provide a high-quality, continuous record of total solar irradiance variability that may be linked with prior measurements and continued into the foreseeable future. This would provide a basis for evaluating the role of variability in solar energy output in climate variability, and allow a clear separation between solar-caused climate change and other causes,

including greenhouse gases released by human industrial activity. Such a clear separation of causes is critical to the assessment of the causes of climate change and predictions of future changes.

2.4.1.2 Radiative energy fluxes—TOA, surface, atmospheric

Satellite remote sensing, in situ data, and models will be brought together under EOS to provide a global, homogeneous data set of observations of radiative fluxes at the TOA, at the surface, at the tropopause, and at intervening layers of the atmosphere (in order of priority). Because of both improved instrumentation and improved techniques for estimating radiative energy fluxes, the radiative flux estimates produced by EOS will be useful in understanding climate and in validating models to predict future climate variability and change. Key contributions will come from improved calibration, improved spatial and spectral resolution of the MODIS solar and IR imager, improved directional information from MISR, improved sampling in space, time, and angle and greater accuracy from CERES, and better methods to incorporate cloud information in flux estimates.

2.4.1.3 Cloud properties

Cloud property detection and monitoring are essential both for understanding the maintenance of the current climate and for observing seasonal and interannual shifts in cloud distributions that may be related to natural or anthropogenic climate variability. Instruments to be flown as part of EOS provide unprecedented capabilities for monitoring the properties of clouds with detail and precision not previously possible. Critical instruments include MODIS, CERES, MISR, and EOSP. They will provide not only improved technology for determining critical cloud properties from space, but also better calibration for determining long-term trends.

2.4.1.4 Precipitation

Global precipitation measurements, currently in a rather unsatisfactory state, will be greatly improved during the EOS era. The combination of visible/infrared imaging, microwave imaging, and rain radar on the TRMM mission will provide a revolutionary data set of precipitation observations in the tropics, and will also lead to improvement in algorithms for precipitation estimation from combined VIS/IR and microwave imaging. Adequate temporal and spatial sampling by better quality microwave imagers such as MIMR and AMSR will improve precipitation estimates over the oceans, and provide a high-quality, long-term data set of the type required for

seasonal-to-interannual and longer-term prediction research and testing.

2.4.2 Understanding of the processes that relate clouds and water vapor to global climate and their effect on climate sensitivity

Critical climate sensitivity mechanisms involve radiation, clouds, and water vapor. The global coverage, high-spatial-resolution, and high-spectral-resolution data from EOS can be used to better understand the processes that lie at the core of these sensitivity mechanisms. EOS will provide accurate global measurements of the exchange of energy between the Earth and space with sufficient spatial resolution and detail so that, when combined with observations of temperature, clouds, and water vapor, also to be provided by EOS, the role of clouds and water vapor in climate can be accurately assessed. The spatial resolution of some of the key instruments will be fine enough that the phenomena (e.g., convective cloud complexes in the tropics) involved in these processes can be resolved and their interactions with the larger-scale environment depicted, particularly those relating to the distribution of water vapor. These observations can be used to test explicit simulations of these phenomena using regional and cloud-scale models, and the observations and regional models together can be used to test and improve the parameterizations required in global climate models. This end-to-end validation of key processes involving clouds and water vapor in global climate models will greatly increase confidence in the validity of seasonal forecasts and predictions of global climate change.

2.4.3 More-accurate treatment of cloud and water vapor and their radiative effects in global climate models

Processes that control cloud properties and the distribution of atmospheric water vapor are critical to climate sensitivity and accurate climate forecasts. Current efforts to include more-explicit treatments of cloud water and ice in global climate models are hampered by insufficient understanding of the key physical processes and lack of adequate data for validation. The observations and associated scientific investigations to be provided by EOS are designed to improve this situation. Key contributions will be made in the areas of tropical mesoscale anvil clouds that accompany deep convection in the tropics. EOS will provide key microphysical and radiative properties of these clouds that will be helpful in determining how to represent the detrainment of ice from cumulus updrafts into anvil clouds. New observations of the ubiquitous and poorly understood thin cirrus that exists at all latitudes

will help to define the source of this cloud and its climatic importance.

Upper troposphere water vapor is maintained by some combination of detrainment from cumulus and synoptic-scale eddy fluxes. The SAGE III, MLS, and HIRDLS instruments that are part of EOS will provide greatly improved sampling of upper tropospheric water vapor, while AIRS will have the capability to derive a water vapor product analogous to that available from the operational satellites, but with greatly improved accuracy and vertical resolution.

Subtropical marine stratus and trade cumulus are important to climate models not only as a source of cloud feedback but also as a key deficiency that causes climate drift in coupled ocean-atmosphere GCMs. EOS will also allow improved analysis of observed relationships between the liquid water content of warm clouds and ambient temperature, a potentially powerful climate feedback mechanism.

A related question for GCMs is how to translate grid-scale predicted cloud water content into cloud albedo, given small-scale inhomogeneities. The 250-m resolution of MODIS is sufficient to capture the most important scales of inhomogeneity, permitting optical thickness probability density functions to be characterized for different cloud types. This combined with MODIS particle size estimates will help define parameterizations for albedo as a function of LWP.

Another particle size issue is the poorly defined indirect effects of aerosols on clouds, both the radiative effect of smaller droplets and the suppression of drizzle. EOSP and MISR will define the tropospheric aerosol distribution, which can be combined with MODIS optical thickness and particle size to isolate the indirect radiative effect. In principle, AMSR can complement this by measuring drizzle rates for stratus, but current microwave algorithms are insensitive to light precipitation.

A key to reducing uncertainty in climate model forecasts is to efficiently incorporate the new observations from EOS into the understanding and methodology that underlie cloud and precipitation parameterizations in climate models. The EOS interdisciplinary investigations will help catalyze a more-effective and productive interaction between theory, observation, and modeling.

2.4.4 Better measurement of precipitation and understanding of the role of precipitation in connecting atmospheric and surface processes, and more-accurate modeling of precipitation in global climate models

With improved measurements of global precipitation from TRMM and advanced microwave imagers such as MIMR

and AMSR, cloud properties from MODIS/MISR/EOSP, temperature and humidity from AIRS/AMSU/HSB, and surface wind patterns from scatterometry, it will be possible to more closely relate precipitation to the large-scale environment. This will enable much more rigorous testing of precipitation simulations in global weather prediction models, seasonal-to-interannual forecast models, and climate models.

2.4.5 Synergism with oceanic and land-surface processes

Radiation, clouds, water vapor, and precipitation are all closely related to important processes at the land surface and in the ocean. Improvements in these areas will interact very positively to improve understanding and simulation of land surface and oceanic processes. The ocean is driven by heat, momentum, and water fluxes at its surface, and these are all closely related to the water and energy budgets of the atmosphere and the processes that maintain them. The character of the land surface and its suitability for habitation are shaped by precipitation and the supply of radiant energy to warm the surface and evaporate water.

2.4.6 Enhanced assessment of global change: Monitoring and trend detection

The long-term (>15 years), accurate, global data sets for total solar irradiance, TOA, surface, and atmospheric radiation fluxes, temperature, humidity, cloud properties, precipitation, and winds that EOS will develop, will provide an unprecedented view of the global climate system that will be essential in developing assessments of climate variability and change. The diurnal, intraseasonal, seasonal, and year-to-year variability within this database will give a needed perspective on the natural variability on these time scales, and the relationships between the variables will provide insight into how the climate system operates. This perspective on the decadal variability of the climate system will be essential in reaching a consensus about what aspects of global change can be attributed to human activities, and what this information implies about future changes and their effects on humanity. In addition, variability on time scales from seasons to a decade is of great practical importance to humanity, and the global, homogeneous, long-term measurements of the climate system to be provided by EOS, together with the associated scientific research efforts, will result in improved ability to predict seasonal and interannual variability.

2.4.7 Improved predictions of future climates and the influence of climate change on humanity

The database to be assembled under the EOS program will provide a global picture of the Earth system from the relatively small scales of convection to the much larger scales of planetary circulation systems. This database will be critical in understanding climate sensitivity processes and assuring that they are adequately treated in global climate models used to predict future climates. Total solar irradiance, exchanges of energy between the Earth and

space, upper-tropospheric humidity, and global precipitation can all be measured very effectively from space and are all central to important climate maintenance and sensitivity mechanisms. These measurements, when combined with in situ measurements, models, and a well-directed program of scientific research, will lead to great enhancements in our ability to understand and predict global climate changes and their effects on human activities.

References

- Ackerman, S. A., W. L. Smith, J. D. Spinhirne, and H. E. Revercomb, 1990: The 28 October 1986 FIRE IFO case study: Spectral properties of cirrus clouds in the 8-12 micrometer window. *Mon. Wea. Rev.*, **118**, 2377–2388.
- Arking, A., and J. D. Childs, 1985: Retrieval of cloud cover parameters from multispectral satellite images. *J. Climate Appl. Meteor.*, **24**, 322–333.
- Arrhenius, S., 1896: On the influence of carbonic acid in the air upon the temperature of the ground. *Phil. Mag.*, **41**, 237–276.
- Baker, G. D. W., F. R. Emmitt, R. M. Robertson, J. E. Atlas, D. A. Molinari, J. Bowdle, R. M. Paegele, R. Hardesty, R. T. Menzies, T. N. Krishnamurti, R. A. Brown, M. J. Post, J. R. Anderson, A. C. Lorenc, and N. McElroy, 1995: Lidar-measured winds from space: A key component for weather and climate prediction. *Bull. Amer. Meteor. Soc.*, **76**, 869–888.
- Ballard, S. P., B. W. Golding, and R. N. B. Smith, 1991: Mesoscale model experimental forecasts of the Haar of northeast Scotland. *Mon. Wea. Rev.*, **119**, 2107–2123.
- Barkstrom, B., E. Harrison, G. Smith, R. Green, J. Kibler, and R. Cess, 1989: Earth Radiation Budget Experiment (ERBE) archival and April 1985 results. *Bull. Amer. Meteor. Soc.*, **70**, 1254–1262.
- Bates, J. J., X. Wu, and D. L. Jackson, 1996: Interannual variability of upper-troposphere water vapor band brightness temperature. *J. Climate*, **9**, 427–438.
- Baum, B. A., B. A. Wielicki, P. Minnis, and L. Parker, 1992: Cloud-property retrieval using merged HIRS and AVHRR data. *J. Appl. Meteor.*, **31**, 351–369.
- Baum, B. A., R. F. Arduini, B. A. Wielicki, P. Minnis, and C. T. Si, 1994: Multilevel cloud retrieval using multispectral HIRS and AVHRR data: nighttime oceanic analysis. *J. Geophys. Res.*, **99**, 5499–5514.
- Bengtsson, L., and J. Shukla, 1988: Integration of space and in situ observations to study global climate change. *Bull. Amer. Meteor. Soc.*, **69**, 1130–1143.
- Betts, A. K., 1990: Greenhouse warming and the tropical water budget. *Bull. Amer. Meteor. Soc.*, **71**, 1464–1465.
- Betts, A. K., and Harshvardhan, 1987: Thermodynamic constraint on the cloud liquid water feedback in climate models. *J. Geophys. Res.*, **92**, 8483–8485.
- Blau, H. H., R. D. Espinosa, and E. C. Reifenstein, 1966: Near-infrared scattering by sunlit terrestrial clouds. *Appl. Opt.*, **5**, 555.
- Bony, S., J. P. Duvel, and H. Le Treut, 1995: Observed dependence of water vapor and clear-sky greenhouse effect on sea surface temperature: comparison with climate warming experiments. *Climate Dynamics*, **11**, 307–320.
- Braun, S. A., and R. A. Houze, Jr., 1994: The transition zone and secondary maximum of radar reflectivity behind a midlatitude squall line: Results retrieved from Doppler radar data. *J. Atmos. Sci.*, **51**, 2733–2755.
- Budyko, M. I., 1969: The effects of solar radiation on the climate of the Earth. *Tellus*, **21**, 611–619.
- Cahalan, R. F., W. Ridgway, W. J. Wiscombe, S. Gollmer, and Harshvardhan, 1994: Independent pixel and Monte Carlo estimates of stratocumulus albedo. *J. Atmos. Sci.*, **51**, 3776–3790.
- Cahalan, R. F., D. Silberstein, and J. B. Snider, 1995: Liquid water path and plane-parallel albedo bias during ASTEX. *J. Atmos. Sci.*, **52**, 3002–3012.
- Cess, R. D., G. L. Potter, J. P. Blanchet, G. J. Boer, A. D. Del Genio, M. Deque, V. Dymnikov, V. Galin, W. L. Gates, S. J. Ghan, J. T. Kiehl, A. A. Lacis, H. Le Treut, Z.-X. Li, X.-Z. Liang, B. J. McAvaney, V. P. Meleshko, J. F. B. Mitchell, J. J. Morcrette, D. A. Randall, L. Rikus, E. Roeckner, J. F. Royer, U. Schlese, D. A. Sheinin, A. Slingo, A. P. Sokolov, K. E. Taylor, W. M. Washington, R. T. Wetherald, I. Yaga, and M.-H. Zhang, 1990: Intercomparison and interpretation of climate feedback processes in nineteen atmospheric general circulation models. *J. Geophys. Res.*, **95**, 16,601–16,615.
- Cess, R. D., G. L. Potter, M.-H. Zhang, J. P. Blanchet, S. Chalita, R. Colman, D. A. Dazlich, A. D. Del Genio, V. Dymnikov, V. Galin, D. Jerrett, E. Keup, A. A. Lacis, H. Le Treut, X.-Z. Liang, J. F. Mahfouf, B. J. McAvaney, V. P. Meleshko, J. F. B. Mitchell, J. J. Morcrette, P. M. Norris, D. A. Randall, L. Rikus, E. Roeckner, J. F. Royer, U. Schlese, D. A. Sheinin, J. M. Slingo, A. P. Sokolov, K. E. Taylor, W. M. Washington, R. T. Wetherald, and I. Yagai, 1991: Interpretation of snow-climate feedback as produced by 17 general circulation models. *Science*, **253**, 888–892.
- Cess, R. D., M. H. Zhang, G. L. Potter, H. W. Barker, R. A. Colman, D. A. Dazlich, A. D. Del Genio, M. Esch, J. R. Fraser, V. Galin, W. L. Gates, J. J. Hack, W. J. Ingram, J. T. Kiehl, A. A. Lacis, H. Le Treut, Z.-X. Li, X.-Z. Liang, J. F. Mahfouf, B. J. McAvaney, V. P. Meleshko, J. J. Morcrette, D. A. Randall, E. Roeckner, J. F. Royer, A. P. Sokolov, P. V. Sporyshev, K. E. Taylor, W. C. Wang, and R. T. Wetherald, 1993: Uncertainties in carbon dioxide radiative forcing in atmospheric general circulation models. *Science*, **262**, 1252–1255.
- Cess, R. D., and 33 co-authors, 1996: Cloud feedback in atmospheric general circulation models: An update. *J. Geophys. Res.*, **101**, 12,791–12,794.
- Chahine, M. T., 1974: Remote sounding of cloudy atmospheres. I. The single cloud layer. *J. Atmos. Sci.*, **31**, 233–243.

- Chahine, M. T., 1992: The hydrological cycle and its influence on climate. *Nature*, **359**, 373–380.
- Charlock, T. P., 1981: Cloud optics as a possible stabilizing factor in climate. *J. Atmos. Sci.*, **38**, 661–663.
- Charlock, T. P., 1982: Cloud optical feedback and climate stability in a radiative-convective model. *Tellus*, **34**, 245–254.
- Charlock, T., and F. Rose 1994: WMO/TD #593.
- Charlock, T., F. Rose, T. Alberta, G. L. Smith, D. Rutan, N. Manalo-Smith, P. Minnis, and B. Wielicki, 1994: Cloud profiling radar requirements: Perspective from retrievals of the surface and atmospheric radiation budget and studies of atmospheric energetics. *Utility and Feasibility of a Cloud Profiling Radar*, WCRP-84, IGPO Publication Series No. 10, Jan. 1994. B10–B21.
- Charlson, R. J., J. Langner, H. Rodhe, C. B. Leovy, and S. G. Warren, 1991: Perturbation of the Northern Hemisphere radiation balance by backscattering from anthropogenic sulfate aerosols. *Tellus*, **43AB**, 152–163.
- Charlson, R. J., S. E. Schwartz, J. M. Hales, R. D. Cess, J. A. Coakley, J. E. Hansen, and D. J. Hofmann, 1992: Climate forcing by anthropogenic aerosols. *Science*, **255**, 423–430.
- Charney, J. G., 1975: Dynamics of deserts and droughts in Sahel. *Quart. J. Roy. Meteor. Soc.*, **101**, 193–202.
- Chen, S. S., 1996: Tropical convection in the active and suppressed phases of TOGA-COARE ISO simulated by a three-dimensional mesoscale model, in prep.
- Chen, S. S., R. A. Houze, Jr., and B. E. Mapes, 1995: Multiscale variability of deep convection in relation to large-scale circulation in TOGA COARE. *J. Atmos. Sci.*, **53**, 1380–1409.
- Chertock, B., R. Frouin, and R. C. J. Somerville, 1991: Global monitoring of net solar irradiance at the ocean surface; climatological variability and the 1982–1983 El Niño. *J. Climate*, **4**, 639–650.
- Chou, M. D., 1991: The derivation of cloud parameters from satellite-measured radiances for use in surface radiation calculations. *J. Atmos. Sci.*, **48**, 1549–1559.
- Chou, M. D., A. Arking, J. Otterman, and W. L. Ridgway, 1995: The effect of clouds on atmospheric absorption of solar radiation. *Geophys. Res. Lett.*, **22**, 1885–1888.
- Coakley, J. A., Jr., and F. P. Bretherton, 1982: Cloud cover from high-resolution scanner data: Detecting and allowing for partially filled fields of view. *J. Geophys. Res.*, **87**, 4917–4932.
- Coakley, J. A., Jr., and R. Davies, 1986: The effect of cloud sides on reflected solar radiation as deduced from satellite observations. *J. Atmos. Sci.*, **43**, 1025–1035.
- Cox, S. K., D. S. McDougal, D. A. Randall, and R. A. Schiffer, 1987: FIRE—The First ISCCP Regional Experiment. *Bull. Amer. Meteor. Soc.*, **68**, 114–118.
- Crommelynk, D., V. Domingo, A. Fichot, and R. Lee, 1994: Total solar irradiance observations from the EURECA and ATLAS experiments. *The Sun as a Variable Star*, IAU Col. 143 proc., J. Pap, C. Frohlich, H. Hudson, and K. Salience, Eds. Cambridge University Press, 63–69.
- Darnell, W. L., W. F. Staylor, S. K. Gupta, N. A. Ritchey, and A. C. Wilber, 1992: Seasonal variation of surface radiation budget derived from International Satellite Cloud Climatology Project C1 data. *J. Geophys. Res.*, **97**, 15,741–15,760.
- Davies, R., W. L. Ridgway, and K. E. Kim, 1984: Spectral absorption of solar radiation in cloudy atmosphere: A 20 cm⁻¹ model. *J. Atmos. Sci.*, **41**, 2126–2137.
- Del Genio, A. D., M. S. Yao, W. Kovari, and K. K. W. Lo, 1996: A prognostic cloud water parameterization for global climate models. *J. Climate*, **9**, 270–304.
- DeMott, P. J., M. P. Meyers, and W. R. Cotton, 1994: Parameterization and impact of ice initiation processes relevant to numerical model simulations of cirrus clouds. *J. Atmos. Sci.*, **51**, 77–90.
- Deser, C., and M. L. Blackmon, 1993: Surface climate variations over the North Atlantic Ocean during winter: 1900–1989. *J. Climate*, **6**, 1743–1753.
- Duda, D. P., and G. L. Stephens, 1994: Macrophysical and microphysical influences on radiative transfer in two-dimensional marine stratus. Atmos. Sci. Paper 565, Colorado State University, 202 pp.
- Duncan, C. H., R. G. Harrison, J. R. Hickey, J. M. Kendall Sr., M. P. Thekaekara, and R. C. Willson, 1977: Rocket calibration of the Nimbus 6 solar constant measurements. *Applied Optics*, **16**, 2690–2697.
- Ebert, E. E., 1987: A pattern-recognition technique for distinguishing surface and cloud types in the polar regions. *J. Clim. Appl. Meteor.*, **26**, 1412–1427.
- Eddy, J. A., 1977: Historical evidence for the existence of the solar cycle. *Solar Output and Its Variation*. (O.R. White, Ed.), Univ. of Colo. Press, Boulder, CO, 51–71.
- Ellingson, R. G., J. Ellis, and S. Fels, 1991: The intercomparison of radiation codes used in climate models: Long wave results. *J. Geophys. Res. D*, **96**, 8929–8953.
- Evans, K. F., and G. L. Stephens, 1995a: Microwave radiative transfer through clouds composed of realistically shaped ice crystals. Part I: Single scattering properties. *J. Atmos. Sci.*, **52**, 2041–2057.
- Evans, K. F., and G. L. Stephens, 1995b: Microwave radiative transfer through clouds composed of realistically shaped ice crystals. Part II: Remote sensing of ice clouds. *J. Atmos. Sci.*, **52**, 2058–2072.
- Feigelson, E. M., 1978: Preliminary radiation model of a cloudy atmosphere. Part I - Structure of clouds and solar radiation. *Beitr. Phys. Atmos.*, **51**, 203–229.
- Foukal, P., and J. Lean, 1986: The influence of faculae on total solar irradiance and luminosity. *Astrophys. J.*, **302**, 826–835.
- Foukal, P., and J. Lean, 1988: Magnetic modulation of solar luminosity by photospheric activity. *Astrophys. J.*, **328**, 347–357.
- Foukal, P., and J. Lean, 1990: An empirical model of total solar irradiance variations between 1874 and 1988. *Science*, **247**, 556–558.
- Fowler, L. D., D. A. Randall, and S. A. Rutledge, 1996: Liquid and ice cloud microphysics in the CSU general circulation model. Part I: Model description and simulated microphysical processes. *J. Climate*, **9**, 489–529.
- Frohlich, C., 1987: Solar oscillations and helioseismology from ACRIM/SMM irradiance data. *New and Exotic Phenomena*, (O. Fackler and J.T.T. Van, Eds.), Gif-sur-Yvette: Editions Frontieres, 395–402.
- Frohlich, C., 1994: Irradiance observations of the sun. *The Sun as a Variable Star*, IAU Col. **143**, (C. Frohlich, H. Hudson, and K. Salience, Eds.), Cambridge University Press, 28–36.
- Fu, R., and B. J. Soden, 1996: Changes of upper tropospheric humidity in the global midlatitudes forced by deep convection in the tropical atmosphere. *Nature*, submitted.
- Fu, R., A. D. Del Genio, W. B. Rossow, and W. T. Liu, 1992: Cirrus-cloud thermostat for tropical sea surface temperature tested using satellite data. *Nature*, **358**, 394–397.
- Fujita, T. T., 1984: Review of the history of mesoscale meteorology and forecasting. Satellite and Mesometeorology Research Paper 208, University of Chicago, 42 pp.
- Gaffen, D. J., R. D. Rosen, D. A. Salstein, and J. S. Boyle, 1995: Validation of humidity, moisture fluxes, and soil moisture in GCMS: Report of AMIP diagnostic subproject 11. Part 2: Humidity and moisture flux fields. Atmospheric Model Intercomparison Project, DoE.
- Gao, B. C., A. F. H. Goetz, and W. J. Wiscombe, 1992: Cirrus cloud detection from airborne imaging spectrometer data using the 1.375 μm water vapor band. *Geophys. Res. Lett.*, **20**, 301–304.
- Gates W. L., 1993: AMIP: The Atmospheric Model Intercomparison Project. *Bull. Amer. Meteor. Soc.*, **73**, 1962–1970.
- Gleckler, P. J., D. A. Randall, G. Boer, R. Colman, M. Dix, V. Galin, M. Helfand, J. Kiehl, A. Kitoh, W. Lau, X.-Y. Liang, V. Lykossov, B. McAvaney, K. Miyakoda, S. Planton, and W. Stern, 1995: Cloud-radiative effects on implied oceanic energy transports as simulated by atmospheric general circulation models. *Geophys. Res. Lett.*, **22**, 791–794.

- Green, R. N., and P. O'R. Hinton, 1996: Estimation of angular distribution models from radiance pairs. *J. Geophys. Res.*, **101**, 16,951-16,959.
- Greenwald, T. J., G. L. Stephens, H. T. H. Vonder and D. L. Jackson, 1993: A physical retrieval of cloud liquid water over the global oceans using Special Sensor Microwave/Imager (SSM/I) observations. *J. Geophys. Res.*, **98**, 18,471-18,488.
- Grell, G. A., J. Dudhia, and D. R. Stauffer, 1993: A Description of the Fifth-Generation Penn State/NCAR Mesoscale Model (MM5). NCAR Tech. Note -398+IA, October 1993.
- Groisman, P. Y., T. R. Karl, and R. W. Knight, 1994: Observed impact of snow cover on the heat balance and the rise of continental spring temperatures. *Science*, **263**, 198-200.
- Gupta, S. K., 1989: A parameterization for longwave surface radiation from sun-synchronous satellite data. *J. Climate*, **2**, 305-320.
- Gupta, S. K., W. L. Darnell, and A. C. Wilber, 1992: A parameterization for surface longwave radiation from satellite data: Recent improvements. *J. Appl. Meteor.*, **31**, 1361-1367.
- Gupta, S. K., C. H. Whitlock, N. A. Ritchey, A. C. Wilber, W. L. Darnell, and W. F. Staylor, 1996: A climatology of surface radiation budget derived from satellite data. International Radiation Symposium, Fairbanks, Alaska, August 19-24.
- Hahn, C. J., S. G. Warren, J. London, R. M. Chervin, and R. Jenne, 1982: *Atlas of simultaneous occurrence of different cloud types over the ocean*. NCAR Technical Note, NCAR/TN-201+STR, NTIS PB83-152074, 212 pp.
- Han, Q., W. B. Rossow, and A. A. Lacis, 1994: Near global survey of effective droplet radii in liquid water clouds using ISCCP data. *J. Climate*, **7**, 465-497.
- Hansen, J. E., and J. B. Pollack, 1970: Infrared light scattering by terrestrial clouds. *J. Atmos. Sci.*, **27**, 265-281.
- Hansen, J. E., W.-C. Wang, and A. A. Lacis, 1978: Mount Agung eruption provides test of a global climate perturbation. *Science*, **199**, 1065-1068.
- Hansen, J., A. Lacis, D. Rind, G. Russell, P. Stone, I. Fung, J. Lerner, and R. Ruedy, 1984: Climate sensitivity: Analysis of feedback mechanisms. *Climate Processes and Climate Sensitivity*, J. E. Hansen and T. Takahashi, Eds., AGU, Washington DC, 130-163.
- Hansen, J. E., M. Sato, R. Reudy, A. Lacis, K. Asamoah, S. Borenstein, E. Brown, B. Cairns, G. Caliri, M. Campbell, B. Curran, S. deCastro, L. Druyner, M. Fox, C. Johnson, J. Lerner, M. P. McCormick, R. Miller, P. Minnis, A. Morrison, L. Pandolfo, L. Ramberran, F. Zaucker, M. Robinson, P. Russell, K. Shah, P. Stone, I. Tegen, L. Thomason, J. Wilder, and H. Wilson, 1994: A Pinatubo climate modelling investigation. *The Effects of the Mt. Pinatubo Eruption on the Atmosphere and Climate*, (G. Fiocco, D. Fua, and G. Visconti, Eds.), Springer-Verlag.
- Harrington, J. Y., M. P. Meyers, R. L. Walko, and W. R. Cotton, 1995: Parameterization of ice crystal conversion processes due to vapor deposition for mesoscale models using double-moment basis functions. Part I: Basic formulation and parcel model results. *J. Atmos. Sci.*, **52**, 4344-4366.
- Harrison, E. F., P. Minnis, B. R. Barkstrom, V. Ramanathan, R. D. Cess and G. G. Gibson, 1990: Seasonal variation of cloud radiative forcing derived from the Earth Radiation Budget Experiment. *J. Geophys. Res.*, **95**, 18,687-18,703.
- Harrison, E. F., P. Minnis, G. G. Gibson, and F. M. Denn, 1992: Orbital analysis and instrument viewing considerations for the Earth Observing System (EOS) satellite. *Astrodynamic 1991, Advances in the Astronautical Sciences*, **76**, (B. Kaufman, Ed.), 1215-1228.
- Harshvardhan, B. A. Wielicki, and K. M. Ginger, 1994: The interpretation of remotely sensed cloud properties from a model parameterization perspective. *J. Climate*, **7**, 1987-1998.
- Hartmann, D.L., 1994: *Global Physical Climatology*, Academic Press, 411 pp.
- Hartmann, D. L., and M. L. Michelsen, 1993: Large-scale effects on the regulation of tropical sea surface temperature. *J. Climate*, **6**, 2049-2062.
- Hartmann, D. L., H. H. Hendon, and R. J. Houze, 1984: Some implications of mesoscale circulations in tropical cloud clusters for large-scale dynamics and climate. *J. Atmos. Sci.*, **41**, 113-121.
- Hartmann, D. L., M. E. Ockert-Bell, and M. L. Michelsen, 1992: The effect of cloud type on Earth's energy balance: Global analysis. *J. Climate*, **5**, 1281-1304.
- Hayasaka, T., N. Kikuchi, and M. Tanaka, 1995: Absorption of solar radiation by stratocumulus clouds: Aircraft measurements and theoretical calculations. *J. Appl. Meteor.*, **34**, 1047-1055.
- Held, I. M., 1993: Large-scale dynamics and global warming. *Bull. Amer. Meteor. Soc.*, **74**, 228-241.
- Held, I. M., R. S. Hemler, and V. Ramaswamy, 1993: Radiative-convective equilibrium with explicit two-dimensional moist convection. *J. Atmos. Sci.*, **23**, 3909-3925.
- Heymsfield, A. J., and L. J. Donner, 1990: A scheme for parameterizing ice-cloud water content in general circulation models. *J. Atmos. Sci.*, **47**, 1865-1877.
- Hickey, J. R., L. L. Stowe, H. Jacobowitz, R. H. Maschoff, F. House, and T. H. Vonder Haar, 1980: Initial solar irradiance determination from Nimbus-7 cavity radiometer measurements. *Science*, **208**, 281-283.
- Horel, J. D., and J. M. Wallace, 1981: Planetary-scale atmospheric phenomena associated with the Southern Oscillation. *Mon. Wea. Rev.*, **109**, 814-829.
- Houghton, J. T., G. J. Jenkins, and J. J. Ephraums, Eds., 1990: *Climate Change: The IPCC Scientific Assessment*. Cambridge University Press, Cambridge, 365 pp.
- Houghton, J. T., L. G. Meira Filho, B. A. Callander, N. Harris, A. Kattenberg, and K. Maskell, Eds., 1996: *Climate Change 1995: The Science of Climate Change*. Intergovernmental Panel on Climate Change, Cambridge, 572 pp.
- Houze, R. A., Jr., 1982: Cloud clusters and large-scale vertical motions in the tropics. *J. Met. Soc. Japan*, **60**, 396-410.
- Houze, R. A., Jr., 1989: Observed structure of mesoscale convective systems and implications for large-scale heating. *Quart. J. Roy. Meteor. Soc.*, **115**, 425-461.
- Houze, R. A., Jr., 1993: *Cloud Dynamics*. Academic Press, 573 pp.
- Hoyt, D. V., H. L. Kyle, J. R. Hickey, and R. H. Maschoff, 1992: The Nimbus 7 solar total irradiance: A new algorithm for its derivation. *J. Geophys. Res.*, **97**, 51-63.
- Hudson, H. S., and R. C. Willson, 1982: Sunspots and solar variability. Conference on Sunspots, Sacramento Peak Observatory, Sunspot, AZ, Sacramento Peak Observatory.
- Huffman, G. J., R. F. Adler, and P. R. Keehn, 1995: Experiments with a technique for combining satellite-based precipitation estimates with gauge and model estimates. Proceedings, *Seventh Conf. on Sat. Meteor. and Oceanogr.* 6-10 June, 1994, Monterey, Amer. Meteor. Soc.
- Inamdar, A. K., and V. Ramanathan, 1994: Physics of greenhouse effect and convection in warm oceans. *J. Climate*, **7**, 715-731.
- Intergovernmental Panel on Climate Change, 1990: *Climate Change: The IPCC scientific assessment*. Cambridge Univ. Press, 365 pp.
- Kahn, R., R. West, D. McDonald, B. Rheingans, and M. I. Mishchenko, 1996: Sensitivity of multi-angle remote sensing observations to aerosol sphericity. *J. Geophys. Res.*, in press.
- Kalnay, E., and R. Jenne, 1991: Summary of the NMC/NCAR reanalysis workshop of April 1991. *Bull. Amer. Meteor. Soc.*, **72**, 1897-1904.
- Kaufman, Y. J., and B. C. Gao, 1992: Remote sensing of water vapor in the near IR from EOS/MODIS. *IEEE Transactions on Geoscience and Remote Sensing*, **30**, 871-884.
- Kelly, K. K., A. F. Tuck, and T. Davies, 1991: Wintertime asymmetry of upper-tropospheric water between the Northern and Southern Hemisphere. *Nature*, **353**, 244-247.

- Kiehl, J. T., and K. E. Trenberth, 1997: Earth's annual global mean energy budget. *Bull. Amer. Meteor. Soc.*, **74**, 21–34.
- King, M. D., 1993: Radiative properties of clouds. *Aerosol-Cloud-Climate Interactions*, **54**, (P. V. Hobbs, Ed.), Academic Press, 123–149.
- Klein, S. A., and D. L. Hartmann, 1993a: Spurious changes in the ISCCP dataset. *Geophys. Res. Lett.*, **20**, 455–458.
- Klein, S. A., and D. L. Hartmann, 1993b: The seasonal cycle of low stratiform clouds. *J. Climate*, **6**, 1587–1606.
- Klein, S. A., D. L. Hartmann, and J. R. Norris, 1995: On the relationships among low-cloud structure, sea surface temperature, and atmospheric circulation in the summertime northeast Pacific. *J. Climate*, **8**, 1140–1155.
- Krueger, S. K., 1988: Numerical simulation of tropical cumulus clouds and their interaction with the subcloud layer. *J. Atmos. Sci.*, **45**, 2221–2250.
- Lau, K. -M., and H. -T. Wu, and S. Bony, 1997: The role of the large-scale atmospheric circulation in the relationship between tropical convection and sea surface temperature. *J. Climate*, **10**, 381–392.
- Lau, K. -M., Y. S. Sud, and J. H. Kim, 1995: Intercomparison of hydrologic processes in global climate models. NASA Tech. Memo. 104617, 161 pp.
- Lau, K. -M., C. H. Sui, M. -D. Chou, and W.-K. Tao, 1994: An inquiry into the cirrus cloud thermostat effect for tropical sea surface temperature. *Geophys. Res. Lett.*, **21**, 1157–1160.
- Lau, K. -M., C. -H. Sui, and W. -K. Tao, 1993: A preliminary study of the tropical water cycle and its sensitivity to surface warming. *Bull. Amer. Meteor. Soc.*, **74**, 1313–1321.
- Lau, N. -C., and M. J. Nath, 1994: A modeling study of the relative roles of tropical and extratropical SST anomalies in the variability of the global atmosphere-ocean system. *J. Climate*, **7**, 1184–1207.
- Lean, J., and D. A. Warrilow, 1989: Climate impact of Amazon deforestation. *Nature*, **342**, 311–313.
- Lean, J., J. Beer, and R. Bradley, 1995: Reconstruction of solar irradiance since 1610: Implications for climate change. *Geophys. Res. Lett.*, **22** (23), 3195–3198.
- Lee, R. B. I., M. A. Gibson, R. S. Wilson, and S. Thomas, 1995: Long-term total solar irradiance variability during sunspot cycle 22. *J. Geophys. Res.*, **100**, 1667–1675.
- Legates, D. R., and C. J. Wilmott, 1990: Mean seasonal and spatial variability in gauge-corrected global precipitation. *Int. J. Climatol.*, **10**, 111–127.
- LeTreut, H., and Z.-X. Li, 1991: Sensitivity of an atmospheric general circulation model to prescribed SST changes: feedback effects associated with the simulation of cloud optical properties. *Clim. Dyn.*, **5**, 175–187.
- Li, Z., and H. LeTreut, 1992: Cloud-radiation feedbacks in a general circulation model and their dependence on cloud modeling assumptions. *Clim. Dyn.*, **7**, 133–139.
- Li, Z., and H. G. Leighton, 1993: Global climatologies of solar radiation budgets at the surface and in the atmosphere from 5 years of ERBE data. *J. Geophys. Res.*, **98**, 4919–4930.
- Li, Z., and F. Becker, 1993: Feasibility of land surface temperature and emissivity determination from AVHRR data. *Remote Sens. Env.*, **43**, 67–85.
- Li, Z., H. G. Leighton, K. Masuda, and T. Takashima, 1993: Estimation of SW flux absorbed at the surface from TOA reflected flux. *J. Climate*, **6**, 317–330.
- Li, Z., C. H. Whitlock, and T. P. Charlock, 1995: Assessment of the global monthly mean surface insolation estimated from satellite measurements using Global Energy Balance Archive data. *J. Climate*, **8**, 315–328.
- Lilly, D. K., 1968: Models of cloud-topped mixed layers under a strong inversion. *Quart. J. Roy Meteor. Soc.*, **94**, 292–309.
- Lindzen, R. S., 1990: Some coolness concerning global warming. *Bull. Amer. Meteor. Soc.*, **71**, 288–299.
- Lipps, F. B., and R. S. Hemler, 1986: Numerical simulation of deep tropical convection associated with large-scale convergence. *J. Atmos. Sci.*, **43**, 1796–1816.
- Liu, W. T., and C. Gautier, 1990: Thermal forcing of the tropical Pacific from satellite data. *J. Geophys. Res.*, **95**, 13,209–13,217.
- Liu, W. T., A. Zhang, and J. K. B. Bishop, 1994: Evaporation and solar irradiance as regulators of sea surface temperature in annual and interannual changes. *J. Geophys. Res.*, **99**, 12,623–12,637.
- Livingston, W., L. Wallace, and O. R. White, 1988: Spectrum line intensity as a surrogate for solar irradiance variation. *Science*, **240**, 1765–1767.
- Luo, G., X. Lin, and J. A. Coakley, Jr., 1994: 11- μm emissivities and droplet radii for marine stratocumulus. *J. Geophys. Res.*, **99**, 3685–3698.
- Manabe, S., and R. T. Wetherald, 1967: Thermal equilibrium of the atmosphere with a given distribution of relative humidity. *J. Atmos. Sci.*, **24**, 241–259.
- Manabe, S., R. J. Stouffer, M. J. Spelman, and K. Bryan, 1991: Transient response of a coupled ocean-atmosphere model to gradual changes in atmospheric CO₂. Part I: annual mean response. *J. Climate*, **4**, 785–818.
- Mapes, B. E., and R. A. Houze, Jr., 1993: Cloud clusters and superclusters over the oceanic warm pool. *Mon. Wea. Rev.*, **121**, 1398–1415.
- Mapes, B. E., and R. A. Houze, Jr., 1995: Diabatic divergence profiles in western Pacific mesoscale convective systems. *J. Atmos. Sci.*, **52**, 1807–1828.
- McCormick, M. P., R. E. Viegas, and W. P. Chu, 1992: Stratospheric ozone profile and total ozone trends derived from the SAGE I and SAGE II data. *J. Geophys. Res.*, **19**, 269–272.
- Minnis, P., 1989: Viewing zenith angle dependence of cloudiness determined from coincident GOES East and GOES West data. *J. Geophys. Res.*, **94**, 2303–2320.
- Minnis, P., and E. F. Harrison, 1984a: Diurnal variability of regional cloud and clear-sky radiative parameters derived from GOES data. Part I: Analysis method. *J. Clim. Appl. Meteor.*, **23**, 993–1011.
- Minnis, P., and E. F. Harrison, 1984b: Diurnal variability of regional cloud and clear sky radiative parameters derived from GOES data. Part II: Cloud distributions. *J. Clim. Appl. Meteor.*, **23**, 1012–1031.
- Minnis, P., and E. F. Harrison, 1984c: Diurnal variability of regional cloud and clear-sky radiative parameters derived from GOES data, Part III: November 1978 radiative parameters. *J. Clim. Appl. Meteor.*, **23**, 1032–1051.
- Minnis, P., D. F. Young, K. Sassen, J. M. Alvarez, and C. J. Grund, 1990: The 27–28 October 1986 FIRE IFO Cirrus Case Study: cirrus parameter relationships derived from satellite and lidar data. *Mon. Wea. Rev.*, **118**, 2402–25.
- Minnis, P., P. W. Heck, D. F. Young, C. W. Fairall, and J. B. Snider, 1992: Stratocumulus cloud properties derived from simultaneous satellite and island-based instrumentation during FIRE. *J. Appl. Meteor.*, **31**, 317–39.
- Mitchell, J. F. B., 1993a: Simulation of climate. *Renewable Energy*, **3**, 421–432.
- Mitchell, J. F. B., 1993b: Simulation of climate change. *Renewable Energy*, **3**, 433–445.
- Mitchell, J. F. B., C. A. Senior, and W. J. Ingram, 1989: CO₂ and climate: A missing feedback? *Nature*, **341**, 132–134.
- Nakajima, T., and M. D. King, 1990: Determination of the optical thickness and effective particle radius of clouds from reflected solar radiation measurements. Part I: Theory. *J. Atmos. Sci.*, **47**, 1878–1893.

- Nakajima, T., M. D. King, J. D. Spinhirne, and L. F. Radke, 1991: Determination of the optical thickness and effective particle radius of clouds from reflected solar radiation measurements. Part II: Marine stratocumulus observations. *J. Atmos. Sci.*, **48**, 728–750.
- National Research Council, 1994: *Solar Influences on Global Change*. National Academy Press, p. 10.
- Nobre, C., P. J. Sellers, and J. Shukla, 1991: Amazonian deforestation and regional climate change. *J. Climate*, **4**, 957–988.
- Norris, J. R., and C. B. Leovy, 1994: Interannual variability in stratiform cloudiness and sea surface temperature. *J. Climate*, **7**, 1915–1925.
- Ohmura, A., and H. Gilgen, 1991: Global Energy Balance Archive GEBA. *The GEBA Database, Interactive Applications, Retrieving Data*, World Climate Program Water Project A7, Report 2, Züricher Geographische Schriften Nr. 44, Geographisches Institut ETH, Zürich.
- Paltridge, G. W., 1980: Cloud-radiation feedback to climate. *Quart. J. Roy. Meteor. Soc.*, **106**, 367–380.
- Peixoto, J. P., and A. H. Oort, 1992: *Physics of Climate*. American Institute of Physics, New York, 520 pp.
- Peixoto, J. P., and A. H. Oort, 1983: The atmospheric branch of the hydrologic cycle and climate. *Variations in the Global Hydrologic Cycle and Climate*. (A. Street-Perrott, M. Beran, and R. Radcliffe, Eds.), Reidel Publ. Co., Holland, 5–65.
- Penner, J. E., R. J. Charlson, J. M. Hales, N. S. Laulainen, R. Leifer, T. Novakov, J. Ogren, L. F. Radke, S. E. Schwartz, and L. Travis, 1994: Quantifying and minimizing uncertainty of climate forcing by anthropogenic aerosols. *Bull. Amer. Meteor. Soc.*, **75**, 375–400.
- Pierrehumbert, R., 1994: Thermostats, radiator fins, and the local runaway greenhouse. *J. Atmos. Sci.*, **52**, 1784–1806.
- Pilewskie, P., and F. P. Valero, 1995: Direct observations of excess solar absorption by clouds. *Science*, **267**, 1626–1629.
- Pinker, R., and I. Laszlo, 1992: Modeling surface solar irradiance for satellite applications on a global scale. *J. Appl. Meteor.*, **31**, 194–211.
- Platt, T., S. Sathyendranath, C. M. Caverhill, and M. R. Lewis, 1988: Ocean primary production and available light: Further algorithms for remote sensing. *Deep Sea Res.*, **35**, 855–879.
- Platt, C. M., S. A. Young, A. I. Carswell, S. R. Pal, M. P. McCormick, D. M. Winker, M. DelGuasta, L. Stefanutti, W. L. Eberhard, M. Hardesty, P. H. Flamant, R. Valentin, B. Forgan, G. G. Gimmestad, H. Jäger, S. S. Khmelevtsov, I. Kolev, B. Kaprieolev, Da-ren Lu, K. Sassen, V. S. Shamaev, O. Uchino, Y. Mizuno, U. Wandinger, C. Weitkamp, A. Ansmann, and C. Woodriddle, 1994: The Experimental Cloud Lidar Pilot Study (ECLIPS) for cloud-radiation research. *Bull. Amer. Meteor. Soc.*, **75**, 1635–1654.
- Prabhakara, C., D. A. Short, and B. E. Vollmer, 1985: El Niño and atmospheric water vapor: Observation from Nimbus 7 SMMR. *J. Climate Appl. Meteor.*, **24**, 1311–1324.
- Prabhakara, C., R. S. Fraser, G. Dalu, M. L. C. Wu, and R. J. Curran, 1988: Thin cirrus clouds: Seasonal distribution over oceans deduced from Nimbus-4 IRIS. *J. Climate Appl. Meteor.*, **27**, 279–299.
- Ramanathan, V., and W. Collins, 1991: Thermodynamic regulation of ocean warming by cirrus clouds deduced from observations of the 1987 El Niño. *Nature*, **351**, 27–32.
- Ramanathan, V., R. D. Cess, E. F. Harrison, P. Minnis, B. R. Barkstrom, E. Ahmad, and D. L. Hartmann, 1989: Cloud-radiative forcing and climate: Results from the Earth Radiation Budget Experiment. *Science*, **243**, 57–63.
- Ramanathan, V., B. Subasilar, G. J. Zhang, W. Conant, R. D. Cess, J. T. Kiehl, H. Grassl, and L. Shi, 1995: Warm pool heat budget and shortwave cloud forcing: A missing physics? *Science*, **267**, 499–503.
- Rasch, P. J., and D. L. Williamson, 1990: Computational aspects of moisture transport in global models of the atmosphere. *Quart. J. Roy. Meteor. Soc.*, **116**, 1071–1090.
- Rasmusson, E. M., and J. M. Wallace, 1983: Meteorological aspects of the El Niño-Southern Oscillation. *Science*, **222**, 1195–1202.
- Raval, A., and V. Ramanathan, 1989: Observational determination of the greenhouse effect. *Nature*, **342**, 758–761.
- Read, W. G., J. W. Waters, D. A. Flower, L. Froidevaux, R. F. Jarnot, D. L. Hartmann, R. S. Harwood, and R. B. Rood, 1995: Upper-tropospheric water vapor from UARS MLS. *Bull. Amer. Meteor. Soc.*, **76**, 2381–2389.
- Rind, D., E. W. Chiou, W. Chu, J. Larsen, O. Oltmans, J. Lerner, M. P. McCormick, and L. McMaster, 1991: Positive water vapour feedback in climate models confirmed by satellite data. *Nature*, **349**, 500–503.
- Rind, D., E. W. Chiou, W. Chu, J. Larsen, S. Oltmans, J. Lerner, M. P. McCormick, and L. McMaster, 1993: Overview of the Stratospheric Aerosol and Gas Experiment II water vapor observations: Method, validation, and data characteristics. *J. Geophys. Res.*, **98**, 4835–4856.
- Roeckner, E., U. Schlese, J. Biercamp, and P. Loewe, 1987: Cloud optical depth feedbacks and climate modeling. *Nature*, **329**, 138–140.
- Ropelewski, C. F., and M. S. Halpert, 1989: Precipitation patterns associated with the high index phase of the Southern Oscillation. *J. Climate*, **2**, 268–284.
- Rossow, W. B., and R. A. Schiffer, 1991: ISCCP cloud data products. *Bull. Amer. Meteor. Soc.*, **72**, 2–20.
- Rossow, W. B., F. Mosher, E. Kinsella, A. Arking, M. Desbois, E. Harrison, P. Minnis, E. Ruprecht, G. Seze, C. Simmer, and E. Smith, 1985: ISCCP cloud algorithm intercomparison. *J. Climate Appl. Meteor.*, **24**, 877–903.
- Rossow, W. B., L. C. Garder, P. J. Lu, and A. Walker, 1991: International Satellite Cloud Climatology Project (ISCCP) documentation of cloud data. *WMO/TD-No. 266 (Revised)*, World Meteorological Organization, Geneva, 76 pp.
- Salathe, E. P., Jr., D. Chester, and Y. C. Sud, 1995: Evaluation of the upper-tropospheric moisture climatology in a general circulation model using TOVS radiance observations. *J. Climate*, in press.
- Saunders, R. W., and K. T. Kriebel, 1988: An improved method for detecting clear sky and cloudy radiances from AVHRR data. *Int. J. Remote Sens.*, **9**, 123–150.
- Schubert, S., C. K. Park, C. Y. Wu, Y. Higgins, Y. Kondratyeva, A. Molod, L. Takacs, M. Seabloom, and R. Rood, 1995: A multilayer assimilation with the GEOS-1 system: Overview and results. NASA Technical Memorandum 104606, Vol. 6, 183 pp.
- Sellers, P. J., and F. G. Hall, 1992: FIFE in 1992: Results, scientific gains, and future research directions. *J. Geophys. Res.*, **97**, 19,091–19,109.
- Sellers, P. J., and D. S. Schimel, 1993: Remote sensing of the land biosphere and biogeochemistry in the EOS era. *Global and Planetary Change*, **7**, 279–297.
- Sellers, W. D., 1969: A climate model based on the energy balance of the Earth-atmosphere system. *J. Appl. Meteor.*, **8**, 392–400.
- Senior, C. A., and J. F. B. Mitchell, 1993: Carbon dioxide and climate: The impact of cloud parameterization. *J. Climate*, **6**, 393–418.
- Shuttleworth, W. J., and R. E. Dickinson, 1989: Comments on “Modeling tropical deforestation: A study of GCM land-surface parameterizations.” *Quart. J. Roy. Meteor. Soc.*, **115**, 1177–1179.
- Simpson, J., Ed., 1988: TRMM: A satellite mission to measure tropical rainfall: Report of the steering group. National Aeronautics and Space Administration, Goddard Space Flight Center, Greenbelt, MD 20771, 94 pp.
- Sinha, A., 1995: Relative influence of lapse rate and water vapor on the greenhouse effect. *J. Geophys. Res.*, **100** (D3), 5095–5103.
- Slingo, A., and M. J. Webb, 1992: Simulation of clear-sky outgoing longwave radiation over the oceans using operational analyses. *Quart. J. Roy. Meteor. Soc.*, **118**, 1117–1144.

- Smith, R. N. B., 1990: A scheme for predicting layer clouds and their water content in a general circulation model. *Quart. J. Roy. Meteor. Soc.*, **116**, 435–460.
- Smith, W. L., and H. M. Woolf, 1976: The use of eigenvectors of statistical covariance matrices for interpreting satellite sounding radiometer observations. *J. Atmos. Sci.*, **33**, 1177–1187.
- Soden, B. J., and F. P. Bretherton, 1993: Upper-tropospheric relative humidity from the GOES 6.7 micron channel: Method and climatology for July 1987. *J. Geophys. Res.*, **98**, 16,669–16,688.
- Soden, B. J., and R. Fu, 1995: A satellite analysis of deep convection, upper-tropospheric humidity and the greenhouse effect. *J. Climate*, **8**, 2333–2351.
- Somerville, R. C. J., and L. A. Remer, 1984: Cloud optical thickness feedbacks in the CO₂ climate problem. *J. Geophys. Res.*, **89**, 9668–9673.
- Stackhouse, P. W., Jr., and G. L. Stephens, 1991: A theoretical and observational study of the radiative properties of cirrus: results from FIRE 1986. *J. Atmos. Sci.*, **48**, 2044–2059.
- Starr, D. O'C., and S. H. Melfi, 1991: The role of water vapor in climate: A strategic plan for the proposed GEWEX Water Vapor Project (GVAP), NASA Conf. Publ. 3120, 50 pp.
- Stephens, G. L., 1990: On the relationship between water vapor over the oceans and sea surface temperature. *J. Climate*, **3**, 634–645.
- Stephens, G. L., and P. J. Webster, 1984: Cloud decoupling of the surface and planetary radiative budgets. *J. Atmos. Sci.*, **41**, 681–686.
- Stephens, G. L., and S. Tsay, 1990: On the cloud absorption anomaly. *Quart. J. Roy. Meteor. Soc.*, **116**, 671–704.
- Stephens, G. L., A. Slingo, M. J. Webb, P. J. Minnett, P. H. Daum, L. Kleinman, I. Wittmeyer, and D. A. Randall, 1994: Observations of the Earth's Radiation Budget in relation to atmospheric hydrology. 4. Atmospheric column radiative cooling over the world's oceans. *J. Geophys. Res.*, **99**, 18,585–18,604.
- Stokes, G. M., and S. E. Schwartz, 1994: The Atmospheric Radiation Measurement (ARM) program: Programmatic background and design of the cloud and radiation test bed. *Bull. Amer. Meteor. Soc.*, **75**, 1201–1221.
- Stone, R. S., G. L. Stephens, C. M. R. Platt, and S. Banks, 1990: The remote sensing of thin cirrus clouds using satellites, lidar, and radiative transfer theory. *J. Appl. Meteor.*, **29**, 353–366.
- Stowe, L. L., C. G. Wellemeyer, T. F. Eck, H. Y. M. Yeh, and the N. C. D. P. Team, 1988: Nimbus-7 global cloud climatology, Part I, Algorithm and validation. *J. Climate*, **1**, 445–470.
- Stowe, L. L., E. P. McClain, R. Carey, P. Pellegrino, G. G. Gutman, P. Davis, C. Long, and S. Hart, 1991: Global distribution of cloud cover derived from NOAA/AVHRR operational satellite data. *Advances in Space Research*, **11**, 51–54.
- Sui, C. H., K. M. Lau, W. K. Tao, and J. Simpson, 1993: The tropical water and energy cycles in a cumulus ensemble model. Part I: equilibrium climate. *J. Atmos. Sci.*, **51**, 711–728.
- Sun, D. Z., and R. S. Lindzen, 1993: Distribution of tropical tropospheric water vapor. *J. Atmos. Sci.*, **50**, 1644–1660.
- Sundqvist, H., 1978: A parameterization scheme for nonconvective condensation including prediction of cloud water content. *Quart. J. Roy. Meteor. Soc.*, **104**, 677–690.
- Susskind, J., D. Reuter, and M. T. Chahine, 1987: Cloud fields retrieved from HIRS2/MSU. *J. Geophys. Res.*, **90**, 11,602–11,608.
- Takano, Y., and K. N. Liou, 1989: Radiative transfer in cirrus clouds. I. Single scattering and optical properties of oriented hexagonal ice crystals. *J. Atmos. Sci.*, **46**, 3–20.
- Tally, L. D., 1984: Meridional heat transport in the Pacific Ocean. *J. Phys. Oceanogr.*, **14**, 231–241.
- Tian, L., and J. A. Curry, 1989: Cloud overlap statistics. *J. Geophys. Res.*, **94**, 9925–9935.
- Tao, W. K., and S. T. Soong, 1986: A study of the response of deep tropical clouds to mesoscale processes: Three-dimensional numerical experiments. *J. Atmos. Sci.*, **43**, 2653–2676.
- Tao, W. K., and J. Simpson, 1993: The Goddard Cumulus Ensemble Model. Part I: Model description. *Terrestrial, Atmospheric and Oceanic Sciences*, **4**, 35–72.
- Tiedtke, M., 1993: Representations of clouds in large-scale models. *Mon. Wea. Rev.*, **121**, 3040–3061.
- Trenberth, K. E., and J. G. Olson, 1988: Evaluation of NMC global analyses: 1979–1987, National Center for Atmospheric Research. NCAR/TN-299+STR, 82 pp.
- Tselioudis, G., W. B. Rossow, and D. Rind, 1992: Global patterns of cloud optical thickness variation with temperature. *J. Climate*, **5**, 1484–1495.
- Udelhofen, P., and D. L. Hartmann, 1995: The influence of tropical cloud systems on the relative humidity in the upper troposphere. *J. Geophys. Res.*, **100**, 423–440.
- Wade, C. G., 1994: Problems with radiosonde humidity in the United States and their effect on climate analysis. *AGU Chapman Conference on Water Vapor in the Climate System*, October 25–28, Jekyll Island, Georgia.
- Wallace, J. M., 1992: Effect of deep convection on the regulation of tropical sea surface temperature. *Nature*, **357**, 230–231.
- Wallace, J. M., and D. Gutzler, 1981: Teleconnections in the geopotential height field during the Northern Hemisphere winter. *Mon. Wea. Rev.*, **109**, 784–812.
- Wang, W. C., R. B. Rossow, M. S. Yao, and M. Wolfson, 1981: Climate sensitivity of a one-dimensional radiative-convective model with cloud feedback. *J. Atmos. Sci.*, **38**, 1167–1178.
- Wang, W. C., G. Y. Shi, and J. T. Kiehl, 1991: Incorporation of the thermal radiative effect of CH₄, N₂O, CFC₁₃, and CF₂C₁₂ into the NCAR community climate model. *J. Geophys. Res.*, **96**, 9097–9103.
- Warren, S. G., C. J. Hahn, J. London, R. M. Chervin, and R. J. Jenne, 1986: *Global distribution of total cloud cover and cloud type amounts over land*. Technical Note, TN-273+STR, National Center for Atmospheric Research, Boulder.
- Warren, S. G., C. J. Hahn, J. London, R. M. Chervin, and R. J. Jenne, 1988: *Global distribution of total cloud cover and cloud type amounts over ocean*. Technical Note, TN-317+STR, National Center for Atmospheric Research, Boulder.
- Washington, W. M., and G. A. Meehl, 1984: Seasonal cycle experiment on the climate sensitivity due to a doubling of CO₂ with an atmospheric general circulation model coupled to a simple mixed-layer ocean model. *J. Geophys. Res.*, **89**, 9475–9503.
- WCRP (World Climate Research Programme), 1982: Cage Experiment: A feasibility study. WCRP-22, Geneva, 95 pp.
- WCRP (World Climate Research Programme), 1991: Radiation and Climate. *Second Workshop on Implementation of the Baseline Surface Radiation Network*. WCRP-64, WMO/TD-No. 453.
- WCRP (World Climate Research Programme), 1994: Utility and feasibility of a cloud profiling radar. WCRP-84, IGPO Publication Series No. 10, 46 pp.
- WCRP (World Climate Research Programme), 1995: CLIVAR: A study of climate variability and predictability: Geneva, World Meteorological Organization.
- Webster, P. J., and R. Lukas, 1992: TOGA-COARE: The Coupled Ocean Atmosphere Response Experiment. *Bull. Amer. Meteor. Soc.*, **73**, 1377–1417.
- Welch, R. M., S. K. Sengupta, A. K. Goroch, P. Rabindra, N. Rangaraj, and M. S. Navar, 1992: Polar cloud and surface classification using AVHRR imagery: An intercomparison of methods. *J. Appl. Meteor.*, **31**, 405–420.
- Wentz, F. J., 1994: *User's Manual SSM/I - 2 Geophysical Tapes*. Tech. Rep. 070194, Remote Sensing Systems, Santa Rosa, California, 20 pp.

- Wetherald, R.T., and S. Manabe, 1986: An investigation of cloud cover change in response to thermal forcing. *Clim. Change*, **8**, 5–23.
- Whitlock, C. H., T. P. Charlock, W. F. Staylor, R. T. Pinker, I. Laszlo, A. Ohmura, H. Gilgen, T. Konzelman, R. C. DiPasquale, C. D. Moats, S. R. LeCroy, and N. A. Richey, 1995: First global WCRP shortwave surface radiation budget data set. *Bull. Amer. Meteor. Soc.*, **76**, 905–922.
- Wielicki, B. A., and J. A. Coakley, Jr., 1981: Cloud retrieval using infrared sounder data: An error analysis. *J. Appl. Meteor.*, **20**, 37–49.
- Wielicki, B. A., B. R. Barkstrom, E. F. Harrison, R. B. I. Lee, G. L. Smith, and J. E. Cooper, 1996: Clouds and the Earth's Radiant Energy System (CERES): An Earth Observing System Experiment. *Bull. Amer. Meteor. Soc.*, **77**, 853–868.
- Wielicki, B. A., and L. Parker, 1992: On the determination of cloud cover from satellite sensors: The effect of sensor spatial resolution. *J. Geophys. Res.*, **97**, 12,799–12,823.
- Wielicki, B. A., J. T. Suttles, A. J. Heymsfield, R. M. Welch, J. D. Spinhirne, M. L. C. Wu, S. K. Cox, D. O'C. Starr, L. Parker, and R. F. Arduini, 1990: The 27-28 October 1986 FIRE IFO Cirrus case study: Comparison of radiative transfer theory with observations by satellite and aircraft. *Mon. Wea. Rev.*, **118**, 2356–2376.
- Wielicki, B. A., R. D. Cess, M. D. King, D. A. Randall, and E. F. Harrison, 1995: Mission to Planet Earth: Role of cloud and radiation in climate. *Bull. Amer. Meteor. Soc.*, **76**, 2125–2153.
- Williams, M., and R. A. Houze, Jr., 1987: Satellite-observed characteristics of winter monsoon cloud clusters. *Mon. Wea. Rev.*, **115**, 505–519.
- Wilson, C. A., and J. F. B. Mitchell, 1987: A doubled CO₂ climate sensitivity experiment with a global climate model including a simple ocean. *J. Geophys. Res.*, **92**, 13,315–13,343.
- Willson, R. C., 1973: Active cavity radiometer type III. *Appl. Optics*, **12**, 810.
- Willson, R. C., 1979: Active cavity radiometer type IV. *Appl. Optics*, **18**, 179.
- Willson, R. C., S. Gulkis, M. Janssen, H. S. Hudson, and G. A. Chapman, 1981: Observations of solar irradiance variability. *Science*, **234**, 1114–1116.
- Willson, R. C., 1982: Solar irradiance variations and solar activity. *J. Geophys. Res.*, **86**, 4319–4326.
- Willson, R. C., 1984: Measurements of solar total irradiance and its variability. *Space Science Reviews*, **38**, 203–242.
- Willson, R. C., and H. S. Hudson, 1986: Long-term downward trend in total solar irradiance. *Science*, **234**, 1114–1117.
- Willson, R.C., and H. S. Hudson, 1988: Solar luminosity variations in solar cycle 21. *Nature*, **332**, 810–812.
- Willson, R. C., and H. S. Hudson, 1991: The sun's luminosity over a complete solar cycle. *Nature*, **351**, 42–44.
- Willson, R. C., 1994: Irradiance Observations of SMM, Spacelab-1, UARS and ATLAS Experiments. *The Sun as a Variable Star*, IAU Col. 143 proc., J. Pap, C. Frohlich, H. Hudson and K. Saliency, Eds., Cambridge University Press, 54–62.
- Willson, R. C., 1995: Science rationale of the EOS/ACRIMSAT mission. *The Earth Observer*, Feb., 1995.
- Woodard, M. F., and H. S. Hudson, 1983: Frequencies, amplitudes, and line widths of solar oscillations from solar total irradiance observations. *Nature*, **318**, 449–450.
- Woodard, M. F., 1984: Upper limit on solar interior rotation. *Nature*, **309**, 530–532.
- Woodard, M. F., and R. W. Noyes, 1985: Change of solar oscillation eigenfrequencies with the solar cycle. *Nature*, **318**, 449–450.
- Wu, X., J. J. Bates, and S. J. S. Khalsa, 1993: A climatology of the water vapor band brightness temperatures from NOAA operational satellites. *J. Climate*, **6**, 1282–1300.
- Wylie, D. P., and W. P. Menzel, 1989: Two years of cloud cover statistics using VAS. *J. Climate*, **2**, 380–392.
- Xu, K. M., and S. K. Krueger, 1991: Evaluation of cloudiness parameterizations using a cumulus ensemble model. *Mon. Wea. Rev.*, **119**, 342–367.
- Yamanouchi, T., K. Suzuki, and S. Kawaguci, 1987: Detection of clouds in Antarctica from infrared multispectral data of AVHRR. *J. Meteor. Soc. Japan*, **65**, 949–962.
- Yang, H., and R. T. Pierrehumbert, 1994: Production of dry air by isentropic mixing. *J. Atmos. Sci.*, **51**, 3437–3454.
- Zhang, M. H., J. J. Hack, J. T. Kiehl, and R. D. Cess, 1994: Diagnostic study of climate feedback processes in atmospheric general circulation models. *J. Geophys. Res.*, **99**, 5525–5537.
- Zhu, T., J. Lee, R. C. Weger, and R. M. Welch, 1992: Clustering, randomness, and regularity in cloud fields: 2. Cumulus cloud fields. *J. Geophys. Res.*, **97**, 20,537–20,558.

Chapter 2 Index

- AATSR 67, 69
 absorption, scattering, and emission,
 aerosol 50
 absorption, scattering, and emission,
 cloud 51-52
 absorption, scattering, and emission,
 Earth's surface 52-55
 absorption, scattering, and emission,
 gas 49-50
 ACRIM 43-47, 66-67, 69, 91, 103
 ADEOS 69, 87, 89
 Agung 48
 AIRS/AMSU/HSB 50, 52, 55, 59, 62,
 67-71, 78-82, 94-99, 102, 105
 AMIP 55, 80, 86
 AMSR 55, 62, 75-76, 79, 87-88, 95,
 97, 101, 104-105
 AMSR-E 52, 62, 67, 72, 75-76, 79, 87-
 88, 96-100
 ARM 50, 55, 72, 90, 91, 94, 102
 ASTER 52-55, 66, 69, 72, 94, 96
 ATLAS 44, 47
 atmospheric chemistry 48
 atmospheric temperature 49, 96-97,
 101
 ATSR 73
 AVHRR 52, 66-67, 75, 87, 90, 94
 biomass burning 50
 boundary layer fog 64
 boundary layer cloud 64
 BRDF 92
 BSRN 55, 70-71, 91, 102
 calibration 46-48, 66-69, 70-74, 82, 86,
 90-94, 99, 102, 104
 carbon cycle 101
 carbon dioxide (CO₂) 48-49, 56, 59,
 61, 65-66, 80, 84, 88, 91
 CART 102
 CEMs 63-64
 CERES 50-55, 62, 66-67, 69-71, 79,
 92-94, 102, 104
 CLIVAR 101-102
 cloud modeling 59-63
 cloud observations 57-58
 cloud property measurements 72, 94,
 104
 COARE 63-64, 83, 101
 convection 43-45, 56-58, 62-65, 77-83,
 87, 104-106
 convection and clouds in climate
 models 56, 80, 82
 CPR 52, 91
 DAAC 68-69
 data assimilation 55-57, 79, 81, 89, 97
 DFA 99
 DMSP 75, 88
 DoD 90
 DoE 102
 Earth's energy balance, cloud effects on
 56-57
 ECLIPS 102
 ECMWF 56, 81, 89
 EDC 54, 69, 72
 El Niño 52, 79, 83, 100
 ENSO 52, 79, 85-87, 103
 ENVISAT 66, 69, 73
 EOS AM 49, 52-54, 66-70, 92, 101-
 102
 EOS PM 55, 66, 75, 82, 88, 92, 101
 EOSDIS 48, 86
 EOSP 50, 52, 59, 62, 67, 72, 75-79, 94-
 97, 102, 104-105
 ERB 43-48, 54, 67-68
 ERBE 44, 49, 51-56, 59, 66-70, 89
 ERBS 44, 46-47
 ESA 46, 66, 72, 87
 ESCC 43
 ESMR 87
 EURECA 44
 FIRE 64, 70-76, 94, 100-101
 fluxes, radiative 48, 50, 52, 54, 65-66,
 71-72, 91, 93, 97, 102, 104-105
 fluxes, surface 48-49, 52, 54, 65, 67-
 70, 79, 83, 93, 104
 fluxes, TOA 51, 59, 66-72, 92-93, 104
 fluxes, within atmosphere 71-73
 FSSP 75
 GCIP 54-55, 91
 GCMs 48, 54, 58, 60-62, 65, 90, 102
 GEBA 70
 GENESIS 58
 GEOS 55-57, 79, 81
 GERB 92
 GEWEX 48, 54, 81, 90, 101
 GHCN 86
 GLAS 52, 66-69, 71-72, 74, 79, 94-96,
 101
 GLI 67, 69
 GMS 87
 GOALS 101
 GOES 80, 82, 87, 90
 GPCP 84-86
 GSFC 68-69
 GVAP 81
 HIRDLS 49, 78, 82, 94
 HIRS 67-68, 78, 82
 HSB 55, 59, 67-71, 78-79, 82, 87, 98-
 99, 105
 humidity 43, 52, 55, 59, 77-82, 88, 92-
 96, 98-99, 103, 105-106
 hydrology 54-55
 ICRCCM 50
 IDS 48, 52, 55, 59, 62-64, 79-80
 interannual variability 43, 48, 52, 81,
 89, 96, 101
 IPCC 50, 84
 IR 66, 81, 86-87, 95, 99, 104
 ISCCP 49, 51-57, 59, 62, 64, 67-74,
 100
 ISLSCP 54
 ITCZ 83-87
 IWP 76
 land processes 103
 lidar 52, 67, 69, 71-74, 82, 89, 94, 96,
 99, 102
 lightning 97
 LIS 62, 97
 LW 48-59, 66-72, 92, 93
 LWP 62, 66, 69, 75-76, 97, 105
 MCS 64, 76-78
 measurement strategy 70
 MERIS 67, 69
 methane (CH₄) 49
 METOP 66, 69, 75, 87, 98, 100
 MIMR 88, 97-100, 104-105
 MISR 50-54, 66-67, 69-74, 79, 92-97,
 102, 104-105
 MLS 49, 77-78, 82, 97-99, 105
 MMS 63-65

modeling 48-49, 52-54, 59-64, 72, 77-80, 83-84, 89-90, 93, 99, 101-102, 105
 MODIS 50-55, 62, 66-76, 79, 92-105
 MOPITT 49
 MSG 92
 NASA 43, 54, 66, 89-90
 NASDA 69, 88
 NCAR 63
 NCDC 86
 NCEP 81
 NEXRAD 86
 NMC 81, 89, 91
 NOAA 67-68, 78, 81, 86-87, 90, 102
 NWP 54, 81
 OLR 49, 53-56, 93
 Pathfinder data 54
 POLDER 66, 69, 73-76
 PR 87
 precipitation 43-106
 PSU 63
 QuikSCAT 24, 89
 radiation in climate models 55
 RAMS 63-64
 RC 48
 SAGE III 78-79, 82, 94-99, 105
 salinity 83
 satellite measurements 87-89, 91, 99
 SCARAB 67-68
 SeaWinds 88, 99, 100
 SMM 43-47
 SMMR 75, 81, 87
 snow cover 83
 SOHO 44-47
 SPCZ 85
 SRB 54, 67-68
 SSM/I 67-68, 75-76, 81, 87-88
 SST 58, 60-61, 65, 80, 86-89, 100, 103
 sulfate 50
 sulfur 50
 surface flux 70, 72, 102
 surface forcing 102
 surface insolation 49
 surface observations 58, 74, 86, 99, 101
 SVAT 54
 SW 48-59, 66-71, 92-93
 temperature profiles 81, 97, 99
 TES 49-50, 96
 TMI 67-68, 75, 87-88
 TOGA 63-64, 83, 101
 topography 64
 TOVS 78-81
 trace gases 48-49
 TRMM 65-70, 75, 87, 92, 94, 97, 99, 101, 104-105
 TSI 43-47, 103
 USGCRP 55, 102
 USGS 54
 validation 54-55, 59-60, 64-75, 81-82, 86, 90-94, 99, 101-104
 variability, trend detection 105
 VIRGO 44, 46-47
 VIRS 52, 66-76, 87, 92, 94
 VIS 87, 104
 water vapor 43-106
 WCRP 51, 70-74, 90, 101-103
 wind 48, 55, 79, 88-89, 99-105
 WOCE 101
 WSR 86

Ocean Circulation, Productivity, and Exchange with the Atmosphere

LEAD AUTHOR D. A. Rothrock

CONTRIBUTING AUTHORS

M. R. Abbott	N. G. Maynard
R. Alley	F. Muller-Karger
P. G. Brewer	P. P. Niiler
O. Brown	J. Parslow
A. J. Busalacchi	E. T. Peltzer
W. E. Esaias	B. E. Schutz
S. K. Esbensen	C. K. Shum
M. H. Freilich	M. Srokosz
J. Frew	R. Stewart
D. M. Glover	T. Strub
J. S. Godfrey	L. J. Walstad
C. Goyet	J. A. Yoder
M. R. Holland	V. Zlotnicki
T. Matsunaga	

CHAPTER 3 CONTENTS

3.1 Overview	117
3.1.1 Organization of this chapter	117
3.1.2 Oceans and climate	117
3.1.3 Oceans and humanity	117
3.2 Major scientific questions	118
3.2.1 Ocean-atmosphere surface coupling	118
3.2.1.1 Momentum exchange	119
3.2.1.2 Thermal fluxes: radiative and turbulent	121
3.2.1.3 Freshwater forcing: evaporation, precipitation, and sea ice	121
3.2.2 Ocean circulation	123
3.2.2.1 Oceans and the global heat balance	123
3.2.2.2 Ocean circulation	124
3.2.2.3 Ocean modeling and data assimilation	126
3.2.3 Global sea-level rise	128
3.2.3.1 Mean ocean surface height	128
3.2.3.2 Ice sheets, glaciers, and continental movements	129
3.2.3.3 Steric change and ocean circulation	129
3.2.3.4 Ocean tides	129
3.2.4 The marine biosphere and ocean carbon system	130
3.2.4.1 Introduction	130
3.2.4.2 Ocean carbon in relation to global carbon cycle	132
3.2.4.3 Air-sea CO ₂ fluxes	132
3.2.4.4 Land/sea interactions and fluxes	133
3.2.4.5 Productivity of the marine biosphere	134
3.2.4.6 The marine ecosystem and climate change	136
3.2.4.7 Modeling the marine biosphere	136
3.3 Required measurements and data sets	138
3.3.1 Satellite observations	138
3.3.1.1 Surface fluxes of momentum, heat, and moisture	138
3.3.1.2 Circulation and sea level	140
3.3.1.3 Biogeochemistry	142
3.3.2 Critical surface observations and field experiments	149
3.3.2.1 WOCE, TOGA, GOALS, and CLIVAR	149
3.3.2.2 JGOFS	149
3.3.2.3 GLOBEC	150
3.4 EOS contributions: Combining the knowledge of ocean and climate systems	151
3.4.1 Air-sea flux plans for EOS	151
3.4.2 Ocean circulation and sea-level plans for EOS	152
3.4.3 Marine biogeochemical research planned in EOS	153
3.4.4 Human dimensions of ocean climate	154
3.4.5 Atmosphere/ocean modeling	155
3.4.6 Improved predictions of seasonal-to-decadal climate variability through global land-atmosphere-ocean models	156
3.4.7 Understanding of ocean's effect on carbon dioxide, the major greenhouse gas	156
References	157
Chapter 3 Index	160

3.1 Overview

3.1.1 Organization of this chapter

Four themes are addressed in this chapter:

- The interaction between the atmosphere and ocean across the sea surface
- The role of the oceans in the Earth's heat and hydrologic cycles
- The causes of sea-level change
- The ocean's biological system and its interplay with the Earth's carbon cycle

The chapter is organized as follows:

- In Section 3.2 we introduce the above four scientific topics and clarify the important issues.
- In Section 3.3 we discuss the observational requirements both from satellite and from other sources.
- In Section 3.4 we lay out the Earth Observing System (EOS) plans for addressing these scientific issues with these data sets.

3.1.2 Oceans and climate

The Earth's climate is driven by heat. Because the world ocean absorbs about half of the solar radiation the Earth receives, the ocean is an equal partner with the atmosphere in the climate system. The climate system redistributes the heat it gains in the tropics towards middle and high latitudes. The ocean again is an equal partner with the atmosphere in this poleward redistribution, yet much about how this climate engine functions, and certainly how its functioning changes over years and decades, remains only qualitatively known; EOS will change this.

Forecasts of the timing and geographic extent of seasonal-to-interannual climate anomalies at least a year in advance are within our reach. Such lead times can be envisaged primarily because the thermal inertia of the coupled climate system rests in the upper ocean, which has a relatively slow response compared to the atmosphere.

Of great influence on the surface climate of the Earth—where people live—is atmospheric transparency to solar radiation and opacity to longwave radiation. Carbon dioxide is typical of the gases that give the atmosphere these properties. The abundance of carbon in the atmosphere is tied to the chemistry and biology of life both on land and in the ocean. Here again, in the Earth's carbon cycle, the ocean's role of absorbing and sequestering CO₂ in ocean sediments is crucial.

These are the motivations for EOS's strong oceanographic component in its plans for Earth system research.

3.1.3 Oceans and humanity

The oceans not only play a role in modulating climate and weather, but they also provide food and mineral resources. The oceans support tourism. They serve as a waste repository. Coastal regions are the center of worldwide population increases; by 2020 over 65% of the world's population will live along continental margins. Changes in climate with their associated changes in sea level, in patterns of temperature and rainfall, have major impacts on the global economy and on the distribution and abundance of oceanic resources and on the industries that pursue them.

In particular, coastal waters are of immense economic and environmental importance. Almost 95% of the world's commerce is transported by ship through coastal waters; waterborne commerce for the U.S. for 1990 is estimated at \$465 billion. Coastal ocean oil and gas extraction currently accounts for about \$16 billion annually. According to estimates of the National Oceanic and Atmospheric Administration's (NOAA's) National Weather Service, the damages due to Hurricanes Hugo (in 1989), Andrew (in 1992), and Iniki (in 1992) caused a cumulative loss in excess of \$40 billion.

In 1992 U.S. commercial fisheries produced \$3.9 billion in revenue to fishermen at U.S. ports, with a total impact on the Gross National Product (GNP) of over \$50 billion. Yet fish populations and their associated fisheries are enormously variable, with interdecadal fluctuations of different fish populations that appear related to basin-wide oceanographic variability. The implication is that climate changes affect this resource in presently unknown ways. Past failures to modify fishing pressure in response to patterns of natural variability have produced disastrous collapses. Sardines off the U.S. west coast are just now recovering, the cod and haddock fishery is virtually closed, and many Northwest salmon species are threatened while Alaskan salmon are at record high levels.

These issues of resource management, marine-centered commerce, and safety are the second motivation for EOS's strong component of both physical and biological oceanographic studies within its investigations of Planet Earth.

3.2 Major scientific questions

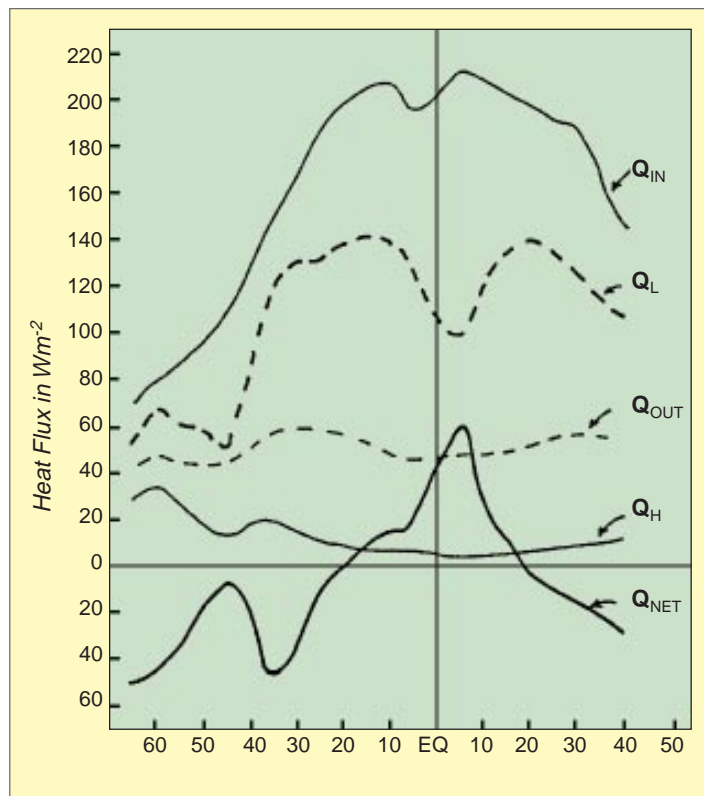
3.2.1 Ocean-atmosphere surface coupling

One of the major scientific requirements of climate research is to quantify the roles of the ocean and atmosphere in regulating the momentum, heat, water, and gas exchange at the air-sea interface. The ocean is not “forced” by the atmosphere but is coupled to it as part of the climate system. Understanding of these exchanges can be conceived of in two parts. The first is the fundamental knowledge of the physics and chemistry of seawater, sea ice, and air, and of the dynamical processes in both atmospheric and oceanic boundary layers. These can be loosely thought of as the “rules of air-sea exchange.” The second part is the large-scale atmospheric and oceanic states that together determine the magnitude and direction of the exchange by setting the relevant variables: near-surface winds, air-sea temperature and humidity differences, atmospheric water content and ensuing precipitation, and clouds that control the net surface radiation balance. Both clarifying the “rules” governing air-sea interaction and understanding the role of this interaction in the coupled atmosphere-ocean climate system are important elements of EOS research.

The linkage between the upper ocean and the lower atmosphere operates on relatively short time scales by processes such as seasonal formation of sea ice, stratification of the ocean through surface warming, and the spring bloom of phytoplankton. However, one of the great challenges in climate research is the coupling between the rapidly-varying upper ocean and the slowly-varying deep ocean. If the ocean were just a shallow layer of water, climate prediction would be much simpler. However, the mid ocean and the deep ocean have time scales of years to centuries. For example, deep water formed in Greenland and Labrador seas may not re-encounter the atmosphere for two centuries. Thus the ocean acts as the “memory” of the ocean/atmosphere system. These long time scales lead to teleconnections between widely-separated regions of the ocean (Trenberth and Hoar 1996) with unexpected impacts on climate and ecological processes. Thus climate studies must include both the short-term processes that couple the lower atmosphere with the upper ocean and the longer-term links between the upper ocean and mid- and deep-ocean processes.

The primary mechanisms of local air-sea interaction are well known and qualitatively understood. Sea-surface evaporation tends to cool and salinify the upper ocean, as well as supplying latent heat and water to the atmosphere. There is a strong feedback between water in the troposphere and ocean surface heating: clouds absorb and re-emit outgoing terrestrial radiation and scatter and absorb incoming solar radiation. They also tend to cool and freshen the near-surface water through rainfall. Ocean circulation depends on the net surface fluxes, which are subtly balanced between large incoming and outgoing components, e.g., the near balance between latent heat loss and the solar radiative gain in the heat budget, or the differences between precipitation and evaporation in the surface freshwater budget. The thermal components have equivalent heat transfers on the order of 100 Wm^{-2} , but the variations and differences necessary to understand many climate problems are on the order of 10 Wm^{-2} . This

FIGURE 3.1



Zonally-averaged heat flux across the air-sea surface (annual meridional profile for three oceans). Q_{IN} is the net incoming solar radiation, Q_{OUT} is the net outgoing longwave radiation, Q_H and Q_L are sensible and latent heat fluxes, and Q_{NET} is the sum of $Q_{IN} - Q_{OUT} - Q_H - Q_L$ (Hsiung 1986).

is a severe requirement for both observations and climate models.

More than half of the annually-averaged solar energy entering the climate system is absorbed by the ocean (Sellers 1965). The fate of that oceanic heating is illustrated in Figure 3.1. Although the upward flux of longwave radiation from the ocean surface is large, it is nearly balanced by the downward flux from the atmosphere, and the net radiative flux is therefore dominated by solar radiation. Ninety percent of the net radiative heating of the global ocean is balanced by evaporative cooling, with the remaining ten percent coming from sensible heat exchange with the atmosphere.

Evaporation plays a major role in the freshwater budget of the ocean (Baumgartner and Reichel 1975). On a global and annually-averaged basis, the ocean loses ten percent more water through evaporation than it gains through atmospheric precipitation. Approximate balance is maintained on an annual basis by river runoff. On longer time scales, gradients of these freshwater and thermal inputs and their mixing with the upper ocean constrain the thermohaline component of ocean circulation.

Spaceborne observations provide unprecedented spatial coverage of air-sea interaction parameters; clearly these are crucial EOS observations. A fundamental condition for developing confidence in the ability of global coupled models to simulate climate change is that they be able to reproduce aspects of the observed fields to within the observational errors. To have a significant impact on climate research, we plan for simultaneous observations of these parameters to be continued for a sufficient period to document synoptic, seasonal, and interannual variability of the climate system, and to begin building the database for exploring decadal-to-centennial variability.

One of the most graphic examples of how air-sea interaction affects people's lives is its role in severe storms. The probabilities and actual occurrences of severe storms are affected by ocean variability. The linkages are complex. The Kuroshio carries warm, equatorial waters along the coast to Japan, then enters the interior of the Pacific. Recent analyses show that planetary (Rossby) waves caused the Kuroshio to shift northward during 1993, changing where the ocean releases heat to the atmosphere. The more-remarkable issue, however, is that the Rossby waves were themselves a consequence of the propagation of Kelvin waves associated with the 1982–83 El Niño—first eastward along the equator, then northward along the coast of North America. This is a striking example of the ocean's memory and the time scales of the coupled ocean-atmosphere system (see Jacobs et al. 1994). Another example occurred in 1993 when the jet stream

became stuck south of its usual path. This allowed intense cyclone activity to propagate directly into the U.S. Midwest, and also allowed the atmosphere to acquire more moisture than usual from the Gulf of Mexico and transport it in storms lasting 122 days into the Mississippi basin and eastern United States, causing disastrous flooding.

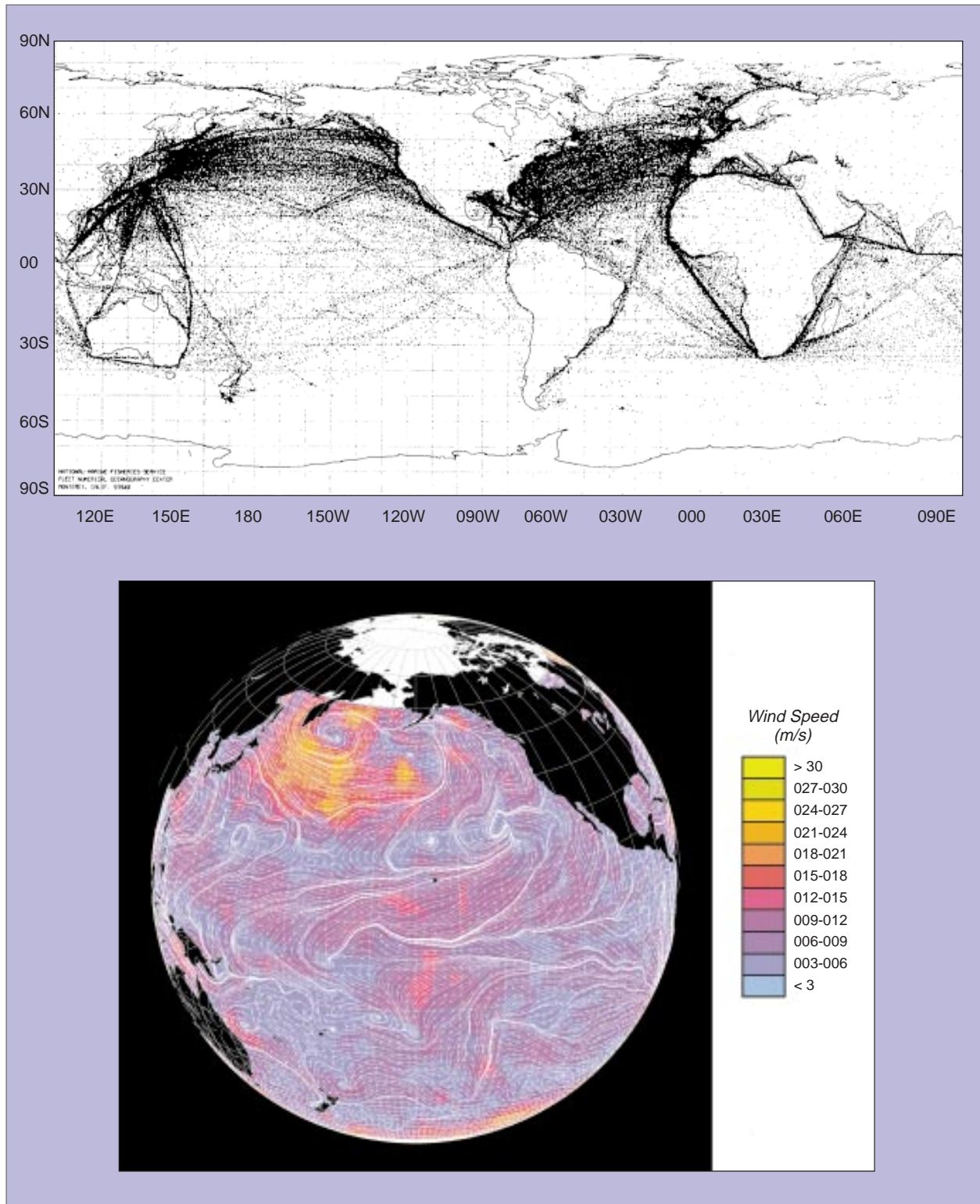
3.2.1.1 Momentum exchange

The exchange of momentum between the atmosphere and the ocean plays a critical role in determining climate (e.g., Gill 1982). Wind stress is the largest single source of momentum to the upper ocean, and air-sea momentum fluxes substantially influence large-scale upper-ocean circulation, smaller-scale mixing, and, through wave generation, the detailed shape of the sea surface on scales from centimeters to hundreds of meters. The wind-dependent roughness (variable geometry) of the surface directly influences the air-sea fluxes of all other quantities (e.g., sensible and latent heat, water, and gases). Air-sea momentum fluxes and near-surface winds thus modulate the coupling between the atmosphere and the ocean. Understanding, measuring, and ultimately predicting air-sea momentum exchange and the partitioning of this momentum between oceanic motions on various scales are thus among the central tasks in climate research.

Most historical estimates of large-scale air-sea momentum fluxes were based on compilations of direct observations of near-surface winds and sea conditions (e.g., Hellerman and Rosenstein 1983). The great hemispherical disparity in ocean surface area (larger in the Southern Hemisphere) and density of shipping tracks (much larger in the Northern Hemisphere) resulted in large geographical differences in the accuracies of these climatologies. Thus, while typical annual-mean global wind stresses are 0.1–0.15 N m^{-2} , statistical uncertainties ranged from less than 0.01 N m^{-2} in the northern midlatitude and tropical oceans to more than 0.05 N m^{-2} in mid and high southern latitudes (Hellerman and Rosenstein 1983). Comparisons between climatologies produced by different investigators yielded differences that were often larger than the error estimates of each of the individual products (Harrison 1989).

More recently, large-scale air-sea momentum flux climatologies have been constructed from operational surface wind analyses produced by weather prediction centers (e.g., Trenberth et al. 1990). Although the analysis/forecast systems include sophisticated physics and attempt to assimilate all available surface and upper-air data, significant differences also exist between and among these climatologies and with conventional and remotely-sensed data sets (e.g., Mestas-Nunez et al. 1994), with the climatically important tropics and high Southern lati-

FIGURE 3.2



The top image shows locations of all ship observations of surface meteorological variables for 100 days beginning 1 July 1978; one acquires the same number of observations, globally distributed, in one day of NSCAT observing (Freilich 1985, JPL Pub. 84-57). The bottom image shows a synoptic wind field derived from interpolated ERS-1 scatterometer data for February 10, 1993. The color in the image represents wind speed, and the streamlines indicate wind direction (courtesy of T. Liu and W. Tang).

tudes exhibiting the largest uncertainties and intercomparison differences. Figure 3.2 illustrates the huge sampling advantage of a satellite.

Differences and errors in the wind stress fields used in ocean and coupled ocean-atmosphere modeling lead to significant differences in the models' predictions. As just one example, a recent comparison of tropical ocean model results driven by three widely-used wind stress climatologies concluded that large differences in the model predictions of equatorial oceanic circulation resulted primarily from differences in the wind-stress forcing (Bryan et al. 1995b). In addition, Milliff et al. (1996) have shown that modern ocean model predictions are sensitive to small-scale wind stress features that are undoubtedly present in the real world but are unresolved in all existing air-sea momentum flux climatologies.

The past two decades have witnessed a great advancement in our ability to measure near-surface winds and air-sea momentum fluxes using satellite-borne instruments. Microwave multichannel radiometers and active scatterometers have been proven capable of acquiring all-weather measurements of wind-stress magnitudes (radiometers) and vector stresses (scatterometers) over extensive areas with high spatial resolution. The accuracies of these measurements (discussed in more detail in Section 3.3) are comparable to those of in situ meteorological buoys, while their global coverage substantially eliminates the geographical disparity in data distribution that dominates historical wind stress climatologies. Construction of consistent, high-resolution, accurate wind-stress (air-sea momentum flux) data sets and their application in ocean and climate modeling represents a crucial component of the EOS science objectives.

3.2.1.2 *Thermal fluxes: radiative and turbulent*

Surface heat exchange can be divided into four components: sensible heat resulting from the vertical thermal gradient, latent heat of evaporation, shortwave radiation from the sun, and longwave radiation from the atmosphere and the ocean. Sensible and latent heat fluxes are transported by turbulence. The parameterization of turbulence in terms of average measurements (wind speed, air temperature, air humidity, and sea-surface temperature [SST]) in routine ship reports has been extensively studied in the last few decades. Spaceborne sensors can measure surface wind speed and SST over the ice-free ocean, but not air temperature and humidity.

The ocean has a thermal inertia that is much greater than that of the atmosphere, but it is an oversimplification to view the atmosphere as a slave to the ocean, consisting of independent vertical columns of air in equilibrium with a local value of the SST. As early as the

mid-1960s, Bjerknes argued that it is likely that decadal-to-centennial variations in the thermohaline circulation depend on exchanges of heat and water with the atmosphere that are explained not solely by local air-sea interaction but more by changing modes of atmospheric and oceanic circulation. His insight is being proved correct. The theory of the El Niño-Southern Oscillation (ENSO), the periodic warming of the southeastern Pacific and all the attendant oceanic and atmospheric changes, depends on the ability of both the atmosphere and ocean to support equatorial waves that form coupled large-scale fluctuations that would not exist in either the ocean or atmosphere alone (Zebiak and Cane 1987).

Some recent theoretical studies have begun to isolate and quantify the most important processes that regulate air-sea exchanges of heat and water. Simple atmospheric boundary layer models containing only large-scale horizontal advection of heat and moisture, surface fluxes, and entrainment of dry air from aloft into the atmospheric boundary layer (Kleeman and Power 1995; Seager et al. 1995), can explain much of the observed pattern of sensible and latent heat fluxes over the global oceans, such as the observed seasonal changes in latent heat flux over the North Atlantic shown in Figure 3.3. Simple ocean-atmosphere column models have been used to explore the subtle relationships between radiation, convection, and large-scale divergent circulations in the ocean and atmosphere, and their role in regulating air-sea exchanges of heat and water (Betts and Ridgway 1989; Sui et al. 1991). EOS will produce data sets and analyses over the global oceans that are necessary to test these working hypotheses. In the data-sparse areas of the southern and tropical oceans, the utilization of satellite observations will provide the first reliable estimates of the near-surface turbulent and radiative fluxes.

3.2.1.3 *Freshwater forcing: evaporation, precipitation, and sea ice*

The sources and sinks of freshwater at the ocean surface are a crucial component of the global water balance which is shown in Figure 3.4. The ocean loses about 10% more freshwater through evaporation than it gains through precipitation (Baumgartner and Reichel 1975). The remaining 10% is contributed by river runoff, with the change in storage of freshwater in the oceans being a much smaller residual. The surface freshwater flux determines upper ocean mixing and the thermohaline component of ocean circulation. The stabilizing effect of a local net freshwater surface input limits the efficiency of ocean-atmosphere communication: it impedes heat exchange with subsurface layers, nutrient transport to the upper ocean, and trace gas exchange with the atmosphere. In the atmosphere these

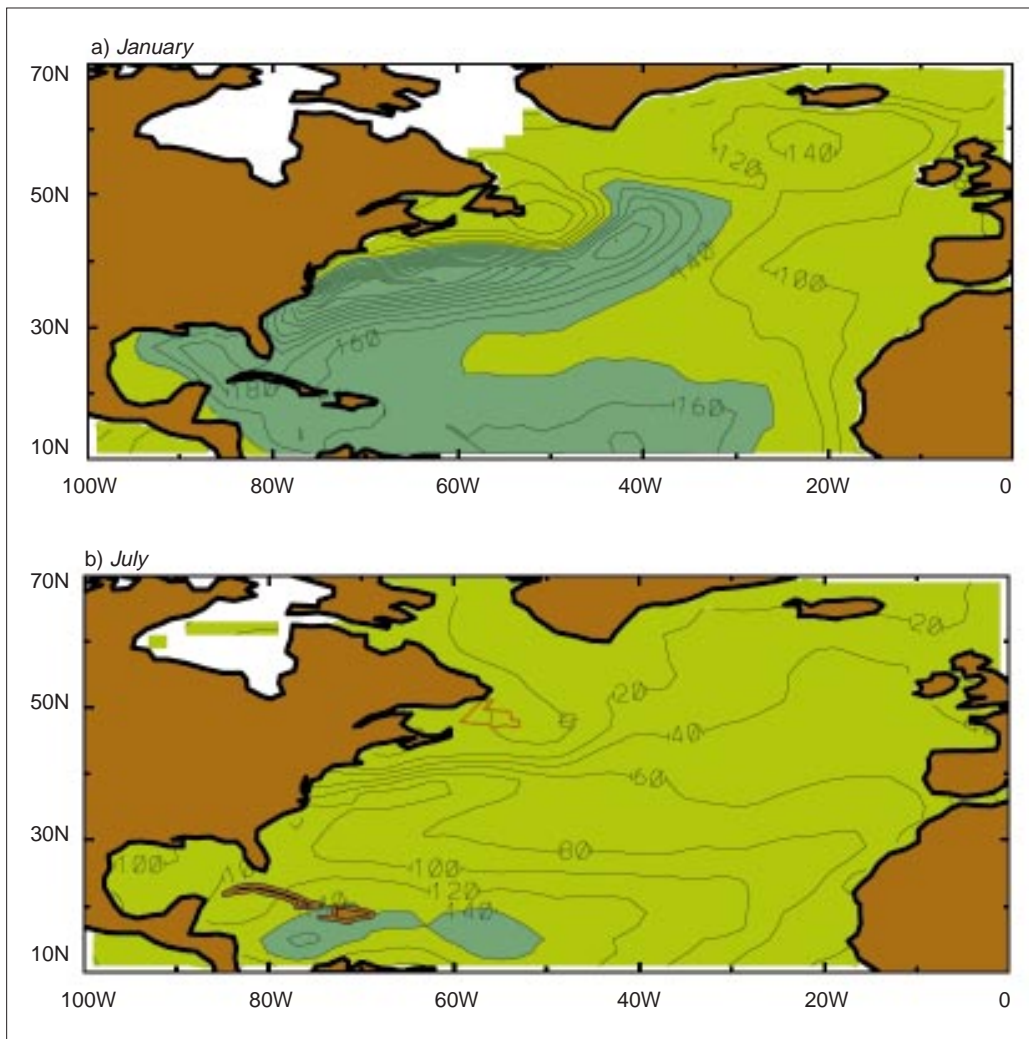
fluxes determine atmospheric moisture content and latent heat that drive tropospheric convection, horizontal advection, and precipitation patterns.

Surface freshwater forcing is believed to play a primary role in setting the background state and timing of the large interannual phenomenon of ENSO. Theory suggests that equatorial upper-ocean heat content and mixed-layer depth are crucial in setting ENSO time scales (Zebiak and Cane 1987). Over the western Pacific warm pool region, the upper-ocean mixed layer is observed to be very shallow, on the order of 30 m, apparently due to a combination of stabilization by precipitation and highly intermittent wind forcing (Lukas and Lindstrom 1991). Long-term observations that permit the accurate estimation of precipitation, evaporation, and wind stress are

therefore likely to be important for an improved understanding of ENSO, and for the development of a quantitative ENSO prediction capability.

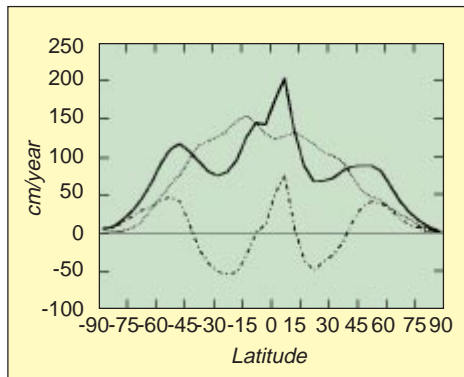
On longer time scales, the present picture of the global thermohaline circulation includes surface processes in both north and south polar seas. Sea ice melts and freezes, forcing the surface freshwater balance in complete analogy with evaporation and precipitation. The Arctic Ocean is a large ice-covered estuary that funnels freshwater from rivers and the North Pacific Ocean across the Pole and into the North Atlantic Ocean. In a sense, the Arctic acts as a global “choke point” for calculating the freshwater budget of the world ocean (Wijffels et al. 1992). Part of this freshwater is converted to sea ice during the winter and exits the Arctic Ocean through Fram Strait;

FIGURE 3.3



Climatological estimates of latent heat flux (Wm^{-2}) over the North Atlantic for January and July by Oberhuber (1988) (courtesy of S. Esbensen).

FIGURE 3.4



Latitudinal distribution of the global surface hydrologic balance, showing evaporation E , precipitation P , and runoff Δf (data from Baumgartner and Reichel 1975).

the remainder stays in liquid form and exits through both Fram Strait and the Canadian Archipelago. This low-salinity Arctic outflow is delicately balanced with respect to the underlying water masses in the subpolar North Atlantic. Small changes in the amount and salinity of the outflow are sufficient to permit or restrain deep convection in the Greenland and Labrador seas, which in turn affects the global thermohaline circulation (Broecker and Denton 1989). Deep convection is thought to be controlled by rapid cooling and freezing of this cold, low-salinity outflow. Recent observations indicate that the formation of North Atlantic Deep Water (NADW) in the Greenland Sea experiences large interannual changes, and in fact may have shut down completely in recent years (Schlosser et al. 1991). In ways not understood at present, the supply of NADW is thought to be linked with the wind stress driving the Antarctic Circumpolar Current in controlling the world ocean's deep thermohaline circulation.

The Southern Ocean is the source of the coldest oceanic deep water, Antarctic Bottom Water (AABW). The density stratification of the Southern Ocean is weak compared to waters at lower latitudes and is largely determined by salinity. The lack of vertical stratification implies that the dynamical scales of ocean eddies in the Southern Ocean are very small and that topographically-induced disturbances extend to the surface. The large-scale geostrophic flow is not sufficient to explain the Southern Ocean heat budget in the AABW source region (de Szoeke and Levine 1981), suggesting that mesoscale eddies may be responsible for supplying the required advective contributions. Similarly, measured sediment fluxes and the apparent new nitrate production that is available for export do not balance (Honjo 1990; DeMaster et al. 1992; Smith and Sakshaug 1990). One possible explanation is

that there may be considerable vertical transport of organic matter that is not explained by gravitational sinking. Thus, in addition to the physical processes associated with the Antarctic sea ice distribution, the freshwater input at the surface is thought to play a role in determining the location and characteristics of ocean disturbances responsible for AABW formation and the biological productivity of the region. Accurate long-term observations of surface thermohaline and mechanical forcing are required to understand such complex interactions between the physical and biological systems over the global oceans.

3.2.2 Ocean circulation

Ocean circulation is important for three reasons:

- horizontal heat transport,
- establishment of surface temperature patterns that are important to air-sea exchange, and
- transport of nutrients, chemicals, and biota for biochemical processes.

3.2.2.1 Oceans and the global heat balance

The oceans play a vital role in the heat balance of the globe by acting as a storage medium of thermal energy and by transporting thermal energy from the tropics to middle and high latitudes. In fact, as Figure 3.5 (pg. 124) shows, the ocean and atmosphere each transport about half of the total poleward heat flux in the global climate energy balance (Trenberth and Solomon 1994). Over large portions of the oceans, seasonal heat storage is very local because thermal energy cannot be transported over great distances during a single season (Gill and Niiler 1973). However, along western boundaries and on the equator a very different picture emerges. There is a net flux of heat into the equatorial oceans due to the intensive solar radiation, and this thermal energy is transported poleward by wind-driven currents of the surface layers (Wyrtki 1982). The poleward transport reaches a maximum in the Horse Latitudes (30-35° N and S), where the western boundary currents become well formed. The warm water moving poleward from these latitudes is intensely cooled by the dry and cold air masses that spill from the continents each winter. In each ocean basin this process is somewhat different; it is most intense in the North Atlantic and results in significant warming of the air in its journey to northern Europe. The British Isles are kept so much warmer than Siberia in winter not by oceanic heat stored locally in summer, but by the great northward flow of heat in the Gulf Stream (Stommel 1979).

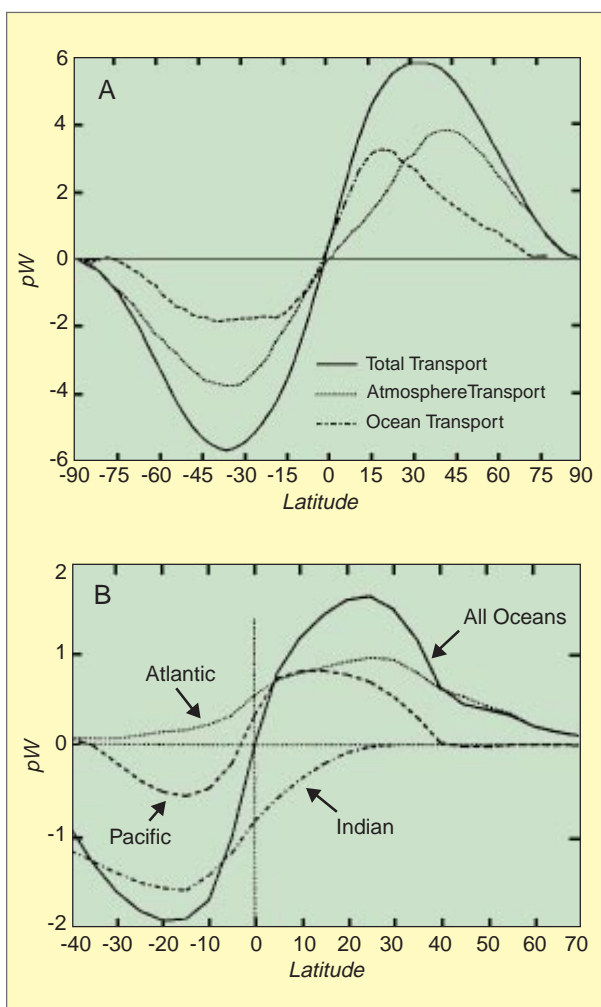
Besides its ability to transport heat, the ocean is simply very efficient at absorbing and storing heat. Compare the situation with land. The ocean thermal capacity

is several orders of magnitude larger than that of land because water is more absorptive to visible radiation, and the turbulent diffusivity of heat in the wind-blown sea is several orders of magnitude larger than that of soil (Niiler 1992). One consequence is that the seasonal range of the air temperature over the ice-free ocean is seldom more than 17°C, while over the continental land masses the seasonal peak can be in excess of 70°C. The exceptions are coastal land areas that possess a milder “maritime” cli-

mate and attract a much-larger population density than continental interiors.

Although the importance of the ocean in determining weather and climate has long been recognized, we are now in the early stages of applying ocean-atmosphere forecasting to such practical uses as crop and fisheries management. For instance, the focus on the interannual variability of air-sea interaction in El Niño is elucidating the mechanisms by which global weather patterns are altered by the ocean. Correlations between El Niño and crop yields are significant; the presence of El Niño appears to cause a 15% crop decrease in the southeast United States. Twelve-month forecasts are leading to experimental efforts at crop selection on a year-by-year basis, for instance, in Brazil and Peru. These forecast techniques are at present a blend of statistical and physical models. The physical basis of these forecasts can be strengthened if better data sets are acquired to improve their initialization and the understanding of the model processes.

FIGURE 3.5



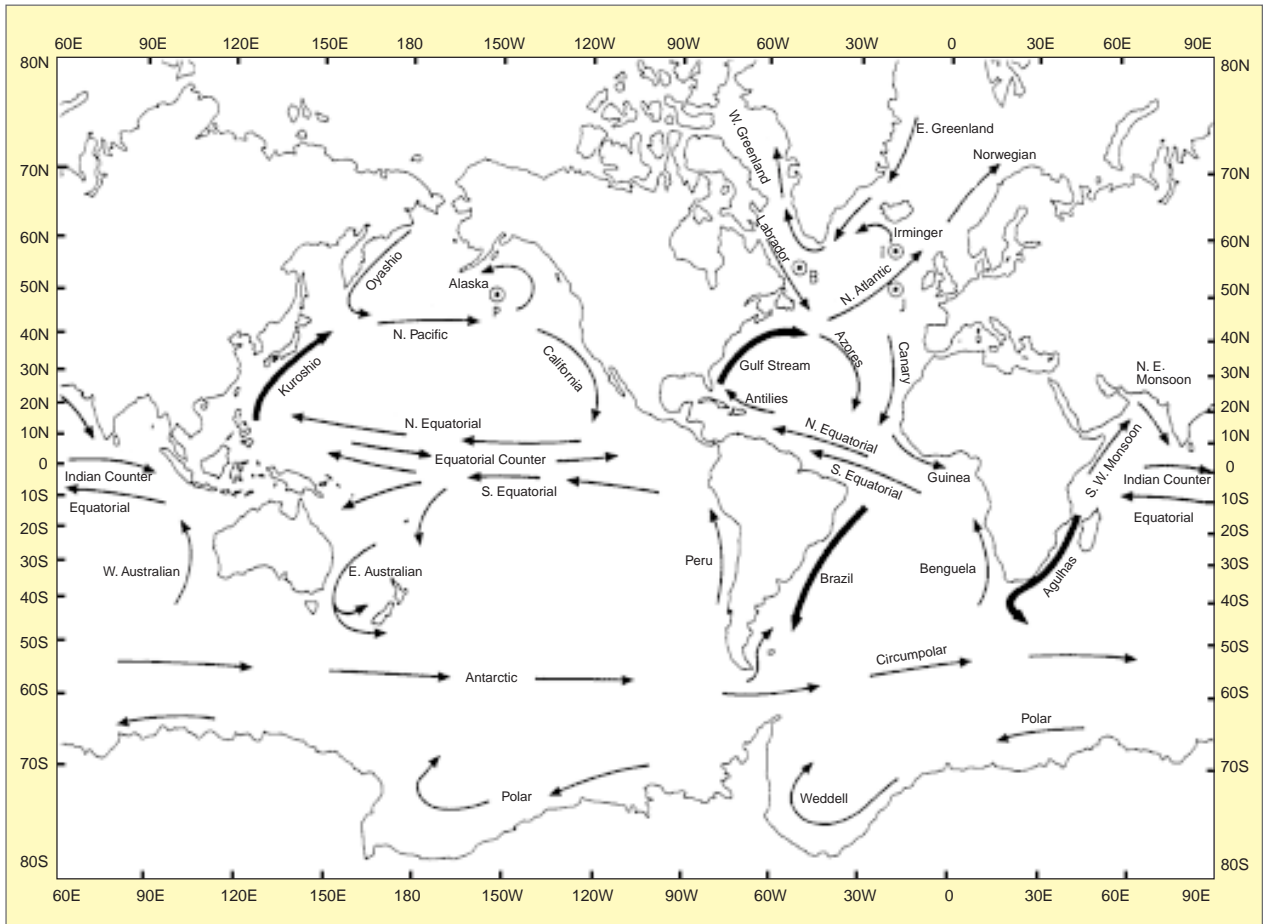
A) Estimates of the annual mean meridional energy transport (positive northward) required by the energy balance at the top of the atmosphere, estimated from atmospheric observations by Peixoto and Oort (1984) and the Earth Radiation Budget Experiment, in petawatts ($=10^{15}$ W). The oceanic transport is obtained by subtracting the atmospheric energy transport from the total transport required by the annual energy balance. B) Meridional profiles of the northward oceanic heat transport for the various oceans, computed indirectly from the surface heat balance (Adapted from Hsiung [1985]).

3.2.2.2 Ocean circulation

The ocean general circulation shown in Figure 3.6A is dominated by vorticity conservation and the mechanisms by which vorticity is generated and dissipated. Vorticity dynamics determine the position of major ocean current systems such as the Gulf Stream, the Kuroshio, and the Antarctic Circumpolar Current. Except near the equator, the horizontal circulation (barotropic or depth-averaged flow) is largely forced by the wind stress curl through Ekman dynamics. Wind stress supplies oceanic vorticity by imparting a convergence (divergence) within the mixed layer in the subtropical (subpolar) gyres. Western boundary currents return water poleward (equatorward) in the major subtropical (subpolar) gyres and provide a means for dissipating vorticity. Within a few degrees of the equator, wind stress, in combination with the variation in the Coriolis parameter, drives the equatorial current system. Bottom topography and coastlines constrain the flow and combine with both the north-south gradient in the Coriolis parameter and wind stress to determine the general circulation. Instability of the large-scale circulation and the interaction of this flow with the bottom topography are primary sources of energy for eddies that move heat poleward in concert with the mean currents. We still need to improve our parameterizations of bottom drag and the effect of unresolved eddies upon the larger-scale flow.

Thermohaline circulation determines the vertical distribution of heat, salt, and momentum. It is the thermohaline circulation that transports deep water formed in the polar regions to low latitudes and eventually to the surface in upwelling regions as shown in Figure 3.6B (pg. 124). Aspects of this transport are becoming known

FIGURE 3.6A



The principal surface currents of the World Ocean. Western boundary currents are shown bold (Mann and Lazier 1991).

through analysis of in situ data, especially of deep tracers.

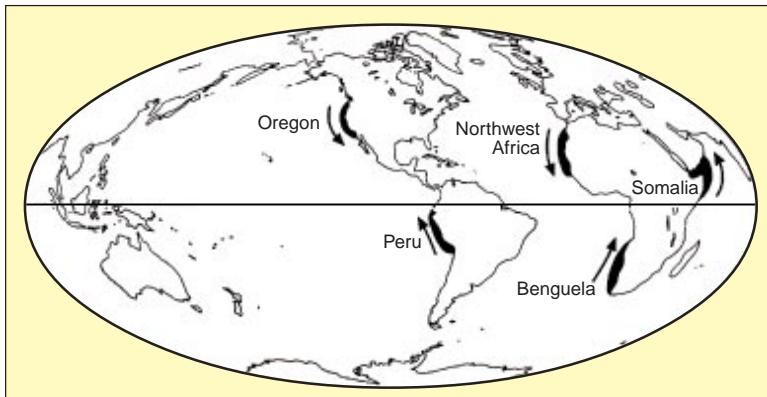
Forcing the thermohaline circulation is an interplay of atmospheric fluxes, solar heating, and oceanic flow that combine to determine the position at which isopycnal surfaces outcrop and largely control the temperature-salinity (T-S) characteristics of deep water during its formation at the surface. Vorticity dynamics remains a crucial element controlling the oceanic response to this forcing, although mixing and diffusive processes are also important. The oceanic mixed layer conveys most of the surface flux to the interior of the water column, and therefore upper-ocean processes are important to the thermohaline circulation. Seasonal cycles and the formation and dissipation of a seasonal thermocline are important in much of the midlatitudes.

Mixing processes that allow the T-S properties of water to be changed away from the ocean surface, although qualitatively understood, must be quantified. These in-

clude roles of topographically generated mixing, internal wave breaking, and background turbulence in the cross-isopycnal mixing needed to raise the buoyancy of deep water so that this water may reach the surface at low latitudes. The role of mesoscale eddies and other transient events in mixing the deep water is not well understood, nor is the importance of seasonal cycles and decadal-scale variability, both as the result of internal processes and as driven by variations in surface thermohaline forcing. An additional aspect of the thermohaline circulation is the prospect of thermohaline catastrophe, a fundamental change in the thermohaline circulation; modeling studies have demonstrated the capacity of the thermocline system to undergo dramatic internal changes in response to small changes in the forcing.

While the general circulation of the upper ocean is known, the deep circulation shown in Figure 3.7 (pg. 127) is more speculative. Also, we do not fully understand the processes involved with specific regional circulation pat-

FIGURE 3.6B



Major coastal upwelling regions, with arrows indicating the prevailing winds (Mann and Lazier 1991).

terns, yet these currents can be important to the meridional heat transport. Deep western boundary currents transport deep water rapidly towards the equator, losing water into the midlatitude gyres and providing a source of deep water to the central gyres. The processes that determine the deep western boundary currents, the rate of flow, and the fate of water entrained into these currents, are not known. Strong upwelling occurs along the equator and in eastern boundary current regions. Both processes are driven by wind stress and significantly alter the local upper-ocean temperature pattern. In midlatitudes, the mean surface heat flux is into the ocean in eastern boundary current regions and into the atmosphere away from them. In the Southern Ocean, the heat balance of the Antarctic Circumpolar Current cannot be reconciled with existing in situ measurements; eddy fluxes have been hypothesized as the missing component of the heat balance. These aspects of the ocean circulation must be resolved and properly represented in climate models.

To understand the thermohaline circulation, we must know not only the wind stress but also surface fluxes of heat and freshwater that force the baroclinic circulation. In concert with mixing and advection, these fluxes produce a rich array of “water masses” with individual, distinguishable T-S properties that are tied to source and history of a parcel of water. Together, these processes constitute the “conveyor belt” that transports warm salty surface water poleward and colder, fresher deep water equatorward. The thermohaline and barotropic circulations are intimately linked, making it difficult to approach them independently.

To quantify temporal changes in the circulation, four measurements from space are essential.

- *Winds at 10 m.* We do not have an adequate global picture of the mean, the seasonal changes, or the daily wind stress curl, the input of vorticity to the oceans (see Section 3.2.1.1).

- *Surface temperature and surface radiative, sensible, and latent heat fluxes.* As argued in Section 3.2.1.3, the latter quantities force the thermohaline component of the circulation; SST is a crucial diagnostic not only of ocean circulation but of the Earth’s climate.

- *Surface salinity and evaporation and precipitation.* Again, the latter quantities force the thermohaline component of the

circulation; salinity is a diagnostic of this surface forcing.

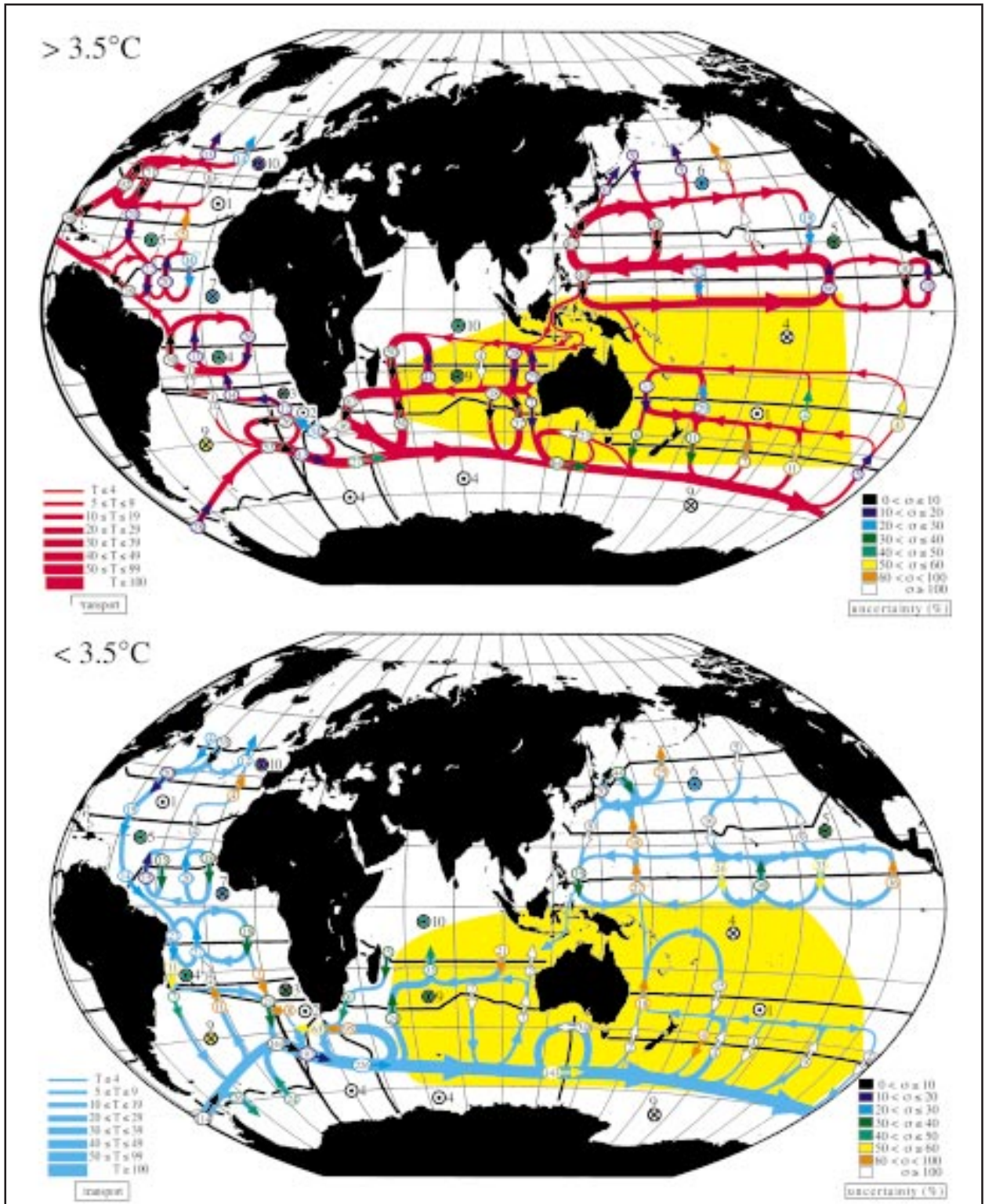
- *Surface geostrophic currents, as observed with altimetry.* They are the “response” to the “forcing,” and through the density stratification they constrain deep currents. It is important to remember the strong correlation between the surface and deeper levels.

3.2.2.3 Ocean modeling and data assimilation

Numerical ocean models embody simplifications of the equations that govern the dynamics and thermodynamics of the oceans. Future versions may incorporate biological processes, and perhaps chemical ones—the transport of possible chemical tracers is already encoded in current numerical models. Two of these simplifications are the quasi-geostrophic (Holland 1986) and the hydrostatic (Marshall et al. 1993), which is embedded in most primitive equation models.

In order to complete a useful simulation in present-day computers, other simplifications are introduced. Global models with relatively coarse spatial resolution are on the verge of resolving mesoscale eddies (e.g., Semtner and Chervin 1992) as some regional models already do (Bryan et al. 1995a). However, the rapid increase in computer power keeps changing the boundary. Another trade-off is the representation of the vertical density structure and associated change of properties. “Level” models (with the vertical quantized by depth) are generally thought to have excessive cross-isopycnal mixing, while layer models (with the vertical quantized by density) impose restrictions in modeling an upper-ocean mixed layer (New and Bleck 1995). Of course, regional models require specifying the flow and other fluxes at the open

FIGURE 3.7



Schematic of the global ocean circulation deduced from the best-estimate model (Macdonald and Wunsch 1996). The two panels (red and blue) illustrate the flow pattern of waters of potential temperatures greater and less than 3.5°C , respectively. The strength of the flows (in 10^9 kg s^{-1}) are indicated where they cross the model sections and are further illustrated by the thickness of the lines. Color shading indicates the uncertainty of the transport values (given as a percentage of the transport value). Circles with dots indicate upwelling within a box through the 3.5°C interface. Circles with crosses indicate downwelling. The yellow shading indicates the deduced region of influence of the Pacific-Indian throughflow (courtesy of A. Macdonald).

boundary, which makes them unsuitable for long-term climate studies.

Lacking actual data for surface fluxes of fresh water and heat, most models simulate these fluxes as proportional to the difference between model values and either climatologically averaged values that drive the model to correct upper-ocean climatology or atmospheric values from an atmospheric general circulation model (GCM).

Assimilation models change the “state” (model variables at all grid nodes) predicted by a numerical model based on data that differ from the model predictions; the modified model state in turn influences the future model evolution (e.g., Bennett and Chua 1994). Various techniques for assimilation are still maturing, and range from simple nudging (Sarmiento and Bryan 1982) to adjoint models (Thacker and Long 1988) and Kalman smoothers (Fukumori et al. 1993). The key practical problem remains the trade-off between computational burden and accurately using information on errors in the data and in the model to give proper weight to both the data and the model predictions.

The key advantage of assimilation is its ability to “propagate” information given by one data type and location to other variables and locations. To the extent that the physical model is accurate, the model, after assimilation, gives a four-dimensional description of the ocean (x, y, z, t) that is consistent with all the data, within their errors, and thus useful to understand the ocean processes responsible for the ocean’s state. By examining the differences between the assimilation and the data, one can determine model deficiencies and what additional data are needed to further constrain the model.

3.2.3 Global sea-level rise

Major climate-related factors that contribute to sea-level rise are thermal expansion in the oceans (steric changes) as well as ablating mountain glaciers and polar ice sheets. Other factors include complex processes of air-sea interaction and ocean circulation, as well as geophysical causes such as the postglacial rebound and ocean basin uplifts. Major uncertainties exist in the contributions of the Greenland and Antarctic ice sheets to recent changes in sea level as well as predicted future changes. The paucity in observational data concerning the mass balance of the polar ice sheets is the primary contributor to these uncertainties. Nevertheless, the polar ice sheets hold the potential for a global sea-level rise of 75 m if they were to experience complete melting.

Even partial shrinkage of the polar ice sheets would inundate the major coastlines of the world and produce serious economic consequences. However, such a collapse does not appear to be imminent, although the West Ant-

arctic ice sheet exhibits unstable characteristics. Of more-immediate concern are the effects of sea-level rise at the present rate of several mm/yr. The economic impact clearly increases as the rise increases. An example of the sensitivity of the coastal ecosystem to sea level is found in Louisiana, where baldcypress trees on fifty thousand acres of wetlands were defoliated in 1993 by an insect to which the trees were made vulnerable by increased salt-water flooding. The exposure of coastal commerce and property to severe storms is clearly worsened by the gradual rise of sea level. A rise of 3 mm/yr sounds immaterial but produces a rise of almost 10 cm in 30 years, a rise that could threaten wetlands and produce increased coastal erosion. A goal of EOS is to reduce the uncertainties in these estimates and provide a capability to predict the future state and human impact of sea level.

3.2.3.1 Mean ocean surface height

During the last Ice Age, 18,000 years ago, the global sea level was more than 100 m lower than at present. Recent studies of global sea-level change (Warrick and Oerlemans 1990) have concluded that the average rate of rise during the last century has been 1 to 3 mm/yr and that sea level by the year 2070 A.D. may be 20 to 70 cm higher than today. The thinking is that the increasing concentration of atmospheric greenhouse gases leads to global warming, which strongly affects the distribution of stored water and ice on the Earth (e.g., Peltier 1988; Warrick and Oerlemans 1990). Nearly half of the predicted sea-level rise would be due to thermal expansion of the oceans. The remainder would be caused by melting of Antarctica, Greenland, and other ice sheets and glaciers and by geophysical processes. Over longer time scales of glacial cycles, the thermal expansion of the oceans can account for a rise or fall of at most several meters.

One basic strategy for testing the notion of greenhouse warming is to detect and monitor global mean sea level. The strategy for EOS is to measure both mean sea level with radar altimeters and ice-sheet volume with laser altimeters.

Until the availability of satellite altimetry, long-term observations of tide gauge measurements have been used to monitor sea-level change. Recent tide gauge measurement studies indicate that the global mean sea level has risen over the last century at a rate of 1-3 mm/yr (Peltier 1988; Douglas 1991), with a suggestion of possible acceleration since the middle of the last century. The poor global distribution of tide gauges (mostly in coastal regions, therefore significantly affected by the effect of postglacial rebound) and the use of a dynamically changing reference make it difficult to separate these effects. However, by coupling satellite measurements with glo-

bal circulation models, these effects can be separated because they are expected to have quite distinct spatial and temporal patterns. The advantage of tide gauges is that they provide a multi-decadal observational record, and they can act as in situ calibration devices for radar altimeters.

Satellite altimetry missions in this decade and beyond (the Earth Remote-sensing Satellite [ERS-1], Ocean Topography Experiment [TOPEX]/Poseidon, ERS-2, Geosat Follow-On [GFO], Environmental Satellite [ENVISAT], and EOS Jason-1) will provide global measurements of long-term mean sea level and its variations with an accuracy approaching 1 mm/yr. The unprecedented accuracy of TOPEX/Poseidon enables a number of studies based primarily on the technique reported by Born et al. (1986). Figure 3.8 (pg. 130) shows that during a 42-month period sea level rises in some regions by up to 60 mm/yr and falls similarly in others while the global mean essentially shows a slight fall at 0 ± 2 mm/yr (Guman et al. 1996). There is evidence that the global-scale sea-level variations are due to dynamical phenomena such as El Niño with time scales of several years. This is a clear case where a monitoring period longer than a decade will greatly clarify our understanding. As the multi-year phenomena are “averaged out,” the secular change in sea level will become more evident. An effort linking operational and scientific altimeters (Geosat, ERS-1, and TOPEX/Poseidon) from 1987 to 1995, with a 4-year data gap between 1989 and 1992, shows that the global mean sea level is rising at a rate of 1 ± 5 mm/yr (Guman et al. 1996). The large uncertainty is primarily due to the inaccurate calibration between Geosat and TOPEX/Poseidon and insufficient knowledge of the instrument drifts. The uncertainty will decrease with improved calibration and longer data span. Figure 3.9 (pg. 131) shows the Pacific mean sea-level variation over 9 years from both altimeters and tide gauges; the trend is 0 ± 2 mm/yr. The agreement between altimeter and tide gauge sea-level measurements is good. EOS will contribute 1) a longer data span and 2) improved modeling of ocean circulation and geophysical effects to allow the separation of the global warming signal and other natural processes.

3.2.3.2 Ice sheets, glaciers, and continental movements

Potentially the largest influences on sea level (up to 80 m of sea-level equivalent) come from land ice. The main reservoirs are mountain glaciers (0.5 m of sea-level equivalent), the Greenland ice sheet (7 m), and the ice sheets in West Antarctica (6 m) and East Antarctica (65 m). In the ordinary view, the sensitivity of the ice sheets to climate change, and the rate at which they are likely to deliver water to the oceans, is inversely related to their

size. However, this generality would fail if dynamic processes destabilized an ice mass, such as the West Antarctic ice sheet.

The scientific challenges are to assess the modern state of balance of the ice masses, and especially to predict their future balance in a modified climate. At present, the combined uncertainties in the mass balances of land ice are larger than the uncertainty in sea-level rise and contributions from other sources, so the ocean is our most sensitive indicator of land-ice mass balance. As we wish to predict sea-level change, this is an unacceptable situation. The goals and requirements for measuring the mass balance of ice sheets and glaciers are described in Chapter 6, “The Cryospheric System.”

3.2.3.3 Steric change and ocean circulation

Overall heating also changes sea level by causing thermal expansion of a column of seawater. In general, these changes give rise to an altered sea surface and ocean density structure. Repeated altimetric observations of the global mean sea-surface height determine the change in the total volume of water in the ocean. For this calculation, the geoid (the shape of the “locally level” sea surface) need not be known. In situ data on changes of the temperature and salinity structure determine what part of the change in the volume of the ocean is due to changes of state in the seawater; any residual should equal the net contribution from melting ice.

In addition to the global mean sea level, there is great practical importance to local mean sea level. To know how local mean sea level is changing requires much more knowledge, including changes in the major current systems. To know these, one needs to know the geoid, and the long-term changes in the ocean surface forcing—winds, and the net surface freshwater and heat fluxes.

3.2.3.4 Ocean tides

The astronomical tides result from the gravitational interaction of the Sun, the Moon, and the Earth. Tidal periods are well known and range from 12 hours to 18.6 years. Because tides are a nearly resonant sloshing of water in a rotating ocean basin with islands, trenches, and shelves, tidal amplitude and phase are difficult to predict accurately from first principles, particularly in coastal regions and semi-enclosed seas. Predictions based on harmonic analysis of tidal data also contain uncertainty, because non-tidal dynamical phenomena have similar natural frequencies.

Progress in quantifying tides depends on assimilating surface-height data into hydrodynamic models. The advent of satellite altimetry in the 1980s, along with space geodetic measurements such as satellite laser ranging

(SLR) to geodetic satellites, and advances in numerical tidal modeling and data assimilation have enabled the prediction of global ocean tides in the deep ocean with unprecedented accuracy. Ten global tide models developed since 1994 agree within 2-3 cm in the deep ocean, and they represent an improvement over the earlier Schwiderski model by approximately 5 cm rms (Shum et al. 1996).

Because tides cause a larger sea-level signal than temporal changes in ocean circulation and sea level, an accurate tidal model is required to remove the tidal signal for studies of ocean circulation with altimetry. Tides do more than contaminate ocean circulation signals; they directly affect the ocean loading of the sea bed and hence the geodetic shape of the Earth and its instantaneous gravity field. Their effect on gravity causes slight perturbations in satellite orbits. So knowledge of tides is crucial for extracting a full range of accurate geometric information from altimetric and geodetic measurements.

Tides have been of immense commercial importance for millennia, especially for coastal commerce. The better known deep water tides are generally used to con-

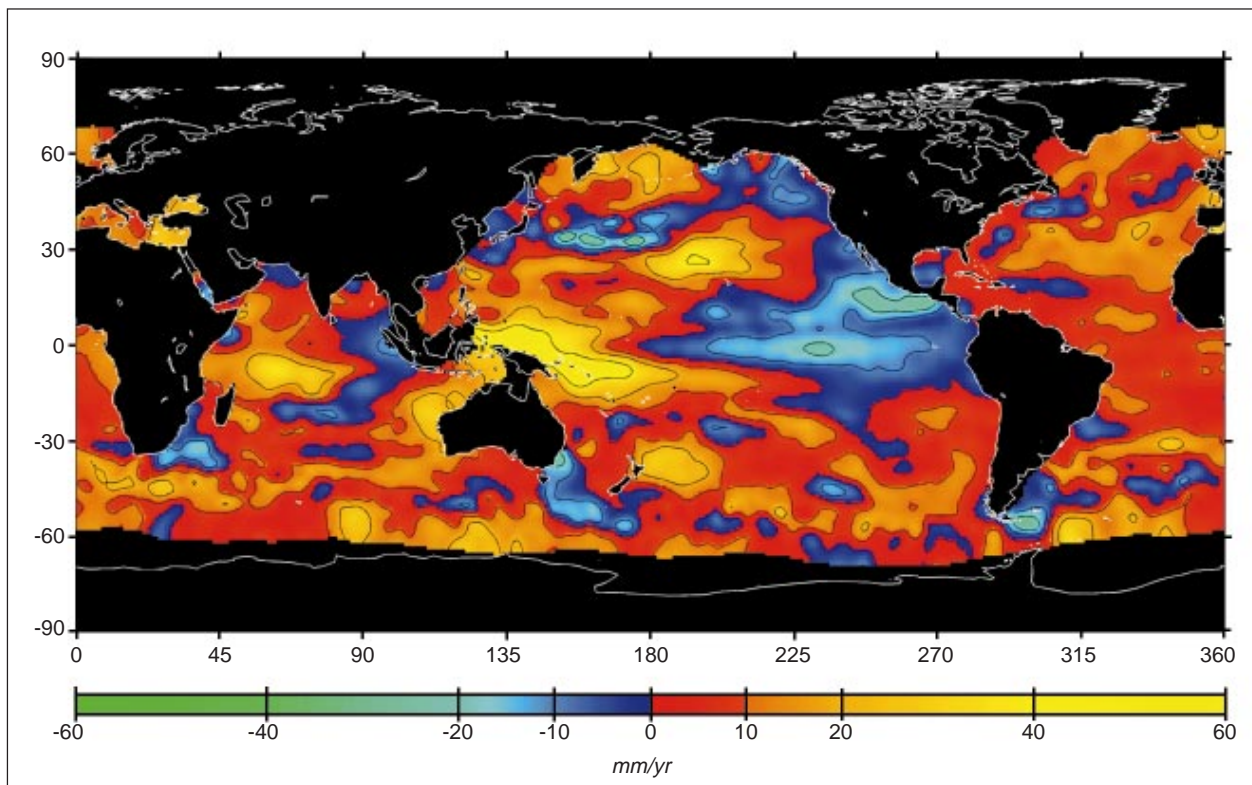
strain very-fine-resolution coastal models at their seaward boundaries. The largest differences in predictions by various tide models occur in precisely those regions most crucial for human activity—shallow coastal waters—where forecasts of waves, eddies, local sea-level changes, and storm surges vitally affect coastal populations, fisheries, and offshore oil exploration and drilling.

3.2.4 *The marine biosphere and ocean carbon system*

3.2.4.1 *Introduction*

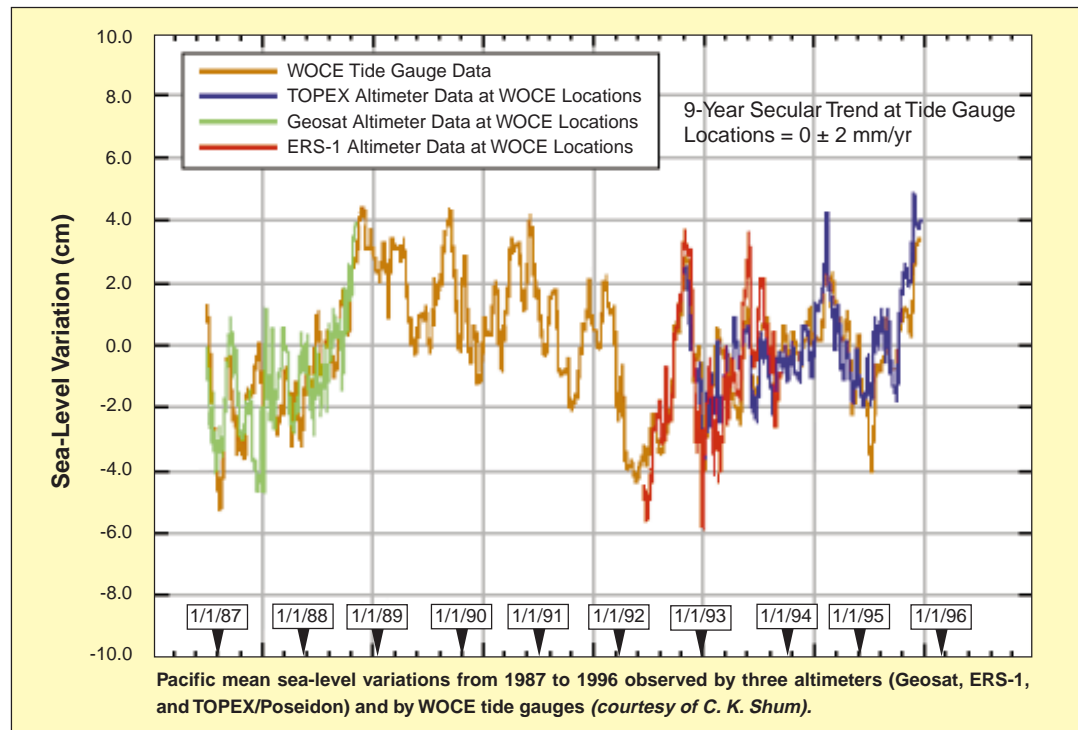
The importance of the ocean in the world carbon cycle is simple in concept: the ocean is an alkaline solution of vast size and in constant motion; carbon dioxide is an acidic gas with a rapidly rising atmospheric signal. The result is a gigantic chemical reaction, whose capacity is governed by the alkalinity of the world ocean, and whose rate is governed by the wind stirring of this solution, and by heating and cooling, with a mean turnover time of about 500 years. The relationship of rates, areas, and chemistry is such that the enormous oceanic presence on the plan-

FIGURE 3.8



Geographical distribution of sea level trends observed by pre-Earth Observing System (EOS) sensor TOPEX/Poseidon altimeter measurements from October 1992 through January 1996. The regional sea level rise and fall over the time span reaches 60 mm/yr (courtesy of C. K. Shum).

FIGURE 3.9



etary surface accounts for the annual uptake of about 40% of the carbon dioxide emissions of humankind.

Due to the complex chemistry, the exchange rate of carbon dioxide with the ocean surface is quite slow; while atmospheric gases such as oxygen or nitrogen reach equilibrium with the upper-ocean mixed layer in about a month; CO_2 takes about a year to equilibrate. This slow rate allows complex patterns of disequilibrium between air and sea to occur. The pre-industrial pattern of this disequilibrium is now overwritten by the signature of human industrial activities. By this time the forcing of the industrial signal is calculated to drive an 8-9 microatmospheres mean difference in CO_2 partial pressure between air and sea, and the signal is climbing. The complex natural pattern means that this signal is hard to detect amidst natural variability.

While oceanic CO_2 cannot be detected directly from space, the forcing terms driving its distribution can. For example, biological activity from photosynthesis is a very large driver of variability and can be remotely sensed as ocean color. Temperature alone is a diagnostic of solubility; however, given enough time, either warm or cold water would reach equilibrium with the atmosphere. It is the rate of temperature change with season or circulation,

relative to the surface gas exchange rate, that is critical in driving variability of CO_2 uptake.

The primary challenge for ocean research is to understand the coupling of the physical, chemical, and biological components, as well as the processes and pathways by which the ocean system interacts with the land and atmosphere. Satellite remote sensing plays a critical role by providing the global view over long time periods and with sufficient temporal and spatial resolution to study the non-equilibrium aspects of the upper ocean. However, many important components of the upper-ocean system, such as gases in the ocean, cannot be remotely sensed. Nonetheless, the exchange of gases, and in particular CO_2 , between air and sea is a crucial part of the climate perturbation equation, and as such is a critical area of research for the EOS program. Interpretation of satellite observations in concert with in situ measurements, laboratory studies, and numerical models provides a comprehensive framework with which we can make predictions about ocean behavior in response to changes in natural and anthropogenic forcing.

Answers to the following questions are required to predict the ocean's biogeochemical response to, and its influence on, climate change:

- How do changes in surface forcing of heat, momentum, and nutrient fluxes affect carbon cycling in the upper ocean?
- What are the fluxes of gases such as CO₂, CO, and dimethyl sulfide (DMS) across the air-sea interface?
- What regulates the presence of nitrogen-fixing and carbonate-producing organisms, and how are they affected by natural and anthropogenic processes?
- What role do organisms play in the production of DMS and subsequent cloud formation?
- How well do SST and pigment-based models predict large-scale seasonal and interannual movements of economically important fish species?
- What are the long-term trends in phytoplankton concentrations in coastal waters off major human population centers, and what is the link, if any, between biomass and eutrophication and between biomass and diseases? How do interannual differences in river discharge affect coastal ecosystems?
- How do these processes vary on seasonal and interannual time scales as well as on mesoscales and basin-wide spatial scales?

These issues are complementary to goals of major international research programs such as the Joint Global Ocean Flux Study (JGOFS), Global Ocean Ecosystem Dynamics (GLOBEC) program, and Land Ocean Interactions in the Coastal Zone (LOICZ).

The second critical application of marine biology is managing and preserving ocean food stocks. World fisheries as a whole are now considered to be fully or excessively exploited. Total catch has declined in recent years, and there have been some spectacular stock collapses, such as the collapse of the Canadian Atlantic cod fishery. Fisheries managers have increasingly recognized the need to understand and account for environmental effects on fish stocks, particularly interannual-to-interdecadal changes in stock recruitment and distribution, which are generally attributed to climate variability. As stocks are fully or over exploited, they become more vulnerable to interannual changes in recruitment. Alternatively, managers need to understand the likely nature and impact of future environmental change in order to set ecologically sustainable policies that properly allow for precautionary principles. The practical short-term problem faced by a manager confronted with sudden

declines in catches or stock size is to decide whether this is due to changes in the habitat or to overfishing. Failure to recognize the interaction of these factors can lead to dramatic and long-term consequences: the collapse of the Peruvian anchovy and California sardine fisheries, as seen in Figure 3.10, are oft-quoted examples.

3.2.4.2 Ocean carbon in relation to global carbon cycle

Although the annual gross uptake of atmospheric CO₂ by the oceans and land is similar (ca. 100 Gigaton [Gt], where 1 Gt = 10¹² kg), carbon pools and exchanges are very different in the two systems. Three unique characteristics of the ocean carbon system are of particular importance to EOS scientific investigations. First, carbonate dissolved in seawater accounts for ca. 35,000 Gt of carbon, a reservoir approximately 20 times greater than the carbon in terrestrial biota, soil, and detritus. The annual net flux of CO₂ into the ocean is now believed to be about 2 Gt per year, and, based on model results, most of this net flux is accumulating in the transient sink of the ocean carbonate system (Sundquist 1993). Second, annual photosynthetic uptake of CO₂ is 10 times greater than the carbon pool size of ocean biota, whereas the reverse is true for terrestrial biota for which photosynthetic carbon uptake is only a small fraction (about 20%) of their biomass. Thus, mean carbon-specific growth is much faster in the ocean than on land. Ocean plants also have much higher nitrogen and phosphorus content relative to carbon than land plants. Global estimates of the mean and time-varying components of ocean photosynthetic carbon production and its relation to nutrient (e.g., nitrogen and iron) cycles differ widely and will not be resolved without sophisticated analyses and models involving both satellite (e.g., from the Moderate-Resolution Imaging Spectroradiometer [MODIS]) and in situ data. Finally, the ocean stores 700 Gt of dissolved organic carbon (DOC), approximately equivalent to the soil and detrital carbon on land. Fluxes between oceanic DOC and ocean biota, and between DOC and the carbonate pool, are not well understood at present, particularly in the upper layers of the ocean where remote sensors can observe the signal from “colored” dissolved organic matter (CDOM). This represents a significant uncertainty in ocean carbon cycle models.

3.2.4.3 Air-sea CO₂ fluxes

Most of the exchange of carbon between the ocean and the atmosphere occurs by continuous CO₂ gas exchange across the ocean-atmosphere interface. However, because of the alkaline nature of seawater, the latter process is relatively slow compared to the rapid input of anthropogenic CO₂ into the atmosphere. Air-sea CO₂ fluxes are controlled by the transfer velocity and the gradient of CO₂

concentration in seawater and at the air-sea interface. A goal of EOS is to combine in situ and remote-sensing measurements with ocean models, and provide quantitative global estimates of sea-surface CO₂ flux. Furthermore, the neW measurements and models will improve the ability to predict the role of the ocean as a moderating influence on the rate of atmospheric CO₂ buildup.

The best estimates of CO₂ flux (F) across the ocean-atmosphere interface are computed from the gas-exchange flux equation (Liss 1983a,b) of the form:

$$F = K ([CO_2]_{air} - [CO_2]_{sea})$$

in which the concentration gradient across the sea surface is multiplied by the transfer velocity K. [CO₂]_{air} is not directly measurable but is derived by multiplying the measured atmospheric pCO₂ in the water-vapor-saturated air above seawater by the solubility of CO₂ gas in seawater (at the temperature of the water at the air-sea interface, using Henry's law). [CO₂]_{sea} represents the concentration of dissolved CO₂ in the ocean mixed layer (upper 10 m) and is estimated by multiplying the measured pCO₂ in the ocean mixed layer by the solubility of CO₂ in seawater at the temperature of the mixed layer.

Although the complex hydrodynamic processes that determine K are poorly understood at a fundamental level, there are empirical equations for K as a function of wind velocity measured at 10 m above sea level (Liss and Merlivat 1986; Upstill-Goddard et al. 1990; Peng and Takahashi 1993; Watson et al. 1991) that have an uncertainty factor of about 1.7. Experiments are now underway to reduce this large uncertainty, which arises from a number of factors, including the influence of surface films, variable fetch, marine boundary layer instabilities, and the short-term variability of surface winds (Erikson 1993). These effects are largely manifested in the spectrum of the small-scale waves. The most promising approach appears to be an empirical parameterization of K in terms of mean-square wave slope (Jahne et al. 1987; Frew 1997). The latter parameter can be derived from backscatter measurements using microwave scatterometers and altimeters (Jackson et al. 1992).

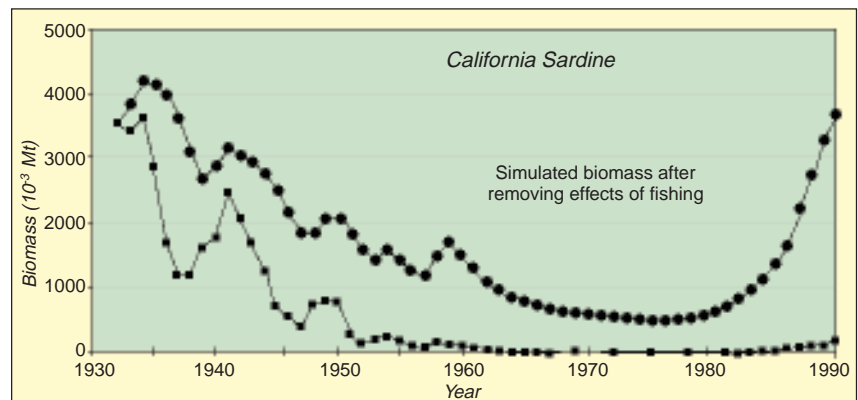
In the troposphere, CO₂ is chemically inert and well mixed. The spatial and temporal variations of pCO₂ in the atmospheric boundary layer are well documented (Komhyr et al. 1985). However, sea surface pCO₂ is dif-

ficult to monitor and is poorly documented (Takahashi 1989); it undergoes large variations (up to 0.15 microatmospheres around atmospheric pCO₂) on short space scales, driven by thermal, biological, and mixing effects. Since temperature can be remotely sensed and biological activity estimated from satellite ocean color scanners, there is now an opportunity to estimate oceanic pCO₂ on a global scale with temporal resolution on the order of a month. In addition, remotely sensed microwave backscatter will simultaneously provide an accurate estimate of gas transfer velocities across the air-sea interface (Wanninkhof et al. 1991; Wanninkhof and Bliven 1991).

3.2.4.4 Land/sea interactions and fluxes

The coastal zone extends from the coastal plains to the outer edges of the continental shelves. This region ap-

FIGURE 3.10



Time series of sardine biomass (1932-1990) obtained from observations of the actual population and from a model simulation that removes the effect of overfishing (courtesy of T. Strub).

proximately matches the area alternatively flooded and exposed in the late Quaternary period due to changes in sea level. The coastal zone encompasses about 8% of the surface area of the Earth and 26% of the biological production (Holligan and deBoois 1993).

Rivers move carbon, nutrients, sediments, and freshwater from the land to the ocean, providing about 0.8 Gt per year of carbonate and organic carbon to the ocean. This is about twice the annual flux of organic carbon and carbonate to deep-sea sediments (Sundquist 1993). Rivers also provide 0.02 to 0.07 Gt per year of nitrogen, the nutrient that generally limits biological production in the ocean. This flux is only a small proportion of the nitrogen flux from deep water to the coastal zone due to upwelling but is a new source relative to the ocean and is greater than annual nitrogen fixation by ocean biota (Wollast 1993). Rivers are also the principal source of sediments and are important sources of phosphorus, sili-

con, and other nutrients. Human activities are directly and indirectly affecting river sources in ways that are presently difficult to quantify on a global scale. For example, widespread farming and deforestation have probably doubled river sediment fluxes compared to the pre-modern era (Meybeck 1993). There is, however, considerable uncertainty in present global estimates as well as the relative importance between large and small rivers (Milliman and Syvitski 1992).

In three very large regions of the ocean, productivity, and hence carbon fixation, is probably limited by the trace nutrient iron (Martin 1990; de Baar et al. 1995). These regions—the Equatorial Pacific, the North Pacific, and the Southern Ocean—are referred to as “High Nutrient, Low Chlorophyll” (HNLC) regions. In all three, substantial amounts of primary nutrients, nitrate and phosphate, are left unused, indicating that phytoplankton carbon assimilation is limited by other factors (Cullen and Lewis 1995). The major source of iron is iron oxide in dust carried on winds from African, South American, and Asian deserts. As aeolian transport is much greater during glacial than interglacial times, iron stimulation of ocean primary production, with subsequent full utilization of primary nutrients in the global ocean, was proposed as a possible mechanism accounting for the drawdown of CO₂ between interglacial and glacial periods (Sarmiento and Toggweiler 1984; Martin 1990). This “iron hypothesis” led to serious proposals to fertilize the Southern Ocean with iron as a biotechnological approach for decreasing the rate of fossil fuel CO₂ accumulation in the atmosphere (Cullen and Lewis 1995). Models show that the iron fertilization could lead to substantial increases in ocean carbon assimilation but would not provide a long-term sink of anthropogenic CO₂ (Sarmiento 1993). Nevertheless, the iron hypothesis is still considered a possible explanation for the HNLC regions, and large-scale field programs in these regions are underway (Cullen 1995). Aerosol fluxes to the open sea and their effects on phytoplankton chlorophyll distributions will be studied using MODIS and other EOS sensors.

The terrestrial biosphere is affected by coastal meteorology through extreme storms, air pollution, and localized patterns of fog, clouds, and precipitation. Until recently, the atmosphere was not considered to be an important conduit of plant nutrients from the land to the ocean, but recent studies contradict this traditional view. In fact, Cornell et al. (1995) show that atmospheric nitrogen deposition ranges from 0.056 to 0.15 Gt of nitrogen annually, which is equivalent to the nitrogen flux to the ocean from rivers. Most of this nitrogen originates from terrestrial sources (e.g., from dust and other aerosols), although human activities (e.g., combustion) may have

increased this nitrogen supply by as much as 0.12 Gt per year (Cornell et al. 1995). If fully assimilated by marine phytoplankton in the Redfield carbon:nitrogen ratio of 6:1, this estimate implies that human modification of atmospheric deposition rates could be generating an additional 0.7 Gt per year of new photosynthetic carbon production in the ocean, and assuming mean nitrogen recycling rates of about 10%, could lead to a 10-to-20% increase in overall ocean primary production.

3.2.4.5 Productivity of the marine biosphere

Plankton. Plankton productivity of the ocean biosphere is principally supported by the primary production of microscopic plants, which grow rapidly compared to terrestrial plants. Since the dominant primary producers are microscopic, and are thus carried passively by ocean currents, time and space distributions of ocean primary production are very closely tied to ocean circulation patterns. Ocean currents transport and mix organisms laterally, and vertical density structure and vertical mixing rates generally determine the local rate of photosynthesis by affecting the light environment and nutrient supply. The close relation between the productivity of the ocean biosphere and ocean circulation means that the time/space patterns of ecosystem productivity are very complex and difficult to quantify at ocean-basin and global scales using traditional oceanographic sampling platforms. The traditional notion of stability based on maps of “average” biomass and productivity is a naive view, and the variability of the planktonic ecosystem is now thought to be of at least equal importance. This is essentially a non-equilibrium view of the marine biology in which variability is a critical component (Figure 3.11).

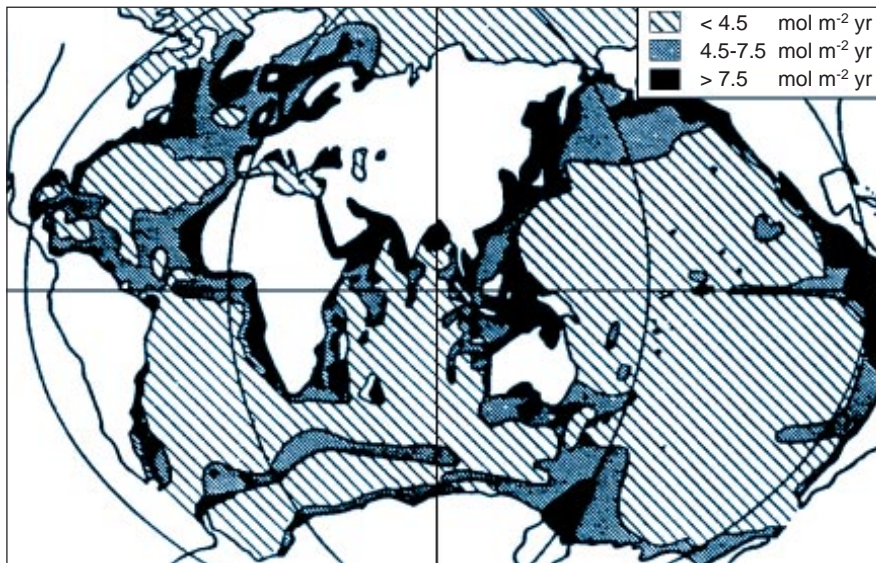
Ocean primary production cannot be directly measured from space, but is calculated from chlorophyll *a* concentration, and, depending on the sophistication of the algorithm, various other remotely-sensed and in situ data and climatologies (Platt and Sathyendranath 1988). Calculations and models, which begin with satellite-derived fields of chlorophyll *a* at daily and longer time scales, are the only practical approach to improve current estimates of mean ocean primary production at basin-to-global scales and to generate new knowledge of the time/space scales of its variability. Primary production is one of the most basic ecological measurements and is an essential component of all studies of trophic relations in the ocean. In addition, primary production is related to most other biologically-mediated carbon fluxes (e.g., the settling flux of organic carbon), including the annual yield of global fisheries (Pauly and Christensen 1995).

Light harvested by phytoplankton can be transformed into chemical energy through photosynthesis, heat, or re-emitted as light through chlorophyll fluorescence. The rate of fluorescence depends in part on the rate of light absorption and the rate of photosynthesis. As phytoplankton become stressed through processes such as nutrient limitation, the quantum yield of fluorescence generally increases. That is, less light energy is utilized in photosynthesis and more is re-emitted as fluorescence. In-water measurements have exploited this process to estimate photosynthesis. However, the variability in fluorescence quantum yield as a function of environmen-

vertical velocities play a critical role in bringing nutrients up into the euphotic zone and regulating primary production. There are three types of regions where upwelling is a persistent factor in enriching the ocean. Along the eastern boundaries of the major basins at low and midlatitudes, winds are equatorward for one or more seasons during the annual cycle, directing Ekman transport offshore and creating coastal upwelling (Smith 1992). For this reason, eastern boundary currents play a large role in global fisheries and most likely in the carbon cycle. The second type of region occurs along the equator where the westward Trade Winds cause surface Ekman transport away from

the equator in each hemisphere, causing equatorial upwelling. Some of the equatorial upwelling areas are limited by low trace nutrients forming HNLC regions. Thirdly, strong positive wind stress curl causes surface divergences and upwelling, for instance, in the Arabian Sea. Any study of the spatial patterns in global primary productivity should place an emphasis on these regions. In the past, the U.S. JGOFS program has examined the equatorial Pacific and the Arabian Sea. The international GLOBEC program on Small Pelagic Fish and Climate Change includes comparative studies of eastern boundary currents as a goal but not yet a

FIGURE 3.11



Geographic distribution of plant productivity in the ocean (Broecker and Peng 1982).

tal variability appears to be a better indicator of the photosynthetic state of the phytoplankton.

A major goal of EOS is to improve current estimates of mean ocean primary production, to describe its variability on regional-to-global spatial scales and from daily-to-interannual time scales, and to understand the basic ocean processes accounting for observed changes in productivity. These activities will build on research begun with Coastal Zone Color Scanner (CZCS) and Sea-viewing Wide Field-of-view Sensor (SeaWiFS) data. Advanced models of primary productivity utilizing the fluorescence bands on MODIS will provide a view with higher temporal and spatial resolution than more-traditional models.

Effects of vertical circulation. In regions where major nutrients in the surface layer are low (not the HNLC regions),

firm plan. A comparison of parts of several eastern boundary currents off Oregon, Peru, and northwest Africa was accomplished in the 1970s, but a truly global comparison has yet to be made.

Since light availability decreases exponentially with depth, photosynthetic organisms such as phytoplankton are constrained to the upper waters. As phytoplankton continue to grow, nutrients become depleted. However, solar radiation is absorbed largely near the surface and stably stratifies the upper layers. Only cooling or large inputs of momentum can overcome this stratification, resulting in entrainment of the cooler, more nutrient-rich waters at depth. Moreover, processes that break down this stratification increase the depths over which phytoplankton are mixed, causing them to spend an increasing amount of time in deep, poorly lit waters. Thus the fundamental challenge for phytoplankton is to balance light availabil-

ity near the surface with nutrition at depth. This coupling between physical and biological processes is fundamental to ocean biogeochemistry. Understanding and predicting these processes will require both in situ observations at depth and the larger-scale horizontal patterns provided by the EOS sensors. Interpreting these data in the context of dynamical models will make it possible to predict the linkages between the ocean and climate change.

Coral reefs. Coral reefs are found along tropical and subtropical coasts. They support the highest biodiversity and productivity among all the ecosystems. At present, however, coral reef ecosystems are being degraded by local and global environmental changes. The increasing impact of human activities in the tropical coast contribute to the crises facing reef ecosystems through eutrophication and sedimentation, as well as direct mechanical destruction. Reef ecosystems are also adversely affected by CO₂ increase, global warming, sea-level rise, and increasing UV exposure, and the adverse effects will increase in the next decade. Our present knowledge of coral reefs and shallow seas is sketchy. In contrast to land, there is no basic map of the various types of ecosystems that cover the shallow seas. A goal of EOS is to provide such a map.

3.2.4.6 *The marine ecosystem and climate change*

The recent report by the Intergovernmental Panel on Climate Change (IPCC) focuses heavily on the responses and feedbacks in the Earth's climate system. In the area of the marine biosphere, the first involves the role of the continental shelves in the carbon cycle. The shelves are burial sites for organic carbon derived from both ocean and terrestrial sources. Increases in anthropogenic nutrient loading (due to effluents and land-use changes) could affect oxygen concentrations (through increased microbial activity), which in turn will have complex effects on nitrogen and carbon cycling. Another feedback results from increases in Ultraviolet-B (UV-B) levels, which can depress phytoplankton growth rates as well as affect the cycling of dissolved organic matter (DOM) in the upper ocean. The response to UV-B is species-dependent so there will be pronounced secondary effects on ecosystem structure and function.

Aside from these direct effects on phytoplankton and primary productivity, there are impacts on higher trophic levels that cannot presently be well quantified. Variations in atmospheric forcing cause changes in oceanic circulation, temperature, mixed-layer depth, stratification, and turbulence intensities that affect the reproduction and survival of early stages of zooplankton and larval fish. Poor survival rates during these larval and juvenile stages is thought to be the primary source of

mortality and a determinate of year-class population sizes for many marine species. The accumulation of year-to-year changes in the early-life survival rates creates strong fluctuations in community structure and food web dynamics of marine ecosystems, resulting in the natural rise and fall of commercially important fish species with periods of years to decades, even in the absence of fishery harvest. For fisheries management to be successful, these fluctuations must be understood. The variations in the environmental conditions named above can involve alterations of the mean levels or changes in the frequency, intensity, and structure of the environmental variability (such as the ENSO multi-year cycle). Unlike terrestrial ecosystems where vegetation is dominated by long-lived species that integrate environmental variability over many decades, many components of oceanic systems respond rapidly to subtle shifts in the environment, making the prediction of these rapid changes more critical.

Thus, an important scientific questions is: "What are the effects of climate change on the distributions, abundances, and productivity of living marine resources in the global oceans?" This is the central question addressed by the GLOBEC program of the International Geosphere-Biosphere Program (IGBP) (see Section 3.3.2.3).

3.2.4.7 *Modeling the marine biosphere*

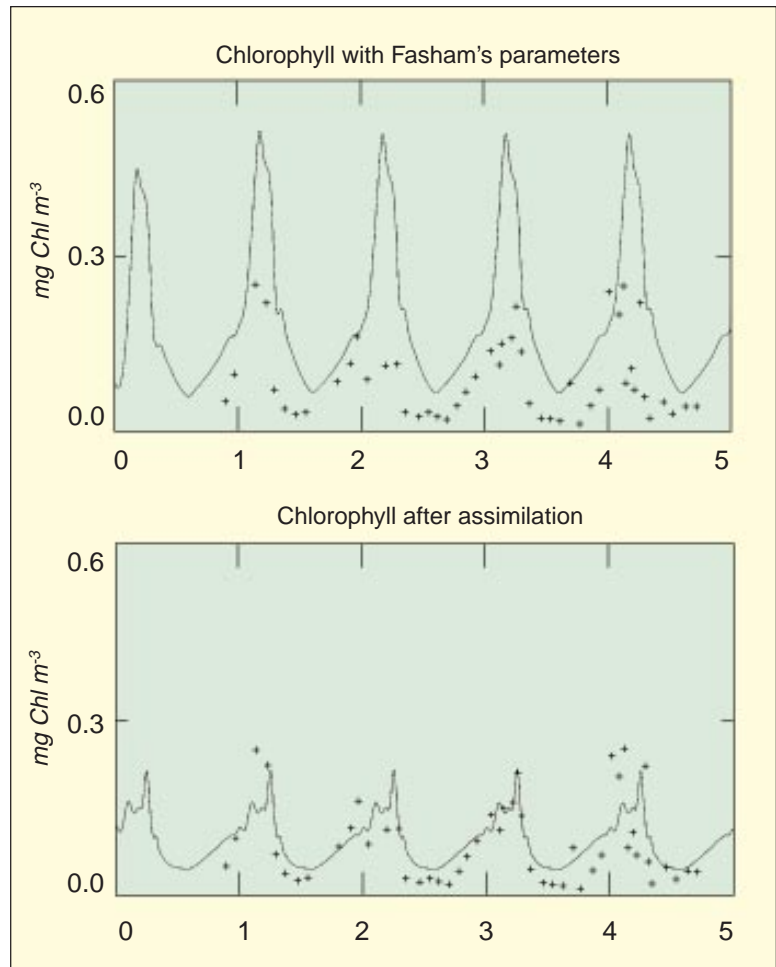
GCMs are in the early stages of linking together the ocean and atmosphere from a purely physical climate point of view. Coupling with biogeochemical models is only just beginning. However, it should be noted that physical circulation models themselves are still in their infancy. For example, different circulation models with identical physical forcing produce widely different fields of vertical velocity, as much as the difference between ENSO and non-ENSO years. As vertical velocity and mixing are critical to biological processes through their impact on light and nutrient supply rates, this suggests that coupling of physical and biogeochemical models must proceed carefully.

Various types of box models are used to study the linkages between climate and biogeochemistry. Models that focus on ecosystem dynamics generally explore specific processes, such as the spring bloom. Most of the present models include only simple ecosystems (one nutrient, one phytoplankton type, and one zooplankton type), but more complex models are beginning to appear. A general limitation of all of these models is that the parameterizations of biological processes have a quite limited domain of applicability. Thus models have tended to focus on short-lived phenomena in specific regions. Models that attempt to study large-scale processes generally degrade in performance over time because of inadequate

characterization of the marine ecosystem. Another handicap has been that the physical models have been developed to study ocean circulation, not biogeochemistry. Thus the time and space scales as well as the model formulation are often inadequate for biogeochemical studies. Simplifications and parameterizations that are appropriate for physical circulation models may be inappropriate for biogeochemical models. For example, isopycnal models have revealed many insights into physical oceanography, but they are difficult to link with mixed-layer dynamics that are crucial for ocean biology. Clearly, coupled climate/biogeochemical models must have their climate and their biogeochemical components joined early in their development.

Data assimilation is just starting to be used in ocean ecosystem models. Phytoplankton-nutrient-zooplankton (PNZ) models have been widely used for the last 20 years. Fasham et al. (1990) have developed a more-advanced version of the basic PNZ model which includes microbial processes as well. However, one of the challenges in these models is estimating the more than two dozen free parameters, many of which cannot be measured directly. Relying on data assimilation techniques, these parameters can be estimated by using long time series of observations of some of the components of the ecosystem model. Figure 3.12 shows the performance of such an assimilation model where the data were assimilated and measured at the JGOFS Bermuda Atlantic Time Series site. The ecosystem model was modified to include a light adaptation function for phytoplankton, and it can be seen that this model fits the data quite well. In the EOS era, satellite measurements, such as phytoplankton chlorophyll, and photoadaptation derived from MODIS, will be used in more-advanced three-dimensional assimilation models.

FIGURE 3.12



A time series of chlorophyll modeled with Fasham's parameters (above) and by assimilating data from in situ observations (below) over a period of five years. The model calculations are given by the solid line, the data by the crosses (courtesy of Yvette Spitz [OSU] and John Moisan [SIO]).

3.3 Required measurements and data sets

3.3.1 Satellite observations

The purpose of this section is to put into a scientific context the oceanic observational requirements of EOS. Following the structure of the science questions addressed above, the observational requirements in this section are broken into the topics of ocean surface fluxes, ocean circulation and sea level, and marine biogeochemistry. Within each topic, a set of observations with accuracies and sampling requirements is listed in tabular form. The last column in the tables refers to an instrument and a product number; more detail about these data products can be obtained from the Algorithm Theoretical Basis Documents prepared by each Instrument Team.

3.3.1.1 Surface fluxes of momentum, heat, and moisture

The atmosphere and the ocean are coupled through air-sea fluxes of momentum, heat, moisture, and a variety of biogeochemically important compounds. Comparisons between predicted and measured air-sea fluxes provide sensitive tests of the accuracies of coupled general circulation and Earth system models; specifications of the fluxes are required as surface boundary conditions if oceanic or atmospheric models are to be examined separately. EOS science requires continuous global estimates of critical air-sea exchange parameters: air-sea momentum flux or “wind stress,” sensible heat flux, net moisture and latent heat flux, and long- and shortwave radiative flux.

The turbulent fluxes of sensible and latent heat and of moisture can only be measured directly by exacting in situ instrumentation, but various parameterizations allow them to be derived from quantities observed globally from satellites. They are commonly estimated with bulk aerodynamic formulae or more-sophisticated boundary layer models; both approaches require surface winds and air-sea differences of temperature and humidity. As a rule, satellites measure surface properties and atmospheric properties aloft, but cannot provide air temperature or humidity at the desired height somewhere between 2 and 100 m above the surface. So the required air-sea differences and the resulting surface fluxes must be inferred from the available data and models. The air-sea temperature difference is a controlling factor because it determines the atmospheric boundary layer stability, which in turn controls the efficiency of these turbulent fluxes. The accuracies of air-sea flux estimates therefore depend jointly on the accuracies of the basic satellite measurements and the validity of the parameterizations used to calculate the fluxes from the measured quantities (Donelan 1990).

Wind stress is an exception. For seasonal and yearly means, analysis of remotely sensed wind stress will provide the best estimates of wind stress. For shorter time scales, the best estimates come from hindcasts by numerical weather prediction models (such as those from the EOS Data Assimilation Office) that wait for all available data and focus upon producing accurate analyses without concern for timeliness. These statements apply more strongly to other near-surface parameters that can only be derived from models that assimilate surface and tropospheric measurements. Direct conventional measurements (e.g., from buoys or ships) are essential to refine and validate the remote-sensing algorithms.

For radiative fluxes, we require the observations of clouds and the atmospheric profiles of temperature, humidity, and aerosols (described in Chapter 2) and the derived estimates of net surface long- and shortwave radiation.

This section outlines the satellite data sets that will contribute to calculation of air-sea turbulent and hydrologic fluxes as well as to prognostic and diagnostic analyses of atmospheric and oceanic circulation and coupling. The required observations are of SST, surface wind velocity, column water vapor for estimating near-surface humidity, precipitation, and sea-surface salinity.

SST. SST plays a crucial role in the global climate system. It is a critical aspect of the coupling between the atmosphere and the ocean (Gill 1982; Peixoto and Oort 1992). The ocean skin provides the lower boundary condition for the upwelling infrared radiation in the marine atmosphere and for boundary layer models that compute the air-sea temperature difference. Accurate satellite measurements also provide the possibility of generating a consistent global climatology of SST that can be used as time progresses to diagnose the rate of climate change.

SSTs are measured from satellites using infrared and passive microwave radiometry. The accuracy of satellite retrievals approaches that of conventional in situ thermometers (i.e. $<0.5\text{K}$) (Mutlow et al. 1994). Satellite measurements have the further advantages of global coverage and higher spatial and temporal resolutions than achievable by other means.

The infrared measurements from which SST is derived are taken in spectral intervals where the atmosphere is most transparent. To achieve accuracies in the derived SST field at a level of a few tenths of a degree, it is necessary that the individual channel radiance measure-

ments, when expressed as brightness temperatures, should have an accuracy much greater than this, i.e., < 0.1 K. Typical spatial resolutions of existing and planned infrared radiometers, about 1 km at the surface, are adequate for most oceanic, weather, and climatic applications requiring SST. For climate studies, global coverage of the oceans is required; this can be achieved with broad-swath instruments every 2-3 days, cloud cover permitting.

Under cloud-free conditions, SST will be derived from the EOS/MODIS infrared channels in the 3.7- μm , 4- μm , 10-to-12 μm , and possibly 8.6- μm intervals (channels 20, 22, 23, 29, 31, and 32). Shorter wavelength channels (visible and near-infrared) will be used to identify cloud and aerosol contamination during daylight. The noise equivalent temperature differences need to be at the 0.05 K level or below to achieve accuracy goals for the derived SST product. Determining the spectral resolution for each band is a trade-off between narrower bands that avoid undesirable spectral lines and broader bands that maximize radiometric sensitivity. The current MODIS specifications (MODIS 1986) represent an achievable balance between these two goals.

Microwave radiometry provides critical and complementary observations of SST. Although the Special Sensor Microwave Imager (SSM/I) instruments presently flying and planned for the remainder of the decade do not include the low-frequency channels (6 to 7 GHz) required to extract SST information, both the European Space Agency (ESA)-supplied Multifrequency Imaging Microwave Radiometer (MIMR) and the National Space Development Agency (NASDA)-supplied Advanced Microwave Scanning Radiometer (AMSR) multichannel microwave radiometers will be capable of extracting all-weather (clear sky and cloudy) SST information with about 60-km resolution and accuracies of 1 to 1.5° C over swaths 1400 to 1500 km wide (Table 3.1, pg. 140).

Surface wind speed and direction. Near-surface winds over the ocean will be acquired under clear and cloudy skies and at night and day by satellite-borne scatterometers, multichannel microwave radiometers, and microwave altimeters. The measurement and analysis techniques are mature and have been successfully tested in space. Time series of wind measurements from all instruments were started in the 1980s and 1990s, well before the launch of the initial EOS instrument suites.

Scatterometers are active microwave instruments designed specifically to measure near-surface wind velocity (both speed and direction) and vector surface stress over the ice-free oceans. They are the only instruments with the demonstrated capability of measuring wind ve-

locity and vector stress (as opposed to scalar wind speed and stress magnitude) in both clear-sky and cloudy conditions. The NASA Scatterometer (NSCAT) dual-swath, Ku-band scatterometer flew as one component of the Advanced Earth Observing System-1 (ADEOS-I) mission and the SeaWinds dual-pencil-beam, wide-swath scatterometer will fly as a NASA-EOS instrument on NASA's EOS QuikSCAT mission (planned for launch November 1998) and on the ADEOS-II mission (planned for launch in February 2000). Dual-swath dedicated C-band scatterometers are planned for flight on the ESA Meteorological Operational (METOP) satellite polar-orbiting spacecraft. All present and planned scatterometer wind measurements have spatial resolution of about 50 km and accuracies of approximately 10 to 12% (rms) in speed and 20 degrees (rms) in direction. Individual instruments achieve near-global coverage in 2 days; the planned constellation (SeaWinds plus an ESA scatterometer) should allow daily global coverage.

Passive microwave radiometers measure the brightness temperature of the Earth/atmosphere system at a variety of carefully chosen frequencies and polarizations. The multiple measurements can be combined to allow simultaneous estimation of many geophysical quantities including wind speed. Recent work (e.g., Wentz 1992, and references therein) suggests that it may also be possible to infer wind direction given proper polarization selections and instrument measurement geometry. However, considerable research is required before such measurements can be considered a substitute for scatterometry. Microwave radiometers (SSM/I) have flown on the operational Department of Defense (DoD) Defense Meteorological Satellite Program (DMSP) spacecraft since June 1987. Two SSM/I instruments are generally operational at any time, yielding nearly daily coverage with 25-to-50-km spatial resolution. Wind speed rms accuracies are 1-to-1.4 m s^{-1} (Wentz 1994), based on comparisons with buoy data. (SSM/I does not include the low-frequency [6-to-7 GHz] channels required to calculate SST, and wind-speed retrieval therefore requires independent knowledge of SST, typically from climatologies). Microwave radiometer wind-speed measurements will be available (through about 2002) from SSM/I instruments on DMSP (or the converged METSAT polar orbiters) as well as from advanced, high-resolution (10 km) radiometers: MIMR on the ESA ENVISAT, and AMSR on NASDA ADEOS-II. A slightly modified copy of the AMSR instrument, designated AMSR-E, is also scheduled to fly on the EOS PM-1 spacecraft. These advanced microwave radiometers will include channels needed to retrieve SST, although the polarizations and measurement geometries will not assure accurate retrieval

of vector winds (direction as well as speed). Similar all-weather wind-speed products (with 50-km spatial resolution, 1600-km wide swath) will be obtained from the Atmospheric Infrared Sounder (AIRS) instruments on the EOS PM-1 spacecraft and possibly on future operational satellites.

Radar altimeters are nadir-viewing active radar instruments designed specifically to acquire accurate measurements of the distance between the spacecraft and the sea surface (see the sea-surface topography observations in Section 3.3.1.2). Empirical models have been developed relating the received backscatter power to wind speed under clear-sky and cloudy conditions. Altimeter wind speed measurements are accurate to 2 m s^{-1} (rms) based on comparisons with buoys, with resolution of 7- to-10 km. Altimeter coverage is restricted to the nadir sub-track only. Altimeters are presently flying onboard the TOPEX/Poseidon and both ERS spacecraft. Future altimeters are planned for the U.S. DoD GFO and EOS Radar Altimeter (now Jason-1) missions and the ESA ENVISAT missions (Table 3.2).

Near-surface humidity. Near-surface specific humidity cannot be directly measured using present or planned satellite instrumentation. However, a variety of column-integrated water, atmospheric water vapor, and liquid water quantities are routinely calculated from satellite-borne microwave radiometers, and empirical models relating near-surface specific humidity to integrated water vapor on monthly mean time scales have been developed (Liu 1986; Liu et al. 1991, Table 3.3)

Precipitation. The small spatial and temporal scales associated with rain events greatly complicates the design of global remote precipitation-measurement systems, yet knowledge of precipitation (especially over the ocean) is required to close the global hydrologic cycle (see Section 3.2.1.3). Accurate space-based measurement of precipitation requires high spatial resolution, frequent coverage, and the combined analysis of co-orbiting active rain radars, passive microwave radiometers, and infrared radiometers. The first such measurement suite is flying as the joint NASA-NASDA Tropical Rainfall Measuring Mission (TRMM) launched in November 1997. TRMM utilizes a low-inclination (35°) orbit to achieve frequent coverage and diurnal resolution, confining observations to tropical and subtropical latitudes. TRMM data will provide the basis for developing and refining accurate remote-sensing rain-rate algorithms and designing future precipitation sensor suites.

Although high-accuracy global precipitation measurements over the ocean are not planned for the period 1995 to 2002, qualitative, low-resolution precipitation estimates with 50% accuracy in rain rate, 1-3 day resolution, and 14 to 100 km spatial resolution will be produced from SSM/I, AMSR, and MIMR microwave radiometer data. In addition, AIRS/Advanced Microwave Sounding Unit (AMSU) data will be used to produce a precipitation index accurate to 2 mm/day and with 50-km resolution (Table 3.4).

Sea-surface salinity. There is very little information about the large-scale variability of ocean surface salinity. About 30% of the $1^\circ \times 1^\circ$ boxes of the ocean surface do not have a single salinity observation. Surface salinity is a major dynamic parameter that influences the density-driven ocean circulation, particularly the convective overturning in the North Atlantic. The ocean's influence on the global hydrological cycle is enormous, and the hydrologic budget cannot be balanced without closing the salt budget of the oceanic mixed layer. Surface salinity is a very strong constraint on the water and energy flux parameterizations of coupled ocean/atmosphere GCMs. Recent results from the Tropical Ocean Global Atmosphere (TOGA)/Coupled Ocean-Atmosphere Response (COARE) indicate that freshwater buoyancy flux in the equatorial warm pool of the western Pacific governs the thickness of the thermodynamically active mixed layer, and thus modulates the transfer of heat between the ocean and atmosphere in this region, which is the spawning ground for ENSO. Low-frequency microwave radiometry holds promise.

3.3.1.2 Circulation and sea level

Studies of ocean circulation and long-term climate change require continual observations of surface geostrophic currents and measurements of mean sea level. These can be provided by satellite-borne microwave altimeters, which directly measure the altimeter's distance above the sea surface. To determine the mean sea level and the mean current, the satellite's orbit must be known accurately, and the Earth's geoid and tidal contributions to the sea-surface height must be subtracted from the altimetric measurements. This section addresses this set of requirements. Other satellite measurements needed in the study of ocean circulation are measurements of the Earth's rotation rate, and, as described in Section 3.3.1.1, those that allow tests and diagnoses of ocean models—SST and salinity—and those that provide estimates of sea-air fluxes of heat, salt, and momentum.

TABLE 3.1

PARAMETER NAME	UNITS	ACCURACY ABS::REL	TEMPORAL RESOLUTION	HORIZONTAL RESOL:: COVER	VERTICAL RESOL::COVER	COMMENTS
Sea_sfc Temperature (SST)	K	0.3-0.5 K :: 0.3-0.5 K	1/day, 1/wk 1/mon	1 km :: Ocean/L	N/A :: Sfc	MODIS (28)
Sea Surface Temperature (SST)	K	1 K ::		60 km :: Ocean	N/A :: Sfc	AMSR/ MIMR (06)
Sea Surface Temperature (SST)	K	<0.2 K ::	1/day	1.0 deg ::	N/A :: Sfc	AMSR/ MIMR (17)

Sea-surface temperature

TABLE 3.2

PARAMETER NAME	UNITS	ACCURACY ABS::REL	TEMPORAL RESOLUTION	HORIZONTAL RESOL:: COVER	VERTICAL RESOL::COVER	COMMENTS
Wind Vectors, Near_Surface	m/s,dg	> of 2 m/s or 10% rms (speed); 20 dg rms (direction) ::	N/A	50 km :: Ocean (1600-km swaths)	N/A :: Sfc	SeaWinds (03)
Wind Speed Sea_sfc	m/s	1.5 m/s* ::		14, 25 km :: Ocean	N/A :: Sfc	AMSR/ MIMR (05)
Wind Speed, Sea_Sfc	m/s	<0.5 m/s* ::	1/day	1.0 deg ::	N/A :: Sfc	AMSR/ MIMR (16)
Wind Speed, Along-track	m/s	2 m/s ::		7 km :: Ocean	N/A :: Sfc	DFA (02)
Wind Speed, Sea_sfc	m/s		2/day	50 × 50 km :: Ocean	N/A :: Sfc	AIRS (06)

Surface wind velocity and speed

TABLE 3.3

PARAMETER NAME	UNITS	ACCURACY ABS::REL	TEMPORAL RESOLUTION	HORIZONTAL RESOL:: COVER	VERTICAL RESOL::COVER	COMMENTS
Precipitable Water	g cm ⁻²	0.2 g cm ⁻² ::		14 km :: Ocean	Column :: Trop	AMSR/ MIMR (04)
Precipitable Water	g cm ⁻²	<0.1 g cm ⁻² ::	1/day	1.0 deg ::	Column :: Trop	AMSR/ MIMR (15)
Precipitable Water	mm	5% :: 3%	2/day [d,n]	50 × 50 km :: G	N/A :: Atmos	AIRS (05)

Column water vapor

TABLE 3.4

PARAMETER NAME	UNITS	ACCURACY ABS::REL	TEMPORAL RESOLUTION	HORIZONTAL RESOL:: COVER	VERTICAL RESOL::COVER	COMMENTS
Precipitation (Ocean, 2 layers)		50% ::		14 km :: Ocean	N/A :: Sfc	AMSR/ MIMR (02)
Precipitation (Ocean)		10% ::	1/day	1.0 deg ::	N/A :: Sfc	AMSR/ MIMR (13)
Precipitation Index	mm/day	2 mm/day :: 1 mm/day	2/day [d,n]	50 × 50 km :: G	N/A :: Trop	AIRS (05)

Precipitation rate

Mean sea-surface height and geoid. Altimetric measurement of the sea-surface height is presently the only method for measuring ocean surface currents over large areas of the ocean every 10 days in a cost-effective and timely manner. Sea-surface height measurements observed by satellite altimetry consist of a mean component (the dynamic topography) and the time-varying component. Improved knowledge of large-scale mean circulation enhances understanding of the internal structure of currents and enables better estimates of global transport. However, the accuracy of the global marine geoid is required to fully make use of the altimetric dynamic topography measurements. To achieve an accuracy of 1 Sverdrup of transport, the geoid needs to be accurate to less than 2 cm over a length scale of shorter than 500 km. The current best geoid model, JGM-3, is accurate only to 11 cm over 3000 km, which enables surface current determination to an accuracy of only 5 cm/sec. Geoid models computed using satellite tracking data, altimetry, and shipboard gravity data will not satisfy the requirement. Future geopotential mapping missions have goals of producing a geoid model to enable surface currents to be computed to an accuracy of 0.5 cm/sec (Table 3.5).

Time-varying dynamic topography. Altimetric satellite orbits were designed so that orbits repeat exactly to within ± 1 km at the equator at a specified interval, for example, 10 days. This allows the dominant marine geoid error to be eliminated when repeat-track analysis of altimetric measurements is conducted. The time-varying component of the sea surface height can be computed with an accuracy of 3 cm rms over a length scale of 7 km along the satellite groundtrack. The variations of the sea-surface height and hence of surface geostrophic currents can be computed directly using altimetric measurements. Eddy kinetic energy of the global ocean currents can be directly computed (Table 3.6).

Precision orbit determination. Accurate knowledge of the position of the altimeter antenna within a well-maintained terrestrial reference system is vital to the interpretation of the altimeter height measurements in terms of sea-surface topography. Improved gravity and tide models, nonconservative force models, and terrestrial reference frame models, and the use of SLR and Doppler Orbitography and Radiopositioning Integrated by Satellite (DORIS) range-rate tracking data, have enabled determination of the TOPEX/Poseidon spacecraft radial position to within 3-4-cm accuracy relative to the center of mass of the Earth. The demonstration of satellite-to-satellite Global Positioning System (GPS) tracking has

shown enormous potential for further enhancement of accuracy of altimetric satellite orbits. Together with the continued improvement of dynamic models and employing dense tracking data (e.g., GPS and SLR), the radial orbits of 2 cm can be achieved for the future altimetric satellite Jason-1 (Table 3.7).

Tidal component of sea-surface height change. Tidal variations in sea-surface height can be aliased into climate-sensitive time scales and therefore must be removed from altimeter measurements. Great care was taken in the choice of the TOPEX/Poseidon orbit to minimize aliasing of important tidal frequencies into climate-sensitive frequencies. In addition, analyses of TOPEX/Poseidon data have generated a number of improved deep-ocean tide models. Shum et al. (1996) have provided an accurate assessment of 10 such models and concluded that the tides in the deep ocean are accurate to 2–3 cm rms. Most global models have spatial resolutions of 1/2 degree (50 km). At present, tides in coastal areas and semi-enclosed seas are poorly modeled. In addition, long-period tides (e.g., Mm, Mf) and tides with meteorological origin are poorly modeled and are difficult to separate from astronomical tides. Improved accuracy from coastal and deep-ocean tidal prediction capabilities can be anticipated by using additional TOPEX/Poseidon data and other current and future altimeter measurements, along with improved methodology to assimilate data into hydrodynamic models. These models can be used to correct sea-surface topography measurements from altimetric missions (Table 3.8).

3.3.1.3 Biogeochemistry

Surface forcing and SST. The observations required for surface fluxes (Section 3.3.1.1) are also required for studies of the interrelationships between the physical state and processes of the ocean and the biological state and processes. In addition, we require, as described below, total incoming solar radiation at the Earth's surface on a daily basis, its spectral composition, including photosynthetically-available radiation (PAR) and ultraviolet radiation. We also require estimates of the fluxes of iron and major plant nutrients (e.g., nitrogen) from the atmosphere to the ocean.

The temperature dependence of the solubility of gases such as CO₂ requires accurate knowledge of the surface temperature of the surface mixed layer, as well as of the surface skin of the ocean. The skin temperature can be slightly cooler than the mixed-layer temperature; ignoring this difference can lead to a significant underestimation of air-sea gas exchanges. This surface

TABLE 3.5

PARAMETER NAME	UNITS	ACCURACY ABS::REL	TEMPORAL RESOLUTION	HORIZONTAL RESOL:: COVER	VERTICAL RESOL::COVER	COMMENTS
Sea_Level Height, Along-track	cm	11 cm :: N/A		3000 km :: Ocean	N/A :: Sfc	[DFA02]
Topography Map, Sea_sfc	cm	5 cm or 10% ::	1/(10 day)	25 km :: Ocean	N/A :: Sfc	DFA03

Local mean dynamic topography

TABLE 3.6

PARAMETER NAME	UNITS	ACCURACY ABS::REL	TEMPORAL RESOLUTION	HORIZONTAL RESOL:: COVER	VERTICAL RESOL::COVER	COMMENTS
Sea_Level Height, Along-track	cm	N/A :: 3cm	1/(10 days)	7 km :: Ocean	N/A :: Sfc	

Time-varying dynamic topography

TABLE 3.7

PARAMETER NAME	UNITS	ACCURACY ABS::REL	TEMPORAL RESOLUTION	HORIZONTAL RESOL:: COVER	VERTICAL RESOL::COVER	COMMENTS
Precision orbit units	cm	2 cm :: N/A		7 km :: Global	N/A :: Sfc	

Precision orbit determination

TABLE 3.8

PARAMETER NAME	UNITS	ACCURACY ABS::REL	TEMPORAL RESOLUTION	HORIZONTAL RESOL:: COVER	VERTICAL RESOL::COVER	COMMENTS
Ocean Tide Model	cm	2 cm :: 2 cm	2/day	50 km :: Ocean	N/A :: Sfc	DFA05

Component of tidal sea-surface height

skin effect, in fact, which is usually not considered in the calculation of the global carbon budget using conventional SST climatologies, can account for ~0.7 Gt C yr⁻¹ of extra carbon flux to the ocean (Robertson and Watson 1992). This can be up to about 50% of the discrepancy between estimates of net oceanic CO₂ uptake derived from models calibrated by tracers when compared to models that integrate the air-sea exchanges over the global oceans.

Surface gas exchange. As discussed above, CO₂ fluxes cannot be measured directly and have to be estimated from various observations. On the global scale, the quantification of CO₂ fluxes across the ocean-atmosphere interface requires two complementary sets of observations: in situ observations of sea-surface pCO₂ on short temporal and spatial scales, and space-based observations of a limited number of parameters (such as ocean color and SST) with a lesser accuracy than in situ observations. Algorithms

developed in the EOS program will couple in situ and proxy space-based observations to quantify the global absorption of CO₂ by the oceans.

Exchanges between the land and the ocean. Rivers are major sources of freshwater, sediments, nutrients, and DOM to the coastal zone, as well as pollutants that may be transported in soluble and particulate forms. Knowledge of the river flux, plume area, and salinity provides valuable information necessary for estimating plume thickness from space, data important to calculating the light field in and beneath the plume. To interpret the ocean color signal in the coastal zone, a significant improvement in the performance of the Land Remote-Sensing Satellite (Landsat) class of sensors is required, with a movement away from hyper-spatial sampling and toward hyper-spectral sampling. Improved signal-to-noise can be achieved by using larger pixels (e.g., 60 to 90 m) and

increased dwell or integration time in order to cope with a need for 10-15-nm sampling with contiguous bands.

Bio-optical measurements. We need spectral measurements from satellite sensors to distinguish important biogeochemical components suspended and dissolved in the upper ocean and to correct for bottom reflectance in coastal waters. We also need in situ measurements to help interpret the satellite signals including water-leaving radiances, chlorophyll *a*, detrital carbon, accessory pigment (e.g., phycoerythrin), and CDOM concentrations. In addition, we need estimates of the abundance in surface waters of certain classes of phytoplankton including coccolithophorids and the floating mats of cyanobacteria, notably *Trichodesmium*. These observational requirements are described below.

Water-leaving radiance, integrated, spectral, surface PAR. Models of biogeochemical cycles in the upper ocean rely on appropriately parameterized mixed-layer physics. For example, solar radiation incident on the sea surface warms and stabilizes the upper ocean. It is also responsible for driving photosynthetic production of organic matter. Transfer of momentum from wind to sea mixes the upper ocean and is responsible for generating turbulence, which mixes nutrients and other dissolved and particulate constituents in the vertical. Excess latent heat losses drive

convective motions responsible for deep water formation and the transport of both organic and inorganic carbon to the deep sea.

For estimates of light utilization by phytoplankton, we need visible and ultraviolet radiative fluxes. Total incoming solar radiation at the Earth's surface as well as PAR are required on a daily basis. Instantaneous PAR is needed for some of the primary productivity models. Ultraviolet radiation will be estimated from a combination of the incoming solar radiation and ozone concentration. These estimates will be made through a combination of visible radiometers (e.g., MODIS) and the Total Ozone Mapping Spectrometer (TOMS) (for ozone concentration) (see Tables 3.9 and 3.10).

*Phytoplankton chlorophyll *a* concentration and fluorescence.* Satellite ocean-color scanners measure ocean radiance, and from these data one derives accurate estimates of phytoplankton chlorophyll *a* concentration (a good proxy for phytoplankton biomass) and other in-water constituents. Algorithms based on the strong blue absorption by phytoplankton chlorophyll *a* work well in open-ocean and most continental-shelf waters but are difficult to implement in optically complicated waters near the coast owing to the interference of other strong blue-absorbing substances. Advanced ocean-color scanners like MODIS will have high signal-to-noise in bands near 683

TABLE 3.9

PARAMETER NAME	UNITS	ACCURACY ABS::REL	TEMPORAL RESOLUTION	HORIZONTAL RESOL::COVER	VERTICAL RESOL::COVER	COMMENTS
Level-2 Radiance, Water-leaving	mW cm ⁻² /sr/μm	5-10% :: 5-10%	1/day, 1/wk, 1/mon	1 km :: Ocean/R,L	N/A :: Sfc	MODIS (18)
Downwelling Irradiance, Sea_sfc	Wm ⁻²	::	1/day	1 km :: Ocean	N/A :: Sfc	MODIS (22)
PAR, Sfc (IPAR) and Incident (IPAR)	quanta m ⁻² sec ⁻¹	0.05 :: 1.05	1/day [d]	1 km :: Ocean	N/A :: Sfc	MODIS (22)
PAR, Daily	Wm ⁻² day ⁻¹	0.1 :: 1.1	1/day	N/A :: G	N/A :: Atmos	MODIS (22)

Water-leaving radiance and photosynthetically active radiation

TABLE 3.10

PARAMETER NAME	UNITS	ACCURACY ABS::REL	TEMPORAL RESOLUTION	HORIZONTAL RESOL::COVER	VERTICAL RESOL::COVER	COMMENTS
Irradiance, UV Solar [1 nm res.]	Wm ⁻²	3-5% :: 1%	1/hr	N/A :: N/A	N/A :: N/A	SOLSTICE (02)
Irradiance, UV Solar [0.001 nm res.]	Wm ⁻²	3-5% :: 1%	1/hr	N/A :: N/A	N/A :: N/A	SOLSTICE (03)

UV radiation

nm to detect the sunlight-stimulated chlorophyll *a* fluorescence signal in coastal waters having relatively high concentrations of phytoplankton biomass (ca. >1.0 mg Chl *a* m⁻³). This capability provides an alternative approach to the absorption-based algorithms to estimate phytoplankton biomass, particularly in coastal waters where the absorption-based algorithms often fail. MODIS measurements at 412 nm will be used to estimate the concentration of marine detritus (dissolved and particulate) and to improve estimates of chlorophyll *a* when these substances significantly affect blue absorption (Table 3.11).

With the CZCS, only total pigment concentrations could be estimated as there was insufficient spectral resolution to separate chlorophyll *a* from its associated degradation products. Several studies have shown that traditional bio-optical algorithms fail in the presence of DOM such as humic acids, which occur in coastal waters and in river plumes and even in the open ocean. SeaWiFS and MODIS will have channels near 412 nm to correct pigment estimates and to estimate the concentration of CDOM. Although there remain challenges for atmospheric correction at these short wavelengths, the availability of these measurements will extend the range of water types that can be observed quantitatively from space. Other accessory pigments, such as phycoerythrin, will require at least the increased spectral resolution of MODIS and probably additional bands between 580 nm and 610 nm.

Extensive airborne data have shown that the phycoerythrin influence can be detected, but measurements at appropriate wavelength bands are required to extract pigment concentration.

Coccolithophorid and cyanobacteria concentrations, and accessory pigments. The concentration of coccolithophorids can be estimated with the next generation of ocean-color sensors, including MODIS. These calcium-carbonate-producing organisms play a critical role in two cycles. First, a shift from silica-producing organisms (such as diatoms) to carbonate-producing organisms may tend to increase the surface pCO₂ of the ocean. However, there is a complex balance between this reaction and the competing effects of sinking of carbonate skeletons. The second role is in the production of DMS. Coccolithophorids produce a precursor, dimethylsulphoniopropionate. DMS is the major natural source of sulphur to the atmosphere and acts as a cloud condensation nucleus. There appears to be a link between DMS production and increased cloud condensation nuclei, but this is a strong function of species composition, total biomass, and ecosystem structure. However, it is clearly an area worth further study.

It is theoretically possible to distinguish relative dominance by some phytoplankton classes based on the absorption characteristics of accessory photosynthetic pigments such as the phycobiliproteins (common in blue-

TABLE 3.11

PARAMETER NAME	UNITS	ACCURACY ABS::REL	TEMPORAL RESOLUTION	HORIZONTAL RESOL::COVER	VERTICAL RESOL::COVER	COMMENTS
Chlorophyll Fluorescence Line Curv	mW cm ⁻² /sr/μm	0.25 :: 1.25	1/day, 1/wk	1 km, 20 km? :: Ocean/R,G	N/A ::	MODIS (20)
Chlorophyll Fluorescence Line Height	mW cm ⁻² /sr/μm	.004 Wm ⁻² sr ⁻¹ :: .004 Wm ⁻² sr ⁻¹	1/day, 1/wk	4 km, 1 km? :: Ocean/G,R,L?	N/A ::	MODIS (20)
Chlorophyll Fluorescence Efficiency	mW cm ⁻² /sr/μm/mg-Chl m ⁻³	TBD :: TBD	1/day, 1/wk	1 km :: Ocean/R,L	N/A ::	MODIS (20)
Chlorophyll _a Pigment Conc, Case II	mg m ⁻³	50%(0.05<[Chl]<1) :: 50%(0.05<[Chl]<2)	1/day, 1/wk, 1/mon	1 km :: Ocean-II/ R	N/A ::	MODIS (21)
Chlorophyll _a Pigment Conc, Case I	mg m ⁻³	30%(0.1<[Chl]<1); 60%(1<[Chl]<10); TBD([Chl]>10) :: 30%(0.1<[Chl]<1); 60%(1<[Chl]<10); TBD([Chl]>10)	1/day, 1/wk, 1/mon	1 km :: Ocean-I/ L	N/A ::	MODIS (21)

Chlorophyll *a* concentration and fluorescence

green algae) and the carotenoids (common in diatoms and dinoflagellates). Some biogeochemically important types of phytoplankton (e.g., coccolithophorids and the blue-green nitrogen-fixer, *Trichodesmium*) significantly affect the scattering properties of ocean waters, and thus semi-quantitative estimates of their abundance will be possible.

The final group of phytoplankton that perhaps can be detected from space are floating mats of cyanobacteria, notably *Trichodesmium*. Some preliminary results with historical CZCS data suggest that these mats can be quantified. As these organisms convert atmospheric nitrogen into organic nitrogen, they play a unique role in both nitrogen and carbon cycling in the upper ocean. Recent field studies suggest that their importance may have been overlooked, and that their abundance may depend strongly on variability in wind stress (Table 3.12).

DOM. The world ocean contains about 35,000 Gt of carbon. While the bulk of this material is in the inorganic form, approximately 700 Gt (2%) is in the form of DOM. Often referred to as DOC, this pool of carbon is comparable in size to all of the carbon contained in all of the living biota on the continents (750 Gt) and to the total atmospheric inventory of carbon (740 Gt) as carbon di-

oxide. The DOC pool likewise dwarfs the amount of carbon contained within the living biota in the ocean, estimated as 1-4 Gt of carbon. (All carbon pool size estimates are from Sundquist 1985.)

The seasonal variations in the size of regional DOC pools suggest that the flux of carbon between the inorganic and organic forms for the global ocean is on the order of 100 Gt annually. This “flux” is the major sink for inorganic carbon in the surface waters of the world ocean and is larger than all other sinks combined. For example, recent estimates of the various sinks of carbon in the equatorial Pacific Ocean suggest that 50-80% of the carbon loss was in the form of DOC (Murray et al. 1994), exceeding the vertical sinking flux of particles from the euphotic zone by a factor of 2-4 in all seasons and more than three times the gas exchange loss to the atmosphere.

Thus, any global model that attempts to define the carbon budget and includes interactions between the ocean and the atmosphere must deal with the process of incorporating carbon into the DOC pool. Most of these exchanges occur in the surface waters of the world ocean and intimately link the flux of carbon between the DOC and dissolved inorganic carbon (DIC) pools with the exchange of carbon between the oceans and the atmosphere.

TABLE 3.12

PARAMETER NAME	UNITS	ACCURACY Abs::REL	TEMPORAL RESOLUTION	HORIZONTAL RESOL::COVER	VERTICAL RESOL::COVER	COMMENTS
Coccolith Conc, Detached	number/ml	25000/ml (10-20%) :: 25000/ml (10-20%)	1/day, 1/wk 1/mon	20 km, 1 km? :: Ocean (in Coccolith Blooms)/G,R,L?	N/A ::	MODIS (25)
Calcite Conc, Estimated	mg-CaCO ₃ cm ⁻³	::	1/day, 1/wk, 1/mon	20 km, 1 km? :: Ocean (in Coccolith Blooms)/G,R,L?	N/A ::	MODIS (25)
Pigment Conc (in Coccolithophore Blooms)	mg m ⁻³	::	1/day, 1/wk, 1/mon	20 km, 1 km? :: Ocean (in Coccolith Blooms)/G,R,L?	N/A ::	MODIS (25)
Pigment Conc	mg m ⁻³	100% (Global); 35% (Case I, Clear Atmos) :: 100% (Global); 35% (Case I, Clear Atmos)	1/day, 1/wk 1/mon	20 km, 1 km? :: Ocean/G,R,L?	N/A ::	MODIS (19)
Phycocyanin Conc	mg m ⁻³	0.5 :: 1.5	1/day, 1/wk 1/mon	1 km :: Ocean /RL	N/A :: Sfc	MODIS (31)
Phycourobilin Conc	mg m ⁻³	0.5 :: 1.5	1/day, 1/wk 1/mon	1 km :: Ocean /RL	N/A :: Sfc	MODIS (31)
Constituent Inherent Optical Properties (CDOM absorption, Chlorophyllous absorption)		::	During overpass of validation regions	1 km :: Ocean /RL	N/A :: Sfc	MODIS (31)

Coccolithophorid and cyanobacteria concentrations

For example, any carbon that gets incorporated into the DOC pool represents a draw-down of the DIC pool and a simultaneous reduction in the partial pressure of CO₂. Furthermore, any sensitivity of these fluxes to changes in temperature or ocean circulation will modify the carbon budget, as these parameters change in association with the global climate.

Developing the models to adequately describe these processes and make reliable predictions of the consequences of future climatic changes in response to various scenarios represents a formidable challenge. Linking satellite observations of ocean color, temperature, and circulation to ship-based observations is our best hope of developing a comprehensive model.

Unfortunately, one of the critical parameters to a comprehensive land-ocean-atmosphere carbon model, DOC, is not directly observable from satellites, although a portion of the DOC pool, the CDOM, is. There has long been an interest in observing CDOM from satellites. Initially, this was driven by the desire to correct estimates of chlorophyll and biomass for the interference by CDOM (Hochman et al. 1995). More recently, there has been an effort to directly observe CDOM from aircraft and satellite data and correlate this with in situ determinations of DOC (Vodacek et al. 1995).

The initial simple relationships between observations (Vodacek et al. 1995) have turned out to be somewhat misleading. Recent work shows the correlations to be quite complex, exhibiting both seasonal and regional variations. In addition, photooxidation reactions in the mixed layer ultimately lead to the degradation of CDOM and the bleaching of its absorption and fluorescence emission

bands. Photobleaching occurs much faster than photooxidation of bulk DOC (Mopper et al. 1991), leading to an inverse correlation between DOC and CDOM in upwelling regions. Thus, on a global basis, one can not even be assured of the sign of the correlation without empirical in situ information.

This leads to the conclusion that the best hope for constraining global estimates of the distribution of DOC and how it impacts the oceanic carbon budget will involve a marriage of satellite observations and in situ (sea-truth) data. By combining the growing database of in situ measurements now becoming available via the JGOFS program with a variety of satellite ocean observations (e.g., SST, winds, and ocean color/chlorophyll), empirical correlations may make it possible to constrain the size of the DOC pool on a global basis and more often than is possible simply by accumulating ship-based observations (Table 3.13).

Water transparency. As noted earlier, bio-optical measurements of water transparency are essential in studies of the upper ocean heat budget. It is well-established that variation in phytoplankton abundance is the primary cause of variations in the light-trapping properties of the upper ocean. The absorption of sunlight is one of the primary processes determining mixed-layer depth. Many recent field and satellite-based studies have confirmed the importance of bio-optical properties for understanding the heat budget (and subsequent air/sea fluxes) of the upper ocean. Ocean-color measurements can be used to estimate water transparency at several wavelengths (Table 3.14, pg. 148).

TABLE 3.13

PARAMETER NAME	UNITS	ACCURACY ABS::REL	TEMPORAL RESOLUTION	HORIZONTAL RESOL::COVER	VERTICAL RESOL::COVER	COMMENTS
Suspended-Solids Conc, Ocean Water	g m ⁻³	0.5 :: 1.5	1/day, 1/wk, 1/mon	20 km, 1 km? :: Ocean/G,R?.L?	N/A ::	MODIS (23)
Organic Matter Conc, Dissolved	g m ⁻³	40%(open ocean best case); 100%(coastal for [Chl]<1) :: 40%(open ocean best case); 100%(coastal for [Chl]<1)	1/day, 1/wk 1/mon	20 km, 1 km? :: Ocean/R	N/A ::	MODIS (24)
Organic Matter Conc, Particulate	mg m ⁻³	TBD :: TBD	1/day, 1/wk	20 km :: Ocean	N/A ::	MODIS (24)

Colored dissolved organic matter

Primary productivity. To understand carbon cycling and the response of the marine biosphere to climate change, we must look beyond static variables of standing stocks to measurements of dynamics. Existing models rely on biomass estimates collected from ocean-color sensors to infer production rates. Empirical methods have been used to estimate light adaptation and other physiological parameters to improve these models. However, there has been much recent progress, and improved models have begun to appear in the scientific literature.

There are two promising lines of research. First, information on the photoadaptive state will significantly improve productivity estimates. Although the relationship of sun-stimulated fluorescence to photoadaptive parameters is not well-understood (especially for surface, light-inhibited populations), fluorescence bands will be included on MODIS, the Global Imager (GLI), and the Medium-Resolution Imaging Spectrometer (MERIS). This information will provide estimates of the physiological state of the phytoplankton and, when coupled with biomass estimates using measurements from other wave-

lengths, should improve productivity models. The availability of morning and afternoon MODIS sensors will allow the study of some aspects of diel variability, at least in regions of the world ocean that are not obscured by glint during one of the passes. Measurement of diel variations in sun-stimulated fluorescence might further improve models of phytoplankton growth rates. However, considerable field work remains before sun-stimulated fluorescence can become a standard tool for estimating productivity. The second line of research relies on productivity models that incorporate biological and physical processes explicitly. Clearly, such an approach must reflect increased understanding of the processes that regulate growth rates. A balance must be maintained between increasing the realism of the productivity models and adding unnecessary detail (Table 3.15).

Coral reef extent and ecosystem type. Current sensors, including Landsat and the Systeme pour l'Observation del la Terre (SPOT), are not able to observe coral reefs adequately. A Coral Reef Satellite Image Database is be-

TABLE 3.14

PARAMETER NAME	UNITS	ACCURACY ABS::REL	TEMPORAL RESOLUTION	HORIZONTAL RESOL:: COVER	VERTICAL RESOL::COVER	COMMENTS
Ocean Water Attenuation Coef@490nm	/m	0.25 :: 1.25	1/day, 1/wk, 1/mon	20 km, 1 km? :: Ocean-I/R,L	N/A ::	MODIS (26)
Ocean Water Attenuation Coef@520nm	/m	0.35 :: 1.35	1/day, 1/wk	1 km :: Ocean	N/A ::	MODIS (26)
Absorption Coef, Total	/m	0.25 :: 1.25		::	::	MODIS (36)
Absorption Coef, Gelbstof	/m	0.25 :: 1.25		::	::	MODIS (36)
Clear Water Epsilon		2% (0.9 to 1.4) :: 2% (0.9 to 1.4)	1/day, 1/wk 1/mon	1 km :: Ocean	::	MODIS (39)

Water transparency

TABLE 3.15

PARAMETER NAME	UNITS	ACCURACY ABS::REL	TEMPORAL RESOLUTION	HORIZONTAL RESOL:: COVER	VERTICAL RESOL::COVER	COMMENTS
Ocean Productivity, Primary, Daily	mg-C/m^2/day	35% (Goal) :: 35% (Goal)	1/day, 1/wk	1 km :: Ocean-I/R,L	N/A ::	MODIS (27)
Ocean Productivity, Primary, Global Annual	GT-C/yr	35% (Goal) :: 35% (Goal)	1/yr	20 km :: Ocean/G,R	N/A ::	MODIS (27)

Primary productivity

ing developed within the Advanced Spaceborne Thermal Emission and Reflection Radiometer (ASTER) project to identify which coral reefs have not been observed by satellites and determine which ones ASTER should observe. This database covers the northwest Pacific Ocean (0° to 31°N, 90°E to 180°) with 0.5° mesh. Each mesh cell has been assigned a probability of finding coral reefs: A (probable), B (possible), or blank (improbable). The database will be expanded to the rest of the world in the near future. ASTER coral reef products will be generated using ASTER-calibrated and atmospherically corrected surface-reflectance products. In a pre-processing stage, the image is classified into "land," "deep sea," "shallow sea," and "cloud and its shadow." Then, by an algorithm that is being developed and validated, "shallow sea" pixels are classified into benthic community classes such as corals, algae, seagrass, and sand.

3.3.2 Critical surface observations and field experiments

Satellite observations are usually only indirectly related to desired geophysical parameters. Algorithms that convert satellite data to geophysical data need testing and improvement by comparison with more direct observations, particularly in situ observations. Furthermore, because of the variability of atmospheric constituents and sea-surface roughness, coincident surface and atmospheric measurements are needed to correct satellite-derived surface parameters. As these parameters become more accurate over time, motivation will grow for a well-designed set of continual in situ observations.

3.3.2.1 World Ocean Circulation Experiment (WOCE), TOGA, Global Ocean-Atmosphere-Land System (GOALS), and Climate Variability and prediction (CLIVAR)

Much of the recent progress in advancing our understanding of seasonal-to-interannual climate variability is due to the TOGA program. This decade-long program focused on understanding and predicting the ENSO phenomenon, long recognized as being the most prominent interannual variation of the coupled climate system and one with global consequences. TOGA successfully implemented a routine in situ observing system across the tropical Pacific basin, mounted a major field campaign (TOGA/COARE), remotely monitored critical parameters of the coupled system (such as SST and sea-surface topography, deep atmospheric convection determined from outward long-wave radiation), and initiated experimental predictions of ENSO events.

The ten-year TOGA program has now been completed and has gone far beyond the original expectations

laid down in 1985. A new national program, GOALS, has been developed to both continue and expand research on seasonal-to-interannual variability. GOALS is a U.S. contribution to the international program, CLIVAR, which is a study of global climate on seasonal-to-centennial time scales. GOALS has an expanded scope of understanding and predicting connections between the tropical Pacific ENSO signal and climatic variations in other parts of the world as well as the predictability of climate variations not directly attributable to ENSO. EOS observations will support the GOALS goal of expanding its focus from the tropical Pacific to the entire global tropics. Related studies will improve understanding of the connections between tropical climate variability and significant climatic events at higher latitudes, with the goal of determining the feasibility of predicting these higher latitude events up from a season to a year in advance.

3.3.2.2 JGOFS

JGOFS, which began over a decade ago, is designed to study biogeochemical processes in the ocean and their role in climate change. The International Science Plan (JGOFS Report No. 5, SCOR, 1990) has set forth two goals:

- 1) To determine and understand on a global scale the processes controlling the time-varying fluxes of carbon and associated biogenic elements in the ocean, and to evaluate the related exchanges with the atmosphere, sea floor, and continental boundaries.
- 2) To develop a capability to predict on a global scale the response of oceanic biogeochemical processes to anthropogenic perturbations, in particular those related to climate change.

To meet these goals, the U.S. JGOFS approach is based on large-scale surveys, time-series stations, process studies, modeling, and data management. The large-scale surveys will provide a basin-scale-to-global-scale view of biogeochemical properties on seasonal time scales. Critical properties include surface pigment, primary production, CO₂, and export fluxes. The time-series stations will provide long-term, consistent observations to study seasonal variability of biogeochemical processes at a few sites. An improved mechanistic understanding of crucial biogeochemical processes is the objective of the process studies. These campaigns are conducted in critical regions of the ocean for a limited duration. Modeling activities will synthesize these data sets to provide a diagnostic understanding of ocean biogeochemistry as well as eventual use in predictive studies of the ocean's response to cli-

mate change. Lastly, these data sets and models will be maintained and managed so that future researchers can have confidence in the quality of the data as well as to facilitate data sharing and intercomparison.

The first three JGOFS process studies were the North Atlantic Bloom Experiment, the Equatorial Pacific program, and the Arabian Sea program. The final process study (Antarctic Environment Southern Ocean Process Study [AESOPS]) began in austral spring, 1996, and will conclude in 1998, just before the launch of the first AM-1 platform. High-quality satellite measurements from all of the ocean sensors (altimetry, scatterometry, visible radiometry, and infrared radiometry) will be available during this study of coupled ocean physical and biogeochemical processes. This represents a unique opportunity to develop and test models using observations analogous to EOS observations.

The next ocean program planned for IGBP is the Surface Ocean Lower Atmosphere Study (SOLAS), which will focus on event-scale processes and their role in air/sea fluxes. At this point, SOLAS is just beginning to be defined, but one of its primary objectives is to exploit the broad range of satellite observations of the ocean that will be available in late the 1990s and early 2000s. Building on JGOFS, SOLAS will expand our understanding of the coupling of physical and biological processes in the ocean. EOS observations will play a critical role.

3.3.2.3 GLOBEC

The U.S. and International GLOBEC programs have the goal of determining how marine animal populations respond to climatic variability and long-term climate change. The focus on zooplankton and higher trophic levels complements the focus of JGOFS on nutrients, primary production, and the carbon cycle. There is an international GLOBEC program and office at the Plymouth Marine Laboratory in the United Kingdom, and a number of national programs, including the U.S. GLOBEC program located at U.C. Berkeley. GLOBEC's approach includes:

- retrospective studies to elucidate the important scales of variability of ecosystem response to climatic change and to formulate hypotheses about mechanisms through which the components of the ecosystem respond,

- process studies to test the hypotheses and quantify the mechanisms, and
- ecosystem models that incorporate these mechanisms and provide a predictive capacity.

The first intensive process study of the U.S. program is a study of zooplankton, cod, and haddock on Georges Bank. The focus is on processes that control retention of larval and juvenile fish over the bank, looking also at their predators and prey. Retention is thought to be a key process in enhancing their survival and recruitment into the adult fish population. The second study is planned in the northeast Pacific (California Current and Alaska Gyre). This study is likely to concentrate on the processes that control mortality of juvenile salmon in the coastal ocean as they emerge from the rivers. Mortality during this period is thought to control ultimate yearly population strength. The general health of the coastal zooplankton ecosystem will also be a target, forming the prey field for the salmon, as will their predators. The survival of larval benthic invertebrate species may also be included, since these may be used as indicators of the health of the offshore zooplankton ecosystem.

These two studies are complemented by the national GLOBEC studies planned by Canada in the Atlantic and Pacific oceans and by Mexico in the Pacific. The international GLOBEC program has initiated modeling studies in the Southern Ocean (in cooperation with JGOFS), is planning field studies in the Southern Ocean concentrating on ecosystem dynamics that control the population of krill (beginning in 1999, following JGOFS), and is in the planning stage for studies in the regions where small pelagic fish (sardine, anchovy, herring, sprats) are the main fishery. Krill form the base of the marine animal food web in the Southern Ocean. Small pelagics are distributed globally, constitute about 1/3 the global fish catch, and cause much of the interannual variability in annual fish catch biomass. It will be important to coordinate GLOBEC process studies with EOS measurements and to combine EOS monitoring with GLOBEC ecosystem modeling in order to gain the most information from the two programs. Similar coordination with field studies carried out by JGOFS and its successor will be equally important.

3.4 EOS contributions: Combining the knowledge of ocean and climate systems

3.4.1 Air-sea flux plans for EOS

The focus of air-sea flux research in EOS is to make significant improvements in space-based observations required for global estimates of the air-sea momentum, heat, and freshwater exchanges, and to use this information to obtain a better understanding of ocean-atmosphere coupling on seasonal-to-interannual time scales.

Air-sea fluxes play crucial roles in six EOS Interdisciplinary Science Investigations—those of Abbott, Hartmann, Lau, Liu, Rothrock, and Srokosz—and are the focus of the Instrument Science Team for SeaWinds. Their combined goals regarding surface fluxes are listed below.

(i) Provide long-term, global, space-based observations of the surface wind stress from direct microwave observations of the ocean surface from both pre-EOS and EOS sensors.

The SeaWinds Instrument Team has the fundamental goal of providing ocean wind stress fields over 90% of the ice-free ocean every 2 days. The team will provide continuing long-term wind stress data for studies of ocean circulation, climate, air-sea interaction, and weather forecasting. The AMSR-E Instrument Team will provide continual observations of wind speed and stress magnitude.

(ii) Provide long-term, global, space-based observations of the variables relevant to the estimation of radiative and turbulent air-sea fluxes.

These observations are detailed in Section 3.3.1.1. The fundamental variables over both oceans and sea ice are surface temperature; temperature and humidity at as low a level in the atmosphere as can be observed (850 mb or lower); cloud water and ice content; radiative properties of the lower troposphere including atmospheric temperature and humidity profiles; and precipitation rates and amounts. Aside from the estimation of fluxes, SST and salinity are needed as diagnostic variables.

(iii) Assimilate surface and lower troposphere data into models that estimate wind stress, water vapor flux, sensible heat flux, and up- and downwelling components of radiation at the surface. Provide long-term global records of these fluxes over oceans and sea ice from both pre-EOS and EOS sensors.

Air-sea fluxes cannot be observed directly from space. Rather, the fluxes must be deduced from estimates

of more-directly-observable meteorological and oceanographic fields as called for in (ii). The problem of estimating climatological air-sea exchanges of momentum, heat, and freshwater may be thought of as a problem in data assimilation, in which observed data are used to tightly constrain the key variables in physical or empirical models of exchange processes. Because flux estimation often requires combining data from more than one sensor, Interdisciplinary Teams are actively developing multi-sensor and data assimilation techniques. Two Interdisciplinary Teams are ensuring that these flux fields extend to the Arctic and Southern oceans with no degradation in quality.

(iv) Apply air-sea flux data sets to the study of oceanic and atmospheric processes that control these fluxes and cause them to vary, and to the study of the role these fluxes play in forcing oceanic and atmospheric circulations and in the global heat and water balance.

Atmospheric processes such as air mass movement, convection and subsidence, formation of marine clouds, and development of storm systems all affect the strength of air-sea fluxes by controlling the temperature and humidity contrast between the sea surface and the atmospheric boundary layer. Similar control is exercised by oceanic processes such as the general ocean circulation, mixing, and upwelling. The contrasting point of view is understanding how surface fluxes transfer heat between the ocean and atmosphere and contribute to the global heat and water cycles. Local seasonal phenomena such as monsoon cycles and hurricane seasons must be characterized in terms of ocean-atmosphere phenomena.

(v) Utilize in situ data of surface and near-surface meteorological conditions to validate air-sea flux models.

Both space-based and in situ data are required to obtain accurate estimates. Space-based data provide global spatial coverage within the limitations of the satellite orbit. In situ data from ships, buoys, aircraft, and island stations provide point measurements of meteorological and oceanographic fields and the related fluxes. Space-based data therefore provide the spatial and temporal coverage needed to reduce sampling errors, whereas the in situ data provide a calibration standard and information on the detailed vertical structure of the atmosphere. There are numerous air-sea flux programs, some with attached field programs, in which EOS investigators are

participants along with a wider community of investigators.

A central aspect of these studies is clarifying sampling issues so that space-based and surface-based flux estimates can be intercompared and jointly utilized in model testing.

(vi) Support the design, building, and validation of an interdecadal climate prediction system that correctly treats air-sea interaction including precipitation.

New knowledge of atmospheric and oceanic boundary layer processes is being used to test and improve model parameterizations. Modeled fields of air-sea fluxes will be thoroughly tested against independent space-based and surface-based flux estimates and estimates of closely related surface variables such as SST and salinity. The goal is a climate model that accurately transfers momentum, heat, and water across the sea surface. Some initial work is directed at examining the air-sea coupling in the Earth system model.

3.4.2 Ocean circulation and sea-level plans for EOS

EOS oceanographers are focussed upon assessing and understanding the distribution of heat and salt within the world oceans, and the ocean circulation. The fundamental task is collection and analysis of remotely sensed data describing the dynamic state of the ocean surface. The essential tools are an array of ocean and atmosphere-ocean models that permit the diagnosis of ocean dynamics and atmosphere-ocean coupling in both “forced” and “data assimilating” modes.

Contributions to studies of ocean circulation are being made by the TOPEX/Poseidon and Jason-1 Altimeter Teams, the MODIS Science Team, the AMSR Science Team, and the NSCAT and SeaWinds Science Teams, and by a number of Interdisciplinary Science Investigations—those of Abbott, Liu, Rothrock, and Srokosz. Their combined goals regarding ocean circulation are as follows:

(i) Determine the marine geoid to an accuracy of 1.5 cm by means of a gravity mission, determine multi-decadal global sea-level variations to an accuracy of 4 mm rms, and determine the long-term trend to <1 mm/yr.

These are fundamental observational goals for defining the mean ocean circulation and climate-driven sea-level change. They will enable the measurement of oceanic transports at the 1 Sv level.

(ii) Provide a multi-decadal record of the seasonal and interannual variability of ocean surface currents and of

surface temperature and salinity, and validate these data with in situ observations.

A multi-decadal record of the sea-surface state is the underpinning of the contribution oceanography needs from satellite observations. Providing and validating this record is the central goal of many instrument and interdisciplinary investigators. Altimeter data together with in situ data are being intercompared in programs such as the TOGA/WOCE Surface Velocity Program and the Global Drifter program.

(iii) Utilize improved observations of surface fluxes, currents, temperature, and salinity to quantify the mean ocean circulation and its seasonal-to-interdecadal variability, assessing in particular the mean and variability of the poleward oceanic heat transport.

The determination of mean currents requires a better geoid. In the meantime, mesoscale processes and variability are being studied using higher-resolution sea-level fields generated by coupling multiple altimeter data sets. Coupled infrared and altimeter observations will be used to calculate high-resolution ocean circulation fields. Investigators are examining the relationship between the temporal and spatial variability of the atmospheric forcing and the variability of the oceanic response. Altimetry and SST data are being combined to study time-dependent eddies and seasonal variations in the position of currents such as the Agulhas Retroflexion. Studies of SST data in the North Atlantic show high variability localized in the Gulf Stream and off Newfoundland. In situ observations of absolute current in the Drake Passage are being used to extend the interpretation of surface-height anomalies from altimetry. The circulation in the Arctic Ocean and its exchange with the North Atlantic are being studied to document variability in the stability of the Greenland and Labrador Seas and how this variability acts to control episodic deep water formation.

(iv) Advance methods for assimilating surface observations into ocean GCMs and into combined atmosphere-ocean and climate system models, and use the resulting improvements in ocean model physics to advance the predictive capability of combined models.

Investigators are developing fully assimilating ocean models. The assimilated variables can include surface height or current, and SST and salinity; over ice-covered oceans they include ice velocity and concentration. Model results are being studied to understand how physical processes regulate primary productivity in the Southern Ocean. These models will be used to understand the linkage between the intense variability observed

on small scales and the larger-scale processes on monthly or longer time scales.

By assimilating data and forcing models with improved surface fluxes investigators will improve eddy-resolving ocean-circulation models, giving a more-realistic 4-D description than possible with present data. New techniques for assimilating sea-surface height data allow one to project the height data to recover the deep-ocean-water properties and circulation by assuming conservation of relative vorticity.

(v) *Understand the role the ocean plays in determining the angular momentum and mass exchange within the Earth system.*

Atmospheric pressure and ground water redistribution play a significant role in exchanging momentum with the ocean and solid Earth; the mechanism is not well understood. Sea-level changes occur from mass redistribution, thermal change, and ocean circulations. Changes in the Earth rotation are attributable to winds, currents, ground-water circulation, and mass redistribution within the Earth system. Changes in the gravity field, which can be inferred from satellite orbit perturbations, arise only from mass redistribution. Combining EOS observations and space geodetic techniques enables one to observe and interpret these global signals, to improve atmospheric and ocean models, and to improve the predictive capabilities of these models. The model improvements can be accomplished by using the global angular momentum, stress torques, and mass variations as a means of calibrating, interpreting, and constraining general ocean-circulation-model outputs.

3.4.3 *Marine biogeochemical research planned in EOS*

We presently lack basic observations of “ocean color” necessary to estimate ocean biogeochemical variables and to develop and test relationships between them in numerical models. Long-time series of well-calibrated satellite optical observations will provide these critical observations and allow us to quantify the linkages between climate and ocean ecology. The approach in EOS is based on a synthesis of ocean and atmosphere circulation models with satellite and in situ measurements of the ocean-surface biogeochemical variables. These studies are being undertaken by the MODIS Instrument Science Team and the Interdisciplinary Science Investigations of Abbott, Goyet, and Srokosz. We are pursuing the following objectives in parallel:

(i) *Acquire long-term, calibrated satellite data sets of ocean biogeochemical variables.*

The biological component of the investigation will utilize MODIS as well as other ocean-color sensors—SeaWiFS, Ocean Color and Temperature Scanner (OCTS), MERIS, and GLI—to obtain basic information on ocean biological processes. These sensors will be used to estimate phytoplankton abundance as well as growth rates based on models that incorporate biomass, fluorescence, and incoming solar radiation.

(ii) *Acquire in situ observations of physical and biogeochemical data to complement satellite observations, to provide variables not observable by satellite, to intercompare with satellite data, and to assess sampling characteristics and accuracy of satellite data.*

Investigators will make field measurements in the Southern Ocean of both biological and physical processes. Bio-optical moorings are planned for the Polar Front in late 1997. A test mooring was deployed at the Hawaii JGOFS Time Series station in early 1995. A cruise in the Weddell Sea used bio-optical drifters and photosynthesis measurements to improve models for estimating primary productivity from fluorescence measurements from MODIS. New buoy-mounted technology for in situ real-time sensing of pCO₂ is being developed to provide short-term and long-term time-series measurements and to gain better understanding of the temporal variations of pCO₂ in surface seawater. In-water optical properties are being related to phytoplankton biomass and pigment concentrations, including accessory pigments, as well as DOM concentrations. Algorithms to determine phytoplankton speciation and distributions are being studied. In addition, improved models for estimating primary production and DOC in the mixed layer from pigment concentrations, SST, mixed-layer depth, and mean incident solar irradiance are being developed. The output of these models will be compared with in situ measurements. Data will be analyzed in terms of the scales of variability from days to years and from kilometers to thousands of kilometers.

(iii) *Quantify the mean and variability of the ocean surface biogeochemical state.*

Models for mapping seawater partial pressure fields of several radiatively active gases are being developed. The field of pCO₂ in the ocean mixed layer will be derived from mixed-layer depth, salinity, SST, and phytoplankton biomass, and constrained by field measurements of alkalinity and TCO₂ from WOCE and JGOFS field observations currently underway.

(iv) *Develop coupled ocean circulation/biogeochemical models, both with and without data assimilation, and utilize satellite and in situ data to provide model forcing and to test and improve model formulation.*

Fluxes of CO₂, DMS, and CO over basin and global scales will be modeled using the air-sea gas-concentration gradients derived from maps of gas transfer velocities. Algorithms for a more-accurate gas-transfer velocity parameterization based on wind speed, CZCS-derived organic matter estimates, and microwave backscatter-derived wave slope measurements are under investigation. New production and the primary production contribution from below the mixed layer will be modeled. The results of these investigations will be incorporated in upper-ocean models: ecosystem models treating phytoplankton, zooplankton, nutrients, and detritus, as well as global eddy-resolving ocean models using sea surface total CO₂ and pCO₂ interpolated from satellite imagery.

(v) *Develop a quantitative understanding of the relationship between the climate and the upper-ocean ecological state—both the mean and its variability.*

Interdisciplinary studies are aimed at 1) understanding and predicting the response of the marine biosphere to variations in physical forcing, with particular emphasis on the Southern Ocean and North Atlantic and 2) understanding and predicting the air-sea exchange and fate of CO₂ and two other radiatively important gases, DMS and CO. Studies will determine processes near the Subtropical Convergence governing “new” production, which is the component of primary productivity supported by the input of nutrients into the ocean’s euphotic zone from deeper waters or from the atmosphere. New production is related to the vertical flux of carbon in the ocean and thus plays a key role in the ocean carbon cycle. The Subtropical Convergence is one of the most important sites in the world ocean for new production and hence for the uptake of atmospheric CO₂. The approach is to use ocean-color observations as well as measurements of physical forcing by EOS altimeters and scatterometers to study the processes controlling the rate of new production. The role of atmospheric forcing and its impacts on ocean circulation and eventually on biological productivity will be analyzed using the full suite of EOS ocean sensors and numerical models.

3.4.4 Human dimensions of ocean climate

EOS will provide for the first time simultaneous observations of the major physical and biological ocean-surface variables. These observations along with simultaneous atmospheric and terrestrial observations will introduce a

new era in predictive modeling capabilities with enormous benefits to oceanic, and, particularly, coastal human activity. Sea level, currents, and waves all affect transportation, oil and gas extraction, property loss through sea-level change and coastal erosion, recreational boating, and search and rescue. Storms and floods in coastal regions destroy infrastructure and living resources. The assimilation of EOS measurements will dramatically improve global and regional atmospheric and oceanic forecasts. Simultaneous and improved atmospheric and oceanic measurements over the open oceans will be especially critical to forecasts along the continental west coasts, where upstream atmospheric information is presently sparse. Specific benefits include:

- Improved prediction of circulation patterns that will aid oil/chemical spill cleanup, allow accurate environmental impact assessments, and improve waste management decisions.
- Improved prediction of coastal effects of storms and other marine hazards that will increase the safety of navigation, improve warnings and evacuations for storms, floods, and tsunamis, and provide guidance for long-term coastal planning.
- Improved prediction of wave heights and directions and of ocean tides will allow more accurate time-series measurements of coastal sea level.
- Improved understanding and modeling of sediment erosion/deposition, land subsidence, and sea-level rise that will allow long-term projections of sea-level change and its impact on coastal populations and economies.

It is critical that we define today’s baseline condition of global coastal environments. EOS data and model products will provide a unique framework for quantitatively addressing changes in freshwater inputs and their relationship to precipitation in catchment areas, and exchanges of water and sediment between estuaries and the coastal ocean. Besides improvements in large-scale models, it is also important that we improve regional models that predict winds and precipitation over variable terrain at the shoreline transition and forecast potential damage caused by winds, waves, floods, and storm surges.

Understanding and predicting the effects of climatic variability on coastal and pelagic fisheries is another critical issue with tremendous human consequences. There is growing evidence that fish populations respond strongly and quickly to local and basin-scale environmental vari-

ability (Hunter and Alheit 1995; US GLOBEC Report Nos. 11, 1994, and 15, 1996). Examples include responses to interannual ENSO fluctuations in the Pacific Ocean and responses to interdecadal fluctuations in conditions in all basins. The affected species range from phytoplankton at the base of the food web to commercially and ecologically important fish, marine birds, and mammals. As a consequence of our ignorance of these natural cycles, we have overfished certain stocks during their natural collapse periods, depleting their stocks to actual or near extinction. A case in point is the California sardine, which is now thought to have been in a period of natural decline in the late 1940s. By overfishing this resource at a critical time, we drove the population to virtually zero off the U.S. west coast. The few remaining fish did respond to a change in oceanic conditions in the late 1970s, but instead of returning to their peak numbers by 1980 (as they would have, if left at natural levels), an additional 15 years were required until they reached moderate levels in the mid 1990s. Other examples include cod and haddock in the Northeast Atlantic and salmon stocks in the Pacific Northwest, although the interplay between natural fluctuations and overfishing in these cases is not yet as clear.

Most commercially important fish and benthic invertebrates, like crabs, begin life as passive larvae, subject to the forces of currents and other oceanic environmental conditions. EOS sensors will either observe or help models predict the environmental influences on their life cycle:

- the wind forcing, including turbulent mixing that affects larval feeding behavior;
- circulation patterns, which carry larvae to locations better or worse suited for their growth and survival;
- temperatures, which affect growth of the larvae and also the abundance of their prey and predators;
- phytoplankton concentration and primary productivity, forming the base of the food chain; and
- mixed-layer depth and stratification, which affect vertical motion and mixing of nutrients that support primary productivity.

In coordination with process studies aimed at specific mechanisms that affect growth and mortality of target species, EOS data sets will be invaluable for formulating and testing biophysical ecosystem models. Benchmarked against environmental changes seen in EOS data, these models will become management tools predicting changes

that lead to natural declines in populations, allowing a rational approach to fishery harvests.

3.4.5 Atmosphere/ocean modeling

For many purposes, the ocean can be treated as an isolated component of the climate system. This is possible when adequate boundary conditions are available from observations for the issue to be studied, that is, when fluxes of momentum, heat, fresh water, and various chemical substances across the sea surface are available. Then numerical models of the oceanic circulation can be used to unravel some of the key processes involved in the ocean's role in climate change. In many circumstances, however, it is not possible to isolate the ocean from the atmosphere. It is, in fact, the interactions that feed from one of these components to another—often in both directions—that contain the essential mechanisms for global climate-change scenarios.

A good example of this is the feedback associated with perturbations within the ocean and atmosphere associated with changes in SST. Because of its small heat capacity the atmosphere quickly restructures its winds and thermal fields in response. This in turn results in changes in the forcing of the ocean that begins to create a new upper ocean structure and SST pattern. The potential for such interactions that can provide both positive feedbacks (leading to the combined system tending to move further from its initial condition) and negative feedbacks (such that the combined response is to damp the system back toward its initial configuration) is at the heart of coupled ocean/atmosphere modeling. Such models must play a central role in any strategy for unraveling the climate puzzle.

The lack of complete, global observations of many important variables and derived quantities presents major challenges to validation of component models of the atmosphere, ocean, and sea ice. In coupled models, concern with interactive system behavior exacerbates validation problems by increasing the available degrees of freedom. However, a great deal of data can provide indirect information about aspects of the coupled system. For example, heat and fresh water budget constraints can be used to validate coupled atmosphere-ocean-sea ice components. Estimates of evaporation minus precipitation from atmospheric measurements or analyses can be used to examine fresh water transports, oceanic salinity, and thermohaline circulation. Similarly, the sum of convergence of heat transports by atmosphere and ocean must balance net radiation at the top of the atmosphere. The combination of local budgets of these quantities in the atmosphere, the ocean, and at the interface produces over-specification,

requiring conciliation among different answers and, thus, provides constraints on system behavior. Models provide another important insight: one can examine model sensitivities and discover which components are critical to the system's proper behavior and then focus upon observing these components and ensuring that they are well represented in the models.

3.4.6 Improved predictions of seasonal-to-decadal climate variability through global land-atmosphere-ocean models

Changes in climate, whether anthropogenic or natural, involve a complex interplay of physical, chemical, and biological processes of the atmosphere, ocean, and land surface. As climate system research seeks to explain the behavior of climate over time scales of years to millennia, focus necessarily turns to behavior introduced by physical, chemical, and biogeochemical interactions among climate subsystems. The need to understand climate as a coupled system is demonstrated by the paleoclimate record, which reveals large and related changes in atmospheric and oceanic circulations and biogeochemistry (e.g., Broecker 1987; Dansgaard et al. 1993). The challenges of modeling the role of anthropogenic emissions of CO₂, of reactive trace gases, and of changing land use in the Earth system likewise require a coupled climate system approach. While knowledge that land-ocean-atmosphere interactions influence climate is not new, the emergence of coupled climate system questions as central scientific concerns of geophysics constitutes a major realignment of the research agendas in atmospheric science, oceanography, ecology, and hydrology.

Two recent books, *Climate System Modeling* (Trenberth 1992) and *Modeling the Earth System* (Ojima 1992), document many aspects of climate system modeling and of the uses of such models for global change research and paleoclimate studies. Key questions include the coupling between processes occurring at different time scales (seasonal to interannual, interannual to decadal) that affect the longer-term behavior of the system. The interaction between seasonal and interannual (ENSO) processes discussed by Tziperman et al. (1994) provides one example. As a related but longer-term example, evidence—in the paleorecord and from models—shows that changes in ENSO frequency are a component of long-term climate variability (Meehl et al. 1993; Thompson et al. 1989). The possible existence of thresholds or multiple equilibria in the climate system arising from the

thermohaline ocean circulation and perhaps related to the carbon cycle is another issue of scientific importance and great relevance to society (Taylor et al. 1993). This is because adaptation to abrupt change would be much more difficult for mankind than acclimatization to continuous change.

Relatively simple models will continue to play an important role in climate system research, but the most credible characterizations of the important processes, as well as the best predictions for future climate change, will come from comprehensive models of the climate system. Many relevant examples of component subsystem models exist, and several groups around the world have produced interesting prototypes for a comprehensive climate system model. However, no mature model of this type yet exists. It is vital therefore, during the EOS years, that such models be further developed vigorously and exercised fully in pursuit of more-complete understanding of climate-change issues.

3.4.7 Understanding of ocean's effect on carbon dioxide, the major greenhouse gas

In order to describe and predict climate variability due to the continuous increase of anthropogenic CO₂ in the atmosphere, it is essential to understand the present-day role of the ocean in the absorption of atmospheric CO₂ gas. Most of this absorption occurs by carbon input from the rivers and by continuous CO₂ gas exchange across the ocean-atmosphere interface.

As mentioned above (in Section 3.2.4.3) CO₂ fluxes cannot be measured directly and have to be estimated from various observations. On the global scale, the quantification of CO₂ fluxes across the ocean-atmosphere interface requires two complementary sets of observations: in situ and remotely-sensed observations.

The in situ observations, typically obtained from oceanographic research cruises, provide accurate sea-surface pCO₂ data sets on short time and spatial scales. The space-based observations provide global spatial coverage at frequent time scales of a limited number of parameters (such as ocean color and SST) with a lesser accuracy than in situ observations. The challenge is to develop algorithms that couple in situ and proxy space-based observations to quantify the global absorption of carbon by the oceans.

Providing a global estimate of the air-sea exchange of CO₂ will be a major contribution to quantifying the Earth climate system.

References

- Baumgartner, A., and E. Reichel, 1975: *The World Water Balance: Mean Annual Global, Continental and Maritime Precipitation, Evaporation and Run-off*. Elsevier, New York, 179 pp.
- Bennett, A. F., and B. S. Chua, 1994: Open-ocean modeling as an inverse problem: The primitive equations. *Mon. Wea. Rev.*, **122**, 1326–1336.
- Betts, A. K., and W. Ridgway, 1989: Climatic equilibrium of the atmospheric convective boundary layer over a tropical ocean. *J. Atmos. Sci.*, **46**, 1326–1336.
- Born, G., B. Tapley, J. Ries, and R. H. Stewart, 1986: Accurate measurement of mean sea level changes by altimetric satellites. *J. Geophys. Res.*, **91**, 11,775–11,782.
- Broecker, W. S., and G. H. Denton, 1989: The role of ocean-atmosphere reorganizations in glacial cycles. *J. Geophys. Res.*, **53**, 2465–2501.
- Broecker, W. S., 1987: Unpleasant surprises in the greenhouse? *Nature*, **328**, 123–126.
- Broecker, W. S., and T. S. Peng, 1982: Tracers in the Sea. Lamont-Doherty Geological Observatory, Columbia University, 690 pp.
- Bryan, F. O., C. W. Boning, and W. R. Holland, 1995a: On the midlatitude circulation in a high-resolution model of the North Atlantic. *J. Phys. Oceanogr.*, **25**, 289–305.
- Bryan, F. O., I. Wainer, and W. R. Holland, 1995b: Sensitivity of the tropical Atlantic circulation to specification of wind stress climatology. *J. Geophys. Res.*, **100**, 24,729–24,744.
- Cornell, S., A. Rendell, and T. Jickells, 1995: Atmospheric inputs of dissolved organic nitrogen to the oceans. *Nature*, **376**, 243–246.
- Cullen, J. J., and M. R. Lewis, 1995: Biological processes and optical measurements near the sea surface: Some issues relevant to remote sensing. *J. Geophys. Res.*, **100**, 13,255–13,266.
- Dansgaard, W., S. J. Johnsen, H. B. Calusen, D. Dahl-Jensen, N. S. Gundestrup, C. U. Hammer, C. S. Hvidberg, J. P. Steffensen, A. E. Sveinbjornsdottir, J. Jouzel, and G. Bond, 1993: Evidence for general instability of past climate from 250-kyr ice-core record. *Nature*, **364**, 218–220.
- deBaar, H. J. W., J. T. M. de Jong, D. C. E. Bakker, B. M. Loscher, C. Veth, U. Bathmann, and V. Smetacek, 1995: Importance of iron for plankton blooms and carbon dioxide drawdown in the Southern Ocean. *Nature*, **373**, 412–414.
- DeMaster, J. D., R. B. Dunbar, L. I. Gordon, A. R. Leventer, J. M. Morrison, D. M. Nelson, C. A. Nittrouer, and W. O. Smith Jr., 1992: Cycling and accumulation of biogenic silica and organic matter in high-latitude environments: The Ross Sea. *Oceanography*, **5**, 146–153.
- de Soeke, R. A., and M. D. Levine, 1981: The advective flux of heat by mean geostrophic motion in the Southern Ocean. *Deep-Sea Res.*, **28**, 1057–1085.
- Donelan, M. A., 1990: Air-sea interaction. *The Sea: Part B - Ocean Engineering Science*, **9**, (B. LeMehaute, and D. Hanes, Eds.), 239–292.
- Douglas, B., 1991: Global sea level rise. *J. Geophys. Res.*, **96**, 6981–6992.
- Erikson, D. J., III, 1993: A stability dependent theory for air-sea gas exchange. *J. Geophys. Res.*, **98**, 8471–8488.
- Fasham, M. J. R., H. W. Ducklow, and S. M. McKelvie, 1990: A nitrogen based model of plankton dynamics in the ocean mixed layer. *J. Mar. Res.*, **48**, 591–639.
- Freilich, M. H., 1985: Science opportunities using the NASA scatterometer on N-ROSS. National Aeronautics and Space Administration, JPL Publication 84-57, 36 pp.
- Frew, N. M., 1997: The role of organic films in air-sea gas exchange. *The Sea Surface and Global Change*, (P. S. Liss and R. A. Duce, Eds.), Cambridge University Press, New York, in press.
- Fukumori, I., J. Benveniste, C. Wunsch, and D. B. Haidvogel, 1993: Assimilation of sea surface topography into an ocean circulation model using a steady state smoother. *J. Phys. Oceanogr.*, **23**, 1831–1855.
- Gill, A. E., 1982: *Atmosphere-Ocean Dynamics*. Academic Press, Inc., San Diego, 662 pp.
- Gill, A. E., and P. P. Niiler, 1973: The theory of the seasonal variability in the ocean. *Deep-Sea Research*, **20**, 144–177.
- Guman, M. D., C. K. Shum, J. C. Ries, and B. D. Tapley, 1996: Mean sea level variations observed using satellite altimetry. Spring American Geophysical Union Meeting, Baltimore, MD, 20–24 May 1996.
- Harrison, D. E., 1989: On climatological monthly mean wind stress and wind stress curl fields over the world ocean. *J. Climate*, **2**, 57–70.
- Hellerman, S., and M. Rosenstein, 1983: Normal monthly wind stress over the world ocean with error estimates. *J. Phys. Oceanogr.*, **13**, 1093–1104.
- Hochman, H., J. J. Walsh, K. L. Carder, A. Sournia, and F. E. Muller-Karger, 1995: Analysis of ocean color components within stratified and well-mixed waters of the western English Channel. *J. Geophys. Res.*, **100**, 10,777–10,787.
- Holland, W. R., 1986: Quasigeostrophic modeling of eddy resolved ocean circulation. *Advanced Physical Oceanographic Numerical Modeling*, (J. J. O'Brien, Ed.), D. Reidel Pub. Co., 203–231.
- Holligan, P. M., and H. deBoois, 1993: Land-Ocean Interactions in the Coastal Zone (LOICZ) Science Plan. *International Geosphere-Biosphere Programme (IGBP) Report No. 25*, 50 pp.
- Honjo, S., 1990: Particle fluxes and modern sedimentation in the polar oceans. *Polar Oceanography: Part B Chemistry Biology, and Geology*, (W. O. Smith Jr., Ed.), Academic Press, Inc., San Diego, 687–739.
- Hsiung, J., 1985: Estimates of global, oceanic meridional heat transport. *J. Phys. Oceanogr.*, **15**, 1405–1413.
- Hsiung, J., 1986: Mean surface energy fluxes over the global ocean. *J. Geophys. Res.*, **91**, 10,585–10,606.
- Hunter, J. R., and J. Alheit, Eds., 1995: International GLOBEC Small Pelagic Fishes and Climate Change Program: Report of the First Planning Meeting, La Paz, Mexico, June 20–24, 1994, *GLOBEC Report #8*, 72 pp.
- Jackson, F. C., W. T. Walton, D. E. Hines, and C. Y. Peng, 1992: Sea surface mean square slope from Ku-band backscatter data. *J. Geophys. Res.*, **97**, 11,411–11,427.
- Jacobs, G. A., H. E. Hurlburt, J. C. Kindle, E. J. Metzger, J. L. Mitchell, W. J. Teague, and A. J. Wallcraft, 1994: Decade-scale trans-Pacific propagation and warming affects of an El Niño anomaly. *Nature*, **370**, 360–363.
- Jahne, B., K. O. Munnich, R. Bosinger, A. Dutzi, W. Huber, and P. Libner, 1987: On the parameters influencing air-water gas exchange. *J. Geophys. Res.*, **92**, 1937–1949.
- Joint Global Ocean Flux Study Report No. 5 Science Plan, 1990: Scientific Committee on Oceanic Research.
- Kleeman, R., and S. B. Power, 1995: A simple atmospheric model of surface heat flux for use in ocean modeling studies. *J. Phys. Oceanogr.*, **25**, 92–105.
- Komhyr, W. D., R. H. Gammon, T. B. Harris, L. S. Waterman, T. J. Conway, W. R. Taylor, and K. W. Thoning, 1985: Global atmospheric CO₂ distribution and variations from 1968–1982 NOAA/GMCC CO₂ flask sample data. *J. Geophys. Res.*, **90**, 5567–5596.
- Liss P. S., and L. Merlivat, 1986: Air-Sea exchange rates: Introduction and synthesis. *The Role of Air-sea Exchange in Geochemical Cycling*, (P. Buat-Menard, Ed.), NATO ASI series, D. Reidel Pub. Co., Boston, 113–127.

- Liss P. S., 1983a: Gas transfer: Experiments and geochemical implications. *Air-sea Exchange of Gases and Particles*, (P. S. Liss, and W. G. N. Slinn, Eds.), D. Reidel Pub. Co., Boston, 241–298.
- Liss P. S., 1983b: The exchange of biochemically important gases across the air-sea interface. *The Major Biogeochemical Cycles and Their Interactions*, (B. Bolin, and R. B. Cook, Eds.), J. Wiley, New York, 411–426.
- Liu, W. T., 1986: Statistical relation between monthly mean precipitable water and surface-level humidity over global oceans. *Mon. Wea. Rev.*, **114**, 1591–1602.
- Liu, W. T., W. Tang, and P. P. Niiler, 1991: Humidity profiles over oceans. *J. Climate*, **4**, 1023–1034.
- Lukas, R., and E. Lindstrom, 1991: The mixed layer of the western equatorial Pacific Ocean. *J. Geophys. Res.*, **96**, 3343–3357.
- Macdonald, A. M., and C. Wunsch, 1996: Oceanic fluxes of mass, heat, and freshwater: A global estimate and perspective. 1996 Ocean Sciences Meeting. Supplement to *Trans. Amer. Geophys. Union*, **76**, U.S. WOCE Contribution Number 361.
- Mann, K. H., and J. R. N. Lazier, 1991: Dynamics of Marine Ecosystems, Blackwell, Oxford, 466 pp.
- Marshall, J. C., A. J. G. Nurser, and R. G. Williams, 1993: Inferring the subduction rate and period over the North Atlantic. *J. Phys. Oceanogr.*, **23**, 1315–1329.
- Martin, J. H., 1990: Glacial-interglacial CO₂ change: The iron hypothesis. *Paleoceanography*, **5**, 1–13.
- Meehl, G. A., G. W. Branstator, W. M. Washington, 1993: Tropical Pacific interannual variability and CO₂ climate change. *J. Climate*, **6**, 42–63.
- Mestas-Nunez, A. M., D. B. Chelton, M. F. Freilich, and J. G. Richmann, 1994: An evaluation of ECMWF-based climatological wind stress fields. *J. Phys. Oceanogr.*, **24**, 1532–1549.
- Meybeck, M., 1993: Land and water interface zones (as global sinks of atmospheric CO₂). *Water, Air, Soil Pollut.* (Dordrecht), **70**, 123–137.
- Milliff, R. F., W. G. Large, W. R. Holland, and J. C. McWilliams, 1996: The general circulation responses of high resolution North Atlantic ocean models to synthetic scatterometer winds. *J. Phys. Oceanogr.*, **26**, (in press).
- Milliman, J. D., and J. P. M. Syvitski, 1992: Geomorphic/tectonic control of sediment discharge to the ocean: The importance of small mountainous rivers. *J. Geol.*, **100**, 525–544.
- MODIS, 1986: MODIS, Moderate-Resolution Imaging Spectroradiometer, Earth Observing System, IIB. *Instrument Panel Report*, National Aeronautics and Space Administration, Washington, D.C., 59 pp.
- Mopper, K., X. Zhou, R. J. Kieber, D. J. Kieber, R. J. Sikorski, and R. D. Jones, 1991: Photochemical degradation of dissolved organic carbon and its impact on the oceanic carbon cycle. *Nature*, **353**, 60–62.
- Murray, J. W., R. T. Barber, M. R. Roman, M. P. Bacon, and R. A. Feely, 1994: Physical and biological controls on carbon cycling in the equatorial Pacific. *Science*, **266**, 58–65.
- Mutlow, C. T., D. T. Llewellyn-Jones, A. M. Zavody, and I. J. Barton, 1994: Sea-surface temperature measurements by the Along-Track Scanning Radiometer (ATSR) on ESA's ERS-1 satellite: Early results. *J. Geophys. Res.*, **99**, 22, 575–22, 588.
- New, A. L., and R. Bleck, 1995: An isopycnic model study of the North-Atlantic. Interdecadal variability of the subtropical gyre. *J. Phys. Oceanogr.*, **25**, 2700–2714.
- Niiler, P. P., 1992: The ocean circulation. *Climate System Modeling*, Cambridge University Press, New York, 117–148.
- Oberhuber, J. M., 1988: The budgets of heat, buoyancy, and turbulent kinetic energy at the surface of the global ocean. Report No. 15, Max-Planck-Institute für Meteorologie, Hamburg.
- Ojima, D., 1992: *Modeling the Earth System: Papers Arising from the 1990 Oies Global Change Institute*. Snowmass, CO, 16–27 July 1990.
- Pauly, D., and V. Christensen, 1995: Primary production required to sustain global fisheries. *Nature*, **374**, 255–257.
- Peixoto, J. P., and A. H. Oort, 1992: Physics of Climate. *American Institute of Physics*, New York, 520 pp.
- Peixoto, J. P., and A. H. Oort, 1984: Physics of Climate. *Reviews of Modern Physics*, **56**, 365–429.
- Peltier, W., 1988: Global sea level and Earth rotation. *Science*, **240**, 895–901.
- Peng T. H., and T. Takahashi, 1993: Ocean uptake of carbon dioxide. Heat Transfer in Turbulent Flows, (R. S. Amano, R. H. Pletcher, S. A. Sherif, R. G. Watts, and A. N. Anand, Eds.), *HTD*, **246**, 117–134.
- Platt, T., and S. Sathyendranath, 1988: Oceanic primary production: Estimation by remote sensing at local and regional scales. *Science*, **241**, 1613–1620.
- Robertson, J. E., and A. J. Watson, 1992: Thermal skin effect of the surface ocean and its implications for CO₂ uptake. *Nature*, **358**, 738–740.
- Sarmiento, J. L., 1993: Ocean carbon cycle. *Chem. and Eng. News*, **71**, 30–43.
- Sarmiento, J. L., and J. R. Toggweiler, 1984: A new model for the role of the oceans in determining atmospheric pCO₂. *Nature*, **308**, 621–624.
- Sarmiento, J. L., and K. Bryan, 1982: An ocean transport model for the North Atlantic. *J. Geophys. Res.*, **87**, 394–408.
- Schlosser, P., G. Bonisch, M. Rhein, and R. Bayer, 1991: Reduction of deepwater formation in the Greenland Sea during the 1980's: Evidence from tracer data. *Science*, **251**, 1054–1056.
- Seager, R. M., B. Blumenthal, and Y. Kushnir, 1995: An advective mixed layer model for ocean modeling purposes: Global simulation of surface heat fluxes. *J. Climate*, **8**, 1951–1964.
- Sellers, W. D., 1965: Physical climatology. University of Chicago Press, Chicago, 272 pp.
- Semtner, A. J., Jr., and R. M. Chervin, 1992: Ocean general circulation from a global eddy-resolving model. *J. Geophys. Res.*, **97**, 5493–5550.
- Shum, C. K., P. L. Woodworth, O. B. Andersen, G. Egbert, O. Francis, C. King, S. Klosko, C. Le Provost, X. Li, J. Molines, M. Parke, R. Ray, M. Schlax, D. Stammer, C. Tierney, P. Vincent, and C. Wunsch, 1996: Accuracy assessment of recent ocean tide models. *J. Geophys. Res.*, submitted.
- Smith, R. L., 1992: Coastal upwelling in the modern ocean. *Upwelling Systems: Evolution Since the Early Miocene*, (Summerhayes, C. P., W. L. Prell, and K. C. Emeis, Eds.), Geological Society Special Publication No. 64, 9–28.
- Smith, W. O., Jr., and E. Sakshaug, 1990: Polar phytoplankton. *Polar Oceanography: Part B Chemistry, Biology, and Geology*, (W. O. Smith Jr., Ed.), Academic Press, Inc., San Diego, 477–525.
- Stommel, H., 1979: Oceanic warming of western Europe. *Proc. Nat. Acad. Sci.*, **76**, 2518–2521.
- Sui, C. H., K. M. Lau, A. K. Betts, 1991: An equilibrium model for the coupled ocean-atmosphere boundary layer in the tropics. *J. Geophys. Res.*, **96**, 3151–3163.
- Sundquist, E. T., 1985: Geological perspectives on carbon dioxide and the carbon cycle. *The Carbon Cycle and Atmospheric CO₂: Natural Variations Archean to Present*, Geophysical Monograph, **32**, American Geophysical Union, Washington, DC, 5–59.
- Sundquist, E. T., 1993: The global carbon dioxide budget. *Science*, **259**, 934–941.
- Takahashi, T., 1989: Could the oceans be the storehouse for the missing gas? *Oceanus*, **32**, 22–29.

- Taylor, K. C., G. W. Lamorey, G. A. Doyle, R. B. Alley, D. M. Grootes, P. A. Mayewski, J. W. C. White, and L. K. Barlow, 1993: The "flickering switch" of late Pleistocene climate change. *Nature*, **361**, 432–435.
- Thacker, W. C., and R. B. Long, 1988: Fitting dynamics to data. *J. Geophys. Res.*, **93**, 1227–1240.
- Thompson, L. G., E. Mosely-Thompson, M. E. Davis, J. F. Bolzani, J. Dai, T. Yao, N. Gunderstrup, X. Wu, L. Klein, and Z. Xie, 1989: Holocene-late Pleistocene climatic ice core records from Quinhai-Tibetan Plateau. *Science*, **246**, 474–477.
- Trenberth, K. E., Ed., 1992: *Climate System Modeling*. Cambridge Univ. Press, New York, 788 pp.
- Trenberth, K. E., and T. J. Hoar, 1996: The 1990-1995 El Niño-Southern Oscillation event: Longest on record. *Geophys. Res. Lett.*, **23**, 57–60.
- Trenberth, K. E., and A. Solomon, 1994: The global heat balance: Heat transports in the atmosphere and ocean. *Climate Dynamics*, **10**, 107–134.
- Trenberth, K. E., W. G. Large, and J. G. Olson, 1990: The mean annual cycle in global ocean wind stress. *J. Phys. Oceanogr.*, **20**, 1742–1760.
- Tziperman, E., L. Stone, M. A. Cane, and H. Jarosh, 1994: El Niño chaos: Overlapping of resonances between the seasonal cycle and the Pacific ocean-atmosphere oscillator. *Science*, **264**, 72–74.
- US GLOBEC, 1994: Eastern Boundary Current Program: A Science Plan for the California Current. US GLOBEC Report 11, 134 pp.
- US GLOBEC, 1995: Report on Climate Change and Carrying Capacity of the North Pacific Ecosystem. US GLOBEC Report 15, 95 pp.
- Upstill-Goddard, R. C., A. J. Watson, P. S. Liss, and M. I. Liddicoat, 1990: Gas transfer velocities in lakes measured with SF₆. *Tellus*, **42**, 364–377.
- Vodacek, A., F. E. Hoge, R. N. Swift, J. K. Yungel, E. T. Peltzer, and N. V. Blough, 1995: The use of in situ airborne fluorescence measurements to determine UV absorption coefficients and DOC concentrations in surface waters. *Limnol. Oceanogr.*, **40**, 411–415.
- Wanninkhof, R. H., and L. F. Bliven, 1991: Relationship between gas exchange, wind speed, and radar backscatter in a large wind wave tank. *J. Geophys. Res.*, **96**, 2785–2796.
- Wanninkhof, R., L. F. Bliven, and D. M. Glover, 1991: Gas transfer velocities and radar backscatter from the water surface. *Air-Water Mass Transfer*, Selected Papers from the Second International Symposium on Gas Transfer at Water Surfaces, (S. C. Wilhelms, and J. S. Gulliver, Eds.), Amer. Soc. Civil Engineers, New York, N. Y., 294–308.
- Warrick, R. A., and H. Oerlemans, 1990: Sea level rise. *Climate Change: The IPCC Scientific Assessment*, (J. T. Houghton, G. J. Jenkins, and J. J. Ephraums, Eds.), Cambridge Univ. Press, Cambridge, 261–281.
- Watson, A. J., R. C. Upstill-Goddard, and P. S. Liss, 1991: Air-sea gas exchange in rough and stormy seas by a dual-tracer technique. *Nature*, **349**, 145–147.
- Wentz, F. J., 1992: Measurement of oceanic wind vector using satellite microwave radiometers. *IEEE Trans. Geosc. Rem. Sens.*, **30**, 960–972.
- Wentz, F. J., 1994: Wind-vector satellite radiometer. *IEEE Geosci. & Remote Sensing Soc.*, **4**, 2405–2406.
- Wijffels, S. E., R. W. Schmitt, H. L. Bryden, and A. Stigebrandt, 1992: Transport of freshwater by the oceans. *J. Phys. Oceanogr.*, **22**, 155–162.
- Wollast, R., 1993: Interactions of C, N, P, and biogeochemical cycles and global change. *Proceedings of the NATO Advanced Research Workshop on Interactions of C, N, P, and S Biogeochemical Cycles*, Melreux, Belgium, 4–8 March 1991, Springer-Verlag, New York, 195–210.
- Wyrski, K., 1982: An estimate of equatorial upwelling in the Pacific. *J. Phys. Oceanogr.*, **11**, 1205–1214.
- Zebiak, S. A., and M. A. Cane, 1987: A model El Niño-Southern Oscillation. *Mon. Wea. Rev.*, **115**, 2262–2278.

Chapter 3 Index

- AABW 123
 ADEOS 139
 AESOPS 150
 AIRS/AMSU 140-141
 AMSR 139-141, 152
 AMSR-E 139, 151
 biodiversity 136
 biogeochemistry 136-138, 149, 156
 bio-optical measurements 145
 calibration 129, 151
 carbon cycle 117, 130, 132, 135, 150, 154, 156
 carbon dioxide (CO₂) 117, 130-136, 142-148, 153-156
 carbon monoxide (CO) 132, 154
 CLIVAR 149
 CO₂ fluxes 132, 143, 156
 COARE 140, 149
 coccolithophorid 145-146
 convection 121-123, 149, 151
 coral reefs 136, 148-149
 cyanobacteria 144-146
 CZCS 145-146, 154
 DFA 141, 143
 DIC 146
 DMS 145, 154
 DMSP 139
 DoD 139-140
 DOM 136, 143-146, 153
 DORIS 142
 ecosystem 128, 132-137, 144, 146, 154-155
 El Niño 119, 121, 124, 129
 ENSO 128, 132, 134, 136-137, 145, 148-150, 154-155
 ENVISAT 129, 139-140
 EOS PM 139
 ERS 120, 129, 131, 140
 ESA 139-140
 freshwater forcing 121-123
 GFO 129, 140
 GLI 148, 153
 GLOBEC 132, 135-136, 150, 155
 GNP 117
 GOALS 149
 GPS 142
 HNLC 134-135
 horizontal energy transport 123
 humidity 118, 121, 138, 140, 151
 hydrology 156
 ice sheets 128-129
 IGBP 136, 150
 interannual variability 119, 124, 149-150, 152
 IPCC 136
 Jason-1 129, 140, 142, 152
 JGOFS 132, 135, 137, 147-149, 150, 153
 LOICZ 132
 marine biosphere 130-138, 142-148
 MERIS 148, 153
 METOP 139
 MIMR 139-141
 modeling 121, 125-126, 129-130, 136, 149-50, 154-156
 MODIS 132-139, 141-148, 152-153
 momentum exchange 119-121
 NADW 123
 NASA 139-140
 NASDA 139-140
 NSCAT 120, 139, 152
 ocean-atmosphere surface coupling 118-123
 ocean circulation 118-119, 123-130, 134-140, 140-141, 147-156
 ocean color 131, 133, 143-148, 153-156
 ocean economics 117
 ocean food stocks 132
 ocean tides 128-130, 142, 154
 OCTS 153
 OSU 137
 PAR 142, 144
 phytoplankton 118, 132-137, 143-148, 153-155
 PNZ 137
 precipitation 138, 140-141, 151-155
 productivity 117-156
 QuikSCAT 139
 salinity 123, 125-126, 129, 138, 140, 143, 151-155
 satellite measurements 128, 137-140, 150
 sea level 117-156
 SeaWiFs 135, 145, 153
 SeaWinds 139, 141, 151-152
 SLR 142
 SOLAS 150
 SOLSTICE 144
 SPOT 148
 SSM/I 139-140
 SST measurements 121, 126, 132, 138-139
 surface flux 118, 125, 142, 151-153
 surface forcing 126, 129, 132, 142
 surface observations 149, 152
 T-S 125-126
 thermal fluxes 121
 thermohaline circulation 121-126
 TOGA 140, 149, 152
 TOPEX/Poseidon 129-131, 140, 142, 152
 topography 124, 129, 140-144, 149
 trace gases 156
 TRMM 140
 validation 146, 152, 155
 vertical circulation 135
 water-leaving radiance 144
 water transparency 147-148
 wind 117-156
 wind fields 121
 WOCE 131, 149, 152-153

CHAPTER 4

Atmospheric Chemistry and Greenhouse Gases

LEAD AUTHOR

D. Schimel

CONTRIBUTING AUTHORS

D. Glover

J. Melack

R. Beer

R. Myneni

Y. Kaufman, C. Justice,

and MODIS ATBD authors

J. Drummond

and MOPITT ATBD authors

CHAPTER 4 CONTENTS

4.1 Earth Observing System (EOS) program objectives	167
4.2 Introduction	168
4.2.1 Science questions	168
4.2.1.1 How does changing land/land use affect fluxes of greenhouse gases such as CO ₂ , methane, and nitrous oxide? How does it affect O ₃ precursors from soil (e.g., NO), plant (e.g., biogenic nonmethane hydrocarbons), emissions, and biomass-burning plumes?	168
4.2.1.2 How does interannual variability in climate affect interannual variability in biogeochemistry?	168
4.2.1.3 How will changing global hydrology and patterns of soil moisture affect fluxes of methane and CO ₂ in wetlands?	169
4.2.1.4 What is the spatial distribution of tropospheric O ₃ ? How do changing surface fluxes of precursor species affect the tropospheric O ₃ budget?	169
4.2.1.5 What is the vertical distribution of tropospheric O ₃ ? What controls this distribution, and how is it affected by stratosphere-troposphere exchange, the changing geography of surface sources of precursors, and by anthropogenic sources (aircraft) in the free troposphere?	169
4.2.1.6 How do physical, chemical, and biological processes interact to control ocean carbon uptake?	169
4.3 EOS data products and synthetic analyses	170
4.3.1 Introduction	170
4.3.2 The carbon cycle	170
4.3.2.1 Quantify land-cover change and convert to carbon changes	170
4.3.2.2 Monitor correlates of terrestrial CO ₂ exchange through photosynthesis and respiration; use models to quantify variability and trends in carbon storage	172
4.3.2.2.1 EOS LAI and FAPAR products	172
4.3.2.2.2 Interannual variations in atmospheric CO ₂	172
4.3.2.2.3 ENSO & NDVI	173
4.3.2.2.4 Interannual variations in Gross Primary Production (GPP)	173
4.3.2.3 Monitor correlates of oceanic CO ₂ change on short time scales (pCO ₂ proxy and wind stress)	173
4.3.2.4 Integrate the above into global synthetic analyses	174
4.3.3 Methane	174
4.3.3.1 Monitor land-use/land-cover correlates: wetland extent and hydrology, including natural wetlands, rice cultivation, and biomass burning	176
4.3.3.2 Delineation of wetland inundation and vegetative cover with microwave remote sensing	176
4.3.4 Nitrous and nitric oxide	177
4.3.4.1 Monitor terrestrial correlates processes that influence N ₂ O and NO emissions	177
4.3.4.2 Monitor soil moisture	178
4.3.4.3 Monitor tropospheric reactive nitrogen levels	178
4.3.5 Ozone: its precursors and fate	178
4.3.5.1 Monitor ozone precursors	178
4.3.5.2 Monitor ozone vertical distribution	179
4.3.5.3 Monitor terrestrial emissions of O ₃ precursors from soils, vegetation, and biomass burning	179

CHAPTER 4 CONTENTS (CONT.)

4.4 EOS algorithms, observations, and required additional data	181
4.4.1 The carbon cycle	181
4.4.1.1 Land measurements	181
4.4.1.1.1 Land cover and land-cover change	181
4.4.1.1.2 Correlates of plant growth: FAPAR, LAI	181
4.4.1.1.3 Biomass burning	181
4.4.1.2 Ocean measurements	181
4.4.1.2.1 Ocean color	181
4.4.1.2.2 Wind stress	181
4.4.2 Methane and nitrous/nitric oxide	181
4.4.2.1 Surface correlates	181
4.4.2.1.1 Land cover and land-cover change	181
4.4.2.1.2 Wetland productivity correlates: FPAR, LAI	181
4.4.2.2 Atmospheric retrieval of column methane	181
4.4.3 Atmospheric chemistry and greenhouse gases	181
4.4.3.1 Methane and CO from MOPITT	181
4.4.3.1.1 Instrument characteristics	182
4.4.3.2 Ozone and ozone precursors from TES	183
4.4.3.2.1 TES	183
4.4.3.2.2 The extraction of concentration profiles from infrared spectra	184
4.4.3.3 Biomass-burning sources of gases (including CO ₂)	184
4.5 Synthesis and integrative modeling: status and needs	185
4.5.1 Introduction	185
4.5.2 An EOS strategy for integrative models of biogeochemistry	185
4.5.2.1 The carbon cycle	185
4.5.2.2 Trace gases	187
References	191
Chapter 4 Index	194

4.1 Earth Observing System (EOS) program objectives

Any effort to study global change must include quantitative inventories of the forcing agents, specifically atmospheric burdens of greenhouse gases. In addition, the sources and sinks that lead to changing atmospheric concentrations must be known. For simple calculation of radiative forcing, the spatially-resolved concentrations of the relevant gases is sufficient, but neither scientific understanding nor policy is served by such limited data. Scientific understanding requires that the relationships between sources, sinks, and atmospheric concentrations be known in order to: 1) establish whether the causes of the atmospheric changes are explained by anthropogenic or natural causes; and 2) ensure that budgets balance in order to, for example, guarantee that no key processes are missing from our understanding and thus our computational models. Policy formulation further requires that sources and sinks be understood, because, in general, anthropogenic changes to greenhouse gases can only be modified by changing sources or sinks (sources such as fossil-fuel combustion, fertilizer use, sinks by manipulating forest growth, etc.). For the most part, the processes discussed in this chapter can be characterized as “biogeochemical” in that they involve the interaction of biological, geochemical, and photochemical processes.

The EOS program addresses a number of problems in this science area in which space-based measurements are required, or in which synergism between remote sensing and modeling is particularly necessary in order to achieve a global perspective. The EOS program contributes to the study of greenhouse gases and atmospheric chemistry, but is not a stand-alone activity. With our current state of knowledge there are many processes that must be measured in situ, including concentrations of a number of important greenhouse gases, biogeochemical processes in soils or the water column that cannot be remotely observed, and marine and terrestrial stocks of carbon.

Principal foci of the EOS program are using remote sensing to understand and quantify key processes in the global CO₂, CO, CH₄, N₂O, and O₃ budgets, and combining remote observations with theory, modeling, and in situ measurements to develop a tested predictive capability. The EOS program contributes in different ways to understanding the cycles of the different greenhouse gas species. For example, CO₂ and N₂O concentrations cannot be remotely observed in the troposphere with sufficient resolution or accuracy to determine rates of change or spatial distributions. However, many important correlates of CO₂ exchange may be sensed remotely; these include:

- Vegetation index-type measurements (see Chapter 5) that correlate with terrestrial photosynthesis;
- Measurements of terrestrial land cover and land-cover change (see Chapter 5); these influence emissions of many of the trace gases, both directly, as in deforestation and biomass burning, and indirectly. For example, many managed ecosystems have higher N₂O emissions than the corresponding forests;
- Frequency, intensity, and areal extent of biomass burning;
- Ocean-color measurements that relate to marine biological productivity (see Chapter 3);
- Ocean wind stress, which influences CO₂ exchange across the air-sea boundary; and
- Surface climate, which influences CO₂ and N₂O exchange by influencing rates of biological processes.

For the important greenhouse gases, methane and O₃, a different strategy may be employed. In addition to monitoring correlates of methane exchange (such as land cover, inundation, and surface climate), the spatial distribution of methane columns in the atmosphere can be determined by the Measurements of Pollution in the Troposphere (MOPITT) sensor with moderate resolution; methane’s oxidation product, CO, can be monitored very accurately (but has many sources in addition to methane related to industrial processes, automobiles, and biomass burning). O₃ is formed in the atmosphere through a complex of photochemical reactions, rather than being emitted from surface sources. Surface sources, biological and anthropogenic, do contribute to O₃ formation by influencing atmospheric NO_x and hydrocarbon concentrations, which form O₃ through a series of reactions. These surface fluxes can be monitored, as they are controlled by many of the same processes that control CO₂, N₂O, and SO₂ exchange. In addition, both O₃ and many of its chemical precursors can be measured in the troposphere directly by the Tropospheric Emission Spectrometer (TES). Key measurements for methane and O₃ include:

- land-cover type and change,
- inundation,
- surface climate,
- methane and CO distributions, and
- O₃ and precursor distributions.

Finally, it must be noted that many processes in the greenhouse gas cycles cannot be monitored directly or by proxy from space and must be quantified globally using models to synthesize multiple data types. Processes such as decomposition or nitrogen turnover that occur in soils and release CO₂, CH₄, and nitrogen trace gases to

the atmosphere must be modeled to obtain global estimates (in situ measurements are not feasible except at intensive research sites). The challenge for the EOS program is to incorporate as much global information into such models as possible in order to increase the accuracy of the results.

4.2 Introduction

The study of the cycles of the greenhouse gases includes a huge number of important scientific questions, which include some of the key science questions in the disparate fields of ecology, atmospheric chemistry, oceanography, and human dimensions studies, and are linked to some of the most important environmental management issues of the day. These include not only global climate change, but also acid precipitation (linked to atmospheric NO_x budgets), oxidant damage (largely tropospheric O₃), and habitat destruction (as land-cover change affects the carbon and trace gas cycles and biological diversity [Skole and Tucker 1993]). Key questions addressed by the EOS program are listed below.

4.2.1 Science questions

4.2.1.1 How does changing land cover/land use affect fluxes of greenhouse gases such as CO₂, methane, and nitrous oxide? How does it affect O₃ precursors from soil (e.g., NO), plant (e.g., biogenic nonmethane hydrocarbons) emissions, and biomass-burning plumes?

Land-cover change is one of the most potent forces affecting global greenhouse gas changes. In the current carbon budget, fossil-fuel burning and cement production add 5.5 Gt C/yr to the atmosphere (1980s average; Schimel et al. 1995). Land-cover change adds another (although highly uncertain) 1-2 Gt C/yr (Houghton 1995; Table 1 in Schimel et al. 1995). Because land-cover change can in principle be detected using Moderate-Resolution Imaging Spectroradiometer (MODIS) data (Townshend personal communication) and quantified using Landsat or Advanced Spaceborne Thermal Emission and Reflection Radiometer (ASTER) time series (Skole and Tucker 1993), EOS can contribute directly to the estimate of areal changes in land cover. Changes in the carbon content of pre-disturbance and modified landscapes currently must

be estimated from in situ data, although radar is a promising alternative for forests.

In addition to influencing CO₂, land-cover changes affect N₂O and NO emissions. In general, forests and undisturbed grasslands have lower rates of nitrogen trace-gas emissions than pastures or croplands (Luizão et al. 1989; Mosier et al. 1991) so land conversion may increase the emissions of these gases. However, emissions decrease with time after conversion (Keller et al. 1993), and so time series of land-cover change are essential to determine time since conversion.

A critical process related to land use is biomass burning. Biomass burning adds CO₂ to the atmosphere as well as a suite of other trace gases. Space-based observations of the extent, frequency, and timing of biomass burning have already proven their value in studies of ecosystem-atmosphere interactions. EOS measurements of biomass burning from MODIS will be a critical feature of future studies of the biogeochemical role of biomass burning.

4.2.1.2 How does interannual variability in climate affect interannual variability in biogeochemistry?

Recently, evidence from global observations of CO₂ and O₂ (Ciais et al. 1995; Keeling et al. 1995), CO, CH₄, and N₂O (Dlugokencky et al. 1994), and satellite data (Braswell 1996; Myneni et al. 1996) have indicated that substantial interannual variability in terrestrial ecology and atmospheric chemistry may result from interannual variability in climate, modulated by the internal dynamics and lags resulting from terrestrial ecosystem and oceanic processes (Schimel et al. 1996). Understanding the origins of interannual variability in sources and sinks of CO₂ is important for us to verify our basic understanding of the carbon cycle, and to probe the processes whereby ecosystems and the oceans respond to climate, the latter being crucial for gaining confidence in predic-

tive models. Whereas global observations of CO₂, its isotopes, and O₂ (from global, ground-based observation networks) are the basic tools for observing interannual variability in the carbon budget, remote sensing is the best available method for understanding the geographic distribution of climate anomalies (which, although they may affect the global mean, are not usually distributed homogeneously over the globe) and the spatial response of the oceans and land ecosystems.

4.2.1.3 *How will changing global hydrology and patterns of soil moisture affect fluxes of methane and CO₂ in wetlands?*

Wetlands are a particularly productive environment, yet the processes and fluxes of trace-gas exchange with the atmosphere are inadequately understood and are only beginning to be measured on a global scale. For example, the methane budget is strongly affected by wetland sources, both natural and anthropogenic (Aselmann and Crutzen 1989; Bartlett and Harriss 1993). Consequently, in order to correctly account for methane terms in global biogeochemical models, it is essential to understand the role of wetlands in methane production as well as the effect of changing wetland distribution.

The extent of wetlands is uncertain because there is no clear basis for identification and classification of wetlands on a global scale. In addition, the areal extent of wetlands is being modified as a result of land-use changes, so that once a globally-consistent classification scheme is established, the areal distribution must be monitored and recompiled. New data are becoming available from remote sensing that provide a global perspective on wetland distribution and classification, but these are not yet reconciled with ground-based ecological and hydrological data.

There have been several remote-sensing studies on characterizing various types of wetlands at differing scales using airborne and spaceborne systems (Hess et al. 1990, 1995; Pope et al. 1992, 1994; Morrissey et al. 1994). Most of these studies have been at a local scale using airborne systems. Current optical and microwave algorithms need to be evaluated and implemented for generating new, improved regional and global data sets on wetland extent and seasonality.

4.2.1.4 *What is the spatial distribution of tropospheric O₃? How do changing surface fluxes of precursor species affect the tropospheric O₃ budget?*

Tropospheric ozone is a key species in atmospheric chemistry and a critical link between atmospheric chemistry and the Earth system. Ozone is produced in the atmo-

sphere by photochemical processes and is derived from precursor gases that have their origin in stratospheric chemistry, the biosphere, oceans, and industrial processes. Changes to the tropospheric ozone budget result from changing sources of precursors arising from fossil-fuel burning, biomass burning, and, possibly, changing biogenic sources in soils and vegetation. Ozone is a key species in the troposphere because it is a potent greenhouse gas in the mid and upper troposphere, and damaging to vegetation and human health at high concentrations near the Earth's surface. Because its distributions in space and time are very heterogeneous, reflecting its short lifetime, global spatial data on its distribution are key to understanding both how global tropospheric chemistry is changing, and how those changes may affect climate and the biosphere. The effects of ozone on UV radiation are also very important and are dealt with elsewhere (see Chapter 7).

4.2.1.5 *What is the vertical distribution of tropospheric O₃? What controls this distribution and how is it affected by stratosphere-troposphere exchange, the changing geography of surface sources of precursors, and by anthropogenic sources (aircraft) in the free troposphere?*

Knowledge of the vertical distribution of ozone is critical. The vertical profile of ozone from the mid-stratosphere to the surface influences the integrated radiative effect of ozone, and, hence, its effects on climate. Since large increases in surface concentrations can occur in areas polluted by automobiles, industry, and biomass burning, information on high surface levels is likewise critical. Understanding how the vertical profile of ozone may change in the future requires knowledge of how the vertical profile could change as the geography of sources changes, if atmospheric convection and mixing change (affecting the rate in which ozone and its precursors are mixed through the troposphere), and with the introduction of anthropogenic sources (e.g., subsonic aircraft). Because understanding the vertical distribution of ozone requires understanding of sources, subsequent chemistry, transport, stratosphere-troposphere exchange, and sinks, accurate predictive models will be extremely difficult to develop and evaluate without strong constraints from global observations.

4.2.1.6 *How do physical, chemical, and biological processes interact to control ocean carbon uptake?*

By continually exchanging heat and greenhouse gases with the atmosphere, the global ocean plays an important role in the regulation of the Earth's climate. The ocean alone

contains about 50 times more carbon than the atmosphere and, paradoxically, because of its large buffering capacity, the ocean has the potential (if instantaneously ventilated to the atmosphere) to absorb approximately 6000 Gt of additional CO₂. This very large number is misleading, however, as it assumes all of the ocean can be brought into contact with the atmosphere at once. In reality, only the surface waters of the ocean are ventilated with the atmosphere, and, because this is a reversible chemical reaction, only a small fraction of this CO₂ would be neutralized by the time a new equilibrium is reached. Much later, on the order of thousands of years, this added CO₂ will react with the CaCO₃ in the ocean, in effect recharging the surface water's neutralizing capacity. In the end, it's not the distribution of CO₂ in the ocean but rather the distribution of the ocean's alkalinity that drives this absorption.

The kinetics of CO₂ gas transfer across the ocean-atmosphere interface is slow, on the order of a year. This

rate is slower than processes such as the biological uptake of carbon that significantly affects seasonal partial pressure of CO₂ (pCO₂) in surface seawater over time scales of days to months. Consequently, the process of CO₂ gas exchange between the ocean and atmosphere is controlled by the complex interactions of biological activities throughout the water column, the chemical buffering capacity of the ocean for CO₂, and ocean circulation dynamics (see Sections 4.1.1.3, 4.2.4.2, 4.2.4.3, and 4.2.4.5). The relative importance of these processes varies both temporally and spatially. New data from atmospheric ¹³CO₂ and O₂ measurements provide a new, globally-integrated view of these processes, but little insight into how and where the processes are occurring. Atmospheric data suggest that only approximately 55% of the anthropogenic CO₂ gas injected into the atmosphere remains there. The remaining and rather variable 45% is taken up by both the ocean and the terrestrial biosphere. What controls this partitioning and its changes in time?

4.3 EOS data products and synthetic analyses

4.3.1 Introduction

This section addresses the specific scientific activities, data products, and algorithms currently in progress within the EOS program. This discussion will describe the specific "deliverables" as we now envision them. The deliverables are grouped under the subheadings: Carbon Cycle, Methane, Nitrous Oxide, and Atmospheric Chemistry and Ozone, but in fact there is considerable synergism between the measurements and models for the different trace gases. In Section 4.4, the space-based observations and algorithms that support these scientific deliverables are described in more detail.

4.3.2 The carbon cycle

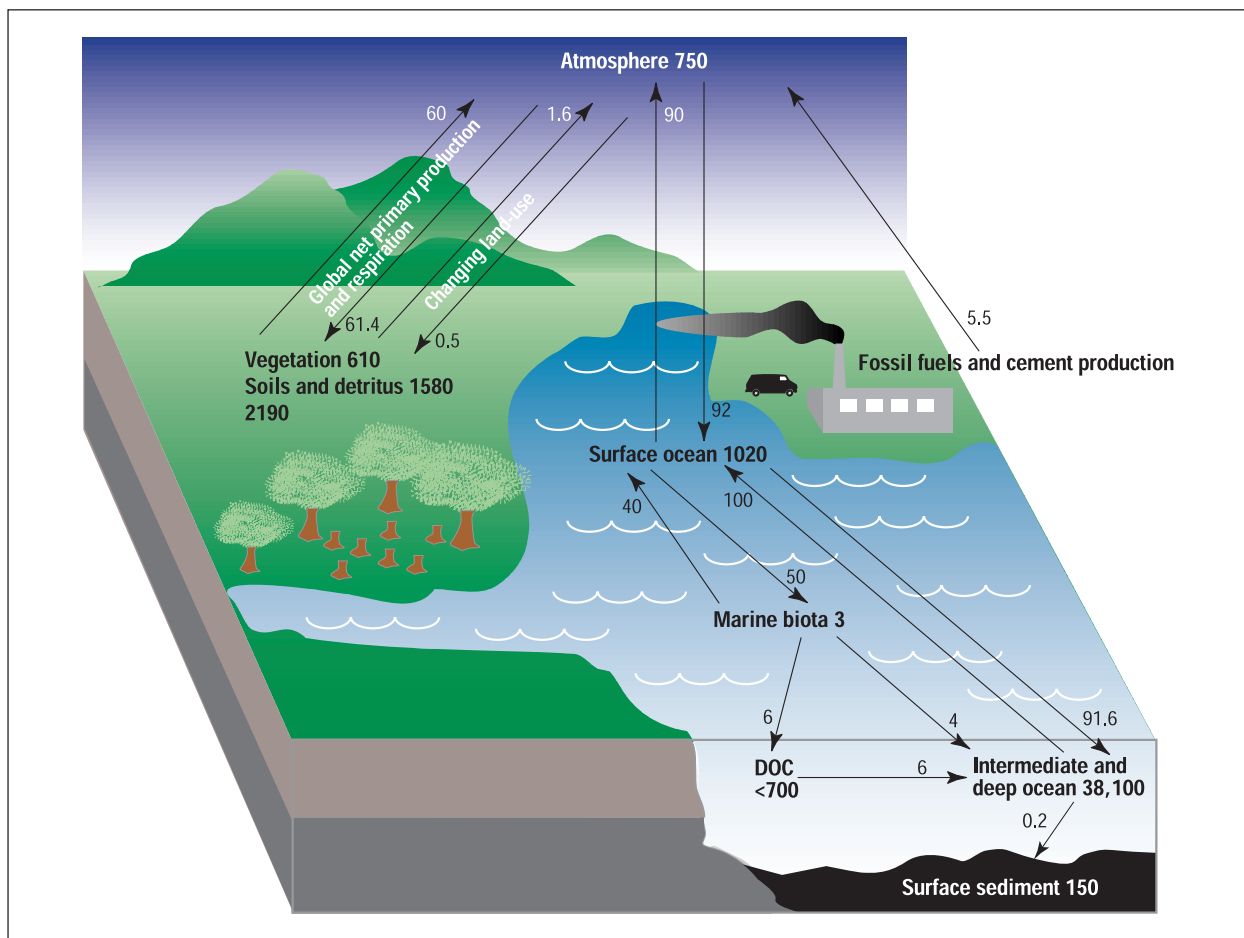
The major fluxes of the carbon cycle on interannual-to-centennial time scales are illustrated in Figure 4.1. This figure does not show some of the millennial-to-longer processes such as calcite dissolution, carbonate mineral formation, and other rock-cycle processes. The processes include background fluxes, characteristic of the undisturbed biosphere, such as the nearly balanced air-sea and terrestrial primary production-respiration exchanges of ~90 and ~60 Gt C/yr, respectively. The figure also illustrates so-called perturbation fluxes that result directly or indirectly from anthropogenic activity. These include fos-

sil fuel plus cement production, fluxes from land-use change, and the imbalances in air-sea exchange (~2 Gt C/yr) and in net primary production (NPP)-respiration exchange (~1.4 Gt C/yr). Components of the EOS program address measurement of both the perturbation fluxes (which are the terms usually referred to as "the global carbon budget") and the magnitude or at least the variability in some of the background fluxes.

4.3.2.1 Quantify land-cover change and convert to carbon changes

Land-cover change is one of the fundamental factors perturbing the global carbon cycle. In the most recent Intergovernmental Panel on Climate Change (IPCC) assessment, conversion of forests to managed systems (pastures and cropland) in the tropics was estimated to release 1.6 (±1) Gt C/yr to the atmosphere. Conversely, the regrowth of midlatitude forests harvested a half-century to a century ago may be absorbing 0.5-1.0 Gt C/yr. (The values given are average rates for the 1980s.) Satellite and other evidence suggests that land conversion may be quite variable from one year to the next. Current efforts in the EOS project and within the Earth Science Enterprise (ESE) (carried out by IDS and Pathfinder teams) are using Landsat, Systeme pour l'Observation de

FIGURE 4.1



The global carbon cycle, showing the reservoirs (in Gt C) and fluxes (Gt C/yr) relevant to the anthropogenic perturbation as annual averages over the period 1980-1989 (Siegenthaler and Sarmiento 1993; Potter et al. 1993; Eswaran et al. 1993). The component cycles are simplified and subject to considerable uncertainty. In addition, this figure presents average values. The riverine flux, particularly the anthropogenic portion, is currently very poorly quantified and so is not shown. Evidence is accumulating that many of the key fluxes can fluctuate significantly from year to year (terrestrial sinks and sources: INPE 1992; Ciais et al. 1995; export from the marine biota: Wong et al. 1993). In contrast to the static view conveyed by figures such as this one, the carbon system is clearly dynamic and coupled to the climate system on seasonal, interannual, and decadal time scales (Schimel and Sulzman 1995).

la Terre (SPOT), Japanese Earth Remote-sensing Satellite (JERS)-OPS, and European Remote-Sensing Satellite (ERS-1) data to quantify rates of land-cover change in selected case-study regions. (The Brazilian Amazon, Thailand, Cambodia, Laos, Vietnam, several West African regions, and Costa Rica are currently under study by a range of investigators.) In addition to identifying primary land conversion, successful efforts are underway to estimate regrowth in secondary forest, a key factor in carbon balances. Future EOS efforts will take advantage of the ASTER, Landsat, and international sensors to continue to build an increasingly global database of high-resolution analyses of land-cover change. These high-resolution

data are also being used to calibrate and validate retrievals of land cover and land-cover change using lower-resolution sensors (such as AVHRR), an effort that will continue with MODIS.

Additionally, MODIS will provide estimates of the timing, frequency, and extent of biomass burning. These retrievals utilize a special MODIS channel, with the appropriate dynamic range not to saturate over biomass-burning sources (<http://eospsp.gsfc.nasa.gov/atbd/modis/atbdmod15.html>). This retrieval, coupled with in situ estimates of biomass density and emission factors (CO₂ released/unit biomass consumed) allows spatially-resolved estimates of the contribution of biomass burning

to atmospheric CO₂. Similar algorithms are used for other trace gases.

4.3.2.2 *Monitor correlates of terrestrial CO₂ exchange through photosynthesis and respiration; use models to quantify variability and trends in carbon storage*

4.3.2.2.1 EOS LAI and FAPAR products

The importance of vegetation in studies of global climate and biogeochemical cycles is now well recognized (Sellers and Schimel 1993). This is especially the case with respect to carbon, as the exchange of carbon between plants and the ambient air involves vast quantities of gaseous carbon dioxide, an important greenhouse gas. In order to estimate carbon fixation by terrestrial vegetation and to prescribe the land surface accurately in global climate models, variables descriptive of surface assimilation area, radiation absorption, plant physiology, and climatology are required. The consensus is that such multi-temporal global data sets can be regularly obtained only from remote sensing. Therefore, several of the instruments scheduled for EOS have land-surface-parameter estimation as major deliverables (Asrar and Greenstone 1995).

Two key variables required in primary production and global climate studies are leaf-area index (LAI) and fraction of photosynthetically-active radiation (0.4 - 0.7 μm) absorbed by the vegetation (FAPAR) (Sellers et al. 1986; Ruimy et al. 1994). Leaf-area index is generally defined as one-sided green-leaf area per unit ground area in broadleaf canopies, and variously (projected or total) in needle canopies. Unlike LAI, FAPAR exhibits diurnal variation. Its use in models with time steps longer than a day requires appropriate time resolution. It has a spatial resolution of 1.1 km. There are two algorithms to derive LAI and FAPAR. The first is a Normalized Difference Vegetation Index (NDVI)-based approach, supported by substantial theoretical and empirical evidence. The second algorithm to derive accurate estimates of LAI and FAPAR is a look-up-table-based approach that is capable of exploiting the spectral nature of MODIS measurements and the angular nature of Multi-Angle Image Scanning Radiometer (MISR) measurements. A comprehensive three-dimensional radiative transfer model for vegetated surfaces is utilized by both algorithms to connect remote observations to surface variables of interest in a manner that is consistent with the spatial scale of the observations. The algorithms require a land-cover classification that is compatible with the radiative-transfer model used in their derivation. Global land covers can be classified into six biome types depending on the canopy structure:

grasslands/cereal crops, shrublands, broadleaf crops, savannas, broadleaf forests, and needleleaf forests. Further details on theoretical aspects, implementation, and accuracy can be found in Myneni et al. (1996).

4.3.2.2.2 Interannual variations in atmospheric CO₂

A measurable link between atmospheric CO₂ drawdown by vegetation and NDVI dynamics was demonstrated by Tucker et al. (1986). Interannual variations in observed atmospheric CO₂ and inferred biospheric carbon exchange since 1980 were discussed recently by Keeling et al. (1995). The biosphere was found to be a source of carbon during the warm events and a sink during cold events. The atmospheric CO₂ anomaly, with respect to a 20-year baseline period (1959-1979), increased from 1980 to late 1988 and has decreased. The global NDVI anomaly, which is indicative of photosynthetic carbon fixation by plants, was mostly negative during the period of increasing atmospheric CO₂ anomaly, and, starting from late 1988 it was positive until mid-1991, when the eruption of Mount Pinatubo corrupted the satellite data (private communication from R. B. Myneni 1996).

While the 1980s experienced well-defined sea-surface temperature (SST) oscillation events both in the equatorial Pacific (Woodruff et al. 1993) and tropical Atlantic (Philander 1986), the situation during the 1990-1995 time period was different. There were three weak warmings in the equatorial Pacific beginning from early 1991 onwards. The strong co-variation between biospheric carbon exchange and NINO3 index observed in the 1980s appears weakened from early 1991 onwards. The decrease in atmospheric CO₂ anomaly from the time of the Mount Pinatubo eruption in mid 1991 until late 1993 was uncharacteristically sharp (Keeling et al. 1995). Although air temperatures decreased following the Mount Pinatubo eruption, the global anomaly is still high, about 0.3°C (Jones et al. 1994), and 1995 was the warmest year so far (Anonymous 1996).

In a recent study, Keeling et al. (1996) reported that the amplitude of the seasonal CO₂ cycle in the Northern Hemisphere increased on an average by about 30% since the early 1960s, thus indicating increased Northern Hemisphere biospheric activity. Moreover, the midpoint in atmospheric CO₂ drawdown between spring and summer was found to be advanced by about 7 days, which they interpret as an indication of a longer growing season. This important result has lately been confirmed from analysis of satellite-derived NDVI data (private communication from R. B. Myneni 1996). Thus, both the radiometric data and the atmospheric CO₂ record seem to indicate that the global carbon cycle has responded to

interannual fluctuations in temperature, which may be small at the global scale but potentially significant at the regional scale.

4.3.2.2.3 ENSO & NDVI

SST in the tropical Pacific is coupled with atmospheric phenomena such as pressure fields, wind fields, large-scale convection of moist air from the ocean to the atmosphere, oceanic and continental rainfall, and other atmospheric processes (Philander 1990). Large-scale SST variations on the order of 2-3°C in the tropical Pacific Ocean are reported to have dramatically perturbed global precipitation and temperature patterns through displacement of major rain-producing convergence zones in the tropics and atmospheric circulation changes, causing torrential rains in some areas and severe droughts in others, with associated crop failures, forest fires, mud slides, floods, and other natural disasters (Glantz et al. 1991).

Several workers have compared surface precipitation records with El Niño Southern Oscillation (ENSO)-cycle SST anomalies, identifying areas where precipitation anomalies were correlated with tropical Pacific SST anomalies (McBride and Nicholls 1983; Ropelewski and Halpert 1987, 1989). Point rainfall frequently does not adequately represent areal rainfall, especially in semi-arid tropical regions where rainfall is often erratically distributed. Thus, accurate estimates of the geographical extent of SST-linked precipitation anomalies have been hampered in many areas. Satellite-derived NDVI data, which several studies have shown to be highly correlated with arid and semi-arid rainfall (Tucker et al. 1991), have been used to correlate tropical Pacific SST anomalies from the NINO3 region (5° S to 5° N latitude and 90° W to 150° W longitude) in order to delineate anomalous rainfall areas through direct measurement of vegetation amount and condition in a spatially-continuous manner for arid and semi-arid areas.

The 1980s experienced well-defined alternating ENSO warm and cold events (Philander 1990). It was found that large areas (between 0.5 and 1.5 million km²) in semi-arid regions experienced rainfall anomalies that were directly correlated to SST anomalies in the equatorial Pacific. Although the warm events of the ENSO cycle were associated with decreased rainfall and the cold events with increased rainfall, this pattern was not always consistent, at least during the 1982-1990 time period. For instance, southeastern South America encompassing regions in southern Brazil, northern Argentina, Paraguay, and Uruguay experienced a strong drought during the 1988-89 cold event of the ENSO cycle (Myneni et al. 1996). This analysis confirmed the disruptive effects of

large-scale SST anomalies on regional-scale precipitation patterns and, therefore, vegetation in arid and semi-arid regions of Africa, Australia, and South America for the time period of 1982-1990.

4.3.2.2.4 Interannual variations in Gross Primary Production (GPP)

GPP denotes the amount of carbon photosynthesized by plants. Some of this carbon is respired, while the rest is invested in plant growth. Seasonal and interannual variations in GPP of terrestrial vegetation are therefore of considerable interest. Monthly GPP estimated from monthly mean global green-leaf area and photosynthetically-active radiation derived from observations made from several geostationary and polar orbiting satellites for the years 1982 through 1990 were recently investigated by Myneni et al. (1995).

Interannual variations in GPP, of the order of 1.6 Pg C, were reported by Myneni et al. (1995). Interestingly, this is in good agreement with results on the interannual variability of atmospheric CO₂ increase (Conway et al. 1994). The largest year-to-year changes in atmospheric CO₂ increase, of the order 2-3 Pg C, occurred during the 1982-1983 and 1986-1987 El Niño/Southern Oscillation events. Similar large year-to-year changes in GPP were also observed (4.3 and 2.3 Pg C, respectively). In fact, the evolution of monthly GPP anomalies was reported to be similar to the atmospheric CO₂ growth rate during 1982-1990. That is, periods of increasing atmospheric CO₂ were coincident with periods of higher-than-average biospheric GPP and vice versa. This was observed both globally and for the 30°-90° N latitudinal band, but not for other latitudes 0-30° N, 0-30° S, and 30°-90° S. If NPP is assumed to be a constant fraction of GPP, then heterotrophic respiration and biospheric NPP must respond similarly but disproportionately to climate in order to match the observed atmospheric CO₂ growth rate (disregarding small variations in net oceanic exchange). This inability of heterotrophic respiration to balance biospheric NPP could be the likely mechanism by which the so-called missing carbon (Tans et al. 1990) is being sequestered into soils, ultimately, via biospheric net fixation. This needs to be confirmed, although some evidence of carbon sequestration in tropical soils has recently been reported (Fisher et al. 1994).

4.3.2.3 Monitor correlates of oceanic CO₂ change on short time scales (*pCO₂* proxy and wind stress)

The atmospheric signal of CO₂ change should now be large in the ocean, hypothesized to correspond to approximately 45 μmol/kg total inorganic carbon in the modern

surface ocean. However, traditional direct oceanic observations are incomplete and cannot unambiguously confirm this hypothesis. The seasonal range in $p\text{CO}_2$ due to biological activity alone can be as large as 200 μatm (corresponding to approximately half the anthropogenic signal). Other confounding changes to the CO_2 concentration of the upper ocean, such as thermal effects, help mask the other half of this signal. We will need answers to pressing global-change problems before this portion of the carbon cycle can be sorted out through more-traditional means.

Thus, continuous, near-synoptic measurements of CO_2 -influencing processes can be a boon to the Earth system science of the global carbon budget. EOS data will help identify, on a global scale, areas of high biological activity (via ocean-color data, see Section 4.3.2.5) and of intense mixing and ocean-atmosphere CO_2 flux due to wind stress (via altimetry and scatterometry, see Sections 4.3.1.1, 4.3.2.3, and 4.3.4.6). Data assimilation of altimetry will improve models of ocean circulation, especially those of the upper ocean where ocean-atmosphere interactions take place (see Section 4.3.1.2). By combining our current knowledge (largely physical) with our EOS-enhanced knowledge (largely biological) we will be able to monitor the behavior of CO_2 in the surface waters of the ocean well enough to separate natural from anthropogenic signals (see relevant sections in Chapter 2).

4.3.2.4 *Integrate the above into global synthetic analyses*

Understanding the global carbon cycle requires the integration of terrestrial, aquatic, and marine exchanges to produce a global budget. It also requires information on the anthropogenic fluxes of CO_2 from fossil-fuel combustion and cement manufacture (data available through the Carbon Dioxide Information and Analysis Center [CDIAC] and the Socioeconomic Data and Applications Center [SEDAC]). Within the EOS program, efforts are being made to develop and intercompare models of the component systems (ocean models and terrestrial biogeochemical models) and to integrate them via atmospheric transport models. Several groups within EOS and in collaboration with EOS have developed and applied models of the carbon cycle. These models have been used in specific case-study modes for intercomparison and validation (Figure 4.2; VEMAP members 1995; Schimel et al. 1996), and in inverse calculations, where the best fit between atmospheric observations and modeled spatial distributions of fluxes is sought using mathematical techniques (Figure 4.3; Ciais et al. 1995; Denning et al. 1995). As more information becomes available, both from atmospheric observations and from space, these integrated

inverse and forward models will become a more-important part of the EOS program.

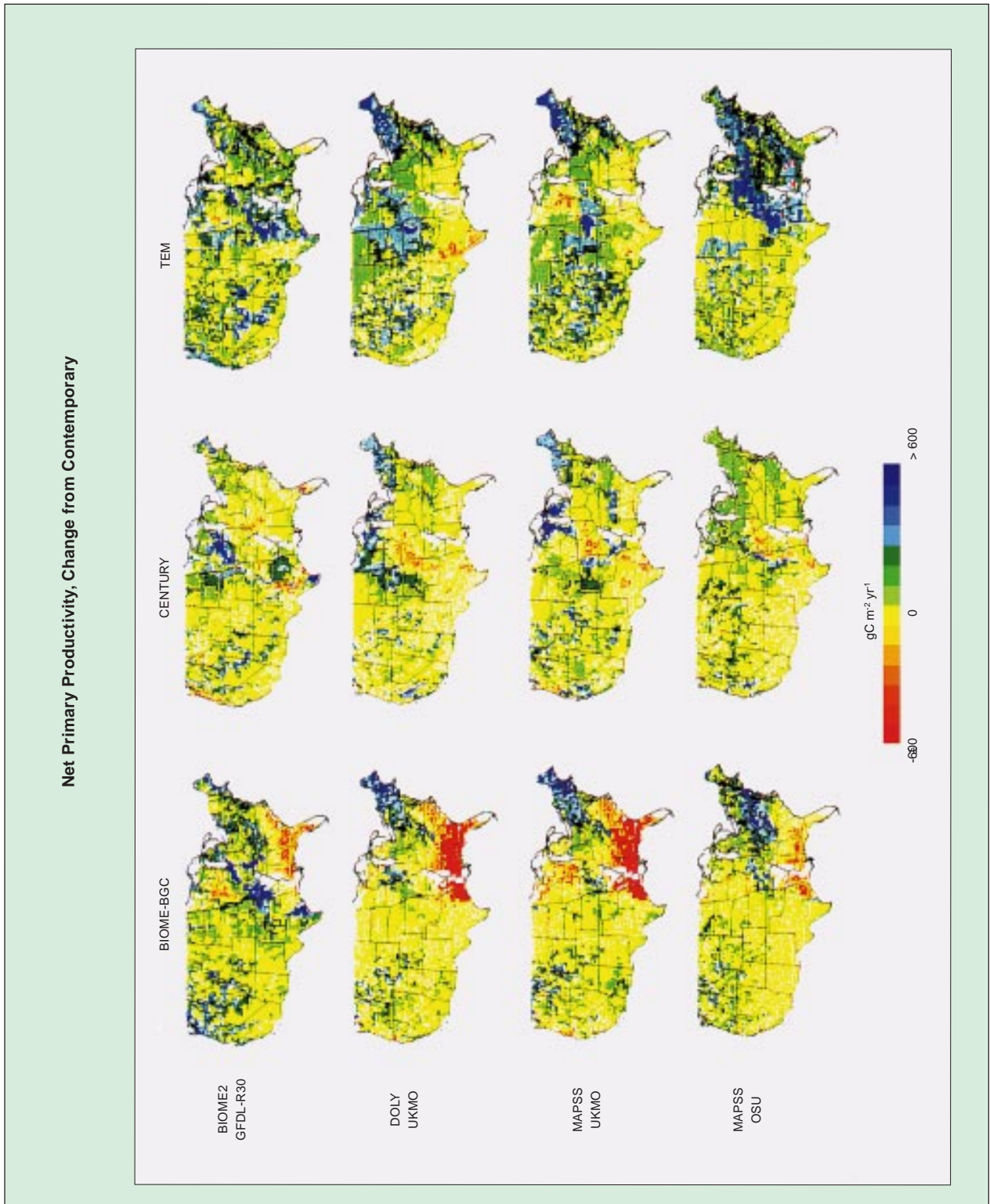
4.3.3 *Methane*

After CO_2 , changing methane is the second largest perturbation of the radiative forcing of the atmosphere (see Chapter 8 for a discussion of the countervailing effects of sulfur gases). Methane is produced via a number of pathways, mostly involving biological processes in reducing (low oxygen) environments. Methane is produced when heterotrophic bacteria have insufficient O_2 to use as electron acceptors in metabolism, and insufficient SO_4 to use sulfur compounds to fuel energy metabolism. Key methanogenic environments include natural wetlands, paddy rice cultivation, the rumens (stomachs) of cattle and other ruminant wild and domestic animals, and landfills. At a process level, methane production in wetlands and rice-growing regions is reasonably well-understood. In these systems, methane production occurs largely during seasons of inundation, where soils are sufficiently flooded that oxygen, which diffuses slowly in water, becomes limiting to microbial metabolism (Paul and Clark 1989). Methane is produced predominantly from recently produced carbon, and so methane production increases, in general, as primary productivity increases (Dacey and Klug 1979; Valentine et al. 1994). Large methane fluxes occur in regions of high primary productivity and prolonged inundation. Thus, intensively managed rice fields may have extremely high rates of methanogenesis, as may some natural wetlands. It is important to note that in our present state of knowledge, the methane budget is not balanced: known sources do not equal known sinks, although the difference is within the uncertainty of the estimates (Prather et al. 1995). This is of concern as it adds uncertainty to estimates of methane's lifetime and leaves open the possibility of an important but unknown process. Thus, spatial analyses of methane dynamics remain of considerable importance.

Also of importance is the fact that methane is oxidized to CO_2 in aerobic soils, although the dominant sink for methane is photochemical oxidation in the atmosphere. In aerobic soils, where oxygen is plentiful, methane oxidation typically occurs at intermediate soil-moisture levels (Mosier et al. 1991). Rates of methane oxidation are typically reduced in derived (pastures and cropland) as compared to native ecosystems (Mosier et al. 1991; Keller et al. 1993). Furthermore, the use of nitrogen fertilizer seems to inhibit methane oxidation (Mosier et al. 1991).

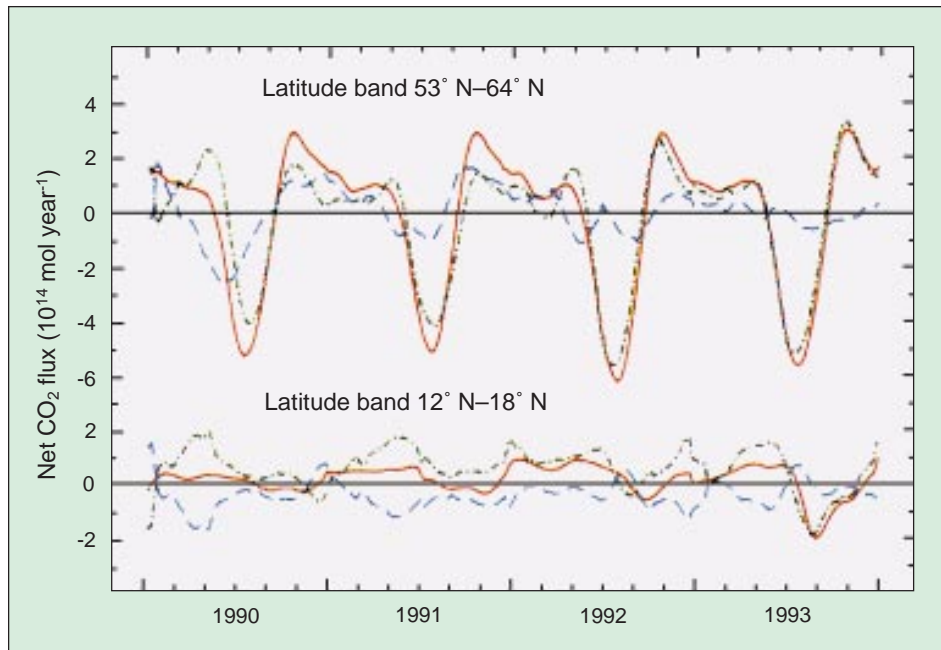
Key EOS products include wetland hydrology (extent and duration of inundation) and land cover and productivity in methanogenic regions and in areas of methane oxidation (using satellite data and models: see

FIGURE 4.2



Comparison of changes in annual net primary productivity (NPP) estimates when biogeochemistry models (BIOME-BGC, CENTURY, TEM) are run with the vegetation distributions of the biogeography models (BIOME2, DOLY, MAPSS) for particular climate scenarios (GFDL-R30, UKMO, OSU) (VEMAP 1995)

FIGURE 4.3



Ocean and land partitioning of CO_2 fluxes as a function of time. Latitude bands in the tropics and at northern midlatitudes are shown as examples. At northern midlatitudes, the lower values for net uptake during 1990 and 1991 are artifacts of the sparser isotopic measurements in those years. When constrained with sufficient data, the seasonality of carbon uptake in the tropics is clearly terrestrial. We note that the mirroring effect of the terrestrial biospheric and oceanic fluxes for the tropical zone may be indicative of a problem with the isotopic data. The solid line shows the annual mean net flux of CO_2 without the contribution of fossil-fuel emissions. The dashed line is the net exchange of CO_2 with the oceans. The dash-dot line is the net exchange on land (Ciais et al. 1995).

MODIS ATBD 17; <http://eosps.gsf.nasa.gov/atbd/modis/atbdmod17new.html>), biomass burning, and direct retrievals of methane. These products can be used in models of atmospheric chemistry to constrain estimates of surface emissions based on atmospheric methane budgets.

4.3.3.1 Monitor land-use/land-cover correlates: wetland extent and hydrology, including natural wetlands, rice cultivation, and biomass burning

4.3.3.2 Delineation of wetland inundation and vegetative cover with microwave remote sensing

Characterization of the areal and temporal extent of wetlands would greatly extend our understanding of trace-gas exchange from these ecosystems and of their significance to global processes. The availability of Synthetic Aperture Radar (SAR) data from airborne and satellite platforms has provided a unique opportunity to study dynamic wetland processes related to biogenic trace-gas exchange by providing information on the type and distribution of wetlands and temporal distribution of inundation. During the past five years a number of ad-

vanced airborne SAR systems have been developed, and five spaceborne SAR systems—ERS-1 and 2, JERS-1, Radarsat, and Shuttle Imaging Radar-C (SIR-C)/X-SAR—have been deployed. Additional spaceborne SARs are likely to be launched throughout the remainder of this decade and into the next.

For most scientific questions involving wetlands, it is necessary to distinguish not only flooded vs. non-flooded areas, but herbaceous vs. woody vegetation. Delineation of both flooding status and vegetation, with accuracies greater than 90% for all categories, has been demonstrated using multi-frequency, polarimetric SAR data sets for wetlands in the southeastern United States (Jet Propulsion Laboratory

Airborne Synthetic Aperture Radar [JPLAIRSAR]) and the central Amazon (SIR-C) (Melack et al. 1994; Hess et al. 1995). Based on these studies, which included extensive field verification, and on modeling studies (Wang et al. 1995), the following generalizations can be made:

- 1) While C-band is adequate for distinguishing flooding in marshes, it can reliably detect forest inundation only where stem densities are low. L-band is required for flood detection in most floodplain forests.
- 2) Horizontal, horizontal polarization (HH) is the best polarization for flood detection in both forests and marshes.
- 3) Two wavelengths are required to reliably separate woody from herbaceous vegetation. The greater the contrast in wavelengths, the better the separation: C and L provide good results, and C and P provide better results; the combination of X and L requires further study. Although L-band HH (LHH) alone can readily distinguish between woody and non-woody vegeta-

tion on non-flooded sites, the situation is more complex where flooding is present, because flooding can increase LHH backscattering from herbaceous vegetation to values nearly identical to those from unflooded forest.

The ability to penetrate the extensive cloud cover and to detect standing water beneath vegetation canopies is unique to SAR (Hess et al. 1990). SAR has proven useful in delineating levels of inundation; backscatter from ERS-1 SAR acquired over Barrow, Alaska, in 1991, is strongly related to the position of the local water table and thus to methane exchange rates (Morrissey et al. 1994). The capability to differentiate wetland source areas and non-wetlands with SAR is further enhanced by the availability of time-series data. While species composition per se usually cannot be detected with SAR, plant communities often can be detected due to differences in vegetation height, density, or architecture (Pope et al. 1994).

A global record of passive microwave observations from satellites is available from 1979 to the present. The Scanning Multichannel Microwave Radiometer (SMMR) was operated on board the Nimbus-7 satellite from 1979 to 1987, with global coverage every six days. The Special Sensor Microwave/Imager (SSM/I) replaced SMMR in 1987 and continues today with three-day global coverage. These microwave emission measurements include both vertical and horizontal polarizations and four frequencies. For wetland studies, the two highest frequencies, 37 GHz (SMMR and SSM/I) and 85.5 GHz (SSM/I only), are the most useful because they offer the best spatial resolution (ca. 30 and 15 km, respectively). Passive microwave emission measurements are expressed as brightness temperatures in kelvins, and the difference between the two polarizations may be referred to as DT. The principal advantages of the passive microwave observations are their frequent global coverage and their ability to reveal certain characteristics of the land surface beneath cloud cover and vegetation. The coarse spatial resolution may be an advantage for global studies because it reduces the data volume, but it is often a limitation for studies of specific sites.

SMMR observations of the 37 GHz DT have been analyzed to determine spatial and temporal patterns of inundation in the extensive floodplains of the Amazon River (Sippel et al. 1994) and the Pantanal wetland (Hamilton et al. 1996) of South America. The utility of passive microwave remote sensing to monitor inundation in other wetlands of the world has yet to be investigated. The coarse spatial resolution limits the application of the technique to large wetlands, or to regions where the cu-

mulative area of smaller wetlands comprises a significant proportion of the landscape. Surface roughness, exposed soil and rock, seasonal vegetation changes, and seasonal snow cover can affect the DT (Choudhury 1989), and these factors may have to be accounted for to quantify the variability in flooded areas using microwave emission.

There have been many investigations of the potential use of passive microwave remote sensing to quantify surface soil moisture (Jackson 1993). Soil-moisture studies have focused on arid and semi-arid regions where bare soils dominate, or in agricultural areas. Jackson and Schmugge (1991) discuss the effects of vegetation on the microwave emission from soils and conclude that there is little chance of reliably estimating soil moisture under forest or shrub canopies, which attenuate the emission from the soil surface. In addition, the lowest frequency available for satellite data is 19.4 GHz, where emission represents less than 1 cm of soil depth, and the satellite measurements have a spatial resolution of about 50 km.

4.3.4 Nitrous and nitric oxide

Nitrous oxide (N_2O) is an important greenhouse gas, with an atmospheric lifetime longer than 100 years. It is produced by microbial processes in soils and increases with intensified land use, especially as a result of fertilization. Nitric oxide (NO), a short-lived, chemically-active species is produced by these same microbial processes, but is not a greenhouse gas; however, increasing levels of NO in the atmosphere lead to higher production of atmospheric O_3 , an important greenhouse gas. Nitrous oxide is increasing in the atmosphere (although its annual rate of growth is low), and soil NO emissions may well be increasing. Changes to the atmospheric N_2O content can be measured directly, but changes in NO are hard to detect globally, because NO's short atmospheric lifetime means that atmospheric concentrations are low and spatial variability is extremely high. However, the NO_x family of compounds (NO, NO_2 , HNO_3 , . . .) can be measured from space, complementing surface observations, which have lower spatial resolution although potentially higher temporal resolution than from space.

4.3.4.1 Monitor terrestrial correlates processes that influence N_2O and NO emissions

This task parallels the tasks described for the carbon cycle. Conversion of forests to other uses such as pasture or cropland will for a time increase nitrogen trace gas emissions. The basic science requirement here is to provide periodic assessments of land cover along with, at a minimum, indicators of regions that are undergoing rapid change (from change-detection algorithms). Relatively frequent assessment of land-cover change will be necessary in areas of

rapid land-cover change because of the dependence of trace-gas emissions on time since disturbance. Both NO and N₂O emissions have been shown to depend upon time since conversion from forest to pasture (Keller et al. 1993), and may depend upon time since conversion from grassland to cropland.

4.3.4.2 Monitor soil moisture

Soil moisture is a key control over nitrogen trace-gas fluxes. Soil moisture content affects both the species of nitrogenous trace gas emitted, and the overall rate of nitrogen trace-gas emissions (Parton et al. 1988). In general, overall NO and N₂O emissions increase with increasing soil moisture up to a maximum level related to the fraction of overall soil volume filled with water (water-filled pore space [WFPS]) (Firestone and Davidson 1989; Davidson 1992). Above the WFPS threshold, emissions of the inert gas N₂ may continue to increase, but emissions of reactive species may decline. In addition, there is evidence that emissions of NO occur in “pulses” immediately following each rainstorm in more-arid conditions (Yienger and Levy 1995), so knowledge of event frequency is itself a useful variable. Whereas there are severe technical problems with remotely measuring soil moisture (a) under dense vegetation and (b) below a few centimeters depth, there are several potential EOS contributions of space-based measurements. First, there is some promise that microwave surface “wetness” retrievals may eventually be correlated with more-quantitative measures of soil moisture. This is hopeful for trace gases as, in many ecosystems, most N metabolism occurs near the soil surface (Schimel et al. 1986). Second, soil-moisture retrievals from 4-Dimensional Data Assimilation (4DDA) may be useful. This latter possibility is crucial, as constrained but physically-based estimates of soil moisture linked to an integrated hydrological calculation could result in critical improvements in global soil-moisture estimates. These techniques are most hopeful for the upper soil layers, where water content is most tightly coupled to the atmosphere.

4.3.4.3 Monitor tropospheric reactive nitrogen levels

In a recent report (<ftp://eosps0.gsfc.nasa.gov/docs/chemistry.pdf>) two key questions were identified relative to tropospheric reactive nitrogen.

- 1) Can we quantify the sources of reactive nitrogen in the upper troposphere, including . . . in situ aircraft emissions, in situ production by lightning, downward transport from the stratosphere, and upward transport of species emitted at the surface?

- 2) Can we improve our knowledge of the distributions of reactive nitrogen compounds in the troposphere through measurements and models . . . ?

Although improved terrestrial source estimates can aid in answering these questions, it is clear that more knowledge of the global distributions than can be obtained using aircraft in situ measurements alone will be required to reduce the uncertainties. Whereas sources of reactive N from biogenic sources (including fertilizers and other ecosystem or agronomic manipulations) can be modeled using EOS data, NO_x from lightning and aircraft cannot be so estimated (although lightning itself will be monitored). In particular, the lightning source is poorly constrained, and global observations of lightning and NO_x will be crucial for improving estimates of this source. In general, only if consistency can be achieved between 1) models of reactive N distributions using source estimates as input, 2) accurate and precise but episodic and regional in situ measurements, and 3) global climatological data from space, can closure of the reactive N budget be assumed. The EOS satellite contribution to this comes from the TES instrument, which can measure reactive N species in the limb-viewing mode. The limb mode will reduce the coverage and increase the minimum average altitude (because of clouds, which block the measurement and the larger footprint in the limb mode) relative to nadir viewing, but is required to achieve the requisite sensitivity.

4.3.5 Ozone: Its precursors and fate

4.3.5.1 Monitor ozone precursors

Ozone is different from the other species discussed earlier in the chapter as it is produced in situ in the atmosphere from precursor compounds, or, alternatively, transported from remote stratospheric sources into the troposphere. This makes understanding the sources, sinks, and distributions of ozone precursors in the atmosphere critical. One such precursor, reactive nitrogen, was discussed above and is particularly crucial. Over a wide range of chemical environments (leaving aside very low NO_x and very polluted air), as NO_x increases, O₃ will increase linearly. Thus the monitoring and development of a NO_x climatology, resolved by altitude, is a critical EOS product.

Other crucial species involved in O₃ formation include CO, CH₄, and the non-methane hydrocarbons (NMHCs), including biogenic isoprene and terpenes, and pollutant species. Of these, several can be monitored from space. CO has been measured successfully from space using a Shuttle instrument (Reichle et al. 1990; Fishman

et al. 1991). The MOPITT instrument on the EOS AM-1 platform will make measurements of CO at four levels in the atmosphere and will be supplemented by missions such as Mir using the MAPS instrument with less-than-global coverage. Figure 4.4 (pg. 180) shows a simplified scheme for tropospheric chemistry, indicating the key species or families of species involved in the tropospheric ozone cycle. The species are coded by whether they are observable or not. In addition, the species that require limb viewing (and so will be observed with lower spatial/temporal resolution, especially in the lower troposphere) are also noted.

Ozone itself must also be monitored. Ozone's horizontal distribution is quite variable, and satellite measurements show typical high ozone in industrially-polluted areas. A surprise finding from early tropospheric ozone measurements from space (using the tropospheric residual technique in which stratospheric ozone is subtracted from column ozone) was the presence of a tropical maximum, now believed to be the result of biomass burning (Andreae et al. 1988; Fishman et al. 1991). Because tropospheric ozone and especially lower-tropospheric ozone can be very variable in time and space, reflecting changing precursor sources and convective mixing upwards, space-based measurements are critical for understanding the climatology and temporal variability of ozone.

4.3.5.2 Monitor ozone vertical distribution

Ozone is distributed vertically in the atmosphere, with the majority (~90%) of atmospheric ozone located in the stratosphere. Because of mixing between the stratosphere and troposphere, the upper troposphere tends to have higher ozone levels than the lower, although this can be extremely heterogeneous because of the relatively short lifetime of ozone and its precursors, and because of the dynamic nature of stratosphere-troposphere exchange. Despite the generally increasing profile of ozone with height in the troposphere, local pollution can cause surface ozone levels as high as or higher than upper tropospheric levels. Ozone poses a different issue at different heights. High ozone in the boundary layer is a serious pollutant and is damaging to human health and ecosystems. Ozone in the mid-to-upper troposphere acts as a strong greenhouse gas, with a radiative forcing (if increases are evenly distributed in the troposphere) of 0.02 Wm⁻² per ppbv change in O₃. Various estimates for the radiative forcing due to historical changes in O₃ are summarized in IPCC 1994 by Shine et al. (1995). Because of ozone's variable distribution in space, its positive radiative forcing effect can be quite localized.

Lower-stratospheric ozone depletion has the opposite effect. A loss of ozone in the lower stratosphere will lead to cooling, although the magnitude and (in extreme cases) the sign of the effect is dependent upon the shape of the ozone profile (Wang et al. 1993; Shine et al. 1995). Because of the sensitivity of the climate system to changes in the vertical distribution of ozone, and because of the biospheric significance of high boundary-layer ozone, vertical profiles of ozone are a key EOS product.

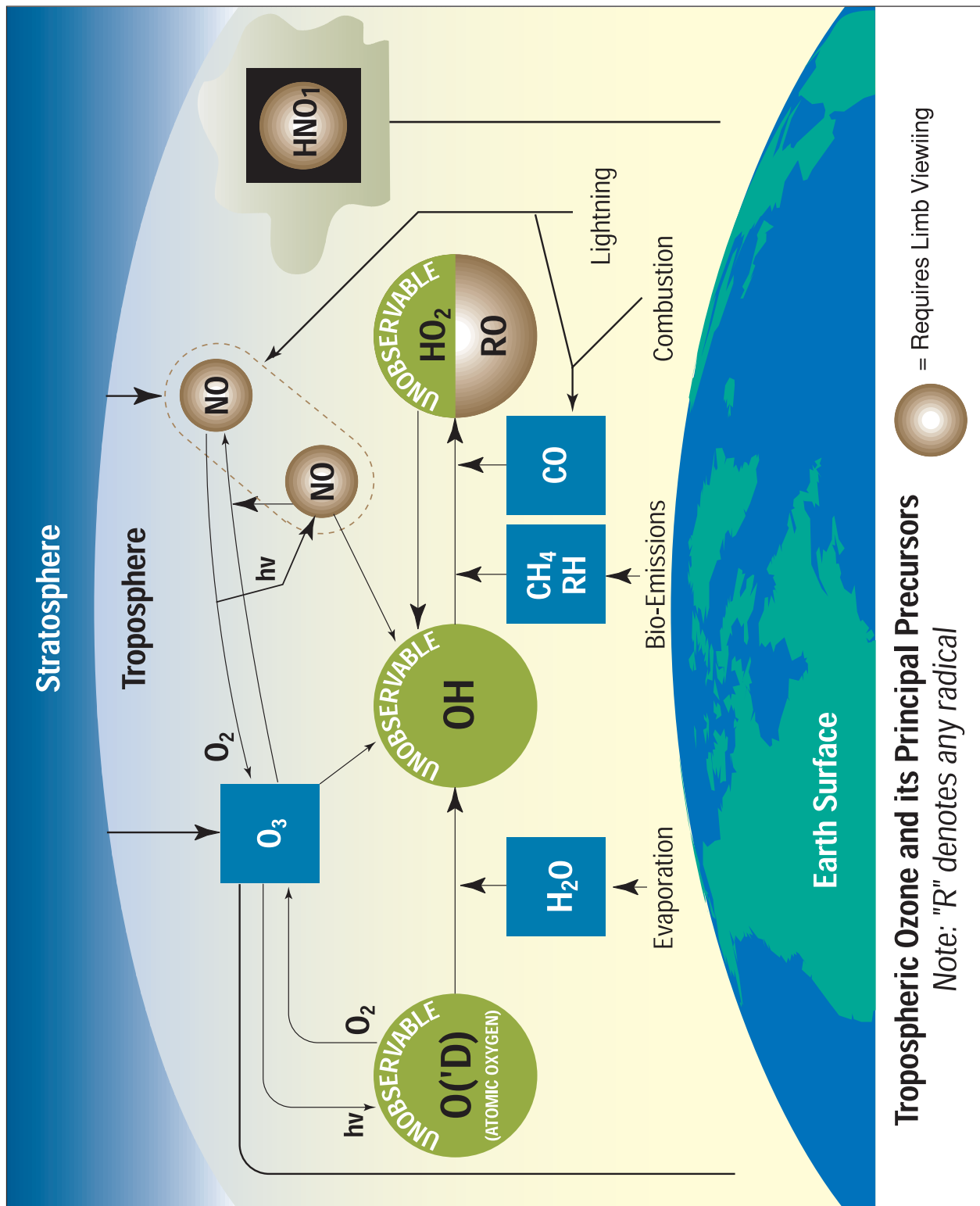
4.3.5.3 Monitor terrestrial emissions of O₃ precursors from soils, vegetation, and biomass burning

Changing terrestrial emissions from changing land use have the potential to alter tropospheric O₃ over much of the globe. As noted above, soil NO is potentially a significant factor, especially in the tropics, where deep convection may lift soil NO from the boundary layer to high altitudes, when otherwise most of it might be re-deposited. As agriculture intensifies globally and nitrogen fertilizer use increases, this source could grow substantially. Terrestrial vegetation emits NMHCs, mainly isoprene and the terpenes, and, in the appropriate (high NO_x) chemical environment, these compounds react to form O₃. Biomass burning also releases a suite of compounds that can react to form ozone (hydrocarbons, methane, NO_x, CO, and the NMHCs), and contributes substantially to tropical ozone formation. In order to understand the contemporary atmosphere, and to monitor changes to sources that may impact atmospheric chemistry, spatial characteristics of terrestrial sources of ozone precursors are important data products. The approaches for NO_x were described above.

NMHC emissions are controlled by the biophysical environment, modified by the plant species considered. Different plant species emit different suites of NMHCs (Monson et al. 1995), with rates varying according to the physical environment of the leaf (Guenther et al. 1993) and the physiological state of the plant (Lerdau et al. 1995). The physical variables controlling leaf-level processes can be monitored as described above in Section 4.3.3, and models of NPP using satellite data form a strong foundation for assessing NMHC emissions. Species-specific emissions, as an input to model rates, require in situ determination, a process underway for many regions.

The basic biomass-burning measurement approaches are described above (4.3.2.1). Conversion of biomass burning detection to the quantification of trace-gas emissions requires the use of "emission factors"—the quantity of trace gas emitted per unit biomass burned or per unit CO₂ emitted. Considerable work has gone into the estimation of biome-specific emission factors for

FIGURE 4.4



A schematic of the tropospheric ozone cycle, indicating the key species or families of species involved. The species are coded by whether they are observable or not. The species that require limb viewing (and so will be observed with lower spatial/temporal resolution, especially in the lower troposphere) are also noted.

many chemical species in the Transport and Chemistry near the Equator over the Atlantic (TRACE-A) and South African Fire—Atmosphere Research Initiative (SAFARI) experiments in Southern Africa and South America; earlier work was done during Dynamique et Chimie de l'Atmosphère en Forêt Equatoriale (DECAFE). These algorithms require information on extent of burning, temperature, and prior biomass levels. EOS data products, together with estimates of emission factors, will allow the production of fields of trace-gas release from biomass burning.

Finally, many O₃ precursors are derived from fossil-fuel combustion or other technological activity. While there is no current proposal to estimate such releases directly from remote sensing, remote observations of atmospheric chemistry (CO from MOPITT and the MAPS missions; O₃, and other compounds from TES) will aid in testing emission factors for surface and airborne sources.

4.4 EOS algorithms, observations, and required additional data

This section is intended to provide information on the anticipated EOS observations and data products supporting research on greenhouse gases and atmospheric chemistry. Many of the required algorithms and data products are documented in the land and hydrology and ocean chapters and we include here only cross-references. Other algorithms are still in development and are not planned for standard production as yet. For some of these only minimal information is now available (this includes especially the measurement of soil moisture and inundation where considerable uncertainty exists about the instrument capabilities and utility of products). Other data sets and algorithms are documented in this chapter.

4.4.1 The carbon cycle

4.4.1.1 Land measurements

4.4.1.1.1 Land cover and land-cover change
(See Chapter 5, “Land Ecosystems and Hydrology.”)

4.4.1.1.2 Correlates of plant growth: FAPAR, LAI
(See Chapter 5, “Land Ecosystems and Hydrology.”)

4.4.1.1.3 Biomass burning
(See 4.4.3.3.)

4.4.1.2 Ocean measurements

4.4.1.2.1 Ocean color
(See Chapter 3, “Oceanic Circulation, Productivity, and Exchange with the Atmosphere.”)

4.4.1.2.2 Wind stress
(See Chapter 3, “Oceanic Circulation, Productivity, and Exchange with the Atmosphere.”)

4.4.2 Methane and nitrous/nitric oxide

4.4.2.1 Surface correlates

4.4.2.1.1 Land cover and land-cover change
(See Chapter 5, “Land Ecosystems and Hydrology.”)

4.4.2.1.2 Wetland productivity correlates: FIPAR and LAI
(See Chapter 5, “Land Ecosystems and Hydrology.”)

4.4.2.2 Atmospheric retrieval of column methane
(See Section 4.4.3, below.)

4.4.3 Atmospheric chemistry and greenhouse gases

4.4.3.1 Methane and CO from MOPITT

This section describes the algorithm for retrieving vertical profiles of CO and the total column amount of CO and CH₄ from thermal emission and reflected solar radiation measurements by MOPITT in the 6.4- μ m and 2.3- μ m band of CH₄. Standard Level 2 products include 1) total column amounts of CO and CH₄ for the sunlit side of the orbit; and 2) vertical profiles of CO with a vertical resolution of about 3 km.

The MOPITT experiment has been described by Drummond (1992). The objective of MOPITT CO measurements is to obtain profiles with a resolution of 22 km horizontally, 3 km vertically, and with an accuracy of 10%

throughout the troposphere. A CO total-column-amount measurement will also be made with a 10% accuracy. For CH₄, the objective is to measure the column in the troposphere to a precision of better than 1%, with a spatial resolution similar to that of the CO measurement. The column amounts of CO and CH₄ will only be available on the sunlit side of the orbit as standard Level 2 MOPITT products.

The concentration of CO in the Earth's atmosphere has been changing mainly because of increased human activities (Khalil and Rasmussen 1994). The full range of the effects of the increased concentration of CO is not fully understood at the present time, but it is believed that CO is photochemically active and plays a major part in the concentration of OH radicals in the troposphere. Increased CO may deplete tropospheric OH radicals, thereby reducing the yearly removal of many natural and anthropogenic trace species. In particular, this effect may add to the increase of CH₄, which in turn could further reduce OH concentration. Increased CO may also indirectly intensify global warming and perturb the stratospheric ozone layer by increasing the lifetime of trace gases such as CH₄, CH₃Cl, CH₃CCl₃, and the HCFCs and HFCs. Global measurements of CO and CH₄ will undoubtedly shed light on the concentration of OH, which is one of the most important and difficult species to measure from space due to its very low concentration. Those measurements will enhance our knowledge of the chemistry of the troposphere and particularly how it interacts with the surface/ocean/biomass systems, atmospheric transports, and the carbon cycle. Global CO and CH₄ measurements from MOPITT will also be used in parallel modeling efforts to advance our understanding of global tropospheric chemistry and its relationship to sources, sinks, and atmospheric transports, which can be determined from other data. Understanding their biogeochemical cycles and their intimate interrelation with each other and with climate will lead to better predictions of possible effects of anthropogenic activities.

The possibility of remotely measuring CO profiles in the troposphere from spaceborne platform observations of thermal-infrared emission/absorption was first suggested by Ludwig et al. in 1974. Success of MAPS on the second Space Transport System engineering test flight (STS-2) of the Shuttle in November 1981 proved the feasibility of inferring the CO profile from measurements by a nadir-viewing instrument (Reichle et al. 1986). The instrument employed is a gas filter radiometer operating in the 4.7- μm region of the CO fundamental band with a passband from 2080 to 2220 cm^{-1} . At the surface, the instantaneous field of view is approximately 20-by-20 km. Successive MAPS experiments provided more global tropospheric CO measurements and further demonstrated the

importance and feasibility of CO measurements from space.

Even though MAPS experiments have provided important global CO measurements for global tropospheric chemistry study, limited coverage, with only the average CO mixing ratio in the middle of the troposphere, is not adequate, and multiple-level CO measurements that would resolve the troposphere into several layers are needed. MOPITT is an instrument designed to meet this requirement and provide global CO measurements of the lower, middle, and upper troposphere and daytime total columns of CO and CH₄. The MOPITT retrieval algorithm is based on proven retrieval techniques, such as the maximum likelihood method (Rodgers 1976), and is designed to maximize scientific return of the MOPITT experiment with state-of-the-art retrieval techniques.

4.4.3.1.1 Instrument characteristics

MOPITT, on the AM-1 platform, measures upwelling thermal emission from the atmosphere and surface in the longwave channels, and reflected solar radiation in the shortwave channels (radiation that has passed through the atmosphere, been reflected at the surface, and been transmitted back up through the atmosphere). Total atmospheric transmittance derived from reflected sunlight measurements is a convenient way to determine the total column amount of a trace gas. This technique requires that the target gas have a spectral band in a region with large solar radiance, and that the total optical depth along such a path not be too large. Methane has an overtone band near 2.2 μm with a measurable but not-too-large total absorption for such a path. Similarly, CO has its first overtone band at 2.3 μm , which is also suitable. For vertical profiling, the requirement is that significant and measurable portions of the signal must originate in different atmospheric layers, which means that there must also be a source of radiation in the atmosphere. Thermal emission is a radiation source, and the CO fundamental band at 4.7 μm has enough opacity to determine atmospheric amounts, as demonstrated by Reichle et al. (1986, 1990).

All three bands are in regions of the spectrum with other bands, and the lines of the gases of interest are mixed with those of interfering species. It would be possible, in principle, to measure the total emission or transmission of the species of interest, and correct for the contributions of interfering species. However, the contributions of other species are often larger than those of the gases of interest, and their amounts are often not known with sufficient accuracy. The uncertainties of the corrections may significantly degrade, or even mask, changes due to the gas of interest.

MOPITT is designed to meet this challenge by enhancing the sensitivity of the instrument to the gas of interest. Since all gases in the atmosphere are emitting/absorbing simultaneously, it is essential that the effect of the gas of interest can be separated out from the general radiation field. Further, the information about the vertical distribution of the gas is contained within the shape, which generally requires high spectral resolution. High spectral resolution leads to low signal-to-noise, which means low instrument sensitivity. Therefore, high-sensitivity and high-spectral-resolution requirements for tropospheric trace species remote sensing are difficult to implement with conventional dispersing instruments.

Correlation radiometry (CR), a non-dispersive spectroscopic technique, offers the promise of high effective spectral resolution with a high signal-to-noise ratio achieved by higher throughput through analog addition of signals from many spectral lines. In CR, a cell containing a sample of the target gas is placed in the optical train ahead of the detector. The gas in the cell absorbs the incoming radiation at the frequencies of its spectral lines. By varying the amount of gas in the cell between a higher and lower amount, a difference signal can be obtained due to the difference in absorption by the target gas lines. The difference signal is identical to the output of a system in which the gas cell and its modulator are replaced by an optical filter which only responds at the frequencies of the target gas lines. A further feature is that if the cell gas pressure is low, the difference is primarily near the center of the line, while for higher cell pressure the difference is in the line wings. This can be used to obtain information on the vertical distribution of the target gas.

MOPITT makes use of two methods to modulate the gas amounts in the cell, depending on cell pressure. For low pressures (< 100 hPa) the pressure is modulated through the use of pressure-modulated cells, described in detail by Taylor (1983). For high pressures, the cells are modulated by changing the length of the gas cell (Drummond, 1989).

4.4.3.2 Ozone and ozone precursors from TES

Figure 4.4 shows the principal pathways through which tropospheric ozone is created, transported, and destroyed. As the figure shows, the chemistry is very complex, and, unfortunately, several key species (notably atomic oxygen in the $O(^1D)$ state and the OH and HO_2 radicals) are unobservable by any current remote sensor; thus, their concentrations must be inferred through a combination of models and observed concentrations of precursor species. Furthermore, the equally important active nitrogen species NO, NO_2 , and HNO_3 , and most of the oxygenated hydrocarbons (“RO”) can only be observed by limb

viewing because of their very low concentrations (typically parts-per-trillion). On the other hand, species such as O_3 itself, H_2O , CO, and the more-abundant simple hydrocarbons can be observed both in the nadir and at the limb. This is important because limb viewing rarely penetrates below about 5 km (because of cloud interference), but many of the critical interactions take place closer to the surface. Thus, while both capabilities are needed to provide inputs to the models, it is essential that the air masses observed in both limb and nadir modes be, as nearly as possible, the same because much of the chemistry is quite localized. TES has been specifically designed to provide this capability.

4.4.3.2.1 TES

TES is an infrared ($650 - 3050$ cm^{-1} ; $3.3 - 15.4$ μm), high-resolution (0.025 cm^{-1}), imaging (1×16 pixels) Connes'-type Fourier Transform Spectrometer intended for the near-simultaneous measurement and profiling of the global three-dimensional concentrations of those molecules key to the production and destruction of tropospheric ozone, with especial emphasis on the reactive nitrogen species (Table 4.1, pg. 190). On regional and local scales, TES may (as a goal) measure additional species that are sporadic or otherwise not well-quantified (Table 4.2, pg. 190). Even more species will certainly be measurable but they are generally of minor interest. Nevertheless, they must be accounted for in the retrieval process because they contribute to the received radiance, and their neglect can compromise the accuracy of the retrieved concentrations of the major species.

TES operates by natural thermal emission ($650 - 2450$ cm^{-1} ; $4.1 - 15.4$ μm) and by solar reflection ($2000 - 3050$ cm^{-1} ; $3.3 - 5.0$ μm) when appropriate. TES will obtain its data in single scans of four seconds each in downlooking (nadir $\pm 45^\circ$) operations and in 16 seconds while staring at the trailing limb (0 - 33 km). Longer integrations (up to 221 seconds) by scan-averaging are possible for improved sensitivity, or multiple scans over the same interval can be used to investigate time variability. Spatial variability can be studied by “stacking” footprints contiguously to generate North-South transects up to 2700 km long. Spatial resolution from the EOS 705-km orbit is interchangeably 0.5 km cross-track \times 5 km in-track or 2.5×25 km in the nadir (per each of 16 contiguous pixels) and 2.3 km high \times 23 km (parallel to the Earth's surface) at the limb, providing 16 simultaneous measurement levels from the surface to about 33 km.

4.4.3.2.2 The extraction of concentration profiles from infrared spectra

Most modern retrieval algorithms for the extraction of concentration profiles operate on similar principles: a “first guess” physical and chemical compositional profile of the atmosphere is set up (the source may be climatology, a previously retrieved set, or, sometimes, sonde profiles), and, incorporating known instrumental properties such as spectral resolution and instrumental line shape, a model spectrum is generated through a forward solution of an appropriate version of the equation of radiative transfer. The model calculation is compared to the actual data and the model is iterated until the two match to within some prescribed limit. The differences among algorithms generally lie in: a) the exact character of the inevitable approximations inherent in any numerical calculation, and b) the methods used to indicate that convergence has occurred. It should further be noted that the problem is ill-conditioned—it can never be demonstrated that the solution is unique (one can “drop” into local minima of the solution space). Thus verification and correlative measurements are a crucial part of the operation.

Measurements in the troposphere can, however, take advantage of the fact that spectral lines formed below about 20 km exhibit significant pressure-broadening (see Figure 4.5). Thus, species whose stratospheric abundance greatly exceeds that in the troposphere (such as O₃ itself) can nevertheless be discriminated provided that the spectral resolution suffices to make this possible.

The shape of pressure-broadened lines is reasonably well described by the Lorentz Function:

$$1) \quad k_L(n - n_0) = \frac{S(n_0)\Sigma a_L}{p\Sigma[(n - n_0)^2 + a_L^2]}$$

where k_L is the absorption coefficient, S is the line strength (tabulated), n is frequency (normally in cm⁻¹), n_0 is the frequency of the line center, and a_L is the broadening coefficient (defined as the half-width at half-maximum of the function).

a_L , which is directly proportional to pressure, is determined empirically through laboratory investigations and is tabulated at STP because it also has a weak (and often unknown) temperature dependence (roughly as $T^{1/2}$). The absorption A ($= 1 - \text{transmission}$) of the gas is related to the absorption coefficient by:

$$2) \quad A(n - n_0) = 1 - \exp[-k(n - n_0) \cdot L]$$

where L is the number of molecules of the particular species in the line of sight (at constant temperature and pressure).

Now, it is a curious (but quantum-mechanically explicable) property of a_L that its value is nearly independent of species and frequency (wavelength) and takes a value of about 0.05 cm⁻¹ near the Earth’s surface. Thus, when the product of k_L and L is small (a so-called “weak line”), the full width at half maximum depth of the spectral line is $2a_L$ (0.1 cm⁻¹) for all molecules anywhere in the spectrum.

There is only one class of spectrometer that meets the requirements of broad spectral coverage and frequency-independent spectral resolution—a Fourier Transform Spectrometer (FTS). Thus, TES has been designed to be an FTS.

As examples of how the retrieval process operates, Figures 4.6 through 4.11 (pp. 186-187) show simulated limb retrievals of many of the species important to tropospheric chemistry (the error bars are based on expected TES performance but do not include any sources of systematic error). Again, it must be emphasized that those profiles that are shown as going to the surface will rarely, in practice, do so because of cloud interference.

4.4.3.3 Biomass-burning sources of gases (including CO₂)

The MODIS fire product uses the special fire channel at 3.9 μm that saturates at 500 K and the high gain of the 11-μm channel. During the night the fire product will use also the 1.65- and 2.15-μm channels. The analysis is based on a 10 × 10-pixel box comparing the fire-apparent temperatures in these spectral bands to the background temperatures and their standard deviation. The product includes daily fire occurrence (day/night), the logical criteria used for the fire selection (day/night), and fire location. For fires that are high enough above the detection limit, the fire spectral apparent temperatures will be converted into the total emitted energy from the fire and the smoldering/flaming ratio. The fires are classified into fire classes based on their strength; for each class the ratio between smoldering and flaming stage is computed from empirical field information. This information is expected to be helpful in estimation of the spatial and temporal distribution of fires in different ecosystems and for the estimation of the emissions of trace gases and particulates from the fires.

The product also includes: composite ten-day-and-night fire occurrence (full resolution); composite monthly day-and-night fire occurrence (full resolution); gridded 10-km summary per fire class (as described above; daily/ten day/monthly) count of the number of fires in each class and the ratio between smoldering and flaming for the combination of all the fires in the class; and gridded 0.5-degree summary of fire counts per class (daily/ten-day/monthly), and smoldering/flaming per class.

4.5 Synthesis and integrative modeling: status and needs

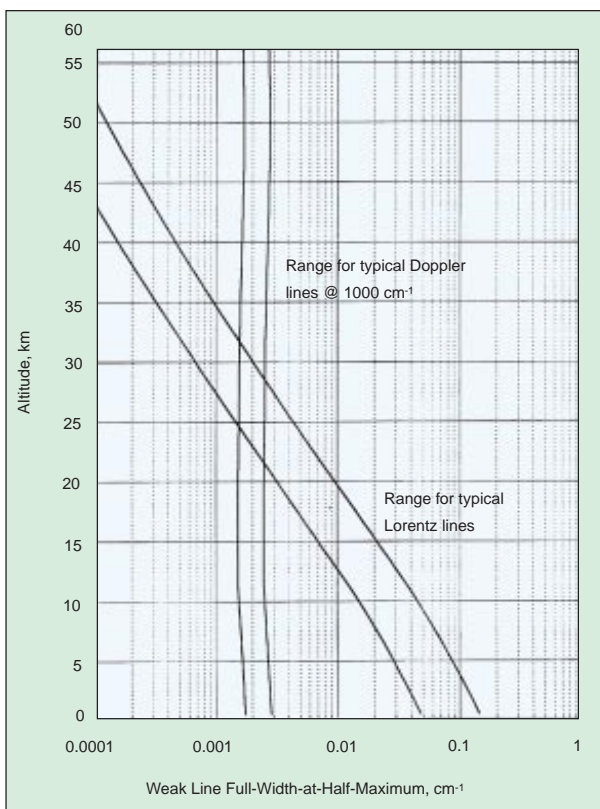
4.5.1 Introduction

The unique aspect of the topics discussed in this chapter is the degree of interdisciplinary integration across the EOS program they require. Even a first-order analysis of the carbon cycle requires addressing fundamental problems of ocean physics and biology, terrestrial ecology and biophysics, and atmospheric transport and measurements. Because the carbon cycle is driven by industrial processes, transportation, energy use, land-use change, and other anthropogenic processes, the human dimensions of the problem are also central. Understanding the changing ozone content of the troposphere is likewise integrative and interdisciplinary. Like the carbon cycle, changing atmospheric chemistry is driven by changing land use and “industrial ecology.” Other sources and many of the sinks for trace gases are biological and require fundamental ecological knowledge in order to understand rates and extrapolate them correctly in time and space (Andreae and Schimel 1989). The effects of ozone on climate and

the biosphere are determined by the horizontal and vertical distribution of O_3 , which is controlled by 1) the geography of sources, 2) chemical reactions in the atmosphere, 3) transport and mixing by physical processes, and 4) physical, biological, chemical, and dynamic (e.g., mixing into the stratosphere, loss at the surface) sinks.

Many of the most critical processes for biogeochemistry in all three domains—oceans, land, and atmosphere—are extremely heterogeneous in time and space, thus requiring global time-series monitoring. These processes are largely invisible to direct remote observation. Such key “invisible” processes include, but are not limited to 1) respiration from dead organic matter on land, 2) mixing of carbon from the surface to deeper ocean layers, and 3) the atmospheric concentrations of the hydroxyl radical. Because of this invisibility, a central tool in the overall strategy is to use available data from remote and in situ sensors to constrain models, and to use models to interpolate in time and space as a means to estimate these invisible processes. This procedure must be continually evaluated against independent observations, made in situ when needed, which, in addition to testing the ability of models to interpolate and estimate additional variables, also allow the diagnosis of errors and biases. This, in turn, provides information that can improve and reduce the uncertainties when models are used in a predictive or extrapolation mode.

FIGURE 4.5



Variation of spectral line widths as a function of altitude (TES Science Team).

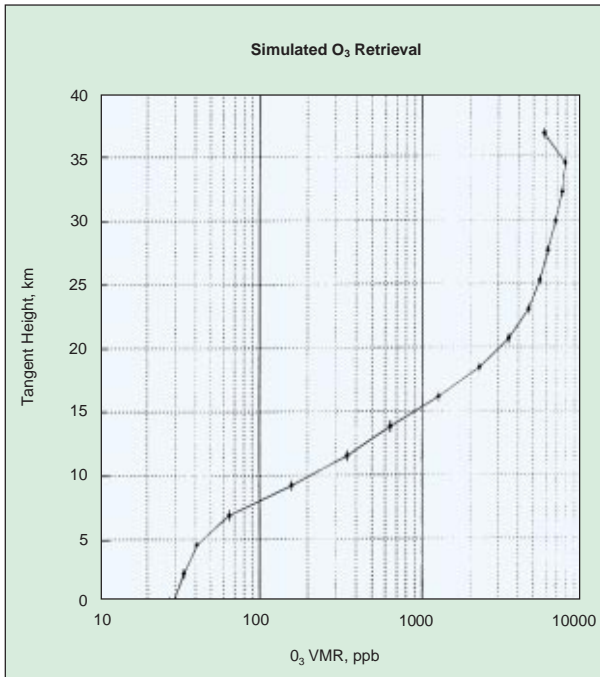
4.5.2 An EOS strategy for integrative models of biogeochemistry

The problems inherent in the carbon cycle and other greenhouse gases require integration not only within the “interdisciplinary” investigations that are a main component of the EOS program, but across multiple IDS teams and with instrument team science and algorithm investigations as well. These problems also require integration of non-EOS in situ data. The components required for CO_2 , methane, N_2O , NO , NMHC, and O_3 modeling and analysis, however, have much in common. Below, we outline two major thrusts to integrate EOS data and large-scale modeling for the carbon and ozone cycles. These do not exhaust the important integrative research and application areas, but exemplify how EOS data, process understanding, and global models can be used synergistically.

4.5.2.1 The carbon cycle

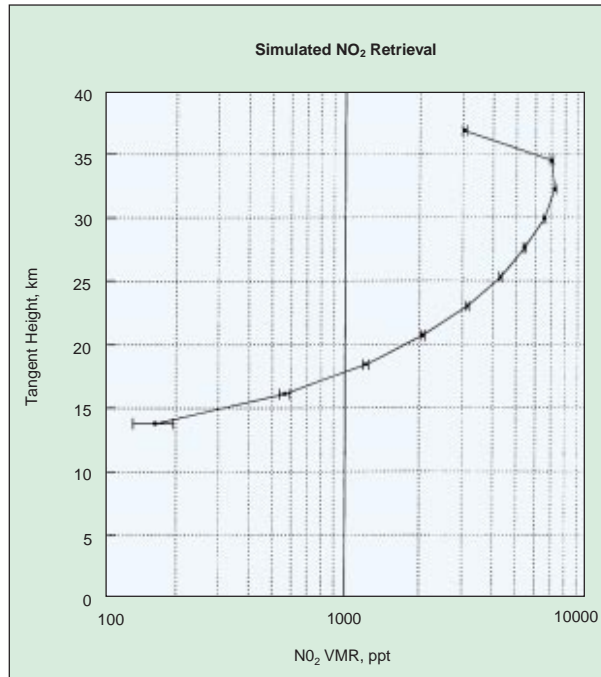
Figure 4.12 (pg. 188) shows how EOS data and models can be integrated. Information on the physical atmosphere provides either direct or assimilated information on the

FIGURE 4.6



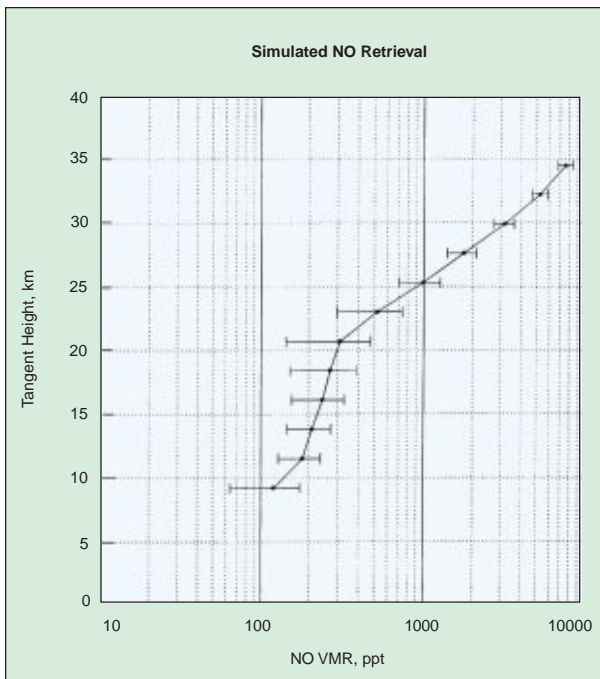
Simulated limb retrieval of ozone. (The error bars are based on expected TES performance but do not include any sources of systematic error.) (TES Science Team.)

FIGURE 4.8



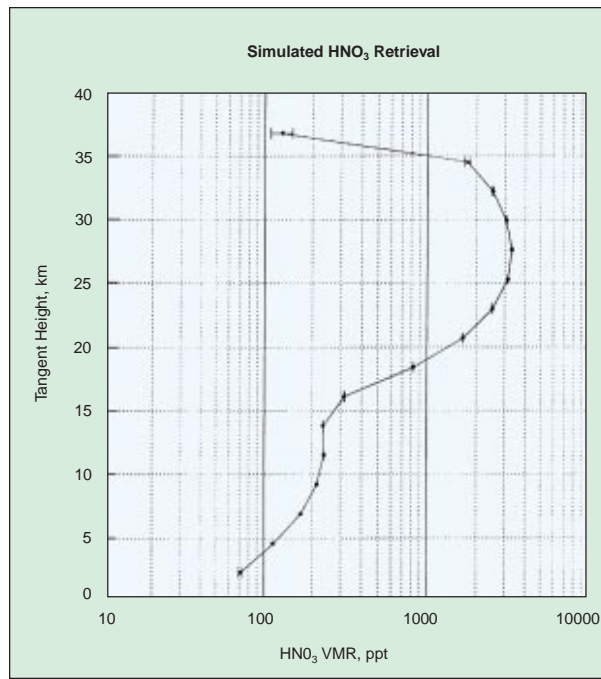
Simulated limb retrieval of NO₂. Error bars as in Figure 4.6. (TES Science Team.)

FIGURE 4.7



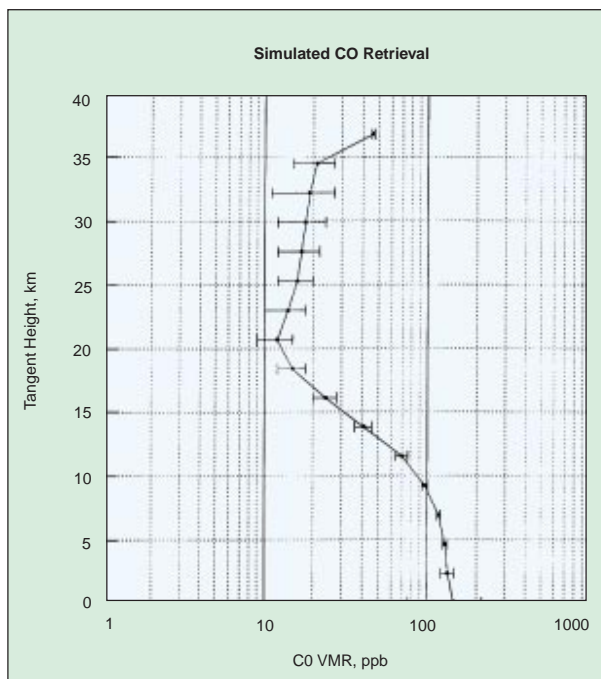
Simulated limb retrieval of NO. Error bars as in Figure 4.6. (TES Science Team.)

FIGURE 4.9



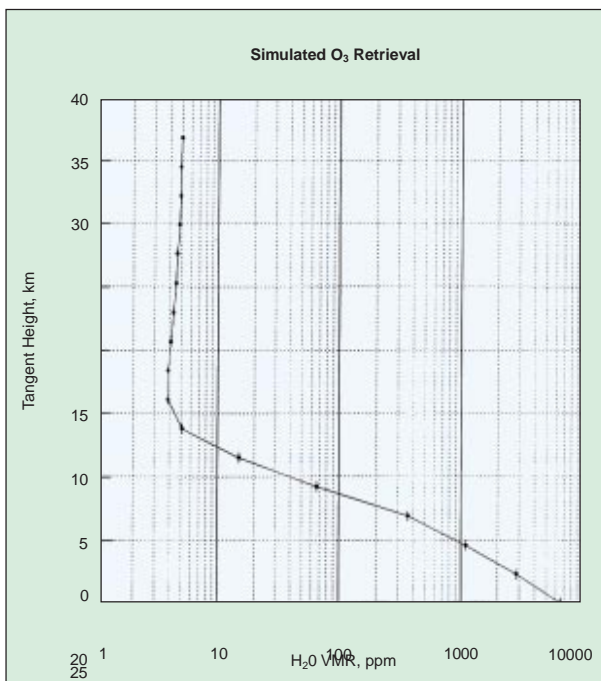
Simulated limb retrieval of HNO₃. Error bars as in Figure 4.6. (TES Science Team.)

FIGURE 4.10



Simulated limb retrieval of CO. Error bars as in Figure 4.6. (TES Science Team.)

FIGURE 4.11



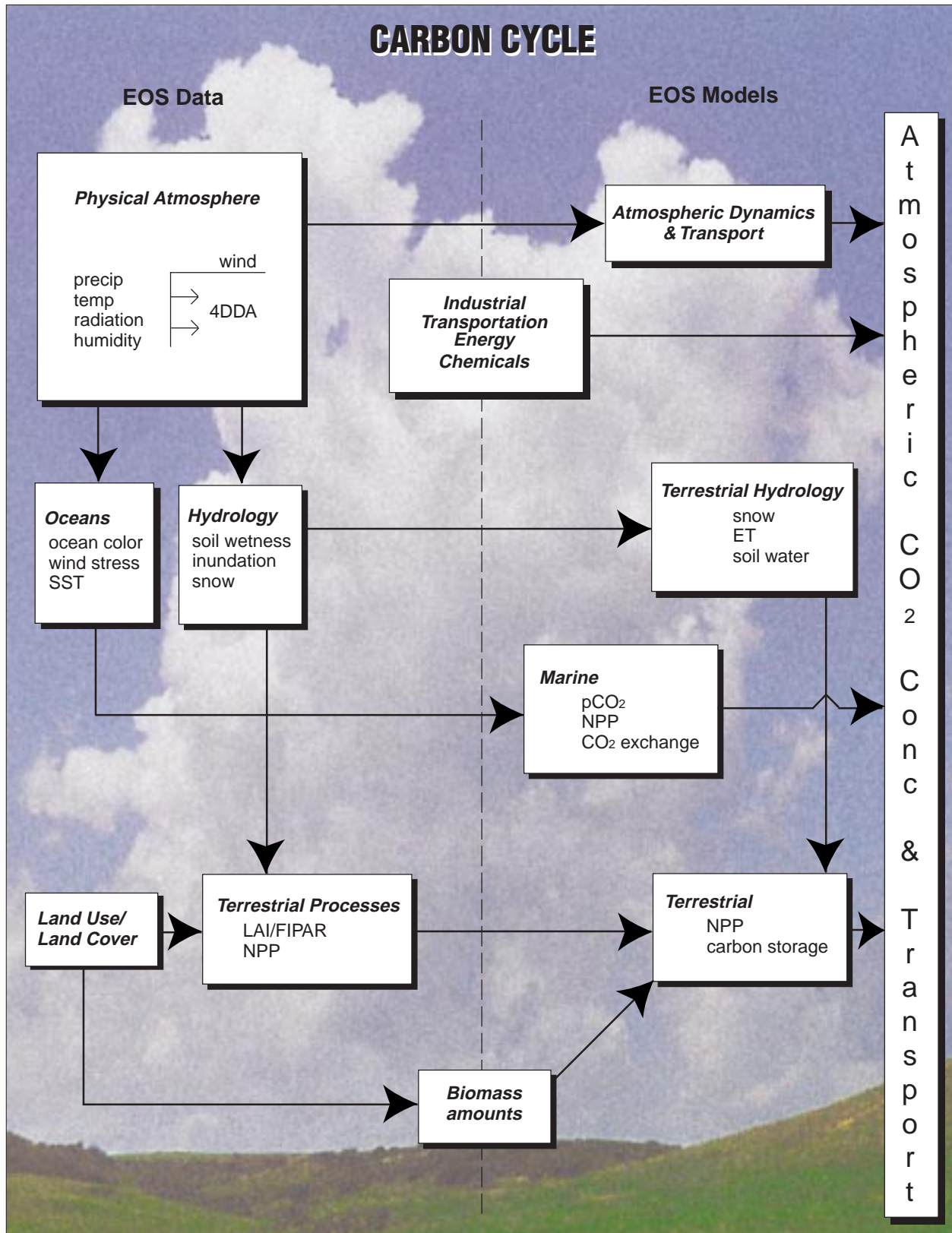
Simulated limb retrieval of H₂O. Error bars as in Figure 4.6. (TES Science Team.)

critical land-surface-climate variables, including temperature, radiation, and precipitation, wind stress, and other factors influencing the terrestrial biophysical and marine gas-exchange environment. For the terrestrial system, these variables, plus snow, surface wetness, and other retrievals, may be further analyzed to produce fields of hydrological variables such as inundation and soil moisture. Remote observations of land cover and land-cover change are combined with either in situ or remote (radar) estimates of biomass to produce a carbon flux from land-use change. Climate information is combined with land-cover data as inputs into ecosystem models to compute terrestrial carbon storage changes. Together, the ocean, ecosystem, and land-use change fluxes are combined to produce spatial maps of terrestrial sources and sinks of CO₂, with fossil-fuel and cement sources also included from statistical data. The distributions of CO₂ in the atmosphere (measured in situ) may then be further analyzed using transport observations from the physical atmosphere for consistency with the modeled sources and sinks. This approach will link the existing land, atmosphere, and ocean activities.

4.5.2.2 Trace gases

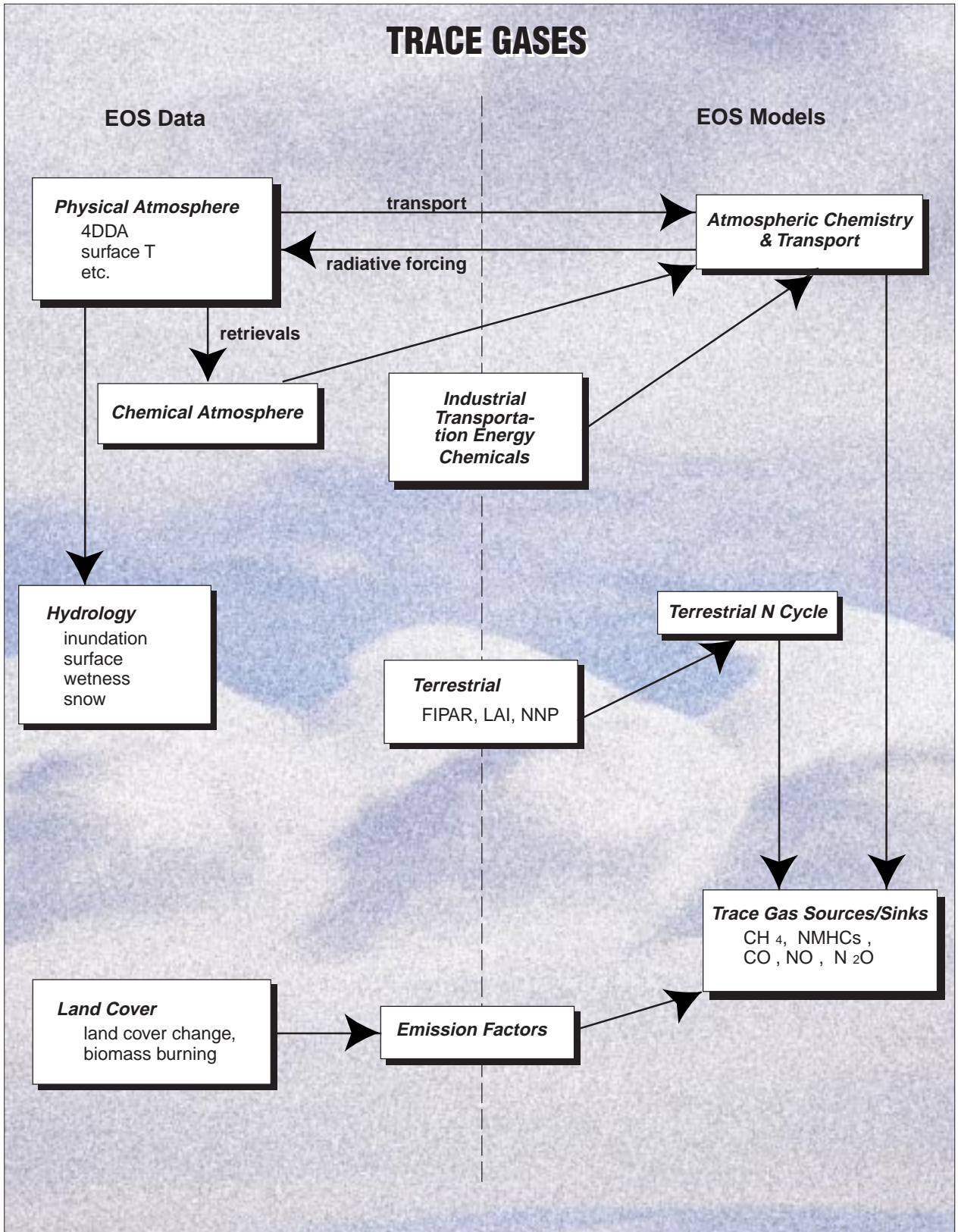
Figure 4.13 (pg. 189) shows a similar scheme for trace gases and the ozone cycle. Information about the physical atmosphere is used to compute biophysical conditions for the land surface and aquatic systems that govern trace-gas emissions, as for the carbon cycle. This information, together with information retrieved about vegetation and ecosystems, is used as input into models of the terrestrial nitrogen cycle and plant physiology. These in turn can be used to compute the fluxes of nitrogen- and carbon-based trace gases, both greenhouse gases and gases involved in the ozone cycle. These fluxes can be used as inputs to atmospheric chemical transport models, possibly coupled to climate models. Direct retrievals of the distributions of greenhouse gases from TES, MOPITT, High-Resolution Dynamics Limb Sounder (HIRDLS), and other instruments can also be passed to the chemical transport models. Finally, anthropogenic gases from industrial, transportation, energy, chemical, and other sectors are also passed to the chemical transport models. This system can address a number of questions, including: 1) Can we explain current distributions of ozone and other key tropospheric gases from known sources and sinks of ozone and precursors? 2) How might changing land use affect future tropospheric chemistry? and 3) How are changing sources, including aircraft, affecting the vertical distribution of ozone?

FIGURE 4.12



Integration of EOS data and models for the carbon cycle.

FIGURE 4.13



Integration of EOS data and models for trace gases.

Table 4.1: TES Standard Data Products

O_x	H_xO_y	C-compounds	N-compounds
O_3 (3 ppb)	H_2O (0.5-50 ppm)	CO (3 ppb) CH_4 (14 ppb)	NO NO_2 HNO_3
Numbers in parentheses are estimated Volume Mixing Ratio (VMR) sensitivities based on a combination of limb and nadir observations; accuracies are expected to be in the 5 - 20% range. Altitude coverage is 0 - 33 km except for NO_y .			

Table 4.2: TES Special Data Products

H_xO_y	C-compounds	N-compounds	Halogen-compounds	S-compounds
H_2O_2	CO_2	HNO_4	HCl^*	SO_2
HDO	C_2H_6	NH_3	HF^*	COS
	C_2H_2	HCN	H_2S^*	
	$HCOH$	N_2O^{**}		
	$HCOOH$			
	CH_3OH			
	PAN			
Sensitivities are TBD; accuracies are expected to be no better than 10% — * Volcanic plume column densities only — ** Control (VMR known)				

References

- Andreae, M. O., and D. S. Schimel, 1989: Exchange of trace gases between terrestrial ecosystems and the atmosphere, *Dahlem Workshop Reports - Life Sciences Research Reports*, **47**, 347.
- Andreae, M. O., E. V. Browell, G. L. Garstang, R. C. Gregory, R. C. Harriss, G. F. Hill, D. J. Jacob, M. C. Pereira, G. W. Sachse, A. W. Setzer, P. L. Silva Dias, R. W. Talbot, A. L. Torres, and S. C. Wofsy, 1988: Biomass-burning emissions and associated haze layers over Amazonia, *J. Geophys. Res.*, **93**, 1509-1527.
- Anonymous, 1996: *World Climate News*, **9**.
- Aselmann, I., and P. J. Crutzen, 1989: Global distribution of natural freshwater wetlands and rice paddies, their net primary productivity, seasonality, and possible methane emissions, *J. Atmos. Chem.*, **8**, 307-358.
- Asrar, G., and R. Greenstone, 1995: *MTPE/EOS Reference Handbook*, NASA, MTPE, EOS, Greenbelt, MD.
- Bartlett, K. B., and R. C. Harriss, 1993: Review and assessment of methane emissions from wetlands, *Chemosphere*, **26**, 261-320.
- Braswell, B. H., 1996: Global terrestrial biogeochemistry: perturbations, interactions, and time scales, Ph.D. Thesis, University of New Hampshire, Department of Earth Sciences, Durham, NH.
- Choudhury, B. J., 1989: Monitoring global land surface using Nimbus-7 37 GHz data, theory and examples, *Int. J. of Remote Sensing*, **10**, 1579-1605.
- Ciais, P., P. P. Tans, M. Trolier, J. W. C. White, and R. J. Francey, 1995: A large Northern Hemisphere terrestrial CO₂ sink indicated by ¹³C/¹²C of atmospheric CO₂, *Science*, **269**, 1098-1102.
- Conway, T. J., P. Tans, L. S. Waterman, K. W. Thoning, D. R. Buanerkitzis, K. A. Masarie, and N. Zhang, 1994: Evidence for interannual variability of the carbon cycle from the NOAA/CMDL global air sampling network, *J. Geophys. Res.*, **99D**, 22831-22855.
- Dacey, J. W. H., and M. J. Klug, 1979: Methane efflux from lake sediments through water lilies, *Science*, **203**, 1253 - 1255.
- Davidson, E. A., 1992: Sources of nitric oxide and nitrous oxide following wetting of dry soil, *Soil Science Society of America Journal*, **56**, 95-102.
- Denning, A. S., I. Y. Fung, and D. Randall, 1995: Latitudinal gradient of atmospheric CO₂ due to seasonal exchange with land biota, *Nature*, **376**, 240-243.
- Dlugokencky, E. J., L. P. Steele, P. M. Lang, and K. A. Masarie, 1994: The growth rate and distribution of atmospheric methane, *J. Geophys. Res.*, **99**, 17021-17043.
- Drummond, J. R., 1989: Novel correlation radiometer: the length-modulated radiometer, *Applied Optics*, **28**, 2451-2452.
- Drummond, J. R., 1992: Measurements of pollution in the troposphere (MOPITT), *The Use of EOS for Studies of Atmospheric Physics*, (J. C. Gille and G. Visconti, Eds.), North Holland, Amsterdam, pp. 77-101.
- Eswaran, H., E. Van den Berg, and P. Reich, 1993: Organic carbon in soils of the world, *Soil Science Society of America Journal*, **57**, 192-194.
- Firestone, M. K., and E. A. Davidson, 1989: Microbiological basis of NO and N₂O production and consumption in soil, *Exchange of Trace Gases between Terrestrial Ecosystems and the Atmosphere*, (M. O. Andreae and D. S. Schimel, Eds.), John Wiley & Sons, New York, pp. 7-22.
- Fisher, M. J., I. M. Rao, M. A. Ayarza, C. E. Lascano, J. I. Sanz, R. J. Thomas, and R. R. Vera, 1994: Carbon storage by introduced deep-rooted grasses in the South American savannas, *Nature*, **371**, 236-238.
- Fishman, J., K. Fakhruzzaman, B. Cros, and D. Nganga, 1991: Identification of widespread pollution in the Southern Hemisphere deduced from satellite analysis, *Science*, **252**, 1693-1696.
- Glantz, M. H., R. W. Katz, and N. Nicholls, (Eds.), 1991: *Teleconnections Linking Worldwide Climate Anomalies: Scientific Basis and Societal Impact*, Cambridge University Press, New York.
- Guenther, A. B., P. R. Zimmerman, P. C. Harley, R. K. Monson, and R. Fall, 1993: Isoprene and monoterpene emission rate variability: model evaluations and sensitivity analyses, *J. Geophys. Res.*, **98**, 12609-12617.
- Hamilton, S. K., S. J. Sippel, and J. M. Melack, 1996: Inundation patterns in the Pantanal wetland of South America determined from passive microwave remote sensing, *Archives of Hydrobiology*, **137**, 1-23.
- Hess, L. L., J. M. Melack, and D. S. Simonett, 1990: Radar detection of flooding beneath the forest canopy: a review, *Int. J. of Remote Sensing*, **5**, 1313-1325.
- Hess, L. L., J. M. Melack, S. Filoso, and Y. Wang, 1995: Delineation of inundated area and vegetation along the Amazon floodplain with the SIR-C synthetic aperture radar, *IEEE Trans Geosci. Remote Sens.*, **33**, 896-904.
- Houghton, R. A., 1995: Effects of land-use change, surface temperature, and CO₂ concentration on terrestrial stores of carbon, *Biotic Feedbacks in the Global Climatic System: Will the Warming Feed the Warming?*, (G. M. Woodwell and F. T. Mackenzie, Eds.), Oxford University Press, New York, pp. 333-350.
- INPE, 1992: Deforestation in Brazilian Amazonia, Instituto Nacional de Pesquisas Espaciais, São Paulo, Brazil.
- Jackson, T. J., and T. J. Schugge, 1991: Vegetation effects on the microwave emission of soils, *Remote Sens. Environ.*, **36**, 203-212.
- Jackson, T. J., 1993: III. Measuring surface soil moisture using passive microwave remote sensing, *Hydrological processes*, **7**, 139-152.
- Jones, P. D., T. M. L. Wigley, and K. R. Briffa, 1994: Global and hemispheric temperature anomalies — land and marine instrumental records, *Trends '93: A Compendium of Data on Global Change*, (T. A. Boden, D. P. Kaiser, R. J. Sepanski, and F. W. Stoss, Eds.), ORNL/CDIAC-65. Carbon Dioxide Information Analysis Center, Oak Ridge National Laboratory, Oak Ridge, Tenn., pp. 603-609.
- Keeling, C. D., J. F. S. Chin, and T. P. Whorf, 1996: Increased activity of northern vegetation inferred from atmospheric CO₂ measurements, *Nature*, **382**, 146-149.
- Keeling, C. D., T. P. Whorf, M. Wahlen, and J. van der Plicht, J., 1995: Interannual extremes in the rate of rise of atmospheric carbon dioxide since 1980, *Nature*, **375**, 666-670.
- Keller, M., E. Veldkamp, A. M. Weltz, and W. A. Reiners, 1993: Effect of pasture age on soil trace-gas emissions from a deforested area of Costa Rica, *Nature*, **365**, 244-246.
- Khalil, M. A. K., and R. A. Rasmussen, 1994: Global decrease of atmospheric carbon monoxide, *Nature*, **370**, 639-641.
- Lerdau, M., P. Matson, R. Fall, and R. Monson, 1995: Ecological controls over monoterpene emissions from douglas-fir (*Pseudotsuga menziesii*), *Ecology*, **76**, 2640-2647.
- Ludwig, C. B., M. Griggs, W. Malkmus, and E. R. Bartle, 1974: Measurement of air pollutants from satellites, 1. Feasibility considerations, *Applied Optics*, **13**, 1494.
- Luizão, F., P. Matson, G. Livingston, R. Luizão, and P. Vitousek, 1989: Nitrous oxide flux following tropical land clearing, *Global Biogeochemical Cycles*, **3**, 281-285.
- McBride, J. L., and N. Nicholls, 1983: Seasonal relationships between Australian rainfall and the southern oscillation, *Mon. Wea. Rev.*, **111**, 1998-2004.
- Melack, J. M., L. L. Hess, and S. Sippel, 1994: Remote sensing of lakes and floodplains in the Amazon basin, *Remote Sensing Reviews*, **10**, 127-142.

- Monson, R. K., M. T. Lerdau, T. D. Sharkey, D. S. Schimel, and R. Fall, 1995: Biological aspects of constructing volatile organic compound emission inventories, *Atmospheric Environment*, **29**, 2989-3002.
- Morrissey, L. A., G. P. Livingston, and S. L. Durden, 1994: Use of SAR in regional methane exchange studies, *Int. J. of Remote Sensing*, **15**, 1337-1342.
- Mosier, A., D. Schimel, D. Valentine, K. Bronson, and W. Parton, 1991: Methane and nitrous oxide fluxes in native, fertilized and cultivated grasslands, *Nature*, **350**, 330-332.
- Myneni, R. B., S. Maggion, J. Jaquinta, J. L. Privette, N. Gobron, B. Pinty, D. S. Kimes, M. M. Verstraete, and D. L. Williams, 1995: Optical remote sensing of vegetation: modeling, caveats, and algorithms, *Remote Sens. Environ.*, **51**, 169-188.
- Myneni, R. B., S. O. Los, and C. J. Tucker, 1996: Satellite-based identification of linked vegetation index and sea surface temperature anomaly areas from 1982-1990 for Africa, Australia and South America, *Geophys. Res. Lett.*, **23**, 729-732.
- Parton, W. J., J. W. B. Stewart, and C. V. Cole, 1988: Dynamics of C, N, P, and S in grassland soils: A model, *Biogeochemistry*, **5**, 109-131.
- Paul, E. A., and F. E. Clark, 1989: *Soil Microbiology and Biochemistry*, 273 pp.
- Philander, S. G. H., 1986: Unusual conditions in the tropical Atlantic ocean in 1984, *Nature*, **322**, 236-238.
- Philander, S. G. H., 1990: El Niño, La Niña, and the Southern Oscillation, *International Geophysics Series*, **46**, 293.
- Pope, K. O., J. M. Rey-Benayas, and J. F. Paris, 1994: Radar remote sensing of forest and wetland ecosystems in the Central American tropics, *Remote Sens. Environ.*, **48**, 205-219.
- Pope, K. O., E. J. Sheffner, K. J. Linthicum, C. L. Bailey, T. M. Logan, E. S. Kasischke, K. Birney, A. R. Njogu, and C. R. Roberts, 1992: Identification of Central Kenyan Rift Valley fever virus vector habitats with Landsat TM and evaluation of their flooding status with airborne imaging radar, *Remote Sens. Environ.*, **40**, 185-196.
- Potter, C. S., J. T. Randerson, C. B. Field, P. A. Matson, P. M. Vitousek, H. A. Mooney, and S. A. Klooster, 1993: Terrestrial ecosystem production: A process model based on global satellite and surface data, *Global Biogeochemical Cycles*, **7**, 811-841.
- Prather, M., R. Derwent, D. Ehalt, P. Fraser, E. Sanhueza, and X. Zhou, 1995: Other trace gases and atmospheric chemistry, in *Climate Change 1994: Radiative Forcing of Climate Change and An Evaluation of the IPCC IS92 Emission Scenarios*, (J. T. Houghton, L. G. Meira Filho, J. Bruce, H. Lee, B. A. Callander, E. Haites, N. Harris, and K. Maskell, Eds.), Cambridge University Press, Cambridge, UK, pp. 75-126.
- Reichle Jr., H. G., V. S. Connors, J. A. Holland, W. D. Hypes, H. A. Wallio, J. C. Casas, B. B. Gormsen, M. S. Saylor, and W. D. Hesketh, 1986: Middle and upper tropospheric carbon monoxide mixing ratios as measured by a satellite-borne remote sensor during November 1981, *J. Geophys. Res.*, **91**, 10865-10887.
- Reichle, H. G., V. S. Connors, J. A. Holland, R. T. Sherrill, H. A. Wallio, J. C. Casas, E. P. Condon, B. B. Gormsen, and W. Seiler, 1990: The distribution of middle tropospheric carbon monoxide during early October 1984, *J. Geophys. Res.*, **95**, 9845-9856.
- Rodgers, C. D., 1976: Retrieval of atmospheric temperature and composition from remote measurements of thermal radiation, *Reviews of Geophysics and Space Physics*, **14**, 609-624.
- Ropelewski, C. F., and M. S. Halpert, 1987: Global and regional scale precipitation patterns associated with the El Niño/Southern Oscillation, *Mon. Wea. Rev.*, **115**, 1606-1626.
- Ropelewski, C. F., and M. S. Halpert, 1989: Precipitation patterns associated with the high index phase of the Southern Oscillation, *J. Climate*, **2**, 268-284.
- Ruimy, A., B. Saugier, and G. Dedieu, 1994: Methodology for the estimation of terrestrial net primary production from remotely sensed data, *J. Geophys. Res.*, **99**, 5263-5283.
- Schimel, D. S., B. H. Braswell, R. McKeown, D. S. Ojima, W. J. Parton, and W. Pulliam, 1996: Climate and nitrogen controls on the geography and time scales of terrestrial biogeochemical cycling, *Global Biogeochemical Cycles*, **10**, 677-692.
- Schimel, D., I. G. Enting, M. Heimann, T. M. L. Wigley, D. Raynaud, D. Alves, and U. Siegenthaler, 1995: CO₂ and the carbon cycle, *Climate Change 1994: Radiative Forcing of Climate Change and An Evaluation of the IPCC IS92 Emission Scenarios*, (J. T. Houghton, L. G. Meira Filho, J. Bruce, H. Lee, B. A. Callander, E. Haites, N. Harris, and K. Maskell, Eds.), Cambridge University Press, Cambridge, UK, pp. 35-71.
- Schimel, D. S., W. J. Parton, F. J. Adamsen, R. G. Woodmansee, R. L. Senft, and M. A. Stillwell, 1986: The role of cattle in the volatile loss of nitrogen from a shortgrass steppe, *Biogeochemistry*, **2**, 39-52.
- Schimel, D., and E. Sulzman, 1995: Variability in the Earth climate system: Decadal and longer timescales, *Rev. Geophys.*, Supplement, U.S. National Report to International Union of Geodesy and Geophysics 1991-1994, 873-882.
- Sellers, P. J., Y. Mintz, Y. C. Sud, and A. Dalcher, 1986: A simple biosphere model (SiB) for use within general circulation models, *J. Atmos. Sci.*, **43**, 505-531.
- Sellers, P. and D. Schimel, 1993: Remote sensing of the land biosphere and biogeochemistry in the EOS era: science priorities, methods and implementation—EOS land biosphere and biogeochemical cycles panels, *Global and Planetary Change*, **7**, 279-297.
- Shine, K. P., Y. Fouquart, V. Ramaswamy, S. Solomon, J. Srinivasan, et al., 1995: Radiative forcing, in *Climate Change 1994: Radiative Forcing of Climate Change and An Evaluation of the IPCC IS92 Emission Scenarios*, (J. T. Houghton, L. G. Meira Filho, J. Bruce, H. Lee, B. A. Callander, E. Haites, N. Harris and K. Maskell, Eds.), Cambridge University Press, Cambridge, UK, pp. 163-203.
- Siegenthaler, U., and J. L. Sarmiento, 1993: Atmospheric carbon dioxide and the ocean, *Nature*, **365**, 119-125.
- Sippel, S. K., S. K. Hamilton, J. M. Melack, and B. Choudhury, 1994: Determination of inundation area in the Amazon River floodplain using the SMMR 37 GHz polarization difference, *Remote Sens. Environ.*, **48**, 70-76.
- Skole, D. and C. Tucker, 1993: Tropical deforestation and habitat fragmentation in the Amazon: Satellite data from 1978 to 1988, *Science*, **260**, 1905-1910.
- Tans, P. P., I. Y. Fung, and T. Takahashi, 1990: Observational constraints on the global atmospheric CO₂ budget, *Science*, **247**, 1431-1438.
- Taylor, F. W., 1983: Pressure modulator radiometry, in *Spectroscopic Techniques, Vol. III*, Academic Press, San Diego, pp. 137-197.
- Tucker, C. J., I. Y. Fung, C. D. Keeling, and R. H. Gammon, 1986: Relationship between atmospheric CO₂ variations and a satellite-derived vegetation index, *Nature*, **319**, 195-199.
- Tucker, C. J., H. E. Dregne, and W. W. Newcomb, 1991: Expansion and contraction of the Sahara Desert from 1980 to 1990, *Science*, **253**, 299-1073.
- Valentine, D. W., E. A. Holland, and D. S. Schimel, 1994: Ecosystem and physiological controls over methane production in northern wetlands, *J. Geophys. Res.*, **99**, 1563-1571.
- VEMAP Members, 1995: Vegetation/ecosystem modeling and analysis project (VEMAP): Comparing biogeography and biogeochemistry models in a continental-scale study of terrestrial ecosystem responses to climate change and CO₂ doubling, *Global Biogeochemical Cycles*, **9**, 407-438.
- Wang, M.-X., S. Xingjian, S. Renxing, R. Wassman, and W. Seiler, 1993: Methane production, emission and possible control measures in rice agriculture, *Advances in Atmospheric Sciences*, **10**, 307-314.

- Wang, Y., S. Filoso, L. Hess, and J. M. Melack, 1995: Understanding the radar backscattering from flooded and nonflooded Amazonian forests: results from canopy modeling, *Remote Sens. Environ.*, **54**, 324-332.
- Wong, C. S., Y.-H. Chan, J. S. Page, G. E. Smith, and R. D. Bellegay, 1993: Changes in equatorial CO₂ flux and new production estimated from CO₂ and nutrient levels in Pacific surface waters during the 1986/87 El Niño, *Tellus*, **45B**, 64-79.
- Woodruff, S. D. et al., 1993: Comprehensive Ocean-Atmosphere Data Set (COADS). Release 1a, NOAA, Washington DC.
- Yienger, J. J., and H. Levy II., 1995: Empirical model of global soil-biogenic NO_x emissions, *J. Geophys. Res.*, **100**, 11,447-11,464.

Chapter 4 Index

- agriculture 179
 AIRSAR 176
 ATBD 176
 AVHRR 171
 biomass burning 176, 181, 184
 BIOME2 175
 carbon cycle 170-177, 181-188
 carbon dioxide (CO₂) 167-173, 176, 181, 184-190
 carbon monoxide (CO) 167-168, 178-183, 187-190
 CDIAC 174
 CH₃Cl 182
 convection 169, 173, 179
 COS 190
 CR 183
 DECAFE 181
 DT 177
 ecosystem 168, 178, 187
 El Niño 173
 ENSO 173
 EOS AM 179
 ERS 171, 176-177
 evapotranspiration (ET) 188
 FAPAR 172, 181
 floodplains 177
 FTS 184
 GFDL 175
 Gross Primary Production (GPP) 173
 HH 176
 HIRDLS 187
 human health 169, 179
 humidity 188
 hydrology 169, 174, 176, 181
 IDS 170, 185
 interannual variability 173
 IPCC 170
 JERS 171, 176
 LAI 172, 181, 188-190
 land cover/land-use change 168, 170-172, 181
 LHH 176-177
 lidar 178
 MAPS 179-182
 methane (CH₄) 167-168, 181-182, 190
 MISR 172
 modeling 172, 185-190
 MODIS 168, 171-172, 184
 MOPITT 167, 179, 181-183, 187
 NDVI 172-173
 nitric oxide (NO) 177-178
 nitrous oxide (N₂O) 168, 170, 177-178
 NMHCs 178-179, 188
 NO_x 167-168, 177-179
 NPP 170, 173
 ocean carbon 169-170, 173-174
 ocean color 167, 174, 188
 OH 182-183
 OSU 175
 ozone precursors 178-181, 183
 RADARSAT 176
 reactive nitrogen 178
 SAFARI 181
 SAR 176-177
 SEDAC 174
 SMMR 177
 snow cover 177
 soil moisture 169, 176-177
 SPOT 171
 SSM/I 177
 STP 184
 sulfur 174
 surface observations 177
 Synthetic Aperture Radar (SAR) 176
 TEM 175
 TES 183, 187
 trace gases 167-168, 170, 172, 178, 182-190
 tropospheric ozone (O₃) 168-169, 178-181
 UKMO 175
 validation 174
 VEMAP 174-175
 wetlands 176-177
 WFPS 178
 wind 167, 173, 174, 181, 187-188
 wind stress 181

Land Ecosystems and Hydrology

CO-AUTHORS S. W. Running
G. J. Collatz
J. Washburne
S. Sorooshian

CONTRIBUTING AUTHORS T. Dunne
R. E. Dickinson
W. J. Shuttleworth
C. J. Vorosmarty
E. F. Wood

CHAPTER 5 CONTENTS

5.1 Introduction	201
5.1.1 Land-climate	201
5.1.2 Land-hydrology	201
5.1.3 Land-vegetation	202
5.2 Major land-surface science issues	202
5.2.1 Land-climate science issues	202
5.2.1.1 The development of land surface models (LSMs)	203
5.2.1.2 Quantifying atmospheric forcings and states	204
5.2.1.3 The role of remote sensing	204
5.2.1.4 AGCM research specifically related to EOS	205
5.2.1.4.1 How will the land surfaces' biophysical controls on the carbon, energy, and water cycles respond to and feed back on climate?	205
5.2.1.4.2 Effects of land-cover change on climate	206
5.2.1.4.3 How will biospheric responses to changing climate and atmospheric CO ₂ levels affect and feed back on atmospheric composition and climate?	208
5.2.1.4.4 How does local-scale heterogeneity in land-surface properties affect regional-to-continental climate?	209
5.2.1.4.5 How do land surface-atmospheric interactions affect weather and climate at seasonal to annual time scales?	210
5.2.2 Land-hydrology science issues	210
5.2.2.1 Quantifying and modeling hydrologic variables	211
5.2.2.1.1 Precipitation	211
5.2.2.1.2 Runoff	213
5.2.2.1.3 Evapotranspiration (ET)	213
5.2.2.1.4 Near-surface soil moisture	215
5.2.2.1.5 Infiltration and deep percolation	216
5.2.2.1.6 Radiation	216
5.2.2.1.7 Near-surface meteorology	217
5.2.2.2 Estimating and validating the land-surface water balance	218
5.2.2.3 Extreme hydrologic events	218
5.2.2.3.1 Introduction	219
5.2.2.3.2 Severe storms	219
5.2.2.3.3 Floods	220
5.2.2.3.4 Floodplains	221
5.2.2.3.5 Droughts	221
5.2.2.3.6 The causes of extreme events	221
5.2.2.4 River biogeochemistry	222
5.2.3 Land-vegetation science issues	223
5.2.3.1 The role of EOS in global change studies of vegetation	223
5.2.3.2 Land cover	223
5.2.3.2.1 Landsat and high-spatial-resolution land science	224
5.2.3.3 Vegetation structure	225
5.2.3.3.1 LAI	225
5.2.3.3.2 FPAR	226
5.2.3.3.3 Vegetation indices	226
5.2.3.4 Vegetation phenology	227
5.2.3.5 Net Primary Production (NPP)	227
5.2.3.5.1 Stem and soil carbon	229
5.2.3.6 Regional weekly application products	230
5.2.3.7 Biogeochemistry	231
5.2.3.8 Predictions of terrestrial biospheric dynamics	232
5.3 Required measurements and data sets for quantifying land-surface attributes	233
5.3.1 Introduction	233
5.3.2 EOS Sensors	233
5.3.2.1 MODIS	233
5.3.2.2 MISR	233

CHAPTER 5 CONTENTS (CONT.)

5.3.2.3	ASTER	234
5.3.2.4	Landsat 7	234
5.3.3	Ancillary data sets	235
5.3.3.1	Soils	235
5.3.3.2	Topography	235
5.3.3.3	River and flood control networks	236
5.3.4	Assimilation data sets	236
5.4	Validation programs for EOS	236
5.4.1	Responsibility hierarchy	236
5.4.2	Global organization of terrestrial observations	237
5.4.3	EOS IDS field sites	238
5.4.3.1	Arid/semi-arid: Sahel and Upper San Pedro River basins	238
5.4.3.2	Biogeochemical analysis of savanna ecosystems	238
5.4.3.3	Humid/coastal: Susquehanna River Basin Experiment (SRBEX)	238
5.4.3.4	Southern Great Plains: Arkansas/Red River basins	239
5.4.3.5	LSM parameterizations from FIFE and BOREAS campaigns	239
5.4.3.6	Tropical: Amazon	240
5.4.3.7	Global biogeochemical cycles	240
5.4.3.8	Canadian studies of carbon and hydrologic cycles	240
5.4.3.9	Cryospheric System (CRYSYS)	240
5.4.3.10	Seasonally snow-covered alpine basins	241
5.4.4	Land-vegetation science	241
5.4.5	Terrestrial validation activity	243
5.4.5.1	Tier 1 major field experiments	243
5.4.5.1.1	Past experiments	243
5.4.5.1.1.1	First ISLSCP field experiment	243
5.4.5.1.1.2	HAPEX-Sahel	243
5.4.5.1.1.3	EFEDA	244
5.4.5.1.1.4	BOREAS	244
5.4.5.1.1.5	OTTER	244
5.4.5.1.2	Opportunities from current and future experiments	244
5.4.5.1.2.1	LBA	244
5.4.5.1.2.2	GCIP	245
5.4.5.1.2.3	CART-ARM	245
5.4.5.1.2.4	CASES	245
5.4.5.1.2.5	NOPEX	245
5.4.5.2	Tier 2-3 validation monitoring for terrestrial fluxes	246
5.4.5.2.1	FLUXNET and EUROFLUX	246
5.4.5.2.2	Carbon America	247
5.4.5.2.2.1	Continuous flux measurements	247
5.4.5.2.3	TRAGNET	247
5.4.5.3	Tier 3-4 permanent ecological field station networks	248
5.4.5.3.1	NSF LTER Project, MODLERS	248
5.4.5.3.2	GLCTS: The Global Land Cover Test Site Program	249
5.4.5.3.3	IGBP terrestrial transects	249
5.4.5.3.4	The Gap Analysis Program	249
5.4.5.3.5	IGBP NPP data initiative	249
5.4.6	EOS-related land science modeling plans	251
5.4.6.1	PILPS: Project for Intercomparison of Land-surface Parameterization Schemes	251
5.4.6.2	VEMAP	251
5.4.6.3	PIK-NPP	252
	References	253
	Chapter 5 Index	258

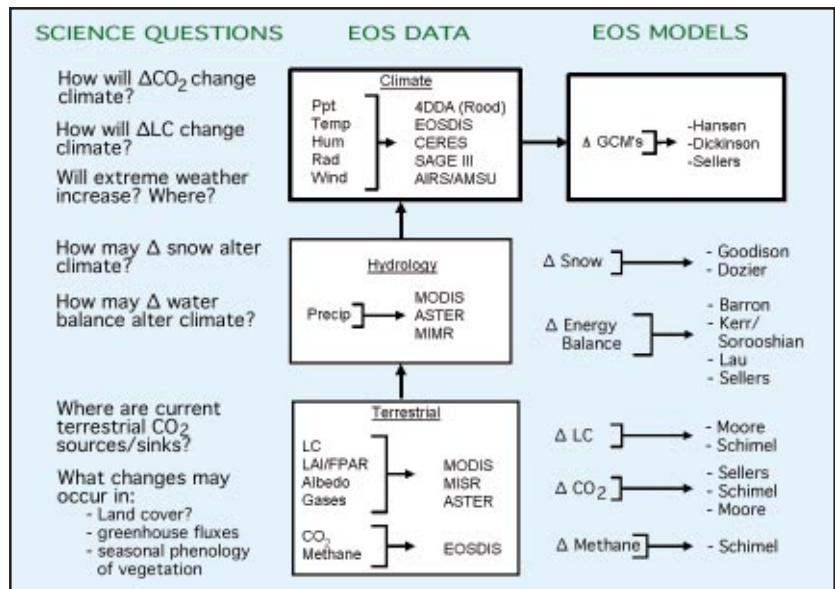
5.1 Introduction

The terrestrial biosphere is an integral component of the Earth Observing System (EOS) science objectives concerning climate change, hydrologic cycle change, and changes in terrestrial productivity. The fluxes of CO₂ and other greenhouse gases from the land surface influence the global circulation models directly, and changes in land cover change the land surface biophysical properties of energy and mass exchange. Hydrologic cycle perturbations result from terrestrially-induced climate changes, and more directly from changes in land cover acting on surface hydrologic balances. Finally, both climate and hydrology jointly control biospheric productivity, the source of food, fuel, and fiber for humankind. The role of the land system in each of these three topics is somewhat different, so this chapter is organized into the subtopics of Land-Climate, Land-Hydrology, and Land-Vegetation interactions (Figures 5.1, 5.2, and 5.3).

The magnitude of spatial and temporal heterogeneity of the global land system is extreme. The range of a simple variable like albedo can be 10-80% over different land surfaces globally, or a single location can change over this same magnitude during an annual cycle. Likewise, land covers range from deserts to rainforests globally, yet an agricultural field can change from bare soil to complete canopy coverage within two months. The EOS satellites will accurately quantify this spatial and temporal variability of critical land-surface attributes. The EOS biospheric models will then ingest these land-surface parameters and calculate important land-surface processes such as fluxes of CO₂ and H₂O, and primary productivity.

exemplified by the Biosphere-Atmosphere Transfer (BATS) model of the Dickinson Interdisciplinary Science Investigation (IDS) team and the Simple Biosphere (SiB) model of the Sellers IDS team. These and other LSP models require a suite of land-surface variables for operation in the AGCMs, including land cover, leaf-area index (LAI), roughness length, and albedo. Some of these variables change seasonally, so EOS sensors will be used to monitor the natural growing season variability of, for example, albedo and LAI. Interannual variability in climate—El Niño events for instance—feed back to cause changes in timing and magnitude of change in these vegetation variables. At decadal time scales, changes in land cover caused by natural and human disturbances may also influence aerodynamic roughness. Land-Climate models also require atmospheric data as described in Chapter 2 for forcing and validation of their AGCM components. These will be supplied by a number of EOS sensors and

FIGURE 5.1



A summary diagram of land-climate research in EOS.

5.1.1 Land-Climate

The Land-Climate interaction section deals with the fluxes of energy and mass between the atmosphere and land surfaces. The central question here for EOS is “How will changes in land-surface processes/properties interact with regional and global climate?” Specifically, this section discusses the scientific questions being addressed through the use of Land-Surface Parameterizations (LSPs) coupled to atmospheric general circulation models (AGCMs), as

the Four-Dimensional Data Assimilation (4DDA) products (see Table 5.1, pg. 207).

5.1.2 Land-Hydrology

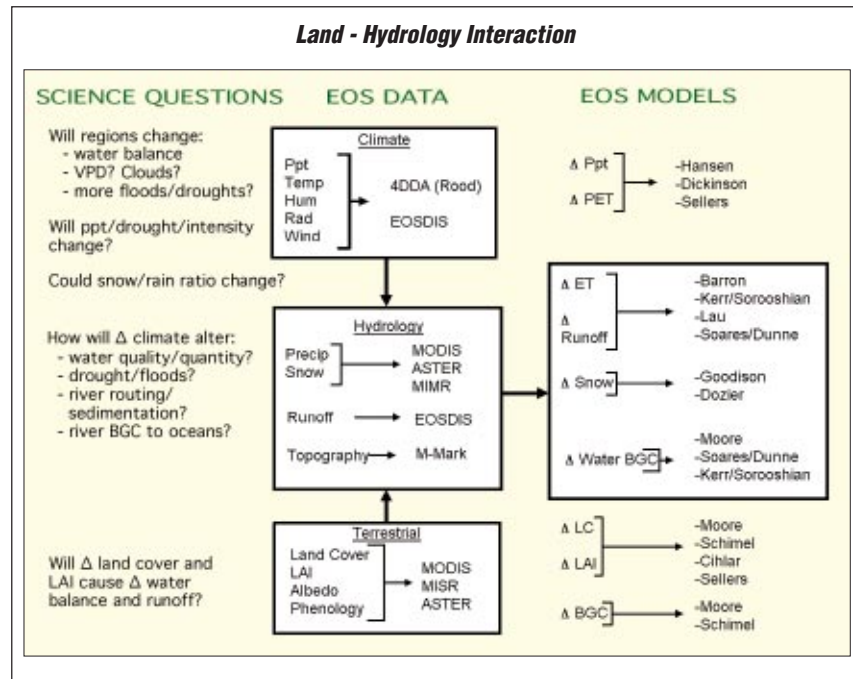
The Land-Hydrology section addresses how changing climate and land-surface characteristics may combine to change precipitation patterns, surface-water partitioning and storage, and river flows. Hydrologically-controlled

land-surface energy partitioning directly feeds back to the climate system. In addition, hydrologic extremes such as droughts and floods have severe human consequences. Terrestrial variables for hydrologic modeling are similar to those required by climate models, but topography and spatial details are more critical for defining hydrologic routing. An additional dimension of hydrologic questions relates to water quality, the land processes that change erosion, sedimentation, and river biogeochemistry—all important to human welfare.

5.1.3 Land-vegetation

The Land-vegetation section addresses responses of terrestrial vegetation at multiple time scales, from daily to decadal. At the first time scale are questions of ecosystem gas-exchange activity. What is the current global terrestrial CO₂ balance? What is the distribution and contribution of different biomes to the global CO₂ flux? Fluxes and dynamics of other greenhouse gases are covered in Chapter 4. At intermediate time scales are questions of interannual climatically-induced variability of vegetation structure and canopy density. Longer-range questions are related to how biome distribution is influenced by changing land cover and climate. Some of the most serious questions of human habitability relate to how the regional distribution and magnitude of crop, range, and forest pro-

FIGURE 5.2



A summary diagram of land-hydrology research in EOS.

ductivity will change with climate and land-use change. Clearly there are important interactions between these vegetation questions and the hydrologic extreme event questions on droughts and floods. If the mean climate changes, the geographic distribution of biomes and agricultural crops will change. EOS satellites will provide regular global monitoring of land cover, LAI, and various spectral vegetation indices that will be used in biospheric carbon balance models to answer these questions.

5.2 Major land-surface science issues

5.2.1 Land-climate science issues

In order to understand these effects we are particularly interested in the following issues related to how the climate is influenced by the land surface. These issues are developed further in Section 5.2.1.4.

- To what extent do land-surface processes affect global, continental, and regional climate?
- Is there a positive feedback between the loss or degradation of vegetation and climate?

- How do changes in radiative forcing from terrestrial greenhouse gases influence climate, and how might land-surface-atmosphere interactions be affected by increasing atmospheric CO₂?
- How do terrestrially-produced aerosols influence climate?
- How might changes in land-surface energy partitioning potentially influence climate?

- How might climate-induced changes in seasonality of surface temperature, snowpack, vegetation phenology, etc., interact with the biosphere and cause changes that feed back to the climate?
 - means
 - extremes
 - regional distribution
- How do land-surfaces characteristics influence the likelihood and severity of extreme weather events?
 - How many droughts/floods change NPP?
 - How may snow duration alter NPP?

Based on the answers to these questions, we would then like to know:

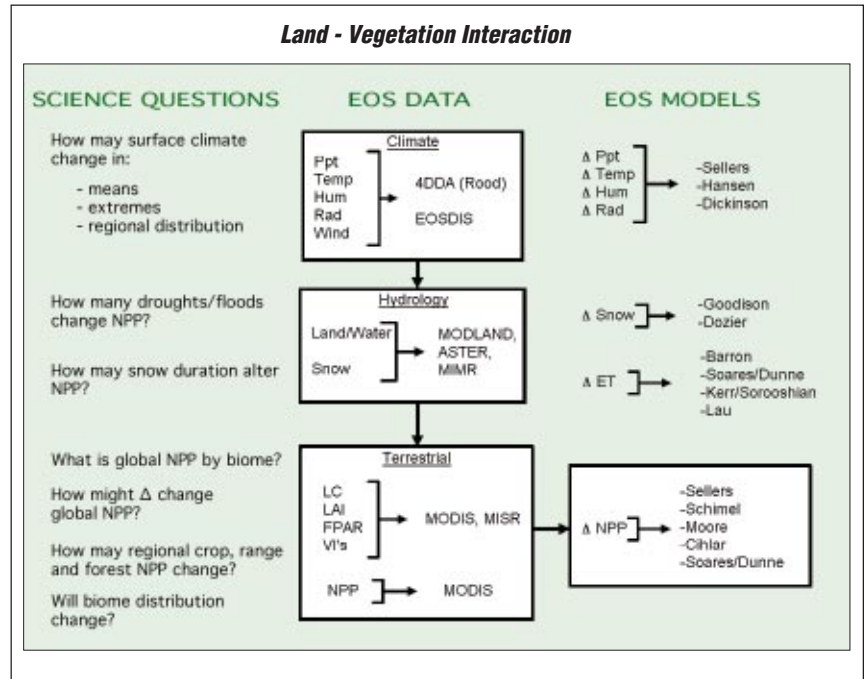
- How might changes in global climate be manifested in terms of regional climates?
- How might changes in regional climates affect agriculture and water resources?
- How might short-term weather forecasting be improved?

In addressing these issues, we recognize that changes in the Earth's climate are a natural part of its evolution; climate changes have occurred in the past and will inevitably be part of its future. However, successful predictions of such changes will enable humans to moderate the influence of climate variations on their well-being and on the well-being of the ecosystems in which they live.

A promising approach to understanding and predicting climate is the use of numerical models of atmospheric circulation. The current generation of AGCMs that are being used to study climate contain representations of land and ocean surface interactions with the atmosphere. With improved models and parameter estimates it will be possible to reduce the uncertainty surrounding the important scientific questions regarding the role of land-surface processes and climate change.

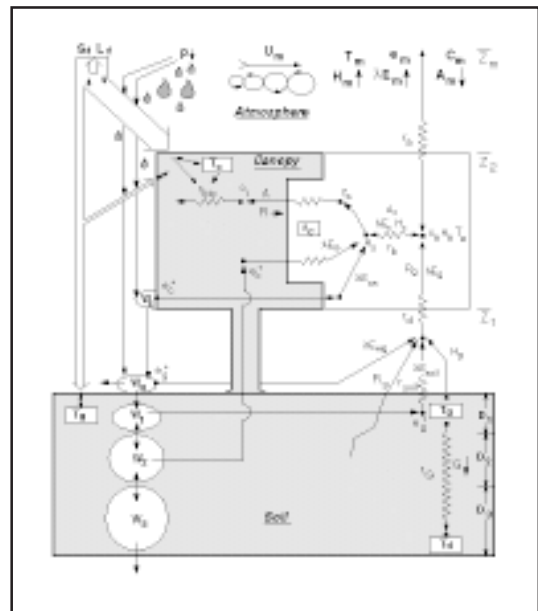
5.2.1.1 *The development of land-surface models (LSMs)*
 Evidence that land-surface processes affect climate comes largely from AGCM sensitivity studies, which have shown that a number of land-surface characteristics influence the continental and global climate; these include albedo

FIGURE 5.3



A summary diagram of land-vegetation research in EOS.

FIGURE 5.4



Schematic diagram depicting most of the processes modeled in SiB 2.

(Charney 1977), soil moisture (Shukla and Mintz 1982), roughness (Sud et al. 1988), and land-cover change (Nobre et al. 1991). Such evidence and the increasing sophistication of atmospheric models have stimulated the development of a new generation of LSMs for implemen-

tation within AGCMs (Dickinson 1984; Sellers et al. 1986; Xue et al. 1991; Thompson and Pollard 1995). These models generally contain formulations that model surface radiation fluxes, turbulent heat and mass fluxes, liquid water fluxes, and the control of water vapor and CO₂ fluxes by vegetation. An example of the structure and processes represented in a typical “state-of-the-art” LSM is illustrated in Figure 5.4 (pg. 203).

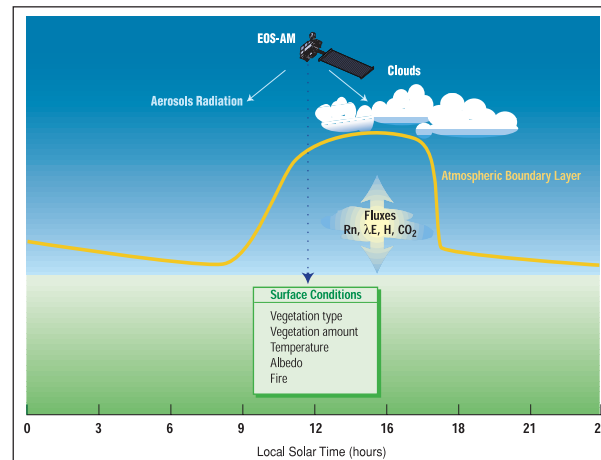
Because of factors related to the nature of atmospheric circulation as well as numerical constraints, coupled LSM-AGCMs are currently operated at short time scales (< hour) and large spatial scales (> 10,000 km²). Although long-time-scale, small-spatial-scale processes associated with ecosystem function and biogeochemistry are recognized as important in understanding and predicting climate, their implementation awaits the next generation of LSMs. Meanwhile, accurate representations of short-time-scale, surface-atmosphere interactions are crucial for improving climate predictions and for the development of integrated Earth system models in which LSMs will be the interface between long-time-scale hydrological, ecological, and geological processes, and the short-time-scale atmospheric circulation. For example, responses of ecosystem structure and function to climate and land-use change might be expressed in LSMs through changes in model parameters (LAI, land-cover type, and surface roughness).

While much progress has been made toward realistic and accurate formulation of LSMs, there is plenty of room for improvement. A recent LSM intercomparison study showed large discrepancies between the predictions made by the various models (Pitman et al. 1993), and it is not clear which formulations are better. Consensus on how LSMs should be formulated and parameterized awaits further testing using local and regional observations.

5.2.1.2 Quantifying atmospheric forcings and states

Land-surface processes are, in large part, controlled by water and energy exchanges with the atmosphere. For many studies these exchanges can be measured, but for comprehensive models used to study and predict changes, they must be determined as part of the model. Perhaps the most important of these exchanges are the temporal and spatial fields of precipitation and surface radiation (Figure 5.5). Unfortunately, these exchanges are also poorly represented in current models as indicated by comparisons between observations and model predictions. For example, radiation is in large part controlled by clouds, which remain a weak element of climate models, and precipitation depends substantially on processes at smaller spatial scales than those resolved by the models. Also important are the near-surface meteorological fields; in par-

FIGURE 5.5



AM-1 Platform diagram showing types of measurements made from the EOS AM-1 satellite platform that will contribute to parameterization and testing of land-surface models. Note that the morning equatorial overpass will improve measurements of surface conditions by avoiding interference from afternoon convective clouds.

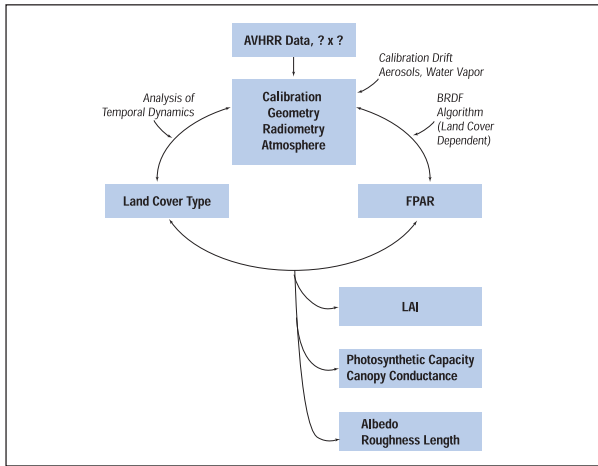
ticular, winds, temperature, and humidity, which are largely determined from parameters related to the land surface (soil moisture and temperature) and the overlying atmosphere.

Improved quantification of these exchanges depends on progress being made in the areas of data assimilation, model parameterization, and model validation. Current procedures for 4DDA do not make use of observations of precipitation and surface radiation, nor do they use observations of near-surface meteorological fields. These fields are constructed internally by the models, and can be seriously in error. One recent exception is the use by the European Centre for Medium-Range Weather Forecasts (ECMWF) of near-surface humidity observations to nudge soil moisture to improve the match between modeled and observed humidities (Viterbo and Beljaars 1995). Further improvements in data assimilation should not be long coming; the World Climate Research Program (WCRP) Surface Radiation Budget (SRB) project has demonstrated how satellite data can be used to provide surface solar radiation, and rapid advances are being made in developing comprehensive observations of precipitation from combinations of surface and satellite observations. EOS cloud, radiation, humidity, and temperature profiles products (see Chapter 2) will provide data needed to validate atmospheric components of climate models as well as that needed for initialization/assimilation.

5.2.1.3 The role of remote sensing

LSM development is constrained to a large extent by the availability of data required to initialize, parameterize,

FIGURE 5.6



Vegetation algorithm diagram representing an approach to specify vegetation type and characteristics using currently-available satellite data. Satellite-derived surface attributes are used to parameterize land-surface models used in global climate simulations.

and test the models. The most promising approach to obtaining these data is the development of algorithms to predict the state of the land surface and the atmosphere from remote-sensing platforms. Intensive, multi-scale field studies such as the First International Satellite Land Surface Climatology Project (ISLSCP) Field Experiment (FIFE), the Hydrological-Atmospheric Pilot Experiment (HAPEX), and the Boreal Ecosystems Atmosphere Study (BOREAS) are examples of such efforts. Satellite observations are the most practical means of supplying LSMs with parameters and validation data (see Figure 5.6) at continental and global scales. EOS instruments will play an important role in this effort by providing high-quality remote-sensing data to complement ground-based observations during the EOS era. Many instrument and IDS teams plan to play major roles in the development and maintenance of several long-term validation/calibration sites.

5.2.1.4 AGCM research specifically related to EOS

The first science question addressed below—that of how land surfaces interact with climate—is related to the others that follow. Better understanding of land-atmosphere feedbacks will provide answers to questions regarding the climatic implications of land-use change, of atmospheric composition, and of land-surface heterogeneity. Work on these and other related questions will in turn further our understanding of land-atmosphere feedbacks. Improvements in land-surface-atmosphere models will produce practical benefits such as better predictions of weather, climate, and biospheric productivity. The EOS program was designed to fill critical gaps in our knowledge in the

land-surface climate system by supplying data that only satellites can provide.

5.2.1.4.1 How will the land surfaces' biophysical controls on the carbon, energy, and water cycles respond to, and feed back on, climate?

There is mounting evidence for the important role of land-atmosphere interaction in determining regional, continental, and global climate. Progress towards accurately forecasting climate from seasons to decades to centuries will depend in part on improving the representation of land surfaces in climate models. The fluxes of energy, mass, and momentum from land surfaces adjust to and alter the state of the atmosphere in contact with land, allowing the potential for feedback at several time and spatial scales. Earlier climate sensitivity simulations in which land-surface properties (such as albedo [Charney et al. 1977], soil moisture [Shukla and Mintz 1982], roughness [Sud et al. 1988]) were changed for the entire Earth showed significant climate alterations. More recently, Bonan et al. (1992), Nobre et al. (1991), and others have shown that continental-scale modifications representing dramatic change in vegetation type cause significant changes in simulated continental-scale climate. Avissar (1995) reviews examples of model and observational evidence showing that regional-scale precipitation patterns are affected by land-surface features such as discontinuities in vegetation type. In some cases positive feedback has been observed between large-scale precipitation patterns and land surface, resulting in the extension of drought or wet periods (Entekhabi 1995). Another example of land-surface atmosphere interaction is the measurable seasonal cycle in trace gases composition of the atmosphere over the Northern Hemisphere that results from the seasonality in the physiological activity of the biosphere, which in turn is controlled by climate (Keeling and Heiman 1986).

Because of this high degree of interaction between land-surface processes and climate, a useful way to study and predict the outcome of feedback is to use an LSM coupled to an AGCM. Several biophysical LSMs have been developed and implemented in AGCMs (Dickinson 1984; Sellers et al. 1986; Bonan 1995; Sellers et al. 1996) for studying surface-climate interactions. LSMs are necessarily simplistic because of: 1) limited knowledge of how relevant processes work, 2) computational constraints, and 3) lack of continuous temporal and spatial information required to characterize the state of the land-surface-atmosphere system. All three limitations are the focus of current research activity.

LSMs have improved in large part due to the increasing availability of observations necessary for

development and testing. Several intensive regional-scale field campaigns have been launched over the last 10 years such as FIFE, HAPEX-Sahel, and BOREAS that were designed to develop and test LSM and remote-sensing models. During these campaigns, teams of scientists observe the state of various components responsible for the energy and CO₂ fluxes from the surface. Models developed and tested using remote sensing from aircraft and satellites provide a way to extend the insights gained to similar ecosystems elsewhere.

The limited number and scale (time and space) of these observational campaigns present a problem for parameterizing and validating global climate models. Long-term measurements of canopy fluxes of energy and carbon such as those pioneered by Wofsy et al. (1993) help to bridge the gap between the time scales of atmospheric turbulence and climate. Two spatial-scale issues are more difficult to resolve: the differences in spatial scale between the sampling footprint of an eddy flux tower (m to km) and the typical AGCM grid cell (100s of km) and, related to this, the small number of measuring sites relative to total global land surface. Satellite observations are the most plausible way of providing continuous global measurements of the state of the land surface and atmosphere (Running et al. 1994; Sellers et al. 1995; Nemani and Running 1995).

EOS contribution: In the pre-EOS era, satellite data largely from the National Oceanic and Atmospheric Administration (NOAA) weather satellites are used to provide global estimates of land-surface conditions for use in land-climate models (Figure 5.6). Specifically the visible, near-infrared, and thermal channels on the Advanced Very High Resolution Radiometer (AVHRR) instrument are being processed into global fields of model parameters and are surrogates for much-improved EOS products to come. The Moderate-Resolution Imaging Spectroradiometer (MODIS) instrument, for instance, has greater spectral resolution, greater number of spectral bands, higher spatial resolution, better viewing time, better calibration, and will make coincident measurements with other instruments on a common platform—characteristics that make it far superior for parameterizing LSMs than existing satellite instruments.

The Sellers IDS Team (Sellers et al. 1996) has processed AVHRR data into seasonally-varying land-surface characteristics needed by LSMs, such as fraction of incident radiation absorbed by vegetation (FPAR), LAI, and surface aerodynamic roughness. They have initially released two years (1987 and 1988) of this data to the Earth scientific community (Figure 5.6). The Dickinson IDS Team is also using existing remote-sensing data in anticipation of the improved EOS instruments (MODIS and

the Multiangle Image Scanning Radiometer [MISR]) to specify vegetation class, structure, and composition in their LSM. The Lau IDS Team is developing continental-scale models that they hope to force and validate using MODIS products (land-surface characteristics, clouds, and surface temperatures) and Multi-frequency Imaging Microwave Radiometer (MIMR)/Advanced Microwave Scanning Radiometer (AMSR) products (atmospheric water, soil water, and precipitation). The Barron IDS Team is likewise using current satellite data (from AVHRR and Landsat) to model atmosphere/hydrology interactions on a regional scale and plans to ultimately use EOS products. Besides providing important model parameters EOS instruments will also measure the state of the atmosphere (temperature, humidity, clouds, radiation, and wind speed) (Table 5.1 and Figure 5.5). These data in conjunction with the 4-D data assimilation products that are to be produced by the Goddard Data Assimilation Office (DAO) will be used to provide atmospheric modelers including all IDS teams involved with land-atmosphere interactions (Lau, Barron, Hansen, Dickinson, Sellers) with data to initialize and test their models. Simultaneous and continuous global measurements of climate-state variables from EOS satellites will provide unprecedented opportunities for evaluating the performance of climate models (Sellers et al. 1995; Nemani and Running 1995).

5.2.1.4.2 Effects of land-cover change on climate

Both natural (floods, fires, volcanoes, solar output, etc.) and human (deforestation, overgrazing, and pollution) influence are known to cause massive changes in the vegetation cover. Imhoff (1994) estimated that 15% of the global forests have been converted to agriculture. Drastic changes in land-surface properties, such as occur due to deforestation or desertification, are likely to have climatic consequences. Satellites are currently providing better estimates of land-surface change than can be obtained by any other method. For instance, Skole and Tucker (1993) using Landsat data were able to improve estimates of deforestation and forest fragmentation in the Amazon Basin. When these estimates were used to parameterize an LSM-general circulation model (GCM), significant decreases in simulated precipitation over the region occurred (Walker et al. 1995). Extensive disturbance of vegetation cover will change the way the land surface interacts with the atmosphere. For example, Bougeault et al. (1991) were able to model, and confirm with observations, the influence of forest-crop boundary on cloud and precipitation patterns. Discontinuities in landscape patterns, as occur when forests are cleared, can affect when clouds form and the amount and distribution of rainfall (Avissar and Chen 1993). Nemani and Run-

ning (1995) have published the first consistent satellite-derived estimate of global land-cover change (Figure 5.7, pg. 208).

Modeling studies have been performed for land-cover changes at continental scales using GCMs. Notable examples include several Amazon deforestation simulations which showed the deterioration of the regional climate caused by deforestation (Nobre et al. 1991; Dickinson and Kennedy 1992; and Henderson-Sellers et al. 1993). Bonan et al. (1992) used an LSM-GCM to examine the impact of the boreal forests on climate. They found that the lower albedo caused by the presence of the

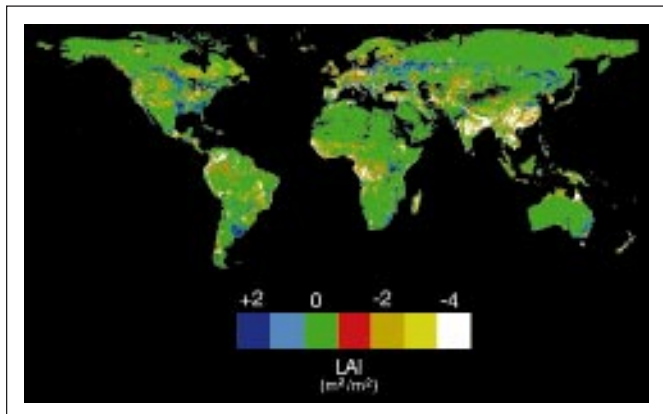
forest caused the boreal climate to be warmer all year round compared to the case in which the forests were converted to tundra. The altered climate simulated by these deforestation experiments is large enough to feed back on the land and alter the recovery response. The ability to simulate vegetation responses in a fully-coupled way with a GCM is yet to be achieved. Initial work has shown that feedbacks between climate and vegetation result in different vegetation and climate distributions from those predicted without considering feedback (Henderson-Sellers and McGuffie 1995).

TABLE 5.1

<i>INSTRUMENT</i>	<i>PRODUCTS</i>	<i>USES</i>
ASTER	Land-surface temperature, snow, cover, cloud characteristics, albedo Visible and near-IR bands, elevation, albedo	forcing parameterization validation
CERES	Albedo, radiation fluxes, precipitable water, cloud forcing characteristics, surface temperature, aerosols, temperature, humidity, and pressure profiles albedo	forcing parameterization validation
MIMR	Precipitation, snow cover, soil moisture albedo, cloud fraction, aerosols, soil moisture, BRDF	forcing parameterization validation
MODIS	Temperature and water-vapor profiles, cloud cover, albedo, surface temperature, snow cover, aerosols, surface resistance/ evapotranspiration, land-cover-classification, vegetation indices, BRDF	parameterization validation
SAGE III	Cloud height, H ₂ O concentration and mixing ratio, temperature and pressure profiles	validation
TRMM	Rainfall profile, surface precipitation (PR,TMI,VIRS)	forcing, validation
Other	4D data assimilation including wind, temperature, and humidity profiles; momentum, energy and precipitation fluxes	forcing, validation

Listing of EOS instruments and products and how they will be used by land-surface climate models.

FIGURE 5.7



Human-induced changes in global land cover estimated by comparing AVHRR NDVI data, expressed as leaf-area index, with potential leaf index computed from long-term climatological data and hydrologic-vegetation equilibrium theory (Nemani et al. 1996).

Severe disturbance of vegetation cover sometimes results in an increase in atmospheric aerosols. The reductions in the surface solar radiation and the heating of the atmosphere as a result of aerosols are expected to alter atmospheric and land-surface processes. The process of deforestation often involves burning of biomass, which may cause significant reductions in the solar radiation incident on the surface (Penner et al. 1992). Disturbance, both natural and human, can lead to soil erosion and increased dust loading of the atmosphere. Using atmospheric transport model and satellite data Tegen et al. (1996) predict that around 50% of the total atmospheric dust is derived from land-surface disturbance. The alterations in the radiation reaching the Earth's surface and the heating of the atmosphere are likely to have climatic impacts that could feed back on land-surface properties and, therefore, must be taken into account when considering the impacts of land-cover change on climate.

EOS contribution: EOS instruments have been designed to measure the nature and extent of changes in land cover. MODIS, for instance, will produce calibrated and corrected global vegetation-cover data at 250-m resolution for over a decade. In particular, vegetation indices and surface radiative temperature will be used to diagnose land-cover change from MODIS data in a similar manner to the analysis Nemani and Running (1995) have done with AVHRR data in Figure 5.7. Sellers IDS team members are measuring deforestation using AVHRR and Landsat data. They are currently prescribing observed interannual variability in vegetation cover in their LSM-GCM to estimate the climatic impacts of such changes. MODIS products will provide better quality data (calibration, atmospheric corrections), higher spatial reso-

lution, and, in the tropics, less cloud contamination (EOS AM-1 series) than current satellite data. MISR products will be used to observe changes in the three-dimensional structure of vegetation cover. The improved quality of EOS data will provide more-realistic estimates of land-cover disturbance for climate sensitivity studies and will support the development of models that predict land-cover change in response to climate change and human activities. Barron, Dickinson, Hansen, Lau, and Sellers IDS teams all have plans to evaluate the impact of land-cover changes on climate using MODIS products as inputs to their LSM-GCMs.

Several EOS instruments (Earth Observing Scanning Polarimeter [EOSP], MODIS, MISR, High Resolution Dynamics Limb Sounder [HIRDLS], Stratospheric Aerosol and Gas Experiment III (SAGE III), and ESA's Polarization and Directionality of the Earth's Reflectance [POLDER]) will provide aerosol estimates which will be useful for land-surface climate studies because of two elements: the impact of aerosols on climate as recently observed in the case of the 1991 eruption of Mt. Pinatubo (McCormick et al. 1995), and, since aerosols interfere with other EOS measurements, accurate estimation will permit better aerosol corrections. Hansen and Sellers IDS teams are currently exploring the impacts of land-cover changes on atmospheric dust and climate using remote-sensing products and GCMs. EOS aerosol products will allow better quantification of the climatic impacts of dust generated from land-cover change.

Fire that causes changes in land cover will be monitored by MODIS. Hansen's team has developed a lightning parameterization for their GCM that can be used to predict lightning-caused fires. MODIS will provide observations of global fire-occurrence data, and the Lightning Imaging Sensor (LIS) (Tropical Rainfall Measuring Mission-1 [TRMM-1]) will supply direct measurements of lightning, both of which will contribute to model validation and further development.

5.2.1.4.3 How will biospheric responses to changing climate and atmospheric CO₂ levels affect and feed back on atmospheric composition and climate?

There are two issues addressed here that are associated with atmospheric composition and land-surface processes: 1) The interaction between the biosphere and atmospheric CO₂ composition, and 2) the interaction between land surface and climate in response to increasing atmospheric CO₂. Land surfaces play an important role in the composition of the atmosphere. Various nitrogen compounds, methane, CO₂, and plant secondary products exchange

between the atmosphere and land. For instance, biological processes occurring on land surfaces significantly affect the CO₂ concentration in the atmosphere. The amount of carbon in the terrestrial biosphere is almost three times greater than in the atmosphere, and on an annual basis about 20% of the atmospheric carbon is removed by photosynthesis and returned through respiration. Anthropogenic CO₂ emissions on the other hand are less than 5% of the photosynthetic flux. Alterations in the balance between photosynthesis and respiration causing changes in the size of the biospheric carbon stores will have dramatic effects on the CO₂ concentration of the atmosphere and, as a result, on the climate.

The seasonal and spatial patterns in the atmospheric CO₂ concentration and its isotopic composition imply that the Northern Hemisphere land surfaces are currently acting as a CO₂ sink (see Figure 5.11 on pg. 220 and Ciais et al. 1995; Tans et al. 1990). These and other studies show that almost a quarter of the anthropogenic CO₂ release is taken up by the terrestrial biosphere causing the atmospheric CO₂ to rise more slowly than predicted by human activities alone. The specific locations and the nature of this biospheric sink are yet to be determined and are the focus of continued research because of the importance of the CO₂ balance of the atmosphere on climate. If in the future the biosphere changes from a net sink for CO₂ to a net source, atmospheric CO₂ will rise much faster than the current rate, possibly leading to faster and greater climate change.

Local-scale experimental studies continue to show that biospheric processes controlling CO₂ and water vapor exchange often respond directly to the atmospheric levels of CO₂. These results imply that, as global atmospheric CO₂ concentrations continue to increase as a result of human activities, the behavior of land surfaces will change due both to the climate change associated with increased radiative forcing and to direct response of the biosphere to CO₂. This opens the possibility for complicated feed-back interaction between the biosphere and climate. The elevated CO₂ scenario has been well studied using GCMs, but only recently have LSMs attempted to incorporate plausible biospheric responses to CO₂. Sellers et al. (1996) have used such an LSM coupled to a GCM for a series of 2 × CO₂ scenarios and observed that biospheric responses to CO₂ cause changes in continental climates that are of similar magnitude to CO₂ radiative forcing effects and continental deforestation effects.

EOS contribution: The Sellers IDS team has committed much effort to developing an LSM with realistic representation of physiological control of CO₂ and water vapor fluxes from the biosphere. Two important findings to date have come from this work. First, the covariance

of the height of the atmospheric boundary layer and photosynthetic activity of the vegetation both diurnally and seasonally has important consequences for the prediction of spatial and temporal variations in atmospheric CO₂ (Denning et al. 1995). Second, the direct response of vegetation to increased atmospheric CO₂ may lead to decreases in evapotranspiration (ET) and to further surface heating beyond that caused by CO₂ radiative forcing effects alone (Sellers et al. 1996). The Sellers and Hansen IDS team members are attempting to predict the location and strength of CO₂ sinks and sources using atmospheric models together with the observed atmospheric CO₂ signal and satellite-derived measurements of vegetation cover. EOS-era land-cover products such as those associated with biospheric productivity will be used by these teams and others in conjunction with ground-based atmospheric composition data and models to identify and monitor feedback between the biosphere and atmospheric composition at regional-to-global scales.

5.2.1.4.4 How does local-scale heterogeneity in land-surface properties affect regional-to-continental climate?

Variations in the properties of vegetation and soil that affect energy and mass exchange between the land surface and the atmosphere are often measured at spatial scales of less than a meter and operate on temporal scales from less than an hour to centuries. Computational constraints as well as the lack of high-spatial-resolution global data sets limit running climate models at resolutions necessary to explicitly include fine-scale heterogeneity. The issue of spatial heterogeneity involves many aspects of model operation. Data required to initialize, force, and validate LSMs such as meteorological conditions, the parameters required by the model to characterize the land surface, and the measured fluxes are generally obtained at individual points. Climate models, on the other hand, predict regionally-averaged forcing and fluxes and require regionally-averaged parameters. Intensive field experiments such as HAPEX, FIFE, and BOREAS were designed to learn how local forcing, model parameters, and surface fluxes can be integrated up to the region.

Mesoscale atmospheric models have been used to study the impacts of surface heterogeneity on atmospheric circulation. Model and observational results show that atmospheric circulation is sensitive to the length scale of the surface patches (Avissar 1995). Model parameters associated with vegetation cover are some of the most important and most variable of those needed by LSMs (Bonan et al. 1993; Li and Avissar 1994). Vegetation cover can be measured by remote sensing of leaves, canopies, and the landscape using sensors that are hand held or mounted to towers, aircraft, and satellites, each level rep-

representing an integration of lower-scale levels of heterogeneity. Recent work has confirmed the applicability of coarse-scale satellite observation as an integrator of heterogeneity as in the amount of solar radiation absorbed by vegetation (Hall et al. 1992). Other encouraging results indicate that it should be possible to scale up from point data to the climate model grid cell using relatively simple rules based on theoretical and observational information (Noilhan and Lacarrere 1995; Sellers et al. 1995), although scaling of soil moisture and mesoscale atmospheric circulation remain problematic.

EOS contributions: Various strategies for dealing with subgrid-scale heterogeneity in global climate models are being pursued by EOS IDS teams (Barron, Lau, Dickinson, Hansen, and Sellers). In particular, Dickinson's team is studying the extent to which surface heterogeneity can affect local circulation systems that produce summer convective precipitation. The Sellers team is testing various techniques of aggregating condition and fluxes using multi-scale data obtained during FIFE and BOREAS. Some important processes controlling the interaction between land and the atmosphere have been shown to be scale-invariant and measurable with spatially-coarse satellite observations.

Certainly, an important step towards resolving issues of heterogeneity is to measure it. Several EOS instruments will provide regional and global products that will measure heterogeneity at various relevant scales. Examples include MODIS and MISR global products at 1 km or less, and the Advanced Spaceborne Thermal Emission and Reflection Radiometer (ASTER) and the Enhanced Thematic Mapper Plus (ETM+) at less than 100-m horizontal resolution. EOS measurements of parameters (vegetation type, FPAR, etc.) and state variables (such as surface temperature, clouds, etc.) at different scales will provide the information that is critically needed to address the questions of accounting for sub-grid-scale heterogeneity in climate models.

5.2.1.4.5 How do land surface-atmospheric interactions affect weather and climate at seasonal-to-annual time scales?

Improved climate forecasts have obvious economic and human welfare benefits. Agriculture and water resource planning are currently limited by currently unpredictable meteorological conditions. With better long-term forecasts mitigation strategies can be implemented far enough ahead to reduce the impact of extreme weather events. Improvement in modeling land-surface atmosphere interactions contributes not only to better long-term climate predictions, but also to better weather prediction at shorter time scales of weeks to years. Much progress has been made in extending weather forecasts with numerical models as

shown by the improved ability to predict the occurrence and intensity of El Niño events. Short-term weather forecasts (days) are more dependent on initialization and less on interaction with land surfaces. But, as forecasts extend to weeks, months, and longer, land-surface processes are expected to play a greater role, and realistic representations of land-surface processes are needed to improve these forecasts. The influence of land-surface cover on cloudiness and precipitation patterns (Avissar 1995) and the feedbacks between soil moisture and precipitation (Entekhabi 1995) are examples of how land-surface processes control weather. Recognizing the importance of land-atmosphere interactions, weather forecasting organizations (the National Aeronautics and Space Administration [NASA]-DAO, National Meteorological Center [NMC], and ECMWF) are currently working on upgrading their LSPs. Large-scale field experiments play an important role in the development of improved LSM formulations. For instance, as a result of analysis of data collected during FIFE, the soil parameterization in the ECMWF model has been improved, resulting in improved weather predictions for the central U.S. (Viterbo and Beljaars 1995). Application of remote-sensing data to parameterization and initialization of weather forecasting models is likely to greatly improve forecasting skill. Satellites can estimate state variables over land that are not available as yet globally at high-enough resolution from ground observations (precipitation, radiation, and biophysical characteristics).

EOS contributions: The availability of high-spatial-and-temporal-resolution surface and atmosphere conditions from EOS sensors will present unique opportunities for parameterization and initialization of weather forecasting models especially over land. EOS instruments will measure a number of important meteorological state variables globally at daily frequencies. Surface and top-of-the-atmosphere conditions will be supplied by MODIS, MISR, AMSR-E, and the Clouds and the Earth's Radiant Energy System (CERES). HIRDLS, SAGE III, the Atmospheric Infrared Sounder (AIRS)/Advanced Microwave Sounding Unit (AMSU)/HSB, and the Tropospheric Emission Spectrometer (TES) will provide profiles of atmospheric conditions above land surfaces. The combination of improved model formulations and assimilation of EOS data products should lead to important practical benefits associated with more-accurate longer range predictions of weather.

5.2.2 Land-hydrology science issues

Hydrologic processes must be understood within a space-time continuum (Figure 5.8), which separates natural linkages between scale and hydrologic response. While

our understanding of global hydrology will only be complete when we understand, can observe, and model hydrologic phenomena from the micro-scale to the global-scale, most land-surface hydrologic phenomena of interest in assessing impacts on humankind are below the GCM and synoptic scales, which have received the greatest scientific investigation to date. The challenge to EOS scientists is to strive to improve our hydrologic understanding at these critical human scales. Section 5.2.1.1 introduced LSMs in the context of land-climate issues and some ways EOS can contribute to their improvement. One important difference between that section and this one is that land-surface hydrology is mainly concerned with processes and events at smaller scales.

Key land-hydrology science issues of interest, particularly in the context of EOS are:

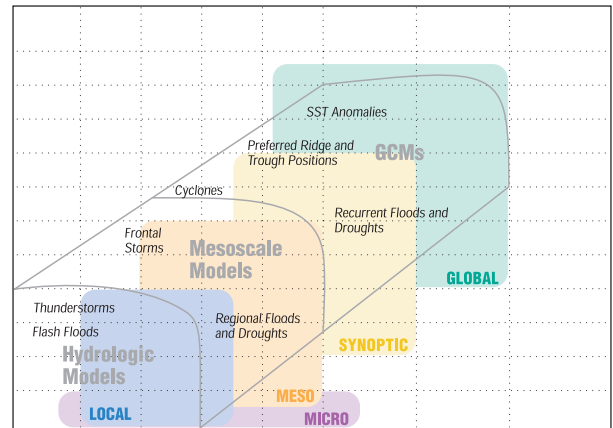
- a) the identification and quantification of key hydrologic variables across a range of scales, and
- b) the development or modification of hydrologic process models to take advantage of operational and realistic data sources.

EOS data and systems present many new opportunities for evaluating global and regional water balances on a regular and objective basis. The wide variety of previously unattainable and potentially useful data that will become available over the next decade is likely to result in significant improvements in the understanding of land-surface hydrology. However, unlike parameters described in many other sections of this report, hydrologic fluxes are not directly observable from space. Thus, another challenge to EOS scientists is to learn how to estimate these fluxes through a combination of satellite, ground, and model data. So far, the only major components of the hydrologic cycle that are estimated operationally using remotely-sensed data are precipitation (indirectly) and snow cover (directly).

The following section will address the two key science issues outlined above. This will be done by concentrating on the most important hydrologic variables and what we stand to learn from them over the next decade. Later sections will discuss the importance of estimating and validating the land-surface water balance, the significance of extreme events to hydrologic analysis, and river biogeochemistry.

5.2.2.1 Quantifying and modeling hydrologic variables
 How are the key hydrologic variables distributed in space and time? How will EOS data be used to derive these variables?

FIGURE 5.8



Space-time scales of interest in hydrology (Hirshboeck 1988).

The global hydrologic cycle is illustrated in Figure 5.9 (pg. 212), showing the importance of moisture transport from the oceans to the land with surface runoff and ET completing the cycle (Lau IDS homepage 1996). The continental water balance is augmented by a 36% surplus of precipitation over ET as a result of this advection. While this aspect of the general circulation is reproducible in the current generation of GCMs (Shaikh 1996), the details of how and where the land surface redistributes this excess remain to be worked out (Avissar 1995).

The primary components of the water balance at the land surface are precipitation, runoff, ET, soil-water, and ground-water storage. An energy balance is often used to derive ET from radiation, near-surface meteorology, and surface temperature. Although each of these components is closely tied to the others, they will be reviewed separately below.

5.2.2.1.1 Precipitation

How is precipitation distributed in time and space?

Importance: Precipitation is the sole mechanism by which water enters the land surface system. While rainfall is the primary form of precipitation in many regions of the world, some regions receive more than half of their precipitation in the form of winter snowfall, which significantly affects energy and mass transfers between the land surface and the atmosphere. Time delays between precipitation events and the redistribution of that water to rivers, the subsurface, and back into the atmosphere are drastically altered as well. To assess, forecast, and predict hydrologic responses, it is important to understand how the amount, rate, duration, and purity of precipitation are distributed in space and time. Such knowledge is also key to improving the specificity, accuracy, and reli-

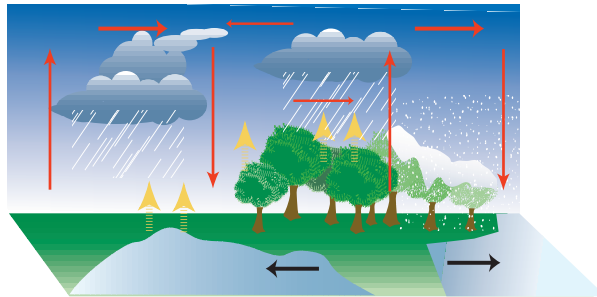
ability of weather/climate forecasts. Precipitation climatology may come to be considered as important as are temperature anomalies in the current debate about climate change and its impact on critical human infrastructures because of those systems' sensitivity to rapid change (Shuttleworth 1996).

There are significant physical contrasts between snow- and non-snow-covered areas, but an assessment of snow properties (such as snow water equivalent [SWE] and depth) is difficult to achieve in topographically rough terrain where typical patch-length scales may be on the order of 100 m. Nonetheless, satellites have and will continue to play a significant role in the real-time monitoring of many cryospheric parameters. The frequency of abnormal weather patterns coupled with the volatility of the spring snow pack make cryospheric variables a sensitive and critical parameter in the context of hydrologic science. More details of cryospheric factors that influence the hydrological cycle can be found in Chapter 6.

Current capabilities: Until recently, data regarding rainfall and snow accumulation were obtained primarily using networks of rain gauges and snow courses. Advanced ground-based radar systems, such as the Next Generation Weather Radar (NEXRAD) Weather Surveillance Radar (WSR)-88D in the U.S. (Crum et al. 1993), now represent the state of the art in precipitation measurement, and techniques for compositing the radar data with ground-level gauge data are under development. These techniques still need improvement (Smith et al. 1996), particularly in mountainous terrains. Outside of the most-developed countries, existing and projected gauge and ground-based radar networks are unable to provide adequate coverage. For this reason satellite methods hold great promise.

EOS capabilities: Remote sensing of precipitation is a key component of Earth Science Enterprise missions such as TRMM and EOS PM-1. Several EOS sensors such as TRMM Microwave Imager (TMI), Visible Infrared Scanner (VIRS), Precipitation Radar (PR), AMSU, and AMSR have been specifically designed for the collection of data relating to precipitation and clouds. The TRMM mission, launched in 1997 and conducted in cooperation with Japan, measures the diurnal variation of precipitation in the tropics. Precipitation is measured at a spatial scale of 4.3 km using a PR (13.8 GHz) between $\pm 30^\circ\text{N}$ (220-km swath) and a 5-channel TMI (10-91 GHz, dual polarization) between $\pm 38^\circ\text{N}$ (760-km swath). Further, a 5-channel visible/infrared imaging radiometer (VIRS) provides data at a nominal 2-km resolution at nadir and 1500-km swath. The mission is expected to provide at least three years of rainfall and climatological observations for the tropics. These unique data sets will facilitate

FIGURE 5.9



A schematic diagram of components of the global hydrologic cycle.

detailed studies of the rainfall climatology in areas dominated by the Inter-Tropical Convergence Zone (ITCZ), continental monsoons, hurricanes, and the El Niño-Southern Oscillation (ENSO) cycle. In addition, because these data will be collected simultaneously with multiple sensors they will facilitate analyses of sensor capabilities leading to improvements in the rainfall estimation techniques that employ data from the geosynchronous Special Sensor Microwave/Imager (SSM/I), the Geostationary Operational Environmental Satellite (GOES), and the NOAA series of satellites.

The EOS PM-1 mission is expected to be equipped with an AIRS (infrared sounder) and two microwave sounders (AMSU and HSB). These three instruments will, together, provide information regarding precipitation volumes, cloud thickness, and cloud water content.

IDS team contributions: Because precipitation combines and interacts with the landscape, topography, land use, and soil moisture with great variability, synoptic and climatological-scale precipitation is of little use in predicting the hydrologic response of the land. Local inferences cannot safely be drawn from regional precipitation climatologies and data sets, regardless of the methods used to build these data sets. Therefore, a top priority of several IDS teams is to investigate methods of distributing observed rainfall in both time and space.

The IDS team led by Kerr and Sorooshian has contributed to this by successfully using historical rainfall climatologies and land-surface topography to distribute subgrid-scale precipitation (Gao and Sorooshian 1994). The IDS team led by Lau is participating in rainfall algorithm development in conjunction with the TRMM mission, using both single and combined satellite sensors. The three IDS teams, led respectively by Barron, Brewer, and Dickinson, will be using the precipitation estimates provided by AMSR and AIRS/AMSU in their modeling studies. The IDS team led by Dozier has been working on estimating snow cover (Rosenthal and Dozier 1996) and

SWE (Shi and Dozier 1995) from remote-sensing data provided by Landsat, Airborne Visible-Infrared Imaging Spectrometer (AVIRIS), and Synthetic Aperture Radar (SAR); they will extend these techniques for subpixel snow mapping using MODIS and ASTER data. Several IDS teams have proposed new land validation sites in Oklahoma (Lau/Wood) and Arizona (Dickinson/Sorooshian). Further details of EOS cloud and precipitation research can be found in Chapter 2.

One area where satellite data will make a strong impact is in our ability to follow and analyze regional trends and patterns in the spatially-distributed precipitation field. How to effectively make use of these patterns is less certain although observed climatologies are likely to replace historical rainfall climatologies in the studies cited above. Another approach to disaggregation is to use climate statistics (Gong et al. 1994). The process preserves subgrid moments but is valid only for average behavior (rather than event-based behavior) and loses relevance under non-stationary (climate change) conditions. Researchers at Pennsylvania State University (PSU) are using neural nets to derive transfer functions from larger-scale circulations to local precipitation based on a 5-year data assimilation effort at Goddard Space Flight Center (GSFC). EOS must help transfer to its scientists the wealth of knowledge from ongoing programs such as the Global Precipitation Climatology Project (GPCP) and similar efforts led by WCRP and the International Geosphere-Biosphere Programme (IGBP).

5.2.2.1.2 Runoff

How will the timing and volume of runoff be affected by climate change?

Importance: Runoff is a unique basin-integrated variable and, as such, is extremely useful for validation of most land-surface modeling schemes. Runoff is a critical component of a regional water balance, the source of agricultural irrigation, many municipalities' water supplies, recreation, and a sustaining factor to the web of ecological interrelationships in wetlands. If climate were to change, the resulting shifts in the timing and volume of runoff could upset the most basic assumptions which underlie every large water diversion and storage project.

Current and EOS capabilities: Ground-based historical records of streamflow are available for almost all the world's major river systems (GRDC 1996). However, with the exception of water contained in the floodplain or in wide, shallow braided channels, it is not clear how runoff can be measured through remote sensing.

IDS team contributions: Hydrologic science has traditionally focused on the development of watershed

models that estimate the production of runoff based on measurements of precipitation. These models need, however, to be modified to function at the larger scales characteristic of LSMs. The original LSMs such as BATS (Dickinson 1995) and SiB2 (Sellers et al. 1986, 1996c) incorporated highly-simplified representations of the runoff mechanisms so as to focus on the modeling of ET feedbacks to the atmosphere. Many new land-surface schemes are currently under development that provide more-realistic representations of the runoff generation mechanisms. The IDS team led by Kerr/Sorooshian is investigating the kinematic wave overland flow, channel routing, and erosion model (KINEROS) (Woolhiser et al. 1990) for application to arid/semi-arid (A/SA) regions. The IDS team led by Barron is developing the Terrestrial Hydrology Model (THM), which includes comparison of the runoff generated by the Green-Ampt and Phillips equations, as well as kinematic wave and Muskingum channel-routing mechanisms. The IDS team led by Lau is investigating the Massachusetts Institute of Technology (MIT) hillslope model, the Princeton Terrestrial Observation Panel (TOP) and the Variable Infiltration Capacity (VIC) models, and the United States Geological Survey (USGS) Modular Modeling System (MMS). The IDS team led by Dunne is investigating how changes in climate and land use in the Amazon Basin are modifying the generation of runoff and its chemical and sediment load. These materials are then routed through the channel and valley-floor network of the basin. C. J. Vorosmarty of the IDS Moore team is assembling a Global River and Drainage Basin Archive, sponsored also by the IGBP-Biospheric Aspects of the Hydrological Cycle (BAHC) project to assemble and reproduce on CD-ROM comprehensive databases of global runoff and related hydrologic variables.

As the EOS program moves forward, the improved understanding of the interaction between land and atmosphere will lead to the development of more effective land-surface schemes with appropriate representations of the runoff processes. Newly-available, globally-consistent river networks (Oki et al. 1995) will further these improvements, particularly at the GCM scale. Much work remains to be done to find common ground between basin observations of runoff and grid (model) estimates (Arnell 1995).

5.2.2.1.3 Evapotranspiration (ET)

Importance: ET is a variable of primary interest to many end-users of hydrologic data because it represents a loss of usable water from the hydrologic supply (e.g., agriculture, natural resources, and municipalities; Miller et al. 1995). ET has an impact on plant water stress and gen-

eration of convective precipitation patterns, and is required to close both the water and energy budgets. ET is a variable of utmost importance in land-surface hydrologic models because it represents direct feedback of moisture to the atmosphere from the land surface. Consequently, evaporation demands on vegetation help limit and define the biological environment and agricultural efficiency. Vegetation adapts to climatic moisture conditions such that LAI alone is insufficient to derive stomatal controls on transpiration. In fact, several biophysical factors exert vastly different controls on the spatial and temporal variability of land-surface ET (Choudhury 1995).

Current capabilities: There are several approaches used to calculate ET. One involves analyzing combinations of remotely-sensed observations in the context of simplifying boundary assumptions. Moran et al. (1996) use a Penman-Monteith model to define a theoretical polygon or area in temperature (T_s - T_a) versus vegetation index (Normalized Difference Vegetation Index [NDVI]) space, from which fractional canopy can be estimated. Carlson et al. (1994) and Moran et al. (1994) have developed similar models. The second approach involves energy-balance modeling based on observations of radiation, near-surface and surface temperature, albedo, and even boundary-layer height (Hall et al. 1992). From these observations, ET is calculated as a residual. These calculations hold the promise of being valid over a wide range of space scales and are useful to bridge the gap between mesoscale and GCM fluxes (Noilhan and Lacarrere 1995). ET is also simulated by complex biospheric models that use satellite-derived biome class and LAI parameterizations, then are driven by regular surface meteorology data. These models compute components of the hydrologic balance—interception, evaporation, and transpiration—and can simulate land-cover change effects on hydrology (Vegetation/Ecosystem Modeling and Analysis Project [VEMAP] 1995; Hunt et al. 1996).

The issue of validation again is extremely important but difficult. Validation of ET calculations at a point can be made through direct measurements (Shuttleworth 1988). Regional-scale estimates can be validated using basin-wide rainfall-runoff measurements (Oki et al. 1995) or using calculations of moisture divergence from balloons or radiosondes (Hippis et al. 1994). Indirect validation of ET as a residual of watershed-discharge measurements is the most common validation for ET, but provides only an annual ET estimate.

EOS capabilities: While these techniques help explain observations at relatively small scales, too little verification and analysis of spatial averages and of values for individual pixels has been done. Miller et al. (1995)

noted that the full suite of environmental observations available through the Earth Observing System Data and Information System (EOSDIS) is required to advance this research. Seasonally-variable surface characteristics and thermal images from high-spectral-resolution MODIS images will be of great interest. Precipitation and atmospheric data are critical to solve the water and energy balances. Thermal emissivity from ASTER (Hook et al. 1992) and a measure of soil moisture will also be useful. The MODIS-Running team plans a simple ET estimate as an EOS PM-1 standard product. This product will compute absorbed shortwave radiation from the FPAR, albedo, and photosynthetically-active radiation (PAR) products, then assign a biome-specific energy conversion factor to complete an estimate of daily ET. This MODIS ET product will be executed at 1 km on the 8-day composite cycle planned for many MODIS land products. Although not a research-quality computation of ET, this product should have good utility for water resource management applications that need a regular ET estimate as part of hydrologic balance calculations.

IDS team contributions: Many of the IDS teams are using environmental data provided by measurement campaigns like FIFE, HAPEX, the Global Energy and Water Cycle Experiment (GEWEX) Continental-Scale International Project (GCIP), and the Atmospheric Radiation Measurement (ARM)-Southern Great Plains (SGP) to test their methods for estimation of ET. The IDS team led by Yann/Sorooshian is studying HAPEX and ARM-SGP. Estimating and making use of partial-vegetation canopy plays a critical role in the semi-arid regions they have studied (Chehbouni et al. 1995). The IDS team led by Lau is studying the Little Washita River Basin. The IDS teams led by Dickinson and Sellers, respectively, are studying FIFE and BOREAS. Dunne's IDS team is computing ET from satellite and ground-level data and will validate the calculations against streamflow and radiosonde data over the Amazon River Basin. In the Susquehanna River Basin, Gillies and Carlson (1995) found that 90% of the variance in surface ET can be explained by spatial variations in fractional cover and surface moisture availability. This suggests that the distribution of surface energy fluxes is insensitive to the distribution of root zone soil water, although their magnitudes might be closely related. Other teams (Dickinson, Barron, and Lau) are planning to use their advanced LSMs coupled with GCMs or mesoscale models to obtain diagnostic analyses of the water-vapor hydrology at the regional and global scale. E. Wood of the IDS Lau team will test the MODIS-derived ET estimate being produced by the MODIS Land (MODLAND)-Running team over the GCIP study area.

5.2.2.1.4 Near-surface soil moisture

How will soil moisture be represented in EOS-era hydrologic models?

Importance: Soil moisture is a critical hydrologic parameter that partitions energy between sensible and latent heat fluxes, and that partitions rainfall between runoff and root-zone storage. Despite its importance, three factors limit its use in most hydrologic models. First, near-surface soil moisture changes more quickly than deeper soil moisture, which makes inferring general soil wetness difficult from surface observations alone. Second, soil moisture exhibits considerable variability in time and space. The importance of soil and soil moisture heterogeneity is unclear but must have some scale-dependent properties (Vinnikov et al. 1996). Third, until now, soil moisture has not been consistently observed at time and space scales useful to large and mesoscale models. The GEWEX Global Soil Wetness Project Report (Sellers et al. 1995) summarizes this issue by stating: “The practical result of this is that soil moisture has not been treated as a measurable variable in any of our current hydrologic, climatic, agricultural, or biogeochemical models.” This situation is frustrating since the prospect for successfully applying microwave techniques to surface soil-moisture detection, at least across areas of minimal canopy cover, is good.

Current capabilities: There are few, mainly local, soil-moisture monitoring networks. Some idea of what continental-scale patterns show can be found in historical data from the Former Soviet Union (Robock et al. 1995) but this network has largely broken down. Other networks exist or are being developed in Illinois (Kunkel 1990) and Oklahoma (ARM-SGP site).

There are two basic microwave approaches; one is based on passive radiometry, the other on active radar. Both approaches utilize the large contrast between the dielectric constant of dry soil and water. There are major differences between these two systems in terms of spatial resolution, swath width, data rate, and power requirements. However, in almost every case, these two systems are complementary in that strengths in one are matched with weaknesses in the other (Kerr and Jackson 1993). NASA-sponsored aircraft studies of soil moisture have been invaluable to assess the potential of remote detection of soil moisture (Schmugge et al. 1994) but various engineering issues have limited the deployment of L-band radars in space.

Today’s microwave efforts rely on the heritage of the Scanning Multichannel Microwave Radiometer (SMMR) and SSM/I radiometer programs, the focus of which was on oceanographic and cryospheric problems

because of existing technology and lower frequency cut-offs of 5.6 GHz and 19 GHz, respectively. Currently, operating satellites include the SSM/I (K-band), the European Remote-sensing Satellite-1 (ERS-1) and the Japanese Earth Remote-sensing Satellite-1 (JERS-1) (C-band), and (Radar Satellite) Radarsat (C-band) systems. Like earlier efforts, only limited resources are being applied to soil-moisture studies using these non-optimal frequencies (Kerr and Njoku 1990; Kerr 1991). Numerous studies have attempted to relate K-band passive microwave radiometer signals to soil moisture, but the physical basis for this is tenuous with most of the signal coming from surface roughness and vegetation. An optimal satellite mission would consist of a multi-polarization L-band radiometer having a 25-km instantaneous field of view (IFOV) and would focus on areas of little or no canopy cover (LeVine 1996).

Without direct satellite observations of soil moisture, options are limited for generating a map of this variable. Many current models approach this problem by setting relatively dry initial conditions and then letting the value follow the model without any real constraints. Satellite data can be used indirectly by looking for cool spots or thermal inertia anomalies in thermal infrared (TIR) data, tracking clouds associated with precipitation, or assuming that as the vegetation index increases, soil moisture stress decreases. Finally, limited ground data, soil maps, satellite data, and model simulations can be combined into an assimilated product. These alternative approaches might prove to be more useful in that the emphasis is on soil water availability rather than surface wetness, which is more closely tied to plant and atmospheric demand.

EOS capabilities: A scaled-back EOS program has missed the opportunity to launch an active microwave soil-moisture sensor, but there are many secondary strategies being pursued to estimate this critical state variable. Current space-based efforts focus on promoting both conventional and experimental (such as inflatable antennas) L-band radiometers under NASA’s Small Satellite and New Millennium Programs, developing algorithms to assimilate mixed polarization and multi-sensor signals, and improved representation of soil moisture in LSMs of sub-humid regions across a variety of scales.

IDS team contributions: Almost every IDS team has proposals to produce soil moisture products, most notably the GSFC Data Assimilation System (DAS), which proposes to produce a 3-hour, 1-degree, and 3-level (shallow, root, and deep) product based on a hydrologic balance model. Other approaches to this problem include soil-moisture nudging of global forecast models (Mahfouf

1991; Bouttier et al. 1993), assimilation of model and satellite microwave data (Houser 1996), and the application of crop-soil models (Maas et al. 1992).

Because of the difficulty of soil moisture measurement, and the important role played by soil moisture in land-surface hydrology, most of the IDS teams studying land-atmosphere interactions are using advanced LSMs instead of a bucket model as the land-surface interface with their climate models. In this way, soil moisture is actively linked with the overlying atmosphere, and the water balance is maintained (note that in the original bucket model, prescribed soil-moisture levels provided unlimited water to the atmosphere). In this regard, the IDS team led by Dickinson is studying appropriate treatments of land-surface parameters to improve calculations of the soil moisture. The IDS team led by Lau is working on a statistical description of soil-moisture distribution at the subgrid scale. The IDS team led by Yann/Sorooshian is investigating soil-moisture measurement in the A/SA regions using remote-sensing data. The IDS team led by Dunne intends to map the inundated areas of the Amazon River Basin with passive microwave imagery and to couple these measurements with routing models to account for the spatial distribution of the stored water within geomorphically-distinct reaches of the valley floor. Koster (1996) has developed a standard model that allows all but the most disparate soil-moisture schemes to be compared.

A major issue that requires further consideration deals with validation. The NASA Soil Moisture Workshop (1994) found that “the potential ease with which remote-sensing instruments can estimate the large-scale distribution of soil moisture is attractive (in sub-humid regions); the difficulty lies in validating such maps and relating them to subpixel distributions and profiles of field soil moisture,” particularly in the root zone. At intermediate space-time scales, Washburne and Shuttleworth (1996) are evaluating the similarities between area-averaged soil moisture across central Oklahoma based on soil-moisture sensor data from the Department of Energy’s (DOE’s) Atmospheric Radiation Measurement program and forecast data from NMC’s Eta-model. Other potential validation data sets include a new network of monthly gravimetric data collected by students under the guidance of EOS-affiliated scientists as part of the Global Learning and Observations to Benefit the Earth (GLOBE) program.

5.2.2.1.5 Infiltration and deep percolation

How much water is lost to long-term storage?

Importance: Arid-region ephemeral streams are characterized by large channel losses, and many coarse Quaternary deposits are active recharge zones. Beyond the scope of this discussion is the general problem of groundwater recharge (representing a significant store of fresh water) but its time constant of change is often decades if not centuries.

Current capabilities: Of primary importance to issues of infiltration and soil storage are knowledge of soil texture and soil depth. The pioneering and comprehensive work of FAO (1978) to define a global soil-classification scheme and produce a global soil map are reflected in the almost exclusive use of their base maps for producing most current soil products. The original FAO map units have been rendered more usable to the modeling community (but not more accurate) by reclassification and gridding (to $1^\circ \times 1^\circ$) as part of ISLSCP’s Initiative I (Sellers et al. 1995d). An example of this product is given for soil depth, Figure 5.10. The main limitations of this product are the assumptions constraining the soil units, a lack of quality control, and low spatial resolution. Its advantages are that it is the only global product of its kind and maintains some uniformity in classification and relative accuracy. There are several active programs to develop the next generation of soil survey products, most notably by the IGBP Soils task force.

EOS contributions: The role EOS will play in this area is not clear. Satellite and ground-based studies of riparian-zone water and energy balances may improve our understanding of some recharge issues, particularly in conjunction with a focused effort to quantify other energy and water fluxes, as has been proposed for the Semi-Arid Land-Surface-Atmosphere (SALSA) Experiment (Wallace 1995). Supporting comprehensive and uniform soil and soil-property mapping is one activity that will benefit the hydrologic community.

5.2.2.1.6 Radiation

How well can we predict surface radiation fields, especially under partly cloudy and hazy (smokey) conditions?

Importance: The spatial and temporal distribution of solar radiation is a primary variable for atmospheric and vegetation systems. Accurate knowledge of these systems is required by energy balance models which complement direct hydrologic reckoning and are mandatory for 4DDA techniques. One of the greatest current uncertainties is with regard to atmospheric radiative transfer, particularly

the effect of aerosols and multiple cloud layers (McCormick et al. 1995; Penner et al. 1992). In addition, fractional cloud cover represents a significant, scale-dependent problem related to the surface-energy budget and hence the important question of cloud-climate radiation feedback. Many of these issues have been addressed in Chapter 2, but the importance of this issue for land-surface studies must be stressed.

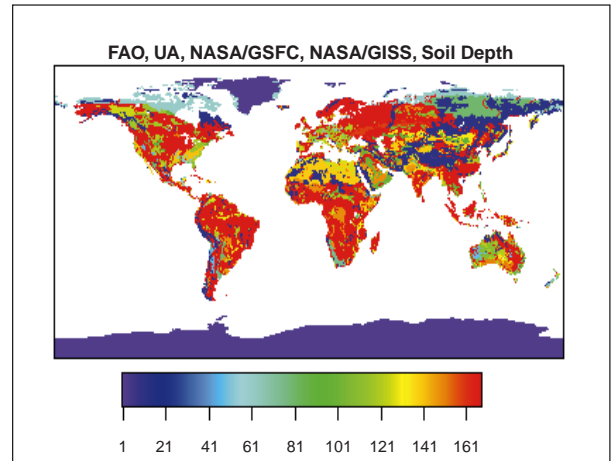
Current capabilities: Two approaches to calculating shortwave fluxes are common (Wielicki et al. 1996). The first involves using a global network of surface stations (Global Energy Balance Archive [GEBA], and Baseline Surface Radiation Network [BSRN]) to adjust simultaneously-observed TOA and surface fluxes. The second involves applying an atmospheric radiative transfer model to observed cloud and TOA fields. Considerable progress has been made in estimating near-surface radiation as an outgrowth of the NASA ERBE, the NOAA GOES program, and the GEWEX ISCCP. Current methodologies for estimating surface shortwave radiation involve sampling the mean and standard deviation of multiple 8-km pixels, applying a cloud filter and 2-stream atmospheric correction to give a product at 50-km and 3-hour resolution (Pinker et al. 1994).

EOS capabilities: Knowledge of the spatial and temporal distribution of radiation will be greatly improved as a result of EOS. While the need for global coverage mandates typical resolutions of 25 km and greater (achieved by CERES), MODIS has the potential for supplying higher-spatial-resolution data on a limited basis. Four observations per day will be achievable, given the deployment of both EOS AM-1 and PM-1, and are required to define the important diurnal component of radiation, cloud, and precipitation fields. This should be considered marginal, and considerable attention and resources must be focused on the use of data from non-EOS geostationary satellites to supplement this information.

Shortwave radiation accuracies of 5 Wm^{-2} should be achievable from the EOS CERES sensor. While larger than estimated climate forcings, they are helpful in light of larger inconsistencies among current GCMs (see Chapter 2). Much better spatial resolution of the general atmospheric models will be possible using the CERES and AIRS sensors. Improved knowledge of bidirectional surface reflectance from MISR will further refine future estimates of net shortwave radiation.

Considerable work needs to be done to improve satellite estimates of the surface net longwave flux. Longwave radiation accuracies of 20 Wm^{-2} or less should be achievable using EOS sensors. Errors are greatly influenced by variable patterns of low-level water vapor and cloud-base heights, which are difficult to obtain from

FIGURE 5.10



A global database of soil depth. This $1^\circ \times 1^\circ$ data set, developed by the ISLSCP Initiative 1 project, is used in global climate, hydrologic, and biogeochemical modeling (Sellers et al. 1996).

space. Again, the AIRS/Humidity Sounder Brazil (HSB) should prove valuable, as well as ASTER to determine longwave surface emissivities (Hook et al. 1992).

IDS team contributions: Observation strategies for determining fractional cloudiness are an important component of the ARM-SGP (Stokes and Schwartz 1994) and Pennsylvania State University (PSU) IDS efforts, using a variety of instruments. Models which realistically simulate continental temperatures of both the annual and diurnal cycle are planned, given adequate observations, where this level of accuracy is still under investigation. Cloud properties will be mapped at scales of 25 km at several atmospheric levels by CERES in support of many IDS investigations. Some studies have shown that no significant spatial variability is discernible below this scale (Pinker and Laszlo 1992) although some researchers find a 250-m scale more valuable for detailed radiation studies (Dubayah 1992).

5.2.2.1.7 Near-surface meteorology

Importance: Near-surface air temperature, humidity, and wind speed are pivotal parameters in many energy balance and satellite flux models, yet relatively little attention has been given to defining regional and local verification data sets for these variables, which vary significantly in space and time. Typical hydrometeorologic applications such as calculating sensible heat flux, estimating partial canopy fraction, and crop stress all depend on being able to calculate the difference between surface and air temperature. Algorithms developed over oceans, which estimate these parameters, cannot be used; land-surface

estimates must rely on the assimilation of ground data and forecast or mesoscale model data. This realistically limits spatial resolutions to 10-50 km with temporal resolutions of 1-3 hours. In some terrains, this may be adequate, but use of these data in mountainous or highly dissected or heterogeneous areas will significantly limit the use of these methods (Li and Avissar 1994).

Current capabilities: Many process-based model studies make an assumption of uniform driving fields across relatively small areas or adjust meteorology using linear adiabatic assumptions. Across larger areas, radiation can be distributed using common geographic adjustments, but atmospheric correction and cloudiness are, at best, often based on a single radiosonde sounding. This approach was taken by Rahman et al. (1996) in conjunction with satellite-derived land-surface characteristics and a Digital Elevation Model (DEM). Another approach is to use a 30-to-50-km gridded forecast meteorological model to drive a distributed hydrologic model. These data are readily available but must be applied judiciously. An effort is currently under way to compare a year of surface model output from NMC's Eta model with area-average fluxes observed over the ARM-SGP site (Washburne and Shuttleworth 1996). Using a nested mesoscale model to drive regional process models is the next level of sophistication but usually requires a major modeling effort.

EOS capabilities: Direct observation of near-surface continental meteorology from space is unlikely in the near future. EOSDIS can play a significant role in this area by making non-EOS data sets (global and regional meteorology assimilations) readily available and by helping to translate data into appropriate EOS formats. Well-defined data standards and a clear appreciation for the critical need these data play in hydrologic modeling are minimum requirements for the EOSDIS system in this area.

IDS team contributions: Application of nested models falls neatly into the overall mission of the Barron IDS, but their effort is likely to be focused on regional areas of interest. The Rood IDS team and the DAO will produce the most basic assimilated data set of surface meteorology for land science application. This 6-hour, near-real-time production of land-surface incident radiation, temperature, precipitation, and humidity will be useful to many hydrology and vegetation models. For many purposes, especially regional calculations, the $2^\circ \times 2^\circ$ gridded data set from the DAO will need to be disaggregated to finer spatial detail using a DEM and appropriate meso- and micro-climate models. The VEMAP ecosystem modeling activity for the continental U.S. illustrates how gridded global climate data sets can

be enhanced for simulations with finer spatial detail data. (VEMAP 1995).

5.2.2.2 *Estimating and validating the land-surface water balance*

How do changes in the water balance feed back and influence the climate and biosphere? How will EOS help monitor these changes? How will we validate models of these changes?

Regional water balances are poorly known in all but a few countries in temperate regions. Major uncertainties regarding the validity of GCM outputs arise because of the sparse nature of rain-gauge, stream-gauge, and other hydrologic data sets. Not only are the day-to-day issues important, but hydrologists must address questions posed by longer-term hydrologic variability and gauge the nuances posed by questions of natural and anthropogenic causes of these events. Additional questions arise because of uncertain model calibrations and the necessity of spatial averaging over large areas. Seasonal and inter-annual storage of moisture in snow packs, soils, groundwater bodies, and large surface water bodies further complicates the picture in ways that are scientifically and societally important, but the paucity of data on these large-scale storage elements continues to degrade modeling computations and predictions of the behavior of regional water resources. The resulting uncertainty in quantification of regional water balances affects calculation of:

- 1) regional evaporation fields,
- 2) land-atmosphere feedback on drought formation,
- 3) the role of antecedent moisture in the flooding of continental-scale rivers, and
- 4) the timing of snowmelt runoff and dry-weather water supply in response to climate change.

Various programs have been proposed to validate both remote sensing data and model fields derived from EOS products. This effort must be international and span a wide range of climates and biomes, and it must be a long-term effort to maintain a strong level of confidence in the data sets.

5.2.2.3 *Extreme hydrologic events*

What changes in the surface water budget may occur with climate change? Will the frequency and magnitude of extreme hydrologic events change? In which direction will the change be, and what effects will it produce?

5.2.2.3.1 Introduction

Like many water resources issues, extreme hydrologic events cover a wide range of spatial and temporal scales. These events can be characterized as instantaneous localized events such as flash floods, hurricanes, and heavy precipitation, or long-duration widespread events such as general floods and droughts. In both cases, extreme hydrologic events can cause significant economic losses as well as social and environmental stresses.

For the past 50 years, scientists have studied extreme hydrologic events, mostly within a probabilistic framework. Numerous reports and studies can be found in the literature regarding the identification, use, and limitations of probability density functions describing the frequency and magnitude of floods and droughts. The apparent increase over the past decade of the frequency and magnitude of extreme hydrologic events is fostering a growing interest in quantifying more process-based relationships between these frequencies and climate variability and climate change.

Many of the analyses concerning the hydrologic impacts of climate variability and long-term climate change are speculative and qualitative; however, quantitative assessments of the second-order social, environmental, and economical impacts are possible at various spatial and temporal scales (AIP 1993). What is more important is the fact that flood levee systems, reservoirs, and water distribution systems have been designed to balance reliability with demand on the basis of historical hydrologic data. In most cases, the design paradigm assumes a stationary climate system in which the point probability of occurrence for extreme events does not change. It is quite possible that the potential water resources impacts from climate change and variability can be significant at local-to-regional scales while larger-scale phenomena and averages remain. Environmental impact models that are unable to transform realistically global average results to local scales will only confuse the public's perception of the issues. These and other topics have been addressed in recent years by several National Research Council (NRC) research reports on estimating extreme hydrological events; for example, NRC (1988) on flood risk estimation, and NRC (1994) on extreme precipitation.

Predicting how hydrologic extreme events may change is very speculative. More severe floods and a change in the distribution and timing of spring snowmelt have been suggested as likely effects of CO₂ doubling that would have significant human impact. At best, GCMs can be used to indicate how the hydrological and meteorological processes may change if global warming takes

place. Macroscale heterogeneity can impede the reliability of regional- and global-scale predictions for localized studies of extreme hydrologic events because of the existing gaps in the spatial resolutions of GCM, mesoscale, and macroscale hydrologic models. Bridging these gaps will result in gains on several fronts, including 1) improving the ability to extend the forecasting lead time, 2) improved understanding of the causes and conditions underlying extreme events, and 3) improving the ability to predict the impacts of climate variability on the frequency and magnitude of extreme events.

Three potential impacts are considered below: increased incidence of severe storms, increased snowmelt-based floods due to rain on snow, and decreased precipitation leading to increased drought.

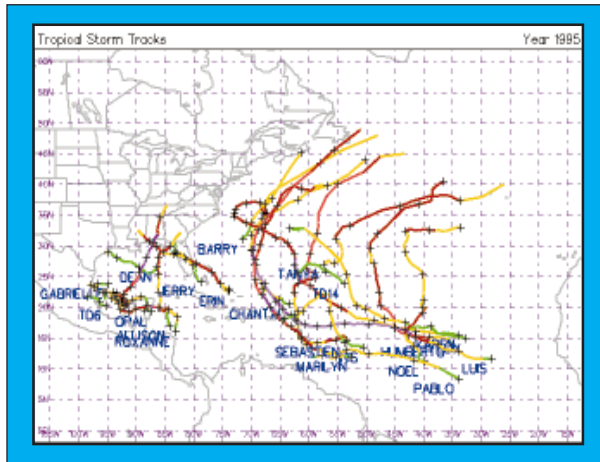
5.2.2.3.2 Severe storms

Will the frequency and intensity of hurricane and severe storms change?

Importance: Hurricanes, tornadoes, hail, and lightning storms can be highly destructive in an urban environment. Loss of lives, severe erosion, wind damage, flooding, crop damage, road and power grid disruption are all common human consequences of these storms. If we focus only on hurricanes, the intensity of a given storm determines its potential for destruction, while the actual amount of damage depends on the density of development, the population, and the economic interests in the impacted coastal areas. Clearly, the increasing urbanization of coastal areas around the world will only intensify the importance of severe cyclonic storms. Additionally, the highly-nonlinear relationship between the wind speed of hurricanes and their potential for destruction indicates that even a minor change in hurricane intensity and frequency can lead to significant increases in damage. The potential for human impact by an especially vigorous tropical storm environment was well documented in the millions of dollars in damage and dislocations as a result of the 1995 storm season along the southeast coast of the U.S. (Figure 5.11, pg. 220, from WPX homepage: <http://thunder.atms.purdue.edu>).

Current capabilities: Presently, the spatial resolution of most GCMs cannot accommodate detailed simulation of hurricanes. GCMs can be used to evaluate the impacts of climate-change scenarios on the tropical disturbances leading to the occurrence of hurricanes. For example, Emanuel (1987) suggests that as sea-surface temperatures (SSTs) rise in doubled CO₂ scenarios, tropical cyclones intensify and winds increase. He reports that a 3°C SST increase would result in a 30-40% increase in

FIGURE 5.11



Tropical storm tracks as observed along the southeast coast of the United States in 1995.

the maximum pressure drop and 15-20% increase in wind speeds. In another study, Haarsma et al. (1992) reported an increase in the number of tropical disturbances under the doubled CO₂ scenario. In general, there is considerable potential for research to better understand the impact of climate change and variability on the frequency and magnitudes of severe storms and hurricanes.

EOS capabilities: EOS instruments such as MODIS will provide high-resolution spatial coverage of SST and higher-level products, such as pressure. Further understanding of the land-surface-ocean processes is also expected to provide insights into the processes associated with the occurrence of severe storms. Recent studies indicate a good correlation between hurricane intensities determined via SSM/I and remotely-sensed SST observed a day earlier; such studies are in their early stages. Further improvements are possible in the forecasting of mid-range tropical cyclones using remotely-sensed outgoing longwave radiation.

5.2.2.3.3 Floods

Will the frequency and magnitude of floods change due to global change? In what direction will the change be, and how will water resources management and infrastructure change or be affected?

Importance: The main difference between flash floods and general floods is in their spatial coverage and temporal duration. Floods may occur due to various combinations of extreme conditions. For example, rain on snow combined with relatively mild ambient temperature accelerates melting. This is one of the primary

processes causing early spring flooding in snowy regions. Other processes such as above-normal winter precipitation which leads to soil saturation followed by early-to-mid-spring heavy rainfall can cause both types of floods. Severe convective storms also cause localized flash floods. Floods such as the Great Flood of 1993 on the Mississippi River can produce a substantial amount of damage. Adding to the economic loss from floodplain agriculture are environmental damages due to severe erosion and overbank deposition.

A definitive assessment of the hydrologic impacts of climate change has yet to be made but many scenarios have been analyzed. Changes in flood frequencies and magnitudes can result from a combination of the hydrologic impacts of climate change as well as from land-use changes and direct anthropogenic factors. Dracup and Kendall (1991) argued that operational policies that require maintaining water in reservoir systems at maximum levels and physical encroachment into the floodplains have contributed to the higher flood stages in the Colorado River. The critical issue of separating impacts of climate variability and those resulting from anthropogenic factors on flood frequency and magnitude must be addressed. This is made even more difficult because of the possible changes in anthropogenic conditions as a response to climate change.

Current capabilities: River runoff is likely to increase as a result of global warming (Revelle and Waggoner 1983). Lettenmaier and Gan (1990) and Running and Nemani (1991) determined that climate change due to global warming would lead to earlier snow melting in the western U.S. and more-frequent rain-on-snow events. Hughes et al. (1993) analyzed two basins in Washington State and showed that for basins in which the floods were snowmelt-dominated, global warming would increase the magnitude of low-occurrence floods, and, for the basin in which floods are rain-dominated, there would be a decrease in magnitude of extreme events. Concerning increases in convective rainfall, which leads to severe local flooding, much of the arguments for increased severity for hurricanes can be used for thunderstorms; i.e., increased heating of the land surface would increase lifting and convergence of moisture and increased storm severity.

EOS capabilities: A primary challenge in the years to come will be to use EOS-era science and data to help furnish the contextual information that will help hydrologists analyze not only the flood event but the global and regional influences behind it. In the arena of predictive advances, we must take a more-cautious approach. As often mentioned, there is a fundamental discontinuity in the predictive capability of GCMs below the length and

time scales of synoptic meteorology, such that important seasonal weather patterns can be resolved, but the watershed and date-specific circumstances that combine in local hydrologic events remain indiscernible. Thus, an important challenge in the years to come will be to take EOS data and model improvements and relate these to issues of particular urgency such as hazard assessment and water resources planning. Whereas anomalous atmospheric circulation patterns can be linked to certain catastrophic floods (Hirschboeck 1988) and the large-scale atmospheric motion is reasonably defined by contemporary GCMs (Barron 1995), it is a much different and difficult task to go from the synthesis of model and observation we will have to the discrete type of events most hydrologists are used to working with. Yet the need for improved climate models and LSPs is real and will undoubtedly advance our ability to better understand and prepare for hydrologic hazards.

5.2.2.3.4 Floodplains

How do floods spread into the complex, low-amplitude topography of alluvial lowlands, such as floodplains, deltas, and other large swamps?

Importance: Inundation of vast alluvial lowlands is a complex process involving local generation of runoff from rainfall or snowmelt, flow from the surrounding highlands, overbank spilling along floodplain channels, and tidal and storm influences near coastlines. The interplay of these processes depends upon the timing of hydrologic events and their alteration by engineered structures. A contributing factor is the intricate geometry of the lowlands themselves, composed of tidal channels, levees, distributory channels, scroll bars, and floodplain lakes.

Current capabilities: Predicting areas of inundation is limited by inaccuracies of hydrologic routing in areas of low relief and by poor spatial resolution of precipitation data.

EOS contributions: These difficulties are being reduced by improved computer models and especially by new satellite information on the extent of inundation. The Soares/Dunne IDS team, studying the Amazon River Basin, is mapping inundation using passive microwave sensors (SMMR and SSM/I), SAR, Landsat Thematic Mapper (TM), and it is exploring the use of AVHRR data. The spatial and temporal patterns of inundation are exceedingly complex because they depend not only on runoff generation but also on subtle details of floodplain topography. These empirical studies to document inundation are combined with model-based investigations of channel-floodplain interactions during floods and the influence of climate and land cover up stream. Significant progress

on this topic will allow hydrologists to study the formation of large floods using space technology and eventually to issue gradually-updated forecasts of where inundation is likely. Satellite altimetry of water surfaces in extensive inundation areas can also assist with understanding the spread of floodwaters and the calibration of hydrodynamical models in other complex flood-prone areas.

5.2.2.3.5 Droughts

Droughts are characterized by their duration and severity. It is unclear how climate change will affect precipitation. Early GCM simulations (Delworth and Manabe 1988) implied that global warming would result in decreases in precipitation and soil wetness, especially in the central portion of large continents. These results must be viewed with extreme caution for two reasons. One, early GCMs had a poor representation of land-surface hydrological processes. It is well known that the lack of vegetation interception storage underestimates land-surface evaporation, thus reducing GCM rainfall (Scott et al. 1996), and a similar argument can be made for single-storage soil-column representations, which lack a surface thin layer that can enhance re-evaporation. The second reason for caution is the generally poor ability of GCMs to reproduce current climate at local-to-regional scales. The characteristics of rain storm and interstorm durations are critical to soil dryness and whether drought occurs. Palmer (1986) reported a strong relationship between global patterns of SST anomalies and drought frequency in the Sahel region.

5.2.2.3.6 The causes of extreme events

More research is required to understand the source of the major weather patterns that lead to floods, droughts, blizzards, tornadoes, and hurricanes (Loaiciga et al. 1996). Teleconnections between widespread hydrologic phenomena, of which ENSO is the most common example, are better left for discussion in Chapters 2 and 3, whose focus is more global, but EOS will make significant contributions to our understanding of these events and how well we monitor them. Anthropogenic influences on the timing or strength of seasonal and longer climate variability are presently speculative but are surely having an effect. More pertinent to this section and chapter is the need to better understand the ties between land-use change and drought, particularly as characterized by reports from the Sahel of Africa. The hope for EOS is that an objective and comprehensive global record of climate and land-sur-

face response will better allow us to discern the causes and effects of critical hydrologic phenomena.

5.2.2.4 River biogeochemistry

What is the role of river biogeochemistry in the Earth system and in affecting water quality and the functioning of aquatic ecosystems?

Importance: An underdeveloped aspect of continental hydrology, but one which is extremely important for understanding both the habitability of valley floors and the ecology and biogeochemistry of wetland and aquatic ecosystems, is the relationship between the regional-scale hydrology of continental-scale watersheds and the flux of water and mobile terrestrial materials (organic and inorganic sediment and solutes) along river networks and into valley floors. These fluxes determine the nutrient loading of river water. The resulting in-channel processing of nutrients causes sedimentation problems, but is also responsible for constructing floodplains and maintaining the biogeochemistry of the associated wetlands. The frequency and duration of flooding affect the oxidation state of the wetlands, and therefore the partitioning of carbon into CO₂, CH₄, and stored particulate forms, with associated effects on the mobility of other nutrients. The rate and form of sedimentation, produced by the basin hydrology and sediment supply, control the nature of floodplain geomorphology, channel shifting, the formation and connection to the river of the various river water bodies, and various engineering problems associated with maintaining the habitability of valley floors. An important task for regional hydrology involves understanding the controls on the flux, processing, and disposition of these mobile terrestrial materials in order to predict their response to large-scale environmental change within continental drainage basins.

The river corridors of a region accumulate the runoff that is the excess of precipitation over ET on the surrounding continental surface. The annual distribution of flow in large rivers is determined by the seasonal variability of the land-surface water balance, transit times, and storage within soils, ground water, and valley floors. Large rivers receive water from source areas with diverse climatology and other hydrologic characteristics, generating extended periods of high runoff that support vast wetlands in the lowlands of the continental-scale river basins. Wetlands may be associated with flowing water, such as river floodplains, or they may be located in areas of low-permeability soils or of constricted drainage on gentle topography.

The Amazon basin, for instance, is a region dominated by the abundance of water. This abundance is evident

in the extensive river and its vast associated areas of periodically inundated land. Junk and Furch (1993) estimate that the floodplain of the Amazon main-stem and primary tributaries covers about 300,000 km², whereas riparian zones of small rivers may cover about 1 million km². Furthermore, savannas exposed to overland flow may account for another 40,000-250,000 km². That is, approximately 15-30% of the area of the basin is subject to periodic saturation and inundation. These periodically or permanently flooded areas play important roles in the hydrology and biogeochemistry of the basin. Because the poorly drained areas often receive transfers of water and materials from nearby and upstream areas, they are subject to indirect impacts as the uplands undergo development. Many of the inundated areas support productive ecosystems including resources such as timber and fish, which are then subject to impacts from the changes which alter the volumes, sediment loads, and chemistry of the regional runoff. The biogeochemistry of these wetlands is driven by the extent, duration, and intensity of their inundation. When saturated, they support anaerobic conditions where microbiological activities such as methane production and denitrification prevail. Hence, an accurate estimate of gas exchange between the land and the atmosphere must consider the vast saturated and flooded regions of river lowlands. In addition, these areas frequently sequester organic carbon and nutrients from the upland environments.

The challenge of global- and continental-scale river biogeochemistry in the EOS program is to link the flow of water through the landscape and down river channels to the ecological and chemical attributes of basins at scales much larger than the relatively-small watersheds that are typically studied. The capability to predict how changes in drainage basins will impact river systems and coastal seas in different parts of the globe can be developed from use of large-scale river models of how changes in land-surface processes will be reflected in the down-river transport and processing of elements and the ultimate marine fate of river-borne materials.

An important task is to collate and check the widespread under-used ground-level data sets on these components of the surface water balance and to interpret them in the context of physics-based mathematical models that accurately represent large-scale hydrologic processes in a way that can be checked against available data such as: stream-flow measurements, satellite-based mapping of inundated areas, and the seasonal condition of vegetation.

Current capabilities: Current predictions of river biogeochemistry involve empirical models of the loading of sediment and nutrients from watershed areas in vari-

ous natural and distributed conditions, and the alteration of these materials during river transport.

EOS capabilities: The availability of satellite information on land-surface characteristics that control the energy and material balances of watersheds holds the possibility of linking large-scale models of hydrology and of primary production and nutrient mobilization, such as the Carnegie-Ames-Stanford Approach (CASA) and Biome-BGC models, over continental-scale watersheds to predict the biogeochemistry of large river basins. Both the IDS Soares/Dunne and IDS Moore teams are specifically working on continental-scale hydrogeochemistry models.

5.2.3 Land-vegetation science issues

5.2.3.1 The role of EOS in global change studies of vegetation

Vegetation responds to climate at virtually all space and time scales. Photosynthetic activity of a leaf changes within seconds when a cloud blocks direct solar illumination. Daily variations in temperature control the CO₂ balance between photosynthesis, respiration, and soil decomposition. The spring-time growth of vegetation is clearly visible continentally by time sequences of NDVI. Interannual variability in atmospheric CO₂ concentrations illustrates that the terrestrial biospheric activity shows high geographic and seasonal dynamics. At decadal time scales land-cover changes, predominantly human-induced, cause measurable changes in terrestrial biogeochemistry.

EOS science questions encompass regional-to-global scales, from the carbon balance of the boreal forest to biospheric net primary production (NPP). The short time scale of vegetation responses to climate considered by EOS will range from following interannual variability in spring phenology, to seasonal changes in daily terrestrial surface CO₂ balance and other greenhouse gas fluxes, to annual NPP and interannual climate-driven variability in NPP. Over multiple years, terrestrial vegetation responds to changing climate with changes in density, which will be quantified as changes in LAI. The most permanent change in vegetation occurs by land-cover change, when one biome type is replaced by another. For example, if climatic warming proceeds, the alpine forest timberline may encroach upon mountain tundra. However, these changes take many decades to occur. The fastest and least predictable changes in global vegetation are caused by direct human activity—cutting forests, draining wetlands, irrigating deserts. EOS has measurements planned to evaluate the terrestrial biosphere at all of these space/time scales.

This section will first cover plans for EOS monitoring of directly-observable vegetation variables, primarily land cover, and land-cover change. Next, derivable biophysical variables, such as LAI, FPAR, albedo, and vegetation indices will be described. Finally the most complex Level 4 products require integration of EOS satellite data with ancillary data to drive biospheric simulation models. These models will produce global estimates of NPP and ET.

5.2.3.2 Land cover

Land cover is the initial variable for parameterizing terrestrial vegetation in virtually all GCM and biospheric models. Land cover does not quantify the vegetation as LAI or biomass does. It only provides a descriptive definition of the biome type present at a given location. The accuracy of global land-cover mapping influences all other biospheric process calculations. Furthermore, the accurate detection of temporal change is one of the most fundamental measures of global change. Ecologically, change in land cover from one biome to another signals the most permanent type of vegetation change, and naturally requires decades to occur. The human-caused changes in land cover, termed land use, are now occurring much faster, and are more relevant to change detection than natural causation. Despite the importance of land cover, it has been poorly quantified (Townshend et al. 1991) and poorly defined (Running et al. 1995) until recently. Nemani and Running (1995) have now estimated from AVHRR 8-km data forest cover of 52.3 million km². They also reported 40% of temperate forests have now been converted to other uses, but only 26% of tropical and 20% of boreal forest land has been cut. These are the first global completely satellite-derived estimates of global deforestation rates.

EOS contribution: Mapping of existing land cover requires satellite data, and a global 8-km current land-cover product from AVHRR is now available (Figure 5.12, pg. 224, Nemani and Running 1995). DeFries et al. (1995) and Nemani and Running (1995) are exploring advanced logic for discriminating biomes with a combination of spectral vegetation indices and surface-temperature thresholds. These groups plan the first full 1-km global land-cover analysis with completion of the AVHRR 1-km Pathfinder data set in 1996. The EOS AM-1 at-launch land-cover product will be derived from 1997 1-km AVHRR data. After launch, the first MODIS-derived 1-km global land cover product will be complete in one year, as an important discrimination criterion for land cover is differences in seasonality of Visible (VIS)/Near Infrared (NIR) spectral reflectances. More-accurate land-cover mapping will be possible as bidirectional reflectance

distribution functions (BRDFs) from MISR are integrated with the MODIS land-cover product. This advanced land-cover product should first be available around 2000 (Lambin and Strahler 1994). Townshend (1996) will produce a MODIS-derived land-cover-change product specifically with the 250-m channels of MODIS for high-resolution tracking of regional land cover and land-use change.

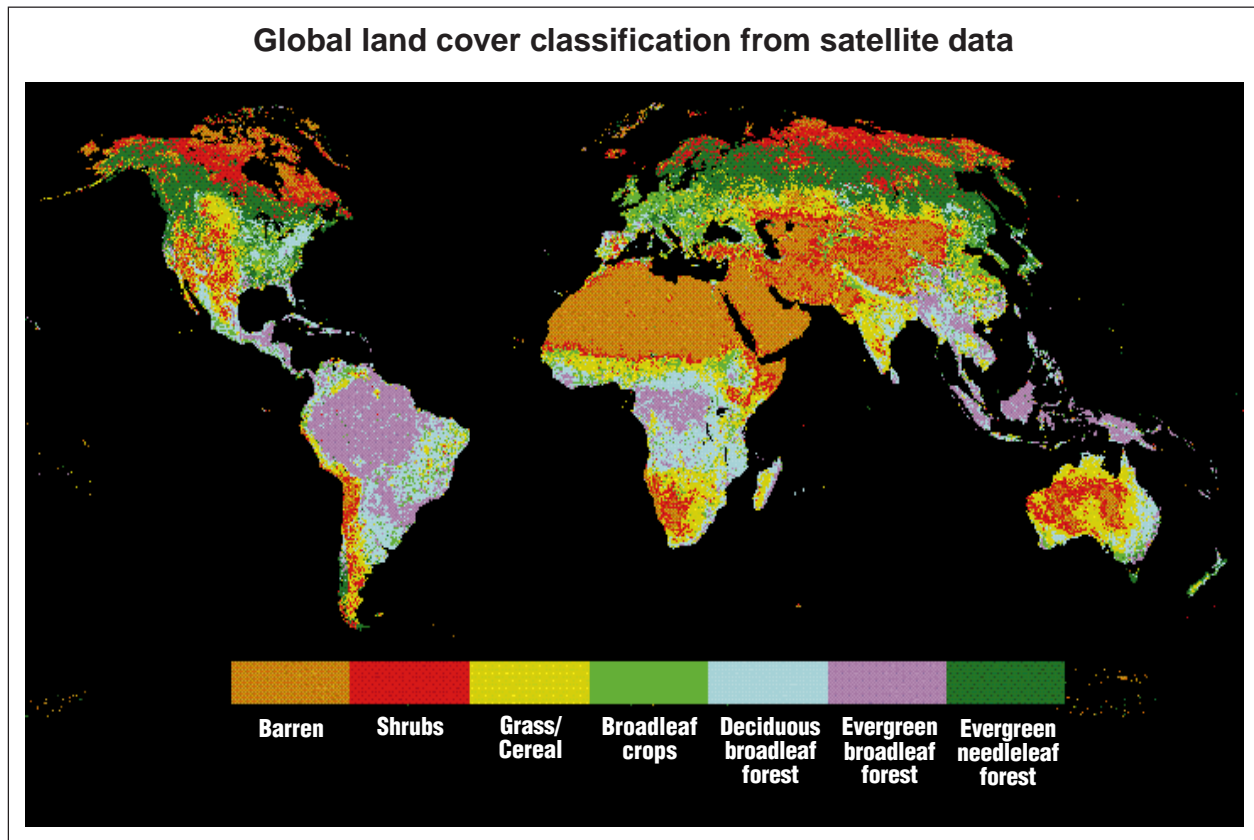
Potential, or climatically-defined land cover is being computed by a number of biogeography models, the most well developed being the Biogeochemical Information Ordering Management Environment (BIOME)2 model (Prentice et al. 1992) and the Mapped Atmosphere-Plant Soil System (MAPSS) model by Nielson (1995). Good definition of potential land cover is a prerequisite for land-cover change analysis and will be used by the Moore-IDS and Schimel-IDS teams for biospheric modeling.

5.2.3.2.1 Landsat and high-spatial-resolution land science

Although EOS is predominantly planned as a global-scale science program, some of the satellites will produce imagery at high spatial resolution. For example, Landsat-7 will produce data at 10- to 30-m spatial resolution with a 16-day repeat cycle. The long history of Landsat science and applications has illustrated that this spatial/temporal combination is best used for regional land-cover mapping. The data volume is too high for global use, and temporal constraints preclude seasonal time-series analysis. However, the high spatial detail makes Landsat-7 the preferred platform for land-cover change detection, particularly where human-induced changes often occur at sub-kilometer scales (Skole and Tucker 1993).

Opportunities to improve mapping of land cover and vegetation structure, such as stem biomass and forest

FIGURE 5.12



The existing global distribution of terrestrial biomes derived from AVHRR data for 1989 (Nemani and Running 1995). These land-cover data sets are used to quantify land-surface characteristics in global climate, hydrology, and carbon-cycling models. Land-cover monitoring is also important for quantifying deforestation/reforestation rates and land-use change and urbanization. EOS will produce a global land-cover product similar to this at 1-km resolution beginning with the EOS AM-1 launch.

density, lie primarily with the high-spatial-resolution sensors like Landsat, and the multi-look-angle MISR sensor. MISR will provide seven looks at a target in one overpass with its multiple-sensor design. As with Landsat, the long repeat time and high data volume will preclude it from routine full global monitoring in the way that MODIS is scheduled, but will allow enhanced capability for detection of vegetation variables and change analysis not possible with MODIS. ASTER will also provide spatial resolution of 15- to 90-m for selected target scenes. MODLAND-Townshend will supplement 250-m MODIS data with Landsat and ASTER data to produce a high-resolution land-cover-change detection that will include a regional change “alarm” to detect areas undergoing very rapid change. This alarm should alert scientists to large land-cover perturbations in uninhabited areas. Dave Skole of the Moore-IDS team will continue to monitor tropical deforestation rates with Landsat and ASTER sensors (Skole and Tucker 1993).

5.2.3.3 *Vegetation structure*

5.2.3.3.1 Leaf-Area Index (LAI)

Plant canopies are the critical interface between the atmosphere and the terrestrial biosphere. Exchanges of energy, mass, and momentum between the atmosphere and vegetation are controlled by plant canopies. When considering the array of global vegetation, there is an infinite variety of plant canopy shapes, sizes, and attributes. Over the last few decades, ecologists have found that a useful way to quantify plant canopies in a simple yet powerful way is by defining the LAI (the projected leaf area per unit ground area). This parameter represents the structural characteristic of primary importance, the basic size of the canopy, while conveniently ignoring the complexities of canopy geometry that make global comparisons impossible otherwise. Characterization of vegetation in terms of LAI, rather than species composition, is considered a critical simplification for comparison of different terrestrial ecosystems worldwide.

Because LAI most directly quantifies the plant canopy structure, it is highly related to a variety of canopy processes, such as interception, ET, photosynthesis, respiration, and leaf litterfall. LAI is an abstraction of a canopy structural property, a dimensionless variable that ignores canopy detail such as leaf-angle distribution, canopy height, or shape. Hence the definition of LAI is used by terrestrial models to quantify those ecosystem processes. FPAR is a radiation term, so it is more directly related to remotely-sensed variables such as Simple Ra-

tio, NDVI, etc., than LAI. FPAR is frequently used to translate direct satellite data such as NDVI into simple estimates of primary production. It does not define plant canopies as directly as LAI, but is more specifically related to the satellite indices.

As remote sensing became an important tool in terrestrial ecology, initial efforts concentrated on measuring LAI by satellite (Asrar et al. 1984; Peterson et al. 1987). Remote sensing of LAI was first attempted for crops and grasslands, correlating spectral reflectances against direct measurement of vegetation LAI. Various combinations of near-infrared and visible wavelengths have been used to estimate the LAI of wheat (Wiegand et al. 1979; Asrar et al. 1984). Peterson et al. (1987) first estimated the LAI of coniferous forests across an environmental gradient in Oregon using airborne Thematic Mapper Simulator data. NDVI is found to vary monotonically with fraction of vegetation cover for various biome types, a variable related to LAI (Price 1992; Huete et al. 1988; Nemani et al. 1993).

In perennial biome types such as forests, LAI reflects climatic optima; warm, wet climates produce forests of high LAI, while colder, drier climates produce lower LAI. Because plants regrow and recycle their canopies on a regular basis, LAI provides a direct measure of the magnitude of biogeochemical cycling of a vegetation type. LAI changes seasonally in crops and annual vegetation types, and the weekly increase in LAI provides a good monitor of crop development. Even in permanent vegetation types such as forests, LAI will change interannually with climatic fluctuations, particularly of water balance. Defining the length of growing season of deciduous vegetation can best be done by tracking spring growth and fall senescence of LAI.

The advanced biospheric models such as TEM, Century, and BIOME-BGC all use LAI as the vegetation structural variable. Neither LAI nor FPAR are critical variables themselves, rather they are both essential intermediate variables used to calculate terrestrial energy, carbon, water cycling processes, and biogeochemistry of vegetation. Although the NPP of grasslands, annual crops, and other seasonal biome types can be estimated by the time integration of observed developing biomass, for biome types such as forests, chaparral, and other evergreen broadleaves, permanent live biomass occupies the site continuously, causing annual NPP to not be visible from orbiting satellites. The current consensus is that LAI will be used preferentially by ecological and climate modelers who desire a representation of canopy structure in their models.

5.2.3.3.2 Fraction of Photosynthetically-Active Radiation (FPAR) FPAR will be preferentially used by remote-sensing scientists to interpret satellite data, and projects interested in simple direct estimates of photosynthetic activity and primary production without using mechanistic biome models. Much of the ambiguity involved in using either LAI or FPAR in global-scale models can be eliminated if one also knows some general details about the basic life form of the vegetation, i.e., whether it is forest, grass, crop, etc. That is why the land-cover product discussed above is a necessary initial step in computation of LAI and FPAR.

FPAR is the radiometric equivalent of the structural variable LAI. The satellite-driven global computations of NPP use FPAR to avoid the inversion to LAI and then re-translation back from a satellite-defined Spectral Vegetation Index. Theoretical studies of canopy radiation penetration theory explore the physics of how light interacts with a plant canopy, in order to better understand remote-sensing data. (Myneni et al. 1992). These studies concentrate on the fate of incoming radiation, not on the canopy structure, and describe their results as intercepted PAR, or FPAR, paying specific attention to spectral differences in radiation absorption and reflection (Goward and Huemmerich 1992). A recent refinement of this logic is to represent the FPAR, the fraction of PAR absorbed relative to the incident spectral radiation. A significant part of the theoretical effort recently has been the unification of theory between description of plant canopies by LAI and by FPAR through the separation of ground cover and clump-leaf area (Asrar et al. 1992; Sellers et al. 1992). Asrar et al. (1992) theoretically showed an important interrelationship amongst LAI, FPAR, and NDVI that improves the utility of these biophysical variables. They found that under specified canopy reflectance properties (for a given biome), FPAR was linearly related to NDVI, and curvilinearly related to LAI, approaching the asymptote at an LAI of 6 where virtually all incident shortwave radiation is absorbed by the canopy. Similar results were shown by Sellers (1985, 1987, 1992) and Myneni and Williams (1994).

Consequently, given a canopy of known structure (land-cover type) and light scattering and absorbing properties, any one measure of the canopy can be used interchangeably with the others with some algebraic manipulation of formulae. Accurate utilization of the NDVI requires that the biome type be known so that the appropriate NDVI-to-LAI-or-FPAR conversion can be made. Further, observational details such as the solar zenith angle, sensor look angle, background (soil) exposure frac-

tion, and extent of uncorrected atmospheric interference change the NDVI-LAI-FPAR relationship significantly (Sellers 1985, 1987; Asrar et al. 1992; Myneni and Williams 1994).

EOS contribution: Satellite definition of LAI uses various VIS and NIR channels for optimum sensitivity for different biome types (Myneni et al. 1996). The regular weekly EOS monitoring of global LAI will be done by MODIS at 1 km, and will use biome-specific algorithms (Figure 5.13). However, the multiple-look angles of MISR will provide improved LAI definition of complex canopies such as forests, but with longer than the monthly repeat times of MODIS. Also, ASTER can provide regional LAI data to 15-m resolution with appropriate algorithms. The Schimel-IDS team is using advanced spectral mixture modeling to improve the LAI estimate of the structurally complex tree/grass savanna mixtures. The MODIS Land team is producing a standard combined LAI/FPAR product weekly at 1 km for the globe. The Sellers-IDS team is researching advanced formulations for deriving FPAR from Spectral Vegetation Indices. The Schimel-IDS team is concentrating on the particular problems of defining LAI and FPAR for the complex savanna canopies. The Cihlar-IDS team is exploring the problems of low-illumination angles at high boreal latitudes on LAI and FPAR retrieval.

5.2.3.3.3 Vegetation indices

The first global vegetation analyses were done with the NDVI from the AVHRR sensor (Tucker et al. 1985; Justice et al. 1985; Goward et al. 1985). A continuous record of consistently-processed terrestrial NDVI from 1981 to the present now exists in the EOS AVHRR Pathfinder program. These data are a priceless archive of the global terrestrial land surface, and have provided valuable lessons on the challenges of processing the volumes of global data that will be generated by EOS (Justice and Townshend 1994).

A number of improvements have been made to the original 2-channel NDVI algorithm (Pinty and Verstraete 1992; Qi et al. 1994). The soil-adjusted vegetation index (SAVI) introduced a soil calibration factor, L , to the NDVI equation to minimize the soil background bias resulting from first-order soil-plant spectral interactions (Huete 1988). This not only minimized soil background effects on the vegetation index (VI), but also eliminated the need for additional calibration for different canopy background conditions. The atmospherically-resistant vegetation index (ARVI) incorporates the blue band into the NDVI equation to stabilize the index to temporal and spatial

variations in atmospheric aerosol content (Kaufman and Tanré 1992).

The MODIS VIs are envisioned as improvements over the current NOAA-AVHRR NDVI as a result of both improved instrument design and characterization and the significant amount of VI research conducted over the last decade. The new indices are based on improved knowledge of atmospheric effects, soil effects, sun- and view-angle effects, surface anisotropy, and canopy radiant transfer models. Improved vegetation sensitivity will be achieved with improved MODIS sensor characteristics and from the optimal utilization of MODIS sensor wavebands. The new MODIS VI will: 1) increase sensitivity to vegetation; 2) further normalize internal and external noise influences, thus improving the vegetation signal-to-noise ratio (external-, internal-, and sensor-caused); and 3) provide new, unique information for vegetation analysis. External variations will be minimized through atmospheric correction algorithms, an atmospherically-resistant NDVI equation, and a level 3 compositing algorithm which incorporates the anisotropic reflectance behavior of vegetated surfaces utilizing directional MISR data.

EOS contribution: The commonly-used 2-channel NDVI algorithm will be produced by the MODIS Land Team as a heritage NDVI to maximize consistency of the continuous record of AVHRR data since 1981 (Huete et

al. 1994). In addition to the heritage NDVI, MODLAND-Huete will also produce advanced Vegetation Indices that correct for variable background and soil reflectance using multiple wavelengths from the 36-channel MODIS sensor and incorporating atmospheric corrections of all channel reflectances done automatically in the MODIS data processing stream.

5.2.3.4 Vegetation phenology

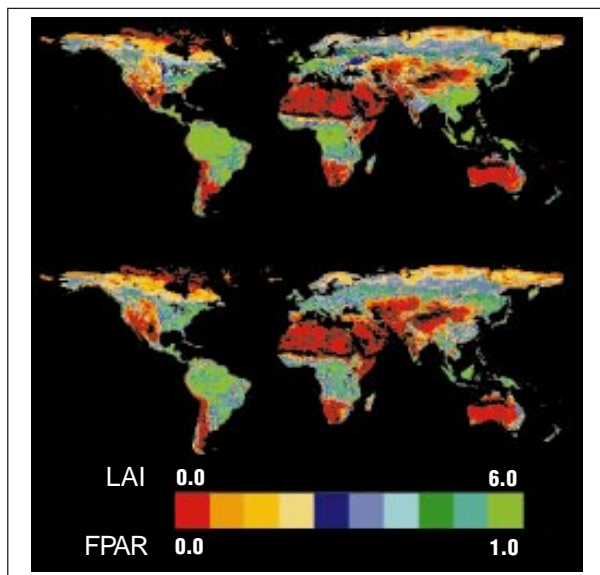
Possibly the most direct and observable response of vegetation to climatic fluctuations is the interannual variability in the timing of spring vegetation growth, primarily, the leafing out of tree canopies and greening of grasses. This seasonal timing, termed phenology, has been found to vary by more than a month. During cool springs, plant development begins later in temperate and boreal latitudes than in warm years. This rather abrupt change in surface albedo, roughness, and wetness measurably changes the energy exchange characteristics of the land surface (Schwartz 1996). Studies have capitalized on the high temporal frequency of AVHRR, and the simple greenness definition provided by NDVI to study phenology at continental scales (Reed et al. 1994).

EOS contribution: During the EOS era MODIS data will be processed at high temporal resolution over certain mid-to-high-latitude cloud-free areas to monitor interannual variability in vegetation phenology. As global climatic change progresses, this phenology monitoring will provide a consistent and rapid measure of vegetation response.

5.2.3.5 Net Primary Production (NPP)

Current best estimates of terrestrial carbon fluxes are 100 to 120 Pg of carbon ($= 10^{15}$ g or a Gigatonne) taken up over a year by photosynthesis, and about 40-to-60 Pg are released over a year by autotrophic respiration for a total terrestrial NPP of about 50 Pg C (Post et al. 1990; Melillo et al. 1993). This averages out to about 370 gC m^{-2} of land surface. Currently about 1.8 Pg of the carbon released by fossil fuel combustion and deforestation are not accounted for by the atmosphere or ocean, and are presumably taken up by terrestrial ecosystems (Tans et al. 1990; Quay et al. 1992; Sundquist 1993). This represents about 4% of the annual NPP, which is well below the amount which may be detected from ground measurements. The spatial variability of NPP over the globe is enormous, from about 1000 gC m^{-2} for evergreen tropical rain forests to less than 30 gC m^{-2} for deserts. With increased atmospheric CO_2 and global climate change, NPP over large areas may be changing. To be sensitive to spatial variability, global NPP is best determined by remote

FIGURE 5.13



Global fields of leaf-area index (LAI) and fraction-absorbed photosynthetically-active radiation (FPAR) computed with AVHRR data for 1982-1991 (Myneni et al. 1996). EOS will produce these products weekly at 1-km resolution from MODIS and MISR data beginning with the EOS AM-1 launch.

sensing, which is one of the key objectives of NASA's Earth Science Enterprise. EOS, and specifically MODIS, were designed in part for the scientific objective of calculating global terrestrial NPP (MODIS Instrument Panel Report 1986).

Goward et al. (1985) was the first study showing a relationship between NPP and NDVI, which was confirmed by Box et al. 1989. Running and Nemani (1988) used a model, the forest-biogeochemistry cycles (FOREST-BGC) model, to show that photosynthesis (PSN) and NPP were also related to NDVI. Sellers (1985, 1987) derived the theoretical relationship between NDVI, the Absorbed Photosynthetically-Active Radiation (APAR), and photosynthesis for unstressed vegetation. Cihlar et al. (1992) showed a similar relationship between PSN and NDVI with the experimental data from the FIFE. Most recently, Runyon et al. (1994), from the Oregon Transect Terrestrial Ecosystem Research (OTTER) experiment, showed NPP to be related to the annual intercepted PAR (about equal to APAR). The advanced MODIS data product of daily PSN more correctly defines terrestrial CO₂ fluxes than simply NDVI to increase understanding on how the seasonal fluxes of net photosynthesis are related to seasonal variations of atmospheric CO₂.

The NPP products are designed to provide an accurate, regular measure of the production activity or growth of terrestrial vegetation. These products will have both theoretical and practical utility. The theoretical use is primarily for defining the seasonally-dynamic terrestrial surface CO₂ balance for global carbon cycle studies such as solving the "missing sink question" of carbon (Tans et al. 1990). The spatial and seasonal dynamics of CO₂ flux are also of high interest in global climate modeling, because CO₂ is an important greenhouse gas (Keeling et al. 1989). Currently, global carbon-cycle models are being integrated with climate models, towards the goal of integrated Earth Systems Models that will represent the dynamic interaction between the atmosphere, biosphere, and oceans. The weekly PSN product is most useful for these theoretical CO₂ flux questions.

The practical utility of the NPP product is as a measure of crop yield, forest production, and other economically and socially significant products of vegetation growth. As our regular global NPP products become well known, we expect a wide variety of derived products to be developed, making regionally-specific estimates of local crop production. NPP is important for a wide variety of uses, from applications like regional crop/range/forest yield forecasting to biospheric carbon cycle increments of biomass sequestration. Regional-to-global NPP may have the highest commercial potential of any EOS variable because it can be used by the agribusiness sector

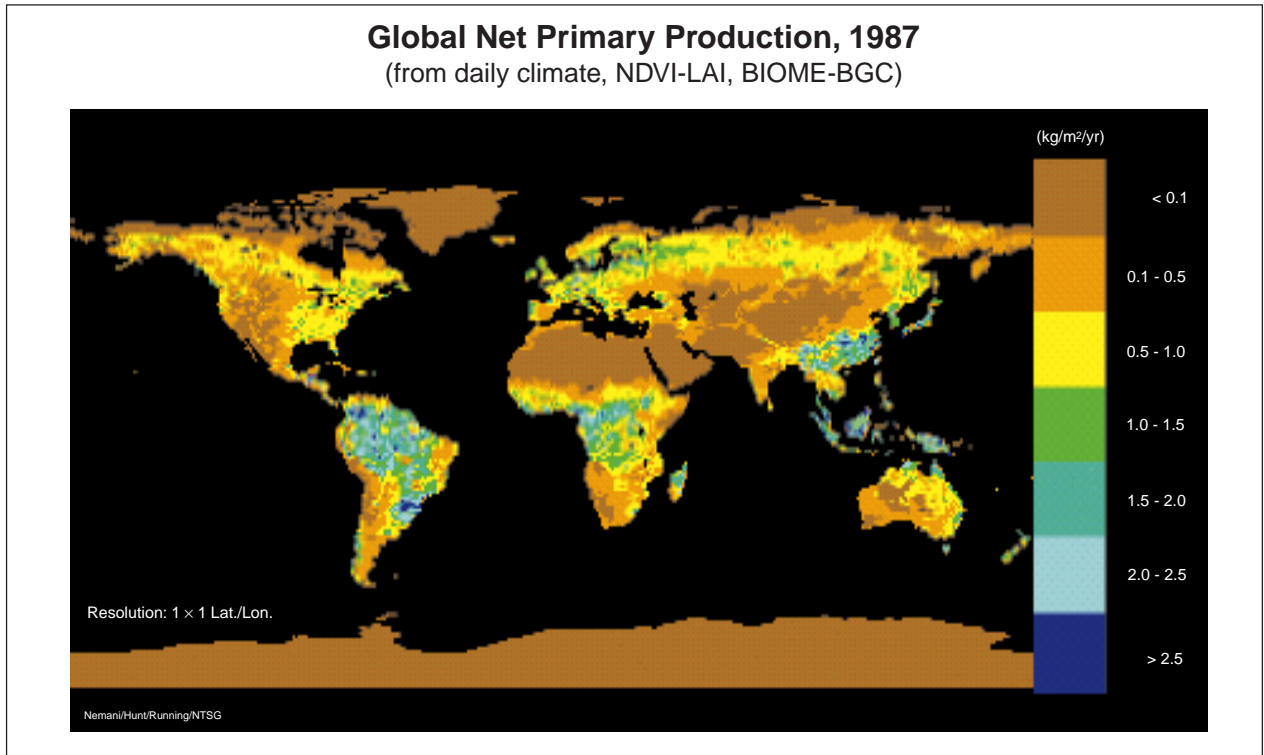
for crop futures commodity planning, disaster insurance analysis, etc.

The algorithms for these products are based on the original logic of J. L. Monteith (1972, 1977), which relates PSN and NPP to the amount of APAR. Spectral Vegetation Indices (SVI) are useful for quantifying the FPAR that is absorbed and the LAI. To implement the algorithms, ancillary data on climate and incident PAR from the Rood-IDS DAO and MODIS land-cover type are required.

The MODIS NPP product is designed to provide a weekly NPP estimate for time-critical activities where the data are only useful if delivered in near-real time (Figure 5.14). Because a comprehensive biospheric model cannot be run every week, this NPP product will be produced from simpler algorithms based on the time-integrated Production Efficiency Model (PEM) logic (Prince and Goward 1995). The weekly MODIS NPP will use the MODIS land cover to define a biome type and a biome-and-seasonally-specific conversion from PAR to NPP. Then the weekly composited FPAR will be generated, and weekly PAR. The weekly MODIS NPP will be available globally at 1-km resolution. The first stage of algorithm development (at launch) will use a simple PEM with temperature and humidity controls on photosynthesis estimated from gridded DAO climate data. With further development (post launch), the efficiency parameter may be determined remotely from the MODIS Vegetation Index (MVI), land-cover type, land-surface temperature, snow/ice cover, surface resistance index, and ancillary meteorological data.

The main problem after computing FPAR and PAR is the determination of the PAR conversion efficiency, ϵ (Field et al. 1995). Prince (1991) summarized values for herbaceous vegetation and found an average from 1.0 to 1.8 gC/MJ for plants with the C₃ photosynthetic pathway, and higher for plants with the C₄ photosynthetic pathway. Running and Hunt (1993) and Hunt (1994) found published values of ϵ for woody vegetation were lower, from about 0.2 to 1.5 gC/MJ. Global variation of the efficiency factor is controlled partially by varying climatic conditions, and partially by inherent physiologic differences of vegetation. Hunt and Running (1992a, 1992b) and Hunt et al. (1996) used a general ecosystem model, BIOME-BGC, to simulate ϵ and found that climate and land-cover types are extremely important factors determining the observed global range of values. Cold temperatures and water stress limit the length of the growing season thereby decreasing conversion efficiency. The maintenance respiration costs of, for example, tree stems, reduces the conversion efficiency for forests and other perennial vegetation.

FIGURE 5.14



The global annual net primary production (NPP) for 1987 computed from AVHRR data. EOS will produce a weekly global NPP at 1 km beginning with the launch of the AM-1 platform. These NPP data will be useful for crop production forecasting, range management, and forest yield estimates.

EOS contribution: The MODIS Land Team will generate a standard weekly EOS NPP product for public use. The Moore-IDS and Sellers-IDS teams will compute global annual NPP as research activities. The Cihlar-IDS team will compute the global boreal forest NPP, and IDS-Schimel the global grassland biome NPP. These IDS teams will use MODIS land-cover and weekly FPAR products, daily 4DDA surface climatology, and EOS ancillary topography and soils databases to parameterize their models. The biospheric simulation models TEM (Moore-IDS), Century (Schimel-IDS), and Biome-BGC (MODLAND-Running) compute NPP as a part of comprehensive ecosystem simulations, which also include photosynthesis-respiration, allocation, litterfall, and decomposition processes, with water and nitrogen cycle controls. Each defined biome type is simulated with biome-specific parameterizations. These advanced models are being developed as components in dynamic Earth Systems Models that will allow accurate future biospheric response forecasting (VEMAP 1995).

An intercomparison test of these terrestrial carbon balance models for the continental U.S. has recently been completed and global model NPP intercomparisons are

underway (Potsdam Institute for Climate Impact Research [PIK]-95, see Section 5.4.6.3). These NPP calculations will be part of global carbon-cycle analyses exploring changes in NPP predicted from climate-change scenarios, answering questions of the “missing sink” in current biospheric carbon-cycle science. Highest priority for these studies is accuracy, so these NPP calculations will be done with year-end EOS data sets that have been error checked, updated, and calibrated. A global database of field-measured NPP from different biomes is being assembled to provide a source of validation data for this NPP product (see Sec 5.4.5.3.5).

5.2.3.5.1 Stem and soil carbon

All computations of terrestrial carbon-cycle balances require input of the live biomass in tree stems that emit CO₂ in maintenance respiration activity, and the dead carbon in soil horizons that release CO₂ from decomposition activity. These ecosystem properties are not directly remote sensible, so a number of inference techniques must be used to provide estimates. Inferences are best done by considering the NPP and biome-specific vegetation life-history characteristics of a region. A forest primarily

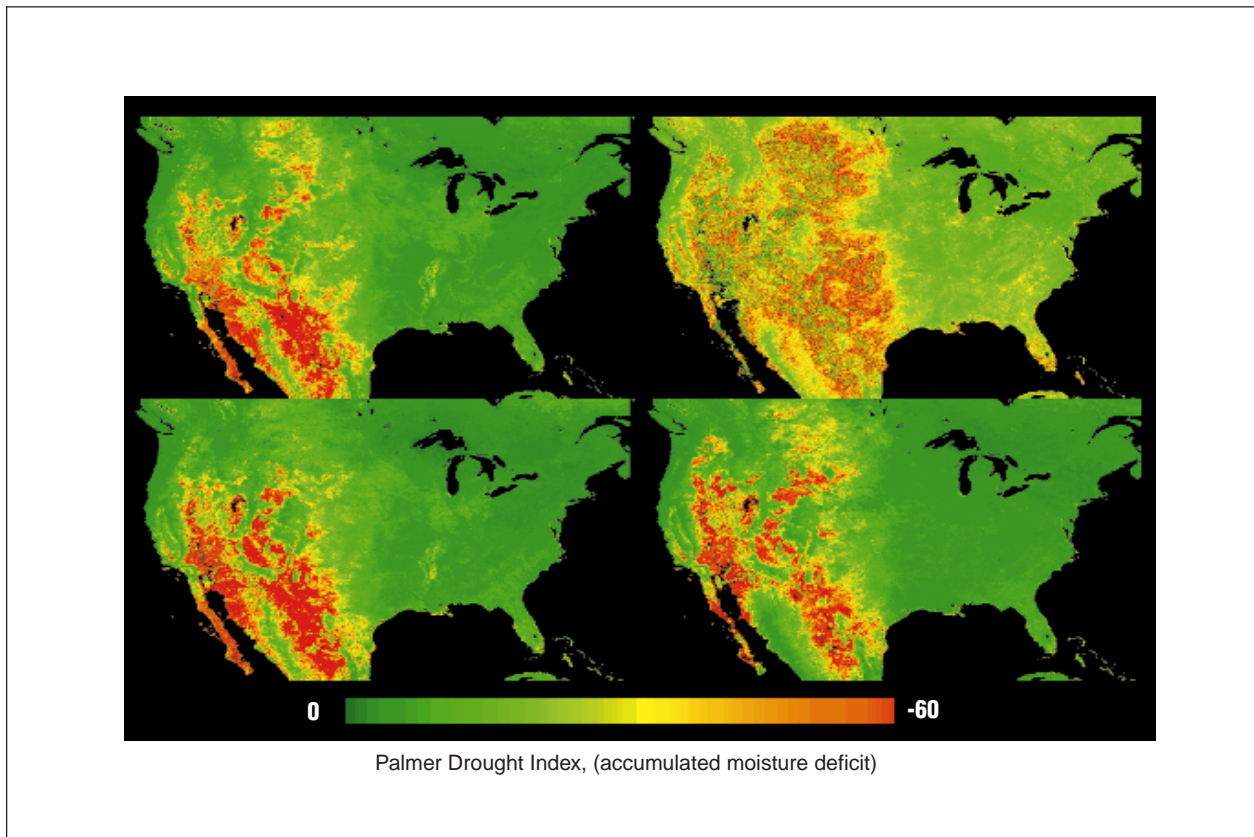
accumulates stem carbon while a grassland accumulates soil carbon. The final step is analysis of the land-cover-change rate for a region. The presumed stem carbon of a mature forest would clearly not be accurate in an area that had been deforested.

EOS contribution: Because of the complicated and biome/region-specific nature of these variables, no standard EOS product generation is planned. Each IDS team is building estimates of stem and soil carbon for research activities in specific areas. The Schimel-IDS team has the most specific research on these problems because grasslands and savanna sequester the highest percentage of annual NPP in soil carbon of any biome type. Boreal forests with low temperature and nutrient-limited decomposition activity are also biomes with high soil carbon sequestration, the focus of the Cihlar-IDS team.

5.2.3.6 Regional weekly application products

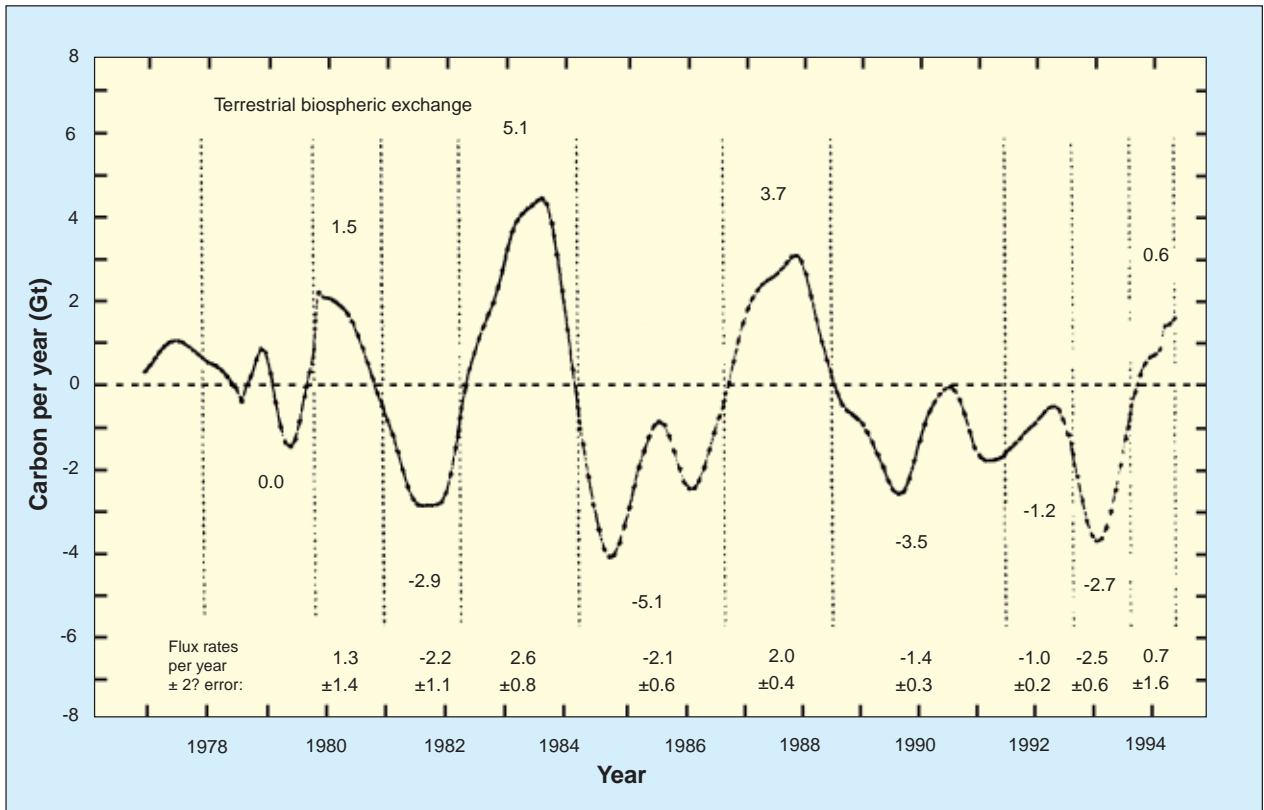
Although much of the EOS datastream is meant for long-term monitoring and global science, some of the terrestrial satellite data can have immediate utility if delivered in real time. The Running-MODLAND team will produce some weekly land products for use by natural resource land managers. Critical to these products is 1 km or better spatial resolution and near-real-time delivery at the end of each weekly computation period. These are crop/range/forest productivity index, drought index (Figure 5.15), and fire danger index. An integrated program for landscape fire management is planned from EOS, which will include fire danger monitoring, mapping ignitions at high frequency and accuracy, tracking fire behavior and movement, computing trace gas emissions, and finally post-fire ecosystem responses (Kaufman et al. 1996). Because all of these indices require the computationally-

FIGURE 5.15



Comparison of the mid-summer drought intensity across the United States for 1988, the year of the Yellowstone Park fires, with the more-normal summer of 1989. This drought index is derived from the NDVI and surface-temperature data from AVHRR using the methodology of Nemani et al. (1993) and Nemani and Running (1989). This satellite-derived drought index will be produced weekly by EOS for applications in agriculture, range and forest management, and for wildfire danger monitoring.

FIGURE 5.16



Interannual variability in terrestrial biospheric net CO₂ exchange, computed from the network of flask sampling of atmospheric CO₂ and an atmospheric transport model (Keeling et al. 1995).

intensive surface resistance product from the PM-1 MODIS sensor and rapid delivery, this product is currently planned to be available only for the continental U.S.

5.2.3.7 Biogeochemistry

The necessity to more accurately quantify global terrestrial vegetation activity was emphasized by attempts in the late 1970s to calculate a global carbon budget. Although it was clear from the Mauna Loa CO₂ concentration record that global atmospheric CO₂ was increasing, the anthropogenic sources did not seem to balance the ocean and terrestrial sinks. In an effort to locate the missing carbon, measured atmospheric CO₂ concentrations around the world were used in global models tracing known sources and sinks (Keeling et al. 1989; Tans et al. 1990). Previously, Tucker et al. (1986) showed NDVI alone can explain much of the global patterns of atmospheric CO₂ concentration. More significantly, this problem underscored the lack of defensible measurement capability of terrestrial primary production at global scales.

CO₂ is the most important carbon cycle flux variable, and because it is a greenhouse gas, is a critical

connecting point between the biosphere and the atmosphere. CO₂ is absorbed by vegetation during photosynthesis, and released by respiration and decomposition processes. Hence, CO₂ flux rates can be positive or negative, depending on the level of activity of the underlying ecosystem processes, and can change hourly as microclimatic conditions change at the surface. Because photosynthesis can only occur during daylight, while respiration and decomposition occur continuously, at global scales, the relative CO₂ balance is influenced by latitude and the seasonal changes in daylength (Ciais et al. 1995). Additionally, CO₂ flux rates are very different for different vegetation types, and stages of vegetation development. The summary of this seasonally-changing vegetation activity is observable in the atmospheric CO₂ concentration records, such as the record for Mauna Loa (Keeling et al. 1989). El Niño interannual climate variations cause measurable perturbations regionally to atmospheric CO₂ signals. The role of climate in controlling interannual variability in biospheric CO₂ balances was dramatically illustrated by the effect the Mt. Pinatubo eruption in 1991 had in slowing the rate of rise in atmo-

spheric CO₂, beginning immediately in 1992 (Figure 5.16) (Keeling et al. 1995).

EOS contribution: All EOS global CO₂ flux research will be model-generated because CO₂ is not directly observable by satellite. The IDS-Sellers team will use SiB2 for global CO₂ flux calculations similar to the work in Sellers et al. (1996) where the influence of vegetation physiological controls on summer air temperatures was studied. Mid-continent air temperatures were found to be higher in the summer when stomatal closure by vegetation was included in the GCM dynamics of the land surface. SiB2 will use MODIS standard products for land cover and LAI/FPAR for initial parameterization. These CO₂ balances from SiB2 will be used in GCMs as part of their greenhouse gas balances. The Schimel-IDS team is emphasizing global grasslands and arid lands in their carbon balance simulations. They find an important conceptual simplification that maximum photosynthetic activity scales linearly with absorbed light in complex multi-storied savannas. This result solidifies the logic for the EOS productivity calculations planned. The Cihlar-IDS team is concentrating on global boreal forest carbon balances. The Cihlar team is currently testing EOS vegetation algorithms under the rather unique conditions of boreal landscapes. Arid and high-latitude regions have been identified as areas where climatic change consequences could be particularly severe. The Moore-IDS team, in addition to computing annual terrestrial CO₂ fluxes, is modeling the transport of carbon via rivers to the oceans.

Other aspects of terrestrial biogeochemistry are also being studied, particularly greenhouse gas dynamics of different biomes. The Schimel-IDS team will calculate methane and N₂O for global grasslands using their Century biospheric model. The Moore-IDS team will assemble a global methane budget from Measurements of Pollution in the Troposphere (MOPITT), TES, and ground data sources for use in their TEM biospheric model.

5.2.3.8 Predictions of terrestrial biospheric dynamics

The only means of predicting future biospheric dynamics is with comprehensive simulation models. Because of the intimate interrelationships amongst the oceans-atmosphere-biosphere, component models cannot effectively provide predictive capability in isolation. Only comprehensive dynamic coupled Earth systems models will provide the predictive accuracy needed by policy makers and society. These models do not yet exist, although prototypes are nearly ready for initial testing. The ultimate accuracy of Earth systems models will rely both on the quality of the models, which are under intensive development now, and the quality and regularity of the

global-monitoring data used by the models to define the Earth system. The role of EOS is clear here: no Earth systems model, no matter how theoretically rigorous and elegant, will have adequate predictive capability without being initialized by accurate, timely, and complete global information.

EOS contribution: The most organized terrestrial modeling programs operating now are VEMAP, a multi-model simulation of the continental U.S., and PIK-NPP, an international effort to improve global NPP models, hosted by PIK. In the VEMAP activity, three GCM climate-change scenarios (United Kingdom Meteorological Office [UKMO], Geophysical Fluid Dynamics Laboratory [GFDL], and Oregon State University [OSU]) are being used to drive coupled biogeography and biogeochemistry models of the U.S., to explore how both potential biome distribution and carbon-cycle processes will change concurrently with doubled CO₂ and resulting climatic change. The biogeography models (BIOME2, Prentice et al. 1992; DOLY [the Dynamic Global Phyto-geography model], Woodward et al. 1995; MAPSS; Neilson 1995) all use climatic indices and thresholds to determine the geographic distribution of biomes. The biogeochemistry models TEM, Century, and BIOME-BGC, calculate the carbon, water, and nutrient cycle balances of the system. The first VEMAP results (VEMAP 1995) suggest high uncertainty on whether continental forest cover may increase or decrease dependent on how precipitation patterns change. The biogeochemistry models all predict a modest overall increase in NPP because the CO₂ enhancement effect counteracts climatic change effects. However, some specific regions may have significant reduction in NPP. Although all of these models are structurally similar, results reflect subtle differences in the theoretical balancing of water, energy, and nutrition in controlling biome distribution and biogeochemistry. These uncertainties must be overcome before trustworthy dynamic Earth systems models can become a reality.

The PIK-NPP project is intercomparing the calculations of global annual NPP made by 18 top research laboratories worldwide. These global NPP models exhibit different logics and theoretical rigor, and rely in varying ways on remote sensing for inputs. Some models are completely defined by the satellite data; others use satellite data to initialize land cover and LAI, then simulate NPP using surface climate data. This intercomparison is an important test of the EOS algorithms for NPP, probably the most important terrestrial vegetation variable generated by the program.

5.3 Required measurements and data sets for quantifying land-surface attributes

5.3.1 Introduction

The derivation of biophysical parameters (net radiation, temperature, precipitation, ET, LAI, non-photosynthetic vegetation, thermal inertia) from remote-sensing data is highly dependent on calibration, spectral and spatial imaging resolution, illumination and measurement geometry, and atmospheric conditions. To determine the impact of these factors on models of hydrology or primary production and nutrient cycling requires that investigators have easy access to Level 1b imaging products. At this level it is possible to analyze images using nominal calibrations and then to perturb calibrations to examine the sensitivity of interpreted biophysical parameters that are entering the model predictions. This level of processing allows screening of data to guarantee specific spatial resolutions and viewing geometries (solar zenith, azimuth, phase, and viewing angles) to minimize uncertainties resulting from extreme viewing angles.

Land-surface remote sensing and modeling is a particularly difficult task. Unlike the world's oceans whose roughness, albedo, heat capacity, and emissivity vary slowly (if at all) and can be estimated accurately, the world's land surface is characterized by considerable spatial and temporal heterogeneity in these basic parameters and additional processes which variably regulate the partitioning and magnitude of near-surface energy and water fluxes. These features are particularly divisive in regions with mixed or partial canopies. The consequence of this for satellite remote sensing and modeling is a requirement for more-accurate and higher-resolution measurements made more often.

5.3.2 EOS sensors

5.3.2.1 MODIS

MODIS will be the primary daily global monitoring sensor on the EOS AM-1 and PM-1 satellites. MODIS is a 36-channel nadir-pointing radiometer covering 0.415–14.235 μm wavelengths, with spatial resolution from 250 m to 1 km at nadir. The global repeat time will be from 1–4 days, depending on latitude and view-angle limits. MODIS will be the primary EOS sensor for providing data on terrestrial biospheric dynamics and vegetation process activity. The suite of global land products planned for EOSDIS implementation includes spectral albedo, land cover, spectral vegetation indices, snow and ice cover, surface temperature and fire, and biophysical variables (LAI and fractional PAR) that will allow computation of global carbon cycles, hydrologic balances,

and biogeochemistry of critical greenhouse gases (Running et al. 1994). The regular global production of these variables will allow accurate land-surface-change detection, a fundamental determinant of global change. The MODIS instrument has the capability to provide measurements to derive most of the parameters required for the global-scale models of interest in hydrology and biogeochemistry on a one-to-two-day period, and, thus would be the primary data source.

Satellite-derived vegetation indices, such as the well known AVHRR NDVI, are used by numerous scientists for quantifying a number of vegetation attributes. The primary EOS vegetation index will be the MODIS Vegetation Index, or MVI, which will be produced weekly at 1 km, with a 2-channel version available at 250 m (Huete et al. 1994). Advanced multi-channel VIs are planned by the MODIS Land science team. MISR will provide BRDF data to improve the nadir VIs of MODIS.

5.3.2.2 MISR

MISR will obtain multidirectional observations of each scene within a time scale of minutes, thereby under virtually the same atmospheric conditions. MISR uses nine separate charge-coupled device (CCD)-based pushbroom cameras to observe the Earth at nine discrete view angles: One at nadir, plus four other symmetrical fore-aft views up to $\pm 70.5^\circ$ forward and afterward of nadir. Images at each angle will be obtained in four spectral bands centered at 0.443, 0.555, 0.67, and 0.865 μm . Each of the 36 instrument-data channels (four spectral bands for each of the nine cameras) is individually commandable to provide ground sampling of 240 m, 480 m, 960 m, or 1.92 km. The swath width of the MISR imaging data is 356 km, providing multi-angle coverage of the entire Earth in 9 days at the equator and 2 days at the poles. MISR images will be acquired in two observing modes, Global and Local. Global Mode provides continuous planet-wide observations, with most channels operating at moderate resolution and selected channels operating at the highest resolution for cloud screening, image navigation, and stereo-photogrammetry. Local Mode provides data at the highest resolution in all spectral bands and all cameras for selected 300×300 km regions.

MISR will be used to monitor global and regional trends in radiatively important optical properties (opacity, single scattering albedo, and scattering phase function) of natural and anthropogenic aerosols—including those arising from industrial and volcanic emissions,

slash-and-burn agriculture, and desertification—and to determine their effect on the solar radiation budget. Over land, the dependence of absolute radiance and scene contrast as a function of angle will be used to retrieve opacity, absorptivity, and phase function. The measured radiances will be directly integrated to yield estimates of reflected flux, hence albedo. For determinations of these quantities at the surface, radiative transfer inversions of the top-of-atmosphere radiances will be used to retrieve multi-angle surface reflectances using aerosol information also derived from MISR data. Automated stereo-image-matching algorithms will be used to derive surface topography and cloud elevations from multi-angle stereoscopic observations. Over the land surface, these data will aid studies of the impact of land-surface processes on climate variables. BRDF measurements of various scene types will be used for the development and validation of models relating soil, snow, and ice angular reflectances to surface albedo. For vegetated terrain, measured angular signatures will be related to canopy structural parameters, will provide improved vegetation cover classifications, and will be used to retrieve surface hemispherical albedos. This information will be used to derive APAR and improved measurements of vegetation canopy photosynthesis and transpiration rates.

5.3.2.3 ASTER

ASTER will operate in three visible and near-infrared (VNIR) channels between 0.5 and 0.9 μm , with 15-m resolution; six short-wavelength infrared (SWIR) channels between 1.6 and 2.5 μm , with 30-m resolution; and five TIR channels between 8 and 12 μm , with 90-m resolution. The instrument will acquire data over a 60-km swath whose center is pointable cross-track $\pm 8.5^\circ$ in the SWIR and TIR, with the VNIR pointable out to $\pm 24^\circ$. An additional telescope (aft pointing) covers the wavelength range of Channel 3. By combining these data with those for Channel 3, stereo views can be created with a base-to-height ratio of 0.6. ASTER's pointing capabilities will be such that any point on the globe will be accessible at least once every 16 days in all 14 bands and once every 5 days in the three VNIR channels. However, global coverage at 15 m might require most of a year to acquire.

ASTER will provide surface reflectances and radiative (brightness) temperatures. The multispectral TIR data can be used to derive surface kinetic temperature and spectral emissivity. This temperature/emissivity information can be used to verify similar procedures employing MODIS data. Surface kinetic temperature can be used to determine elements of surface process models, sensible heat flux, latent heat flux, and ground heat conduction.

Surface temperatures are also related to thermophysical properties (such as thermal inertia), vegetation health, soil moisture, temporal land classification (wet vs. dry, vegetated vs. bare soil), and ET.

Both ASTER and MISR image data will be used to assist in defining spectral trajectories associated with atmospheric variations that are not visually resolvable in MODIS data. Several specific sites will be selected to aid in calibrating and defining adaptive filters that minimize the effect of spectrally complex areas on biophysical parameter estimates. In forested areas the spectral measurements of vegetation are not useful as a measure of cover (all areas are 100% covered by vegetation), but rather correspond largely to canopy architecture and foliar anatomy. Both ASTER and MISR data sets are useful because they can provide a series of measurements over a range of look angles. Differences in the seasonal phenology of different forest community types can be detected using measurements that characterize the photometric function.

5.3.2.4 Landsat-7

The Earth-observing instrument on Landsat-7, the ETM+, replicates the capabilities of the highly successful TM instruments on Landsats-4 and -5*. The ETM+ also includes new features that make it a more-versatile and efficient instrument for global-change studies, land-cover monitoring and assessment, and large-area mapping than its design forebears. The primary new features on Landsat-7 are:

- a panchromatic band with 15-m spatial resolution;
- on-board, full aperture, 5% absolute radiometric calibration; and
- a thermal IR channel with 60-m spatial resolution.

Landsat-7 and ETM+ will have the following characteristics:

The instrument will be supported by a ground network that will receive ETM+ data via X-band direct downlink only at a data rate of 150 Mbps. The primary receiving station will be at the USGS's Earth Resources Observation System (EROS) Data Center (EDC) in Sioux Falls, South Dakota. Substantially cloud-free land and coastal scenes will be acquired by EDC through real-time downlink, and by playback from an on-board, solid-state, recording device. The capacities of the satellite, instrument, and ground system will be sufficient to allow for continuous acquisition of all substantially cloud-free scenes at the primary receiving station. In addition, a worldwide network of receiving stations will be able to receive real-time, direct downlink of image data via

X-band. Each station will be able to receive data only for that part of the ETM+ ground track where the satellite is in sight of the receiving station.

The Landsat-7 system will ensure continuity of TM-type data into the next century. These data will be made available to all users through EDC at the cost of fulfilling user requests. Browse data (a lower-resolution image for determining image location, quality, and information content) and metadata (descriptive information on the image) will be available, on-line, to users within 24 hours of acquisition of the image by the primary ground station. EDC will process all Landsat-7 data received to "Level 0R" (i.e., corrected for scan direction and band alignment but without radiometric or geometric correction) and archive the data in that format. A systematically-corrected product (Level 1G) will be generated and distributed to users upon request. The user will have the option of performing further processing on the data on user-operated digital processing equipment or by employing a commercial, value-added firm.

<http://geo.arc.nasa.gov/sge/landsat/17.html>

5.3.3 Ancillary data sets

These data are critical to any investigation of the surface but represent static data sets whose need and responsibility cut across many groups.

5.3.3.1 Soils

Soils data are required by virtually every climate, hydrology, or ecosystem model, although again, different variables are important to the different disciplines. Surface albedo is required for energy balance models and for vegetation radiative transfer models. Soil depth, water-holding capacity, and texture or drainage characteristics are needed by all models to quantify the retention and release of water by soils to the atmosphere, hydrologic systems, and vegetation. In water-abundant regions, soil capacitance partially defines the time constant of flood-water dynamics. In water-limited areas, soil water depletion regulates the increase of sensible heat partitioning that feeds back to climate models and produces the drought effects that reduce vegetation primary production. The ecosystem models also require some measure of soil carbon and nutrient content for biogeochemical modeling. However, beyond some general definition of parent materials, global soil nutritional estimates can best be estimated by biospheric models specializing in soil biogeochemical dynamics such as Century (Schimel et al. 1994).

The EOS soils data set planned for AM-1 at-launch use is being developed as part of an IGBP-led project to compile and unify soils data sets from every country. Globally-relevant pedo-transfer functions are being built to translate a global pedon database into the soil physical and geochemical properties required. The final global soils database from the IGBP-DIS Global Soils Data Task will be gridded at 5° resolution, and will include soil carbon, soil nitrogen, water-holding capacity, and thermal properties.

The distribution of rock types constitutes the first-order influence on spatial patterns of soils and topography, and therefore on regional hydrologic responses, erosion rates, and natural hazards. Construction of consistent global maps of lithology through digitizing currently available national maps and augmenting with Landsat or ASTER would provide an extraordinary resource for interpreting many of the land-surface characteristics that will be used in models of vegetation, hydrology, and biogeochemistry.

5.3.3.2 Topography

The most important ancillary data set required by EOS land science is global topography. However, the resolution of topographic data needed differs among climate, hydrology, and vegetation disciplines. While 1-km horizontal resolution DEMs are adequate for LSM parameterizations of 1° × 1°, hydrology and vegetation scientists working with 1 km and finer sensor data require the full 100-m horizontal resolution and 1-m vertical resolution possible with best current technology. Hydrologists use topographic data for microclimate corrections, snow-melt models, and for river-drainage-network delineation, and coastline identification. Vegetation scientists use topographic data to correct raw sensor radiances for elevational pathlength and topographic shading corrections, slope-related pixel illumination corrections, and geolocation corrections. For MODIS land products at 1-km, 500-m, and 250-m resolution, and ASTER and MISR land products of even finer resolution, consistent global topographic data of highest possible accuracy will improve these land products.

The Global Land 1-km Base Elevation project plans a 1-km/100-m horizontal/vertical resolution global data set as the best topographic database possible for at-launch AM-1 requirements of January 1998 delivery to EOSDIS. Although higher detail DEMs are available for some parts of the world, such as the U.S. and Europe, no globally-consistent database of higher accuracy is possible with current national databases. Future efforts, possibly includ-

ing a Shuttle Radar Topography Mission may provide data for resolution to 30-m/16-m horizontal/vertical resolution by mid-1999.

NASA is currently sponsoring the Digital Topography Program to evaluate different technologies for the production and use of DEMs. Under this program, DEMs generated from airborne (Topographic SAR [TOPSAR]) and spaceborne (ERS-1, Shuttle Imaging Radar-C [SIR-C]) radars are being compared with topographic models derived via traditional photogrammetric techniques, as well as state-of-the-art global positioning system (GPS) arrays such as real-time kinematic (RTK-GPS). Numerous field sites are located within the U.S., including the Mississippi River, the southwestern desert, and volcanic terrains in Hawaii, plus additional sites in the Philippines and Japan. These studies are also precursors to the Shuttle Radar Topographic mission scheduled for 1999/2000 and data from the Environmental Satellite's (ENVISAT's) Advanced Synthetic Aperture Radar (ASAR) and the Advanced Land Observation Satellite (ALOS).

5.3.3.3 River and flood control networks

Topographic data alone are not adequate to define river runoff routing. Man has placed control structures such as levees and dams along many of the world's major streams, and their ability to confound comparisons between satel-

lite rainfall and model runoff is extreme without an effort to compile or link stage/discharge and flow records in such a way that the data are accessible. EOS or EOSDIS can contribute to efforts to overcome these problems by making this type of information available for U.S. waterways and putting forward a template for collecting this information from abroad. The Global River and Drainage Basin Archive now being assembled (led by Charles Vorosmarty of the Moore-IDS team) will include a reservoir and dam database.

5.3.4 Assimilation data sets

The most critical assimilation data set for land science will be the surface meteorology provided by the Rood-IDS team and the Goddard DAO. The 6-hour near-real-time production of land-surface incident radiation, temperature, precipitation, and humidity will be required by all hydrology and vegetation models. For many purposes, especially regional calculations, the $2^{\circ} \times 2.5^{\circ}$ gridded data set from the DAO will need to be disaggregated to finer spatial detail, using the topographic data set and appropriate meso- and micro-climate models. The VEMAP ecosystem modeling activity for the continental U.S. illustrates how gridded global climate data sets can be enhanced for simulations with finer spatial detail (VEMAP 1995).

5.4 Validation Programs For EOS

5.4.1 Responsibility hierarchy

Global-scale monitoring and validation will be very complicated, both scientifically and politically. For this reason it is imperative for every plan that it be clear who is responsible for execution of the work and what funding is provided. Five fundamental levels of responsibility have been identified that need to be dealt with:

- 1) *Individual*: Each EOS team member takes responsibility within their own EOS funding to do certain measurements at certain field sites.
- 2) *Sensor team*: Each sensor science team, for example the MODIS Land Team, may collectively agree to do certain joint validation activities, again, within their current funding.
- 3) *EOS project*: The EOS project may organize certain activities with joint cooperation from members of appropriate sensor and IDS teams. These activities will be executed solely with funding controlled by NASA.
- 4) *United States*: Some activities may be pursued jointly with agencies outside of NASA. For example, work with NOAA and the CO₂ flask network, DOE and the Free-Air Carbon dioxide Enrichment (FACE) program, and the National Science Foundation (NSF) with the Long-Term Ecological Research (LTER) program are logical and desirable. We must be very aware that these plans require ongoing interagency agreement on objectives, funding level etc., and are therefore much more difficult than activities sponsored from within NASA alone.

- 5) *Global*: The final most difficult activities will be international networks of sites and measurements requiring standardized measurement protocols, equipment calibration, archiving plans, etc. These programs can only be organized by international science organizations such as IGBP, WCRP, the International Hydrological Program (IHP), etc. Because the participation of each nation is both essential for global coverage but totally voluntary, these global networks are simultaneously both the most important yet most difficult aspect of EOS validation and monitoring.

Validation of vegetation variables: The Global Terrestrial Observing System (GTOS) and the terrestrial section of the Global Climate Observing System (GCOS) have been developing a 5-Tier approach to defining the level of financial and scientific activity required for different types of validation effort. These tiers recognize the joint necessity of large but temporary projects like FIFE, HAPEX, and BOREAS for certain EOS validations, but more-permanent geographically-distributed facilities like national resource station networks for other global validation activities. This organizing vision is essential for EOS to produce globally-consistent and representative validations of the full suite of land-science products.

5.4.2 Global organization of terrestrial observations

<http://www.wmo.ch/web/gcos/gcoshome.html>

GCOS/GTOS TOP: GCOS was established to provide the observations needed to meet the scientific requirements for monitoring the climate, detecting climate change, and for predicting climate variations and change. It was initiated via a Memorandum of Understanding (MOU) among WMO, the Intergovernmental Oceanographic Commission (IOC) of the United Nations Educational, Scientific, and Cultural Organization (UNESCO), the United Nations Environment Program (UNEP), and the International Council of Scientific Unions (ICSU), which set up a Joint Scientific and Technical Committee (JSTC) and a Joint Planning Office (JPO) located in WMO Headquarters in Geneva to develop the plans and strategy for implementation of the system. The Terrestrial Observation Plan (TOP) is a joint panel established by GCOS and GTOS to assure that a coordinated plan is produced and implemented. The panel made significant progress on drafting the initial terrestrial observation plan which was presented to the JSTC in October 1995. The strategy for implementing the plan is being developed in conjunction with the WCRP and IGBP.

The plan will provide the necessary climate requirements for GTOS and the terrestrial requirements for GCOS. The objective of the plan is to provide a rationale for the structure and implementation of the initial operational system. Following an introductory chapter, the plan describes the uses of the data, provides a rationale for selection of specific variables, describes a design for sampling sites, a rationale for site selection, a short description of the GCOS data and information system, and lays out specific tasks to be completed to implement the system.

The TOP for climate includes elements of hydrosphere, cryosphere, and biosphere. Shifts in temperature and precipitation will affect energy and water balances, which in turn will cause changes in distribution and abundance of vegetation. Shifts in vegetation patterns then feed back directly to climate. Consequently, understanding the interactions between hydrosphere, cryosphere, and the biosphere is important both from the point of view of understanding and predicting climate change and from understanding the effects of climate change on terrestrial ecosystems. One of the most significant accomplishments at the TOP meeting was to agree on a sampling design for the ecological variables. Many hundreds of variables are potential candidates for global climate monitoring, and there are many thousands of potential sample locations. It is neither feasible nor desirable to measure everything, everywhere, all the time. Most variables have characteristic time-and-space domains in which they should be monitored.

Infrastructure Hierarchy: The GCOS/GTOS observation network planning team developed a 5-Tier approach for defining the relative role, capability, and permanence of different research programs and facilities in different countries. These tiers are:

- *Tier 1*: Major experiment sites such as FIFE or BOREAS. Intensive but usually short-term measurements. Global availability < 20
- *Tier 2*: Major permanent research facilities such as the ARM-Cloud and Radiation Testbed (CART) site with complete instrument suite and comprehensive on-site staff. Global availability ~ 30
- *Tier 3*: Permanent research networks such as the U.S. LTER network. Permanent facilities but measurements of regular meteorology, vegetation, hydrology only. Global availability ~ 300
- *Tier 4*: Temporary sampling points for specific variable acquisition. No permanent on-site facilities, but

may be coordinated from a Tier 2-3 station. Global availability ~10,000

- *Tier 5:* Sensor calibration sites with stable radiometry such as White Sands or Railroad Playa

When planning different measurement/monitoring activities, it is useful to suggest the Tier that each site would best fall into for purposes of organizing activities appropriate to the infrastructure required.

5.4.3 EOS IDS field sites

Various programs have been proposed to validate both remotely-sensed data and model fields derived from EOS products. This effort must be international and span a wide range of climates and biomes, and it must be a long-term effort to maintain a level of confidence in the data sets. A number of basin-to-regional-scale validation and process study efforts and how they fit into each IDS team's overall effort are summarized below. Of primary importance in these investigations is the continuing need and support required to carefully validate satellite observations, algorithms, and model results with comparable-scale ground observations.

5.4.3.1 A/SA: Sahel and Upper San Pedro River basins

IDS: Utilization of EOS data in quantifying the processes controlling the hydrologic cycle in A/SA regions

PIs: Y. Kerr and S. Sorooshian

Two EOS IDS teams were combined to better study hydrologic processes of A/SA regions. The U.S. team has been developing process models starting at the local-watershed-to-regional scale while the French team is more concerned with large-scale operational remote-sensing issues, using existing and planned satellite missions (both EOS and international). Each team is working toward linking their findings at intermediate scales. A degree of model simplification has been achieved by considering the discontinuous nature of storm and interstorm processes that are common in A/SA environments.

Both teams devote considerable resources toward maintaining regional calibration/validation sites and activities in the African Sahel (Hapex-Sahel; Prince et al. 1995) and southeast Arizona (Upper San Pedro and Walnut Gulch; Kustas and Goodrich 1994) regions. An international, multi-agency, trans-border effort called the SALSA Program is being organized to study regional issues and mesoscale modeling with significant leadership

and participation by this group (Wallace 1995). Areas of primary interest include scaling, remote sensing, and process studies in semi-arid mixed grass-shrub watersheds including: geographic information system (GIS) development (particularly around riparian stream corridors), retrospective land-use studies, mesoscale modeling, rainfall-runoff modeling, and soil moisture data assimilation, and collaboration with the United States Department of Agriculture (USDA) Walnut Gulch Experimental watershed, the SALSA project, and EOS Instrument Team (IT)/IDS calibration/validation efforts. The nested approach followed by this group involves calibration and validation activities at a range of scales from the 10^2 km² Walnut Gulch watershed to the 10^6 km² Lower Colorado watershed (Figure 5.17; Michaud and Sorooshian 1994).

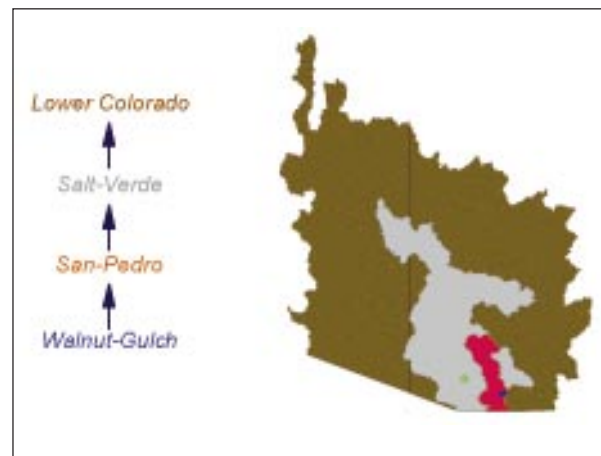
5.4.3.2 Biogeochemical analysis of savanna ecosystems

IDS: Using multi-sensor data to model factors limiting the carbon balance in global arid and semi-arid lands

PI: Dave Schimel

The Schimel-IDS team is studying the responses of global grasslands to global change. This team is emphasizing carbon-cycle processes, primary productivity, and biogeochemical cycling. The team uses the Century ecosystem model and specializes in soil carbon and nutrient cycling limits on global grasslands (Parton et al. 1993; Schimel et al. 1994). Savanna ecosystems cause special problems for estimating FPAR and LAI for tree/

FIGURE 5.17



Use of nested watersheds to provide a multiple-scale analysis of hydrologic processes from 10^2 to 10^6 km² in the southwestern United States (Michaud and Sorooshian 1994).

grass mixtures. A primary research site is the La Copita savanna in the Rio Grande Plains of Texas with secondary sites in Africa and China. Applications of this research will have high value for range resource management worldwide. The team also is developing global biospheric models, and is participating in the VEMAP project for model intercomparisons (VEMAP 1995).

5.4.3.3 *Humid/coastal: Susquehanna River Basin Experiment (SRBEX)*

IDS: Global water cycle—extension across the Earth sciences

PI: E. Barron

A series of nested and coupled models spanning a range of scales will be used to translate large-scale GCM results to shorter space-time scales. The goal is to produce global-change predictions at a spatial scale which is appropriate to assess their impact. A primary task in this effort is the collection of useful initialization/validation data sets and the integration of regional studies. To date, much of the emphasis of the project has been in conjunction with SRBEX. This team has an extensive and on-going study looking at technology and management issues in this humid, mixed-use coastal region including: comprehensive GIS development; hydrologic and meteorologic studies; remote sensing; and evaluation of a soil hydrology model, mesoscale atmospheric model, and a GCM to study scale and parameter issues. Water chemistry and human influences are also being studied.

5.4.3.4 *SGP: Arkansas/Red River basins*

IDS: Hydrologic processes and climate

PI: W. Lau

This group is focusing ground validation efforts in the Arkansas-Red River basins, which include most of Oklahoma. A rich cache of pre-EOS satellite and ground data sets exist in this area for scale and process-model studies including: AVHRR, SSM/I, GOES, NEXRAD, river stage, atmospheric structure, and soil moisture. The approximately coincident CART-ARM and Oklahoma Mesonet networks provide an especially rich base level of meteorologic and atmospheric information. Local-scale remote-sensing studies have been made across the Little Washita sub-watershed (Schmugge et al. 1994). Other activities planned in this central semi-humid grassland

province include: comprehensive GIS development, rainfall-runoff modeling, collaboration with USDA Chickasaw and Little Washita Experimental watershed, DOE CART-ARM SGP study area, the proposed Cooperative Atmosphere-Surface Exchange Study (CASES) Walnut Creek site, soil moisture studies, and EOS IT/IDS calibration/validation.

This IDS investigation has a significant land-atmosphere sub-group working on a variety of model and data issues. The larger group is focused on developing a better understanding, improved models, and linkages between the major hydrologic domains of atmosphere, ocean, and land. E. Wood is working with the MODLAND-Running team to develop and validate the MODIS standard ET and surface resistance products using field data from the Arkansas/Red River basin area.

5.4.3.5 *LSM parameterizations from FIFE and BOREAS campaigns*

IDS: Biospheric-atmospheric interactions

PIs: P. Sellers and H. Mooney

The unique approach adopted by this group has been to link canopy-scale processes to leaf-scale properties. Not only have they helped investigate fundamental processes but they have worked hard to link these with remotely-sensed data such that their modeling domain is global (Sellers et al. 1994). In support of the modeling effort, field validation measurements have been made of a humid grassland (FIFE; Sellers et al. 1995a) and the boreal forest of Canada (BOREAS; Sellers et al. 1995b). Each of these studies has been well-supported with a wide range of ground, aircraft, and satellite measurements of surface energy fluxes, CO₂, and vegetation parameters. Additional validation studies are planned in collaboration with GCIP and the Large Scale Biosphere-Atmosphere Experiment in Amazonia (LBA). This group has refined the Simple Biosphere (SiB) model (Sellers et al. 1996a) and has been able to calibrate it in many environments, particularly those dominated by an active canopy. The current model, SiB2-GCM, realistically simulates energy, water, and carbon exchanges from short-to-interannual time scales. It incorporates a state-of-the-art canopy photosynthesis-conductance model and uses vegetation boundary conditions extracted from global satellite data. Future plans call for linking SiB2 with the CASA carbon model.

5.4.3.6 *Tropical: Amazon*

IDS: Patterns and processes of change in the Amazon River Basin - The EOS Amazon Project

PIs: J. Soares and T. Dunne

The EOS Amazon Project is collating and mapping ground-level data on precipitation and stream flow to estimate regional-scale rainfall-runoff relationships and evaporation fields. Mathematical models of hydrologic processes at three scales (10^7 , 10^2 - 10^4 , and 1-10 km^2) then allow the analysis of flow paths, storage, and water yields, and their alteration through climate change and anthropogenic disturbance. These models require the collation of ground-level and remotely-sensed data on vegetation, soils, radiation, and air and canopy temperature with other data generated by atmospheric models. Validation of the hydrologic models is presently accomplished through comparisons of measured and predicted streamflow, but the era of EOS missions holds out the promise of incorporating temporal and spatial distributions of canopy characteristics and valley-floor water storage into the validation. The next phase of this Project will involve a mesoscale (10^2 - 10^4 km^2) comparison of two basins in western Brazil. One retains a more-or-less pristine forest cover, while the other is massively deforested.

5.4.3.7 *Global biogeochemical cycles*

IDS: Changes in biogeochemical cycles

PI: B. Moore

The Moore-IDS team has as its ultimate goal the generation of a dynamic Earth System Model incorporating full atmosphere-ocean-terrestrial coupling. In the land-science domain, B. Moore has coordinated the PIK-NPP project of intercomparisons of terrestrial NPP models (Moore and Cramer 1996). J. Melillo has led the VEMAP project intercomparing GCM-driven biogeography and biogeochemistry models, participating with their TEM (VEMAP 1995). C. Vorosmarty is assembling a Global River and Drainage Basin Archive Series for use with continental-scale hydrologic models. This series will include all archived river-discharge data, lake levels, sediment and water quality records, and related socioeconomic data for all major global rivers. The Water Balance Model has been used to study biogeochemical transport via river discharge from terrestrial sources to oceanic sinks (Vorosmarty et al. 1996; Vorosmarty and White 1996).

These component models will be assembled in the EOS era to provide fully coupled global modeling capabilities.

5.4.3.8 *Canadian studies of carbon and hydrologic cycles*

IDS: Northern biosphere observation and modeling experiment

PI: J. Cihlar

The Northern Biosphere Observation and Modeling Experiment (NBIOME) project is evaluating responses of northern latitude ecosystems to globally-changing conditions of climate, atmospheric chemistry, and human activity. Climatic change is predicted to be largest at high latitudes. Chen and Cihlar (1996) have addressed the special problems of extracting vegetation biophysical properties from optical sensors under the extreme illumination angles of high latitudes. A regional-scale computation of forest productivity for the entire province of Quebec using FOREST-BGC parameterized by AVHRR data has been recently completed (Liu et al. 1996). Extrapolation of these same technologies to the circumpolar boreal forest is planned after the launch of the EOS AM-1 platform. Understanding the role of boreal biomes as sources or sinks of CO_2 will be one result of these studies.

5.4.3.9 *Cryospheric System (CRYSYS)*

IDS: CRYSYS used to monitor global change in Canada

PI: B. Goodison

Every aspect of CRYSYS is under investigation by an IDS team hosted by Canadian agencies and universities. Its objective is an improved understanding of the climate system through monitoring, modeling, and process studies within the Canadian cryosphere. A challenge to EOS is to take these products developed in a uniquely Canadian environment and supply comparable products globally. Snow-cover and snow-climatology studies are the most critical components from the land-surface hydrology perspective. Existing techniques that estimate snow cover from satellite (microwave) data have been improved. New, operational techniques for detecting permafrost and for deriving SWE from SSM/I data have been developed. In support of climate monitoring and validation activities, key historical, operational, and research data sets have been assembled and analyzed. Based on

these observations, most Canadian valley glaciers appear to have receded over the last century. Snow validation sites are being maintained across the Canadian Prairie Region and in collaboration with the BOREAS field sites.

5.4.3.10 Seasonally snow-covered alpine basins

IDS: Hydrology, hydrochemical modeling, and remote-sensing in seasonally snow-covered alpine drainage basins

PI: J. Dozier

This investigation involves working on the challenging problems associated with monitoring the source areas and hydrology of much of our fresh-water supply—seasonally snow-covered alpine drainage basins. This group will supply improved algorithms and process models to EOS, including useful code for calculating insolation in topographically-complex regions, snowmelt modeling, and using Landsat data to estimate fractional snow-covered area (Rosenthal and Dozier 1996). There are several operational efforts to measure snow, forecast runoff, and evaluate atmospheric deposition in relation to global climate. Field studies in support of this effort are being conducted in the Sierra Nevada, Rocky Mountains, Austrian Alps, Tien Shen, and Andes. This group will depend heavily on new and high-resolution DEMs supplied by EOS. Unlike many other EOS teams, this group's focus is local, and many standard global-resolution satellite products are unusable. Thus, many of their results emphasize developing technologies at high spatial, temporal, and spectral resolution that will not be supplied by EOS platforms. Considerable effort has been made to adapt to other satellite platforms such as Radarsat, ERS-2, and the Lewis Hyperspectral Imaging system. One particularly relevant result is that a two-frequency, co-polarized SAR is needed to map important snow properties through cloud cover (Shi and Dozier 1995).

5.4.4 Land-vegetation science

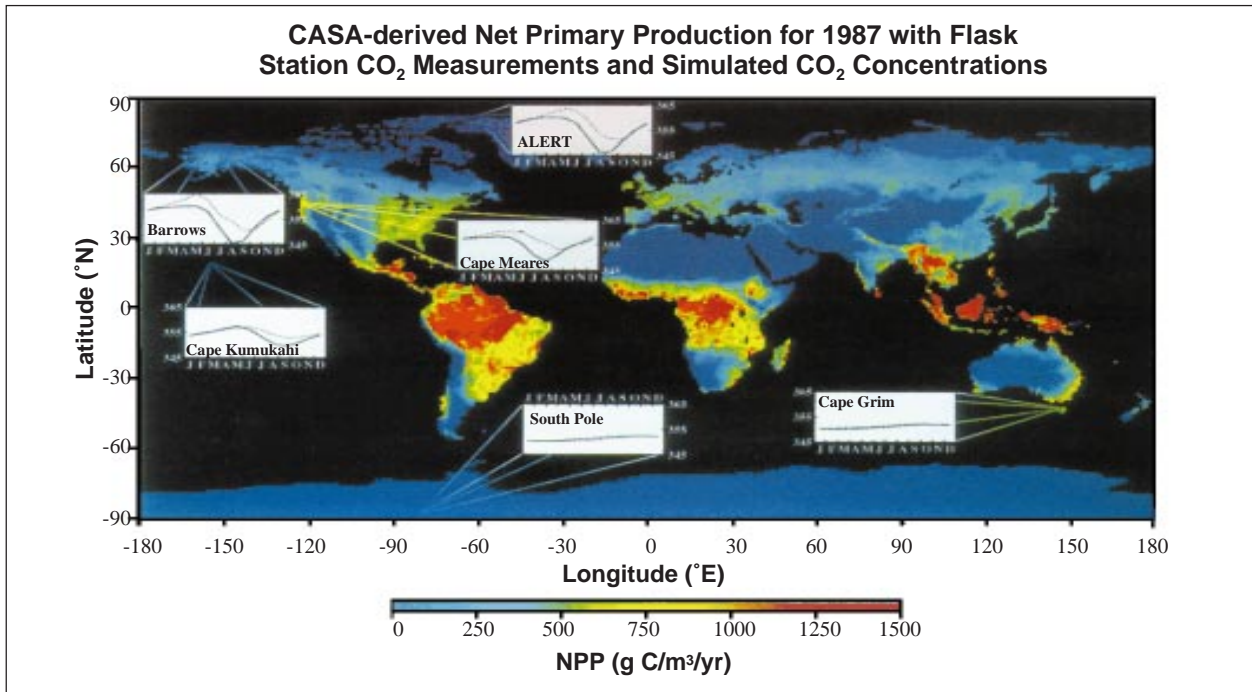
Biogeochemistry: At global scales, possibly the most easily validated terrestrial carbon-cycle variable will be seasonal and interannual variability in land surface CO₂ fluxes as monitored by atmospheric CO₂ concentrations (Figure 5.18, pg. 242). To convert the surface fluxes simulated by the terrestrial models to atmospheric concentrations, atmospheric transport models are used for CO₂ source-sink mixing (Heimann and Keeling 1989), then comparisons with the observed dynamics measured at the global CO₂ networks are made (Tans NOAA net-

work and Keeling network). For this strategy to be effective, a higher density of monitoring stations will be needed, with emphasis on mid-continental locations, possibly with very tall (1000 m+) towers. Original locations were chosen to sample oceanic air uninfluenced by local CO₂ sources such as cities. A new effort to organize a more-advanced tower eddy-correlation-based CO₂/H₂O flux network (FLUXNET) globally is under way (Baldocchi et al. 1996). A flux network allows more direct validation of the CO₂ and H₂O fluxes simulated by the terrestrial biogeochemical models, and avoids the large uncertainties brought about by the atmospheric transport modeling used for the CO₂ concentration-based validations. This IGBP-led network acknowledges that there already are almost a dozen continuously operating flux towers globally, needing only international coordination and centralized data archiving. Once established, at least 20 more sites are possible from research teams already active in this research.

Vegetation structure: Global validation of vegetation structural variables will be a tremendous task requiring international cooperation and leadership of groups like IGBP and WCRP. An initial effort is being made beginning in 1996 to identify, organize, geolocate, and digitize all published NPP data for global ecosystems, and to archive them with IGBP-DIS (see Section 5.4.5.3.5). Because vegetation structure is highly heterogeneous in both space and time, and sampling is typically labor intensive, and not easily automated, a large number of study sites will be required. Projects like the Global Landcover Test Site Initiative (GLCTS) are attempting to get high-spatial-resolution (Landsat TM) data for a global array of test sites established by 1997. A project with the NSF Long-term Ecological Research Sites plans to develop sampling procedures for measuring land cover, LAI, and NPP over tens of kilometers efficiently with standard field instrumentation in different biome types represented by the network in the U.S. The IGBP is planning a suite of global climatic/biome gradient transects, such as tropical-desert Australia, that will cross critical continental ecotones between major biomes and measure a variety of climatic and vegetation variables important to EOS.

Terrestrial ecosystems are highly variable in space for two reasons. First, vegetation is inherently controlled by microclimate and soils influences that change at the kilometer level across the Earth's surface. Second, human activity has dramatically changed the landscape down to even the hectare scale. Terrestrial ecosystems are equally variable in time, particularly at higher latitudes. The seasonal germination, growth, maturation, and se-

FIGURE 5.18



Use of the global flask network of seasonal atmospheric CO₂ trends to validate the global NPP map for 1987 produced by the CASA terrestrial biogeochemical cycle model (Field et al. 1995).

nescence (or harvest) of vegetation is well known, and illustrates that certain measures of vegetation may need to be repeated as often as monthly for any accuracy. Perennial vegetation such as forests are fortunately not as variable temporally, although deciduous forests have a very seasonal canopy cover.

Consequently, any terrestrial validation measurements must be very explicit about the size of area being represented by the data, and the temporal frequency required for remeasurement. It appears that there are two primary categories of terrestrial vegetation measurements possible for EOS validation over multi-kilometer scales. One class is the vegetation structural measurements that can be taken by field crews using routine field ecology techniques. These include land cover, LAI, and NPP. The other class of measurements is the automated atmospheric CO₂ monitors and eddy correlation flux towers.

While the measurement of the structural variables is straightforward in the field on sub-hectare-size plots, they are samples that require extrapolation to at least kilometer scales for use as EOS validations. Also these measures have varying temporal stability. The plan is to treat land cover as a rather conservative variable, needing remeasures only every five years. Various land-cover maps have been created for large areas, even entire coun-

tries. The only usable ones for EOS validation are databases derived from satellite data so that they are measuring existing, not potential vegetation, and are relatively current and repeatable, as land cover changes over time (Running et al. 1994).

LAI may require at least two measures per year, a winter minimum and a summer maximum. The time sequence of LAI through the growing season is a useful validation for APAR models of NPP. However the remeasure frequency would need to be at least monthly, so it is feasible only at the most intensive study sites. The spring greenup or canopy leafout, often termed spring phenology is a very sensitive measure of climate-vegetation interactions, and can be observed and monitored with particular accuracy over large areas. Fall canopy senescence and leaf drop is much more complicated ecologically and much less observable.

NPP is the single most measured field ecology variable, and so a large global database exists of expected values. The critical difficulty is that nearly all reported measurements are on tiny study plots, often 0.1ha. NPP may be most easily represented as accumulated NPP at the end of the growing season although that misses some seasonal dynamics in certain biome types.

The tower-based measurements are able to represent ecosystem carbon-cycle biogeochemical dynamics over larger areas that are difficult to define; the reference area is a function of the height of the tower and upwind dynamics. In general, these techniques are the only real possibility for regional-scale carbon-balance monitoring. They measure net ecosystem production as the difference between net CO₂ uptake by photosynthesis and net ecosystem CO₂ evolution from plant respiration and soil litter decomposition. However, these measurements cannot separate the components of the system CO₂ flux—biospheric models are used for that deconvolution.

Measurement or monitoring of radiometric variables to validate products such as surface reflectance, BRDF, and MVIs require very different plans because of the extreme temporal and spatial variability of solar radiation delivered to the terrestrial surface.

5.4.5 Terrestrial validation activity

5.4.5.1 Tier 1 major field experiments

Global terrestrial carbon models have progressed from simple aggregate budget calculations to relatively mechanistic models including key processes of photosynthesis, respiration, and decomposition specific to given biome types. Major large-scale experiments have been run in a number of biomes to build understanding and tools for spatial scaling. HAPEX, FIFE, the European International Project on Climate and Hydrological Interactions between Vegetation, Atmosphere, and Land Surfaces (ECHIVAL), OTTER, the BOREAS, amongst others, have all had the common objective of developing biophysical techniques and remote sensing to spatially upscale terrestrial surface processes to regional landscapes. These major experiments measure both vegetation structural variables and flux variables from towers. However, these projects typically have intensive field seasons for 1-3 years followed by data analysis and modeling; they are not designed as long-term monitoring programs. The Tier 2 permanent research facilities are better suited for biospheric monitoring programs.

5.4.5.1.1 Past experiments

5.4.5.1.1.1 First ISLSCP Field Experiment (FIFE)

FIFE was conducted across a 15- × 15-km patchwork of burned and unburned prairie near Manhattan, Kansas, during four intensive field campaigns (IFCs) between 1987 and 1989. The objectives of this experiment were two-fold: 1) to test and improve the upscaling of micrometeorological models from scales of 1 m to 1 km

and 2) to investigate the use of satellite remote sensing to infer climatologically-significant land-surface parameters. Fluxes of heat, moisture, CO₂, and radiation were measured across the surface and in the air using a wide variety of instrumentation and compared with estimates from satellite sensors. Many of these results have been reported in two special issues of *Journal of Geophysical Research* (Sellers et al. 1992 and 1995).

Soil moisture, photosynthetic capacity, canopy density, and conductance were among the most important variables identified by FIFE scientists. At a larger scale, precipitation, topography, and the diurnal variability of radiative forcing significantly affect surface fluxes. However, surface physiological feedbacks are more important than variable atmospheric forcings in controlling surface fluxes. This result emphasizes the need to physically characterize the vegetation surface and not expect that the atmosphere will control the fluxes: "...vegetation physiology actively damps out large variations in surface energy budget forced by diurnal variations in atmospheric conditions...." Soil respiration and photosynthetic rates appeared to be closely coupled. Soil moisture is particularly important below the wilting point, where it starts to affect stomatal conductance, and above field capacity as soil evaporation begins to dominate transpiration.

5.4.5.1.1.2 HAPEX-Sahel

HAPEX-Sahel (Hydrologic Atmospheric Pilot Experiment in the Sahel) was an international program focused on the soil-plant-atmosphere energy, water, and carbon balance in the west African Sahel (Prince et al. 1995). It was intended to improve our understanding of the interaction between the Sahel and the general atmospheric circulation, both at present and in the future, providing a baseline for studies of climate change. It was carried out in a 1° × 1° area of west Niger over a 3-to-4-year period with an 8-week intensive observation period from August to October 1992. HAPEX-Sahel was funded by a wide range of agencies in seven participating countries. Over 170 scientists visited and worked in the field. An interdisciplinary approach was adopted with contributed studies in hydrology and soil moisture; surface fluxes and vegetation; remote-sensing science; and meteorology and mesoscale modeling. Detailed field measurements were concentrated at 3 ancillary sites. Four aircraft were used for remote sensing and flux measurement. Observations from space were acquired from nine sensors on seven different satellite platforms.

5.4.5.1.1.3 *ECHIVAL Field Experiment in Desertification-Threatened Areas (EFEDA)*

EFEDA addressed global-change issues, mainly land degradation and desertification processes in the semi-arid region of Castilla la Mancha in southern Spain. Interactions of land-surface processes, mesoscale atmospheric circulations, and impacts of human activities (like rapidly falling groundwater levels) were assessed. From the experiment conclusions may be drawn for a sustainable use of the natural resources in the Mediterranean and other semi-arid regions. EFEDA has made available data for the regions that cover a wide range of hydrological, vegetation, and atmospheric information. Through these data the representation of energy, water, and CO₂ fluxes between vegetation and the atmosphere has been improved substantially for semi-arid regions.

5.4.5.1.1.4 *BOREAS*

BOREAS is a large-scale international field experiment that has the goal of improving our understanding of the exchanges of radiative energy, heat, water, CO₂, and trace gases between the boreal forest and the lower atmosphere (Sellers et al. 1995). An important objective of BOREAS is to collect the data needed to improve computer simulation models of the processes controlling these exchanges so that scientists can anticipate the effects of global change.

From August 1993 through September 1994, a continuous set of monitoring measurements—meteorology, hydrology, and satellite remote sensing—were gathered over the 1000 × 1000-km BOREAS study region that covers most of Saskatchewan and Manitoba, Canada. This monitoring program was punctuated by six campaigns that saw the deployment of some 300 scientists and aircrew into the field, supported by 11 research aircraft. The participants were drawn primarily from U.S. and Canadian agencies and universities, although there were also important contributions from France, the United Kingdom, and Russia. The field campaigns lasted for a total of 123 days and saw the compilation of a comprehensive surface-atmosphere flux data set supported by ecological, trace gas, hydrological, and remote-sensing science observations. The surface-atmosphere fluxes of sensible heat, latent heat, CO₂, and momentum were measured using eddy correlation equipment mounted on a surface network of ten towers complemented by four flux-measurement aircraft. All in all, over 350 airborne missions (remote sensing and eddy correlation) were flown during the 1994 field year.

Preliminary analyses of the data indicate that the area-averaged photosynthetic capacity of the boreal forest is much less than that of the temperate forests to the

south. This is reflected in very low photosynthetic and carbon drawdown rates, which in turn are associated with low transpiration rates (< 2 mm day⁻¹ over the growing season for the coniferous species in the area). The strong sensible fluxes generated as a result of this often lead to the development of a deep dry planetary boundary layer over the forest, particularly during the spring and early summer. The effects of frozen soils and the strong physiological control of ET in the biome do not seem to be well represented in most operational GCMs of the atmosphere.

Analyses of the data have continued through 1995 and 1996. Some limited revisits to the field are anticipated.

5.4.5.1.1.5 *OTTER*

The OTTER project in Oregon studied a climatic gradient that represents nearly the global range of LAI of evergreen forests but with small study plots (Peterson and Waring 1994). This gradient is 200-km long from the ocean into the desert, and provides three land covers (crop, evergreen forest, and shrubland). The objective of the OTTER study was to test the ability to use remotely-sensed vegetation biophysical variables to accurately parameterize an ecosystem biogeochemical simulation model for landscape-scale processes. The intensive study period was summer 1990, and included acquisitions from satellite- and aircraft-mounted sensors. Remote sensing of forest LAI and canopy chemistry was tested, and model simulations of NPP and stand biomass development were executed. Details are available in a special issue of *Ecological Applications* (Peterson and Waring 1994).

5.4.5.1.2 Opportunities from current and future experiments

5.4.5.1.2.1 *The Large Scale Biosphere-Atmosphere Experiment in Amazonia (LBA)*

LBA is an international research initiative led by Brazil. It is designed to create the new knowledge needed to understand the climatological, ecological, biogeochemical, and hydrological functioning of Amazonia, the impact of land-use change on these functions, and the interactions between Amazonia and the Earth system. LBA is centered around two key questions that will be addressed through multi-disciplinary research, integrating studies in the physical, chemical, biological, and human sciences:

- How does Amazonia currently function as a regional entity?
- How will changes in land use and climate affect the biological, chemical, and physical functions of

Amazonia, including the sustainability of development in the region and the influence of Amazonia on global climate?

In LBA, emphasis is given to observations and analyses which will enlarge the knowledge base for Amazonia in six general areas: physical climate, carbon storage and exchange, biogeochemistry, atmospheric chemistry, hydrology, and land use and land cover. The program is designed to address major issues raised by the Climate Convention of Rio de Janeiro in 1992. It will help provide the basis for sustainable land use in Amazonia, using data and analysis to define the present state of the system and its response to observed perturbations, complemented by modeling to provide insight into possible changes in the future.

<http://yabae.cptec.inpe.br/LBA/>

5.4.5.1.2.2 GCIP

As part of an overall scientific strategy of the WCRP and GEWEX to improve global climate predictability, the GEWEX Continental-Scale International Project (GCIP) was formed in 1990. The overall goal of GCIP is to improve climate models by bridging the gap between small scales appropriate for modeling discrete processes over land and large scales practical for modeling the global climate system. The primary objectives of GCIP are to determine the variability of the Earth's hydrological cycle and energy exchange budget over a continental scale; to develop and validate techniques for coupling atmospheric and surface hydrological processes in climate models; and to provide a basis for translating the effects of future climate change to impacts on regional water resources.

The Mississippi River basin was selected as the GCIP study site because of its extensive hydrological and meteorological observation network. Part of the initial phase of GCIP is to build up the science base and technical expertise on regional, continental-scale processes. Included in this first phase are plans for a 5-year period of enhanced observations commencing in late 1995. The surface-based, model-derived, and spaceborne data will be used to develop models that couple complex atmospheric and surface hydrological processes that can operate on a wide range of space scales. A second phase of GCIP will focus on extending this capability to the global scale, using observations that will be forthcoming towards the turn of the century from the next generation of Earth observing satellite systems.

http://www.ncdc.noaa.gov/gcip/gcip_home.html

5.4.5.1.2.3 CART-ARM

The Atmospheric Radiation Measurement (ARM) Program is a multi-laboratory, interagency program that was created in 1989 with funding from the U.S. DOE. The ARM Program is part of DOE's effort to resolve scientific uncertainties about global climate change with a specific focus on improving the performance of GCMs used for climate research and prediction. These improved models will help scientists better understand the influences of human activities on the Earth's climate. In pursuit of its goal, the ARM Program establishes and operates field research sites, called CARTs, in several climatically-significant locales. Scientists collect and analyze data obtained over extended periods of time from large arrays of instruments to study the effects and interactions of sunlight, radiant energy, and clouds on temperatures, weather, and climate.

<http://info.arm.gov/>

5.4.5.1.2.4 CASES

A CASES site is being established within the ARM-CART research area to provide a facility for scientists to study mesoscale processes of meteorology, hydrology, climate, ecology, chemistry, and their complex linkages, and to serve as a focal point to provide field experience for students of the natural sciences. The location of the CASES site is the upper Walnut River watershed north of Winfield, Kansas. Here, boundary layer instrumentation can be deployed such that it coincides with the natural boundaries of the Walnut River watershed. Thus, the boundary layer instrumentation, in conjunction with WSR-88D radars, stream gauges, soil moisture data, topographic and land-use data, mesonet surface data, and atmospheric-hydrologic models, will allow for a detailed description of the hydrologic cycle between the watershed and the atmosphere above. Once fully established, CASES is projected to have a minimum lifetime of three years with possible continuance for the duration of ARM-CART.

5.4.5.1.2.5 Northern Hemisphere Climate-Processes Land-Surface Experiment (NOPEX)

NOPEX is devoted to studying land-surface-atmosphere interaction in a northern European forest-dominated landscape. The NOPEX main study region was selected to represent the southern part of the boreal zone. Central

Sweden is situated in the middle of the densest part of the northern European boreal forest zone. The main NOPEX region is centrally situated in the Baltic Sea drainage basin, the study region for the Baltic Sea Experiment (BALTEX) project. NOPEX is specifically aiming at investigating fluxes of energy, momentum, water, and CO₂—and the associated dynamics—between the soil, the vegetation, and the atmosphere, between lakes and the atmosphere, as well as within the soil and the atmosphere on local-to-regional scales ranging from centimeters to tens of kilometers.

5.4.5.2 Tier 2-3 validation monitoring for terrestrial fluxes

5.4.5.2.1 FLUXNET and EUROFLUX

Strategies for Monitoring and Modeling CO₂ and Water Vapor Fluxes over Terrestrial Ecosystems (IGBP Core Projects BAHC, Global Change in Terrestrial Ecosystems [GCTE], International Global Atmospheric Chemistry [IGAC]).

New micrometeorological technologies have recently been perfected that allow continuous flux

measurements, and a few sites have begun this data collection. Relative to the high cost of the spatial scaling studies, these continuous flux studies are modest in financial requirement. Since these continuous time CO₂ flux data sets have immense value for global carbon and climate modeling, continuous flux measurements should be encouraged in an array of biomes and climates worldwide. Additionally, an organized flux network with standard measurement and data presentation protocols, and an active centralized archive would make these data, critical for validation and testing carbon balance simulation models, available to the wider global science community most quickly.

Although the primary science justification offered here is carbon-balance-related, hydrologic balances are also of high importance, and will be an integral component of flux network measurements (as they were previously in the large-scale experiments described above). As for the carbon cycle, the non-growing season is also critical for hydrologic balances. The continuous measurements of the terrestrial hydrologic balance and ET, and the vegetation (carbon cycle) controls will con-

TABLE 5.2

SIMPLE INTEGRATED TOWER CONCEPT				
COMPONENT TOWER VARIABLES	VARIABLE DEPENDENCIES			
	EB	ATM	BRDF	TG
- Energy Budget/Surface Meteorology (Euroflux, Fluxnet, etc.)	O	X	X	-
- Atmospheric Corrections, Aerosols (Sun Photometer, Shadow-Band Radiometer, Lidar)	X	O	X	-
- Bidirectional Spectral Radiances (Sun Photometer, CCD Camera)	X	X	O	-
- Trace Gas Fluxes/Concentrations (Carbon America, Tragnet, etc.)	X	X	X	O
FOOTPRINT (100 KM²) VEGETATION ANALYSIS				
- Land Cover	X	X	X	X
- LAI/FPAR	X	X	X	X
- Net Primary Production	X	X	X	X
- Stem and Soil Carbon	X	X	X	X

tribute equally to producing better global hydrologic models.

5.4.5.2.2 Carbon America

Goal: Determine the location and magnitude of regional CO₂ sources and sinks in North America and develop an understanding of the mechanisms for terrestrial carbon storage or loss.

The strategy consists of three elements: 1) monitoring of mixing ratios in the vertical dimension, 2) monitoring of surface fluxes in specific ecosystems with co-located additional measurements relevant to the biogeochemical cycle of carbon, and 3) continental-scale modeling of the carbon cycle and atmospheric transport.

By observing the spatial patterns in more detail than ever before, persistent source/sink regions can be identified so that targeted process studies can be planned. Furthermore, by observing the large flux changes known to occur (from studies of global concentration variations and from continuous flux measurements) as a result of regional climate variations, we can uncover major driving forces of short-term terrestrial C storage.

The general feasibility of uncovering regional fluxes through repeated aircraft sampling, based on an analysis of the signal-to-noise of atmospheric measurements, has been shown in “*A feasible global carbon cycle observing system*” (Tans et al. 1996, NOAA/Climate Monitoring and Diagnostics Laboratory [CMDL]). It is envisioned that these measurements are carried out for an initial period of five years spanning one El-Niño cycle, in order to make use of and characterize interannual variations. The frequency of the flights should be once or twice per week.

5.4.5.2.2.1 Continuous flux measurements

The first continuous long-term flux measurements have been performed at the Harvard Forest site. These measurements enable us to calculate the net fluxes integrated over the entire year and, more importantly, to study specific mechanisms controlling the rates of C uptake and loss. The true value of continuous flux measurements can only be realized if the measurements are used to test and develop regionally-specific models of the terrestrial carbon cycle, and the observational data sets on which the models are based. In this way the local results of the flux measurements can be extrapolated to regional scales. Such a strategy calls for many additional measurements to be performed at each flux site. A partial list of additional projects would be a good ecological characterization of the site including the soil, soil humidity and temperature, PAR, N-deposition, meteorological variables, and fluxes. Land-use histories are also crucial in order to allow the

separation of land-use or management-associated fluxes (forest regrowth) from fluxes associated with climate, nitrogen deposition, CO₂ fertilization, or other unknown processes. There is potential to use isotopic measurements in the atmosphere to infer biological processes (photosynthesis and respiration), in which case the isotopic signatures of precipitation, soil water, new plant material, and microbial respiration must be obtained via field studies at the monitoring sites.

5.4.5.2.3 The United States Trace Gas Network (TRAGNET)

The atmospheric concentrations of greenhouse gases such as carbon dioxide (CO₂), methane (CH₄), and nitrous oxide (N₂O) are increasing substantially. These increases are expected to result in global warming and changes in precipitation patterns, and may directly affect terrestrial ecosystems. TRAGNET is tasked with accomplishing the following two goals:

- Document contemporary fluxes of CO₂, CH₄, and N₂O between regionally-important ecosystems and the atmosphere
- Determine the factors controlling these fluxes and improve our ability to predict future fluxes in response to ecosystem and climate change

The proposed network is designed to contribute to our understanding of trace gas fluxes to the atmosphere through six principal objectives.

- 1) The network will promote the comparability of trace gas flux measurements. As discussed later in this report, the network will provide guidance on sampling designs that are site-appropriate; provide suggestions and updated information on appropriate analytical and sample collection methods; and facilitate intercomparisons and intercalibrations.
- 2) The network will provide for more-extensive coverage of ecosystem variability. Identification of regions where no long-term measurements are available, or where replication is needed, will be assessed; the network participants can then encourage the development of research sites in such areas.
- 3) Data synthesis will be facilitated by the network. Data collected from sites that span a range of controlling factors or that represent a range of ecoregions will be available to the group for synthesis and hypothesis setting.

TABLE 5.3

SPECIFIC VARIABLES MEASURED
<p><i>Surface meteorology</i></p> <ul style="list-style-type: none"> - incoming and outgoing shortwave radiation, diffuse, and direct - incoming and outgoing longwave radiation - temperature (air, soil, surface temperature + profile) - canopy and soil heat fluxes - wind speed and direction - relative and absolute humidity - barometric pressure <p><i>Atmospheric properties and corrections</i></p> <ul style="list-style-type: none"> - spectral aerosol optical thickness - total precipitable water vapor - particle size distribution - phase function - single scattering albedo <p><i>Bidirectional spectral radiances</i></p> <ul style="list-style-type: none"> - spectral albedos - vegetation indices - directional reflectances - seasonal reflectance dynamics <p><i>Trace gas fluxes</i></p> <ul style="list-style-type: none"> - eddy correlation fluxes of CO₂ and H₂O - flask measures of isotopic ratios of C, H, and N - CH₄ and N₂O <p><i>Footprint terrestrial ecology</i></p> <ul style="list-style-type: none"> - land-cover class - leaf-area index - net primary production - stem and soil carbon storage

- 4) Interactions between measurement and modeling groups will be facilitated by the network. Data collection at appropriate frequency and spatial scales will allow model development and model testing. Hypotheses generated from the model synthesis activities will foster new field research.
- 5) Intercomparisons of model results will be facilitated. It will be possible to make comparisons that utilize

identical estimates of input and output. In addition, model modularity will be developed where possible, facilitating the identification of reasons models produce different results.

- 6) A long-term data archive for trace gas flux and other ecosystem processes will be established as a component of the network. The purpose of the network is to foster a better understanding of midlatitude trace gas contributions to the global budget by facilitating data access and interactions among those measuring and modeling gas fluxes.

5.4.5.3 Tier 3-4 permanent ecological field station networks

5.4.5.3.1 NSF LTER Project, MODLERS

This project brings together 14 LTER Network sites and NASA's MODLAND Science Team for the purpose of locally validating EOS-era global data sets. Using several standardized methods that incorporate extensive ground data sets, ecosystem models, and remotely-sensed imagery, each LTER site is developing local maps of land-cover class, LAI, and above-ground net primary productivity for a 100 km² area at a grain size of 25 m. A nested, hierarchical ground-based sampling scheme will help establish error bounds on the variable estimates. These sites represent evergreen forests, deciduous forests, grasslands, croplands, shrublands, deserts, and alpine mountains for a reasonable sampling of biome types for MODLAND tests.

A number of different strategies are being used to spatially aggregate the fine-grain site maps to a coarse grain (1 km) so that they can be compared to coincident portions of global maps of the same three biosphere variables developed by the MODLAND Science Team. This coordinated, multi-site grain-size aggregation exercise presents us with an opportunity to grapple with one of the most vexing current problems in ecology: effects of scaling from a fine grain to a coarse grain on estimates of important biosphere variables. We are using several spatially-explicit, geostatistical methods to address this issue, with the intent of determining how best to maintain crucial information among grain sizes. Additionally, we are characterizing similarities and differences among the multiple sites and biomes and between the MODLAND maps and the site maps at each grain size, in terms of the three mapped biosphere variables.

<http://atlantic.evsc.virginia.edu/~jhp7e/modlers/>

5.4.5.3.2 GLCTS: The Global Land Cover Test Site Program

The Global Land Cover Test Site (GLCTS) project is developing a multitemporal data set of satellite imagery for a globally-distributed set of test sites. This data set will provide a resource for research on land-cover characterization and the testing of algorithms for EOS. The selected test sites will represent a wide range of land-cover types and will be well characterized on the ground, have ongoing field-based observation programs, and be of interest to the international global change research community. GLCTS development is being coordinated with a number of affiliated organizations. It is currently proposed that between 40-80 sites be developed for broad land-cover representation. The initial site selection process has identified a set of established and emerging long-term monitoring sites where there is in-situ expertise and infrastructure to facilitate research. Candidate sites under consideration are displayed on the GLCTS homepage. The database to be created for each of the selected sites will consist of a common set of Landsat, AVHRR, land-cover, and elevation data.

<http://glcts.maxey.dri.edu/glcts/index.html>

5.4.5.3.3 IGBP terrestrial transects

The IGBP Terrestrial Transects are a set of integrated global-change studies consisting of distributed observational studies and manipulative experiments coupled with modeling and synthesis activities organized along existing gradients of underlying global-change parameters, such as temperature, precipitation, and land use. The global-change issues that can best be addressed with the gradient approach include questions where a long period of prior equilibration is required, spatial context is essential, identification of thresholds along a continuum is important, and gradient-driven processes are important. The transect approach also promotes collaborative, interdisciplinary research and leads to an efficient use of scarce scientific resources.

The IGBP Terrestrial Transects consist of a set of study sites arranged along an underlying gradient; they are of order 1000 km in length and are wide enough to encompass the dimensions of remote-sensing images. The transects can be visualized most easily where they represent a simple gradient of a single controlling factor that varies in space, for example, the gradient in precipitation from moist tropical forest to dry savanna. In addition to relatively straightforward transects in which a single environmental factor varies continuously in space, a set of IGBP Terrestrial Transects has been identified in which the underlying gradient is one of land use.

The initial set of IGBP Terrestrial Transects is located in four key regions, with three or four existing, planned, or proposed transects contributing to the set in each region.

IGBP - <http://www.ciesin.org/TG/HDP/igbp.html>
 BAHC - <http://www.PIK-Potsdam.DE/~bahc/>
 GCTE - <http://jasper.stanford.edu/GCTE/main.html>
 GAIM - <http://pyramid.sr.unh.edu/csrc/gaim/>
 IGAC - <http://web.mit.edu/afs/athena.mit.edu/org/igac/www/>

5.4.5.3.4 The Gap Analysis Project (GAP)

Gap Analysis provides a quick overview of the distribution and conservation status of several components of biodiversity. It seeks to identify gaps (vegetation types and species that are not represented in the network of biodiversity management areas) that may be filled through establishment of new reserves or changes in land management practices. Maps of existing vegetation are prepared from satellite imagery (Landsat) and other sources and entered into a GIS. Because entire states or regions are mapped, the smallest area identified on vegetation maps is 100 ha. Vegetation maps are verified through field checks and examination of aerial photographs.

Although Gap analysis is coordinated by the National Biological Survey, it is composed of (to date) over 200 collaborating organizations from businesses, universities, and state, local, and federal governments. Thirty-seven states are currently developing GAP analysis maps of land-cover habitat types. When these maps are complete, the land-cover classes can be aggregated into MODLAND land-cover classes which, being for global use, are much more general. The GAP maps will then provide a TM-scale validation of the MODLAND land covers for these areas of the US.

<http://www.nr.usu.edu/gap>

5.4.5.3.5 IGBP NPP data initiative

Global modeling and monitoring of NPP is currently a high-priority issue because of increasing concern over issues such as the consequences of perturbations in the carbon cycle, the impacts of global land-use change, global climate change, and global food security. Monitoring primary production provides information on many inter-related ecological processes as well as the flux of carbon dioxide from the atmosphere. Georeferenced estimates of NPP, including seasonal and interannual variability, are

key components for modeling of the terrestrial carbon cycle and its response to climate change and CO₂ fertilization.

During the past few years, a coordinated strategy to improve global estimates of terrestrial primary production through measurements and modeling has emerged. An essential part of this effort is compiling a reference database of NPP ground-based data to parameterize and validate global ecosystem models. Such data are important to diagnostic-parametric models (using satellite remote sensing), correlative-empirical models (based on

climate regressions), or more mechanistic biogeochemical models. The need for NPP reference data has been endorsed by IGBP's scientific committees of Data and Information System (DIS); Global Analysis, Interpretation, and Modeling (GAIM); GCTE; BAHG; and by the ICSU Scientific Committee on Problems of the Environment (SCOPE).

In addition, the Global Terrestrial Net Primary Productivity First Model Intercomparison Workshop, hosted by PIK at Potsdam, Germany, in July 1994, resulted in a recommendation to develop and distribute a database of

TABLE 5.4

<i>PI/DURATION</i>	<i>INSTITUTE</i>	<i>FIELD SITE</i>	<i>VEGETATION</i>
Wofsy/4yrs+	Harvard Univ	Harvard Forest, MA	temperate deciduous forest
Wofsy/1yr+	Harvard Univ.	Thompson, Manitoba	boreal spruce forest
Jensen/5yrs+	RISO	Roskilde, Denmark	crops
Valentini/2yrs+	Univ. Tuscia	Appenines, Italy	beech forest
Baldocchi/2yrs+	NOAA/ATDD	Oak Ridge, TN	temperate deciduous forest
Verma/1yr+	Univ. Nebraska	Valentine, NE	wetlands
Hollinger/6mo+	USFS	Howland, ME	conifer
Meyers/3mo+	NOAA/ATDD	Little Washita, OK	rangeland
Black/1yr	Univ. British Columbia	Prince Albert, Sask.	boreal aspen
Grace	Univ. Edinburgh	Manaus, Brazil	tropical forest
Black	Univ. British Columbia	Prince Albert, Sask.	boreal aspen
Black	Univ. British Columbia	Vancouver, B.C.	Douglas fir
den Hartog	Atmos. Environ. Service	Borden, Ontario	temperate deciduous forest
Field	Carnegie Inst. Wash	Stanford, CA	grassland
Dunin	CSIRO	WaggaWagga, Australia	crops
Desjardins	Agric. Canada	Ottawa, Ontario	crops
Anderson	USGS	Trout Lake, WI	mixed forests
Bakwin	NOAA/CMDL	North Wisconsin	mixed forests
Jarvis	Univ. Edinburgh	Prince Albert, Sask.	boreal spruce
Oechel	San Diego State Univ.	Northern Alaska	tundra
Gholz	Univ. Fla	Florida	slash pine
Miranda		Brazil	cerrado
Kelliher	Landcare	Southern New Zealand	Pinus radiata
Ham	Kansas State Univ.	Manhattan, KS	Konza prairie
Valentini et al.	EUROFLUX project	15 sites in Europe	conifer and broadleaf forests
Baldocchi	NOAA/ATDD	Western Oregon	Ponderosa pine

List of investigators conducting long-term studies of carbon and water vapor exchange over vegetated ecosystems using the eddy covariance method (+ denotes ongoing operation).

NPP data. The goals of the PIK Workshop, held again in 1995, were to advance the development of terrestrial carbon modeling on global scales through the intercomparison of terrestrial NPP simulation models. Twenty global ecosystem models of NPP have been evaluated in the workshops. The workshops compiled NPP baseline data sets, established intercomparison methodology and protocols, and executed the intercomparison of the model outputs. Comparing the model outputs indicated both spatial and temporal differences and identified a need for validation data.

As a result of the PIK Workshop recommendation, the Global Primary Production Data Initiative Project Description (IGPPDI) (Prince et al. 1995) was prepared and has been endorsed by a steering committee of representatives from the international groups listed above. The initiative will identify and compile reliable NPP data and associated environmental data for field sites and will interpret the data to a range of spatial scales to provide parameterization and validation data needed in support of modeling global primary production and other applications. The IGPPDI includes: 1) identifying and compiling field data sets; 2) scaling field observations to larger grid cells; and 3) storing and distributing data.

These tasks are divided between several institutions, including the Oak Ridge National Laboratory (ORNL), Oak Ridge, Tennessee, U.S. (natural systems); the University of Maryland, College Park (UMCP), College Park, Maryland, U.S. (estimating NPP for grid cells); Laboratoire d'Études et de Recherches en Teledetection Spatiale (LERTS)/Centre d'Études Spatiales de la Biosphère (CESBIO), Toulouse, France (managed systems); and the PIK, Potsdam, Germany (meteorology and other physical variables for the selected sites and cells).

http://www-eosdis.ornl.gov/npp/npp_igbp.html

5.4.6 EOS-related land science modeling plans

5.4.6.1 Project for Intercomparison of LSP Schemes (PILPS)

PILPS is a WCRP project operating under the auspices of GEWEX and WCRP. It has been designed to be an ongoing project. Since its establishment in 1992, PILPS has been responsible for a series of complementary experiments with focuses on identifying parameterization strengths and inadequacies. About 30 land-surface-process modeling groups have been participating in PILPS.

“PILPS is a project designed to improve the parameterization of the continental surface, especially

hydrological, energy, momentum, and carbon exchanges with the atmosphere. The PILPS science plan incorporates enhanced documentation, comparison, and validation of continental surface parameterization schemes by community participation. Potential participants include code developers, code users, and those who can provide data sets for validation and who have expertise of value in this exercise. PILPS is an important exercise because existing intercomparisons, although piecemeal, demonstrate that there are significant differences in the formulation of individual processes in the available land-surface schemes. These differences are comparable to other recognized differences among current global climate models such as cloud and convection parameterizations. It is also clear that too few sensitivity studies have been undertaken, with the result that there is not yet enough information to indicate which simplifications or omissions are important for the near-surface continental climate, hydrology, and biogeochemistry. PILPS emphasizes sensitivity studies with, and intercomparisons of, existing land-surface codes and the development of areally extensive data sets for their testing and validation.” (Henderson-Sellers et al., 1993).

<http://www.cic.mq.edu.au/pilps-rice/pilps.html>

5.4.6.2 VEMAP

The overall objective of the VEMAP project is to make an initial determination of the ability of the U.S. vegetation to sequester carbon in a changed global climate. In order to make a fast-track evaluation, a set of leading ecological models was designated to make this assessment. Three biogeochemistry models have been selected, one of them being the BIOME-BGC model (Running and Coughlan 1988; Running and Gower 1991; Running and Hunt 1993). The other biogeochemistry models in the project are Century by Schimel from NCAR and TEM by Melillo from Woods Hole. For objective one, each biogeochemistry model will be run under a current climate and $2 \times \text{CO}_2$ changed-climate scenarios from three GCMs: OSU, GFDL, and UKMO models. Annual NPP, plant and soil carbon sequestration, and ET will be simulated for the continental U.S. objective. The results from each biogeochemistry model will be compared to assess the level of consistency currently possible from leading ecological models for continental-scale carbon-balance questions. In objective three, the simulations from each GCM scenario will also be compared to determine the relative level of uncertainty that can be ascribed to climate modeling versus ecological modeling when asking these continental-scale vegetation response questions.

In a second aspect of the project, three biogeography models will be also run with current and GCM-based changed climate scenarios to assess the possibilities of vegetation biome shifts in the U.S. These are MAPSS by Nielson from OSU, BIOME2 by Prentice from Sweden, and DOLY by Woodward from Britain. In Objective 4, the final set of simulations, the biome distribution changes simulated by these models, will be used to initialize the three biogeochemistry models for the U.S. The BIOME-BGC model will be initialized in turn with MAPSS vegetation, BIOME2 vegetation, and DOLY vegetation, and the results from each model compared, and with each GCM climate base for the continental U.S. These simulations will produce the most comprehensive assessment yet made of the potential response of the U.S. terrestrial vegetation to climatic change because it will entail the three sequentially-linked simulations of global climate—biogeography—biogeochemistry responses.

<http://www.cgd.ucar.edu:80/vemap/>

5.4.6.3 PIK-NPP

Global primary production of ecosystems on land and in the oceans is a crucial component of biogeochemical model development within IGBP. The second in a series

of IGBP GAIM-DIS-GCTE workshops, “Potsdam ’95,” on global modeling of net primary productivity was held at PIK, June 20-22 1995. The purpose of Potsdam ’95, like Potsdam ’94, was to support a series of model intercomparisons by the various modeling teams around the globe that are currently modeling the terrestrial biosphere at large scales.

A focus of the intercomparison was net primary productivity. Global primary productivity of ecosystems is a crucial component of biogeochemical model development within IGBP. The subject is complex and central to models of the global carbon cycle. The importance of this subject rests upon the fact that most terrestrial carbon-cycle models, as well as terrestrial models that treat energy and water fluxes, must address in a fundamental manner either gross primary productivity (GPP) and/or NPP. There are significant differences in the calculation of NPP within current global terrestrial models, and Potsdam ’95 was held in order to compare model parameters and outputs. One important aspect of the ongoing PIK-NPP project is compilation of a comprehensive database of published NPP measurements globally for all biome types (Prince et al. 1995).

<http://pyramid.sr.unh.edu/csdc/gaim/NPP.html>

Region	Contributing transects in initial set
Humid tropics	Amazon Basin/Mexico Central Africa/Miombo Southeast Asia/Thailand
Semiarid tropics	Savannas in the Long Term (West Kalahari Southern Africa) Northern Australia Tropical Transect
Midlatitude semiarid	Great Plains (USA) Argentina North East China Transect
High latitudes	Alaska Boreal Forest Transect Case Study (Canada) Scandinavia Siberia

References

- AIP (1993). The World at Risk: Natural Hazards and Climate Change, Bras, R. (ed), AIP Conf. Proceedings 277, American Institute of Physics, New York, 352 pp.
- Arnell, N. W., 1995: Grid mapping of river discharge. *J. Hydrology*, **167**, 39-56.
- Asrar, G., B. J. Myneni, and B.J. Choudhury, 1992: Spatial heterogeneity in vegetation canopies and remote sensing of absorbed photosynthetically active radiation: A modeling study. *Remote Sens. Environ.*, **41**, 85-103.
- Asrar, G., M. Fuchs, E. T. Kanemasu, and J. L. Hatfield, 1984: Estimating absorbed photosynthetic radiation and leaf-area index from spectral reflectance in wheat, *Agronomy Journal*, **76**, 300-306.
- Avissar, R., 1995: Recent advances in the representation of land-atmosphere interactions in general circulation models, *Rev. Geophys.*, **2**, 1005-1010.
- Avissar, R., and F. Chen, 1993: Development and analysis of prognostic equations for mesoscale kinetic energy and mesoscale (subgrid-scale) fluxes for large scale atmospheric models. *J. Atmos. Sci.*, **50**, 3751-3774.
- Baldocchi, D., R. Valentini, S. Running, W. Oechel, and R. Dahlman, 1996: Strategies for measuring and modeling carbon dioxide and water vapour fluxes over terrestrial ecosystems, *Global Change Biology*, **2**, 159-168.
- Barron, E. J., 1995: Climate Models: How reliable are their predictions?, *Consequences*, **1**(3), 17-27.
- Bonan, G. B., 1995: Land atmosphere CO₂ exchange simulated by a land-surface process model coupled to an atmospheric general circulation model, *J. Geophys. Res.*, **100**, 2817-2831.
- Bonan, G. B., D. Pollard, and S. L. Thompson, 1993: Influence of subgrid-scale heterogeneity in leaf-area index, stomatal resistance and soil moisture on grid-scale land-atmosphere interactions. *J. Climate*, **6**, 1882.
- Bonan, G. B., D. Pollard, and S. L. Thompson, 1992: Effects of boreal forest vegetation on global climate, *Nature*, **359**, 716-718.
- Bougeault, P., B. Bret, P. Lacarrere, and J. Noilhan, 1991: An experiment with an advanced surface parameterization in a mesobeta-scale model. Part II: the 16 June 1986 simulation. *Mon. Wea. Rev.*, **119**, 2374-2392.
- Bouttier, F., J-F. Mahfouf, and J. Noilhan, 1993: Sequential assimilation of soil moisture from atmospheric low-level parameters, part I: Sensitivity and calibration studies, *J. Appl. Meteor.*, **32**(8), 01335-1351.
- Box, E. O., B. N. Holben, and V. Kalb, 1989: Accuracy of the AVHRR vegetation index as a predictor of biomass, primary productivity and net CO₂ flux, *Vegetatio*, **80**, 71-89.
- Carlson, T. N., R. R. Gillies, and E. M. Perry, 1994: A method to make use of thermal infrared temperature and NDVI measurements to infer soil water content and fractional vegetation cover, *Rem. Sens. Rev.*, **52**, 45-59.
- Charney, J.G., W. J. Quirk, S. H. Chow, and J. Kornfield, 1977: A comparative study of the effects of albedo change on drought in semi-arid regions, *J. Atmos. Sci.*, **34**, 1366-1385.
- Chehbouni, A., E. G. Njoku, J.-P. Lhomme, and Y.H. Kerr, 1995: Approaches for averaging surface parameters and fluxes over heterogeneous terrain, *J. Climate*, **8**, 1386-1393.
- Chen, J.M., and J. Cihlar, 1996: Retrieving leaf-area index of boreal forests using Landsat TM images, *Remote Sens. Environ.*, **55**, 153-162.
- Choudhury, B. J., 1995: Relations between evaporation coefficients and vegetation indices studied by model simulation, *Remote Sens. Environ.*, **50**, 1-17.
- Ciais, P., P. Tans, M. Trolier, J. W. C. White, and R. J. Francey, 1995: A large Northern-Hemisphere terrestrial CO₂ sink indicated by the C-13/C-12 ratio of atmospheric CO₂, *Science*, **269**, 1098-1102.
- Cihlar, J., P. H. Caramori, P. H. Schuepp, R. L. Desjardins, and J. I. MacPherson, 1992: Relationship between satellite-derived vegetation indices and aircraft-based CO₂ measurements, *J. Geophys. Res.*, **97**, 18515-18522.
- Crum, T.D., R. L. Alberty, and D. W. Burgess, 1993: Recording, archiving and using WSR-88D data, *Bull. Amer. Meteor. Soc.*, **74**(4), 645-653.
- Delworth, T.L., and S. Manabe, 1988: The influence of potential evaporation on the variabilities of simulated soil wetness and climate, *J. Climate*, **1**, 523-547.
- DeFries, R. S., M. Hansen, and J. Townshend, 1995: Global discrimination of land cover types from metrics derived from AVHRR pathfinder data, *Remote Sens. Environ.*, **54**, 209-222.
- Denning, A.S., I. Y. Fung, and D. Randall, 1995: Latitudinal gradient of atmospheric CO₂ due to seasonal exchange with land biota, *Nature*, **376**, 240-243.
- Dickinson, R. E., 1995: Land processes in climate models, *Remote Sens. Environ.*, **51**, 27-38.
- Dickinson, R. E., and P. J. Kennedy, 1992: Impacts on regional climate of Amazon deforestation, *Geophys. Res. Lett.*, **19**, 1947.
- Dickinson, R.E., 1984: Modeling evapotranspiration for three-dimensional global climate models, Climate Processes and Climate Sensitivity, J. E. Hansen and T. Takahashi, Eds., American Geophysical Union, Washington, DC, 58-72.
- Dracup, J. A., and D. R. Kendall, 1991: Climate uncertainty: implications for operations of water control systems, Managing Water Resources in the West under Conditions of Climate Uncertainty, Nat. Acad. Press, 177-216.
- Dubayah, R., 1992: The topographic distribution of annual incoming radiation in the Rio Grande River basin, *Geophys. Res. Lett.*, **19**(22), 2231-2234.
- Emanuel, K., 1987: The dependence of hurricane intensity on climate, *Nature*, **326**, 483-485.
- Entekhabi, D., 1995: Recent advances in land-atmosphere interaction research, *Rev. of Geophys.*, **2**, 995-1003.
- FAO Soil Map of the World (1978), scale 1:5,000,000, UNESCO, Paris, Vols. I-X.
- Famiglietti, J. S., and P. Houser, 1995: Spatially-distributed hydrological modeling with soil moisture remote sensing applications at Walnut Gulch, AZ, Presented at Fall AGU, San Francisco.
- Field, C. B., J. T. Randerson, and C. M. Malmstrom, 1995: Global net primary production: Combining ecology and remote sensing. *Remote Sens. Environ.*, **51**, 74-88.
- Gao, X., and S. Sorooshian, 1994: A stochastic precipitation disaggregation scheme for GCM applications, *J. Climate*, **7**(2), 238-247.
- Gillies, R. R., and T. N. Carlson, 1995: Thermal remote sensing of surface soil water content with partial vegetation cover for incorporation into climate models, *J. Appl. Meteor.*, **34**, 745-756.
- Gong, G., D. Entekhabi, and G. Salvucci, 1994: Regional and seasonal estimates of fractional storm coverage based on station precipitation observations, *J. Climate*, **7**, 1495-1505.
- Goward, S. M., and K. E. Huemmerich, 1992: Vegetation canopy PAR absorptance and the Normalized Difference Vegetation Index: An assessment using SAIL model, *Remote Sens. Environ.*, **39**, 119-140.

- Goward, S. N., C. J. Tucker, and D. G. Dye, 1985: North American vegetation patterns observed with the NOAA-7 Advanced Very High Resolution Radiometer. *Vegetatio*, **64**, 3-14.
- GRDC, 1996: Activities of the global runoff data center, GEWEX SSG meeting, Irvine CA, 1/15-19/96.
- Haarsma, R., J. Mitchell, and C. Senior, 1993: Tropical disturbances in a GCM, *Climate Dynamics*, **8**, 247-257.
- Hall, F. G., F. Huemmrich, S. J. Goetz, P. J. Sellers, and J. E. Nickeson, 1992: Satellite remote sensing of surface energy balance: Success, failures, and unresolved issues in FIFE, *J. Geophys. Res.*, **97**, 19061-19089.
- Heimann, M., and C.D. Keeling, 1989: A three-dimensional model of atmospheric CO₂ transport based on observed winds: 2. Model description and simulated tracer experiments, Peterson, D.H. (ed), Aspects of climate variability in the Pacific and the Western Americas, American Geophysical Union, Washington, DC, p. 165-236.
- Henderson-Sellers, A. and K. McGuffie, 1995: Global climate models and 'dynamic' vegetation changes, *Global Change Biology*, **1**, 63-75.
- Henderson-Sellers, A., R. E. Dickinson, T. B. Durbidge, P. J. Kennedy, K. McGuffie, and A. J. Pitman, 1993: Tropical deforestation: Modeling local- to regional-scale climate change. *J. Geophys. Res.*, **98**, 7289.
- Hipps, L. E., E. Swiatek, and W. P. Kustas, 1994: Interaction between regional surface fluxes and the atmospheric boundary layer over a heterogeneous watershed, *Water Resour. Res.*, **30(5)**, 1387-1392.
- Hirschboeck, K., V. R. Baker, R. C. Kochel, and P. C. Patton, eds., 1988: Flood Hydroclimatology, *Flood Geomorphology*, John Wiley & Sons, pp. 27-49.
- Hook, S.J., A. R. Gabell, A. A. Green, and P. S. Kealy, 1992: A comparison of techniques for extracting emissivity information from thermal infrared data for geologic studies, *Remote Sens. Environ.*, **42**, 123-135.
- Houser, P. R., 1996: Remote-sensing of soil moisture using four-dimensional data assimilation, PhD., Univ. Arizona, Dept. of Hydrology, 391 pp.
- Huete, A.R., 1988: A soil-adjusted vegetation index (SAVI), *Remote Sens. Environ.*, **25**, 295-309.
- Huete, A.R., C. Justice, and H. Lui, 1994: Development of vegetation and soil indices for MODIS-EOS, *Remote Sens. Environ.*, **48**, 1-11.
- Hughes, J. P., D. P. Lettenmaier, and E. F. Wood, "An approach for assessing the sensitivity of floods to regional climate change", in Bras, Rafael (editor) *The World at Risk: Natural Hazards and Climate Change*, AIP Conference Proceedings 277, American Institute of Physics, New York, 1993, pp. 112-124.
- Hunt, E. R., Jr., S. C. Piper, R. R. Nemani, C. D. Keeling, R. D. Otto, and S. W. Running, 1996: Global net carbon exchange and intra-annual atmospheric CO₂ concentrations predicted by an ecosystem process model and three-dimensional atmospheric transport model, *Global Biogeochemical Cycles*, **10(3)**, 431-456.
- Hunt, E. R., Jr., 1994: Relationship between woody biomass and PAR conversion efficiency for estimating net primary production from NDVI, *Int. J. Remote Sensing*, **15(8)**, 1725-1730.
- Hunt, E. R., Jr., and S. W. Running, 1992: Simulated dry matter yields for aspen and spruce stands in the North American boreal forest, *Canadian J. Remote Sensing*, **18**, 126-133.
- Hunt, E. R. Jr., and S. W. Running, 1992: Effects of climate and lifeform on dry matter yield from simulations using BIOME-BGC, International Geosciences and Remote Sensing Symposium IGARSS 92, 1631-1633.
- Imhoff, M. I., 1994: Mapping human impacts on the global biosphere, *Bioscience*, **44**, 598.
- Junk, W. J., and K. Furch, 1993: A general review of South American floodplains, *Wetlands Ecology and Management* **2**, (4), 231-238.
- Justice, C. O., and J. R. Townshend, 1994: Data sets for global remote sensing: lessons learned, *Int. J. Remote Sensing*, **15(17)**, 3621-3639.
- Justice, C. O., J. R. G. Townshend, B.N. Holben, and C. J. Tucker, 1985: Analysis of the phenology of global vegetation using meteorological satellite data, *Int. J. Remote Sensing*, **6**, 1271-1318.
- Kaufman, Y. J., C. O. Justice, L. Flynn, E. Prins, D. E. Ward, P. Menzel, and A. Setzer, 1996: Monitoring global fires from EOS-MODIS, (in press).
- Kaufman, Y. J., and D. Tandré, 1992: Atmospheric resistant vegetation index, *IEEE Geosci. and Rem. Sens.*, **30**, 261-270.
- Keeling, C. D., T. P. Whorf, M. Wahlen, and J. van der Plicht, 1995: Interannual extremes in the rate of rise of atmospheric carbon dioxide since 1980, *Nature*, **375**, 666-670.
- Keeling, C. D., R. B. Bacastow, A. F. Carter, S. C. Piper, T. P. Whorf, M. Heimann, W. G. Mook, and H. Roeloffzen, A three-dimensional model of atmospheric CO₂ transport based on observed winds, 1, Analysis of observational data, Aspects of Climate Variability in the Pacific and the Western Americas, *Geophys. Monogr. Ser.*, **55**, edited by D.H. Peterson, pp. 165-236, AGU, Washington, D.C., 1989a.
- Keeling, C. D., and M. Heimann, 1986: Meridional eddy diffusion model of the transport of atmospheric carbon dioxide; 2, Mean annual carbon cycle, *J. Geophys. Res.*, **91**, 7782-7796.
- Kerr, Y. H., and E. G. Njoku, 1990: A semiempirical model for interpreting microwave emissions from semiarid land surfaces as seen from space, *IEEE Geosci. and Rem. Sens.*, **28**, 384-393.
- Kerr, Y. H., 1991: The multi-frequency imaging microwave radiometer (MIMR): Applications to land-surface parameter retrieval, Proc. IGARSS '91, 2365-2368.
- Kerr, Y. H., and T. Jackson, T. (eds.), 1993: Soil moisture working group report, Saint-Lary ESA/NASA Workshop, Available from authors.
- Koster, R. D., and P. C. D. Milly, 1996: The interplay between transpiration and runoff formulations in land-surface schemes used with atmospheric models, *J. Climate*, (in press).
- Kunkel, K. E., 1990: Operational soil moisture estimation for the midwestern United States, *J. Appl. Meteor.*, **29**, 1158-1166.
- Kustas, W. P., and D. C. Goodrich, 1994: Preface to the special section on MONSOON '90, *Water Resour. Res.*, **30(5)**, 1211-1225.
- Lambin, E. F., and A. H. Strahler, 1994: Change-vector analysis in multitemporal space: A tool to detect and categorize land-cover change processes using high temporal-resolution satellite data, *Remote Sens. Environ.*, **48**, 231-244.
- Lettenmaier D. P., and T. Y. Gan, 1990: Hydrologic sensitivities of the Sacramento-San Joaquin River basin, CA, to global warming, *Water Resour. Res.*, **26(1)**, 69-86.
- Le Vine, D. M., 1996: Strawman Proposal for the Global Land Observation (GLO) satellite, NASA.
- Liu, J., J. M. Chen, J. Cihlar, and B. Park, 1996: A process-based boreal ecosystem simulator using remote sensing inputs, *Remote Sens. Environ.*, (in press).
- Li, B., and R. Avissar, 1994: The impact of spatial variability of land-surface characteristics on land-surface heat fluxes, *J. Climate*, **7**, 527.
- Loaiciga, H. A., J. B. Valdes, R. Vogel, J. Garvey, and H. Schwarz, 1996: Global warming and the hydrologic cycle, *J. Hydrology*, **174**, 83-127.
- Mahfouf, J. F., 1991: Analysis of soil moisture from near-surface parameters: A feasibility study, *J. Appl. Meteor.*, **30(11)**, 1534-1547.
- Maas, S. J., M. S. Moran, and R. D. Jackson, 1992: Combining remote sensing and modeling for regional resource monitoring, Part II: A simple model for estimating surface evaporation and biomass production, Proc. ASPRS/ACSM Conv., 225-233.

- McCormick, M. P., L. W. Thompson, C. R. Trepte, 1995: Atmospheric effects of the Mt. Pinatubo eruption, *Nature*, **373**, 399-404.
- Melillo, J. M., A. D. McGuire, D. W. Kicklighter, B. Moore III, C. J. Vorosmarty, and A. Schloss, 1993: Global climate change and terrestrial net primary production, *Nature*, **363**, 234-240.
- Michaud, J. and S. Sorooshian, 1994: Comparison of simple versus complex distributed runoff models on a mid-sized semiarid watershed, *Water Resour. Res.*, **30(3)**, 593-605.
- Miller, D., J. Washburne, E. Wood, 1995: EOS Workshop on land-surface evaporation and transpiration, *The Earth Obs.*, **7(4)**, 52-56.
- Monteith, J. L., 1972: Solar radiation and productivity in tropical ecosystems, *J. Applied Ecology*, **9**, 747-766.
- Monteith, J. L., 1977: Climate and the efficiency of crop production in Britain. *Philosophical Transactions of the Royal Society of London*, **B 281**, 277-294.
- Moore & Cramer: 1996. (in press).
- Moran, M. S., T. R. Clarke, Y. Inoue, and A. Vidal, 1994: Estimating crop water deficit using the relation between surface-air temperature difference and spectral vegetation index, *Remote Sens. Environ.*, **49**, 246-263.
- Moran, M. S., A. F. Rahman, J. C. Washburne, D. C. Goodrich, M. A. Weltz, and W.P. Kustas, 1996: Combining the Penman-Monteith equation with measurements of surface temperature and reflectance to estimate evaporation rates of a semiarid grassland, *Ag. and Forest Meteor.*, (submitted).
- Myneni, R. B., R. R. Nemani, and S. W. Running, 1996: Algorithm for the estimation of global landcover, LAI and FPAR based on radiative transfer models, IEEE (in review).
- Myneni, R. B., and D. L. Williams, 1994: On the relationship between FAPAR and NDVI, *Remote Sens. Environ.*, **49**, 200-211.
- Myneni, R. B., G. Asrar, D. Tanré, and B. J. Choudhury, 1992: Remote sensing of solar radiation absorbed and reflected by vegetated land surfaces, *IEEE Trans. Geosci. Remote Sens.*, **30**, 302-314.
- NASA Soil Moisture Workshop, 1994: M-Y Wei (ed), NASA Conf. Pub. 3319, 77 p.
- National Research Council, Estimating Bounds on Extreme Precipitation Events, National Academy Press, Washington, DC, 1994, 25 pp.
- National Research Council, Estimating Probabilities of Extreme Floods—Methods and Recommended Research, National Academy Press, Washington, DC, 1988, 141 pp.
- Nielson, R. P., 1995: A model for predicting continental-scale vegetation distribution and water balance, *Ecological Applications*, **5**, 362-385.
- Nemani, R. R., and S. W. Running, S.W., 1995: Satellite monitoring of global land cover changes and their impact on climate, *Climatic Change*, **31**, 395-413.
- Nemani, R., S. W. Running, R. A. Pielke, and T. N. Chase, (1996). Global vegetation cover changes from coarse resolution satellite data, *J. Geophys. Res.*, **101(D3)**, 7157-7162.
- Nemani, R., L. Pierce, S. Running, and L. Band, 1993: Forest ecosystem processes at the watershed scale: sensitivity to remotely-sensed leaf-area index estimates, *Int. J. Remote Sensing*, **14(13)**, 2519-2534.
- Nobre, C. A., P. J. Sellers, and J. U. Shukla, 1991: Amazonian deforestation and regional climate change, *J. Climate*, **4**, 957-987.
- Noilhan, J., and P. Lacarrere, 1995: GCM grid-scale evaporation from mesoscale modeling, *J. Climate*, **8**, 206-223.
- Oki, T., K. Musiake, H. Matsuyama, and K. Masuda, 1995: Global atmospheric water balance and runoff from large river basins, *Hydro. Proces.*, **9**, 655-678.
- Palmer, T. N., 1986: Influence of the Atlantic, Pacific, and Indian Oceans on Sahel Rainfall, *Nature*, **322**, 251-253.
- Parton, W. J., J. M. O. Scurlock, D. S. Ojima, T. G. Gilmanov, R. J. Scholes, D. S. Schimel, T. B. Kirchner, J. C. Menaut, T. Seastedt, E. Garcia Moya, A. Kammalrut, and J. Kinyamario, 1993: Observations and modeling of biomass and soil organic matter dynamics for the grassland biome worldwide, *Global Biogeochemical Cycles*, **7**, 785-809.
- Penner, J. E., R. E. Dickinson, C. A. O'Neill, 1992: Effects of aerosol from biomass burning on the global radiation budget, *Science*, **256**, 1432-4.
- Peterson, D. L., and R.H. Waring, 1994: Overview of the Oregon Transect Ecosystem Research Project, *Ecological Applications*, **4(2)**, 211-225.
- Peterson, D. L., M. A. Spanner, S. W. Running, and L. Band, 1987: Relationship of Thematic Mapper Simulator data to leaf-area index, *Remote Sens. Environ.*, **22**, 323-341.
- Pinker, R. T., and I. Laszlo, 1992: Modeling surface solar irradiance for satellite applications on a global scale, *J. Appl. Meteor.*, **31**, 194-211.
- Pinker, R. T., W. P. Kustas, I. Laszlo, M. S. Moran, and A. R. Huete, 1994: Basin-scale solar irradiance estimates in semiarid regions using GOES 7, *Water Resour. Res.*, **30(5)**, 1375-1386.
- Pinty, B., and M. M. Verstaete, 1992: GEMI: A non-linear index to monitor global vegetation from satellites, *Vegetatio*, **101**, 15-20.
- Pitman, A. J., et al., 1993: Project for intercomparison of land-surface parameterization schemes (PILPS), Results from off-line control simulations (Phase 1a). IGPO #7, World Climate Research Program.
- Post, W. M., T. -H. Peng, W. R. Emanuel, A. W. King, V. H. Dale, and D. L. DeAngelis, 1990: The global carbon cycle, *American Scientist*, **78**, 310-326.
- Prentice, I. C., W. Cramer, S. P. Harrison, R. Leemans, R. A. Monserud, and A. M. Solomon, 1992: A global biome model based on plant physiology and dominance, soil properties and climate, *J. Biogeogr.*, **19**, 117-134.
- Price, J. C., 1992: Estimating vegetation amount from visible and near infrared reflectances, *Remote Sens. Environ.*, **41**, 29-34.
- Prince, S. D., Y. H. Kerr, J. -P. Goutorbe, T. Lebel, A. Tinga, P. Bessemoulin, J. Brouwer, A. J. Dolman, E. T. Engman, J. H. C. Gash, M. Hoepffner, P. Kabat, B. Monteny, F. Said, P. Sellers, and J. Wallace, 1995: Geographical, biological, and remote sensing aspects of the hydrologic atmospheric pilot experiment in the Sahel (HAPEX-Sahel), *Remote Sens. Environ.*, **51**, 215-234.
- Prince, S. D., R. J. Olson, G. Dedieu, G. Esser, and W. Cramer, 1995: Global Primary Production Land Data Initiative Project Description, IGBP-DIS Working Paper No. 12, IGBP-DIS, Paris.
- Prince, S. D., and S. N. Goward, 1995: Global primary production: A remote sensing approach, *J. Biogeogr.*, **22**, 815-835.
- Prince, S. D., 1991: A model of regional primary production for use with coarse resolution satellite data, *Int. J. of Remote Sensing*, **12**, 1313-1330.
- Qi, J., A. Chehbouni, A. R. Huete, Y. H. Kerr, and S. Sorooshian, 1994: A modified soil adjusted vegetation index, *Remote Sens. Environ.*, **48**, 119-126.
- Quay, P. D., B. Tilbrook, and C. S. Wong, 1992: Oceanic uptake of fossil fuel CO₂: Carbon-13 evidence, *Science*, **256**, 74-79.
- Rahman, A. F., J. C. Washburne, M. S. Moran, and A. K. Batchily, 1996: Regional-scale surface flux estimation by combined use of remote sensing and meteorological data, *Water Resour. Res.*, (submitted).
- Reed, B. C., J. F. Brown, D. VanderZee, T. R. Loveland, J. W. Merchant, and D. O. Ohlen, 1994: Measured phenological variability from satellite imagery, *J. Vegetation Science*, **5**, 703-714.
- Revelle, R.R., and P. E. Waggoner, 1983: Effects of climate change on water supplies in the Western United States, in: Changing Climate, Nat. Acad. Sci., Washington, DC.

- Robock, A., K. Y. Vinnikov, C. A. Schlosser, N. A. Speranskaya, and Y. Xue, 1995: Use of midlatitude soil moisture and meteorological observations to validate soil moisture simulations with biosphere and bucket models, *J. Climate*, **8**, 15-35.
- Rosenthal, W., and J. Dozier, 1996: Automated mapping of montane snow cover at subpixel resolution from the Landsat Thematic Mapper, *Water Resour. Res.*, (in press).
- Running, S. W., T. R. Loveland, L. L. Pierce, R. R. Nemani, and E. R. Hunt, Jr., 1995: A remote sensing based vegetation classification logic for global land cover analysis, *Remote Sensing Environ.*, **51**, 39-48.
- Running, S. W., C. O. Justice, V. Salomonson, D. Hall, J. Barker, Y. J. Kaufmann, A. H. Strahler, A. R. Huete, J.-P. Muller, V. Vanderbilt, Z. M. Wan, P. Teillet, and D. Carneggie, 1994: Terrestrial remote sensing science and algorithms planned for EOS/MODIS, *Int. J. Remote Sensing*, **15**, 3587-3620.
- Running, S. W. and E. R. Hunt, Jr., 1993: Generalization of a forest ecosystem process model for other biomes, BIOME-BGC, and an application for global-scale models, pp. 141-158, IN: *Scaling Processes Between Leaf and Landscape Levels*. J.R.Ehleringer and C.Field eds., Academic Press.
- Running, S. W., and R.Nemani, 1991: Regional hydrologic and carbon balance responses of forests resulting from global climate change, *Climatic Change*, **19**, 349-368.
- Running, S. W., and R. R. Nemani, 1988: Relating seasonal patterns of the AVHRR vegetation index to simulated photosynthesis and transpiration of forests in different climates, *Remote Sens. Environ.*, **24**, 347-367
- Running, S. W., and S. T. Gower, 1991: FOREST-BGC, a general model of forest ecosystem processes for regional applications II, Dynamic carbon allocation and nitrogen budgets, *Tree Physiology*, **9**, 147-160.
- Running, S. W., and J. C. Coughlan, 1988: A general model of forest ecosystem processes for regional applications, *Ecological Modelling*, **42**, 125-154.
- Runyon, J., R. H. Waring, S. N. Goward, and J. M. Welles, 1994: Environmental limits on above-ground production: observations for the Oregon transect, *Ecological Applications*, **4**, 226-237.
- Schimel, D. S., B. Braswell Jr., B. H.Holland, E. A. McKeown, D. S. Ojima, T. H. Painter, W. J. Parton, and A. R.Townsend, 1994: Climatic, edaphic, and biotic controls over carbon and turnover of carbon in soils, *Global Biogeochemical Cycles*, **8**, 279-293.
- Schmugge, T., T. J. Jackson, W. P. Kustas, R. Roberts, R. Perry, D. C. Goodrich, S. A. Amer, and M. A. Weltz, 1994: Push broom microwave radiometer observations of surface soil moisture in Monsoon '90, *Water Resour. Res.*, **30(5)**, 1321-1328.
- Schwartz, M. D., 1996: Examining the Spring discontinuity in daily temperature ranges, *J. Climate*, **9**, 803-808.
- Scott, R., R. Koster, D. Entekhabi, and M. Suarez, 1996: "Effect of a canopy interception reservoir on hydrological persistence in a general circulation model, *J. Climate*, **8**, 1917-1922.
- Sellers, P. J. (ed.), 1995: The GEWEX Global Wetness Project Report, WCRP-IGPO report **xxxx**.
- Sellers, P. J., D. A. Randall, G. J. Collatz, J. Berry, C. Field, D. A. Dazlich, C. Zhang, 1996a: A revised land-surface parameterization (SiB2) for atmospheric GCMs. Part 1: Model formulation, *J. Climate*, **9**, 738-763.
- Sellers, P. J., S. O. Los, C. J. Tucker, C. O. Justice, D. A. Dazlich, G. J. Collatz, and D. A. Randall, 1996b: A revised land-surface parameterization (SiB2) for atmospheric GCMs. Part 2: The generation of global fields of terrestrial biophysical parameters from satellite data, *J. Climate*, **9**, 706-737.
- Sellers, P. J., L. Bounoua, G. J. Collatz, D. A. Randall, D. A. Dazlich, S. Los, J. A. Berry, I. Fung, C. J. Tucker, C. B. Field, T. G. Jensen, 1996c: Comparison of the radiative and physiological effects of doubled atmospheric levels of CO₂ on climate, *Science*, **271**, 1402-1406.
- Sellers, P. J., M. D. Heiser, F. G. Hall, S. J. Goetz, D. E. Strebel, S. B. Verma, R. L. Desjardins, P. M. Schuepp, and J. I. MacPherson, 1995a: Effects of spatial variability in topography, vegetation cover and soil moisture on area-averaged surface fluxes: A case study using the FIFE 1989 data, *J. Geophys. Res.*, **100**, 25607-25629.
- Sellers, P. J., F. Hall, H. Margolis, B. Kelly, D. Baldocchi, G. denHartog, J. Cihlar, M. G. Ryan, B. Goodison, P. Crill, K. J. Ranson, D. Lettenmaier, and D. Wickland, 1995: The Boreal Ecosystem—Atmosphere Study (BOREAS): An overview and early results from the 1994 field year, *Bull. Amer. Meteor. Soc.*, **76(9)**, 1549-1577.
- Sellers, P. J., W. W. Meeson, F. G. Hall, G. Asrar, R. E. Murphy, R. A. Schiffer, F. P. Bretherton, R. E. Dickinson, R. G. Ellingson, C. B. Field, K. F. Huemmrich, C. O. Justice, J. M. Melack, N. T. Roulet, D. S. Schimel, and P. D. Try, 1995: Remote sensing of the land surface for studies of global change: Models-algorithms-experiments, *Remote Sens. Environ.*, **51**, 3-26.
- Sellers, P. J., C. J. Tucker, G. J. Collatz, S. O. Los, C. O. Justice, D. A. Dazlich, and D. A. Randall, 1994: A global 1° by 1° NDVI data set for climate studies. Part2: The generation of global fields of terrestrial biophysical parameters from the NDVI, *Int. J. Remote Sensing*, **15**, 3519-3545.
- Sellers, P. J., J. A. Berry, G. J. Collatz, C. B. Field, and F. G. Hall, 1992: Canopy reflectance, photosynthesis, and transpiration. III. A re-analysis using improved leaf models and a new canopy integration scheme, *Remote Sens. Environ.*, **42**, 187-216.
- Sellers, P. J., Y. Mintz, Y. C. Sud, and A. Dalcher, 1986: A simple biosphere model (SiB) for use within general circulation models, *J. Atmos. Sci.*, **43**, 505-531.
- Shaikh, M.J., 1996: Precipitation simulation in global climate models: Impact of horizontal resolution and improved land-surface scheme, Ph.D., Univ. of Arizona, 246 p.
- Shi, J., and J. Dozier, 1995: Inferring snow wetness using C-band data from SIR-C's polarimetric synthetic aperture radar, *IEEE trans. Geosci. and Rem. Sens.*, **33(4)**, 905-914.
- Shukla, J., and Y. Mintz, 1982: Influence of land-surface evapotranspiration on the Earth's climate, *Science*, **215**, 1498-1501.
- Shuttleworth, W. J., 1988: Macrohydrology - The new challenge for process hydrology, *J. Hydrology*, **100**, 31-56.
- Shuttleworth, W. J., 1996: The challenges of developing a changing world, *EOS*, **77(36)**, 347.
- Skole, D., and C. J. Tucker, 1993: Tropical deforestation and habitat fragmentation in the Amazon: Satellite data from 1978 to 1988, *Science*, **260**, 1905-1910.
- Smith, J. A., D. J. Seo, M. L. Baeck, and M. D. Hudlow, 1996: An intercomparison study of NEXRAD precipitation estimates, *Water Resour. Res.*, **32(7)**, 2035-2045.
- Stokes, G. M., and S. E. Schwartz, 1994: The Atmospheric Radiation Measurement (ARM) program: programmatic background and design of the Cloud and Radiation Testbed (CART), *Bull. Amer. Meteor. Soc.*, **75(7)**, 1201-1221.
- Sud, Y. C., J. Shukla, and Y. Mintz, 1988: Influence of land-surface roughness on atmospheric circulation and precipitation: A sensitivity study with a General Circulation Model, *J. Climate*, **2**, 105-125.
- Sundquist, E. T., 1993: The global carbon dioxide budget, *Science*, **259**, 934-941.

- Tans, P. P., P. S. Bakwin, and D. W. Guenther, 1996: A feasible global carbon cycle observing system: a plan to decipher today's carbon cycle based on observations, *Global Change Biology*, **2**, 309-318.
- Tans, P. P., I. Y. Fung, and T. Takahashi, 1990: Observational constraints on the global atmospheric CO₂ budget, *Science*, **247**, 1431-1438.
- Tegen, I., A. A. Lacis, and I. Fung, 1996: The influence of mineral aerosols from disturbed soils on climate forcing, *Nature*, (in press).
- Thompson, S. L., and D. Pollard, 1995: A global climate model (GENESIS) with a land-surface-transfer scheme (LSX). Part 1: present climate simulation, *J. Climate*, (in press).
- Townshend, J. T., C. Justice, W. Li, C. Gurney, and J. McManus, 1991: Global land cover classification by remote sensing: Present capabilities and future possibilities, *Remote Sens. Environ.*, **35**, 243-255.
- Tucker, C. J., I. Y. Fung, C. D. Keeling, and R. H. Gammon, 1986: Relationship between atmospheric CO₂ variations and a satellite-derived vegetation index, *Nature*, **319**, 195-199.
- Tucker, C.J., J. R. G. Townshend, and T. E. Goff, 1985: African land cover classification using satellite data, *Science*, **227**, 369-374.
- VEMAP, 1995: Vegetation/ecosystem modeling and analysis project (VEMAP): Comparing biogeography and biogeochemistry models in a continental-scale study of terrestrial ecosystem responses to climate change and CO₂ doubling, *Global Biogeochemical Cycles*, **9(4)**, 407-437.
- Vinnikov, K. Y., A. Robock, N. A. Speranskaya, and C. A. Schlosser, 1996: Scales of temporal and spatial variability of midlatitude soil moisture, *J. Geophys. Res.*, **101(D3)**, 7163-7174.
- Viterbo, P., and A. C. M. Beljaars, 1995: An improved land surface parameterization scheme in the ECMWF model and its validation, *J. Climate*, **8**, 2716-2748.
- Vorosmarty, C. J., and R. W. White, 1996. Suspended sediment delivery from the continental land mass to the coastal ocean: GIS based analysis for South America, *J. Hydrology*, (in press).
- Vorosmarty, C. J., C. J. Wilmott, B. J. Choudury, A. L. Schloss, T. K. Stearns, S. M. Robeson, and T. J. Dorman, 1996: Analyzing the discharge regime of a large tropical river through remote sensing, ground-based climatic data and modeling, *Water Resour. Res.*, (in press).
- Walker, G.K., Y. C. Sud, and R. Atlas, 1995: Impact of the ongoing Amazonian deforestation on local precipitation: A GCM simulation study, *Bull. Amer. Meteor. Soc.* **76**, 346-361.
- Wallace, J., 1995): Multidisciplinary program studies land-atmosphere interactions in semi-arid regions, *EOS*, **76(46)**, 465-469.
- Washburne, J., and J. Shuttleworth, 1996 NMC Eta model surface fluxes —Are they an accurate representation for hydrologic models over the CART-ARM/GCIP-SW region, Presented at the 2nd GEWEX Sci. Conf., Washington, DC.
- Wiegand, C. L., A. J. Richardson, E. T. Kanemasu, 1979: Leaf-area index estimates for wheat from Landsat and their implications for evapotranspiration and crop modeling, *Agronomy Journal*, **71**, 336-342.
- Wielicki, B. A., R. D. Cess, M. D. King, D. A. Randall, and E. F. Harrison, 1996: Mission to Planet Earth: Role of Clouds and Radiation in Climate, *Bull. Amer. Meteor. Soc.*, **76(11)**, 2125-2153.
- Wofsy, S. C., M. L. Goulden, J. W. Munger, S.-M. Fan, P. S. Bakwin, B. C. Daube, S. L. Bassow, and F. A. Bazzaz, 1993: Net exchange of carbon dioxide in a midlatitude forest, *Science*, **260**, 1314-1317.
- Woolhiser, D. A., R. E. Smith, and D. C. Goodrich, 1990: KINEROS, A kinematic runoff and erosion model: Documentation and users manual, U.S.D.A. Ag. Research Service, ARS-77.
- Woodward, F. I., T. M. Smith, and W. R. Emanuel, 1995: A global land primary productivity and phytogeography model, *Global Biogeochemical Cycles*, **9**, 471-490.
- Xue, Y., P. J. Sellers, J. L. Kinter, and J. Shukla, 1991: A simplified biosphere model for global climate studies, *J. Climate*, **4**, 345-364.

Chapter 5 Index

- 4-D assimilation 207
 4DDA 204, 207, 216
 A/SA 216, 238
 aerosols 208
 agriculture 203, 206, 210, 213, 220, 230, 234, 238
 AIRS/AMSU/HSB 210, 212, 217
 ALOS 236
 AMSR 206, 212
 APAR 228, 234, 242
 ARM 215, 217-218, 245
 assimilation data sets (see 4DDA)
 ASTER 210, 213-214, 217, 234
 atmospheric forcings 204
 AVHRR 206, 208, 221-229, 233, 239-240, 249
 AVIRIS 213
 BAHC 213, 246, 249-250
 BATS 201, 213
 biodiversity 249
 biogeochemistry, river 222-223
 biogeochemistry, terrestrial 231-232
 BIOME2 232, 252
 biospheric responses-dynamics 208-209, 232
 BOREAS 237, 239, 241-244
 BRDF 207, 233-234, 243, 246
 calibration 205-206, 221, 226, 233-234, 237-239
 Carbon America 247
 carbon cycle 228-229, 231-232, 238, 241, 243, 246-249, 252
 carbon dioxide (CO₂) 201-209, 219-238, 240-251
 CART 237-239, 245
 CART-ARM 239, 245
 CASES 239, 245
 CCD 233, 246
 CERES 207, 210, 217
 CESBIO 251
 CMDL 247, 250
 convection 251
 cryosphere 237, 240
 CRYSYS 240
 DAO 206, 210, 218, 228, 236
 DoE 236, 239, 245
 droughts 221, 230
 ECMWF 204, 210
 ecosystem 202-204, 214, 218, 225, 228-231, 235-238, 243-244, 247-251
 EDC 234-235
 EFEDA 244
 El Niño 201, 212, 231, 247
 ENSO 212, 221
 EOS instrument products 205-206, 208
 EOS AM 204, 208, 217, 223, 233, 240
 EOS PM 212, 214
 EOSDIS 214, 218, 233, 236, 251
 EOSP 208
 EROS 234
 ERS 215, 236, 241
 ETM+ 234-235
 evapotranspiration (ET) 209-214, 222-225, 233-234, 239, 244, 246, 251
 extreme hydrologic events-severe storms, floods, droughts 218-222
 FAO 216-217
 FIFE 205-206, 209-210, 214, 228, 237-239, 243
 fires 206
 floodplains 220-222
 FLUXNET and EUROFLUX 241, 246-247
 FPAR 206, 210, 214, 223, 225-226, 246
 GCIP 214, 239, 245
 GCMs 201, 203, 205-210, 219, 221
 GCOS/GTOS TOP 237-238
 GCTE 246, 249-251
 GEBA 217
 GEWEX 214-217, 245, 251
 GFDL 232, 251
 GIS 238-239, 248
 GISS 217
 GLCTS 241, 249
 GLOBE 216
 GOES 212, 217, 239
 GPCP 213
 GPS 236
 GRDC 213
 GSFC 213, 215, 217
 HAPEX-Sahel 206, 238, 243
 heterogeneity 209-210
 HIRDLS 208, 210
 HSB 210, 212, 217
 humidity 204, 206-207, 217-218, 228, 236, 247-248
 hydrology 201, 252
 ICSU 237, 250
 IDS 201-252
 IDS field sites 238
 IFOV 215
 IGAC 246
 IGBP 213, 216, 235, 237, 241, 246
 IGPPDI 251
 IHP 237
 infiltration and deep percolation 216
 interannual variability 201, 208, 223, 227, 231, 241, 249
 IOC 237
 IR 207, 234
 ISLSCP 205, 217, 243
 IT 238-239
 ITCZ 212
 JERS 215
 JPO 237
 KINEROS 213
 LAI 201-206, 214, 223-233, 238, 241-244, 248
 land-climate interaction 201-210
 land hydrology 201-233
 land-surface water balance 218
 land-vegetation 223-232, 241-243
 Landsat-7 224-225, 234-235
 LBA 239, 244-245
 LERTS 251
 lidar 208, 246
 lightning 219
 LIS 208
 LSMs 203-206, 208-210, 239
 LSPs 201, 210, 221
 LTER 236-237, 248
 MAPSS 224, 232, 252
 methane (CH₄) 222, 247-248
 MIMR 206-207
 MISR 206, 208, 210, 217, 224-227, 233-234
 MIT 213
 MMS 213
 modeling 213-217, 224-228, 232-252
 MODIS 208, 210, 213-214, 217, 220, 223-229, 231-233
 MODLAND 248
 MODLERS 248

- MOPITT 232
 MOU 237
 MVI 228, 233
 NASA 215-217, 236
 NBIOME 240
 NCAR 251
 NDVI 214, 223, 233
 near-surface meteorology 217-218
 NEXRAD 212, 239
 NIR 223, 226
 NMC 210
 NOAA 206, 212, 217, 227, 236, 241, 247, 250
 NOPEX 245-246
 NPP 223, 227-229, 241-242, 249-251
 NRC 219
 NSF 236, 241, 245
 ORNL 251
 OSU 232, 251-252
 OTTER 228, 243-244
 PAR 204, 214, 226, 228, 233, 247
 PEM 228
 PIK-NPP 232, 250-252
 PILPS 251
 POLDER 208
 PR 207, 212
 precipitation 211-213, 233, 236-243, 247-249
 PSU 213, 217
 RADARSAT 215, 241
 radiation 216-217
 runoff 213
 SAGE III 208, 210
 SALSA 216, 238
 SAR 213, 221, 236, 241
 SAVI 226
 SCOPE 250
 SiB 201, 203, 239
 SMMR 215
 snow cover 207, 211, 240
 soil moisture 215-216
 soils data 216, 235-236
 SRB 204
 SRBEX 239
 SSM/I 215, 239-240
 SST 219-221, 241
 stem and soil carbon 229-230
 surface observations 215
 SWE 212-213, 240
 SWIR 234
 TEM 225, 229, 232, 240, 251
 THM 213
 TIR 215, 234
 TM 221, 234-235, 241, 249
 TMI 207, 212
 TOA 217
 topography 202, 212, 221-222, 229, 234-236, 243
 TOPSAR 236
 tower sites 246
 TRAGNET 246-247
 TRMM 212
 UKMO 232, 251
 UMCP 251
 UNEP 237
 UNESCO 237
 USDA 238-239
 USGS 213, 250
 validation 201, 204-208, 213-216, 229, 234-252
 vegetation indices 202, 207-208, 223, 226-227
 vegetation phenology 203, 223, 227, 234, 242
 vegetation structure 241-243
 VEMAP 214, 218, 229, 232, 236, 239, 240, 251-252
 VIC 213
 VIRS 207, 212
 VIS 223, 226
 VNIR 234
 volcanoes 206
 WCRP 204, 213, 237, 241, 245, 251
 wind 206-207, 217, 219-220, 248
 WMO 237
 WSR 212, 245

Cryospheric Systems

LEAD AUTHORS B. E. Goodison
 R. D. Brown
 R. G. Crane

CONTRIBUTING AUTHORS

R. Alley	D. K. Hall
R. Bales	R. Harrington
D. Barber	J. Kargel
R. Barry	H. Kieffer
C. Bentley	S. Munro
T. Carrol	C. Parkinson
D. Cline	B. Raup
C. R. Duguay	A. Rothrock
G. M. Flato	M. Sharp

CHAPTER 6 CONTENTS

6.1 Overview	263
6.1.1 Rationale for studying the cryosphere	263
6.1.2 Components of the cryosphere	264
6.1.2.1 Snow	266
6.1.2.2 Sea ice	267
6.1.2.3 Lake ice and river ice	268
6.1.2.4 Frozen ground and permafrost	269
6.1.2.5 Glaciers and ice sheets	269
6.2 Major scientific questions	271
6.2.1 Representation of cryospheric processes in climate and hydrological models	271
6.2.1.1 Snow cover	271
6.2.1.2 Sea ice	273
6.2.1.3 Lake ice	274
6.2.1.4 Frozen ground and permafrost	275
6.2.1.5 Glaciers and ice sheets	275
6.2.2 Cryosphere-climate linkages and feedbacks	278
6.2.2.1 Freshwater cycle	279
6.2.2.2 Surface energy balance	279
6.2.2.3 Observed and modeled feedbacks	280
6.2.3 Cryospheric variability and change	281
6.2.3.1 Snow	281
6.2.3.2 Sea ice	283
6.2.3.3 Lake ice	284
6.2.3.4 Frozen ground and permafrost	284
6.2.3.5 Glaciers and ice sheets	285
6.3 Required measurements, data sets, and parameterizations	287
6.3.1 Satellite observations	287
6.3.1.1 Snow cover	287
6.3.1.2 Sea ice	291
6.3.1.3 Lake ice	293
6.3.1.4 Frozen ground and permafrost	295
6.3.1.5 Glaciers and ice sheets	296
6.3.2 Related international science programs	297
6.3.2.1 BOREAS: Boreal Ecosystem-Atmosphere Study	297
6.3.2.2 ACSYS: Arctic Climate System Study	297
6.3.2.3 SHEBA: Surface Heat Budget of the Arctic Ocean	297
6.3.2.4 IABP: International Arctic Buoy Program	297
6.3.2.5 SCICEX: Submarine Arctic Science Cruise Program	297
6.3.2.6 PARCA: Program for Arctic Regional Climate Assessment	297
6.4 EOS contributions	298
References	300
Chapter 6 Index	307

6.1 Overview

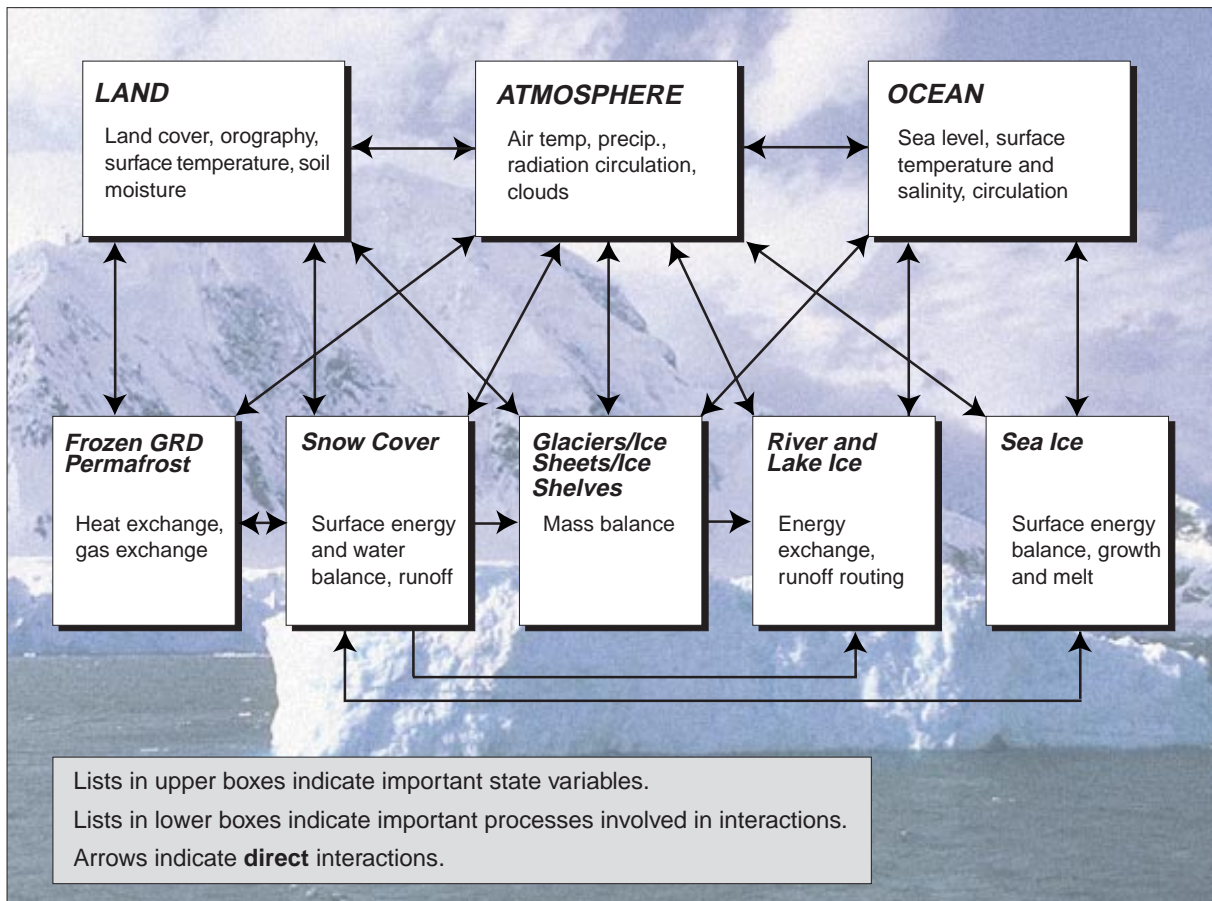
6.1.1 Rationale for studying the cryosphere

The term “cryosphere” traces its origins to the Greek word *kryos* for frost or icy cold. It collectively describes the portions of the Earth’s surface where water is in a solid form and includes sea ice, lake ice, river ice, snow cover, glaciers, ice caps and ice sheets, and frozen ground (which includes permafrost). The cryosphere is an integral part of the global climate system with important linkages and feedbacks generated through its influence on surface energy and moisture fluxes, clouds, precipitation, hydrology, and atmospheric and oceanic circulation (Figure 6.1). Through these feedback processes, the cryosphere plays a significant role in global climate and in climate model response to global change.

A further concern of global warming is that melting ice sheets will cause sea level to rise. Even modest increases in sea level (~ 30 cm) are significant for coastal

communities and coastal engineering (Asrar and Dozier 1994), and the economic and societal implications are immense. The Intergovernmental Panel on Climate Change (IPCC) expects that projected climate warming will lead to rapid and pronounced reductions in seasonal snow cover, permafrost, and glaciers (Fitzharris 1996). While the time scale for this response is uncertain, these changes can be expected to have widespread and significant impacts since the cryosphere is closely intertwined in the natural and economic fabric of many midlatitude and northern countries. In Canada, for example, most regions experience at least 3 months of snow cover each winter; nearly all navigable waters (with the exception of the west coast) are affected by an ice cover for some period during the winter; more than half of the country is underlain by continuous or discontinuous permafrost; and Canadian terrestrial ice masses constitute the most exten-

FIGURE 6.1



Schematic diagram outlining a number of the important interactions between the cryosphere and other major components of the global climate system. (G. Flato.)

sive permanent ice cover in the Northern Hemisphere outside of Greenland (Goodison and Brown 1997).

Because of the sensitivity of the cryosphere to temperature changes, accurate information on the rate and magnitude of changes in cryospheric elements is essential for policy and decision making, particularly over the high latitudes of the Northern Hemisphere, where climate warming is projected to be the greatest. Global climate models (GCMs) do not yet provide accurate simulations of the current climate over the Arctic (Bromwich et al. 1994). Significant improvements in the representation of cryospheric processes and in the understanding of cryosphere-climate linkages and feedbacks are required to reduce the uncertainties in high-latitude climate simulations. Satellite data are indispensable for this task because of their unique combination of capabilities such as repeat coverage over data-sparse areas, all-weather sensing, and the ability to derive information on important surface geophysical properties. Satellites also have the ability to obtain information on horizontal and vertical displacements and other changes, using repeat coverage and specialized techniques such as Synthetic Aperture Radar (SAR) interferometry.

The importance of the cryosphere is clearly reflected in the Earth Observing System (EOS) program. For example, EOS includes a dedicated cryospheric data archiving center, launch of new sensors and algorithm development activities for improved monitoring of snow, ice, and glaciers, and several Interdisciplinary Science Investigation (IDS) activities undertaking research to improve understanding and modeling of cryospheric processes, cryospheric variability, and cryosphere-climate interactions. The following sections provide background information on the important characteristics of the main components of the cryosphere, before moving on to look at the scientific rationale for cryospheric research and monitoring activities within EOS (Section 6.2). Section 6.3 looks at the measurements needed to answer the key science questions, and summarizes the cryospheric data measurement activities of EOS and associated international science programs. The chapter concludes (Section 6.4) with a summary of important EOS contributions to improved understanding and monitoring of the cryosphere.

6.1.2 Components of the cryosphere

Frozen water occurs on the Earth's surface primarily as snow cover, freshwater ice in lakes and rivers, sea ice, glaciers, ice sheets, and frozen ground and permafrost (perennially-frozen ground). The residence time of water in each of these cryospheric sub-systems varies widely. Snow cover and freshwater ice are essentially seasonal,

and most sea ice, except for ice in the central Arctic, lasts only a few years if it is not seasonal. A given water particle in glaciers, ice sheets, or ground ice, however, may remain frozen for 10-100,000 years or longer, and deep ice in parts of East Antarctica may have an age approaching 1 million years. The concept of residence time (flux/storage) is important for the climate system. Water with short residence times participates in the fast-response regime of the climate system (atmosphere, upper-ocean layers, and land surface) that determines the amplitude and regional patterns of climate change. Long-residence-time components (e.g., ice sheets and the deep ocean) act to modulate and introduce delays into the transient response (Chahine 1992). However, the possibility of abrupt changes in the slow-response components of the climate system cannot be overlooked.

The majority of the world's ice volume is in Antarctica (Table 6.1), principally in the East Antarctic ice sheet. In terms of areal extent, however, Northern Hemisphere winter snow and ice extent comprise the largest area, amounting to an average 23% of hemispheric surface area in January. The large areal extent and the important climatic roles of snow and ice, related to their unique physical properties, indicate that the ability to observe and model snow- and ice-cover extent, thickness, and physical properties (radiative and thermal properties) is of particular significance for climate research.

There are several fundamental physical properties of snow and ice that modulate energy exchanges between the surface and the atmosphere. The most important properties are the surface reflectance (albedo), the ability to transfer heat (thermal diffusivity), and the ability to change state (latent heat). These physical properties, together with surface roughness, emissivity, and dielectric characteristics, have important implications for observing snow and ice from space. For example, surface roughness is often the dominant factor determining the strength of radar backscatter (Hall 1996). Physical properties such as crystal structure, density, and liquid-water content are important factors affecting the transfers of heat and water and the scattering of microwave energy.

The surface reflectance of incoming solar radiation is important for the surface energy balance (SEB). It is the ratio of reflected to incident solar radiation, commonly referred to as albedo. Climatologists are primarily interested in albedo integrated over the shortwave portion of the electromagnetic spectrum (~0.3 to 3.5 μm), which coincides with the main solar energy input. Typically, albedo values for non-melting snow-covered surfaces are high (~80-90%) except in the case of forests (see textbox on pg. 266). The higher albedos for snow

TABLE 6.1

COMPONENT	AREA (10 ⁶ KM ²)	ICE VOLUME (10 ⁶ KM ³)	SEA LEVEL EQUIVALENT ^a (M)
Land Ice			
East Antarctica ^b	9.9	25.9	64.8
West Antarctica	2.3	3.4	8.5
Greenland	1.7	3.0	7.6
Small Ice Caps and Mountain Glaciers	0.68	0.18	0.5
Permafrost (excluding Antarctica)			
Continuous	7.60	0.03	0.08
Discontinuous	1.73	0.07	0.18
Sea Ice			
Northern Hemisphere^c			
Late March	14.0	0.05	
Early September	6.0	0.02	
Southern Hemisphere^d			
September	15.0	0.02	
February	2.0	0.002	
Land Snow Cover^e			
Northern Hemisphere			
Late January	46.5	0.002	
Late August	3.9		
Southern Hemisphere			
Late July	0.85		
Early May	0.07		

Volumetric and areal extent of major components of the cryosphere.

- a 400,000 km³ of ice is equivalent to 1 m global sea level.
- b Grounded ice sheet, excluding peripheral, floating ice shelves (which do not affect sea level). The shelves have a total area of 0.62 x 10⁶ km² and a volume of 0.79 x 10⁶ km³ (Drewry 1982).
- c Actual ice areas, excluding open water. Ice extent ranges between approximately 9.3 and 15.7 x 10⁶ km².
- d Actual ice area excluding open water (Gloersen et al. 1993). Ice extent ranges between approximately 3.8 and 18.8 x 10⁶ km². Southern Hemisphere ice is mostly seasonal and generally much thinner than Arctic ice.
- e Snow cover includes that on land ice, but excludes snow-covered sea ice (Robinson et al. 1993).

and ice cause rapid shifts in surface reflectivity in autumn and spring in high latitudes, but the overall climatic significance of this increase is spatially and temporally modulated by cloud cover. (Planetary albedo is determined principally by cloud cover, and by the small amount of total solar radiation received in high latitudes during winter months.) Summer and autumn are times of high-average cloudiness over the Arctic Ocean so the albedo feedback associated with the large seasonal changes in sea-ice extent is greatly reduced. Groisman et al. (1994a) observed that snow cover exhibited the greatest influence on the

Earth radiative balance in the spring (April to May) period when incoming solar radiation was greatest over snow-covered areas.

The thermal properties of cryospheric elements also have important climatic consequences. Snow and ice have much lower thermal diffusivities than air (see text box). Thermal diffusivity is a measure of the speed at which temperature waves can penetrate a substance. As shown in the box, snow and ice are many orders of magnitude less efficient at diffusing heat than air. Snow cover insulates the ground surface, and sea ice insulates the

Typical Ranges for Surface Albedo:

Fresh, dry snow	0.80 to 0.90
Melting ice/snow	0.25 to 0.80
Melting sea ice with puddles	0.30 to 0.40
Snow-covered forest	0.25 to 0.40
Snow-free vegetation/soil	0.10 to 0.30
Water (high solar elevation)	0.05 to 0.10

underlying ocean, decoupling the surface-atmosphere interface with respect to both heat and moisture fluxes. The flux of moisture from a water surface is eliminated by even a thin skin of ice, whereas the flux of heat through thin ice continues to be substantial until it attains a thickness in excess of 30 to 40 cm. However, even a small amount of snow on top of the ice will dramatically reduce the heat flux and slow down the rate of ice growth. The insulating effect of snow also has major implications for the hydrological cycle. In non-permafrost regions, the insulating effect of snow is such that only near-surface ground freezes and deep water drainage is uninterrupted (Lynch-Stieglitz 1994).

While snow and ice act to insulate the surface from large energy losses in winter, they also act to retard warming in the spring and summer because of the large amount of energy required to melt ice (the latent heat of fusion, $3.34 \times 10^5 \text{ J kg}^{-1}$ at 0°C). However, the strong static stability of the atmosphere over areas of extensive snow or ice tends to confine the immediate cooling effect to a relatively shallow layer, so that associated atmospheric anomalies are usually short-lived and local to regional in scale (Cohen and Rind 1991). In some areas of the world such as Eurasia, however, the cooling associated with a heavy snowpack and moist spring soils is known to play a role in modulating the summer monsoon circulation

**Typical Thermal Diffusivities:
(after Oke 1987)**

	$\text{m}^2 \text{ s}^{-1} \times 10^{-6}$
Fresh snow	0.10
Old snow	0.40
Pure ice (0°C)	1.16
Air (still 10°C)	21.50
Air (turbulent)	$\sim 10^7$

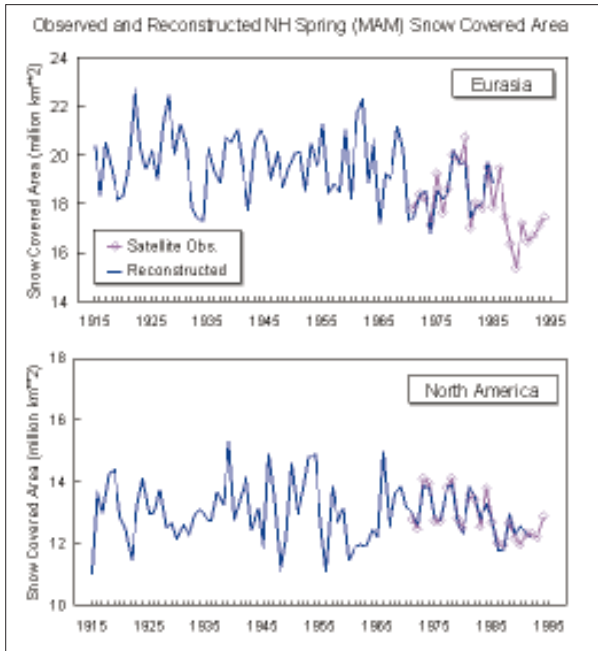
(e.g., Vernekar et al. 1995). Gutzler and Preston (1997) recently presented evidence for a similar snow-summer circulation feedback over the southwestern United States.

The role of snow cover in modulating the monsoon is just one example of a short-term cryosphere-climate feedback involving the land surface and the atmosphere. From Figure 6.1 it can be seen that there are numerous cryosphere-climate feedbacks in the global climate system. These operate over a wide range of spatial and temporal scales from local seasonal cooling of air temperatures to hemispheric-scale variations in ice sheets over time-scales of thousands of years. The feedback mechanisms involved are often complex and incompletely understood. For example, Curry et al. (1995) showed that the so-called "simple" sea ice-albedo feedback involved complex interactions with lead fraction, melt ponds, ice thickness, snow cover, and sea-ice extent. One of the main goals of EOS cryospheric research is to further the development of methods and models to observe and better understand interannual variations in cryospheric elements and their interactions with the global climate system. Further discussion of cryospheric variability and cryosphere-climate interactions is provided in the following subsections, which describe the key characteristics of the main components of the cryosphere, and in Section 6.2.1.

6.1.2.1 Snow

Snow cover has the largest areal extent of any component of the cryosphere, with a mean maximum areal extent of approximately 47 million km^2 . Most of the Earth's snow-covered area (SCA) is located in the Northern Hemisphere, and temporal variability is dominated by the seasonal cycle; Northern Hemisphere snow-cover extent ranges from 46.5 million km^2 in January to 3.8 million km^2 in August (Robinson et al. 1993). North American winter SCA has exhibited an increasing trend over much of this century (Brown and Goodison 1996; Hughes et al. 1996) largely in response to an increase in precipitation (Groisman and Easterling 1994). However, the available satellite data show that the hemispheric winter snow cover has exhibited little interannual variability over the 1972-1996 period, with a coefficient of variation ($\text{COV}=\text{s.d./mean}$) for January Northern Hemisphere snow cover of < 0.04 . According to Groisman et al. (1994a) Northern Hemisphere spring snow cover should exhibit a decreasing trend to explain an observed increase in Northern Hemisphere spring air temperatures this century. Preliminary estimates (Figure 6.2) of SCA from historical and reconstructed in situ snow-cover data suggest this is the case for Eurasia, but not for North America, where spring snow cover has remained close to current levels over most

FIGURE 6.2



Reconstructed SCA from PC analysis of in situ snow-cover data over North America and Eurasia (Brown, 1997).

of this century (Brown 1997). Because of the close relationship observed between hemispheric air temperature and snow-cover extent over the period of satellite data (IPCC 1996), there is considerable interest in monitoring Northern Hemisphere snow-cover extent for detecting and monitoring climate change.

Snow cover is an extremely important storage component in the water balance, especially seasonal snowpacks in mountainous areas of the world. Though limited in extent, seasonal snowpacks in the Earth's mountain ranges account for the major source of the runoff for stream flow and groundwater recharge over wide areas of the midlatitudes. For example, over 85% of the annual runoff from the Colorado River basin originates as snowmelt. Snowmelt runoff from the Earth's mountains fills the rivers and recharges the aquifers that over a billion people depend on for their water resources. Further, over 40% of the world's protected areas are in mountains, attesting to their value both as unique ecosystems needing protection and as recreation areas for humans. Climate warming is expected to result in major changes to the partitioning of snow and rainfall, and to the timing of snowmelt, which will have important implications for water use and management. These changes also involve potentially important decadal and longer time-scale feed-

backs to the climate system through temporal and spatial changes in soil moisture and runoff to the oceans (Walsh 1995). Freshwater fluxes from the snow cover into the marine environment may be important, as the total flux is probably of the same magnitude as desalinated ridging and rubble areas of sea ice (Prinsenberg 1988). In addition, there is an associated pulse of precipitated pollutants which accumulate over the arctic winter in snowfall and are released into the ocean upon ablation of the sea-ice cover.

Variations in snowfall have also been shown to be important in the climate of polar regions since snow on sea ice affects both the thermodynamic and radiative characteristics of the ocean-sea ice-atmosphere interface. Brown and Cote (1992) demonstrated that the insulating effect of snowfall was the most important factor in determining the interannual variability of fast-ice thickness in the Canadian Arctic. In the coupled climate-sea-ice model of Ledley (1991, 1993), the albedo effect was found to dominate, and the effect of additional snowfall was to delay ice break-up and produce a cooling over the Arctic Basin. However, recent model sensitivity studies (Flato and Brown 1996; Harder 1997) suggest that the insulating effect is more important. In reality, it is extremely difficult to assess the baseline range of snow-thickness effects on the thermodynamic coupling between snow and sea ice because of a nearly complete lack of spatially-distributed estimates of snow cover on sea ice. EOS researchers are in the process of developing microwave algorithms for estimating snow-water equivalent over sea ice, which will address this problem (Cavalieri and Comiso 1997).

The snow-cover control of shortwave (SW) energy exchange at the surface also affects the availability of sub-ice photosynthetically-active radiation (PAR); an essential determinant of lower trophic level productivity. The evolution of the marine ecosystem is such that small perturbations in the availability of PAR have dramatic impacts on the initial production of epontic (sub-ice) algae (Welch 1992).

6.1.2.2 Sea ice

Sea ice covers much of the polar oceans and forms by freezing of sea water. Satellite data since the early 1970s reveal considerable seasonal, regional, and interannual variability in the sea-ice covers of both hemispheres. Seasonally, sea-ice extent in the Southern Hemisphere varies by a factor of 5, from a minimum of 3-4 million km² in February to a maximum of 17-20 million km² in September (Zwally et al. 1983; Gloersen et al. 1992). The seasonal variation is much less in the Northern Hemisphere where the confined nature and high latitudes of the Arctic Ocean

result in a much larger perennial ice cover, and the surrounding land limits the equatorward extent of wintertime ice. Thus, the seasonal variability in Northern Hemisphere ice extent varies by only a factor of 2, from a minimum of 7-9 million km² in September to a maximum of 14-16 million km² in March (Parkinson et al. 1987; Gloersen et al. 1992).

The ice cover exhibits much greater regional-scale interannual variability than it does hemispherical. For instance, in the region of the Seas of Okhotsk and Japan, maximum ice extent decreased from 1.3 million km² in 1983 to 0.85 million km² in 1984, a decrease of 35%, before rebounding the following year to 1.2 million km² (Gloersen et al. 1992). The regional fluctuations in both hemispheres are such that for any several-year period of the satellite record some regions exhibit decreasing ice coverage while others exhibit increasing ice cover (Parkinson 1995). The overall trend indicated in the passive microwave record from 1978 through mid-1995 shows that the extent of Arctic sea ice is decreasing 2.7% per decade (Johannessen et al. 1995). Subsequent work with the satellite passive-microwave data indicates that from late October 1978 through the end of 1996 the extent of Arctic sea ice decreased by 2.9% per decade while the extent of Antarctic sea ice increased by 1.3% per decade (Cavalieri et al. 1997).

While small in terms of area, leads and polynyas are very important components of the sea-ice regime because of the dominant role they play in exchanges of heat and moisture to the atmosphere during the polar winter. Thermodynamically, polynyas have been observed to affect climate both at the local and regional scales (Steffen and Ohumura 1985), and the continuous ice production in polynyas is an important contribution to thermohaline circulation (Martin et al. 1992). Radiatively, polynyas become "oases" of biological production because of the significant absorption of PAR within the water column. This stimulates primary production, thereby creating a local abundance in biomass.

6.1.2.3 *Lake ice and river ice*

Ice forms on rivers and lakes in response to seasonal cooling. The sizes of the ice bodies involved are too small to exert other than localized climatic effects. However, the freeze-up/break-up processes respond to large-scale and local weather factors, such that considerable interannual variability exists in the dates of appearance and disappearance of the ice. Long series of lake-ice observations can serve as a proxy climate record, and the monitoring of freeze-up and break-up trends may provide a convenient integrated and seasonally-specific index of climatic perturbations. Information on river-ice conditions is less

useful as a climatic proxy because ice formation is strongly dependent on river-flow regime, which is affected by precipitation, snow melt, and watershed runoff as well as being subject to human interference that directly modifies channel flow, or that indirectly affects the runoff via land-use practices. For various reasons including the small scale of river-ice processes, there is currently no specific river-ice research component within EOS. This may change in the future, but, for the moment, river ice is excluded from further discussion in this chapter.

Lake freeze-up depends on the heat storage in the lake and therefore on its depth, the rate and temperature of any inflow, and water-air energy fluxes. Information on lake depth is often unavailable, although some indication of the depth of shallow lakes in the Arctic can be obtained from airborne radar imagery during late winter (Sellman et al. 1975) and spaceborne optical imagery during summer (Duguay and Lafleur 1997). The timing of breakup is modified by snow depth on the ice as well as by ice thickness and freshwater inflow.

The appearance and disappearance of lake ice are readily observed in the visible band (Maslanik and Barry 1987; Wynne et al. 1996) and microwave sensors are particularly well-suited to monitoring important lake-ice characteristics such as freeze-up, break-up, freeze-to-bottom, and surface-melt onset (Hall 1993). Even small lakes (of a few square kilometers) can be monitored because freeze-up usually occurs after the development of a snow cover, and break-up after the disappearance of snow. Because ice freeze-up and break-up dates exhibit a close relationship to surface air temperatures at local and regional scales, monitoring of these readily observable events by satellite data offers the potential to monitor surface air-temperature anomalies in major data-sparse areas of the globe (Barry and Maslanik 1993). Recent closure or automation of many high-latitude stations increases the desirability of lake-ice monitoring via satellite in order to provide adequate spatial coverage of temperature trends in subarctic and Arctic regions. There are two major research activities being carried out in the Cryospheric System (CRYSYS) IDS to develop methods for using passive (Walker and Davey 1993) and active (Duguay and Lafleur 1997) microwave satellite data to monitor important lake-ice parameters.

Useful empirical relationships have been developed between temperature indices and the date of ice formation. In general, freeze-up and break-up correlate well with air temperature or freezing-degree days as used by Williams (1971). In general, empirical studies suggest an air temperature sensitivity of ice freeze-up/break-up of ± 5 to 10 days per $\pm 1^\circ\text{C}$ seasonal change in air temperature (Palecki and Barry 1986). Thawing-degree days are less

satisfactory indicators of breakup, especially where river inflow and wind are important factors or where there is considerable year-to-year variability in the depth of snow pack on the ice. Physical models of lake-water temperature and ice-cover growth and ablation (e.g., Fang and Stefan 1996) are a more-satisfactory way to proceed since these provide useful information on key processes and sensitivity to climate change, and are less restricted by the need to develop locally-calibrated statistical relationships.

6.1.2.4 *Frozen ground and permafrost*

Permafrost (perennially frozen ground) may occur where mean annual air temperatures (MAAT) are less than -1 or -2°C and is generally continuous where MAAT are less than -7°C . In addition, its extent and thickness are affected by ground moisture content, vegetation cover, winter snow depth, and aspect. The global extent of permafrost is still not completely known, but it underlies approximately 20% of Northern Hemisphere land areas. Thicknesses exceed 600 m along the Arctic coast of northeastern Siberia and Alaska, but, toward the margins, permafrost becomes thinner and horizontally discontinuous. The marginal zones will be more immediately subject to any melting caused by a warming trend. Most of the presently existing permafrost formed during previous colder conditions and is therefore relic. However, permafrost may form under present-day polar climates where glaciers retreat or land emergence exposes unfrozen ground. Washburn (1973) concluded that most continuous permafrost is in balance with the present climate at its upper surface, but changes at the base depend on the present climate and geothermal heat flow; in contrast, most discontinuous permafrost is probably unstable or "in such delicate equilibrium that the slightest climatic or surface change will have drastic disequilibrium effects" (Washburn 1973, p. 48).

Under warming conditions, the increasing depth of the summer active layer has significant impacts on the hydrologic and geomorphic regimes. Thawing and retreat of permafrost have been reported in the upper Mackenzie Valley and along the southern margin of its occurrence in Manitoba, but such observations are not readily quantified and generalized. Based on average latitudinal gradients of air temperature, an average northward displacement of the southern permafrost boundary by 50-to-150 km could be expected, under equilibrium conditions, for a 1°C warming.

Only a fraction of the permafrost zone consists of actual ground ice. The remainder (dry permafrost) is simply soil or rock at subfreezing temperatures. The ice volume is generally greatest in the uppermost permafrost layers and mainly comprises pore and segregated ice in

Earth material. Measurements of bore-hole temperatures in permafrost can be used as indicators of net changes in temperature regime. Gold and Lachenbruch (1973) infer a $2\text{-}4^{\circ}\text{C}$ warming over 75 to 100 years at Cape Thompson, Alaska, where the upper 25% of the 400-m thick permafrost is unstable with respect to an equilibrium profile of temperature with depth (for the present mean annual surface temperature of -5°C). Maritime influences may have biased this estimate, however. At Prudhoe Bay similar data imply a 1.8°C warming over the last 100 years (Lachenbruch et al. 1982). Further complications may be introduced by changes in snow-cover depths and the natural or artificial disturbance of the surface vegetation.

The potential rates of permafrost thawing have been established by Osterkamp (1984) to be two centuries or less for 25-meter-thick permafrost in the discontinuous zone of interior Alaska, assuming warming from -0.4 to 0°C in 3-4 years, followed by a further 2.6°C rise. Although the response of permafrost (depth) to temperature change is typically a very slow process (Osterkamp 1984; Koster 1993), there is ample evidence for the fact that the active-layer thickness quickly responds to a temperature change (Kane et al. 1991). Whether, under a warming or cooling scenario, global climate change will have a significant effect on the duration of frost-free periods in both regions with seasonally- and perennially-frozen ground.

6.1.2.5 *Glaciers and ice sheets*

Ice sheets are the greatest potential source of global freshwater, holding approximately 77% of the global total. This corresponds to 80 m of world sea-level equivalent, with Antarctica accounting for 90% of this. Greenland accounts for most of the remaining 10%, with other ice bodies and glaciers accounting for less than 0.5% (Table 6.1). Because of their size in relation to annual rates of snow accumulation and melt, the residence time of water in ice sheets can extend to 100,000 or 1 million years. Consequently, any climatic perturbations produce slow responses, occurring over glacial and interglacial periods. Valley glaciers respond rapidly to climatic fluctuations with typical response times of 10-50 years (Oerlemans 1994). However, the response of individual glaciers may be asynchronous to the same climatic forcing because of differences in glacier length, elevation, slope, and speed of motion. Oerlemans (1994) provided evidence of coherent global retreat in glaciers which could be explained by a linear warming trend of 0.66°C per 100 years.

While glacier variations are likely to have minimal effects upon global climate, their recession may have contributed one third to one half of the observed 20th-century rise in sea level (Meier 1984; IPCC 1996). Furthermore, it is extremely likely that such extensive gla-

cier recession as is currently observed in the Western Cordillera of North America (Pelto 1996), where runoff from glacierized basins is used for irrigation and hydropower, involves significant hydrological and ecosystem impacts. Effective water-resource planning and impact mitigation in such areas depends upon developing a sophisticated knowledge of the status of glacier ice and the mechanisms that cause it to change. Furthermore, a clear understanding of the mechanisms at work is crucial to interpreting the global-change signals that are contained in the time series of glacier mass-balance records.

Combined mass-balance estimates of the large ice sheets carry an uncertainty of about 20%. Studies based on estimated snowfall and mass output tend to indicate that the ice sheets are near balance or taking some water out of the oceans (Bentley and Giovinetto 1991). Marine-based studies (Jacobs et al. 1992) suggest sea-level rise from the Antarctic or rapid ice-shelf basal melting. Some authors (Paterson 1993; Alley 1997) have suggested that the difference between the observed rate of sea-level rise (roughly 2 mm y^{-1}) and the explained rate of sea-level rise from melting of mountain glaciers, thermal expansion of the ocean, etc. (roughly 1 mm y^{-1} or less) is similar to the modeled imbalance in the Antarctic (roughly 1 mm y^{-1} of sea-level rise; Huybrechts 1990), suggesting a contribution of sea-level rise from the Antarctic.

Relationships between global climate and changes in ice extent are complex. The mass balance of land-based glaciers and ice sheets is determined by the accumulation of snow, mostly in winter, and warm-season ablation due primarily to net radiation and turbulent heat fluxes to melting ice and snow from warm-air advection (Munro 1990; Paterson 1993; Van den Broeke 1996). However, most of Antarctica never experiences surface melting (Van den Broeke and Bintanja 1995). Where ice masses terminate in the ocean, iceberg calving is the major contributor to mass loss. In this situation, the ice margin may extend out into deep water as a floating ice shelf, such as that in the Ross Sea. Despite the possibility that global warming could result in losses to the Greenland ice sheet being offset by gains to the Antarctic ice sheet (Ohmura et al. 1996), there is major concern about the possibility of a West Antarctic ice-sheet collapse. The West Antarctic ice sheet is grounded on bedrock below sea level, and its collapse has the potential of raising the world sea level 6-7 m over a few hundred years.

Most of the discharge of the West Antarctic ice sheet is via the five major ice streams (faster flowing ice) entering the Ross Ice Shelf, the Rutford Ice Stream entering Ronne-Filchner shelf of the Weddell Sea, and the Pine

Island Glacier entering the Amundsen Ice Shelf. Opinions differ as to the present mass balance of these systems (Bentley 1983, 1985), principally because of the limited data. The West Antarctic ice sheet is stable so long as the Ross Ice Shelf is constrained by drag along its lateral boundaries and pinned by local grounding.

Over the last few decades, a number of major programs have significantly improved understanding of the Greenland ice sheet (e.g., Expédition Glaciologique Internationale au Groenland (EGIG), Camp Century, Dye 3, Greenland Ice Sheet Program [GISP]). Reeh (1989) concluded that the Greenland ice sheet as a whole is close to a balanced state with slight thinning of some marginal sectors likely being compensated for by a slight thickening in the central area. Koerner (1989) provided evidence that the Greenland ice sheet experienced extensive melt during the last interglacial 100,000 years ago, which suggests that the current ice sheet is not a relic from a previously colder climate. This was confirmed in an ice-sheet modeling study when, after removal, the ice sheet re-formed on bare bedrock under present or slightly warmer climatic conditions (Letréguilly et al. 1991). The model experiments also revealed that the ice sheet was relatively stable, and that it took temperature rises of at least 6°C for the ice sheet to disappear completely. A recent doubled- CO_2 simulation of the ice sheet with the Global Environmental and Ecological Simulation of Interactive Systems (GENESIS) GCM (Thompson and Pollard 1997) indicated that the net annual mass balance decreased from $+0.13$ to -0.12 m a^{-1} . However, there are still major uncertainties involved in such modeling exercises, particularly in the area of how atmospheric circulation and precipitation will change. Ice-sheet-model sensitivity to accumulation parameterization was highlighted in Fabre et al. (1994), where, for a temperature increase of 5°C , one accumulation parameterization yielded only slight margin retreat while the other resulted in the complete collapse of the ice sheet.

Satellites are playing an increasingly important role in furthering understanding of the Greenland ice sheet mass balance by providing accurate surface-elevation data, ice-flow velocity data (Joughin et al. 1995; Rignot et al. 1995), and surface-ablation information. For example, Abdalati and Steffen (1995) used passive microwave data to observe an increasing trend in ablation area of 3.4% per year since 1978. This trend was temporarily interrupted by the aerosol loading from the eruption of Mt. Pinatubo in 1991, which underscores the sensitivity of the mass balance to perturbations in incoming solar radiation.

6.2 Major scientific questions

As outlined in IPCC (1996, p. 46) the most urgent scientific problems requiring attention are 1) determining the rate and magnitude of climate change and sea-level rise, 2) the detection and attribution of climate change, and 3) the regional patterns of climate change. Addressing these questions requires an improved understanding and ability to model the entire coupled atmosphere-ice-ocean climate system, as well as systematic observations of key climate variables such as snow and sea-ice extent. Improved representation of the cryosphere is vital given documented weaknesses in GCM climate simulations over high latitudes, the area expected to exhibit the greatest warming in response to increased levels of greenhouse gases. With regard to the cryosphere the key areas are:

- improved representation of cryospheric processes and cryosphere-climate interactions in climate and hydrological models, and
- improved ability to monitor and understand variability and change in important components of the cryosphere such as major ice sheets and hemispheric snow and sea-ice extent.

The following sections elaborate the current state of cryospheric science in these key areas and outline the ways in which EOS will contribute to improved understanding of the cryosphere.

6.2.1 Representation of cryospheric processes in climate and hydrological models

Previous evaluations of the performance of GCMs at simulating the present Arctic climate (e.g., Walsh and Crane 1992; Bromwich et al. 1994; McGinnis and Crane 1994) documented numerous shortcomings such as incorrect seasonal variation in cloud cover, excessive atmospheric moisture transport, poor simulation of atmospheric circulation patterns around Greenland, and an excessive dominance of winter-season circulation patterns. Bromwich et al. (1994) noted that the poor simulation of atmospheric circulation around Greenland is greatly improved with higher-resolution representations of Greenland topography by T42 coupled models. However, the problem of excessive northern-latitude precipitation persists in T42 models (Bromwich and Chen 1995). Battisti et al. (1997) concluded that most of the GCMs used to evaluate climate change have an artificially dampened natural variability in the Arctic, and that this was primarily linked to inadequate treatment of sea-ice pro-

cesses (e.g., snow, albedo, heat storage, and conduction). Another cryospheric link to poor climate-model performance was highlighted by Tao et al. (1996) who found that a lack of vegetative masking of snow albedo in some Atmospheric Model Intercomparison Project (AMIP) models resulted in a 3.3°C cold bias in spring air temperatures over northern Eurasia. A high priority for cryospheric research is to improve the representation of the cryosphere in hydrologic models and in global and regional climate models.

6.2.1.1 Snow cover

Snow cover in climate models

The realistic simulation of snow cover in climate models is essential for correct representation of the SEB (albedo, surface temperature, heat and moisture fluxes) ground temperatures, and hydrology. Snow cover has a number of important effects on the hydrological cycle. First, it acts as a major store for winter precipitation, which is subsequently released in the spring. Second, the insulating properties of snow cover are such that in all but permafrost regions, frost penetration into the soil is limited to surface layers, which allows deep water drainage to continue throughout the year (Lynch-Stieglitz 1994). In early GCMs (e.g., the National Center for Atmospheric Research [NCAR]-CCM0A), snow cover was specified from a monthly snow-cover climatology, and the only impact of snow cover was through changes in surface albedo. Studies of GCM performance with and without physically-based snow-cover models (Marshall et al. 1994, Lynch-Stieglitz 1994) have highlighted the need to include an adequate treatment of snow cover to model correctly the hydrological cycle. Lynch-Stieglitz (1994) concluded that the inability to correctly model snow cover cast doubt upon year-round model calculations of runoff.

The energy and mass-balance model of Anderson (1976) is probably one of the most complete snowpack models developed to date. However, this model is too computationally-intensive for GCMs, which have rather severe computational constraints. A review of current GCM snow-cover models (Verseghy 1991; Loth et al. 1993; Marshall et al. 1994; Lynch-Stieglitz 1994) suggests that the following processes must be properly represented in order to provide realistic simulations of the snowpack:

- Snow metamorphism or aging: Snow experiences major changes in physical properties (density, albedo,

thermal conductivity) once it reaches the surface due to a number of processes such as melt/freezing, settling, compaction, and water vapor diffusion. These changes are time- and temperature-dependent and need to be taken into account in order to model correctly the energy balance of the snowpack. A number of empirically-based parameterizations are available which describe these processes, and the verification results appear to be good for the few case studies presented in the literature to date (Lynch-Stieglitz 1994).

- Ability to resolve vertical gradients: Both Loth et al. (1993) and Lynch-Stieglitz (1994) conclude that a multi-layer representation of the snowpack is essential to model the steep temperature gradient at the snow surface and to take account of depth-varying snow properties. Lynch-Stieglitz (1994) recommended that the depth of the surface layer be no greater than the thermal-damping depth of snow (~6-10 cm) to resolve diurnal fluctuations in heat content.
- Snow-rain separation: GCMs employ a variety of schemes for determining precipitation phase (see Table 2 in Randall et al. 1994). Loth et al. (1993) tested several rain/snow criteria and found that the modeled snow cover and runoff (for a midlatitudinal maritime climate) were highly sensitive to the particular criterion used.

Of the various GCM snowpack models published in the literature to date, the multi-layer model of Loth et al. (1993) is the most detailed and potentially the most realistic for 1-D snowpack simulations. However, Lynch-Stieglitz (1994) obtained excellent results with a simplified three-layer snow-cover model, which suggests that important snowpack processes can be captured without a great deal of vertical resolution. It should be noted that most GCM snowpack-model evaluations carried out to date have assessed performance at a single point; none have been validated systematically over a full range of snow-cover climate regimes such as those identified by Sturm et al. (1995). A general lack of suitable evaluation data is a major contributing factor. EOS products from the Moderate-Resolution Imaging Spectroradiometer (MODIS), such as surface temperature, albedo, and snow cover, as well as snow-water equivalent and depth from the EOS Advanced Microwave Scanning Radiometer (AMSR-E), will greatly assist this task.

A major challenge for GCM snow-cover modelers is inclusion of important physical processes, and topographic and land-cover factors affecting the spatial and temporal distribution of snow cover and its properties.

For example, Pomeroy et al. (1997) demonstrated that winter precipitation alone was insufficient to calculate snow accumulation in Arctic regions, and that blowing-snow processes and landscape patterns were the key factors governing the spatial distribution of snow-water equivalent in winter. A recent validation of a point snowpack model highlighted the problem of ignoring wind redistribution processes (Yang et al. 1997). In this case, the model validation results were worse when corrected gauge-catch data were used as the performance standard, because the model did not account for blowing-snow losses. Stochastic approaches can be used to account for sub-grid-scale variations in vegetation (Woo and Steer 1986) and topography (Stieglitz et al. 1997; Walland and Simmonds 1996). In the latter case, the parameterization of sub-grid-scale topographic variability in a GCM snow sub-model yielded more-accurate simulations of seasonal variation in Northern Hemisphere SCA, and solved the characteristic GCM problem of retarded spring snow-cover retreat noted by Frei and Robinson (1995). GCMs also exhibit a general tendency to overestimate snow cover over the Tibetan Plateau and China, but this problem is probably due more to atmospheric model difficulties simulating temperature and precipitation in the lee of a major mountain barrier than to systematic errors in simulating snowpack processes.

The evidence suggests that the multi-layer-snow energy-balance models used in GCMs are able to capture the essential one-dimensional character (surface temperature, depth, snow-water equivalence, density, and snowmelt) of a midlatitudinal snowpack, and that current GCMs are able to provide, for the most part, reasonable simulations of seasonal and year-to-year variation in continental-scale SCA (Foster et al. 1996). However, many of the important processes affecting regional-to-local-scale variations in snow cover and snow properties are not taken into account in current GCM snow models. These shortcomings have important consequences for local-regional-scale hydrology and climate, particularly as the spatial resolution of GCMs increases. EOS satellites will play a major role in helping to address these problems by providing higher-quality land-cover data sets, and higher-resolution snow-water-equivalent observations from sensors such as AMSR-E for model validation and investigation of scaling issues.

Snow cover in hydrological models

The above discussion applies to coarser-scale GCM representations of snow cover. However, in order to predict watershed response to changes in climate or atmospheric pollution, one needs a sensitive, accurate modeling capability that adequately captures the major processes

controlling snowmelt, runoff, and chemical changes in soil and lakes. This information is needed at a scale corresponding to the scale of variability in watershed geology, soils, and vegetation that is important in controlling these changes. While empirical snowmelt-runoff models have been useful for operational runoff-volume forecasts, they provide little information on the timing, rate, or magnitude of discharge, and they are inappropriate in situations outside the boundary conditions governing the development of the relevant empirical parameters. Thus, they may fail to predict water yield adequately in extreme or unusual years, and they cannot be reliably used in investigations examining snowmelt responses to climate variability and change. These problems, and the increasing importance of understanding intrabasin snowmelt dynamics for environmental analysis of such factors as basin ecology (Baron et al. 1993), water chemistry (Wolford et al. 1996), and hillslope erosion (Tarboton et al. 1991), have motivated the development of physically-based, spatially-distributed snowmelt models in recent years. Such models require information on the spatial distribution of snowpack water storage. But, mountain snowpacks are spatially heterogeneous, reflecting the influences of rugged topography on precipitation, wind redistribution of snow, and surface energy fluxes during the accumulation season (Elder et al. 1991).

Snowmelt drives the hydrology in alpine basins and snow-cover changes over the melt season are of primary interest to water managers in the western U.S. A distributed snowmelt model consists of two general components: a model for calculating melt at a single point (given a set of prescribed snowpack and meteorological conditions), and a method of developing the requisite snowpack and meteorological data for all points within the basin. Snowmelt-modeling efforts require several steps necessary to couple basin-wide energy-balance snowmelt models with remote sensing and flow routing. The model TOPORAD (Dozier and Frew 1990) uses information on watershed topography (i.e., a Digital Elevation Model [DEM]) to distribute radiation spatially. Simpler models are used to determine the spatial distribution of other energy-balance components. These radiation maps are then used as inputs to models that estimate the distribution of snow around the basin prior to snowmelt (i.e., initial conditions for melt), and as inputs to the point snowmelt model. To predict the biogeochemical response of catchments, models such as AHM (Wolford et al. 1996) use calculations of water generated at the snow surface coupled with a model of elution of water and chemical species from the snowpack, and routes that water through the basin to estimate, or predict, streamflow and its chemical concentrations.

One of the main obstacles to physically-based modeling is the accumulation of the necessary meteorological and snow-cover data to run, calibrate, and validate such models. For example, basin discharge has frequently been used as the sole physical criterion of model calibration and performance assessment for conceptual snowmelt models. But as basin discharge is an integrated response to melt and runoff, it does not discriminate among the various effects of a multiplicity of data inputs that drive physical models. Distributed snow-cover data are required if one is to properly assess model performance in such complex terrain (Bloschl et al. 1991a; Bloschl et al. 1991b). No widely suitable method yet exists to directly map snow-water equivalence in rugged mountain regions. However, the higher-resolution snow products generated through EOS will help address this issue. Estimates of snow-covered area based on remote-sensing data can significantly improve the performance of even simple snowmelt models in alpine terrain (Kite 1991; Armstrong and Hardman 1991). Rango (1993) reviewed the progress that has been made incorporating remote-sensing data into regional hydrologic models of snowmelt runoff. For operational purposes, empirical approaches using remote-sensing data to estimate snow-covered area and snow-depth networks to estimate snow-water equivalence are continuing to improve (Martinec and Rango 1991; Martinec et al. 1991).

Both visible and near-infrared, and passive microwave remote-sensing data are being used to develop estimates of snow-covered area for operational forecasting of snowmelt. Development of accurate snow-cover information for areas with steep, variable topography requires higher-resolution data than are currently available from operational remote-sensing instruments. Models using the higher-resolution satellite data expected during the next decade show good results with test data acquired from aircraft platforms. Determination of other snowpack properties in alpine areas, such as grain size and albedo (from visible/infrared) and snow-water equivalence (from active microwave) are topics of continuing research. Progress in both algorithm development and testing with field data sets shows that obtaining these properties is achievable. The volume-integrating capability of microwave remote sensing has received much attention, because it offers the possibility of remote determination of whole snowpack properties. However, the lack of multipolarized SAR will limit the ability to reliably estimate snow-water equivalence in alpine areas.

6.2.1.2 *Sea ice*

Model simulations of the climatic impact of increasing greenhouse gases typically show enhanced warming at

high latitudes, largely as a result of positive feedbacks involving sea ice. A concern is that sea ice has been treated rather simply in climate models. In particular, sea ice in GCMs has generally been approximated as a motionless thermodynamic slab. Inclusion of sea-ice dynamics—advection and deformation—is necessary to account for the freshwater provided by melting sea ice advected from the Arctic into the Greenland and Norwegian Seas, and to reproduce dynamic/thermodynamic feedback effects involving open-water “leads.” A further motivation for improving the representation of sea ice in climate models is that sea-ice changes have a major impact on the availability of moisture and the mass balance of major ice sheets, especially Antarctica (Rind et al. 1995). Of the 16 GCMs summarized in the recent IPCC report (Gates et al. 1996), only six included any form of ice motion. Of those six, only three included a real ice dynamics scheme (based on solution of the sea-ice momentum equation); the remaining three simply transported ice with the ocean-surface current.

Experiments with stand-alone sea-ice models (e.g., Hibler 1984; Lemke et al. 1990) have shown that thermodynamic-only models are more sensitive to changes in thermal forcing than those that include dynamics. The reason is, at least in part, the constant formation of open-water leads, which dominate overall ice growth. Recent GCM experiments by Pollard and Thompson (1994) have shown that inclusion of sea-ice dynamics produced more-realistic ice extent and reduced the model’s globally-averaged CO₂-induced warming, with the effect most pronounced around Antarctica.

Including a more-realistic dynamical formulation is the principal improvement currently being made to the sea-ice component of many GCMs. The two approaches most widely used are the “viscous-plastic” model of Hibler (1979) and the simpler “cavitating fluid” model described by Flato and Hibler (1992). Both schemes produce similar large-scale thickness build-up and transport, but they differ in the details of their treatment of internal ice stresses. An important scientific question is “what is the optimal sea-ice dynamics model for use in climate simulations?” This question is being addressed in part through the World Climate Research Program (WCRP) Arctic Climate System Study (ACSYS) project (see Section 6.3.2.1) in the form of the Sea Ice Model Intercomparison Project (SIMIP) (Lemke et al. 1996). SIMIP involves comparison of a hierarchy of sea-ice models to one another and to available observations, using the same forcing and boundary conditions, in order to illustrate the advantages and disadvantages of various parameterizations and their suitability for use in global climate modeling. Such an effort requires accurate specification of atmospheric

and oceanic forcing, along with observations of ice thickness, concentration, velocity, and its spatial derivatives (i.e., deformation). Observations of these same quantities are also required for studies of the ice mass balance and its variability as outlined in Section 6.3.1.2.

Sea-ice thermodynamic schemes used in climate models also tend to be rather crude. In particular, the surface-albedo parameterization (Barry 1996) and the calculation of heat conduction and internal heat storage are typically highly idealized. Surface albedo is highly variable owing to the mixture of open water and ice, some of which may be covered by snow (which itself has a range of albedos). In spring, this situation is further complicated by the presence of melt ponds that arise from surface melt and subsequently evolve in both depth and areal extent due to absorption of radiation and drainage. Storage and release of heat within the ice cover affects the timing of growth and melt. Because of the short summer-melt season, and the large solar radiative fluxes in summer, this effect can have a substantial impact on the ice mass balance. Recent studies by Bitz et al. (1996) and Battisti et al. (1997) have investigated the role of ice thermodynamics in a single-column climate model. Their results indicate that relatively modest changes in thermodynamic parameterizations may have a disproportionate effect on simulated ice-thickness variability, and that this in turn has a major impact on the simulated climate variability. Development and validation of sea-ice thermodynamic parameterizations suitable for use in global climate simulations is therefore a further scientific challenge for EOS.

6.2.1.3 Lake ice

Lakes are important components of many ecosystems, particularly in northern boreal and tundra environments, where lakes and standing water occupy a significant fraction (~25%) of the total land cover. Lakes influence local energy and water exchanges, and the freezing and thawing of lake ice has important consequences for physical, chemical, biological, and hydrological processes (Heron and Woo 1994). Physical models have been developed that are able to simulate lake-water temperatures and ice cover over long periods, e.g., Fang and Stefan (1996). However, most lakes are not resolved in current GCMs, and, according to Arpe et al. (1997), the neglect of frozen water stored in lakes and rivers has led to incorrect simulation of the seasonal cycle of discharge from the Mackenzie River, and to an incorrect supply of freshwater to the Arctic Ocean in coupled models. With increasing resolution of Numerical Weather Prediction (NWP) and regional climate models, there is growing interest in explicit representation of lake processes. For example, the

CLASS Land Surface Process (LSP) model will incorporate a lake-model component in 1998 (D. Verseghy, personal communication 1997).

A number of EOS initiatives are being carried out to understand the physical processes and structural factors affecting the microwave signatures of ice-covered lakes (e.g., Walker and Davey 1993; Hall et al. 1994; Jeffries et al. 1994; Duguay and Lafleur 1997). These initiatives are providing important validation data for lake-ice-model development and testing (conventional shore-based ice observations are inadequate for this purpose). In addition, the coupling of numerical ice-growth models and SAR data has provided important ancillary information such as the depth distribution of northern lakes.

6.2.1.4 *Frozen ground and permafrost*

Frozen ground plays a significant role in the terrestrial portion of the hydrological cycle because it restricts moisture exchanges between surface water and deep ground water (Prowse 1990). The occurrence of frozen ground and permafrost is, therefore, an important factor controlling drainage and the areal and spatial distribution of wetlands (Rouse et al. 1997). Permafrost is also important for modeling snow cover as the cold sub-surface layer increases the amount of energy required to melt the snowpack and delays melt (Marsh 1991).

A recent example highlighting the insights that can be gained through application of 1-D models was provided by Zhang et al. (1996), who used a 1-D finite-difference heat-transfer model to investigate the sensitivity of the ground thermal regime to variations in the depth-hoar content of the overlying snow cover. Depth hoar (or sugar snow) is a relatively low-density ($\sim 150\text{--}250\text{ kg m}^{-3}$) layer of snow with large rounded grains that forms near the ground surface in response to steep temperature gradients. The depth-hoar fraction can be over 50% in tundra snow, and can represent up to 80% of the snowpack for taiga snow (Sturm and Johnson 1991). Zhang et al. (1996) showed that changes in the depth-hoar fraction from 0 to 60% could increase daily ground-surface temperatures by 12.8°C and mean annual surface temperatures by 5.5°C . This result underscores the importance of including realistic simulations of vertical snow-density variations in climate and hydrological models.

To date, few hydrological or climate models include frozen-ground processes in any detail, which results in poor performance at simulating the hydrological cycle in northern environments. The inclusion of frozen soil in hydrological models is a major objective of the Canadian Global Energy and Water Cycle Experiment (GEWEX)

program. In LSP models with multi-layer treatments of soil heat and water flow (e.g., CLASS, Verseghy 1991), soil freezing and thawing can be simulated theoretically. However, accurate simulation of permafrost processes such as active-layer development will require LSP schemes to include additional soil layers and better understanding of heat and water flow in organic soils (Woo, personal communication, 1997). There are still LSP schemes in use that ignore soil freezing completely (Verseghy, personal communication, 1997).

EOS permafrost research activities are focusing on the development of techniques for mapping the spatial distribution of permafrost using remotely-sensed and ancillary data, and the development of algorithms for detecting changes in active-layer depth and terrain features characteristic of degrading permafrost such as ground-ice slumps and thaw lakes. These activities will generate high-resolution information on frozen-ground extent for input and validation of LSP schemes and distributed hydrological models.

6.2.1.5 *Glaciers and ice sheets*

Of the roughly 7 mm y^{-1} of sea-level equivalent that is added to the surfaces of the great ice sheets, less than 1 mm y^{-1} is returned to the sea as meltwater running off the upper surfaces. The great majority of return to the oceans is by ice flow, either as icebergs broken off the coastal regions or as melting from the undersides of floating extensions of the ice sheets called ice shelves. Furthermore, as discussed below, much larger changes in ice flow are possible that are likely to affect surface-balance estimates. Should large changes occur, rapid ice-sheet thinning and sea-level rise could result, but not rapid ice-sheet thickening or sea-level drop. This inherent asymmetry of ice behavior, slow growth but rapid decay, has dominated the ice-age cycles of the last million years (Imbrie et al. 1993) and figures prominently in the view of the future.

Ice outflow is driven by gravity acting on regions with sloping ice surfaces. Gravitational-driving stress increases with surface slope and the ice thickness. Ice responds to this stress by deforming internally and by moving over its substrate (Paterson 1994). The rate of internal deformation increases with temperature and with the cube of stress (Paterson 1994), and depends on the physical properties produced by the history of deformation (Alley 1992). First principles indicate small uncertainties in deformation-rate estimates; tuned models closely match observations. Motion over the bed is much more complex and may account for only a small fraction of total velocity, but in regions called ice streams, which have exceptionally lubricated beds, ice velocity may be 100 times higher than for adjacent ice with similar

stress. Basal velocity is achieved by sliding over the substrate, or by deformation within the substrate (Alley and Whillans 1991).

Internal deformation responds slowly to perturbations. Increased snowfall causes the ice to thicken. This increases the driving stress and the thickness through which the ice flows, both of which increase the ice flux until it matches the increased accumulation and a new steady state is reached. Increased surface temperature eventually warms and softens the ice, which increases ice outflow, thinning the ice and reducing the driving stress until a new steady state is reached. However, because most deformation occurs in deep ice, heat must penetrate near the bed before it causes significant changes. Marginal retreat steepens the ice sheet, which increases the gravitational stress and the ice flow, forcing a wave of thinning that propagates inland. For existing ice sheets, adjustments to changes in snowfall and marginal position require a few thousand years, and the response to temperature changes is somewhat longer. Assessment of internal deformations indicates that of the modern ice sheets, Greenland responds most rapidly and East Antarctica most slowly (Whillans 1981; Alley and Whillans 1984). The Greenland ice sheet has almost completely adjusted to the end of the last ice age, West Antarctica has adjusted for the most part, although further changes can be expected, and East Antarctica has completed only initial responses. Internal deformations appear to be unstable for large ice masses because rapid deformation creates heat, which softens the ice for further deformation; however, this is probably not a dominant process (Clarke et al. 1977; Huybrechts and Oerlemans 1988).

Basal processes are much more difficult to model and predict. Bifurcations and instabilities certainly exist. For example, a glacier frozen to its bed does not move rapidly over that bed, but a thawed-bed glacier can (MacAyeal 1993a, 1993b). Where the bed is thawed, frictional heating increases water supply, thus increasing basal velocity up to some maximum value. Beyond that point basal velocity may decrease with further increases to water supply as the flow system transforms from a distributed one that lubricates ice motion, to a channelized one that does not (Weertman 1972). Most ice motion may occur through deformation of subglacial sediments (Alley and Whillans 1991), but large uncertainties still exist in the understanding and modeling of such processes.

Of great interest is the likelihood that the extreme variations in ice-sheet behavior from place to place also occur at one place over time. Mountain glaciers with thawed, or partly thawed beds are known to experience large, rapid switches in velocity, called surges, that are primarily associated with basal processes (Paterson 1994).

Observations in West Antarctica have shown exceptionally large time evolution, with some regions thickening and others thinning (Alley and Whillans 1991). Glacial-geological evidence shows major changes in ice-marginal positions over very short times for former ice sheets (Clark 1994), and evidence from marine sediments (the Heinrich events; Broecker 1994) indicates large ice surges from Hudson Bay and other ice sheets during the most recent North American glaciation. However, work on such flow instabilities remains in the explanatory rather than the predictive stage.

The most widely discussed instability is that of marine ice sheets (Mercer 1968; Weertman 1974). In the simplest model, an ice sheet with a bed below sea level that deepens towards the center of the ice sheet is inherently unstable. Either its grounding line, which separates ice that is too thick to float free of the bed from floating ice, must advance to the edge of the continental shelf, or it must retreat to the center of the ice sheet, collapsing the ice and raising sea level. Some stability can be provided if the floating extension is not free to spread in the ocean because it runs aground on islands or is constrained in an embayment. The modern West Antarctic ice sheet has a bed which deepens towards the center around most of the coast, and it has constrained ice shelves around much of its coast. In the disaster scenario, warmed waters circulating beneath the ice shelves would melt them partially or completely, reducing their constraint on the grounded ice and triggering a collapse that would raise sea level meters in centuries. The possibility of such a disaster remains; the likelihood is debated (IPCC 1990, 1996; Huybrechts 1990).

Other mechanisms of instability include thawing of frozen regions (Clarke et al. 1984), and loss or narrowing of interstream ridges that now provide much restraint on fast-moving ice streams (Whillans et al. 1993). As for marine instability, present knowledge does not allow exclusion or prediction of such behavior.

The prevailing view of ice-sheet response to climatic change (IPCC 1990, 1996) holds that a coming global warming will enhance melting of the Greenland ice sheet and enhance snowfall on the Antarctic ice sheet, with little net effect on sea-level change. If Greenland ice sheet melt is offset by growth in the Antarctic ice sheet, then the contribution of small glaciers to sea-level rise is not merely significant, as indicated by Meier (1984); it has the potential to be the principal cryospheric agent for sea-level change (Ohmura et al. 1996). Thus the impacts of small-glacier retreat in mountainous areas extend well beyond implications for local water supply.

But predictions about the great ice sheets are disseminated with large, asymmetric error bars that allow

the small, but significant possibility of ice-sheet collapse in West Antarctica. A “Delphic oracle” assessment of the possibility of ice-sheet collapse leads to a somewhat higher probability of rapid sea-level rise than suggested in the IPCC documents (Titus and Narayanan 1995). Whole-ice-sheet models which parameterize accumulation to increase with temperature (Letréguilly et al. 1991; Huybrechts 1993) typically yield slow, steady ice-sheet adjustment occurring over millennia, or longer. The changes in snow-fall and surface melting then dominate the contribution to sea-level change over the century—or centuries-long “planning horizons” adopted. Modeled warming of more than 6°C removes the Greenland ice sheet entirely over 10,000 years (Letréguilly et al. 1991). Over roughly a 10,000-year period, a model warming of 8–10°C will remove the West Antarctic ice sheet, while increasing this amount to approximately 20°C suffices to remove the East Antarctic ice sheet (Huybrechts 1993). These models, however, typically lack the “fast physics” of basal velocity (occurring through sliding or bed deformation) that is strongly sensitive to small perturbations. One model of the West Antarctic ice sheet that included such “fast physics,” when integrated through ten 100,000-year ice-age cycles, frequently produced rapid volume changes, and complete ice-sheet collapse during three of the ten cycles (MacAyeal 1992).

Major uncertainties in projecting future behavior include:

- significant uncertainty in current ice-sheet and glacier mass-balance estimates, particularly as they apply to areal representation;
- questions of how future climate change will be manifested regionally and amplified in polar and alpine regions;
- the difficulty of predicting how atmospheric circulation and precipitation will change in response to global warming;
- the uncertainties of how the “fast physics” of ice flow works, and how to incorporate it into models; and
- the questions of whether future perturbations (perhaps through ice-shelf basal melting) or past perturbations (perhaps through the ongoing penetration of the post-ice-age warmth to the ice-sheet beds) can trigger rapid changes in ice flow and sea level.

Glaciers and ice sheets in climate models

Theoretically, fully-coupled GCMs have the potential to simulate the main processes (precipitation, accumulation, ablation) affecting the mass balance of glaciers and ice sheets, and to capture important feedbacks (such as changes in oceanic and atmospheric circulation) that would accompany a significant reduction in land-ice volume. Until recently, one of the main obstacles to simulating ice-sheet mass balances in GCMs was that of scale (Thompson and Pollard 1997). Accurate representation of the topography of ice sheets (e.g., steep edge slopes) is critical for mass-balance calculations because it affects a host of parameters and processes such as surface temperature, precipitation, and topographic interactions with atmospheric circulation. Recent higher-resolution GCMs (~200-km grid spacing) have been able to provide much-more-realistic simulations of the Antarctic and Greenland ice-sheet mass balances (e.g., Ohmura et al. 1996; Thompson and Pollard 1997). The other main obstacle to simulating ice sheets in GCMs is that, to date, they have not explicitly included ice-flow dynamics and processes such as re-freezing of meltwater. This is less of a shortcoming over short time scales, but is important for examining issues such as sea-level change beyond the end of the next century when ice-sheet dynamic response is significant (Huybrechts et al. 1991). Early attempts to couple GCMs with dynamical ice-sheet models (e.g., Verbitsky and Saltzman 1995) were hampered by the coarse resolution of GCMs, which adversely affected precipitation simulations over the major ice sheets. The inclusion of parameterizations for elevation effects on surface meteorology and for the refreezing of meltwater in the GENESIS GCM (Thompson and Pollard 1997) was found to produce much more realistic simulations of ice-sheet mass balance.

The IPCC (1996) report indicates four major knowledge gaps that need to be addressed in order for climate models to provide better estimates of glacier and ice-sheet mass balance and contributions to sea-level change:

- 1) Inclusion of the processes and feedbacks linking meteorology to mass balance and dynamic response.
- 2) Extension of glacier modeling and process research to a broader spectrum of glacier environments, in particular the larger glaciers mountains of Alaska, central Asia, and the ice caps of Patagonia and the Arctic.
- 3) Quantification of the process of meltwater refreezing.

- 4) Increased understanding of the process of iceberg calving.

EOS satellites will play a major role in helping to reduce these uncertainties: The Advanced Spaceborne Thermal Emission and Reflection Radiometer (ASTER) will provide the capability for glacier mass-balance monitoring at a global scale (Global Land Ice Monitoring from Space [GLIMS]); Earth Science Enterprise (ESE) altimetry data are providing detailed surface topography information for input to atmospheric and ice-sheet models (Ice, Clouds, and Land Elevation Satellite [ICESat]); SAR interferometric methods are being applied to data from the European Remote-Sensing Satellite-1/2 (ERS-1/2) and the Radar Satellite (Radarsat) to generate detailed observations of surface topography and ice-flow rates (e.g., Vachon et al. 1996), and passive-microwave and visible-satellite data from EOS satellites will provide critical information for monitoring and understanding key processes such as surface melt.

Glaciers and ice sheets in hydrological models

One of the major links between glaciers and ice sheets and the global climate system is through runoff. The ability to correctly model glacier-runoff processes is, therefore, essential for realistic simulation of future mass-balance and sea-level changes, and the thermohaline circulation. The importance of runoff is further underscored through the coupling of glacier hydrology and glacier flow dynamics (Iken 1981; Iken and Bindshadler 1986; Kamb 1987; Alley 1989; Harbor et al. 1997). This is mediated by the status of subglacial drainage, which is thermomechanically controlled. Where subglacial drainage occurs, the key questions to address are the configuration of the drainage system (channelized/distributed), how it evolves on various time scales, and exactly where the drainage pathways are located. Answers to these questions hold the key to understanding seasonal and subseasonal variations in glacier velocity, surge-type behavior, the formation of ice streams, and the detailed distribution of velocity in glacier cross sections.

Insofar as glacier response to climate forcing involves an immediate mass-balance response and a longer-term dynamic response, glacier hydrology may be important for the dynamic response (Kamb and Engelhardt 1991; Arnold and Sharp 1992; Alley 1996). Its role could be linked to changes in glacier thermal regime resulting from the combined effects of changing glacier geometry and atmospheric boundary conditions, changes in the length of the summer melt season, changes in runoff volume, changes in runoff regime (e.g., amplitude of diurnal cycles changing in response to thinning or thickening of

snow cover, eradication of firm reservoirs), or changes in the distribution of subglacial drainage pathways (linked to changing glacier geometry). All of these could alter the existence, longevity, character, and distribution of subglacial drainage systems, and the nature of the water-storage regime within them, with implications for ice-flow dynamics.

An improved understanding of glacier hydrology is also needed with respect to glacier hazards. Outburst floods from supraglacial, ice marginal, and englacial/subglacial sources are a concern in high-mountain and volcanically-active areas, and there is a need to document possible source reservoirs (location and size, and frequency of flood release). The existence of very large lakes beneath ice sheets raises the possibility of long-interval, high-magnitude events that might be significant for global sea level and for ocean, circulation, and climate.

Improved understanding and modeling of glacier hydrology is also crucially important from a water-resources perspective. Glaciers are an important source of water for human and livestock consumption, irrigation, and hydro-power in high mountain regions. This is especially true at certain critical times of the year, such as the growing season, when water demand peaks and glacier runoff accounts for a significant fraction of the available water supply. For example, during August in the Bow River, Alberta, Young et al. (1996) determined that glacier ice wastage contributed almost one quarter of the total flow during low-flow years. Variations in glacier extent affect the magnitude of this resource in complex ways. It is important in this regard to understand that times of unusually high meltwater supply may also be times of accelerated ice-resource loss, and that effective water-supply planning must be done with the expected long-term status of the resource clearly in view.

Glacier and ice-sheet runoff are also important from an ecological perspective (e.g., habitat sustainability, wildlife management) through influences on stream-water turbidity and temperature (Brugman et al. 1997). Other water-quality-related ecology issues include the effects of supraglacial runoff. This runoff may be isolated from contact with soils which can buffer acid runoff, and as a result could produce severe acid shock in meltwater streams (Johannessen and Henriksen 1978).

6.2.2 Cryosphere-climate linkages and feedbacks

Reducing the uncertainties in projections of rates and regional patterns of climate change requires improved representation of climate processes in models, especially feedbacks associated with water vapor, clouds, oceans, ice and snow, and land-surface/atmosphere interactions (IPCC 1996). The most obvious cryosphere-climate feed-

backs involve modifications to the SEB (albedo and insulating effects) and to moisture exchanges with the overlying atmosphere. There are also less obvious, but important indirect linkages between the cryosphere and the climate system that operate through the movement and storage of water in the freshwater cycle. Freshwater storage in the cryosphere occurs over a range of time scales as indicated in Section 6.1, and is therefore involved in climate variability over a similar range of time scales. In recent years, a growing body of evidence has accumulated suggesting that the climate of the North Atlantic is highly sensitive to variations in freshwater input, and that the climatic response can be sudden and dramatic (Walsh and Chapman 1990; Weaver and Hughes 1994).

Cryosphere-climate feedbacks can be classified into two main categories: feedbacks working through the freshwater cycle, and feedbacks working through the SEB. These are discussed in more detail below.

6.2.2.1 *Freshwater cycle*

The cryosphere is intimately connected to the freshwater cycle through the storage and transport of freshwater in solid form. Freshwater storage in the cryosphere occurs over a range of time scales and, therefore, is involved in climate variability over a similar range of time scales.

On short time scales (seasonal, annual), the accumulation and melting of snow dominates the hydrological cycle of many alpine and high-latitude drainage basins. In populated areas near glacier-fed river systems, such as the Bow, the Columbia, the Fraser, and the North Saskatchewan, the amount and timing of snowmelt-induced spring runoff has direct human consequences in terms of hydroelectric power generation, water supply, and flooding. Furthermore, valley glaciers respond rapidly to climatic fluctuations, such as those induced by increasing amounts of atmospheric carbon dioxide (Oerlemans 1986), so significant changes in length and volume may occur on the time scale of a few decades.

On annual-to-decadal time scales, sea ice can store freshwater and transport it from one region to another as ice drifts under the influence of winds and currents. This occurs because as sea ice freezes it expels most of the salt, leaving the ice relatively fresh; when ice forms in one location, is transported, and melts in another, the ocean experiences an imbalance in surface salt flux. This process is particularly important in the Northern Hemisphere as ice is transported out of the Arctic into the North Atlantic where it melts, thus forming a stabilizing freshwater layer at the surface. The freshwater layer may moderate deep convection in the North Atlantic and thereby affect the global "conveyor belt" circulation, which is important for transporting oceanic heat northward and

sequestering carbon dioxide in the deep ocean. Variations in this export of sea ice may excite variability in oceanic deep convection and global thermohaline ocean circulation (Halekinen 1993).

On still-longer time scales, large glaciers and ice sheets can play an even more dramatic role, storing and releasing freshwater in amounts that may substantially raise or lower global sea level, thus posing problems for coastal settlements. Because of their vast size, climatic perturbations produce slow responses in these ice masses, on the time scale of glacial-interglacial periods. Recent modeling work (Chen et al. 1997) has highlighted the important role of topographically-related feedbacks between major ice sheets and atmospheric circulation. They presented evidence for a possible feedback between topographically-induced lee cyclogenesis and the mass balance of a large ice sheet, which has significant implications for warmer-world simulations of the Greenland ice sheet.

There are also important feedbacks between permafrost and the climate system through the hydrological cycle. Because the hydraulic conductivity of permafrost is significantly lower than unfrozen soil, this limits ground-water flow and is an important factor controlling drainage patterns and the spatial distribution of wetlands in northern ecosystems (Rouse et al. 1997). Permafrost is also a significant store of CO₂ and methane, which are released when ground thaws; and ground ice represents an important freshwater store for contribution to sea-level rise.

A major scientific challenge is to quantify the exchanges of freshwater between the hydrosphere and cryosphere, and to understand the role of such exchanges in climate variability and change. EOS will contribute to meeting this challenge through an improved ability to observe and simulate the mass budget of sea ice, glaciers, and ice sheets.

6.2.2.2 *SEB*

Perhaps the most direct and dramatic effect of the cryosphere on the climate system is its role in modifying the SEB, over both land and ocean. The two principal mechanisms involving ice and snow cover (Randall et al. 1994) are insulation of land and ocean surfaces from the atmosphere, or outgoing longwave radiation (OLR) feedback, and enhancement of the surface albedo, or shortwave feedback.

The SW feedback comes about through the classic positive feedback between temperature and albedo, where an increase in air temperature enhances melt, thus reducing ice and snow cover, which then decreases albedo, thus leading to greater absorbed energy and warmer tempera-

tures. This feedback is an important issue in climate modeling insofar as it amplifies errors in the parameterization of the processes involved. It is also an important reason that GCMs predict enhanced warming in the polar regions as a result of increasing greenhouse gases. Recent climate-model results indicate that about 37% of a simulated global temperature increase caused by carbon dioxide doubling was the result of direct or indirect sea-ice feedbacks (Rind et al. 1995). In reality, the ice-albedo feedback is considerably more complex than described above. Curry et al. (1995) showed that the sea-ice-albedo feedback involves interactions with lead fraction, melt ponds, ice-thickness distribution, snow-cover and sea-ice extent, and that all the processes should be correctly parameterized in order for a climate model to yield the correct sensitivity to external forcing.

The ice-albedo feedback is inextricably linked with cloud-radiation feedbacks (Shine and Crane 1984; Curry et al. 1996), particularly over snow cover, where increases in cloud cover may increase the atmospheric emissivity sufficiently to offset the positive albedo feedback. The interaction of clouds and radiation with summertime melting of snow and sea ice is considered to be an important area of scientific uncertainty in understanding clouds and radiation in the Arctic (Curry et al. 1996). Over land the presence or absence of snow alters the surface albedo and hence the surface-radiation balance. This effect is much larger over bare soil or grasslands than over forested areas, where the effect of snow albedo is reduced by standing vegetation (see list of typical albedo values in Section 6.1.2).

The low thermal conductivity of snow slows the winter heat loss from the surface, which results in a lower OLR to the atmosphere. An ice cover also exerts a major influence on the exchange of sensible and latent heat with the atmosphere, allowing less heat loss from water as the ice cover thickens. Open water within the polar ice pack, which may be long, narrow leads, or irregular openings between floes, occupies only a small fraction of the ice-covered area (typically less than 10%), but dominates the SEB (Maykut 1978). This open water also contributes to the albedo-temperature feedback responsible for much of the polar amplification of greenhouse-gas warming obtained by climate models. Some estimates of the sensitivity of a climate model to open-water fraction are provided by Flato and Ramsden (1997) and references therein.

Snow and ice also affect the energy balance through the latent heat required to melt ice. The largest SEB feedbacks occur during the spring period, when incoming solar radiation to snow and ice cover is increasing, but heat gain at the ground is hindered by both the high albedo and the latent heat of fusion required to melt the cover.

There are also numerous indirect feedbacks operating through the hydrological cycle (e.g., soil moisture and clouds) although these can still be considered as SW and OLR feedbacks. A good example of this is the role of snow in a monsoon-type circulation. One view (e.g., Barnett et al. 1989; Yang et al. 1997) is that a heavy spring snowpack reduces land-sea contrasts (i.e., higher albedo and soil moisture \rightarrow cooler surface temperatures), which weakens the summertime land-surface heating driving the monsoon. As outlined in Meehl (1994) however, increased soil moisture also provides a moisture source for increased precipitation, so that soil moisture has two competing monsoon effects through increased evaporation and cooler surface temperatures. The insulating effect of snow on sea-ice growth has been shown to be an important climate feedback through its role in modulating sea-ice volume (Harder 1997).

6.2.2.3 *Observed and modeled feedbacks*

Numerous empirical studies have been carried out to quantify the effect of snow cover on temperature and large-scale circulation anomalies (see reviews by Cohen and Rind [1991] and Leathers and Robinson [1993]). These studies reveal that snow cover is associated with local temperature decreases in the range of 1°-6°C, and below-normal geopotential heights. Leathers and Robinson (1993) showed that snow cover could promote significant temperature perturbations well away from the area of anomalous snow cover through large-scale modification of air masses. As noted by Cohen and Rind (1991), a major difficulty with empirically-based studies is to separate the thermodynamic effect of snow cover from the dynamical influence of the regime which produced the snow cover in the first place. Is a winter with positive snow-cover anomalies colder than normal because of the snow cover, or is there more snow cover because of the colder temperatures? This separation is possible with GCMs where experiments can be run that isolate the effect of snow cover on climate. For example, Cohen and Rind (1991) applied the Goddard Institute for Space Studies (GISS) GCM to this problem and found that positive NH snow-cover anomalies in March caused only short-term local decreases in surface temperature. They proposed a negative feedback mechanism to explain these results, whereby the increased atmospheric stability caused by the snow cover acted to suppress the latent and sensible heat flux away from the surface, resulting in a gain in net heating and enhanced removal of the snow-cover anomaly.

Results from a single GCM, however, are insufficient for rendering a convincing picture of the snow-climate feedback. Evaluation of snow-climate feed-

backs in several GCMs (Cess et al. 1991; Randall et al. 1994) revealed that the feedback differed markedly between models, ranging from a weak negative, to a strong positive feedback. One reason for the divergence in the results was that the snow feedback was observed to be associated with a number of complex effects caused by cloud interactions. In one experiment, for example (Cohen and Rind 1991), changes in cloud cover tended to offset much of the impact due to changes in snow cover. They found that although the change in surface albedo at 51° N between the high- and low-snow-cover runs was more than 20%, the absolute difference in planetary albedo at 51° N was only 2% due to the masking influence of cloud cover. In light of the acknowledged weakness of GCMs, with respect to representing clouds and cloud-climate feedbacks (IPCC 1990), GCMs may not yet adequately capture the full complexities of snow-climate feedbacks.

Satellites provide the capability to directly measure cryosphere-climate feedbacks through observations of the global extent of snow and ice cover as well as the main components of the Earth radiation budget. For example, Groisman et al. (1994a) used satellite-derived snow cover and Earth Radiation Budget Experiment (ERBE) data to obtain direct estimates of the snow-cover feedback on the radiation balance at the top of the atmosphere. Their results showed significant spatial and seasonal variations in the magnitude and sign of the feedback. In the fall and winter, the OLR-reduction effect of snow cover dominated, resulting in a positive radiation feedback. For clear-sky conditions, the cooling albedo effect only began to dominate the warming influence from reduced OLR in February and reached a maximum during the spring (March-May). The zones of maximum snow-cover feedback were located over Siberia and the eastern Arctic region of Canada. Groisman et al. (1994a) estimated that the impact of snow cover on Northern Hemisphere extratropical latitudes between high (1979) and low (1990) snow-cover years was 0.9 W m^{-2} , which corresponds to an increase of about 0.5°C in annual surface-air temperature, or about half the observed temperature change between the two years.

An important scientific challenge is to improve the ability to simulate the important geophysical properties and processes controlling energy exchanges in the cryosphere, e.g., melt-pond formation, leads, surface-cloud radiative exchanges, snow density, ice-thickness distribution. EOS observations will play a major role in this process through provision of data for validating process models and through the direct observation of feedback processes.

6.2.3 Cryospheric variability and change

The ability to observe the natural variability of key cryospheric parameters such as sea-ice volume, snow and ice mass, and the area of snow and ice is critical for understanding climate-cryosphere feedbacks, for validation of climate models, and for climate-change detection. EOS satellites will be contributing to an enhanced ability to observe the cryosphere, which is a major objective of the WCRP Global Climate Observing System (GCOS). A summary of the GCOS requirements for cryospheric data is presented in Cihlar et al. (1997). For most cryospheric variables, however, the period of available satellite data is too short to provide insights into the decadal and longer time-scale variability known to be important in the climate system. This will require the application of techniques to combine in situ observations, physical models, and satellite data. The following sections outline current understanding and knowledge gaps in observing cryospheric variability and change.

6.2.3.1 Snow

Satellites are well suited for mapping global-scale variations in snow cover, and two important databases exist for investigations of spatial and temporal variability in hemispheric and global snow cover: the weekly National Oceanic and Atmospheric Administration (NOAA) visible satellite-based snow-cover analysis from 1972¹ (Robinson et al. 1993), and Scanning Multispectral Microwave Radiometer (SMMR) and Special Sensor Microwave/Imager (SSM/I) passive microwave brightness temperature data from 1978, which can be used to derive information on snow extent (Chang et al. 1987), depth (Foster et al. 1984), and snow-water equivalence (Goodison 1989; Chang et al. 1991). The spatial and temporal character of these two data sets is relatively coarse (190.5-km polar stereographic grid and 1/week for the NOAA data set, and ~25-km resolution and 1/day for the passive microwave data) but this is sufficient for monitoring key properties such as snow extent, dates of snow-cover onset and disappearance, and peak accumulation, which are known to be important indicators of change (Barry et al. 1995). The NOAA data set is known to have a number of shortcomings in areas with persistent cloud cover, low solar illumination, dense forest, patchy snow, and mountainous regions (Robinson et al. 1993). However, the most important characteristic of the

¹ Regular satellite monitoring of NH snow cover began in November 1966 (Dewey and Heim, 1982), but the sub-point resolution of the pre-1972 satellites was ~4.0 km compared to 1.0 km with the VHRR launched in 1972 (Robinson et al., 1993). A project to re-chart and digitize the pre-1972 data was recently completed at Rutgers U., which will extend the NOAA record back to 1966 (D. Robinson, personal communication 10/30/97).

data set for studying snow-cover variability is that the analysis methodology has been relatively stable for over 25 years (Basist et al. 1996). The passive microwave data are not limited by solar illumination or cloud cover, and offer a higher resolution. The problem is applying snow algorithms that give reliable results over a range of land-cover types and snow-cover conditions. Evaluations of hemispheric maps of SSM/I-derived snow-water equivalence (Foster et al. 1996) and snow extent (Basist et al. 1996) report systematic biases related to vegetation effects and melting snow. Some of these problems can be overcome by including a wet-snow indicator (e.g., Walker and Goodison 1993) and applying land-cover-specific algorithms following Goita et al. (1997). The development and validation of snow algorithms is a major EOS activity during the pre-launch period for MODIS (Hall et al. 1996) and AMSR-E (Chang and Rango 1996). An automated snow-cover analysis scheme based on SSM/I was implemented by the National Environmental Satellite Data and Information Service (NESDIS) in November 1997 but will be run in parallel with the manual analysis for a period of 18 months to determine possible impacts on the homogeneity of the existing database.

The existing satellite snow databases are currently too short to provide information on the natural variability in continental-scale snow cover needed for climate-change detection and for validating transient simulations of GCMs. Regular in-situ daily snow-depth observations are available in some regions of the world from as early as the late 1800s. However, there are few stations with complete records prior to the early 1900s. Historical snow-cover data sets suitable for studies of snow-cover variability are available for the United States (Easterling et al. 1997; Hughes and Robinson 1996), Canada (Brown and Goodison 1996) and the former Soviet Union (Fallot et al. 1997). Typical problems encountered when working with historical snow data include inconsistent observing practices, inhomogeneities, and bias in observing networks. In spite of this, it appears that useful information on continental-scale variability in snow cover can be obtained from in situ data sets, particularly for variables such as seasonal snow-cover duration, which can be approximated from daily temperature and precipitation data, and which exhibit high spatial coherence (Brown and Goodison 1996). For example, Brown (1997) applied principal-component analysis to observed and reconstructed in situ snow-cover-duration data to reconstruct spring SCA over North America and Eurasia from 1915 to 1985 (Figure 6.2). (See Section 6.1.2.1.) The reconstruction method was able to explain 81% of the springtime variance in satellite-observed SCA over North America and 67% over Eurasia. The results suggested

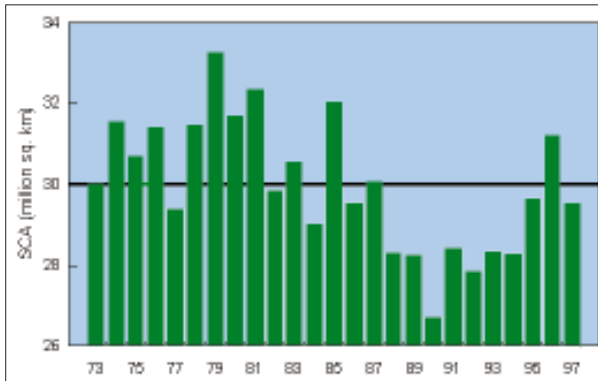
spring SCA had decreased significantly over Eurasia this century, but there was no evidence of a similar long-term decrease in North America. These results are consistent with observed 20th century midlatitudinal spring air-temperature trends over the same period that show a statistically significant increase over Eurasia, but not over North America. Further efforts are needed to develop other methods and approaches for integrating in situ and satellite data to obtain additional independent estimates of historical variation in hemispheric snow cover.

Documenting the spatial and temporal variability of snow depth and snow water-equivalence poses more of a challenge than SCA or snow-cover duration. Snow-water-equivalence algorithms are still being developed and tested for forested environments (Goita et al. 1997), deep snowpacks (de Sève et al. 1997), and over sea ice (Markus and Cavalieri 1997). SAR offers potential for high-resolution mapping of wet or melting snow, which is important for operational monitoring of mountain snowpacks and for integration into runoff models (Hall 1996). EOS researchers are also investigating methods for extracting snow-water-equivalence information from dry and shallow snowpacks using Radarsat data (Bernier and Fortin 1998). Historical data sets of in situ snow-water-equivalence data are available over some regions of the world (e.g., the Former Soviet Union) from 1966-1990 (Armstrong and Krenke 1997) and over Canada from ~1960 (Braaten 1997). While spatially and temporally constrained, these data sets are important for model validation (e.g., Yang et al. 1997). The development and validation of passive microwave snow-water-equivalence algorithms is a key activity for understanding spatial and temporal variability in snow-water equivalence and is vital for snow-cover-validation activities being carried out under AMIP. The collection of detailed validation data sets is an important contribution to understanding spatial and temporal variability in snow cover, and for the correct representation of this variability in climate models.

Given the decadal and long-term variability known to be important in the climate system, it is misleading to present trends of hemispheric snow cover based on the short period of available satellite data, unless appropriately qualified. Groisman et al. (1994a) reported a 10% decrease in Northern Hemisphere annual snow cover over the 1972-1991 period using the NOAA weekly snow-cover data set which was quoted in the recent IPCC (1996) assessment of climate change. More-recent satellite data show that the rapid decrease in Northern Hemisphere spring SCA that characterized the 1980s appears to have reversed itself during the 1990s (Figure 6.3).

Longer historical snow-cover time series indicate that regional snow cover exhibits considerable variabil-

FIGURE 6.3



Annual variation in NH spring (MAM) SCA in million km² derived from NOAA weekly snow-cover analyses. The horizontal line is the mean spring SCA over the 1973-1997 period. (Data from NOAA Climate Prediction Center.)

ity on time scales from years to decades (e.g., Koch and Rüdell 1990; Brown and Goodison 1996; Hughes and Robinson 1996; Fallot et al. 1997). Proxy data can also yield useful information on snow-cover variability. For example, Lavoie and Payette (1992) documented a 20th-century increase in snow cover over subarctic Québec of 0.4 m based on increases in the level of windblown snow abrasion on Black Spruce. Palaeo data on lake levels (Vance et al. 1992) and flood frequency (Knox 1993) suggest that snow cover and snowmelt over the continental interior of North America have likely undergone large and rapid changes in response to abrupt changes in temperature and precipitation that occurred ~5000 years ago (warm and dry), ~3,300 years ago (cool and wet), during the Medieval Warm Period (warm and dry), and again during the Little Ice Age (cool and wet). In conclusion, no single sensor or method alone can provide the information needed to observe spatial and temporal variability in snow cover at the scales required for climate-change monitoring and detection (Barry et al. 1995). Various sensor systems have advantages and disadvantages, and integration of satellite data, in situ observations, and physical models is needed to document the natural variability in the cryospheric system.

6.2.3.2 Sea ice

Changes in the energy balance, as might accompany climatic warming, would affect the ice-mass balance. In addition to possible climatic feedbacks, changes in ice thickness or areal coverage have direct consequences for maritime transportation, offshore oil and gas developments, and the marine ecosystem. Observations of the sea-ice mass balance are needed to quantify its variabil-

ity so that significant changes can be identified, to understand the processes which contribute to variability and change, and to verify the representation of sea ice and its interactions in climate models.

Determining the mass or volume of sea ice from observations requires measurements of both areal coverage and thickness. There are two aspects to areal coverage: ice concentration and ice extent. Concentration is defined as the fraction of area, in a given location, covered by ice; the remainder being open water. Ice extent is defined as the area enclosed by the ice edge, which is often defined as the 15% concentration isoline. Rather good observations of ice concentration, and hence ice extent, have been available from satellite passive microwave radiometry since the 1970s. However, complications arise in interpreting the satellite data, a primary one being the matching of records from different instruments (Bjorgo et al. 1997). It thus becomes desirable for EOS to obtain long records from the same instrument and to have overlap periods with alternative records. Some alternative sources include aircraft and shipborne observations assembled primarily for operational ice analysis and forecasting. Despite problems of spatial coverage and quality, these observations allow assembly of longer time series, such as that produced by Walsh (1978) which, for the Arctic, extends back to 1900. AMSR-E will be the most important EOS instrument for continuing the satellite record of sea-ice concentration and extent.

So far there is no method available to measure ice thickness from satellites, and techniques like airborne electromagnetic surveys are still experimental. A recent development in satellite remote sensing designed to address this issue is the Radarsat Geophysical Processor System (RGPS) housed at the Alaska SAR facility in Fairbanks, Alaska. This system is designed to ingest SAR data of the entire Arctic Basin. These data will be georectified onto a Lagrangian model grid, and displacement statistics will be computed for each of the Lagrangian grids. This procedure will produce weekly ice thickness as a function of ice kinematic histories (openings and closings) throughout the annual cycle at the kilometer scale (Kwok et al. 1995). The first fields of ice-thickness data from RGPS will be available in the third quarter of 1997. At present, the only "operational" method of surveying ice thickness is via upward-looking sonar. Examples of submarine sonar compilations of ice draft are given by Bourke and Garrett (1987) and McLaren et al. (1992). It should be noted that ice thickness varies dramatically over scales as small as a few tens of meters, from open water to ridged ice, which may be greater than 20 m in thickness. Thickness observations and models of ice-thickness evolution are therefore couched in terms of the "ice-thick-

ness distribution” (the probability density of ice thickness [e.g., Thorndike et al. 1975]). The mean of this thickness distribution is most relevant to the sea-ice mass balance, and model studies like that of Flato (1995) may be of use in developing a measurement strategy. A pressing scientific need is to promote access to, and analysis of, submarine thickness data, along with data from moored upward-looking sonar instruments, to complement EOS observations. Considerable progress has been made in this regard through joint efforts of Vice President Al Gore of the United States and Prime Minister Viktor Chernomyrdin of Russia. As a result of their initiative, considerable Arctic submarine data from both countries have been declassified and are being made available to the science community (Belt 1997).

In addition to simply observing the amount of sea-ice mass, it is also important to observe the principal fluxes that enter the mass balance. On a “basin scale”, these include thermodynamic growth and melt, ridging, and transport. These fluxes, and the processes which determine them, are often the means by which the cryosphere interacts with other parts of the climate system. For example, the transport of sea ice out of the Arctic and into the Greenland Sea, where it melts, is a mechanism whereby the cryosphere affects water-mass-formation rates and ventilation of the deep ocean.

To summarize, a complete sea-ice mass budget requires observations of ice-covered area and thickness, the net SEB, and ice transport and deformation. In addition to mass balance, however, it is also important to quantify the spatial and temporal variability in the other characteristics of the ice cover that are significant in terms of ice-climate interaction (e.g., surface albedo, surface temperature, lead distribution). The distribution of open water within the pack and its variability through time can be measured using SAR data, while both ice albedo and surface temperature will be provided from MODIS.

6.2.3.3 *Lake ice*

Lake-ice freeze-up and break-up, particularly break-up, have been found to be useful indicators of regional climate change (Palecki and Barry 1986; Reycraft and Skinner 1993). Records of lake- or river-ice break-up spanning 100 or more years exist in a number of locations with some extending back to the 16th century (Kuusisto 1993). More dense networks of lake-break-up observations are available from ~1950 (Canada) and from the 1920s for Scandinavia.

The combination of physical lake models, in situ observations, and satellite data is required to document natural variability in lake-ice cover over large areas. The major advantage of satellite data is that they provide ob-

jective information on lake freeze-up/break-up over the entire lake surface, unlike shore-based observations. Satellite observations are therefore particularly valuable for validating/calibrating physical lake-ice models, which provide the link for combining satellite and in situ records of lake freeze-up/break-up. Satellite-derived lake-ice information can be obtained from a range of sensors including visible imaging systems such as the Advanced Very High Resolution Radiometer (AVHRR), passive microwave systems, and SAR. ICEMAP (using MODIS) will produce sea-ice-duration information for the larger inland lakes. The use of passive microwave data is limited to the larger lakes, but has the advantage of all-weather capability. SAR, however, may be useful for measuring freeze-up and break-up conditions over small lakes.

6.2.3.4 *Frozen ground and permafrost*

Since climate is the dominant factor influencing the continental distribution of permafrost, the monitoring of permafrost conditions and geographic extent should be useful for deriving information on high-latitude climate change (Leverington and Duguay 1996). Satellites are ideally suited for monitoring the vast, uninhabited areas underlain by permafrost. However, there are several characteristics of permafrost that pose serious challenges for the remote observation of permafrost extent and change. Permafrost conditions cannot be directly observed by orbiting sensors in the way that exposed cryosphere elements such as snow cover, sea-ice and lake-ice cover, or glacier extent can be. First, permafrost is a sub-surface feature, which means that extent and change have to be indirectly deduced from related micro-climate and surface-vegetation characteristics that can be detected with remote-sensing techniques (Hall and Martinec 1985). Second, permafrost responds to the ground heat flux, which is affected by a host of local factors (e.g., vegetation cover, snow cover, sub-surface thermal properties) in addition to external climatic factors, and the response involves significant time lags on the order of decades (Leverington and Duguay 1996).

A number of studies have been able to successfully discriminate frozen/unfrozen ground and the depth of the late-summer active layer with high-resolution multispectral imagery such as is obtained by Landsat Thematic Mapper (TM) (e.g., Morrissey et al. 1986; Peddle et al. 1994; Leverington and Duguay 1996; Leverington and Duguay 1997). This success, however, is closely linked to local training data. Leverington and Duguay (1997) found that classification performance dropped from 90% to 60% when a trained neural-net classification scheme was transferred to a similar area a few tens of kilometers away from the training site (the change in surficial de-

posits being the key factor behind the difference in permafrost-surface relations between the two study areas).

On the basis of their research, Leverington and Duguay (1996) concluded that remotely-sensed monitoring of permafrost has a number of obstacles to overcome before it can be used for large-scale climate monitoring over high latitudes. These include:

- the vertical resolution in estimates of depth to frozen ground is currently insufficient for detecting changes over time;
- land-cover permafrost correlative relationships may change over time;
- the significant time lag between changes in climate, and change in surface cover and permafrost (this time lag may be on the order of decades).

In spite of these problems, remotely-sensed classification of frozen ground remains a powerful tool for regional-scale permafrost research, environmental management, and hydrological modeling. With nearly 50% of Canada, 80% of Alaska, and roughly 25% of the continents underlain by permafrost, extensive ground surveys of permafrost conditions are precluded owing to expense, logistical difficulties, short field seasons, and time constraints. On the other hand, many numerical heat-transfer models have been used in understanding the detailed physics of permafrost-climate relationship. However, these models are impractical beyond the site scale because of the extremely limited database characterizing the microclimates of a broad range of vegetation and terrain conditions. Satellite remote sensing provides the means to spatially distribute the models (local to regional) and therefore more effectively evaluate the impact of climate change on permafrost.

High-resolution remote-sensing imagery is particularly useful for monitoring thermokarst features and the annual freeze-thaw cycle of the landscape. This type of imagery is particularly relevant in the context of climate change. As the greatest amounts of ground ice are usually found near the permafrost table, it is expected that thermokarst features could occur at the beginning of climatic warming within a period of only a few decades (Koster 1993). For example, optical (Landsat TM and Systeme pour l'Observation de la Terre MLA/PLA) and active microwave (Airborne Synthetic Aperture Radar [AIRSAR], ERS-1) data have been used successfully to map permafrost thaw features (e.g., retrogressive thaw slumps, active-layer detachment slides, and thaw lakes (Lewkowicz and Duguay 1995; Duguay et al. 1997)). Also,

multi-temporal SAR observations (e.g., ERS-1) have shown to be a particularly effective means for monitoring the seasonal freeze/thaw cycle of boreal forests (Rignot and Way 1994) and subarctic tundra and forest (Duguay et al. 1998). Multidimensional SAR configurations (i.e., multi-frequency, -temporal, -polarization, -incidence angle) are currently being utilized together with optical sensors to improve the approaches developed thus far, so that permafrost maps of other sites in the discontinuous and continuous permafrost zones can be produced. EOS ASTER data used in concert with spaceborne SAR (ERS-1/2 and Radarsat) data will provide the best configuration to date for mapping frozen ground and associated features.

EOS data will enhance the several innovative approaches that have been adopted for sensing permafrost and ground-ice features from space. However, in situ measurements of ground temperatures remain a significant data source for monitoring permafrost conditions and change. For example, long-term programs of monitoring climate-change effects on permafrost and related phenomena in periglacial mountain belts are being carried out in Argentina, Canada, China, Germany, Italy, Japan, Kazakhstan, Norway, Russia, and Switzerland (Haerberli et al. 1995). These and other permafrost data are being entered into a Global Geocryology Database (GGD) to identify, acquire, and disseminate information on permafrost and frozen ground (Barry and Brennan 1993). A pilot GGD is being established at the World Data Center-A (WDC-A) for Glaciology with funding from the U.S. National Science Foundation (NSF). This will enable the archiving of priority Russian data sets and allow the WDC-A to inventory, retrieve, and organize selected priority data sets from other International Permafrost Association members. Increased recognition is also being given to the monitoring of active layer through such initiatives as the Circumpolar Active Layer Monitoring (CALM) project. The available long-term ground-temperature measurements from deep boreholes demonstrate a distinct, but heterogeneous warming trend in lowland permafrost areas (Fitzharris 1996) with some of the largest warmings (2-4°C/100 yr) occurring over northern Alaska (Lachenbruch and Marshall 1986; Osterkamp 1994).

6.2.3.5 *Glaciers and ice sheets*

The volumetric mass balance of glaciers or ice sheets is determined by changes to their surface mass balance, basal melting, and, where ice flows into standing water, losses due to calving. The key factors in surface mass balance include mass gains, principally due to winter snow accumulation, and mass losses due to meltwater runoff and sublimation. Small amounts of mass transfer occur

through rain freezing on snow, frost accumulation, drifting snow, and avalanches. To the extent that large volumes of ice are involved, change implies global sea-level change, with attendant impacts upon coastal zones. The small ice volumes of individual valley glaciers seem insignificant in this regard until they are grouped together (Meier 1984), but impacts upon local freshwater resources may be highly significant. Also, as noted by Oerlemans (1986), small glaciers can be particularly sensitive to increasing amounts of carbon dioxide in the atmosphere.

The dominant part of change to the volumetric mass balance of a glacier is tied up in its surface mass balance. Data on surface mass balance and volume change are available for about 25 glaciers (Meier 1983, 1984), some of which span more than 50 years since direct measurements first began in 1945. These records are concentrated in the midlatitudes of the Northern Hemisphere, thus rendering them somewhat unrepresentative of global changes to the cryosphere. Midlatitude locations are, however, among those where concentrations of people in search of freshwater resources are likely to be found. Because glaciers are a vital constituent of the freshwater resources of such localities, it is crucial to understand what variations in the surface mass balance imply for the volume of the resource.

There are more-numerous and longer records of glacier advance and retreat (Haerberli 1995), but these are unreliable indicators of volume change. Furthermore, as accurate as good mass-balance measurements in situ can be, the ability to measure volumetric change is moot to water-resource managers if the volume of the ice in question is not known. The significance of change is best understood in relative terms when one is assessing the long-term viability of a resource. There is field evidence that small glaciers in the Rocky Mountains may have lost as much as 75% of the ice volume they had a century ago (Lawby et al. 1995). The volumes of many glaciers, spanning the full size range found in the midlatitudes, must be known in order to assess the significance of such a finding. There is little prospect of accomplishing such a task through field measurement programs.

Much of the current uncertainty about glacier and ice-sheet responses to climate change is generated by the need to make inferences about extensive areas from a few sites where there are field research programs. EOS promises great advances in reducing such uncertainty by virtue of the extensive spatial reach of satellite data. Currently, mass balance can be estimated in the field, either by measuring changes in the thickness and area of grounded ice, or by measuring the seasonal components of the net mass balance. These are often done concurrently with energy

exchange and hydrological studies to explain the processes at work. Therefore, existing field research sites, with their potential to calibrate satellite information, are important places in which to concentrate satellite data analysis. Nevertheless, the choice of new sites in which to conduct process studies can benefit from guidance to key areas identified by satellite, and from satellite data on surface characteristics, elevations, ice extent, and atmospheric conditions.

Areal extent and thickness of ice are clearly the key parameters to measure in order to determine volume. The determination of surface area and differentiation into cover classes is a reasonably straightforward task, as illustrated in studies using TM data for Athabasca Glacier (Gratton et al. 1994) and AVHRR data for the Greenland Ice Sheet (Zuo and Oerlemans 1996). The determination of ice-thickness distribution by satellite is a more-challenging problem, though the use of SAR data may eventually prove to be useful here. The possibility that data from ICESat and SAR may prove to be effective for measuring small changes in surface elevation offers prospects for merging satellite data with historical mass-balance records, such as those which have recently been reported for White Glacier (Cogley et al. 1996). Successful merging of the records with satellite data is crucial to the task of using satellites for regional mass-balance assessments of valley glaciers.

Remote sensing has, and will continue to play, an important role in research to improve the understanding and modeling of glacier hydrology. Examples of key contributions are:

- 1) Accurate representation of topography—DEMs derived from satellite altimetry or SAR interferometry may be crucial as inputs to detailed energy-balance-based melt models. These incorporate effects of slope angle, aspect, and shading on radiation receipts and melt-energy availability. DEMs are also essential for calculation of meltwater routing over and under ice masses.
- 2) Initialization of melt models—A key issue here is representation of the snow-water-equivalent distribution at the onset of a model run. As yet there is no easy way to find this—on an ice-sheet scale there may be some application for microwave techniques—but current resolution is too coarse at the glacier scale. Surface DEMs may also help define surface-roughness features such as sastrugi, which are likely associated with local variability in snow-water equivalence—and which might determine patchiness of melting snow

cover, which has important implications for albedo and for energy fluxes between adjacent areas of contrasting albedo.

- 3) Albedo parameterizations—Performance of energy-balance melt models is critically dependent on performance of albedo parameterizations, which have to be applied in a distributed fashion. Remote sensing offers the only realistic prospect for mapping albedo on an ice-mass scale at regular intervals. This is essential for creating databases which will allow development of effective parameterizations—and for testing their performance when ported to sites or years other than those for which they were developed.
- 4) Meltwater freezing—This is as critical for glacier hydrology as it is for mass balance—especially in the Arctic. Meltwater which refreezes has to be melted at least twice before it runs off—thus adding to effective accumulation. This process delays runoff response to atmospheric temperature changes. Winter warming may not affect melt rates directly, but, by warming surface layers of ice, may reduce the degree of refreezing which occurs, thus promoting more runoff in subsequent summers. Remotely-sensed mapping of distribution of snow/ice facies on ice masses may allow documentation of extent of zones of refreezing—providing a means of testing model performance. Mapping end-of-season snowline positions is also a key means of testing model performance.
- 5) Glacier outburst hazards—Remote sensing offers a means of locating supraglacial and ice marginal reservoirs, which are potential sources for catastrophic outburst events. It also offers the possibility of recording drainage events, measuring reservoir volume (by comparison of topography of basins in drained and pre-drainage states), and identifying flood routeways (from surface-collapse features or surface-velocity response) and outburst locations. Long records allow documentation of outburst-event frequency. Large subglacial reservoirs may be detected from high-resolution measurements of surface topography of ice masses, and there may be some prospect for determining major subglacial flow paths the same way.
- 6) Occurrence of subglacial drainage—Where ice margins are floating, emergence of turbid plumes from ice margins provides evidence of subglacial drainage and helps to locate meltwater efflux points. For land-terminating ice masses, turbidity of meltwater streams may provide some insight into balance of supraglacial/subglacial runoff. In remote areas, remote sensing may allow documentation of distribution of major meltwater input points to oceans—and also provide evidence of timing/duration of these inputs.

6.3 Required measurements, data sets, and parameterizations

6.3.1 Satellite observations

6.3.1.1 Snow cover

A major theme in snow hydrological research over the past decade has been the expanded use of remote sensing for determining snow properties which are used to estimate snow distributions and snowmelt runoff. There has also been a move toward development of physically-based snowmelt models to use with these emerging data, particularly for alpine areas. The coupling of remote sensing and physically-based approaches will enable more-accurate basin-scale forecasts, and will also provide spatially-distributed estimates of snowmelt.

Table 6.2 (pg. 288) summarizes the snow-cover information needed to address the cryospheric-science issues raised in Section 6.2 and to satisfy operational users of EOS data.

Snow extent

Snow-cover-extent information is needed for a wide variety of uses including monitoring and change detection, input to NWP and hydrological models, and for validation of GCMs. The spatial- and temporal-resolution requirements for snow information depend on the application. Continental-scale monitoring of snow cover can be effectively carried out with daily-weekly data at 25-100-km resolution, while spatially-distributed snowmelt and runoff modeling in mountainous terrain requires spatial resolution finer than 1 km. Other useful information can be derived from snow-cover data such as the altitude of the snow line, which can be incorporated into snowmelt forecast models in mountainous areas, e.g., Hartman et al. (1995).

TABLE 6.2

PARAMETER NAME	UNITS	ACCURACY NEED/AVAIL	TEMPORAL RESOLUTION	SPATIAL RESOLUTION	VERTICAL RESOLUTION	SOURCE
Snow extent	—	10%	1/day	30 - 100 m 1/wk, 1/mon	N/A	Radarsat, Landsat
Snow extent	—	10%	1/day, 1 wk, 1/mon	1 km, 12 km, 25 km	N/A	MODIS, AMSR-E, SSM/I
Snow depth	cm	10%	1/day, 1 wk	30 m - 12 km	5 cm	AMSR-E, SSM/I, Radarsat
Snow-water equivalent	mm	10%	1/day, 1 wk	30 - 100 m 12 km	5 mm	Radarsat, AMSR-E, SSM/I
Snow wetness	Yes/ No	—	1/day, 1 wk	30 m - 12 km	—	Radarsat, AMSR-E, SSM/I
Albedo	%	5%	daily	1 km	—	MODIS

Required snow-cover observations to address EOS research and operational requirements. (WCRP 1997.)

NOAA AVHRR data have been routinely used for classification of snow-covered versus snow-free area (Matson et al. 1986; Matson 1991; Xu et al. 1993). Like AVHRR, MODIS will provide near-daily global coverage, but at spatial resolutions ranging from 250 m to 1 km. Only two channels in the visible and near-infrared spectral bands will be available at 250-m resolution; five channels in the visible, near-infrared, and short-wave infrared will be available at 500-m resolution, and the remaining 29 MODIS channels will have a spatial resolution of 1 km, and may not be suitable for snow mapping because they were designed for use over ocean or atmosphere targets. MODIS has onboard visible/near-infrared calibrators while the AVHRR does not, thus we will be able to derive radiances of snow using some of the MODIS sensors. At least one of the visible MODIS channels will not saturate over snow. This will be an advancement over the AVHRR and TM sensors that experience significant saturation over snow and ice targets in the visible channels. The at-launch MODIS snow and ice products will consist of 500-m or 1-km resolution binary maps of snow and ice cover, respectively, produced on a global, daily basis in most months (Hall et al. 1995). In addition, the MODIS cloud mask will be used to derive global maps of cloud cover (Ackerman et al. 1996). After the first EOS launch, techniques initially carried out with Landsat data can be extended to subpixel snow mapping from MODIS and ASTER. But end-member selection needs to be done

for each scene. With such analyses, MODIS will also be useful in alpine regions. SAR investigations that are now being pursued with advanced aircraft-mounted systems may be continued using simplified techniques with single-frequency, single-polarization SAR instruments such as ERS-1, the Japanese Earth Remote-Sensing Satellite-1 (JERS-1), and Radarsat to provide useful snow-mapping data.

SSM/I-derived information on snow extent is being used operationally by NESDIS for generation of the weekly snow-cover analysis product. AMSR-E will continue to provide a weekly snow-extent product, which will allow the combination of SMMR, SSM/I, and AMSR-E to provide a continuous time series of snow extent from 1978. The higher spatial resolution of AMSR-E (10 km) relative to SMMR and SSM/I will improve the ability to map snow cover in forested and mountainous regions. AMSR-E snow-cover information will complement snow products from other EOS sensors such as MODIS, Multi-angle Imaging Spectroradiometer (MISR), and ASTER. This will provide EOS researchers with detailed, multi-sensor information on snow-cover extent, albedo, and surface temperature (Chang and Rango 1996).

Snow depth

Snow depth is an important parameter for input to NWP snow-cover analyses and for validating GCM simulations. For example, the most frequently used GCM snow-vali-

dation standard is the United States Air Force (USAF) global snow-depth data set of Foster and Davy (1988). This data set is based on in situ snow-depth observations, which are not available in many sparsely-populated areas of the world. A global snow-depth map will be produced as a special product from AMSR-E (Chang and Rango 1996). This will most likely apply a density climatology to the AMSR-E snow-water-equivalence map product since snow density exhibits considerably less spatial and temporal variability than snow-water equivalence. The accuracy of this product will depend on the success of snow-water-equivalence-algorithm development activities to account for forest and land-cover effects on brightness temperatures.

Snow-water equivalence

Regular observations of snow-water equivalence are needed to satisfy a wide range of requirements in research and operations, e.g., validation of climate and hydrological models (e.g., AMIP), water resource monitoring (e.g., Goodison and Walker 1994), and input to flood-forecast models. Accurate basin-wide snow-water-equivalence estimates are especially critical in the western U.S. where much of the annual runoff and groundwater recharge comes from melting of the mountain snow pack each spring. The lack of a reliable global snow-water-equivalence climatology for validating GCM climate simulations is a critical data gap that also needs to be addressed. Determining snow-water equivalence directly from remotely-sensed data has been an objective within the remote-sensing community for some time; although operational gamma radiation methods have been developed for areas with gentle topography, aircraft flight height constraints and gamma signal extinction problems in smaller, rugged mountain basins with deep snowpacks generally prevent the use of this method in these areas. SAR at multiple frequencies and polarizations has yielded promising results for snow-water-equivalence measurement (Shi et al. 1990), but operational satellites do not provide the necessary data. At present, the measurement of the spatial distribution of snow-water equivalence and total snow volume within a basin must be performed by intensive field sampling to attempt to represent the large spatial variability of mountain snowpacks. Logistical and safety limitations generally restrict the number of field samples that may be so obtained (Elder et al. 1991). Thus, the problem of determining the volume and distribution of snowpack water storage within mountain basins remains acute.

Estimation of distributed snow-water equivalence is challenging because of the many factors that affect its distribution, and the small correlation length of the snow-

water-equivalence spatial distribution. Further, difficulties associated with accurately determining the time of maximum accumulation present a problem for snowmelt-runoff forecasters. The simplicity of regression models makes them an attractive means of estimating snow-water equivalence because of the large amount of work required to make direct measurements of snow-water equivalence on the catchment scale. An approach to modeling spatially-distributed snowmelt in steep, alpine basins was proposed using net potential radiation, distributed across the basin using a DEM, as the main factor determining relative snowmelt (Elder et al. 1991). Such an approach enables the use of a detailed, physically-based snowmelt model for each physically different subregion of the basin at the scale of interest. Testing this approach on the 1.2 km² Emerald Lake basin in California's Sierra Nevada suggests that little information is lost in going from a 5-m to 25-m grid, but that use of a 100-m grid may result in significant inaccuracies (Bales et al. 1992).

Remote sensing allows estimation of several of the important hydrologic variables for snowmelt modeling from space or aircraft. From Landsat one can map snow at subpixel resolution, to an accuracy as good as with aerial photographs. From hyperspectral sensors (currently the Airborne Visible and Infrared Imaging Spectrometer [AVIRIS]) one can estimate snow-grain size, albedo, liquid-water content in the surface layer, and subpixel coverage. Using two-frequency, co-polarized SAR, one can map snow through thick cloud cover to an accuracy of 80%, and estimate liquid-water content to about 2%. Work on estimation of snow-water equivalence is continuing, with promising results from the Shuttle Imaging Radar-C (SIR-C)/X-Band Synthetic Aperture Radar (X-SAR), from photogrammetry, and from snowmelt modeling with time-series SCA data. A fully automated method of subpixel snow-cover mapping uses Landsat TM data to map snow cover in the Sierra Nevada and make quantitative estimates of the fractional snow-covered area within each pixel (Rosenthal and Dozier 1996). TM scenes are modeled as linear mixtures of image end-member spectra to produce the response variables for tree-based regression and classification models. The algorithm has been tested on a different TM scene and verified with high-resolution, large-format, color aerial photography. Snow-fraction estimates from the satellite data can be as accurate as those attainable with high-resolution aerial photography, but they are obtained faster, at much lower cost, and over a vastly larger area.

The development and validation of snow-water-equivalence algorithms for use with AMSR-E is a major EOS activity. A detailed discussion of the snow-water-equivalence-algorithm development and validation

process for AMSR-E is provided in Chang and Rango (1996). Figure 6.4 documents the multiple steps required to generate a snow-water-equivalence estimate. Detailed field observations of snow properties and corresponding microwave signatures over a variety of terrain and land-cover categories are an essential component of this process. This is an important contribution of snow research activities within the CRYSYS IDS (Goodison and Brown 1997).

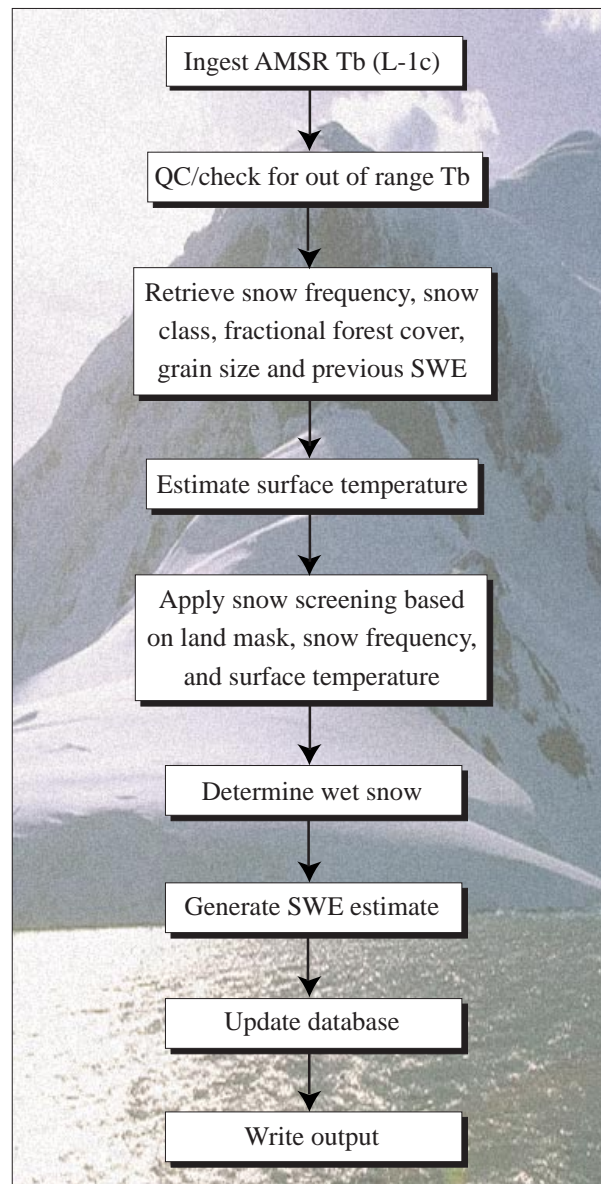
It is also possible to infer snow-water equivalence after the fact from measurements of snow-cover depletion. With a time series of snow cover, e.g., from TM imagery, one can tell when the snow cover disappears, i.e., when snow-water equivalence goes to zero. Then, using a spatially-distributed snowmelt model, one can back calculate from the time snow cover disappears at a point, and then infer the starting value of snow-water equivalence. This method has been implemented using TM scenes for a small watershed in the Sierra Nevada, California (Cline 1997). In this first test, the inferred initial snow-water equivalence agreed well with snow-survey measurements. The reverse approach can be used with a dense time series of remote-sensing scenes, such as will be available from MODIS, to forecast potential snowmelt; such a forecasting approach could set aside the need to estimate snow-water equivalence, and would rely on properties more readily measured from remote-sensing platforms, including SCA and reflectivity.

Snow wetness and albedo

Snow wetness provides important hydrological information such as the onset of melt, and may be a particularly sensitive indicator of change given that climate warming would likely be associated with more frequent rain-on-snow events and more frequent thaw events. Snow-wetness information can be derived from both active and passive microwave data.

Snow-surface albedo is needed for a multitude of uses including climate-change monitoring (e.g., Robinson et al. 1993), understanding snow-cover-climate feedbacks (e.g., Groisman et al. 1994a), input to NWP and hydrological models, and validation of GCMs. Global coverage of snow albedo at 1-km resolution will be provided by MODIS. For finer resolution requirements such as snow ablation in hydrological models, surface-albedo information can be derived from ASTER and the Enhanced Thematic Mapper+ (ETM+) for defined target areas at a horizontal resolution of 15-30 m over the visible and infrared portions of the spectrum.

FIGURE 6.4



Schematic flow diagram of AMSR-E SWE algorithm. (Chang and Rango 1996).

6.3.1.2 *Sea ice*

Sea-ice models, especially those used in climate simulations, treat many processes in a very idealized manner. The reasons include inadequate knowledge of the physics involved, inadequate observational data to define certain key parameters, and the computational expense of including more-realistic treatments. Some process parameterizations which are particularly in need of improvement are listed below, along with the associated observational requirements.

Sea-ice momentum balance—As indicated in Section 6.1.3, GCMs often ignore sea-ice motion, although the trend is now to include a sea-ice dynamical scheme. Physical parameters that arise in such models are shear and compressive strength and drag coefficients. Since strength parameters cannot be measured directly, they are generally inferred by comparisons of observed and modeled buoy drift (e.g., Hibler and Walsh 1982; Flato and Hibler 1992, 1995). More-detailed ice-motion fields, such as those provided by sequential satellite imagery, should allow discrimination between various proposed strength parameterizations, more specifically, the shape of the plastic-yield curve (see, e.g., Ip et al. 1991; Ip 1993). Observations of ice roughness, which is dominated by ridging intensity, may allow more-realistic drag parameterization, which in turn affects a model’s ability to reproduce observed ice drift. Required observations include ice motion and deformation. The accuracy and resolution requirements, along with the data sources, are provided in Table 6.3. Some encouraging results on observed ice drift have recently been obtained through wavelet analysis of satellite ERS-1 SAR images (Liu et al. 1997), and the wavelet technique is now being applied by Liu to the passive microwave data of the Defense Meteorological Satellite Program (DMSP) Special Sensor Microwave Imager (SSM/I).

SEB—Because of its important role in the SEB and climate feedback, it is crucial to parameterize sea-ice al-

bedo accurately. Such parameterization is confounded by both spatial inhomogeneity and the dramatic drop in albedo accompanying snow melt and surface-melt-pond formation in spring (e.g., Morassutti 1989; Barry 1996). More-complete parameterizations, which explicitly include melt ponding, are being developed (Ebert and Curry 1993), and large-scale estimates of surface albedo based on DMSP and AVHRR satellite observations (Scharfen et al. 1987; Lindsay and Rothrock 1994) should aid in this development. Other terms in the sea-ice surface-energy budget are also uncertain, and the available parameterizations are in need of more-comprehensive validation. Data sets required to develop and validate parameterizations of the surface-energy-exchange process include profiles of atmospheric quantities (for radiation calculations), surface quantities like albedo, temperature, and roughness, and ice concentration. Specific requirements are provided in Table 6.4.

Ice mass balance—Continuous deformation, growth, and melt ensure that a region of sea ice contains a range of ice thickness from open water through newly-formed and multi-year ice, to pressure ridges tens of meters thick. Although a theoretical framework to describe this thickness distribution has been available for some time (Thorndike et al. 1975), it has not been widely used owing to computational complexity and uncertainty regarding key parameters. On the other hand, ocean-atmosphere heat exchange is very sensitive to details of the thin portion of the thickness distribution (Maykut 1982), and the time scale of temporal variability in Arctic ice volume is dominated by the long survival time of thick ridged ice (Flato 1995). Hence, some account of the thickness distribution should be made in climate models. The most common approach so far is to consider only two thickness categories, open water and the mean thickness (e.g., Hibler 1979; Parkinson and Washington 1979; Flato and Hibler 1992), but this is rather crude. Parameterizations required to describe ridge redis-

TABLE 6.3

PARAMETER NAME	UNITS	ACCURACY NEED/AVAIL	TEMPORAL RESOLUTION	SPATIAL RESOLUTION	VERTICAL RESOLUTION	SOURCE
Ice displacement	m	1 km/300 m	2/week	5 km	N/A	MODIS, Radarsat, buoys
Ice deformation	s ⁻¹	.5% / .1%	2/week	5 km	N/A	MODIS, Radarsat, buoys

Accuracy and resolution requirements to observe sea-ice momentum balance (WCRP 1997).

TABLE 6.4

<i>PARAMETER NAME</i>	<i>UNITS</i>	<i>ACCURACY NEED/AVAIL OR ABSOLUTE::REL</i>	<i>TEMPORAL RESOLUTION</i>	<i>SPATIAL RESOLUTION OR HORIZONTAL RESOLUTION::COVER</i>	<i>VERTICAL RESOLUTION</i>	<i>SOURCE</i>
Sea-ice concentration	%	7%	daily	20 km	—	AMSR-E
Floe-size statistics	—	10%	weekly	100 km	—	MODIS, Radarsat
Ridge statistics	—	10%	weekly	100 km	—	Radarsat
Cloud fraction	—	4% / 30%	daily	1 km	—	MODIS, climatology, stations
Cloud optical depth	—	15%	daily	1 km	—	MODIS, aircraft
Cloud particle phase	—	—	daily	1 km	—	MODIS, aircraft
Cloud effective particle radius	—	25%	daily	1 km	—	MODIS, aircraft
Cloud top temperature	—	6%	daily	1 km, 100 km	—	AIRS, AMSU, MODIS
Cloud top pressure	—	6%	daily	100 km	—	AIRS, AMSU, HSB
Atmos. ice crystal precip.	—	—	—	—	—	ICESat, aircraft
Atmospheric aerosol	—	—	—	—	—	ICESat, aircraft
Surface albedo	—	0.05 / 0.1	daily	1km	—	MODIS, climatology
Ice surface	—	1 K / 2 K	daily	1 km, 100 km	—	MODIS, AIRS, buoys, stations
Surface roughness	—	—	—	—	—	laser, survey
Humidity profile	g/kg	10% (goal)::5%	2/day (d, n)	50 x 50 km::G	2 km::Atmos	AIRS (05), HSB
Temperature profile	K	1.0 K::0.4 K	2/day (d, n)	50 x 50 km::G	2 km::Atmos	AIRS (07)

Data sets required to develop and validate parameterizations of the surface-energy-exchange process (WCRP 1997).

tribution and strength in the Thorndike et al. (1975) scheme have been investigated numerically by Flato and Hibler (1995). Most of the observations used in such studies are from submarine upward-looking sonar profiles. However, some applicable remote-sensing observations are being assembled from sequential SAR imagery (Kwok et al. 1995; Stern et al. 1995). The quantities of interest here are the ice-thickness distribution, concentration and type, snow thickness, and ridge and floe statistics. Specific requirements are provided in Table 6.5.

Observing the fraction of open water within the ice pack is a priority, both in terms of monitoring and understanding variations which might occur, and in terms of improving the representation of open-water effects in sea-ice and climate models. Since open-water fraction is simply one minus the ice concentration, observations from passive microwave satellites are in principle available from the mid 1970s onward. However, the errors inherent in concentration estimates, roughly 2-7% (Cavalieri 1992), imply errors in open water estimates of nearly 100%! Improving these errors will be a challenge for scientists using future EOS sensors. Nevertheless, the long time series of existing ice-concentration data (Zwally et al. 1983; Parkinson et al. 1987; Gloersen et al. 1992) pro-

vide a useful measure of seasonal and interannual variability in open-water fraction.

6.3.1.3 Lake ice

The freeze-up/break-up of lakes can be readily monitored by satellite. Barry and Maslanik (1993) describe the potential use of passive microwave data for monitoring large water bodies. Small lakes can be readily mapped from visible and infrared data for cloud-free conditions, which are generally more common in spring. Dates determined by remote sensing generally compare well with surface observations (Wynne et al. 1996). SAR data have also been used to study lake-ice processes (freeze-up/break-up, freezing of ice to the lake bed, and ice thickness [Hall et al. 1994; Jeffries et al. 1994; Morris et al. 1995; Jeffries et al. 1996; Duguay and Lafleur 1997]).

With EOS instruments we can exploit the synergism between optical and microwave spaceborne imagery for lake-ice monitoring. As shown in Table 6.6, satellite data should ideally be acquired on a daily basis to determine, with as much precision as possible, the timing of fall freeze-up and spring break-up. Although the sensors identified in this table are well suited for lake-ice studies on large lakes, they lack the spatial resolution needed to

TABLE 6.5

PARAMETER NAME	UNITS	ACCURACY NEED/AVAIL OR ABS::REL	TEMPORAL RESOLUTION	HORIZONTAL RESOLUTION ::COVER	VERTICAL RESOLUTION ::COVER	COMMENTS
Ice thickness distribution	m ⁻¹	thickness: 10% / 50%	—	—	—	sonar, models, Radarsat
Snow depth	m	5 cm / 20 cm	—	—	—	climatology
Sea ice	%	7%::	—	12 km :: Ocean/Cryo	N/A :: Sfc	AMSR-E (11)
Sea-ice type	%	11%::	—	12 km :: Ocean/Cryo	:: Sfc	AMSR-E (12)

Data sets and accuracy required for estimating sea-ice mass balance (WCRP 1997).

TABLE 6.6

PARAMETER NAME	UNITS	ACCURACY	TEMPORAL RESOLUTION	SPATIAL RESOLUTION	VERTICAL RESOLUTION	SOURCE
Freeze-up/ break-up date	Julian Day	1 day	daily	1 km 5 km		MODIS, AMSR-E, SSM/I

Required lake-ice observations for cryospheric monitoring and change detection (WCRP 1997).

TABLE 6.7

PARAMETER	EOS INSTRUMENT	ACCURACY ABSOLUTE:: RELATIVE	TEMPORAL RESOLUTION	HORIZONTAL RESOLUTION ²	VERTICAL RESOLUTION	COMMENTS
Land cover / land use	ASTER, ETM+	10%::	1/year (late July - early August)	15 - 30 m (VIS, NIR, IR)	—	SPOT (useful), MODIS and AVHRR (resol. limiting)
Snow cover	ASTER, ETM+	10%::	8/year (mid-March to mid-June)	15 - 30 m (VIS, NIR, MIR)	—	ERS, JERS, Radarsat, SPOT (useful). AMSR, MODIS, and SSM/I (resol. limiting)
Snow depth	ASTER, ETM+	—	8/year (mid-March to mid-June)	15 - 30 (VIS, NIR, MIR)	—	ERS, JERS, Radarsat (useful). AMSR, SSM/I (resol. limiting)
Soil moisture	ASTER, ETM+	—	6/year (mid-June to late August)	15 - 90 m (VIS, NIR, MIR, TIR)	—	ERS, JERS, Radarsat (useful). AMSR, MODIS, AVHRR (resol. limiting)
Surface reflectance and albedo	ASTER, ETM+	4%::1%	8/year (early May to late August)	15 - 30 m (VIS, NIR, MIR)	—	MISR, MODIS, AVHRR (resol. limiting)
Surface brightness temperature	ASTER, ETM+	1-2 K :: 0.3 K	8/year (early May to late August)	60 - 90 m (TIR)	—	AMSR, MODIS, AVHRR, SSM/I (resol. limiting)
Surface kinetic temperature	ASTER	1-4 K :: 1%	8/year (early May to late August)	90 m (TIR)	—	MODIS (resol. limiting)
Digital elevation model	ASTER	5-10 m ::	1/year (mid-July to early August)	15 m (PAN)	1 m	SPOT and SAR (useful)
Permafrost surface displacement features	ASTER, ETM+	—	1/year (mid-July to early August)	15 - 30 m (VIS, NIR, MIR)	—	SPOT, ERS, JERS, and Radarsat (useful)
Freeze / thaw cycle (vegetation/soil)	—	—	1/week (complete year)	—	—	ERS, JERS, Radarsat, (useful) AMSR and SSM/I (resol. limiting)

Note: Permafrost extent and active-layer thickness cannot currently be extracted directly using remotely-sensed data. (Instruments offering spatial resolutions coarser than 100 m may not be useful for most permafrost investigations.)

Required satellite observations for monitoring and change detection of permafrost¹ and seasonally-frozen ground (WCRP 1997).

monitor freeze-up and break-up on small (shallow) lakes, which are found at many locations in subarctic and arctic regions. Radarsat and ERS-2 SAR sensors, and ASTER visible/infrared spectral bands are seen as important data sources for lake-ice-process studies on shallow lakes, even though the temporal resolution is of the order of one week to a month (depending on the latitude of the study site and number of incidence angles available). However, as indicated by Morris et al. (1995), shallow lakes represent promising sites for long-term monitoring and the detection of changes related to global warming and its effects on polar regions.

6.3.1.4 Frozen ground and permafrost

As shown in Table 6.7, monitoring of permafrost conditions requires the observation of several parameters. Some of these (local environmental factors) are required as input or transfer functions in ground thermal models. Because permafrost conditions are strongly controlled by

local factors, and permafrost features (i.e., surficial expressions) are also local in scale, ASTER will provide the best overall configuration for permafrost mapping and monitoring efforts (i.e., high-spatial resolution, stereo capabilities, and wide range of spectral bands), followed by ETM+ to be flown on Landsat-7.

Local environmental factors—Local factors (i.e., vegetation cover, snow cover, elevation/slope/aspect, and soil-moisture conditions) commonly override the influence of larger scale macroclimatic factors on ground thermal conditions. These factors will be derived from ASTER to complete ongoing regional permafrost mapping efforts at several permafrost study sites (i.e., mapping the presence/absence and active-layer depth), and to determine their influence on the thermal regime of permafrost (by coupling the ASTER-derived variables to a heat transfer model). While Visible and Near Infrared (VNIR) (including the stereo capabilities for the production of DEMs) and short-wavelength infrared (SWIR)

TABLE 6.8

PARAMETER NAME	UNITS	ACCURACY NEED/AVAILABLE	TEMPORAL RESOLUTION	SPATIAL RESOLUTION	VERTICAL RESOLUTION	SOURCE
Ice surface topography	m	0.5 - 5 m /?	yearly	10 - 100 m	1 - 10 m	ICESat, SAR
Area covered by ice	km ²	0.01 - 0.5 km ² /0.001 km ²	yearly	100 m - 1 km	—	ASTER, AVHRR, ETM, MODIS, TM
Ice-thickness distribution	m	0.5 - 5 m /?	yearly	100 m - 1 km	1 - 10 m	SAR
Ice-flow velocity	m d ⁻¹	0.05 - 0.5 m d ⁻¹ /?	daily, yearly	0.1 - 1 m	—	ICESat, SAR
Seasonal ice/snow cover	km ²	0.01 - 0.5 km ² /0.001 km ²	daily, yearly	10 m - 1 km	—	ASTER, AVHRR, ETM, MODIS, TM
Snow-depth distribution	m	- 0.25 m	daily, yearly	10 m - 1 km	0.05 - 0.5 m	ASTER, SSM/I
Snow-water equivalent	mm	2.5 - 25 mm	daily	10 m	5 - 50 mm	SAR
Surface temperature	K	0.5 K / 2 K	daily	10 m - 1 km	—	ASTER, AVHRR, ETM, MODIS, TM
Albedo distribution	%	1% /5-10%	daily	10 m - 1 km	—	ASTER, AVHRR, ETM, MODIS, TM, CERES
Cloud cover	%	10%	daily	1 - 10 km	—	
Meltwater runoff	Yes /No	— /—	daily	1 - 100 m	—	ASTER, TM, ETM

Data sets and accuracy required to monitor glacier and ice-sheet responses to changing climate (WCRP 1997).

channels are planned to be used to derive the local factors, the thermal infrared (TIR) channels will be utilized to test the heat transfer model. The ground-surface temperature in such models is usually approximated using N-factors (factors applied as transfer functions between the air temperature and the temperature at the ground surface, to account for the local influence of vegetation and snow cover). The TIR channels will likely provide an improvement over the current N-factors approximation. SAR sensors, such as those onboard Radarsat, will also be useful, in particular, for deriving information on snow and soil-moisture conditions.

Permafrost features—Features indicative of permafrost degradation such as thaw lakes, active-layer detachment slides, and retrogressive thaw slumps will be mapped and monitored (VNIR and SWIR channels in particular). These features are particularly good indicators of climate warming. Other surface features, known to have an impact on permafrost conditions, such as new human settlements and forest fires (the after effect, i.e., burned areas), can also be mapped with ASTER. Active microwave SAR imagery acquired by other non-EOS sensors is also likely to be useful (whether used alone or in combination with ASTER data) for mapping thermokarst features.

Seasonally frozen ground—Global warming may significantly alter the duration of the freeze-thaw periods at high- and mid-latitude locations. A modification of the length of the frost-free period could have significant ecological, hydrological, engineering, and economical implications. Active and passive microwave imagery have been shown to be particularly useful for monitoring the freeze-thaw cycle of the landscape (Table 6.7).

6.3.1.5 *Glaciers and ice sheets*

Surface topography, area of ice cover, the spatial distribution of its thickness, surface flow velocity, areas covered by snow and exposed ice during melt periods, snow-depth distribution, its water equivalent, the distributions of surface temperature and albedo, and the presence or absence of meltwater runoff are all important parameters to use in identifying the responses of glaciers and ice sheets to climatic change. They are also needed to assess implications of these responses for sea-level rise and regional water resources. The temporal, spatial, and vertical resolutions stated in Table 6.8 vary according to the scale of the ice involved and the task at hand. The lower ends of the spatial- and vertical-resolution ranges apply to small valley glaciers; the upper ends to large glaciers and ice sheets. Yearly resolution is needed for monitoring responses to climatic change. Daily resolution is ideal to estimate mass-balance responses to short-term weather variations, such

as winter accumulation in the snow pack and summer release of meltwater runoff to streams. Daily resolution, however, with acceptable spatial resolution for small glaciers, cannot be obtained with current satellite scanning systems.

The EOS experiment most closely associated with ice-sheet mass balance is ICESat. By accurately measuring ice surface topography, improved ice-flow models are possible. By measuring it repeatedly, changes in surface elevation are revealed. After correction for small changes caused by evolution of snow-density profiles and of bed-rock motions, the residual is the change in ice-sheet mass balance and hence the contribution of ice sheets to sea-level change. Such experiments are aided by radar altimetry, but laser precision is needed to allow accurate, ice-sheet-wide assessment of mass balance over years rather than decades. Repeat laser altimetry will also identify those regions that are changing especially rapidly, thus identifying important locations for process studies.

Landsat TM data, available in six shortwave bands with spatial resolution of 30 m and one thermal band with 120-m resolution since 1972, are an important source of glacier information pertaining to area covered by ice, as well as its differentiation into seasonal ice/snow cover, so they play a prominent role in Table 6.8. AVHRR has an advantage over TM in that it can provide daily resolution, but its spatial resolution of 1.1 km makes it most suitable for use over large ice sheets (Zuo and Oerlemans 1996). MODIS, with near-daily temporal resolution over a few bands at 250-to-500-m spatial coverage, may prove useful in modeling meltwater discharge from large valley glaciers and small ice sheets, thus providing an effective blend of spatial and temporal resolution.

Increased spatial and spectral resolution over that of the TM is to be gained from the ETM and from ASTER. ASTER, with 14 bands in the visible, near-infrared, and TIR, will have the added benefit of monochromatic stereo imaging. Furthermore, the estimation of snow-depth distribution is possible from ASTER, as it is with SSM/I. It should also be possible to determine the seasonal timing of meltwater runoff from most ice-covered areas with the enhanced resolution.

The spectral characteristics of the foregoing sensors provide the keys to detailed mapping of the components of radiative exchange on glaciers (Gratton et al. 1994) because their data are useful for determining surface temperature and the albedo distribution. Furthermore, it is possible to determine separate albedo values for the visible and near-infrared parts of the solar spectrum, and to validate them against similar measurements in situ over ice (Cutler and Munro 1996) and snow (Cutler and Munro 1996; Marks and Dozier 1992). As

indicated in earlier modeling work by Munro and Young (1982), and shown more recently in situ by Van de Wal et al. (1992), albedo is a powerful determinant of the ablation which supplies meltwater at the ice surface. If such information is to be used effectively in regional hydrological modeling, then it will also be necessary to have satellite cloud-cover data as well, such as can be provided by the Clouds and the Earth's Radiant Energy System (CERES).

Since the 1991 launch of the ERS-1 satellite and its C-band SAR, glacier monitoring has been possible to spatial resolutions of approximately 30 m through cloud cover and darkness. Since October 1995, Radarsat has offered SAR data with 9-m resolution. SAR data reveal information about subsurface glacier processes and features, imaging buried crevasses and the location of the equilibrium line through winter snow cover. SAR's capability of looking so deeply into the ice suggests possibilities for measuring ice-thickness distribution as well. Another unique attribute of SAR is that careful repeat imaging spaced a few days or weeks apart can be used in an interferometric mode. Under optimum conditions, radar interferometry allows precise ice-flow-velocity determinations over short intervals. There is also the possibility that SAR will one day yield the snow-water equivalent of the snow pack as it changes with the seasons, but satellites do not yet provide the necessary data.

6.3.2 *Related international science programs*

6.3.2.1 *The Boreal Ecosystem-Atmosphere Study (BOREAS)*

is a large-scale international interdisciplinary experiment in the northern boreal forests of Canada. Its goal is to improve our understanding of the boreal forests—how they interact with the atmosphere, how much CO₂ they can store, and how climate change will affect them. BOREAS wants to learn to use satellite data to monitor the forests and to improve computer simulation and weather models so scientists can anticipate the effects of global change (<http://boreas.gsfc.nasa.gov/>).

6.3.2.2 *ACSYS*

ACSYS is a WCRP project aimed at improved understanding of the role of the Arctic in the climate system, and of the effects of global climate change and variability on the Arctic. Specific scientific goals of ACSYS include improving the representation of the Arctic in climate models, developing plans for monitoring Arctic climate, and determining the role of the Arctic in climate sensitivity and variability. These scientific goals are closely aligned with EOS goals. Of particular interest to EOS are in situ ob-

servations of Arctic Ocean hydrography, cloud-radiation interactions, observations of ice thickness and Lagrangian motion, and the assembly of historical oceanographic and hydrological data sets (many of which are currently held in Russia). More information can be obtained from WCRP (1994) or via the ACSYS web page (<http://www.npolar.no/acsys/>).

6.3.2.3 *Surface Heat Budget of the Arctic Ocean (SHEBA)*

SHEBA is a multi-national project whose goals are to develop and test models of Arctic ocean-ice-atmosphere interactions and to improve the interpretation of satellite remote-sensing data in the Arctic. Both of these will be based in large part on detailed observations to be made during the 1997-1998 field experiment from the ship frozen in the Beaufort Sea and from associated camps. The very comprehensive annual-cycle data set to be collected during the field program will be especially valuable to EOS for calibration and validation of remote-sensing algorithms and for improving model parameterizations of various energy-exchange processes. More details are available in Moritz et al. (1993) or via the SHEBA web page (<http://sheba.apl.washington.edu/>).

6.3.2.4 *International Arctic Buoy Program (IABP)*

IABP oversees and monitors a network of automatic data buoys which have been repeatedly deployed across the Arctic since 1979. These buoys measure surface pressure, temperature, and ice motion. Climatological and synoptic data from the IABP buoys provide information on large-scale winds, ice drift, and deformation. Further details can be found via the IABP web page (<http://iabp.apl.washington.edu/>).

6.3.2.5 *Submarine Arctic Science Cruise (SCICEX) program*

The SCICEX program is a five-year multi-agency program that makes use of U.S. Navy nuclear submarines as research platforms. The aim of this program is to increase our fundamental understanding of processes in the Arctic Ocean. The Office of Naval Research (ONR) and the NSF co-fund this unclassified basic research mission. Further details can be found via the web page (<http://www.nsf.gov/od/opp/arctic/logistic/whatsnew.htm#scicex>).

6.3.2.6 *Program for Arctic Regional Climate Assessment (PARCA)*

PARCA is a NASA project formally initiated in 1995 by combining into one coordinated program various investigations associated with efforts starting in 1991 to assess whether airborne laser altimetry could be applied to mea-

sure ice-sheet-thickness changes. It has the prime goal of measuring and understanding the mass balance of the Greenland ice sheet. The main components of the program are:

- Periodic, airborne-laser-altimetry surveys along precise repeat tracks across all major ice-drainage basins. The first survey was completed in 1993/1994, with repeat flights along selected routes in 1995 and 1996, when flights were also made over ice caps in eastern Canada, Svalbard, and Iceland.
- Ice-thickness measurements along the same flight lines.
- Monitoring of various surface characteristics of the ice sheet using satellite radar altimetry, SAR, passive microwave, AVHRR, and scatterometer data.
- Surface-based measurements of ice motion at 30-km intervals along the 2000-meter contour completely around the ice sheet, with interpolation of local relative ice motion using interferometric SAR.
- Shallow ice coring (10-200 meters) at many locations to infer recent climate history, atmospheric chemistry, and interannual variability of snow-accumulation rates and to measure temperature and vertical ice motion at various depths.
- Investigations of SEB and factors affecting snow accumulation and surface ablation. This program is a collaborative effort with NSF and includes the installation of automatic weather stations (AWS) at the deeper drill-hole sites.
- Estimating snow-accumulation rates by model analysis of column water vapor obtained from radiosondes and TIROS Operational Vertical Sounder (TOVS) data.
- Detailed investigations of individual glaciers and ice streams responsible for much of the outflow from the ice sheet.
- Development of a thermal probe to measure various ice characteristics at selected depths in the ice sheet.
- Continuous monitoring of crustal motion using Global Positioning System receivers at coastal stations.

6.4 EOS contributions

The cryosphere plays a significant role in the global climate and hydrologic systems over a wide range of time and space scales, and cryospheric feedback processes dominate the high-latitude response of GCM climate-change experiments. Furthermore, snow cover and mountain glaciers provide important sources of freshwater and hydro-electric power for large populations, particularly in the western United States, Canada, northern Europe, and parts of Asia. Changes in the mass balance of the major ice sheets also have the potential for significant impacts on global sea level over the next few centuries.

The cryosphere, through its interactions with other components of the Earth system, contributes to the feedback processes that modify the global and regional response to climate change. At the same time, global climate change is likely to produce cryospheric changes that will have significant ecosystem and societal impacts at the regional scale. Understanding and quantifying

cryosphere-climate interactions, improving their representation in numerical models, and monitoring changes in cryospheric parameters are, therefore, the objectives of several international research programs. EOS will provide a major contribution to all three areas.

Several EOS instruments (e.g., AMSR-E, ASTER, GLAS on ICESat, MODIS) will enable improved monitoring and measurement of the cryosphere from space. These instruments either improve on current measurement capabilities or, as in the case of GLAS, will provide measurements that are not possible on a routine basis with current systems.

Examples of the type of research that will be possible with EOS are seen in the EOS IDS investigations that have a particular cryospheric focus:

- Use of CRYSYS to Monitor Global Change in Canada. Principal Investigator, Barry E. Goodison (<http://www.tor.ec.gc.ca/CRYSYS/>).

- Polar Exchange at the Sea Surface (POLES): The Interaction of Ocean, Ice, and Atmosphere. Principal Investigator, D. Andrew Rothrock (<http://psc.apl.washington.edu/POLES/>).
- Hydrology, Hydrochemical Modeling, and Remote Sensing in Seasonally Snow-covered Alpine Drainage Basins. Principal Investigator, Jeff Dozier (<http://www.ices.ucsb.edu/hydro/hydro.html>).
- Global Water Cycle: Extension across the Earth Sciences. Principal Investigator, Eric J. Barron (<http://eoswww.essc.psu.edu/gwchome.html>).
- Interdisciplinary Determination of Snow Accumulation Patterns on the Greenland Ice Sheet: Combined Atmospheric Modeling and Field and Remote-Sensing Studies. Principal Investigator, Robert Bindshadler.
- In addition, the National Snow and Ice Data Center (NSIDC), is one of eight archives participating in the Earth Observing System Data and Information System (EOSDIS) as a Distributed Active Archive Center (DAAC). The NSIDC DAAC exists to help broaden understanding of snow and ice, of their properties, characteristics, and contexts, and of their significance for human activity. The Center archives analog and

digital snow and ice data, creates and distributes data products, and maintains a large library collection in support of snow and ice research. Established in 1982, NSIDC is co-located with the WDC-A for Glaciology and, through the Polar DAAC Advisor Group (PoDag), serves an important coordinating role in snow and ice research (<http://www-nsidc.colorado.edu/NASA/GUIDE/index.html>).

The enhanced measurement capability represented by EOS will improve our ability to monitor and forecast changes in cryospheric parameters that have significant societal consequences. EOS products such as snow-water equivalence are important for water-resource planning. Similarly, information on sea-ice concentration is significant for ship routing and fisheries. EOS data will realize other major benefits to society by helping to reduce the uncertainties associated with climate change. EOS data and EOS-sponsored research activities will improve the representation of cryospheric processes in hydrological and climate models (e.g., mountain snowpacks and sea-ice dynamics), and improve our understanding of the coupling between atmosphere-ocean-cryosphere and the combined impact of cryospheric changes on sea level. Cryospheric data sets currently available for model boundary conditions or validation will be greatly enhanced by EOS satellite data and EOS-related products (Barry 1997a, b).

References

- Abdalati, W., and K. Steffen, 1995: Passive microwave-derived snow melt regions on the Greenland ice sheet. *Geophys. Res. Lett.*, **22**, 787-790.
- Ackerman, S., K. Strabala, P. Menzel, R. Frey, C. Moeller, L. Gumley, B. Baum, C. Schaaf, G. Riggs, and R. Welch, 1996: *Discriminating Clear-Sky from Cloud with MODIS*. Algorithm Theoretical Basis Document ATBD-MOD-06, NASA Goddard Space Flight Center, 119 pp. [http://modarch.gsfc.nasa.gov/MODIS/ATBD/atbd_mod06.pdf].
- Alley, R. B., and I. M. Whillans, 1984: Response of the East Antarctic ice sheet to sea-level rise. *J. Geophys. Res.*, **89**(C), 6487-6493.
- Alley, R. B., 1989: Water pressure coupling of sliding and bed deformation: I. Water system. *J. Glaciology*, **35**, 108-118.
- Alley, R. B., and I. M. Whillans, 1991: Changes in the West Antarctic ice sheet. *Science*, **254**, 959-963.
- Alley, R. B., 1992: Flow-law hypotheses for ice-sheet modeling. *J. Glaciology*, **38**, 245-256.
- Alley, R. B., 1996: Towards a hydrologic model for computerized ice sheet simulations. *Hydrological processes*, **10**, 649-660.
- Alley, R. B., 1997: Antarctica and sea-level change. *Antarctic Journal of the U.S.* (in press).
- Anderson, E. A., 1976: *A point energy balance model of a snow cover*. Office of Hydrology, National Weather Service, NOAA Tech. Rep. NWS 19, 150 pp.
- Armstrong, R. L., and M. Hardman, 1991: Monitoring global snow cover. *Proc. Western Snow Conference*, 59th Annual Meeting, 103-108.
- Armstrong, R. L., and A. Krenke, 1997: *Former Soviet Union Hydrological Snow Surveys, 1966-1990*. National Snow and Ice Data Center/World Data Center - A for Glaciology. Digital data available from nsidc@kryos.colorado.edu, University of Colorado, Boulder, Colorado.
- Arnold, N., and M. Sharp, 1992: Influence of glacier hydrology on the dynamics of a large Quaternary ice sheet. *J. Quaternary Science*, **7**, 109-124.
- Arpe, K., H. Behr, and L. Dümenil, 1997: Validation of the ECHAM4 climate model and re-analyses data in the Arctic region. *Proc. Workshop on the implementation of the Arctic Precipitation Data Archive at the Global Precipitation Climatology Centre*, WCRP-98, WMO/TD No. 804, 31-40.
- Asrar, G., and J. Dozier, 1994: *EOS: Science Strategy for the Earth Observing System*. NASA, 119 pp.
- Bales, R., R. Galarraga, and K. Elder, 1992: Distributed approach to modeling snowmelt runoff in alpine catchments. *Proc. Workshop on the Effects of Global Climate Change on Hydrology and Water Resources at the Catchment Scale*, Tsukuba, Japan, Feb. 3-6, 1992, 207-217.
- Barnett, T. P., L. Dümenil, V. Schlese, E. Roeckner, and M. Latif, 1989: The effect of Eurasian snow cover on regional and global climate variations. *J. Atmos. Sci.*, **46**, 661-685.
- Baron, J., L. E. Band, S. W. Running, and D. W. Cline, 1993: The effects of snow distribution on the hydrologic simulation of a high elevation Rocky Mountain watershed using Regional HydroEcological Simulation System, RHES Sys. *EOS. Transactions*, American Geophysical Union, Supplement, **74**, 237.
- Barry, R. G., 1996: The parameterization of surface albedo for sea ice and its snow cover. *Progr. Phys. Geogr.*, **20**, 61-77.
- Barry, R. G., 1997a: Satellite-derived data products for the polar regions. *EOS*, **78**(5), 52.
- Barry, R. G., 1997b: Cryospheric data for model validations: Requirements and status. *Ann. Glaciol.*, in press.
- Barry, R. G., and J. A. Maslanik, 1993: Monitoring lake freeze-up, breakup as a climatic index. In: R. G. Barry, B. E. Goodison and E.F. LeDrew (eds.), *Snow Watch '92*, Glaciology Data Report, GD-25. WDC-A for Glaciology, University of Colorado, Boulder, p. 66-79.
- Barry, R. G., and A. M. Brennan, 1993: Towards a permafrost information system. In: *Permafrost, Sixth International Conference Proceedings, Vol. 1*. South China University of Technology Press, Wushan Guangzhou, China.
- Barry, R. G., J. -M. Fallot, and R. L. Armstrong, 1995: Twentieth-century variability in snow cover conditions and approaches to detecting and monitoring changes: status and prospects. *Prog. in Phys. Geog.*, **19**, 520-532.
- Basist, A., D. Garrett, R. Ferraro, N. Grody, and K. Mitchell, 1996: A comparison between snow cover products derived from visible and microwave satellite observations. *J. Appl. Met.*, **35**, 163-177.
- Battisti, D. S., C. M. Bitz, and R. E. Moritz, 1997: Do general circulation models underestimate the natural variability in the Arctic climate? *J. Climate*, **10**, 1909-1920.
- Belt, D., 1997: An Arctic Breakthrough. *National Geographic*, 191(2), 36-57.
- Bentley, C. R., 1983: The west Antarctic ice sheet: diagnosis and prognosis. *Proc. Carbon Dioxide Research Conference: Carbon Dioxide, Science and Consensus*. (Berkeley Springs, W. VA., September 19-23, 1982).
- Bentley, C. R., 1985: Glaciological evidence: the Ross Sea sector. Glaciers, ice sheets, and sea level: effect of a CO₂-induced climatic change. Report of a workshop held in Seattle, Washington September 13-15, 1984, United States Department of Energy, Washington, D.C., 178-196.
- Bentley, C. R., and M. B. Giovinetto, 1991: Mass balance of Antarctica and sea level change. In: G. Weller, C. L. Wilson and B. A. B. Severin (eds.), *Polar regions and climate change*. University of Alaska, Fairbanks, p. 481-488.
- Bernier, M., and J. P. Fortin, 1998: The potential of time series of C-band SAR data to monitor dry and shallow snow cover. *IEEE Transactions on Geoscience and Remote Sensing*, **36**, 1-18.
- Bitz, C. M., D. S. Battisti, R. E. Moritz, and J. A. Beesley, 1996: Low-frequency variability in the arctic atmosphere, sea ice, and upper-ocean climate system. *J. Climate*, **9**, 394-408.
- Björge, E., O. M. Johannessen, and M. W. Miles, 1997: Analysis of merged SSMR-SSMI time series of Arctic and Antarctic sea ice parameters 1978-1995. *Geophys. Res. Lett.*, **24**, 413-416.
- Blöschl, G., R. Kirnbauer, and D. Gutknecht, 1991a: Distributed snowmelt simulations in an Alpine catchment 1. Model evaluation on the basis of snow cover patterns. *Water Resour. Res.*, **27**(12), 3171-3179.
- Blöschl, G., D. Gutknecht, and R. Kirnbauer, 1991b: Distributed snowmelt simulations in an Alpine catchment 2. Parameter study and model predictions. *Water Resour. Res.*, **27**(12), 3181-3188.
- Bourke, R. H., and R. P. Garrett, 1987: Sea ice thickness distribution in the Arctic Ocean. *Cold Regions Science and Technology*, **13**, 259-280.
- Braaten, R. O., 1997: *The Canadian snow water equivalent dataset*. Contract report prepared for Atmospheric Environment Service, Montreal, Canada, March 1997, 28 pp.
- Broecker, W. S., 1994: Massive iceberg discharges as triggers for global climate change. *Nature*, **372**, 421-424.
- Bromwich, D. H., R. -Y. Tzeng, and T. R. Parish, 1994: Simulation of the modern arctic climate by the NCAR CCMI. *J. Climate*, **7**, 1050-1069.

- Bromwich, D. H., and B. Chen, 1995: Intercomparison of simulated polar climates by global climate models (Diagnostic Subproject 8). Abstracts of the First International AMIP Scientific Conference, Monterey, California, 33.
- Brown, R. D., and P. Cote, 1992: Interannual variability in landfast ice thickness in the Canadian High Arctic, 1950-89. *Arctic*, **45**, 273-284.
- Brown, R. D., and B. E. Goodison, 1996: Interannual variability in reconstructed Canadian snow cover, 1915-1992. *J. Climate*, **9**, 1299-1318.
- Brown, R. D., 1997: Historical variability in Northern Hemisphere spring snow covered area. *Annals of Glaciology*, **25** (in press).
- Brugman, M., and P. Raistrick and A. Pietroniro, 1997: Glacier related impact of doubling CO₂ on British Columbia and Yukon. In *Proc. of Workshop on "Responding to Global Climate Change in British Columbia and the Yukon"*, February 27-28, 1997, Vancouver, B.C., E. Taylor and W. Taylor (eds.), Environment Canada and British Columbia Ministry of Environment, Lands and Parks, pp. xx-xx [M. Brugman e-mailed 26/11].
- Cavalieri, D. J., 1992: The validation of geophysical products using multisensor data. In *Microwave Remote Sensing of Sea Ice*, F.D. Carsey (ed.), Am. Geophys. Union, Washington, 233-242.
- Cavalieri, D. J., and J. C. Comiso, 1997: *Algorithm theoretical basis document (ATBD) for the AMSR sea ice algorithm*. NASA Internal Report, 44 pp. [<http://wwwghcc.msfc.nasa.gov/AMSR/atbd-amsr-seaice.pdf>]
- Cavalieri, D. J., P. Gloersen, C. L. Parkinson, J. C. Comiso, and H. J. Zwally, 1997: Observed hemispheric asymmetry in global sea ice changes. *Science*, **278**, 1104-1106.
- Cess, R. D., and 32 others, 1991: Interpretation of snow-climate feedback as produced by 17 General Circulation Models. *Science*, **253**, 888-892.
- Chahine, M. T., 1992: The hydrological cycle and its influence on climate. *Nature*, **359**, 373-380.
- Chang, A. T. C., J. L. Foster, and D. K. Hall, 1987: Nimbus-7 derived global snow cover parameters. *Annals of Glaciology*, **9**, 39-44.
- Chang, A. T. C., J. L. Foster, and A. Rango, 1991: Utilization of surface cover composition to improve the microwave determination of snow water equivalent in a mountainous basin. *Intl. J. Remote Sensing*, **12**, 2311-2319.
- Chang, A. T. C., and A. Rango, 1996: Algorithm Theoretical Basis Document (ATBD) for the AMSR snow water equivalent algorithm. NASA Internal Report, Version 1.0, November 15, 1996. [http://wwwghcc.msfc.nasa.gov/AMSR/snow_ATBD.html]
- Chen, Q., D. H. Bromwich, and L. Bai, 1997: Precipitation over Greenland retrieved by a dynamic method and its relation to cyclonic activity. *J. Climate*, **10**, 839-870.
- Cihlar J. et al., 1997: GCOS/GTOS plan for terrestrial climate-related observations. Version 2.0, June 1997, GCOS-32, WMO/TD No. 796. [http://www.wmo.ch/gcos/pub/topv2_1.html]
- Clark, P. U., 1994: Unstable behavior of the Laurentide ice sheet over deforming sediment and its implications for climate change. *Quaternary Research*, **41**, 19-25.
- Clarke, G. K. C., U. Nitsan, and W. S. B. Paterson, 1977: Strain heating and creep instability in glaciers and ice sheets. *Reviews of Geophysics and Space Physics*, **15**, 235-247.
- Clarke, G. K. C., S. G. Collins, and D. E. Thompson, 1984: Flow, thermal structure, and subglacial conditions of a surge-type glacier. *Canadian Journal of Earth Sciences*, **21**, 232-240.
- Cline, D., 1997: Snow surface energy exchanges and snowmelt at a continental, midlatitude Alpine site. *Water Resour. Res.*, **33**, 689-701.
- Cohen, J., and D. Rind, 1991: The effect of snow cover on the climate. *J. Climate*, **4**, 689-706.
- Cogley, G. J., W. P. Adams, M. A. Ecclestone, F. Jung-Rothenhauser, and C. S. L. Ommanney, 1996: Mass balance of White Glacier, Axel Heiberg Island, N.W.T., Canada, 1960-91. *J. Glaciology*, **42**(142): 548-563.
- Curry, J. A., J. L. Schramm, and E. E. Ebert, 1995: Sea ice-albedo climate feedback mechanism. *J. Climate*, **8**, 240-247.
- Curry, J. A., W. B. Rossow, D. Randall, and J. E. Schramm, 1996: Overview of Arctic cloud and radiation characteristics. *J. Climate*, **9**, 1731-1764.
- Cutler, P. M., and D. S. Munro, 1996: Visible and near-infrared reflectivity during the ablation period on Peyto Glacier, Alberta, Canada. *J. Glaciology*, **42**(141), 333-340.
- de Sève, D., M. Bernier, J.-P. Fortin, and A. Walker, 1997: Preliminary analysis of snow microwave radiometry using SSM/I passive microwave data: the case of the La Grand River watershed (Quebec). *Annals of Glaciology*, **25**, 353-361.
- Dewey, K. F., and R. Heim, Jr., 1982: A digital archive of Northern Hemisphere snow cover, November 1966 through December 1980. *Bull. Amer. Met. Soc.*, **63**, 1132-1141.
- Dozier, J., and J. Frew: Rapid calculation of terrain parameters for radiation modeling from digital elevation data. *IEEE Transaction on Geoscience and Remote Sensing*, **28**, 963-969.
- Drewry D. J., 1982: Antarctica unveiled. *New Scientist*, **1315**, 246-251.
- Duguay, C. R., and P. M. Lafleur, 1997: Monitoring ice freeze-up and break-up of shallow tundra lakes and ponds using ERS-1 SAR data. *Proceedings GER '97 - International Symposium: Geomatics in the Era of Radarsat*, May 24-30, 1997, Ottawa, Ontario (CD-ROM Vol. 1)
- Duguay, C. R., D. W. Leverington, and H. McNairn, 1997: Land cover information content of polarimetric SAR data of a boreal forest, central Yukon Territory. *Proceedings GER '97 - International Symposium: Geomatics in the Era of Radarsat*, May 24-30, 1997, Ottawa, Ontario (CD-ROM, Vol. 1).
- Duguay, C. R., W. R. Rouse, P. M. Lafleur, D. L. Boudreau, Y. Crevier, and T. Pultz, 1998: Analysis of multi-temporal ERS-1 SAR data of subarctic tundra and forest in the northern Hudson Bay Lowland and implications for climate studies. *Canadian J. of Remote Sensing* (in review).
- Easterling, D. R., P. Jamason, D. Bowman, P. Y. Hughes, and E. H. Mason, 1997: Daily snowdepth measurements from 195 stations in the United States. ORNL/CDIAC-95, NDP-059.
- Ebert, E. E., and J. A. Curry, 1993: An intermediate one-dimensional thermodynamic sea ice model for investigating ice-atmosphere interactions. *J. Geophys. Res.*, **98**(C6), 10,085-10,109.
- Elder, K., J. Dozier, and J. Michaelsen, 1991: Snow accumulation and distribution in an alpine watershed. *Water Resour. Res.*, **27**, 1541-1552.
- Fabre, A., A. Letréguilly, C. Ritz, and A. Mangeney, 1994: Greenland under changing climates: sensitivity experiments with a new three-dimensional ice-sheet model. *Annals of Glaciology*, **21**, 1-7.
- Fallot, J.-M., R. G. Barry, and D. Hoogstrate, 1997: Variations of mean cold season temperature, precipitation and snow depth during the last 100 years in the former Soviet Union (FSU). *Hydrological Sciences*, **42**, 301-327.
- Fang, X., and H. G. Stefan, 1996: Long-term lake water temperature and ice cover simulations/measurements. *Cold Regions Sci. and Technol.*, **24**, 289-304.
- Fitzharris, B., 1996: The Cryosphere: Changes and their Impacts. In: *Climate Change 1995, Impacts, Adaptations and Mitigation of Climate Change: Scientific-Technical Analyses*, Cambridge University Press, 241-265.

- Flato, G. M., and W. D. III. Hibler, 1992: Modeling pack ice as a cavitating fluid. *J. Physical Oceanography*, **22**, 626-651.
- Flato, G. M., and W. D. III. Hibler, 1995: Ridging and strength in modeling the thickness distribution of Arctic sea ice. *J. Geophys. Res.*, **100**(C9), 18,611-18,626.
- Flato, G. M., 1995: Spatial and temporal variability of Arctic ice thickness. *Annals of Glaciology*, **21**, 323-329.
- Flato, G. M., and R. D. Brown, 1996: Variability and climate sensitivity of landfast Arctic sea ice. *J. Geophys. Res.*, **101**(C10), 25,767-25,777.
- Flato, G. M., and D. Ramsden, 1997: Sensitivity of an atmospheric general circulation model to the parameterization of leads in sea ice. *Annals of Glaciology*, **25** (in press).
- Foster, D. J.Jr., and R. D. Davy, 1988: *Global snow depth climatology*. USAF publication USAFETAC/TN-88/006, Scott Air Force Base, Illinois, 48 pp.
- Foster, J. L., D. K. Hall, A. T. C. Chang, and A. Rango, 1984: An overview of passive microwave snow research and results. *Reviews of Geophysics*, **22**, 195-208.
- Foster, J., G. Liston, R. Koster, R. Essery, H. Behr, L. Dumenil, D. Verseghy, S. Thompson, D. Pollard, and J. Cohen, 1996: Snow cover and snow mass intercomparisons of general circulation models and remotely sensed datasets. *J. Climate*, **9**, 409-426.
- Frei, A., and D. A. Robinson, 1995: Northern Hemispheric snow cover extent: comparison of AMIP results to observations. *Proc. First Int'l AMIP Scientific Conference*, Monterey, CA, U.S.A., 15-19 May, 1995. WMO TD No. 732, 499-504.
- Gates, W. L., and 9 others, 1996: Climate Models - Evaluation. Chapter 5 in IPCC (1996).
- Gloersen, P., W. J. Campbell, D. J. Cavalieri, J. C. Comiso, C. L. Parkinson, and H. J. Zwally, 1992: Arctic and Antarctic Sea Ice, 1978-1987: Satellite Passive-Microwave Observations and Analysis. NASA SP-511, National Aeronautics and Space Administration, Washington, D.C., 290 pp.
- Gloersen, P., W. J. Campbell, D. J. Cavalieri, J. C. Comiso, C. L. Parkinson, and H. J. Zwally, 1993: Satellite passive microwave observations and analysis of Arctic and Antarctic sea ice, 1978-1987. *Annals of Glaciology*, **17**, 149-154.
- Goita, K., A. E. Walker, B. E. Goodison, and A. T. C. Chang, 1997: Estimation of snow water equivalent in the boreal forest using passive microwave data. Proc. GER'97 (International Symposium: Geomatics in the Era of Radarsat), May 24-30, 1997, Ottawa, Ontario (CD-ROM Vol. 1).
- Gold, L. W., and A. H. Lachenbruch, 1973: *Thermal conditions in permafrost—a review of North American literature*. Permafrost: North American contribution to the Second International Conference, Yakutsk, U.S.S.R., Washington, D.C., National Academy of Sciences, 3-25.
- Goodison, B. E., 1989: Determination of areal snow water equivalent on the Canadian prairies using microwave radiometry. *Proc. IGARSS'89*, Vancouver, July 1989, **3**, 1243-1246.
- Goodison, B. E., and A. E. Walker, 1994: Canadian development and use of snow cover information from passive microwave satellite data. *Proc. EAS/NASA International Workshop on Passive Microwave Remote Sensing Research Related to Land-Atmosphere Interactions*, St. Lary, France, January 11-15, 1993, 245-262.
- Goodison, B. E., and R. D. Brown, 1997: CRYSYS - Use of the cryosphere system for monitoring global change in Canada. *Proc. GER'97* (International Symposium: Geomatics in the Era of Radarsat), May 24-30, 1997, Ottawa, Ontario (CD-ROM Vol. 1).
- Gratton, D. J., P. J. Howarth, and D. J. Marceau, 1994: An investigation of terrain irradiance in a mountain glacier basin. *J. Glaciology*, **40**(136): 519-526.
- Groisman, P. Ya, T. R. Karl, and R. W. Knight, 1994a: Observed impact of snow cover on the heat balance and the rise of continental spring temperatures. *Science*, **263**, 198-200.
- Groisman, P. Ya, T. R. Karl, and R. W. Knight, 1994b: Changes of snow cover, temperature and radiative heat balance over the Northern Hemisphere. *J. Climate*, **7**, 1633-1656.
- Groisman, P. Ya, and D. R. Easterling, 1994: Variability and trends of total precipitation and snowfall over the United States and Canada. *J. Climate*, **7**, 184-205.
- Gutzler, D. S., and J. W. Preston, 1997: Evidence for a relationship between spring snow cover in North America and summer rainfall in New Mexico. *Geophys. Res. Lett.*, **24**, 2207-2210.
- Haeberli, W., D. Barsch, A. E. Corte, A. P. Gorbunov, S. A. Harris, M. Hoelzle, L. King, G. K. Lieb, R. S. Oedegard, J. L. Sollid, D. Trombotto, and D. Vonder Mühl, 1995: Monitoring of mountain permafrost: a review of ongoing programmes. International Permafrost Association workshop 'Our Current Understanding of Processes and Ability to Detect Global Change', Hanover, New Hampshire, 9-11 December 1995.
- Haeberli, W., 1995: Glacier fluctuations and climate change detection - operational elements of a worldwide monitoring strategy. *WMO Bulletin*, **44**, 23-31.
- Halekainen, S., 1993: An Arctic source for the Great Salinity Anomaly: A simulation of the Arctic ice-ocean system. *J. Geophys. Res.*, **98**, 16,397-16,410.
- Hall, D. K., and J. Martinec, 1985: *Remote sensing of snow and ice*. Chapman and Hall, New York, USA, 189 pp.
- Hall, D. K., 1993: Active and passive microwave remote sensing of frozen lakes for regional climate studies. *SNOW WATCH '92 - Detection Strategies for Snow and Ice*. World Data Center A for Glaciology, Glaciological Data Report GD-25, 80-85.
- Hall, D. K., D. B. Fagre, F. Klasner, G. Linebaugh, and G. E. Liston, 1994: Analysis of ERS 1 synthetic aperture radar data of frozen lakes in northern Montana and implications for climate studies. *J. Geophys. Res.*, **99**(C11), 22,473-22,482.
- Hall, D. K., G. A. Riggs, and V. V. Salomonson, 1995: Development of methods for mapping global snow cover using moderate resolution imaging spectroradiometer data. *Rem. Sens. of Environ.*, **54**, 127-140.
- Hall, D. K., and 5 others, 1996: Algorithm Theoretical Basis Document (ATBD) for the MODIS snow-, lake ice- and sea ice-mapping algorithms. NASA Internal Report, Version 3.0, November 1, 1996. [http://modarch.gsfc.nasa.gov/MODIS/ATBD/atbd_mod10.pdf].
- Hall, D. K., 1996: Remote sensing applications to hydrology: imaging radar. *Hydrological Sciences*, **41**, 609-624.
- Harbor, J., M. Sharp, L. Copland, B. Hubbard, P. Nienow, and D. Mair, 1997: Influence of subglacial drainage conditions on the velocity distribution within a glacier cross section. *Geology*, **25**, 739-742.
- Harder, M., 1997: Role of precipitation in numerical simulations of arctic sea ice and related freshwater balance. *Proc. Workshop on the implementation of the Arctic Precipitation Data Archive at the Global Precipitation Climatology Centre*, WCRP-98, WMO/TD No. 804, 26-30.
- Hartman, R. K., A. A. Rost, and D. M. Anderson, 1995: Operational processing of multi-source snow data. *Proc. Western Snow Conference*, 147-151.
- Heron, R., and M-K. Woo, 1994: Decay of a high Arctic lake-ice cover: observations and modeling. *J. Glaciology*, **40**, 283-292.
- Hibler, W. D. III, and J. E. Walsh, 1982: On modeling seasonal and interannual fluctuations of Arctic sea ice. *J. Physical Oceanography*, **12**, 1514-1523.
- Hibler, W. D. III., 1979: A dynamic thermodynamic sea ice model. *J. Physical Oceanography*, **9**, 817-846.

- Hibler, W. D. III., 1984: *Ice dynamics. Sea ice, dynamics, pressure ridges*. U.S. Army CRREL, Monograph 84-3, Vol. 3, Hanover, N.H., U.S. Army CRREL, 52 pp.
- Hughes, M. G., and D. A. Robinson, 1996: Historical snow cover variability in the Great Plains region of the USA: 1910 to 1993. *Int. J. Climatology*, **16**, 1005-1018.
- Hughes, M. G., A. Frei, and D. A. Robinson, 1996: Historical analysis of North American snow cover extent: merging satellite and station-derived snow cover observations. *Proc. 53rd Eastern Snow Conference*, Williamsburg, Virginia, 21-31.
- Huybrechts, P., 1990: The Antarctic ice sheet during the last glacial-interglacial cycle: a three-dimensional experiment. *Annals of Glaciology*, **14**, 115-119.
- Huybrechts, P., A. Letréguilly, and N. Reeh, 1991: The Greenland Ice Sheet and greenhouse warming. *Palaeogeography, Palaeoclimatology, Palaeoecology*, **89**, 399-412.
- Huybrechts, P., 1993: Glaciological modeling of the late Cenozoic East Antarctic ice sheet: stability or dynamism? *Geografiska Annaler*, **75A**, 221-238.
- Huybrechts, P., and J. Oerlemans, 1988: Evolution of the East Antarctic ice sheet: a numerical study of thermo-mechanical response patterns with changing climate. *Annals of Glaciology*, **11**, 52-59.
- Iken, A., 1981: The effect of the subglacial water pressure on the sliding velocity of a glacier in an idealised numerical model. *J. Glaciology*, **27**, 407-421.
- Iken, A., and R. A. Bindschadler, 1986: Combined measurement of subglacial water pressure and surface velocity of Findelengletscher, Switzerland: conclusions about drainage system and sliding mechanism. *J. Glaciology*, **32**, 101-119.
- Imbrie, J., and 18 others, 1993: On the structure and origin of major glaciation cycles: 2. The 100,000-year cycle. *Paleoceanography*, **8**, 699-735.
- Ip, C. F., W. D. III. Hibler, and G. M. Flato, 1991: On the effect of rheology on seasonal sea-ice simulations. *Annals of Glaciology*, **15**, 17-25.
- Ip, C. F., 1993: *Numerical investigation of different rheologies on sea ice dynamics*. Ph.D. thesis, Thayer School of Engineering, Dartmouth College, Hanover, N.H., 242 pp.
- IPCC, 1990: *Climate Change - The IPCC Scientific Assessment*. J. T. Houghton, G. J. Jenkins and J. J. Ephraums (eds.), Cambridge University Press, Cambridge, UK, 365 pp.
- IPCC, 1996: *Climate Change 1995: The Science of Climate Change*. Houghton, J. T., L. G. Meira Filho, B. A. Callander, N. Harris, A. Kattenberg, and K. Maskell (eds.), Contribution of WGI to the Second Assessment Report of the Intergovernmental Panel on Climate Change. Cambridge University Press, Cambridge, UK, 572 pp.
- Jacobs, S. S., H. H. Helmer, C. S. M. Doake, A. Jenkins, and R. M. Frohlich, 1992: Melting of ice shelves and the mass balance of Antarctica. *J. Glaciology*, **38**, 375-387.
- Jeffries, M. O., K. Morris, and G. E. Liston, 1996: A method to determine lake depth and water availability on the north slope of Alaska with spaceborne imaging radar and numerical ice growth modeling. *Arctic*, **49**(4), 367-374.
- Jeffries, M. O., K. Morris, W. F. Weeks, and H. Wakabayashi, 1994: Structural and stratigraphic features and ERS 1 synthetic radar backscatter characteristics of ice growing on shallow lakes in NW Alaska, winter 1992-1992. *J. Geophys. Res.*, **99**(C11), 22,459-22,471.
- Johannessen, M., and A. Henriksen, 1978: Chemistry of snowmelt: changes in concentration during melting. *Water Resour. Res.*, **14**, 615-619.
- Johannessen, O. M., M. Miles, and E. Björge, 1995: The Arctic's shrinking sea ice. *Nature*, **376**, 126-127.
- Joughin, I. R., D. P. Winebrenner, and M. A. Fahnestock, 1995: Observations of ice-sheet motion in Greenland using satellite radar interferometry. *Geophys. Res. Lett.*, **22**, 571-574.
- Kamb, B., 1987: Glacier surge mechanism based on linked cavity configuration of the basal water conduit system. *J. Geophys. Res.*, **92**, 9083-9100.
- Kamb, B., and H. Engelhardt, 1991: Antarctic ice stream B: conditions controlling its motions and interactions with the climate system. *IAHS Publication 208*, 145-154.
- Kane, D. L., L. D. Hinzman, and J. P. Zarling, 1991: Thermal response of the active layer to climatic warming in a permafrost environment. *Cold Regions Science and Technology*, **19**, 111-122.
- Kite, G. W., 1991: A watershed model using satellite data applied to a mountain basin in Canada. *J. Hydrol.*, **128**(1-4), 157-169.
- Knox, J. C., 1993: Large increases in flood magnitude in response to modest changes in climate. *Nature*, **361**, 430-432.
- Koch, E., and E. Rüdell, 1990: Mögliche Auswirkungen eines verstärkte Treibhauseffekte auf die Schneeverhältnisse in Österreich. *Wetter und Leben*, **45**, 137-153.
- Koerner, R. M., 1989: Ice core evidence for extensive melting of the Greenland Ice Sheet in the last interglacial. *Science*, **244**, 964-968.
- Koster, E. A., 1993: Introduction - Present global change and permafrost, within the framework of the International Geosphere-Biosphere Programme. *Permafrost and Periglacial Processes*, **4**, 95-98.
- Kuusisto, E., 1993: Lake ice observations in Finland in the 19th and 20th Century: any message for the 21st? In: R.G. Barry, B.E. Goodison and E.F. LeDrew (eds.), *Snow Watch '92*, Glaciology Data Report, GD-25. WDC-A for Glaciology, University of Colorado, Boulder, 57-65.
- Kwok, R., D. A. Rothrock, H. L. Stern, and G. F. Cunningham, 1995: Determination of the age distribution of sea ice from Lagrangian observations of ice motion. *IEEE Transactions on Geoscience and Remote Sensing*, **33**, 392-400.
- Lachenbruch, A. H., J. H. Sass, B. V. Marshall, and T. H. Jr. Moses, 1982: Permafrost, heat flow, and the geothermal regime at Prudhoe Bay, Alaska. *J. Geophys. Res.*, **87**(B11), 9301-9316.
- Lachenbruch, A. H., and B. V. Marshall, 1986: Changing climate - geothermal evidence from permafrost in the Alaskan arctic. *Science*, **234**, 689-696.
- Lavoie, C., and S. Payette, 1992: Black Spruce growth forms as a record of changing winter environment at treeline, Quebec, Canada. *Arctic and Alpine Res.*, **24**, 40-49.
- Lawby, C. P., D. J. Smith, C. P. Laroque, and M. M. Brugman, 1995: Glaciological studies at Rae Glacier, Canadian Rockies. *Physical Geography*, **15**(5), 425-441.
- Leathers, D. J., and D. A. Robinson, 1993: The association between extremes in North American snow cover extent and United States temperatures. *J. Climate*, **6**, 1345-1355.
- Ledley, T. S., 1991: Snow on sea ice: competing effects in shaping climate. *J. Geophys. Res.*, **96**, 17,195-17,208.
- Ledley, T. S., 1993: Variations in snow on sea ice: a mechanism for producing climate variations. *J. Geophys. Res.*, **98**(D6), 10,401-10,410.
- Lemke, P., W. B. Owens, and W. D. III. Hibler, 1990: A coupled sea-ice mixed-layer pycnocline model for the Weddell Sea. *J. Geophys. Res.*, **95**, 9513-9525.
- Lemke, P., L. Anderson, R. Barry, and V. Vuglinsky (eds.), 1996: *Proceedings of the ACSYS Conference on the Dynamics of the Arctic Climate System*, Goteborg, Sweden, 7-10 November 1994, WCRP-94, WMO/TD 602, no. 760, 483 pp.
- Letréguilly, A., P. Huybrechts, and N. Reeh, 1991: Steady-state characteristics of the Greenland ice sheet under different climates. *J. Glaciology*, **37**, 149-157.

- Leverington, D. W., and C. R. Duguay, 1996. Evaluation of three supervised classifiers in mapping "depth to late-summer frozen ground", central Yukon Territory. *Canadian J. Remote Sensing*, **22**, 163-174.
- Leverington, D. W., and C. R. Duguay, 1997: A neural network method to determine the presence or absence of permafrost near Mayo, Yukon Territory, Canada. *Permafrost and Periglacial Processes*, **8**, 205-215.
- Lewkowicz, A. G., and C. R. Duguay, 1995: Assessment of SPOT panchromatic imagery in the detection and identification of permafrost features, Fosheim Peninsula, Ellesmere Island, N.W.T. *Proceedings of the 17th Canadian Symposium on Remote Sensing*, Saskatoon, Saskatchewan, June 13-15, pp. 8-14.
- Lindsay, R. W., and D. A. Rothrock, 1994: Arctic sea ice albedo from AVHRR. *J. Climate*, **7**, 1737-1749.
- Liu, A. K., S. Martin, and R. Kwok, 1997: Tracking of ice edges and ice floes by wavelet analysis of SAR images. *J. Atmos. Ocean. Tech.*, **14**, 1187-1198.
- Loth, B., H.-F. Graf, and J. M. Oberhuber, 1993: Snow cover model for global climate simulations. *J. Geophys. Res.*, **98**(D6), 10,451-10,464.
- Lynch-Stieglitz, M., 1994: The development and validation of a simple snow model for the GISS GCM. *J. Climate*, **7**, 1842-1855.
- MacAyeal, D. R., 1992: Irregular oscillations of the West Antarctic ice sheet. *Nature*, **359**, 29-32.
- MacAyeal, D. R., 1993a: A low-order model of growth/purge oscillations of the Laurentide Ice Sheet. *Paleoceanography*, **8**, 767-773.
- MacAyeal, D. R., 1993b: Binge/purge oscillations of the Laurentide Ice Sheet as a cause of the North Atlantic's Heinrich events. *Paleoceanography*, **8**, 775-784.
- Marks, D., and J. Dozier, 1992: Climate and energy exchange at the snow surface in the alpine region of the Sierra Nevada. 2. Snow cover energy balance. *Water Resour. Res.*, **28**, 3043-3054.
- Markus, T., and D. J. Cavalieri, 1997: Snow depth distribution over sea ice in the Southern Ocean from satellite passive microwave data. American Geophysical Union Antarctic Research Series. M. Jeffries (ed.). (in press)
- Marsh, P., 1991: Water flux in melting snow covers. In: *Advances in Porous Media, Vol. 1*. M.Y. Corapcioglu (ed.), Elsevier, Amsterdam, 61-124.
- Marshall, S., J. O. Roads, and G. Glatzmaier, 1994: Snow hydrology in a general circulation model. *J. Climate*, **7**, 1251-1269.
- Martin, S., K. Steffen, J. Comiso, D. Cavalieri, M. R. Drinkwater, and B. Holt, 1992: Microwave remote sensing of polynyas. In: Carsey, F. D. (ed.), *Microwave remote sensing of sea ice*, Washington, DC, American Geophysical Union, 1992, 303-311.
- Martinez, J., and A. Rango, 1991: Indirect evaluation of snow reserves in mountain basins. In: H. Bergmann, H. Lang, W. Frey, D. Issler, and B. Salm (eds.), International Association of Hydrological Sciences. IAHS/AISH Publication 602, no.205. *Proc. International Symposium on Snow, Hydrology and Forests in High Alpine Areas*, Vienna, 11-14 August 1991, 111-119.
- Martinez, J., K. Seidel, U. Burkart, R. Baumann, H. Bergmann, H. Lang, W. Frey, D. Issler, and B. Salm (eds.), 1991: Areal modeling of snow water equivalent based on remote sensing techniques. Snow, hydrology and forests in high alpine areas. Proceedings of an international symposium held during the 20th General Assembly of the International Union of Geodesy and Geophysics at Vienna, 11-24 August 1991, IAHS Press, Wallingford, Oxfordshire, 121-129.
- Maslanik, J. A., and R. G. Barry, 1987: Lake ice formation and breakup as an indicator of climate change: potential for monitoring using remote sensing techniques. In: S.I. Solomon, M. Beran, and W. Hogg (eds.), *Influence of Climate Change and Climatic Variability on the Hydrologic Regime and Water Resources*, Proceedings of the Vancouver Symposium, IAHS Publication no. 168, 153-161.
- Matson, M., 1991: NOAA satellite snow cover data. *Palaeogeography, Palaeoclimatology, Palaeoecology* (Global and Planetary Change Section), **90**(1-3), 213-218.
- Matson, M., C. F. Ropelewski, and M. S. Varnadore, 1986: *An atlas of satellite-derived Northern Hemisphere snow cover frequency*, National Weather Service, Wash., D.C., 75 pp.
- Maykut, G. A. 1982: Large-scale heat exchange and ice production in the central Arctic. *J. Geophys. Res.*, **87**(C10), 7971-7984.
- Maykut, G. A., 1978: Energy exchange over young sea ice in the central Arctic. *J. Geophys. Res.*, **83**(C7), 3646-3658.
- McGinnis, D. L., and R. G. Crane, 1994: A multivariate analysis of Arctic climate in GCMs. *J. Climate*, **7**, 1240-1250.
- McLaren, A. S., J. S. Walsh, R. H. Bourke, R. L. Weaver, and W. Wittmann, 1992: Variability in sea-ice thickness over the North Pole from 1977 to 1990. *Nature*, **358**, 224-226.
- Meehl, G. A., 1994: Influence of the land surface in the Asian summer monsoon: external conditions versus internal feedbacks. *J. Climate*, **7**, 1033-1049.
- Meier, M. F., 1983: Snow and ice in a changing hydrological world. *Hydrological Sciences Journal*, **28**, 3-22.
- Meier, M. F., 1984: Contribution of small glaciers to global sea level rise. *Science*, **226**, 1418-1421.
- Mercer, J. H., 1968: *Antarctic ice and Sangamon sea level*. International Association of Hydrological Sciences, Publication No. 179, 217-225.
- Morassutti, M. P., 1989: Surface albedo parameterization in sea-ice models. *Prog. Physical Geography*, **13**, 348-366.
- Morris, K., M. O. Jeffries, and W. F. Weeks, 1995: Ice processes and growth history on arctic and sub-arctic lakes using ERS-1 SAR data. *Polar Record*, **31**(177), 115-128.
- Morrissey, L. A., L. Strong, and D. H. Card, 1986: Mapping permafrost in the boreal forest with thematic mapper satellite data. *Photogrammetric Engineering and Remote Sensing*, **52**, 1513-1520.
- Moritz, R. E., J. A. Curry, A. S. Thorndike, and N. Untersteiner, 1993: *SHEBA—a research program on the Surface Heat Budget of the Arctic Ocean*. Arctic System Science, Ocean-Atmosphere-Ice Interactions (ARCSS OAI) Science Management Office, 34 pp.
- Munro, D. S., 1990: Comparison of melt energy computations and ablatometer measurements on melting ice and snow. *Arctic and Alpine Research*, **22**, 153-162.
- Munro, D. S., and G. J. Young, 1982: An operational net shortwave radiation model for glacier basins. *Water Resour. Res.*, **18**(2), 220-230.
- Oerlemans, J., 1986: Glaciers as indicators of a carbon dioxide warming. *Nature*, **320**, 607-609.
- Oerlemans, J., 1994: Quantifying global warming from the retreat of glaciers. *Science*, **264**, 243-245.
- Ohmura, A., M. Wild, and L. Bengtsson, 1996: A possible change in mass balance of the Greenland and Antarctic ice sheets in the coming century. *J. Climate*, **9**, 2124-2135.
- Oke, T. R., 1987: *Boundary Layer Climates*. Second Edition, Routledge, 435 pp.
- Osterkamp, T. E. 1984. Potential impact of a warmer climate on permafrost in Alaska. In: McBeath, J.H. (ed.), *Potential effects of carbon dioxide-induced climatic changes in Alaska*, The proceedings of a conference. Fairbanks, University of Alaska, March 1984, 106-113.

- Osterkamp, T. E., 1994: Evidence for warming and thawing of discontinuous permafrost in Alaska. *EOS*, **75**, 85.
- Palecki, M. A., and R. G. Barry, 1986: Freeze-up and break-up of lakes as an index of temperature changes during the transition seasons: A case study in Finland. *J. Climate and Appl. Meteorology*, **25**, 893-902.
- Parkinson, C. L., 1995: Recent sea-ice advances in Baffin Bay/Davis Strait and retreats in the Bellinshausen Sea. *Annals of Glaciology*, **21**, 348-352.
- Parkinson, C. L., and W. M. Washington, 1979: A large-scale numerical model of sea ice. *J. Geophys. Res.*, **84**(C1), 311-337.
- Parkinson, C. L., J. C. Comiso, H. J. Zwally, D. J. Cavalieri, P. Gloersen, and W. J. Campbell, 1987: Arctic Sea Ice, 1973-1976: Satellite Passive-Microwave Observations, NASA SP-489, National Aeronautics and Space Administration, Washington, D.C., 296 pp.
- Paterson, W. S. B., 1994: *The Physics of Glaciers*, Third Edition. Pergamon Press, Oxford.
- Paterson, W. S. B., 1993: World sea level and the present mass balance of the Antarctic ice sheet. In: W.R. Peltier (ed.), *Ice in the Climate System*, NATO ASI Series, I12, Springer-Verlag, Berlin, 131-140.
- Peddle, D. R., G. M. Foody, A. Zhang, S. E. Franklin, and E. F. LeDrew, 1994: Multi-source image classification II: An empirical comparison of evidential reasoning and neural network approaches. *Can. J. Remote Sensing*, **20**, 396-407.
- Pelto, M. S., 1996: Annual net balance of North Cascade Glaciers, 1984-94. *J. Glaciology*, **42**, 3-9.
- Pollard, D., and S. L. Thompson, 1994: Sea-ice dynamics and CO₂ sensitivity in a global climate model. *Atmosphere-Ocean*, **32**(2), 449-467.
- Pomeroy, J. W., P. Marsh, and D. M. Gray, 1997: Application of a distributed blowing snow model to the Arctic. *Hydrological Processes*, **11**, 1451-1464.
- Prinsenberg, S. J. 1988: Ice-cover and ice-ridge contributions to the freshwater contents of Hudson Bay and Foxe Basin. *Arctic*, **41**, 6-11.
- Prowse, T. D., 1990: Northern hydrology: an overview. In: Northern Hydrology: Canadian Perspectives, T. D. Prowse and C. S. L. Ommanney (eds.), *NHRI Science Report No. 1*, National Hydrology Research Institute, Environment Canada, Saskatoon, Saskatchewan, 1-36.
- Randall, D. A., and 26 others, 1994: Analysis of snow feedbacks in 14 general circulation models. *J. Geophys. Res.*, **99**(D10), 20,757-20,771.
- Rango, A., 1993: Snow hydrology processes and remote sensing. *Hydrological Processes*, **7**, 121-138.
- Reeh, N., 1989: *Dynamic and climatic history of the Greenland Ice Sheet*. Chapter 14 in Quaternary Geology of Canada and Greenland, R.J. Fulton (ed.); Geological Survey of Canada, Geology of Canada, no. 1, 795-822.
- Reycraft, J., and W. Skinner, 1993: Canadian lake ice conditions: an indicator of climate variability. *Climatic Perspectives*, **15**, 9-15.
- Rignot, E., and J. Way, 1994. "Monitoring freeze-thaw cycles along north-south Alaskan transects using ERS-1 SAR." *Remote Sensing of Environment*, **49**, 131-137.
- Rignot, E., K. C. Jezek, and H. G. Sohn, 1995: Ice flow dynamics of the Greenland Ice Sheet from SAR. *Geophysical Res. Lett.*, **22**, 575-578.
- Rind, D., R. Healy, C. Parkinson, and D. Martinson, 1995: The role of sea ice in 2 x CO₂ climate model sensitivity. Part I: The total influence of sea ice thickness and extent. *J. Climate*, **8**, 449-463.
- Robinson, D. A., K. F. Dewey, and R. R. Heim, 1993: Global snow cover monitoring: an update. *Bull. Amer. Meteorol. Soc.*, **74**, 1689-1696.
- Rosenthal, W., and J. Dozier, 1996: Automated mapping of montane snow cover at subpixel resolution from the LANDSAT Thematic Mapper. *Water Resour. Res.*, **32**, 115-130.
- Rouse, W. R., and 9 others, 1997: Effects of climate changes on the fresh waters of Arctic and subarctic North America. *Hydrological Processes*, **11**, 873-902.
- Scharfen, G., R. G. Barry, D. A. Robinson, G. Kukla, and M. C. Serreze, 1987: Large-scale patterns of snow melt on Arctic sea ice mapped from meteorological satellite imagery. *Annals of Glaciology*, **9**, 1-6.
- Sellman, P. V., W. F. Weeks, and W. J. Campbell, 1975: *Use of side-looking airborne radar to determine lake depth on the Alaskan North Slope*. Special Report No. 230. Hanover, New Hampshire: Cold Regions Research and Engineering Laboratory.
- Shi, J. C., J. Dozier, and R. E. Davis, 1990: Simulation of snow-depth estimation from multi-frequency radar. Proc. IGARSS 1990, IEEE No. 90CH2825-8, 1129-1132.
- Shine, K. P., and R. G. Crane, 1984: The sensitivity of a one-dimensional thermodynamic sea ice model to changes in cloudiness. *J. Geophys. Res.*, **89**, 10,615-10,622.
- Steffen, K., and A. Ohmura, 1985: Heat exchange and surface conditions in North Water, northern Baffin Bay. *Annals of Glaciology*, **6**, 178-181.
- Stern, H. L., D. A. Rothrock, and R. Kwok, 1995: Open water production in Arctic sea ice: Satellite measurements and model parameterizations. *J. Geophys. Res.*, **100**(C10), 20,601-20,612.
- Stieglitz, M., D. Rind, J. Famiglietti, and C. Rosenzweig, 1997: An efficient approach to modeling the topographic control of surface hydrology for regional and global climate modeling. *J. Climate*, **10**, 118-137.
- Sturm, M., and J. B. Johnson, 1991: Natural convection in the subarctic snow cover. *J. Geophys. Res.*, **96**(B7), 11,657-11,671.
- Sturm, M., J. Holmgren, and G. E. Liston, 1995: A seasonal snow cover classification system for local to global applications. *J. Climate*, **8**, 1261-1283.
- Tao, X., J. Walsh, and W. Chapman, 1996: An assessment of global climate model simulations of arctic air temperatures. *J. Climate*, **9**, 1060-1076.
- Tarboton, D. G., M. J. Al-Adhami, and D. S. Bowles, 1991: A preliminary comparison of snowmelt models for erosion prediction. *Proc. 59th Western Snow Conference*, 79-90.
- Thompson, S. L., and D. Pollard, 1997: Greenland and Antarctic mass balances for present and doubled atmospheric CO₂ from the GENESIS Version-2 global climate model. *J. Climate*, **10**, 871-900.
- Thorndike, A. S., D. A. Rothrock, G. A. Maykut, and R. Colony, 1975: The thickness distribution of sea ice. *J. Geophys. Res.*, **80**, 4501-4513.
- Titus, J. G., and V. K. Narayanan, 1995: The probability of sea level rise. United States Environmental Protection Agency, EPA 230-R-95-008.
- Van den Broeke, M. R., 1996: The atmospheric boundary layer over ice sheets and glaciers. Utrecht, Universiteit Utrecht, 178 pp.
- Van den Broeke, M. R., and R. Bintanja, 1995: The interaction of katabatic wind and the formation of blue ice areas in East Antarctica. *J. Glaciology*, **41**, 395-407.
- Van de Wall, R. S. W., J. Oerlemans, and J. C. van der Hage, 1992: A study of ablation variations on the tongue of Hintereisferner, Austrian Alps. *J. Glaciology*, **38**, 319-324.
- Vance, R. E., R. W. Mathewes, and J. J. Clague, 1992: 7000 year record of lake-level change on the northern Great Plains: a high resolution proxy of past climate. *Geology*, **20**, 879-882.

- Vachon, P. W., D. Geudtner, K. Mattar, A. L. Gray, M. Brugman, and I. Cumming, 1996: Differential interferometry measurements of Athabasca and Saskatchewan glacier flow rate. *Can. J. Remote Sensing*, **22**, 287-296.
- Verbitsky, M. Ya., and B. Saltzman, 1995: Behavior of the East Antarctic ice sheet as deduced from a coupled GCM/ice-sheet model. *Geophys. Res. Lett.*, **22**, 2913-2916.
- Vernekar, A. D., J. Zhou, and J. Shukla, 1995: The effect of Eurasian snow cover on the Indian monsoon. *J. Climate*, **8**, 248-266.
- Verseghy, D., 1991: CLASS A Canadian land surface scheme for GCMs. I: Soil model. *Intl. J. Climatology*, **11**, 111-133.
- Walker, A. E., and M. R. Davey, 1993: Observation of Great Slave Lake ice freeze-up and break-up processes using passive microwave satellite data. *Proc. 16th Canadian Symp. on Remote Sensing*, Sherbrooke, Quebec, 7-10 June, 1993, 233-238.
- Walker, A. E., and B. E. Goodison, 1993: Discrimination of wet snow cover using passive microwave satellite data. *Annals of Glaciology*, **17**, 307-311.
- Walland, D. J., and I. Simmonds, 1996: Sub-grid-scale topography and the simulation of Northern Hemisphere snow cover. *Intl. J. Climatology*, **16**, 961-982.
- Walsh, J. E., 1978: *A data set of northern hemisphere sea ice extent, 1953-76*. Glaciological Data. Report GD-2, National Snow and Ice Data Center, University of Colorado, Boulder, CO., 49-51.
- Walsh, J. E., and W. L. Chapman, 1990: Arctic contribution to upper-ocean variability in the North Atlantic. *J. Climate*, **3**, 1462-1473.
- Walsh, J. E., and R. G. Crane, R., 1992: A comparison of GCM simulations of Arctic climate. *Geophys. Res. Lett.*, **19(1)**, 29-32.
- Walsh, J. E., 1995: Continental snow cover and climate variability. In: *Natural Climate Variability on Decadal-to-Century Time Scales*. National Academy Press, Washington, D.C., 49-58.
- Washburn, A. L., 1973: *Periglacial processes and environments*. Edward Arnold, London, 320 pp.
- WCRP, 1994: Initial implementation plan for the Arctic Climate System Study (ACSYS). WCRP-85 (WMO/TD-No. 627), Geneva.
- WCRP, 1997: GCOS/GTOS Plan for Terrestrial Climate-Related Observations. Version 2.0. *GCOS*, **32** (WMO/TD No. 796), Geneva.
- Weaver, A. J., and T. M. C. Hughes, 1994: Rapid interglacial climate fluctuations driven by North Atlantic ocean circulation. *Nature*, **367**, 447-450.
- Weertman, J., 1972: General theory of water flow at the base of a glacier or ice sheet. *Reviews of Geophysics and Space Physics*, **10**, 287-333.
- Welch, H. E., 1992: Energy flow through the marine ecosystem of the Lancaster Sound region, Arctic Canada. *Arctic*, **45**, 343.
- Whillans, I. M., 1981: Reaction of the accumulation zone portions of glaciers to climatic change. *J. Geophys. Res.*, **86(C5)**, 4274-4282.
- Whillans, I. M., M. Jackson, and Y-H. Tseng, 1993: Velocity pattern in a transect across ice stream B, Antarctica. *J. Glaciology*, **39**, 562-572.
- Williams, G. P., 1971: Predicting the date of lake ice breakup. *Water Resour. Res.*, **7**, 323-333.
- Wolford, R. A., R. C. Bales, and S. Sorooshian, 1996: Development of a hydrochemical model for seasonally snow-covered alpine watersheds: application to Emerald Lake watershed, Sierra Nevada, California. *Water Resour. Res.*, **32**, 1061-1074.
- Woo, M -K., and P. Steer, 1986: Monte Carlo simulation of snow depth in a forest. *Water. Resour. Res.*, **22**, 864-868.
- Wynne, R. H., M. K. Clayton, T. M. Lillesand, and D. C. Rodman, 1996: Determinants of temporal coherence in the satellite derived 1978-1994 ice breakup dates of lakes on the Laurentian Shield. *Limnology and Oceanography*, **41**, 832-838.
- Xu, H., J. O. Bailey, E. C. Barrett, and R. E. J. Kelly, 1993: Monitoring snow area and depth with integration of remote sensing and GIS. *Intl. J. Remote Sensing*, **14**, 3259-3268.
- Yang, Z -L., R. E. Dickinson, A. Robock, and K. Ya. Vinnikov, 1997: Validation of the snow submodel of the Biosphere-Atmosphere Transfer Scheme with Russian snow cover and meteorological observational data. *J. Climate*, **10**, 353-373.
- Young, G. J., M. C. English, and C. Hopkinson, 1996: *Changes in glacier dimensions 1951-1994 in the Bow River Basin above Banff*. CRYSYS Collaborative Research Agreement Report to Atmospheric Environment Service, Cold Regions Research Centre, Wilfrid Laurier University, 35 pp.
- Zhang, T., T. E. Osterkamp, and K. Stamnes, 1996: Influence of the depth hoar layer of the seasonal snow cover on the ground thermal regime. *Water Resour. Res.*, **32**, 2075-2086.
- Zuo, Z., and J. Oerlemans, 1996: Modeling albedo and specific balance of the Greenland Ice Sheet: calculations for the Sondre Stromfjord transect. *J. Glaciology*, **42(141)**, 305-317.
- Zwally, H. J., J. C. Comiso, C. L. Parkinson, W. J. Campbell, F. D. Carsey, and P. Gloersen, 1983: *Antarctic Sea Ice, 1973-1976: Satellite Passive-Microwave Observations*. NASA SP-459, National Aeronautics and Space Administration, Washington, D.C., 206 pp.

Chapter 6 Index

- ACSYS 274, 297
 AIRS/AMSU/HSB 292
 AIRSAR 285
 AMIP 271, 282, 289
 AMSR-E 283, 289, 292-293, 298
 ASTER 275, 285, 288, 290, 294-296, 298
 AVHRR 284-288, 291, 294-298
 AVIRIS 289
 AWS 298
 BOREAS 297
 calibration 273, 292
 CALM 285
 carbon dioxide (CO₂) 270-271, 274, 279, 286, 297
 CERES 295, 297
 CLASS 275
 convection 279
 COV 266
 cryosphere 263-267, 271, 278-279, 281, 284, 286, 298-299
 cryosphere albedo 264
 cryosphere-EOS instruments-measurements 264-266, 287-298
 cryosphere-EOS interdisciplinary investigations 298
 cryosphere-freshwater 279
 cryosphere modeling 264, 271-278, 280-281
 cryosphere-related programs-ACSYS, BOREAS, PARCA, SCICEX, SHEBA 297
 cryosphere-sea-level rise 263
 cryosphere-thermal diffusivity 264
 cryosphere volume 264-266
 cryospheric climate linkage 264, 278-279
 cryospheric variability 266, 281-287
 CRYSYS 268, 290, 298
 DAS 279
 DEM 273, 289
 DMSP 291
 ecosystem 267, 270, 283, 297-298
 EGIG 270
 EOSDIS 299
 ERBE 281
 ERS 285, 288, 291, 294-297
 ETM+ 294-295
 freshwater cycle 279
 frozen ground (permafrost) 269, 275, 295-296
 GCOS/GTOS TOP 281
 GEBA 268
 GENESIS 268, 270, 277
 GEWEX 275
 GGD 285
 GISP 270
 GISS 217, 280
 GLAS 295
 GLIMS 278
 GOES 290
 GSFC 297
 HSB 292
 humidity 292
 IABP 297
 ice mass balance 274, 277, 283, 291-293
 ice sheets 263-264, 266, 269-270, 275-278, 285-287, 296-298
 ICESat 278, 286, 292, 295-296, 298
 interannual variability 265-268, 293, 298
 IPCC 263, 267, 271, 274, 276-277, 281-282
 IR 294
 JERS 288, 294
 lake ice 263, 268-269, 274-275, 284, 293-295
 Landsat-7 295
 MAAT 269
 measurement strategy 284
 MISR 288, 294
 modeling 270, 273-278, 282, 289, 296-299
 MODIS 272, 284, 288, 291-295, 298
 NASA 299
 National Snow and Ice Data Center 299
 NESDIS 282, 288
 NH 280, 283
 NIR 294
 NOAA 281-283, 288
 NSF 285, 297-298
 NSIDC 299
 NWP 74, 287-290
 OLR 279-281
 ONR 297
 PAR 265, 267
 PARCA 297
 POLES 299
 precipitation 263, 266, 268, 270-273, 280-283
 RADARSAT 278, 282-283, 285, 288, 291-296
 RGPS 283
 river ice 268-269
 SAR 264, 273, 275, 278, 282-298
 SCA 266-267, 272, 282-290
 SCICEX 297
 sea ice 267-268, 273-274, 283-284, 291-293
 SEB 264, 271, 279-280, 284, 291, 298
 SHEBA 297
 SIMIP 274
 snow cover 263-267, 271-273, 281-283, 287
 snow-water equivalence 267, 272-273, 281-290, 295, 297
 SPOT 294
 SSM/I 282, 288, 294-296
 surface energy balance (SEB) 270, 279, 280, 291
 SW 267, 279-280
 SWE 290
 SWIR 295-296
 TIR 294, 296
 TM 284-290, 295-296
 topography 271-273, 277-278, 286-289, 295-296
 TOVS 298
 USAF 289
 validation 272, 274-275, 281-282, 287, 289-291, 297, 299
 VHRR 281
 VIS 294
 VNIR 295-296
 WCRP 274, 281, 288
 WDC-A 293, 297, 299
 wind 269, 272

Ozone and Stratospheric Chemistry

LEAD AUTHOR

M. R. Schoeberl

CONTRIBUTING AUTHORS

A. R. Douglass
J. C. Gille
J. A. Gleason
W. R. Grose
C. H. Jackman
S. T. Massie
M. P. McCormick
A. J. Miller
P. A. Newman
L. R. Poole
R. B. Rood
G. J. Rottman
R. S. Stolarski
J. W. Waters

CHAPTER 7 CONTENTS

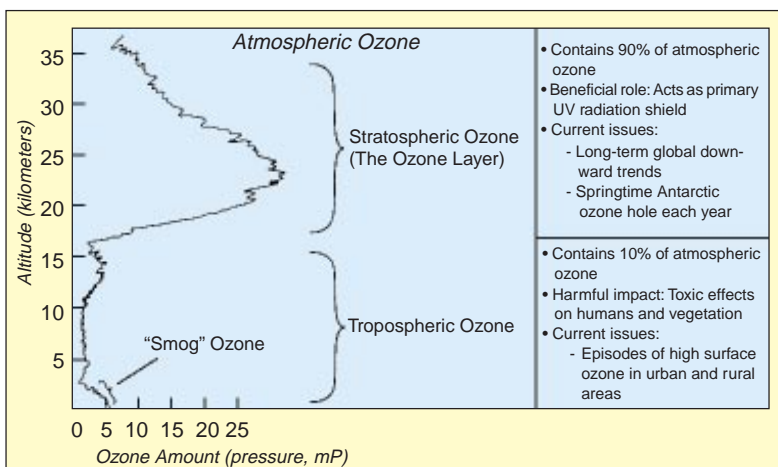
7.1 Stratospheric ozone - background	311
7.1.1 Why is understanding stratospheric ozone important?	311
7.1.1.1 Location of the ozone layer and climatology	311
7.1.1.2 Ozone and UV—biological threat	311
7.1.1.3 Ozone and climate change	311
7.1.2 Observed ozone changes	312
7.1.2.1 Polar ozone changes	312
7.1.2.2 Mid-latitude ozone loss	313
7.1.3 The stratospheric ozone distribution	314
7.1.3.1 Chemical processes	314
7.1.3.2 Transport	315
7.1.3.3 Aerosols and Polar Stratospheric Clouds (PSCs)	315
7.1.3.3.1 Aerosols	316
7.1.3.3.2 Polar stratospheric clouds	316
7.1.3.4 Solar ultraviolet and energetic particles	316
7.1.4 Modeling the ozone distribution, assessments	317
7.1.4.1 Two-dimensional models	317
7.1.4.2 Three-dimensional models	318
7.2 Major scientific issues and measurement needs	319
7.2.1 Natural changes	319
7.2.1.1 Interannual and long-term variability of the stratospheric circulation	319
7.2.1.2 External influences (solar and energetic particle effects)	319
7.2.1.3 Natural aerosols and PSCs	319
7.2.2 Man-made changes	320
7.2.2.1 Trends in chlorine source gases	320
7.2.2.1.1 Historical trends in chlorine source gases	320
7.2.2.1.2 Stratospheric chlorine	321
7.2.2.1.3 Depletion of ozone by stratospheric chlorine	321
7.2.2.2 Effects of aircraft exhaust	322
7.2.3 Summary of science issues	322
7.3 Required measurements and data sets	322
7.3.1 Meteorological requirements	323
7.3.2 Chemical measurement requirements	324
7.3.2.1 Science questions	324
7.3.2.2 Key trace gas measurements	325
7.3.3 Stratospheric aerosols and PSCs	326
7.3.4 Solar ultraviolet flux	327
7.3.5 Validation of satellite measurements	327
7.4 EOS contributions	328
7.4.1 Improvements in meteorological measurements	328
7.4.1.1 Global limb temperature measurements	328
7.4.1.2 Higher horizontal resolution temperature profiles	328
7.4.2 Improvements in chemical measurements in the stratosphere	328
7.4.3 Improvements in measurements of aerosols	330
7.4.4 Improvements in measurements of the solar ultraviolet flux	331
7.4.5 Advanced chemical/dynamical/radiative models	331
7.4.6 Full meteorological and chemical assimilation of EOS data sets	333
7.5 Foreign partners and other measurement sources	333
References	334
Chapter 7 Index	337

7.1 Stratospheric ozone - background

7.1.1 Why is understanding stratospheric ozone important?

Ozone is one of the most important trace species in the atmosphere. Ozone plays two critical roles: it removes most of the biologically harmful ultraviolet light before the light reaches the surface, and it plays an essential role in setting up the temperature structure and therefore the radiative heating/cooling balance in the atmosphere, especially the stratosphere (the region between about 10 and 60 km).

FIGURE 7.1



The distribution of atmospheric ozone in partial pressure as a function of altitude.

7.1.1.1 Location of the ozone layer and climatology

Ozone is mainly found in two regions of the atmosphere. Most of the ozone can be found in a layer between 10 and 60 km above the Earth's surface (Figure 7.1). This ozone region located in the stratosphere is known as the "ozone layer." Some ozone can also be found in the lower atmosphere (below 10 km) in the region known as the troposphere. Although chemically identical to stratospheric ozone, tropospheric ozone is quite distinct and geophysically different from stratospheric ozone, and the science issues concerning tropospheric ozone are discussed in Chapter 4.

7.1.1.2 Ozone and UV—biological threat

Ozone is produced by the photolysis of molecular oxygen, O_2 . The oxygen atom, O , produced by this photolysis recombines with O_2 to form ozone, O_3 . Ozone formation

primarily occurs in the tropical upper stratosphere, where it is transported poleward and downward by the large-scale Brewer-Dobson circulation. The global distribution of total ozone is shown in Figure 7.2 (pg. 312). This figure represents the 13-year average of the total ozone measurements taken by the Nimbus-7 Total Ozone Mapping Spectrometer (TOMS) instrument.

The formation of ozone by the photolysis of molecular oxygen removes most of the incident sunlight with wavelengths shorter than 200 nm. The wavelengths between 200 and 310 nm are removed

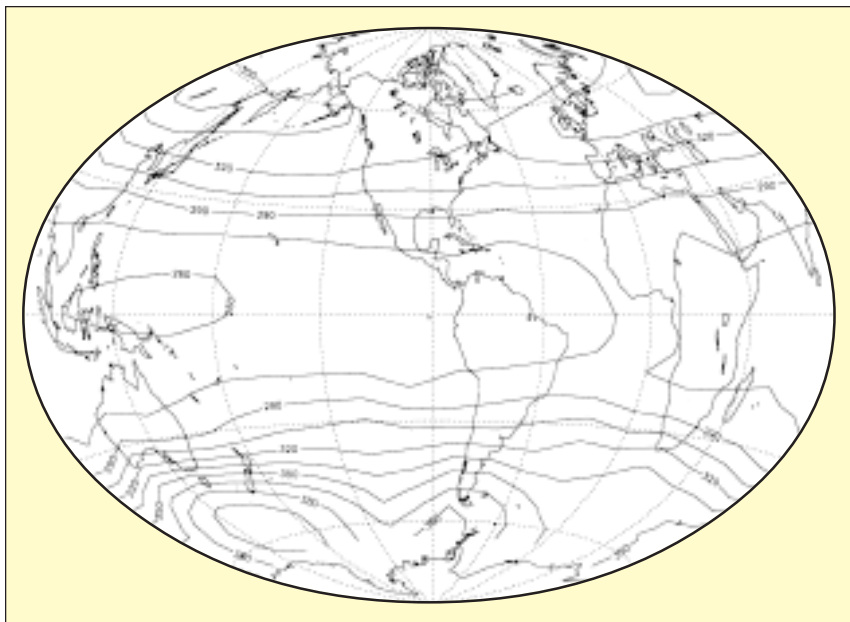
by the photolysis of ozone itself. This photolysis of ozone in the stratosphere is the process by which most of the biologically damaging ultraviolet sunlight (UV-B) is filtered out.

As this filtering process occurs, the stratosphere is heated. This heating is responsible for the temperature structure of the stratosphere, where the temperature increases as the altitude increases. Without this filtering, larger amounts of UV-B would reach the surface. Numerous studies have shown that excessive exposure to UV-B is harmful to plants, animals, and humans (WMO 1992).

7.1.1.3 Ozone and climate change

If ozone in the stratosphere were to be removed, the stratosphere would cool. How a cooler stratosphere affects radiative balance in the rest of the atmosphere has been the subject of many detailed studies. These studies have been reanalyzed and integrated into the latest Intergovernmental Panel on Climate Change (IPCC) report, "Climate Change 1994: Radiative Forcing of Climate Change" (1995). The conclusion of that report is that stratospheric ozone loss leads to a "small but non-negligible offset to the total greenhouse forcing from CO_2 , N_2O , CH_4 , CFCs..." It is ironic that the size of the negative radiative forcing from ozone loss is nearly equal to the positive radiative forcing from chlorofluorocarbons (CFCs), the source of the stratospheric ozone loss. The size of the radiative forcing due to stratospheric ozone loss has also been shown to be very sensitive to the profile shape assumed for that loss.

FIGURE 7.2



The global distribution of column or total ozone averaged over the 13 years of Nimbus-7 TOMS data in Dobson Units (DU).

7.1.2 Observed ozone changes

While the global amount of ozone is fairly constant, there are significant local, seasonal, and long-term changes. The causes of these changes are discussed in detail in Section 7.1.3.

The seasonal ozone changes are basically determined by the winter-summer changes in the stratospheric circulation. Since ozone has a lifetime of weeks to months in the lower stratosphere, the amount of ozone can strongly vary due to transport by stratospheric wind systems. Since weather conditions in the stratosphere, as in the troposphere, vary from year to year, there is also interannual variability in ozone amounts. Interseasonal changes in ozone are also linked to the 11-year solar cycle in UV output and the amount of volcanic aerosols in the stratosphere. Changes in ozone have also been linked to anthropogenic pollutants, especially the release of man-made chemicals containing chlorine. In the section below we describe the more-significant recent global changes in ozone observed by a variety of instruments.

7.1.2.1 Polar ozone changes

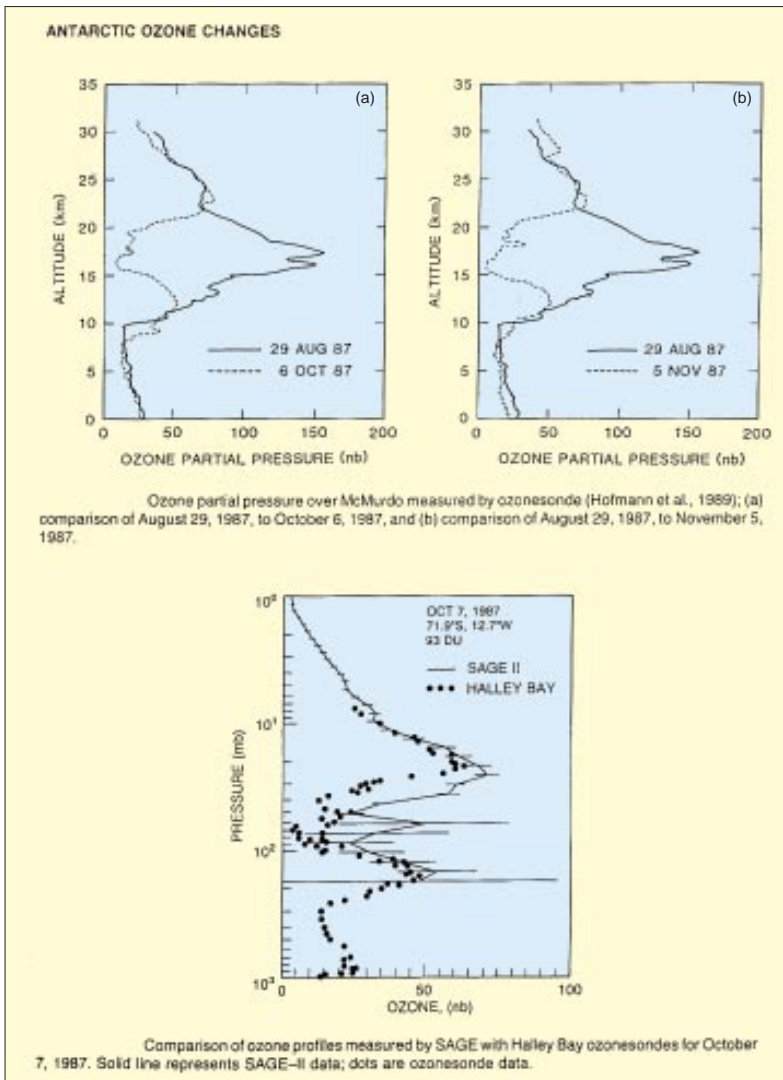
The first ozone measurements in the Antarctic were made during the 1950s. A Dobson instrument was installed at Halley Bay in late 1956 in preparation for the Interna-

tional Geophysical Year in 1957. One of the first discoveries made by this instrument was that the seasonal cycle of ozone in the south polar region is very different from that which had been observed in the north. This was noted in a review article by Dobson (1966), which pointed out that its cause was a difference in the circulation patterns of the Antarctic relative to the Arctic. In the Arctic, the total ozone amount grew rapidly in the late winter and early spring to about 500 Dobson Units (DU). (A DU is one milliatmosphere-cm of pure ozone; a layer of pure ozone that would be 0.001-cm thick under conditions of Standard Temperature and Pressure [STP].) In contrast, the Antarctic early springtime amounts remained near 300 DU.

The Dobson instrument at Halley Bay continued to make measurements each year. Farman et al. (1985) showed that the springtime ozone amounts over Halley Bay had declined from nearly 300 DU in the early 1960s to about 180 DU in the early-to-mid 1980s. This result has been confirmed at a number of other stations and shown using satellite data to occur over an area larger than the Antarctic continent (Stolarski et al. 1986). These large ozone changes implied that losses must be taking place in the lower stratosphere where most of the ozone exists. This was shown to be true in a series of ozonesonde measurements (see, e.g., Hofmann et al. 1989 and Figure 7.3). More-recent sonde measurements have shown instances of near-zero concentrations of ozone over a 5-km altitude range (Hofmann et al. 1994). Aircraft measurements (Proffitt et al. 1989) and satellite measurements (McCormick et al. 1988) confirm and show further details of these ozone changes.

The 1996-1997 Northern Hemisphere winter experienced a significant ozone depletion over the Arctic and subsequent total ozone values achieved record low values in the spring. Long term records of the Total Ozone Mapping Spectrometer (TOMS) (Newman et al., 1997) and ground based observations (Fioletov et al., 1997) show a downward change over the past several years occurring mostly in February and March and confined to the lower

FIGURE 7.3



Balloonsonde ozone measurements made at McMurdo and SAGE II measurements for 1987.

stratosphere (Manney et al. 1997) similar to the depletion over the Antarctic. Total ozone changes for both polar regions are shown in Figure 7.4 (pg. 314) (Newman, Private communication). Chlorine radicals have been conclusively identified as the causes of ozone depletion now in both hemispheres. Measurements of ClO by the UARS MLS instrument (Santee et al., 1997) observed elevated levels in late February over Northern Hemisphere polar regions. The winter of 1996-1997, showed extremely low temperatures in the Stratosphere. These cold temperatures led to the formation of polar stratospheric clouds whose particles shift chlorine gas away from its HCl reservoir to active ClO through heterogeneous chemistry. This is the primary mechanism producing the Antarctic

ozone hole (Anderson et al., 1991, Solomon, 1990, and others). Although the buildup of chlorine has occurred approximately uniformly in both hemisphere the unusually low temperatures reached in high northern latitudes mostly likely precipitated the concurrent ozone losses over the Arctic.

7.1.2.2 Midlatitude ozone loss

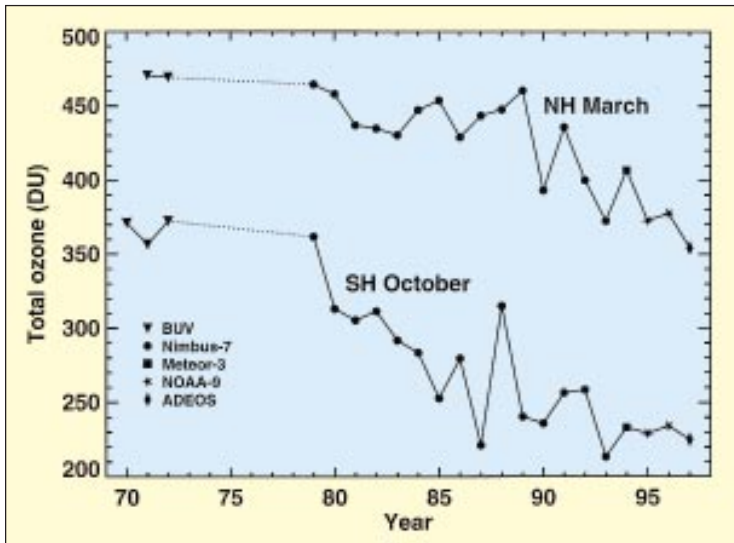
Midlatitude ozone loss estimates must be extracted from long time series using statistical models (see, e.g., Report of the International Ozone Trends Panel 1990). The longest time series of total ozone data is from Arosa in Switzerland. This time series, which dates back to 1926, is shown in Figure 7.5 (pg. 314). The Arosa data show a relatively constant amount of ozone for over 4 decades and a decrease in the last decade and a half. Analysis of a more-extensive network of 30+ stations which have been in operation for about 35 years shows negative trends over the last 1.5 decades, especially in the winter and early spring (see, e.g., Reinsel et al. 1994).

High-quality global satellite data records began in November 1978 with the launch of the Nimbus-7 Solar Backscatter Ultraviolet (SBUV) radiometer and TOMS instruments. These data show midlatitude trends in the Northern Hemisphere which are largest in the winter and early spring, peaking at about 6-8% per decade at

40°-50° N in February (see, e.g., Randel and Cobb 1994; Hollandsworth et al. 1995). These satellite trends are in the process of being updated with a version 7 algorithm for the TOMS and SBUV instruments.

Changes in the profile of ozone with altitude can be deduced from sonde data or from the Stratospheric Aerosol and Gas Experiment (SAGE) satellite measurements. Analyses of sonde data (e.g., Logan 1994) show ozone decreases between the tropopause and about 24-km altitude. Analyses of SAGE data show larger decreases than those derived from sondes. SAGE results show negative ozone trends in the lower stratosphere in the tropics. Column ozone changes deduced from SBUV and TOMS show only small downward trends. Hollandsworth et al.

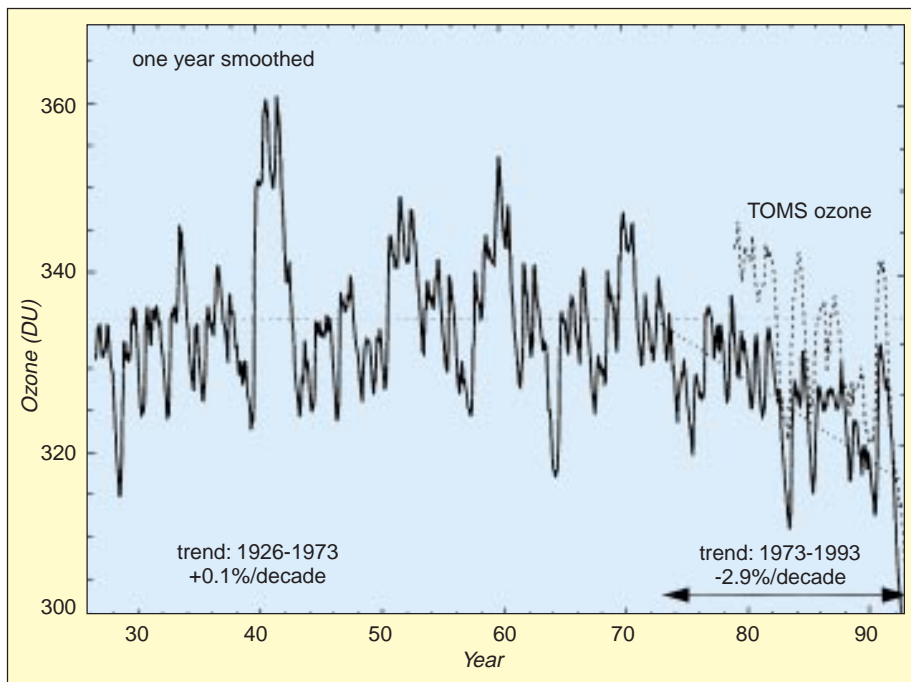
FIGURE 7.4



63° - 90° total ozone average

(1995) used SBUV profile and total ozone trends to deduce that ozone in the tropics below 32 hPa has increased slightly over the last decade. The resolution of the uncertainty in the magnitude of lower stratospheric and upper tropospheric ozone trends is an important measurement and analysis issue for the coming years.

FIGURE 7.5



Time series of column ozone measurements at Arosa, Switzerland, in DU.

7.1.3 The stratospheric ozone distribution

7.1.3.1 Chemical processes

Ozone is being continuously created and destroyed by the action of ultraviolet sunlight. The overall amount of ozone in the global stratosphere is determined by the magnitude of the production and loss processes and by the rate at which air is transported from regions of net production to those of net loss.

Production of ozone requires the breaking of an O₂ bond, with the extra or “odd” oxygen atom attaching to another O₂ to form O₃. This most frequently occurs via the photodissociation of O₂ by solar ultraviolet radiation. In the lower stratosphere and troposphere ozone can also be produced by photochemical smog-like reactions. In these reactions H or CH₃ or higher hydrocarbon

radicals attach to an O₂ forming HO₂ or CH₃O₂, etc., which then react with NO. This reaction breaks the O₂ bond by forming NO₂ (which is really ONO). When NO₂ is photolyzed an O atom is formed which reacts with O₂ to form O₃. Loss of ozone occurs when an O atom reacts with O₃ to re-form the O₂ bond. More importantly, this loss process is catalyzed by the oxides of hydrogen, nitrogen, chlorine, and bromine. These oxides are produced in the

stratosphere from long-lived, unreactive molecules released at the surface of the Earth. The major source molecules for HO_x (HO_x is chemical shorthand for the sum of all the hydrogen radicals—OH and HO₂, mostly) are methane (CH₄) and water vapor (H₂O). The main source of NO_x (NO_x is chemical shorthand for the sum of all nitrogen radicals—NO, NO₂, N₂O₅, NO₃, mostly) is nitrous oxide (N₂O). The major sources of chlorine are industrially-produced CFCs (such as CFC-11, which is CFCl₃, and CFC-12, which is CF₂Cl₂) and naturally-occurring methyl chloride (CH₃Cl). The major

sources of bromine are methyl bromide (CH_3Br) and the halons (CF_3Br and CF_2ClBr). These source molecules are transported to the stratosphere where they react or are photodissociated to produce the catalytically-active oxide radicals.

The catalytic efficiency of hydrogen, nitrogen, chlorine, and bromine oxides is determined by a set of interlocking reactions which convert the active oxides to catalytically-inactive temporary reservoirs, such as HNO_3 , HCl , ClONO_2 , H_2O , HOCl , HOBr , and BrONO_2 , and vice versa. In the lower stratosphere, the balance between catalytic oxides and temporary reservoirs is strongly affected by reactions on the surfaces of stratospheric aerosols. The balance is even more profoundly affected in the polar winter by reactions on the surface of Polar Stratospheric Cloud (PSC) particles. In the early spring, the chlorine balance is shifted to almost 100% ClO_x (ClO_x is shorthand for the sum of all chlorine radicals, ClO , Cl_2O_2 , Cl) (Brune et al. 1989; Waters et al. 1993). This shift in the chemical balance results in a large calculated chemical sensitivity of ozone towards chlorine perturbations and a relatively small calculated sensitivity of ozone towards nitrogen oxide perturbations.

Although the basic outline of the chemistry controlling stratospheric ozone is now known, many important aspects of the problem remain to be solved. The primary difference between the Northern and Southern Hemispheric polar ozone loss regions appears to be a result of the “denitrification” that occurs in the Antarctic winter. Denitrification means the removal of nitrogen oxides and HNO_3 by large particles which fall into the troposphere. Denitrification takes place when temperatures are cold enough to form large stratospheric ice crystals.

When springtime comes there are no nitrogen oxides to convert ClO_x to ClONO_2 and slow down the rate of ozone depletion. There is some evidence for denitrification when temperatures are not cold enough to form ice crystals. Under those conditions the mechanism for denitrification is not completely understood.

7.1.3.2 Transport

Much of the currently-observed ozone interannual variability in the stratosphere is controlled by dynamical processes. In particular, this variability is driven by such processes as the quasi-biennial oscillation (QBO), El Niño-Southern Oscillation, tropospheric weather systems which extend into the stratosphere, and long-term fluctuations in planetary wave activity. The annual cycle of total ozone is largely driven by transport effects. As shown in Figure 7.2, relatively low values of ozone are observed in the tropics and high values are observed in the extratropics. These low tropical ozone values occur in spite

of the large ozone production rates in the tropics. If ozone production were precisely balanced by ozone loss everywhere, total ozone would have extremely high values in the tropics. The observed tropical low values result from vertical advection of low-ozone air from the tropical troposphere into the tropical stratosphere, and the subsequent transport of this air poleward and downward into the extratropics and polar regions. This advective circulation is known as the Brewer-Dobson circulation.

The redistribution of ozone from the production region at low latitudes to extratropical latitudes is modulated by a variety of processes. Foremost among these processes is the annual cycle in the circulation. It is now recognized that the Brewer-Dobson circulation is primarily controlled by large-scale waves in the winter stratosphere. As these waves propagate through the westerly winds that dominate the winter stratosphere, they exert a westward zonal drag, which through the Coriolis force leads to a poleward and downward transport circulation, which in turn drives the temperatures away from radiative equilibrium. The large-scale waves breaking in the winter upper stratosphere also produce lifting in the tropics. Since the lifetime of ozone increases with pressure, the poleward downward circulation causes ozone to accumulate in the lower stratosphere over the course of the winter. Since the large-scale waves are not present in the summer, the poleward and downward circulation is significantly weakened, and ozone amounts which have built up during winter begin to decrease due both to transport into the troposphere and to photochemistry.

The exchange of mass between the troposphere and the stratosphere is the focus of considerable current research (Holton et al. 1995). Stratosphere-troposphere exchange is important for the budget of ozone in the lower stratosphere as well as the ozone budget in the troposphere. Upward transport occurs in the tropics, but the exact mechanism controlling the transport is not clear. Current research is focussing on the role of subvisible cirrus and the radiative impact of infrared (IR) heating of subvisible cirrus (Jensen et al. 1997). Downward transport (stratosphere to troposphere) takes place in midlatitudes through jet stream folds—but the frequency and amount of mass irreversibly moving through these folds is still not understood (Holton et al. 1995).

7.1.3.3 Aerosols and Polar Stratospheric Clouds (PSCs)

It is now known that knowledge of stratospheric aerosols and PSCs is very important to our understanding of stratospheric ozone. The surfaces of aerosols and PSCs are sites for heterogeneous reactions which can convert chlorine from reservoir to radical forms. Likewise, radical nitro-

gen forms can be sequestered as nitric acid to shift the chemical loss process (WMO 1995).

7.1.3.3.1 Aerosols

The long-term stratospheric aerosol record reveals at least three components: episodic volcanic enhancements, PSCs and clouds just above the tropical tropopause, and a background aerosol level. At normal stratospheric temperatures, aerosols are most likely super-cooled solution droplets of $\text{H}_2\text{SO}_4\text{-H}_2\text{O}$, with an acid weight fraction of 55 to 80%. The primary source of stratospheric aerosols is volcanic eruptions that are strong enough to inject SO_2 buoyantly into the stratosphere. Aerosol sizes range from hundredths of a micrometer to several micrometers. Although there is some variability, especially just after a volcanic eruption, a log-normal size distribution of spherical particles appears to aptly describe the aerosol. Just after an eruption, the size distribution becomes bimodal, and some particles are nonspherical because of the addition of crustal material. After an eruption, the SO_2 is converted to H_2SO_4 , which condenses to form stratospheric sulfuric acid aerosols, with a time scale of about 30 days. Subsequently, aerosol loading decreases due to a combination of sedimentation, subsidence, and exchange through tropopause folds. The loading decreases with an e-folding time of 9-to-12 months, although this appears quite variable with altitude and latitude.

The net effect of this post-volcanic dispersion and natural cleansing is a greatly enhanced aerosol concentration in the upper troposphere after a major eruption, especially poleward of about 30° latitude. Except immediately after an eruption, stratospheric aerosol droplets tend to be concentrated into 3 distinct latitudinal bands—one over the equatorial region (to 30°) and the other over each high-latitude region, 50° to 90° N and S. Following a low-latitude eruption, aerosol is dispersed into both hemispheres, whereas following a mid-to-high-latitude eruption, aerosols tend to stay primarily in the hemisphere of the eruption. Potential sources of a background aerosol component include carbonyl sulfide (OCS) from the oceans, low-level SO_2 emissions from volcanoes, and various anthropogenic sources, including industrial and aircraft emissions. Also, it is not clear whether there is an upward trend in this background aerosol, as has been hypothesized and linked to increasing aircraft emissions, since any increase may be due to incomplete removal of past volcanic aerosol.

Stratospheric aerosol loading in 1979 was approximately $0.5 \times 10^{12}\text{g}$ (0.5 Mt), thought to be representative of background aerosol conditions. The present status of the aerosol is one of enhancement due to the June 1991 eruption of Pinatubo (15.1° N, 120.4° E), which produced

on the order of $30 \times 10^{12}\text{g}$ (30 Mt) of new aerosol in the stratosphere, about 3 times that of the 1982 eruption of El Chichón. This perturbation appears to be the largest of the century, perhaps the largest since the 1883 eruption of Krakatoa. By early 1993, stratospheric loading decreased to approximately 13 Mt, about equal to the peak loading values after El Chichón (McCormick et al. 1995). Measurements in 1995 showed that the aerosol levels were approaching background levels.

7.1.3.3.2 Polar Stratospheric Clouds (PSCs)

The interannual variability in PSC sightings has been addressed by Poole and Pitts (1994), who analyzed more than a decade of data from the spaceborne Stratospheric Aerosol Measurement (SAM) II sensor (Figure 7.6). They found noticeable variability in PSC sightings in the Antarctic from year to year, even though the southern polar vortex is typically quite stable and long-lived. This variability was found to occur late in the season and can be explained qualitatively by temperature differences. Poole and Pitts found even more year-to-year variability in SAM II Arctic PSC sighting probabilities. This was expected since the characteristics and longevity of the northern polar vortex vary greatly from one year to the next. The year-to-year variability in Arctic sighting probabilities can also be explained qualitatively by differences in temperature, e.g., zonal mean lower stratospheric temperatures in February 1988 were as much as 20 K colder than those one year earlier.

7.1.3.4 Solar ultraviolet and energetic particles

Since ozone formation is fundamentally linked to the levels of ultraviolet radiation reaching the Earth, natural variations in that radiation must be understood in order to detect trends. The ultraviolet comprises only one-to-two percent of the total solar radiation, but it displays considerably more variation than the longer wavelength visible radiation. For example, from 1986 to 1990 the solar UV increased with onset of the 11-year solar cycle and resulted in an increase of global total ozone of almost 2%. This natural increase in ozone is comparable to the suspected anthropogenic decrease and needs to be understood in order to totally separate the anthropogenic decrease from this natural change. Studies of total ozone trends typically subtract solar cycle and other natural changes from the total ozone record in trend resolution (see WMO 1992; WMO 1995; Stolarski et al. 1991; and Hood and McCormack 1992). Thus, more-quantitative knowledge of this natural solar-cycle-induced total ozone change would be especially valuable.

Changes in energetic particle flux from the sun penetrate into the middle atmosphere and may also drive

the natural ozone variations. A series of solar flares in 1989 spewed solar particles into the Earth's polar cap regions (greater than 60° geomagnetic latitude) and led to polar ozone depletion (Jackman et al. 1993). Further studies related to the very large solar particle events (SPEs) of October 1989 have predicted ozone depletions lasting for several months after the SPEs (Reid et al. 1991; Jackman et al. 1995). Although SPEs of this magnitude occur infrequently (only two have been observed in the past 25 years), they need to be understood more completely to be able to separate natural from anthropogenic ozone effects.

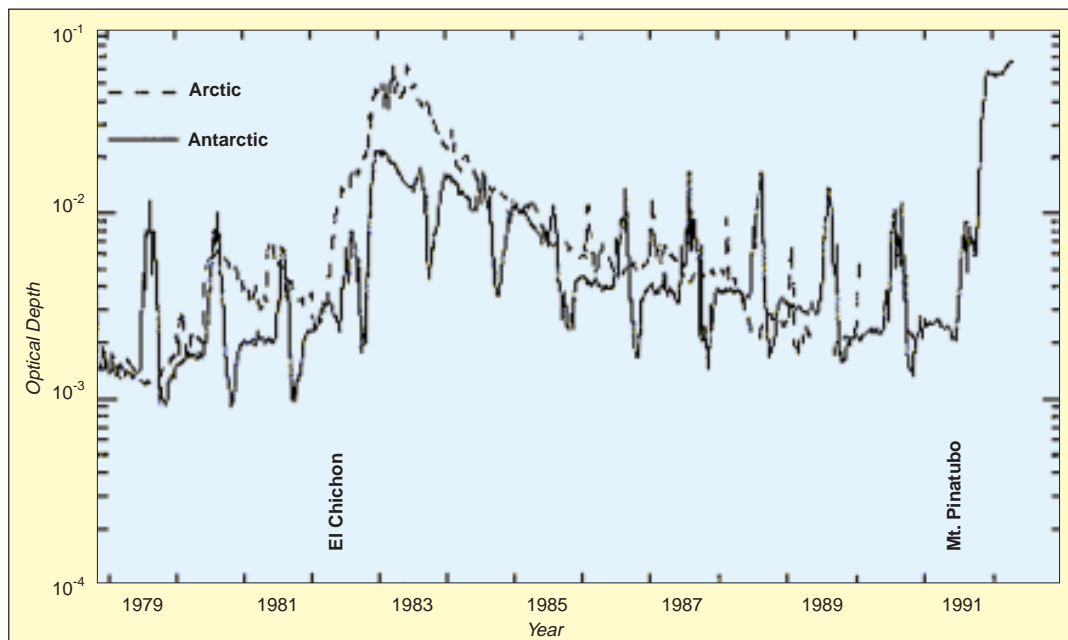
Relativistic electron precipitations (REPs) have been predicted to contribute substantially to the odd nitrogen budget of the stratosphere and, therefore, have been predicted to play a large role in controlling ozone in this region (Callis et al. 1991a, 1991b). Another investigation (Aikin 1992) has failed to find any REP-caused ozone depletion. Further work (Gaines et al. 1995) determined that REPs in May 1992, the largest measured relativistic electron flux precipitating in the atmosphere between October 1991 and July 1994, added only about 0.5 to 1% of the global annual source of odd nitrogen to the stratosphere and mesosphere. The actual importance of REPs in regulating ozone is thus not well understood nor characterized, and further work on REPs is required to thoroughly determine their importance regarding modulation of stratospheric ozone.

7.1.4 Modeling the ozone distribution, assessments
Models of the stratosphere provide the only means to attempt quantitative prediction of global change, or to evaluate the impact of natural or anthropogenic changes in composition on the stratospheric ozone and climate. In addition, models provide a means to integrate observations and theory, to provide tests of mechanisms for chemical, dynamical, or radiative changes, and to enable interpretation of observations from different platforms.

7.1.4.1 Two-dimensional models

Two-dimensional (2-D) models are used by several research groups. The models predict the behavior of ozone and other trace gases in reasonable agreement with measurements (WMO 1992; WMO 1995). Because of these favorable comparisons to measurements, these models have been utilized recently in many atmospheric studies, for example: 1) the response of the middle atmosphere due to solar variability was studied by Brasseur (1993), Huang and Brasseur (1993), and Fleming et al. (1995); 2) the influence of the Mt. Pinatubo eruption on the stratosphere was studied by Kinnison et al. (1994a, b) and Tie et al. (1994); and 3) the effects of proposed stratospheric aircraft on atmospheric constituents were studied by Pitari et al. (1993), Weisenstein et al. (1993), Considine et al. (1994), and Considine et al. (1995).

FIGURE 7.6



SAM II measurements of vertical optical depth data in the stratosphere over the Arctic and Antarctic. The measurements show the impact of volcanic eruptions over the period 1979-1992 along with seasonal effects in the local winters due to Polar Stratospheric Clouds (PSCs). The data are weekly averages at a wavelength of 1000 nm.

These 2-D models have also been used to produce multi-year simulations of the response of stratospheric ozone to perturbations of the source gases such as CFCs from which chlorine radicals are produced (WMO 1992; WMO 1995). An outstanding issue regarding simulations of the stratospheric ozone response to chlorine increases is the lack of ability of 2-D models to accurately predict the ozone trend in the middle and high northern latitudes over the 1980-to-1990 time period. Since the 2-D models predict a smaller trend than observed, it is believed that the models do not adequately model all of the relevant processes and thus require further development.

7.1.4.2 Three-dimensional models

The three-dimensional (3-D) (or general circulation) model with full interaction between chemical, dynamical, and radiative processes remains elusive. The present generation of general circulation models (GCMs) generates unrealistic temperature fields which, in turn, alter the photochemistry. The unrealistic temperatures are related to problems with the model transport circulation. For example, the polar regions are persistently cold in GCMs, which suggests that there is insufficient adiabatic heating (or descent) in the winter polar region. Correspondingly, there will be insufficient ascent in the tropics, which weakens the transport from the troposphere into the stratosphere.

Subtle changes in the general circulation of the atmosphere in 3-D models can alter and distort the chemical feedbacks. For example, Rasch et al. (1995) report on a two-year simulation using version 2 of the National Center for Atmospheric Research (NCAR) Middle Atmosphere Community Climate Model (MACCM2). A chemical scheme for 24 reactive species, or families, is run as part of this simulation. This model is partially coupled in that the water vapor predicted by MACCM2 is connected to the chemical source of water through oxidation of methane. Prescribed ozone is used in the radiative calculation. In this simulation, the calculated upper stratospheric ozone is substantially lower than is observed; much of the difference is attributed to the lower CH_4 , compared to observations by the UARS Halogen Occultation Experiment (HALOE). This bias leads to excessive ClO and excessive destruction of O_3 . In effect, the error in this long-lived trace gas, which results from the weak transport circulation, leads to noticeable errors in ozone.

The difficulties described above show why most 3-D modeling efforts have focused on “off-line” calculations, i.e., use of chemistry and transport models (CTMs) in which the wind and temperature fields are input from a GCM (e.g., Eckman et al. 1995) or from a data assimila-

tion system (e.g., Rood et al. 1991; Lefevre et al. 1994). For either approach, there are computational advantages, as the same set of winds and temperatures is used many times. Furthermore, the effects of modifications to the chemical scheme can be isolated, and their effects understood, without the complications caused by feedback processes. A further advantage of the use of assimilated winds and temperatures is that the results of constituent simulations may be compared directly with observations with no temperature biases such as those found in GCMs. This is particularly important for the study of processes which have a temperature threshold, such as heterogeneous reactions on PSC surfaces. The most information is gleaned when the model is sampled in a manner consistent with the satellite sampling (Geller et al. 1993).

The “off-line” approach has been used successfully for many years and is used to test chemical and transport mechanisms, as well as to interpret observations. These tests include:

- 1) assessment of the importance of transport of air with high levels of reactive chlorine to middle latitudes (Douglass et al. 1991);
- 2) assessment of the rate of ozone loss within the Northern Hemisphere vortex and identification of the variables to which the calculation is sensitive (Chipperfield et al. 1993);
- 3) determination of the importance of upper tropospheric synoptic-scale systems on the vortex temperature, as well as their influence on the transport and mixing of air which has experienced temperatures cold enough for PSC formation (Douglass et al. 1993); and
- 4) examination of the impact of ozone transport following the breakup of the Antarctic polar vortex on the global ozone budget (the “ozone dilution” effect).

These 3-D studies provide a picture of the important physical processes which control polar ozone loss. However, because of computer resource restrictions, it is not yet possible to make full 3-D model long-range predictions, including possible influence of the ozone loss on lower stratospheric temperature and climate. For example, future temperature changes may have a significant impact on the Northern Hemisphere vortex. The full 3-D model, with all relevant chemical, dynamical, and radiative processes and feedbacks among them, has yet to be developed.

7.2 Major scientific issues and measurement needs

Changes in the ozone layer can be divided into two categories: natural changes and man-made changes. Separating these components is the goal of much ozone and trace gas research. Since ozone can be transported by stratospheric winds, there is significant interannual variability in column ozone amounts. Ozone is likewise influenced by aerosol amounts (through heterogeneous chemistry) (Solomon et al. 1996), the formation of nitrogen radicals associated with high-energy particles, and variations in the ultraviolet radiation from the sun. Man-made changes generally include increased chlorine and hydrogen amounts from industrial gases and increased aerosols and nitrogen radicals from airplane exhaust. Many of our current scientific issues and future measurement needs center around the interaction of the ozone layer with these pollutants and separating natural changes in the ozone layer from man-made processes.

7.2.1 Natural changes

7.2.1.1 Interannual and long-term variability of the stratospheric circulation

Because the stratospheric circulation is strongly dependent on the dissipation of large-scale waves in the stratosphere, interannual variability of the wave amplitudes has an important impact on ozone transport (see Section 7.1.3.2). Winds and temperatures derived from 3-D GCMs and assimilation models include such interannual variability and can be used to assess the impact on ozone transport. 2-D models can incorporate prescribed variability to simulate interannual ozone transport (see Section 7.1.4.1). Accurate assessment of the large-scale waves and the transport circulation is necessary for understanding the variability of ozone trends.

One of the failures of the 3-D models is inadequate simulation of the QBO. The QBO is a 24-30-month oscillation of the zonal wind in the tropical lower stratosphere that is driven by tropical waves. The QBO affects the stratospheric temperature distribution and produces a secondary circulation which transports trace gases and aerosols. For ozone, the QBO can generate variations from the climatological mean of 5-10 DU in the tropics. There is also a QBO-ozone signal outside the tropics of 10-20 DU.

The QBO provides one of the largest components of the interannual variability of the column ozone values. Because the geostrophic relationship breaks down in the tropics, direct tropical wind measurements are critical to precisely measuring the QBO and for understanding the

effects of the QBO on the circulation. Data-sparse regions and infrequent sampling of wind fields all preclude good quantitative studies of the tropical circulation and its effect on ozone.

7.2.1.2 External influences (solar and energetic particle effects)

As discussed in Section 7.1.3.4 solar ultraviolet radiation and precipitating energetic particles can strongly influence ozone amounts. In order to understand the anthropogenic changes in ozone, we must maintain reliable measurements of the solar ultraviolet input to the middle atmosphere. Solar variations in the UV produce ozone changes on the same order of magnitude as the current observed midlatitude changes. Proxies for the UV changes have been historically used to estimate the response of ozone to solar ultraviolet changes. With direct measurements from UARS, these proxies have been shown to inadequately represent changes in ultraviolet flux.

Particle events generate NO_x compounds which catalytically destroy ozone, but these events tend to be confined to the upper stratosphere. Large events, which tend to be more episodic, may affect polar ozone at lower levels. The impact of NO_x generation through particle precipitation on the natural ozone layer is a major scientific question.

7.2.1.3 Natural aerosols and PSCs

As discussed in Section 7.1.3.3, aerosols and PSCs are believed to play a major (although indirect) role in ozone loss. Irregular volcanic inputs of SO₂ with the subsequent formation of sulfate aerosols have an impact on the ozone layer. There is some evidence suggesting that increasing amounts of background aerosols are a result of subsonic aircraft emissions in the lower stratosphere. A major scientific question is whether the background amounts of these aerosols are increasing and, if so, determining their origin. Monitoring the aerosol amounts within the stratosphere and determining their trend is a primary measurement requirement to understand ozone loss.

During the 1980s it became apparent that aerosols play an important role in the chemistry of the stratosphere. Observations of large decreases in ozone over Antarctica during the Southern Hemisphere spring were not accounted for by theory, until several researchers hypothesized that heterogeneous reactions on PSCs might be converting inactive chlorine compounds into reactive forms (Solomon et al. 1986; McElroy et al. 1986; Toon et

al. 1986). In a similar fashion to PSCs, heterogeneous reactions upon sulfuric acid droplets at midlatitudes convert N_2O_5 into HNO_3 and shift the ratio of HNO_3 to NO_2 normally present in the stratosphere. Throughout the stratosphere, reactions on and inside aerosol particles are therefore important.

To understand the effectiveness of the heterogeneous (gas phase/aerosol phase) reactions, it is important to know:

- a) the temperatures of the aerosol particles;
- b) the surface and volume densities of the aerosol particles, which are derived from the aerosol extinction, and a knowledge of the size distribution;
- c) the composition (the mixing ratios of H_2O , H_2SO_4 , and HNO_3 in ppbv) and phase (liquid/solid/amorphous solid solution) of the aerosol particles;
- d) the concentration of the reactants in the aerosol (e.g., the concentration of HCl); and
- e) the duration of time over which the heterogeneous reactions occur.

A theoretical framework, by which heterogeneous rates of reaction are quantified, is given in Hanson et al. (1994).

An important research goal is the ability to observe the yearly episodes of ozone loss in the polar regions (e.g., the Antarctic ozone hole), to measure this loss as reservoir chlorine levels change with time, and to be able to relate the changes in observed ozone to a quantitative understanding of heterogeneous processes.

In principle, one should be able to identify the composition of stratospheric aerosol from multi-wavelength extinction data. Multi-wavelength observations of midlatitude sulfuric acid droplets have an extensive history. Observations of El Chichón aerosol (Pollack et al. 1991), post El Chichón aerosol (Osborn et al. 1989; Oberbeck et al. 1989), and of Mt. Pinatubo aerosol (Grainger et al. 1993; Massie et al. 1994; and Rinsland et al. 1994) yield spectral data consistent with theoretical expectation. Analysis of multi-wavelength observations of PSCs is a developing research topic. Recent attempts to use spectra to determine PSC composition are illustrated by Toon and Tolbert (1995).

Several years ago, ice and nitric acid trihydrate (NAT) particles were thought to be the primary composition of PSCs. Recent studies have shown that some PSC particles are liquid (the ternary solution of $\text{HNO}_3/\text{H}_2\text{O}/\text{H}_2\text{SO}_4$), and not that of crystalline NAT (Carslaw et al. 1994; Drdla et al. 1994). As additional laboratory cold-temperature measurements of the indices of refraction of

PSC composition candidates become available, the ability to classify PSC composition from spectra will improve.

Although PSCs are now known to be instrumental in polar ozone loss, their amounts and types must be monitored. The major difference between the Antarctic ozone depletion and the less-severe Arctic depletion appears to be the result of a lack of denitrification in the Arctic (Schoeberl et al. 1993). Fundamentally, denitrification is a function of temperature and the size of PSCs. Above frost point the PSC size is generally too small to precipitate nitric acid from the stratosphere. If temperatures reach frost point, larger PSCs form, which are able to remove nitrogen acid from the lower stratosphere. The temperature history of the air parcel may play an important role in the PSC size distribution as well (e.g., Murphy and Gary 1995). Photolysis of the nitric acid is key to halting the ozone depletion during winter.

With the increase of greenhouse gases, the stratosphere is expected to cool and thus increase the probability of PSC formation as well as increase the surface area and heterogeneous reaction rates on sulfate aerosols. Preliminary studies (Austin et al. 1992) suggest greenhouse gas increase could have a major role in polar ozone depletion through increased probability of PSC formation. Monitoring stratospheric aerosol loading and PSC amounts is critical for understanding ozone loss.

7.2.2 Man-made changes

Man-made changes in ozone mostly arise from the manufacture of unreactive chlorine-containing compounds such as the CFCs (chlorine source gases). These compounds reach stratospheric altitudes where photolysis by ultraviolet radiation releases chlorine with subsequent destruction of ozone through catalytic cycles. Aviation also has an impact on ozone through the release of nitrogen radicals in aircraft exhaust. Both of these anthropogenic effects are discussed below.

7.2.2.1 Trends in chlorine source gases

As mentioned earlier, chlorine source gases and their respective trends are the major drivers behind decreases in stratospheric ozone. A comprehensive discussion of chlorine source gases is contained in WMO (1995). This report may be consulted for more detail and appropriate references.

7.2.2.1.1 Historical trends in chlorine source gases

All chlorine in the stratosphere comes from tropospheric sources, predominantly the man-made CFCs and chlorocarbons. The man-made sources account for about 7/8th of the total stratospheric chlorine. CFCs are cur-

rently being phased out in favor of the hydrochlorofluorocarbons (HCFCs). Extensive measurements of the chlorofluorocarbons CFC-11 (CCl_3F), CFC-12 (CCl_2F_2), and CFC-113 ($\text{CCl}_2\text{FCClF}_2$) have indicated a steady increase in their tropospheric mixing ratios for more than a decade. Most recent data suggest that the growth rate for these species has begun to decrease. Measurements taken from Tasmania suggest that levels of the important chlorocarbon CCl_4 in the troposphere are also decreasing.

As HCFCs are introduced as substitutes for CFCs, it may be expected that their mixing ratios in the troposphere will increase well into the next century. HCFC-22 (CHClF_2) data show a near-linear growth rate in recent years. HCFC-141b and HCFC-142b have been available only recently as CFC replacements. These species are clearly increasing in the troposphere, but further data is required to get reliable growth rates for long-term studies.

CH_3CCl_3 data also indicate a reduced growth rate that is a result of recently-reduced emissions, but also possibly due in part to increasing hydroxyl (OH) levels. Data for dichloromethane (CH_2Cl_2), methyl chloride (CH_3Cl), and chloroform (CHCl_3) currently exhibit no long-term trends. Continued tropospheric measurements of these gases are required to estimate ozone depletion potential.

7.2.2.1.2 Stratospheric chlorine

An extensive compilation of measurements of chlorine source gases in the stratosphere can be found in Fraser et al. (1994). The most comprehensive suites of simultaneous measurements of chlorine constituents in the stratosphere include the Atmospheric Trace Molecule Spectroscopy (ATMOS) experiments of 1985, 1992, and 1993, and the Airborne Arctic Stratospheric Expedition II (AASE II) measurements of 1991, 1992. The data from these missions have provided invaluable information on the stratospheric chlorine burden and the partitioning among the various chlorine species.

Based upon the 1985 ATMOS data, Zander et al. (1992) determined a total stratospheric chlorine level of 2.55 ± 0.28 ppbv. Further, they concluded that above 50 km most of the inorganic chlorine was in the form of hydrogen chloride (HCl), and that the partitioning of the chlorine among sources, sinks, and reservoir species was consistent with that level of total chlorine.

From the 1992 ATMOS flights, total stratospheric chlorine (based upon HCl data above 50 km) was estimated to be 3.4 ± 0.3 ppbv, an increase of approximately 35% in seven years (Gunson et al. 1994). This increase is consistent with that predicted by models (e.g., WMO 1992). Schauffler et al. (1993) inferred total chlorine lev-

els of 3.50 ± 0.06 ppbv from the AASE II data near the tropopause, a value which is in excellent agreement with the 1992 ATMOS values.

Recent HCl data (55 km) from HALOE on UARS (Russell et al. 1996) reveal a trend of 3.4% per year in HCl for the period from UARS launch in 1991 to early 1995 (Figure 7.7).

Of the total stratospheric burden, only about 0.5 ppbv is estimated to arise from natural sources in the troposphere (WMO 1995), but these estimates have yet to be confirmed by direct or remote observations. HCl emissions from major volcanic eruptions (El Chichón, 1982, and Mt. Pinatubo, 1991) provided negligible perturbations to the levels of HCl in the stratosphere (Mankin and Coffey 1984; Wallace and Livingston 1992; and Mankin et al. 1992).

7.2.2.1.3 Depletion of ozone by stratospheric chlorine

Estimates of the severity of ozone depletion in the future can only be determined by atmospheric model simulations. The level of confidence in these models is based upon their ability to simulate present atmospheric distributions and their ability to simulate recent (decadal) trends. A discussion of the strengths and weaknesses of current assessment models is contained in WMO (1995) and Section 7.1.4.1.

Model simulations of ozone change spanning the period 1980 to 2050 were conducted as part of the WMO (1995) assessment process. Two scenarios were adopted for the assessment studies: 1) the emissions of halocarbons follow the guidelines in the Amendments to the Montreal Protocol, Scenario I; and 2) partial compliance with the guidelines, Scenario II (see WMO [1995] for specific details of the scenarios and models).

Figure 7.8 (pg. 324) summarizes the results of the model calculations for Scenario I. This figure shows the percent change (relative to 1980) in the ozone column at 50° N in March for each of the models participating in the assessment. Decreases of up to approximately 6.5% are seen to occur just prior to 2000. The recovery time to 1980 levels varies widely for the different models, from as early as 2020 to well past 2050. The individual models all showed reasonable agreement among themselves for the present-day ozone distributions, but begin to differ substantially as the atmosphere is perturbed away from its existing state by increasing levels of nitrous oxide, methane, halocarbons, and other influences.

Uncertainties in the absolute levels of depletion predicted by the models are difficult to evaluate for these long-term scenario calculations. The trends in the source gases are changing, and the trends in the stratospheric reservoir gases, which are dependent on transport into the

stratosphere, will respond. Thus, measurements of the chlorine source and stratospheric reservoir gases must be made to test models against observations. Critical gases in the suite of required measurements are the reservoirs HCl and ClONO₂. The predictive capability of these assessment models directly rests on additional measurements of chlorine source gases, reservoir gases, and gases which are sensitive to transport processes.

7.2.2.2 *Effects of aircraft exhaust*

Long-lived source gases (e.g., N₂O, CH₄) are unreactive in the troposphere and hence can enter the stratosphere at the ambient tropospheric concentrations. In the stratosphere, these gases undergo photolysis or react with radicals to release their potential ozone-destroying catalytic agents. In contrast, aircraft flying in the stratosphere will directly inject catalytic agents into the stratosphere. The primary agents for potential ozone change which have been considered in studies of aircraft exhaust are the nitrogen oxides (NO_x) and water vapor (which leads to HO_x). Now that heterogeneous reactions on background aerosols and PSCs are known to play an important role in the ozone balance of the stratosphere, the evaluation of the effects on ozone of NO_x from supersonic aircraft flying in the stratosphere has changed significantly.

The impact on column ozone of a fleet of supersonic transports (now referred to as High Speed Civil Transports [HSCTs]) is now calculated to be of the order of 1% or less. An important possibility is that the sulfur in the exhaust will lead to the generation of numerous small particles which will add to the aerosol surface area. An increase in surface area will enhance the conversion of chlorine from its reservoirs to ClO_x and thus could lead to an increased loss rate for ozone. Another possibility is that the other condensibles in the exhaust, water vapor, and nitric acid (from NO_x) could impact the formation or duration of PSCs. Initial calculations show this effect to be small (Conside et al. 1995), and transport studies show that injection into the polar vortex is unlikely (Sparling et al. 1995), but there is still uncertainty about what will happen as the stratosphere cools with increasing CO₂ concentrations.

All of the chemical effects of HSCT exhaust depend on how much of the exhaust products accumulate in the stratosphere and where they accumulate. The same is true for the exhaust of the subsonic fleet, which is released in the upper troposphere and lower stratosphere. The three major potential effects of the subsonic fleet of aircraft are ozone increase due to the smog-like photochemistry of NO_x, CO₂ increase due to fuel consumption, and cirrus cloud formation from the water vapor. The importance of aircraft NO_x to ozone generation in the upper troposphere

and lower stratosphere is not completely understood. Aircraft NO_x sources have to be compared to the NO_x sources due to lightning, stratospheric intrusions, and the lofting of ground-level pollution in cumulus clouds. Thus the role of aircraft as a source of upper tropospheric NO_x and its impact on lower stratospheric ozone is uncertain. Also uncertain is whether heterogeneous chemistry on ice crystals plays a significant role in the NO_x budget.

Understanding the impact of supersonic and subsonic aircraft exhaust on the stratospheric chemical balance is a complex problem. Knowledge of meteorological conditions is required to compute exhaust dispersion. Knowledge of aerosol chemistry is required to understand the aerosol formation process (from sulfur in fuels) and its impact on the background conditions. Finally, a good understanding of the lower stratosphere chemistry is required to understand the direct impact of the NO_x pollutants.

7.2.3 *Summary of science issues*

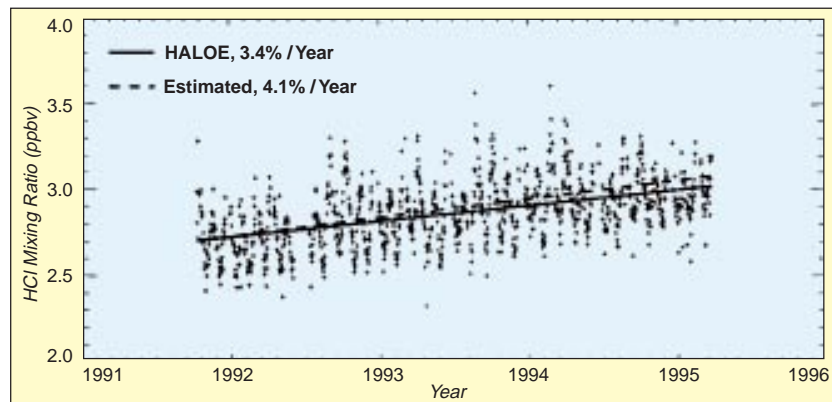
The investment by the scientific community in instrument and model development has produced a significant increase in the understanding of stratospheric chemical and dynamical processes. Although some fundamental questions of ozone loss have been answered, new questions have arisen. For example, the long-term response of the ozone layer to natural fluctuations (QBO, El Niño, volcanoes) is still not well understood (Section 7.2.1.1). The secular decrease in ozone following the eruption of Mt. Pinatubo was clearly associated with aerosol loading of the stratosphere—but the nearly one-year delay in the appearance of maximum ozone loss is still not explained. More fundamentally, the midlatitude trend in column ozone loss reported by Stolarski et al. (1991) is still not explained (although it is probably connected with the increase in stratospheric chlorine and the stratospheric chemistry associated with aerosols, see Section 7.1.3.3). Our understanding of the more-subtle chemical processes is still quite incomplete, which increases our uncertainty in the forecast predictions.

Under the Atmospheric Effects of Aviation Program (AEAP) the impact of stratospheric and tropospheric aircraft pollution on stratospheric ozone is now being investigated (Section 7.2.2.2). The research studies have reemphasized that our understanding of stratospheric transport is not complete with regard to transport, especially the containment of the pollutants within the midlatitude release regions and the distribution and magnitude of stratosphere-troposphere exchange, especially exchange of ozone. Many of the issues associated with the stratospheric circulation (Section 7.2.1.1) are above the observing range of current stratospheric aircraft (i.e.,

above 70 hPa). The analysis of UARS measurements has also revealed the tremendous advantages of global chemical data sets.

Finally, the most extensive observations of solar UV and energetic particle impact on ozone have been made recently by UARS. Unfortunately, these observations have been made during the declining phase of the solar cycle, and we have not developed a long-enough baseline of measurements to quantify the impacts of changing solar conditions. Long-term measurements of solar UV and total solar irradiance are needed during the waxing phase of the solar cycle.

FIGURE 7.7



Trend in HALOE HCl vs. time at 55 km compared with the estimated trend based on tropospheric emissions from Russell et al. (1996).

7.3 Required measurements and data sets

The measurement requirements are discussed below. Table 7.1 (pg. 326) summarizes the minimum measurements, their accuracies, and the instruments which will make the measurements. Often, key measurements will be made by more than one instrument, which gives the whole measurement suite a level of robustness in case of instrument failure.

7.3.1 Meteorological requirements

An understanding of the photochemistry of the stratosphere is clearly contingent on high-quality observations of temperature. The temperature field affects stratospheric physical processes in a number of ways. First, temperature fields are used to calculate geopotential heights and winds via the hydrostatic and geostrophic approximations. Second, temperatures affect the radiation field, particularly in relation to the longwave cooling in the stratosphere. Third, temperatures affect the chemistry via temperature-dependent reaction rates, and via the formation of PSCs (the indirect cause of the ozone hole). Hence, accurate and precise temperatures provide a basic foundation for stratospheric chemistry, radiation, dynamics, and transport.

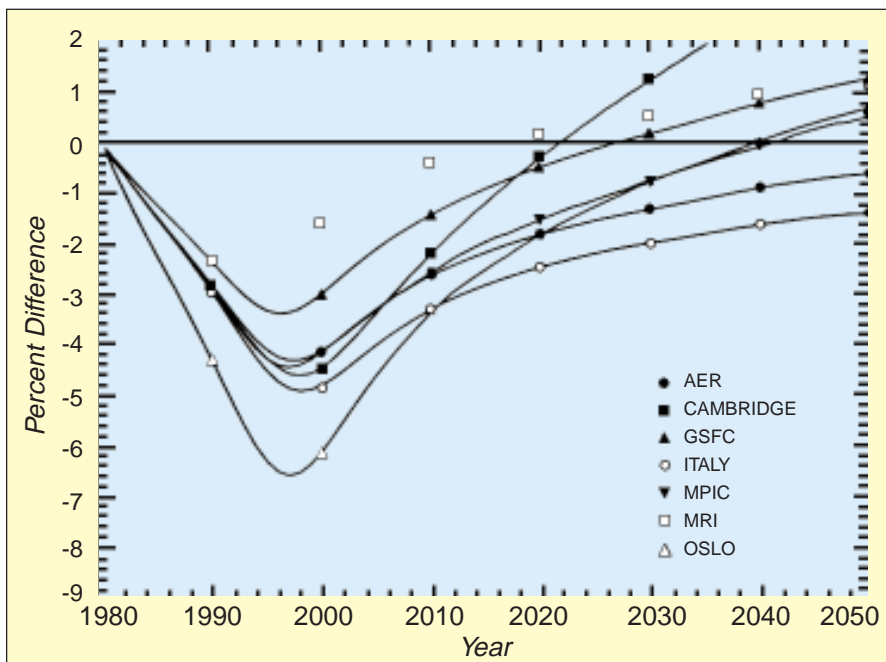
As stated in section 7.2.1.1 low-quality tropical meteorological observations are an impediment to our understanding of the interaction of the tropics and the middle latitudes.

The National Plan for Stratospheric Monitoring 1988-1997 (1989) set down the minimum requirements for meteorological variables between 1000 and 0.1 hPa. Their requirements were: 2.7-km vertical resolution; 12-hour time resolution; 1-K precision for temperature, and 5 m s^{-1} precision for winds.

Current radiosonde and rawinsonde measurements have precisions of a few tenths of a kelvin and 1-4 m s^{-1} wind speed in precision (Nash and Schmidlin 1987). Unfortunately, the balloon-borne rawinsonde system is limited to altitudes below 30 km. For higher altitudes, the meteorological rocket network provided some data, but the network has been effectively discontinued. Satellite systems are now relied upon to provide all of the meteorological information above 30 km.

The National Oceanographic and Atmospheric Administration (NOAA) TIROS Operational Vertical Sounder (TOVS) (Microwave Sounding Unit [MSU], Stratospheric Sounding Unit [SSU], and High-Resolution Infrared Sounder [HIRS]) SSU instrument has an error of 2 K at 10 hPa rising to 4 K at 1 hPa. The TOVS weighting functions are about 10-12-km deep. Later NOAA sounders use the Advanced Microwave Sounding Unit (AMSU) instead of MSU/SSU. The AMSU weighting functions are about half the depth of the TOVS functions. AMSU temperature measurements are limited to the atmosphere below 50 hPa.

FIGURE 7.8



A summary of model calculations of the percent change in column ozone versus time for March at 50° N for Scenario 1 (reproduced from Fig. 6-12 of WMO 1995).

The UARS Microwave Limb Sounder (MLS) has a vertical resolution of a few km, although its horizontal coverage is inferior to nadir-sounding TOVS and AMSU instruments. Improved understanding of stratospheric chemistry and heterogeneous processing suggests that improvement of temperature measurements will have an impact on our ability to predict where the heterogeneous reactions will take place.

Lower stratospheric temperature measurements made during the numerous polar aircraft missions suggest that the meteorological analyses (based upon TOVS) in the Southern Hemisphere are warm biased by about 2 K. This suggests that the Earth EOS stratospheric temperature accuracy requirements should be less than 0.5 K. It is also important that good temperature measurements be made near the tropical tropopause, especially in cloudy regions where air is entering the stratosphere through the tropopause.

Direct stratospheric wind data are needed where the divergence fields are significant (e.g., the tropics). The current wind requirement for assimilation models is an unbiased horizontal wind field accuracy of 2-5 m s⁻¹. These should be global measurements with a vertical resolution of a few kilometers. Presently, the UARS High Resolution Doppler Imager (HRDI) satellite wind instrument makes these measurements at the upper end of the limit.

A joint effort between NOAA, the Department of Defense, and NASA will produce the National Polar Orbiting Environmental Satellite System. This system will take needed operational data and certain long term observations for climate studies (Integrated Program Office, IPO, 1996, 1998). This system will be in place after 2008. The requirements for meteorological variables between 1000 and 1 mb include the following: temperatures accuracies of better than 1.5 K with vertical resolutions of 1 to 5 km from the ground to the mesosphere. The local revisit time is 6 hours and horizontal cell size of about 50 km. The NPOESS also has operational requirements for total column and profile ozone, aerosols and winds

(IPO, 1996, 1998).

7.3.2 Chemical measurement requirements

Atmospheric composition measurements form a cornerstone of any global change strategy. Chemical and dynamical measurements must be made in both the stratosphere and the troposphere. Indeed, chemical measurements around the upper troposphere and lower stratosphere should be among those with the highest priority.

7.3.2.1 Science questions

The science questions for stratospheric processes are mostly focused on the changes in the stratosphere expected to take place as anthropogenic pollutants accumulate in the middle atmosphere. Greenhouse gases are expected to substantially increase during the EOS period. Stratospheric halogens are expected to increase until 1999, then level off and slowly decline as a result of international regulations. The increases in these gases should produce chemical and dynamical changes. The magnitude of the stratospheric cooling in response to increasing greenhouse gases should far exceed the tropospheric warming because there are fewer feedback mechanisms (such as clouds) which buffer the radiative interaction. Increases in chlorine and bromine will cause decreases in stratospheric ozone. The ozone decrease could be exacerbated by colder

lower stratospheric temperatures caused by increasing greenhouse gas concentrations. For example, the colder stratospheric temperatures may lead to an expansion of the extent of PSCs and, hence, polar ozone depletion.

The complex chemistry of the stratosphere can only be understood in detail by measuring a broad range of species over varying conditions with global coverage and over at least an annual cycle. The first area which merits further observational and theoretical study is polar chemistry processes. Direct, simultaneous measurements of HOCl (or a proxy such as ClO), HNO₃, and N₂O₅ are critical since these gases are believed to be involved in PSC surface chemistry. Also, polar night observations, above 20 km, of the chemically-active species, along with PSC measurements, are needed in understanding polar ozone depletion. These regions are not presently accessible with balloons and aircraft.

In order to understand the large ozone depletion at midlatitudes (see Section 7.1.2.2), simultaneous measurements of N₂O₅, HOCl, HNO₃, and HCl are needed to assess the role of heterogeneous chemistry on background aerosols. Since OH and HO₂ drive the chemistry of the lower stratosphere, global measurements of these gases are required to evaluate ozone losses, especially any zonal asymmetries. Also, lower mesosphere observations of OH and HO₂, along with O₃ and temperature, are likely to be key links in understanding the large O₃ decrease expected to occur near 40 km as chlorine levels continue to rise. It is clear that full understanding of these changes requires not just O₃ and ClO measurements, but HO_x and NO_x measurements as well. Measurements in the lower mesosphere, where the chemistry is more simple, may provide the best data set for this analysis.

7.3.2.2 Key trace gas measurements

There are several scientific requirements to address middle-atmosphere chemistry issues:

- 1) The self-consistency between the source gases and the resulting active reservoir gases needs to be tested for the four major families that are important to ozone chemistry. The four families and most important species measurements required are: oxygen family (O₃), hydrogen family (H₂O, CH₄, OH, HO₂, H₂O₂), nitrogen family (N₂O, NO₂, HNO₃, N₂O₅), and chlorine family (CFCl₃, CF₂Cl₂, HCl, ClO, ClONO₂). Stratospheric chlorine is predicted by atmospheric models to increase by 20% in the next five years; thus, our understanding of the production and partitioning among the individual family constituents needs to be verified.
- 2) The changes in the Antarctic/Arctic lower stratosphere constituents (O₃, H₂O, ClO, OClO, HCl, BrO, N₂O, NO₂, HNO₃, N₂O₅, and aerosols) during the ozone hole period in the winter and spring need to be monitored. Since significant changes have been detected during the 1980s and 1990s in the polar regions, these geographical areas require special attention and monitoring.
- 3) There are a few chemical process studies which require investigation as indicated below.
 - a. The HO_x family (OH, HO₂, H₂O₂) is fundamentally important in stratospheric chemistry, but the database for that group remains one of the poorest in the atmosphere. Global measurements of the latitudinal, seasonal, and diurnal variation in the HO_x family and related species, H₂O and O₃, are needed to address this deficiency.
 - b. Models for the past decade have predicted less ozone in the upper stratosphere than is measured. Several species (O₃, O, NO₂, OH, and ClO) need to be measured in the upper stratosphere to help resolve this difficulty (see Section 7.1.4.1).
 - c. Models, in general, predict less odd nitrogen in the lower stratosphere than observed. Measurements of odd nitrogen species, NO₂, HNO₃, N₂O₅, and ClONO₂ in the lower stratosphere will help to deal with this problem.
 - d. Another odd nitrogen species, HNO₃, is not modeled accurately in the wintertime in the mid-to-high latitudes. A measurement of HNO₃, N₂O₅, H₂O, and aerosols should help confront this problem.
- 4) Global observations of ozone in the lowermost stratosphere (tropopause to about 20 km) with high horizontal, vertical, and temporal resolution are needed in order to quantify the ozone budget in that region of the atmosphere and, in particular, to determine the spatial and temporal distribution of ozone fluxes from the lowermost stratosphere to the troposphere. These fluxes, which are presently known only to within about a factor of two, are important for the ozone budget of the lowermost stratosphere and are crucial for understanding the ozone budget of the upper troposphere.

The measurement requirements to attack these science questions are outlined in Table 7.1. Generally, the

TABLE 7.1

MEASUREMENT	ACCURACY	EOS INSTRUMENT
Meteorology		
Temperature	1K	MLS, HIRDLS, SAGE III
Winds	2-5 m/s	(none)
Chemistry		
O ₃ (column)	15 milli-atm-cm	TOMS, OMI
O ₃ (profile)	0.2 ppm	MLS, HIRDLS, SAGE III
H ₂ O	0.5 ppm	MLS, HIRDLS, SAGE III
CFC-11 / 12	0.2 ppb	HIRDLS
N ₂ O	20 ppb	MLS, HIRDLS
CH ₄	0.1 ppm	HIRDLS
HCl	0.1 ppb	MLS
ClONO ₂	0.1 ppb	HIRDLS
HNO ₃	1.0 ppb	HIRDLS, MLS
NO ₂ / NO	0.2 ppb	HIRDLS, SAGE III
ClO	50 ppt	MLS
BrO	5 ppt	MLS
OH	0.5 ppt	MLS
N ₂ O ₅	0.2 ppb	HIRDLS
Aerosols	Surface area within 10%	SAGE III, HIRDLS
Solar Flux	100-400 nm to 4%	SOLSTICE

Stratospheric chemical and dynamical measurement requirements. Requirements include vertical resolution of 1-2 km through the tropopause into the lower stratosphere. Horizontal resolution is minimally that of UARS (2700 km), but increased horizontal resolution vastly improves the science. HIRDLS scanning will achieve a horizontal resolution of 400 km. AMLS may achieve a horizontal resolution of 100 km with MMIC array technology.

accuracies needed are 5-10% of the ambient concentrations found in the lower stratosphere.

7.3.3 Stratospheric aerosols and PSCs

The remote sensing of the composition of aerosol at midlatitudes is fairly straightforward. However, remote sensing of the composition and phase of the aerosol particles, for the case of the PSCs, is a developing topic of research. One research goal is to see to what extent it is possible to estimate the composition, phase, area, and volume densities from orbital observations. It is known that the volume densities of NAT and ternary particles are different. Carslaw et al. (1994) and Drdla et al. (1994) have shown that ternary solutions best describe some of the NASA High-Altitude Research Aircraft (ER-2) data. For

example, Figure 7.9 shows a graph of temperature versus volume density for several aerosol compositions. Beginning with a sulfuric acid droplet core, the volume density of the aerosol increases as temperatures become colder. These equilibrium curves were calculated using different amounts of ambient HNO₃ (5, 10, and 15 ppbv). Remote-sensing observations of temperature versus volume density (and/or aerosol extinction) will likely help classify the composition and phase of the PSC particles. It is also known that HNO₃ is incorporated in ternary, nitric acid dihydrate (NAD), and NAT particles as a function of temperature (i.e., curves of temperature versus the equilibrium gas phase of HNO₃ differ for the three compounds). Therefore, the simultaneous observation of aerosol extinction and HNO₃ gas mixing ratios should

help one to classify regions of PSCs as to composition and phase.

Since the microphysics of PSC particles is very temperature sensitive, absolute temperatures need to be measured to plus-or-minus 2 K, since curves of temperature versus volume density for NAT, ternary, and NAD particles (Figure 7.9, pg. 329) differ by only a few kelvins. Remote-sensing observations also average over many kilometers along a horizontal ray path. Vertical coverage is usually on the order of several km. Thus, the fine-scale structure of PSCs, as sampled by ER-2 instruments, cannot be resolved by the remote sounder. Another complication is due to present limitations in the theoretical understanding of how PSCs form, which compositions are formed, and the need for additional laboratory work to quantify at cold stratospheric temperatures the rates at which realistic PSC particles convert inactive to active chlorine compounds, and the need for additional laboratory measurements of the refractive indices of PSC and sulfuric droplets. Current research will see to what extent it is possible to refine present capability to quantify the mechanisms of PSC chemistry, as observed from orbit.

7.3.4 Solar ultraviolet flux

Solar radiation at wavelengths below about 300 nm is completely absorbed by the Earth's atmosphere and becomes the dominant direct energy input, establishing the composition and temperature through photodissociation, and driving much of the dynamics as well. Even small changes in this ultraviolet irradiance will have important and demonstrable effects on atmospheric ozone. Radiation between roughly 200 and 300 nm is absorbed by ozone and becomes the major loss mechanism for ozone in the middle atmosphere. Likewise, solar radiation < 200 nm is absorbed predominantly by molecular oxygen and becomes a dominant source of ozone in the middle atmosphere, so changes in these ultraviolet wavelengths will have, to first order, an inverse influence on ozone. These two atmospheric processes, driven by solar radiation, become the major natural control for ozone in the Earth's stratosphere and lower thermosphere. To fully understand the ozone distribution will require many coordinated observations and, in particular, a precise measurement of the solar ultraviolet flux.

The visible portion of solar radiation originates in the solar photosphere and has been accurately measured for about fifteen years (Willson and Hudson 1991). Apparently, this radiation varies by only small fractions of one percent over the 11-year activity cycle of the sun, with comparable variation over time scales of a few days. The ultraviolet portion of the solar spectrum comprises only about 1% (approximately 10 W m^{-2}) and originates

from higher layers of the photosphere. As we move to shorter and shorter wavelengths, the emission comes from higher and higher layers of the solar atmosphere. Unlike the solar photosphere, these higher levels are much more under the influence of solar activity, as manifested, for example, by increasing magnetic field strength. As the magnetic activity increases or disappears, the solar radiation, especially the ultraviolet, undergoes dramatic variations modulated by the 27-day rotation period of the sun. Near 120 nm the variation over time periods of days to weeks can be as large as 50%, and over the longer 11-year solar cycle the variation can be as large as a factor of two (Rottman 1993). Toward longer wavelengths, the solar variability decreases to levels of about 10% at 200 nm (Figure 7.10) and finally to only about 1% at 300 nm. Longward of 300 nm, the intrinsic solar variability is probably only on the order 0.1%, roughly commensurate with measurements of total solar radiation.

The challenge during the EOS time period is to provide measurements of the solar ultraviolet with a precision and accuracy capable of tracking the changes in the solar output. Ideally, the instrument will be capable of measuring changes as small as one percent throughout the EOS mission. This requirement is extremely challenging for solar instruments, especially those making observations at the ultraviolet wavelengths, which are notoriously variable. The harsh environment of space, coupled with the energetic solar radiation, rapidly degrades optical surfaces and usually makes the observations suspect. Some manner of in-flight calibration is required to unambiguously separate changes in the instrument response from true solar changes.

7.3.5 Validation of satellite measurements

The role of validation of satellite-based chemical measurements cannot be over stressed. Validation measurements, especially measurements of the same species using two different techniques, have proved to be invaluable for understanding satellite trace species measurements. The very successful UARS validation campaign has contributed a great deal to understanding the individual UARS measurements. The validation campaigns perform two major functions. First, they test the ability of a satellite instrument to make a measurement by giving an independent data point to compare against. Second, if the validation measurements are performed as part of a larger, coordinated campaign, the validation measurements done using aircraft and ground-based measurements can be used to link the small-scale geophysical features that they can observe with the large-scale geophysical features observable from space.

7.4 EOS contributions

7.4.1 Improvements in meteorological measurements

7.4.1.1 Global limb temperature measurements

The tropopause, the boundary between the upper troposphere (UT) and lower stratosphere (LS), is critical for understanding many important processes in the atmosphere. The tropopause is defined by a sharp change in the vertical temperature gradient, taking place over a few hundred meters at most. Below the tropopause, the troposphere is a region of active vertical mixing. Above the tropopause, the stratosphere is very stable with little vertical mixing. The match between these dissimilar regions, troposphere and stratosphere, modulates the processes that permit the exchange of mass, trace gases, momentum, potential vorticity, and energy between the two regions.

Unfortunately, present observing systems do not observe the UT-LS region with sufficient detail. The NOAA operational temperature sensors are characterized by vertical resolution of the retrievals of the order of 10-12 km. The detailed structure of the tropopause is much too thin to be seen by operational systems. However, their cross-track scanning capability gives them the ability to observe horizontal scales of about 100 km (Figure 7.11, pg. 381).

Temperature profiles with much higher vertical resolution can be obtained by observing the atmospheric limb, or horizon. The improvement results from the geometry, since most of the ray path through the atmosphere is within 1-2 km of the lowest, or tangent, point. In addition, the atmospheric signal is seen against the cold background of space. These factors can reduce the height of the vertical weighting functions to 3-4 km, and the effective resolution to ~ 5 km.

EOS limb sounders (MLS and the High-Resolution Dynamics Limb Sounder [HIRDLS] on the EOS Chemistry Mission [CHEM]) will greatly improve the accuracy, precision, and resolution of temperature measurements in the tropopause region. HIRDLS will determine temperatures with a resolution of 1-1.5 km, through a combination of a narrow (1 km) vertical field of view (FOV), low noise, and oversampling. MLS will make limb temperature measurements with a resolution of 2-3 km.

7.4.1.2 Higher horizontal resolution temperature profiles

Previous limb scanners have retrieved temperatures with higher vertical resolution, but, because the vertical scans are made at a single azimuth relative to the orbital plane, the horizontal resolution was limited to the orbital spac-

ing, or about 25°. This is sufficient to resolve only about 6 longitudinal waves. However, the UT-LS is a region in which smaller-scale waves from the troposphere are present. The horizontal resolution of previous limb sounders did not allow these smaller-scale systems to be measured. Figure 7.11 shows that the consistent scaling between vertical and horizontal scales suggests that higher horizontal resolution is required to sample geostrophic motions. The figure shows that HIRDLS has the ability to observe and retrieve with a 1-km vertical resolution and 4° horizontal resolution by scanning from side to side. This resolution allows all horizontal waves, up to ~ wavenumber 45, to be observed with the appropriate vertical resolution. Furthermore, the high vertical resolution of HIRDLS together with the high horizontal resolution and daily observations will for the first time provide accurate global mapping of the distribution of ozone in the lowermost stratosphere, a measurement that is crucial for determining the distribution of the flux of ozone to the troposphere, which in turn is crucial for understanding the budget of tropospheric ozone.

Recently a technological innovation has been proposed for the MLS instrument. Instead of a single heterodyne receiver, Microwave Monolithic Integrated Circuit (MMIC) arrays have been proposed at two frequencies. The array system (Array MLS [AMLS]) would allow 100-km × 100-km horizontal resolution temperature, ozone, N₂O, and water with lower power and weight. This proposed system is currently being studied by NASA.

7.4.2 Improvements in chemical measurements in the stratosphere

EOS instruments will give significantly improved stratospheric chemical measurements by having better measurement precision, particularly in the lower stratosphere, and a more-complete suite of collocated measurements, especially chemical radicals. The accuracy of the proposed instruments is close to that set down in Table 7.1. The major improvements in these chemical measurements are from MLS and HIRDLS. These two instruments (especially AMLS) are very synergistic in that HIRDLS will have high resolution in longitude as well as latitude (discussed in the previous section) while MLS will be able to make measurements in high-aerosol or cloudy regions. In addition, high-latitude coverage will be obtained on each orbit from both HIRDLS and MLS, a significant improvement from UARS, which had monthly gaps in high-latitude coverage and did not sample important periods.

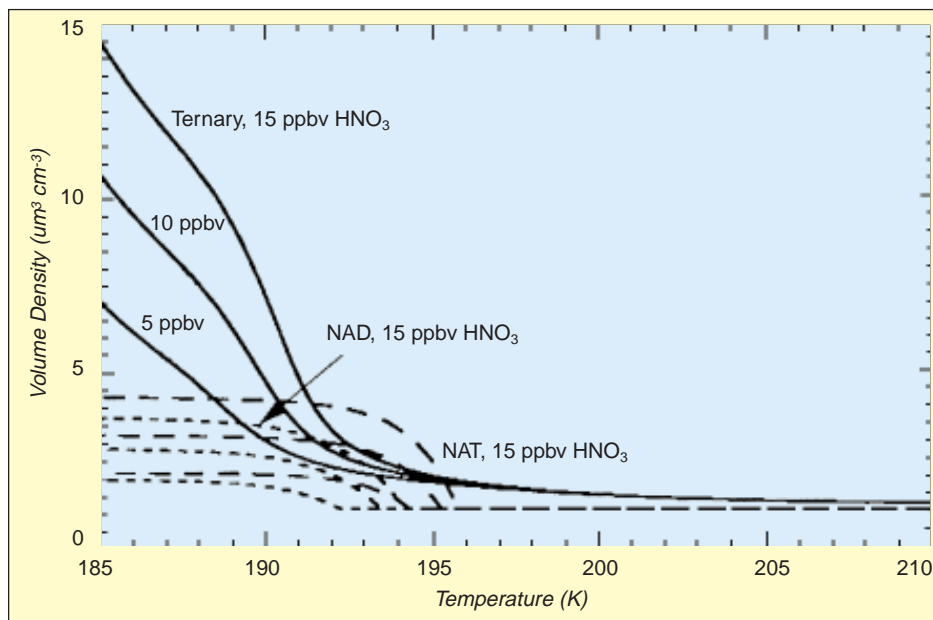
The high-vertical and horizontal-resolution coverage in the upper troposphere and lower stratosphere by HIRDLS (and AMLS) is extremely important because atmospheric waves with smaller horizontal scales can penetrate to these altitudes, creating variations on small scales that are critical to our understanding of wave breaking, mixing, stratosphere-troposphere exchange of mass constituents, and perhaps chemical processing.

Compared with UARS, EOS MLS has tremendous improvements in precision of lower stratospheric measurements due to its increased spectral bandwidth and choice of stronger spectral lines. Whereas UARS MLS was designed primarily for the middle and upper stratosphere, EOS MLS emphasizes the lower stratosphere. Improvements over UARS are summarized in Table 7.2.

Inclusion of the OH measurement in MLS is a major qualitative improvement in the suite of global stratospheric measurements which EOS will provide. This measurement is possible because of recent submillimeter-wavelength technology advances, which were not available for UARS. The OH measurement will extend to the lowest and the highest regions of the stratosphere, where HO_x chemistry is thought to be the dominant ozone loss mechanism on a global scale. It will cover regions where OH is thought to control the conversion of CH₄ to H₂O, to control the rates of SO₂ and OCS oxidation to sulfate aerosol, and to be an essential player in controlling the balance between radical and reservoir species in the nitrogen and chlorine families. The global OH measurements over the complete stratosphere by EOS will give unprecedented new information on stratospheric chemistry, and are especially valuable in being made simultaneously with that of the many other EOS chemistry measurements. MLS will also likely be able to measure HO₂ in the upper stratosphere, further testing and improving our understanding of stratospheric hydrogen chemistry.

HIRDLS NO₂ measurements provide an important component of NO_x, and, because of its reactions with ClO

FIGURE 7.9



Temperature versus volume density for several aerosol compositions expected in the stratosphere.

(measured by MLS), the formation of ClONO₂, also measured by HIRDLS. HIRDLS measurements of N₂O₅ and HNO₃, along with the ClONO₂, provide a fairly complete set of measurements of the NO_y (NO_y is chemical shorthand for the sum of all nitrogen reservoir and radical species, NO_x plus HNO₃, mostly) species. Note that the ratio of NO₂/HNO₃ provides an additional way of deriving the OH concentration.

MLS will also measure middle- and upper-stratospheric BrO, the dominant radical in the bromine chemical family. No global stratospheric bromine measurements have been made to date, and the BrO measurement will be important to test our understanding of this chemistry.

Other important improvements in the suite of chemical measurements include the simultaneous and commonly-calibrated measurement of HCl and ClO by MLS. This allows very accurate monitoring of the ClO/HCl ratio, which provides a sensitive indicator of our understanding of chlorine chemistry and early detection of changes. The MLS and HIRDLS N₂O measurements will allow much more accurate distinction between chemical and dynamical changes in the atmosphere.

Total ozone measurements using TOMS will continue with a flight on a Russian Meteor satellite in 2000. Total ozone measurements will continue with an advanced Ozone Monitoring Instrument (OMI) contributed to EOS Chem by the Netherlands. OMI is a hyperspectral imaging spectrometer operating in the ultraviolet and visible. Its hyperspectral capabilities will improve the precision

and accuracy of the total ozone measurements by better estimates of cloud heights and aerosols effects. OMI will make additional measurements which will be highly complementary to EOS Chem and SAGE, such as column amounts of NO_2 , background SO_2 , OClO , BrO , aerosols, and derived UV-B. After EOS-Chem, total and profile ozone will be monitored by the NPOESS using an advanced TOMS and a separate profiling instrument capable of high vertical resolution measurements in the lower stratosphere.

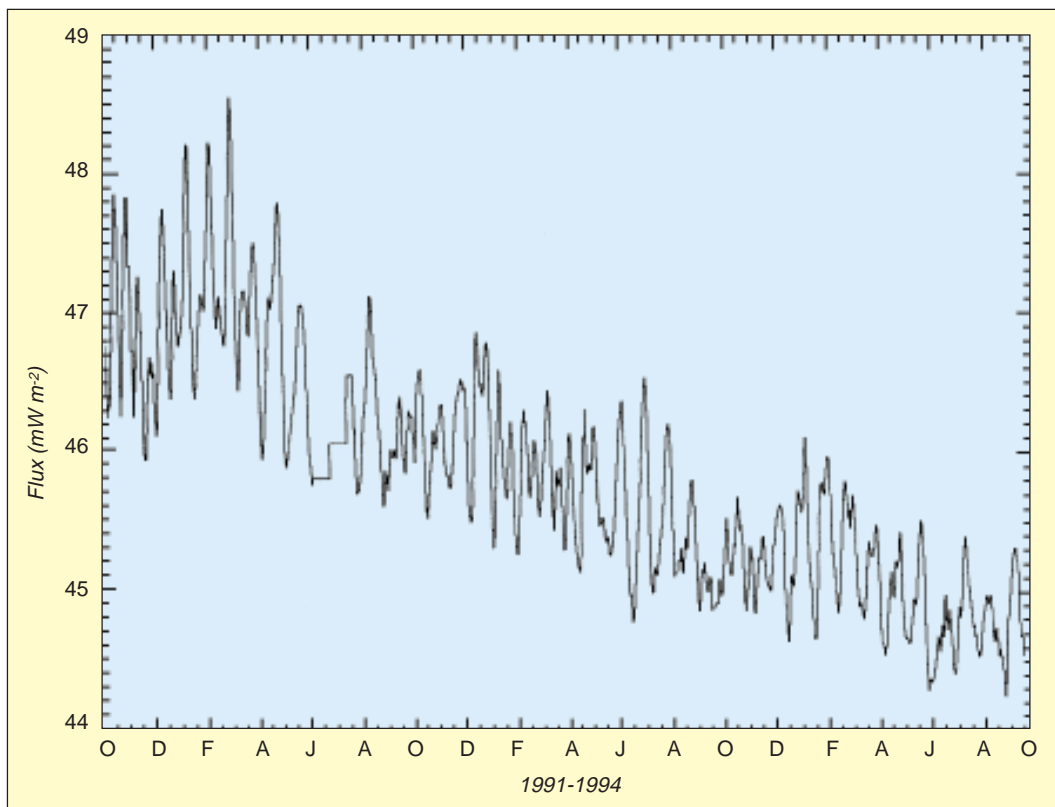
7.4.3 Improvements in measurements of aerosols

EOS instruments will improve upon the ability demonstrated by UARS for several reasons. Temperature retrievals will be more refined, and the horizontal and vertical resolution will be better. HIRDLS resolution will be on the order of 1 km in the vertical coordinate, and 4° latitude-by- 4° longitude in the horizontal coordinate, and will retrieve temperatures with an accuracy of 1K at altitudes below 50 km (Gille and Barnett 1992). The HIRDLS experiment has four spectral channels which are specifically dedicated to obtaining aerosol extinction measurements, but will obtain aerosol information from many of the other channels as well. The measurements

will observe and distinguish midlatitude sulfuric acid droplets and PSCs. H_2O and HNO_3 , two gases which are incorporated into stratospheric aerosols, will be retrieved by HIRDLS. In addition, ClONO_2 and N_2O_5 , species important in heterogeneous processing, are retrieved by HIRDLS.

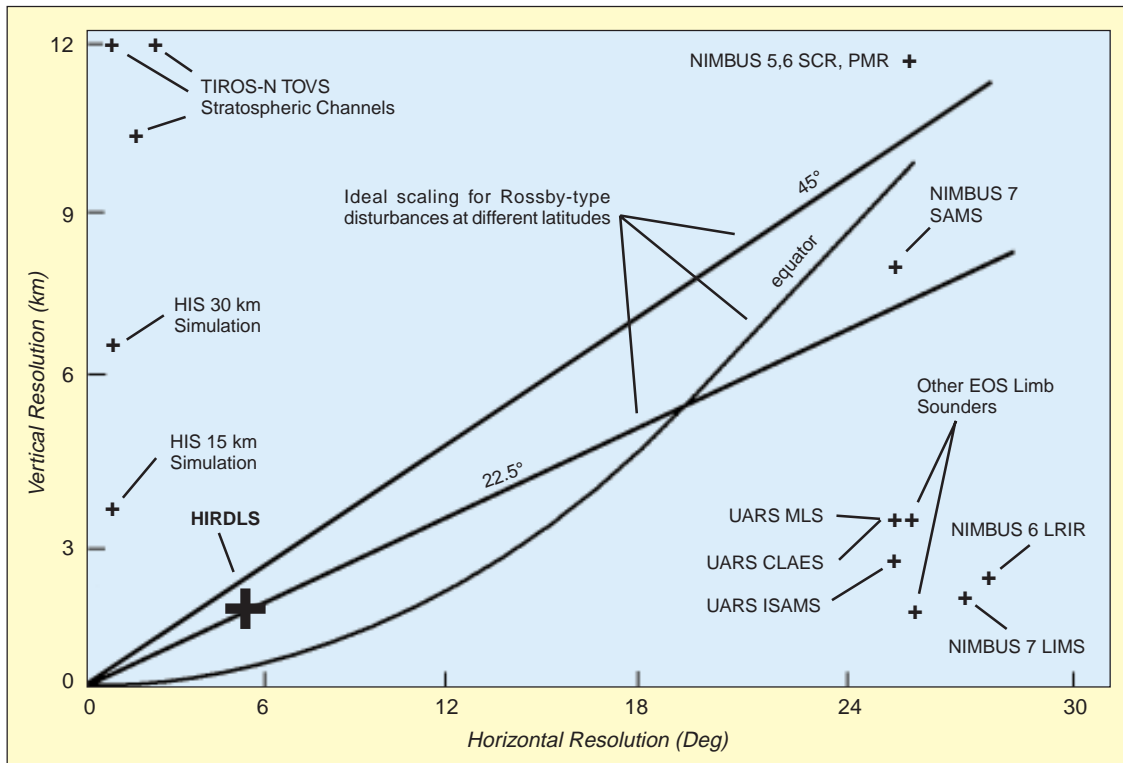
The SAGE III aerosol data will consist of vertical profiles of aerosol extinction at seven wavelengths extending in altitude range from the lower troposphere or cloud top to about 40-km altitude, with vertical resolution of 1 km. From the seven-wavelength aerosol extinction measurements, parameters describing the aerosol physical size distribution, such as volume density and surface area density, can be estimated with good accuracy, with uncertainties of the order of 10%. The wide spectral extinction behavior from the SAGE III measurements should also provide sufficient information to distinguish between a single-modal versus a bimodal aerosol size distribution, especially important immediately after volcanic eruptions. The SAGE III instrument will provide better tropospheric aerosol measurements with extinction measurements with multiple wavelengths through the mid-troposphere, and at least at two wave-

FIGURE 7.10



Changes in solar ultraviolet flux (200-205 nm) versus time from the UARS SOLSTICE instrument (Rottman et al. 1993).

FIGURE 7.11



A comparison of the vertical and horizontal resolutions of various limb- and nadir-sounding satellite instruments. Lines indicate the ideal observation scale for Rossby waves.

lengths down to sea level. For the measurements of PSCs, SAGE III will be the first satellite instrument to provide size distribution information.

The SAGE III aerosol information will be key to understanding the role played by stratospheric aerosols and PSCs in heterogeneous chemical reactions and ozone depletion and will be indispensable for understanding aerosol radiative forcing.

7.4.4 Improvements in measurements of the solar ultraviolet flux

The EOS Solar Stellar Irradiance Comparison Experiment (SOLSTICE) has the unique capability of observing bright, blue stars employing the very same optics and detectors used for the solar observations. With the assumption that these stars are extremely stable, the response of SOLSTICE could be accurately monitored by observing a single star. However the calibration plan uses twenty or more of these reference stars, and it is the average flux from the entire ensemble of stars that provides an even more reliable reference for the solar observations. Repeated observation of the stars should yield an average flux level that is unchanging in time. A decrease in the

level is an indication of loss in instrument sensitivity and adjustments are made accordingly. Since the same optics and detectors are used for the solar observations, the same corrections apply, and the resulting solar measurement is reliable and free of any instrumental effects. The large dynamic range between the stellar and solar signals is on the order of eight to nine orders of magnitude, and is easily accommodated by changing the entrance apertures, spectral bandpass, and integration times (Rottman et al. 1993).

7.4.5 Advanced chemical/dynamical/radiative models

EOS is currently funding a U.S. effort and cooperates with a foreign effort to build fully interactive chemical/dynamical models for interpretation of EOS data. The first effort, the Schoeberl Interdisciplinary Science Investigation (IDS), currently uses data assimilation winds and temperatures (see Section 7.4.6) along with a chemical transport model to simulate the stratospheric system. The results of this model are then used to compare with observations such as those from UARS, SAGE, and TOMS. Full coupling and feedback between the meteorology and

TABLE 7.2

<i>MEASUREMENT</i>	<i>INSTRUMENT</i>	<i>MAJOR IMPROVEMENTS OVER UARS</i>
O ₃ (profile)	HIRDLS, MLS, OMI, SAGE III	Much better spatial resolution, much better precision (especially in lower stratosphere), continuous coverage of both hemispheres, column measurement obtained simultaneously with profile, 5× improvement in precision in lower stratosphere over UARS MLS
OH	MLS	Not measured on UARS
H ₂ O	HIRDLS, MLS, SAGE III	Much better spatial resolution, much better sensitivity in the tropopause region, continuous coverage of both hemispheres. 2× improvement in precision
CH ₄	HIRDLS	Much better spatial resolution, much better precision, continuous coverage of both hemispheres
ClO	MLS	Much better sensitivity, continuous coverage of both hemispheres with 5× improvement in precision over UARS
BrO	MLS	Not measured on UARS
OCIO	SAGE III	Not measured on UARS
HCl	MLS	Continuous coverage of both hemispheres, measurement not degraded by aerosols
ClONO ₂	HIRDLS	Much better spatial resolution and precision, continuous coverage of both hemispheres
CFCl ₃	HIRDLS	Much better precision than on UARS
Temperature	MLS, HIRDLS, SAGE III	10× improvement in precision over UARS
CF ₂ Cl ₂	HIRDLS	Much better spatial resolution and precision, continuous coverage of both hemispheres
NO ₂	HIRDLS, SAGE III	Much better spatial resolution, improved precision, continuous coverage of both hemispheres
NO ₃	SAGE III	Not measured on UARS
HNO ₃	HIRDLS, MLS	Much better spatial resolution and precision, measurements in presence of aerosols, cirrus, and PSCs, continuous coverage of both hemispheres, 20× improvement in precision over UARS
N ₂ O ₅	HIRDLS	Much better spatial resolution, coverage and precision, continuous coverage of both hemispheres
N ₂ O	HIRDLS, MLS	Much better spatial resolution and precision, measurements in presence of aerosols and cirrus, continuous coverage of both hemispheres
SO ₂	MLS	Continuous coverage of both hemispheres
CO	MLS	Much better sensitivity and continuous coverage of both hemispheres
HO ₂	MLS	Not measured on UARS
HOCl	MLS	Not measured on UARS

Improvements in EOS Chemistry measurements over UARS.

chemistry do not occur at this stage. Later, the chemical/transport model will be used along with the EOS chemical data to produce an assimilated chemical data set. The full coupling will occur through the assimilation system. The observations of motion of long-lived trace species can be inverted to make better estimates of stratospheric winds. The forecast of temperatures from the assimilation modeling effort will increase the accuracy of the retrieved trace gases.

The second effort, the Pyle IDS (United Kingdom), uses a full GCM and chemical package. The GCM and chemical/radiation/transport system will be fully linked. The objectives are to examine the sensitivity of the atmosphere to the chemical/radiative/dynamical feedback systems. This foreign effort consists of a full-fledged EOS IDS team but is not funded by NASA.

7.4.6 Full meteorological and chemical assimilation of EOS data sets

The Data Assimilation Office (DAO) at NASA/Goddard Space Flight Center (GSFC) already provides routine support to the stratospheric aircraft missions planned to study stratospheric ozone. Daily analyses are produced for the Stratospheric Tracers of Atmospheric Transport (STRAT) mission, and, given the duration of this mission, this will evolve into the operational support of the EOS Morning Platform (AM-1). During the aircraft deployment periods, forecasts are produced to aid in-flight planning. These forecasts enhance the ability of the mission planners to target air of specific chemical characteristics.

The current DAO meteorological analyses have a large impact on stratospheric chemistry studies. The wind fields are of sufficient quality to remove the dynamical uncertainty from trace observations. This allows a high-caliber examination of chemical processes, a benefit that has been realized for satellite, balloon, and aircraft data. There are active efforts of the DAO to improve the subtropical winds and the deep vertical motions that link the stratosphere and mesosphere.

Future plans call for a straightforward extension of the application of winds from the DAO assimilation to more-general problems. This includes stratospheric-tropospheric exchange, as well as broader issues of tropospheric chemistry. Advanced assimilation systems will directly assimilate constituent observations. First, long-lived tracers will be assimilated. Initial studies of N₂O from UARS show that assimilation can in fact provide verifiable global information from the non-global UARS coverage pattern. An important goal of the DAO constituent effort is to improve wind estimates, especially in the tropics. Wind inversion techniques are being actively investigated. In addition, at least two university proposals have been recently submitted to attempt to assimilate aerosol observations within the DAO system. These proposals are examples of the long-term efforts to assimilate the complete chemical suite of measurements, with the goal of bringing to bear the quantitative analysis of data assimilation on the internal consistency of the chemical observations of UARS and CHEM.

7.5 Foreign partners and other measurement sources

Foreign partners are critical to the scientific success of the global stratospheric measurements program. The scale of collaboration ranges from individual science teams, to collaborative instruments, to reciprocal flights of instruments, to mission planning. The timing of the EOS CHEM mission has been structured to follow the launch of the European Space Agency's (ESA's) Environmental Satellite I (ENVISAT I). This mission, to be launched in 2000, follows the successful NASA UARS mission. ENVISAT will make many critical trace species measurements in the time period of maximum stratospheric chlorine. This long-term data set, UARS-ENVISAT-CHEM, will be ab-

solutely critical to our understanding of the role of trace species in controlling ozone in the stratosphere.

Other international space platforms will carry a few stratospheric instruments: The French Systeme pour l'Observation de la Terre (SPOT) satellite will carry the Polar Ozone Aerosol Measurements II (POAM II) aerosol and ozone measuring system. The Russian MIR space station will fly the Fourier Transform Spectrometer, DOPL.

In addition to these space instruments, several stratospheric aircraft campaigns are planned for the next few years (e.g., the STRAT campaign).

References

- Aikin, A. C., 1992: Stratospheric evidence of relativistic electron precipitation. *Planet. Space Sci.*, **40**, 413–431.
- Anderson, J.G., D.W. Toohey, and W.H. Brune, 1991: Free radicals within the Antarctic vortex: The role of CFC's in the Antarctic ozone loss. *Science*, **251**, 39–46.
- Austin, J., R. R. Garcia, J. M. Russell III, S. Solomon, and A. F. Tuck, 1986: On the atmospheric photochemistry of nitric acid. *J. Geophys. Res.*, **91**, 5477–5485.
- Austin, J., N. Butchart, and K. P. Shine, 1992: Possibility of an Arctic ozone hole in a doubled-CO₂ climate. *Nature*, **360**, 221–225.
- Brasseur, G., 1993: The response of the middle atmosphere to long-term and short-term solar variability: A two-dimensional model. *J. Geophys. Res.*, **98**, 23,079–23,090.
- Brune, W. H., J. G. Anderson, and K. R. Chan, 1989: In situ observations ClO in the Antarctic: ER-2 aircraft results from 54 S to 72 S latitude. *J. Geophys. Res.*, **94**, 16649–16663.
- Callis, L. B., D. N. Baker, J. B. Blake, J. D. Lambeth, R. E. Boughner, M. Natarajan, R. W. Klebesadel, and D. J. Gorney, 1991a: Precipitating relativistic electrons: Their long-term effect on stratospheric odd nitrogen levels. *J. Geophys. Res.*, **96**, 2939–2976.
- Callis, L. B., R. E. Boughner, M. Natarajan, J. D. Lambeth, D. N. Baker, and J. B. Blake, 1991b: Ozone depletion in the high latitude lower stratosphere: 1979–1990. *J. Geophys. Res.*, **96**, 2921–2937.
- Carslaw, K. S., B. P. Luo, S. L. Clegg, Th. Peter, P. Brimblecombe, and P. J. Crutzen, 1994: Stratospheric aerosol growth and HNO₃ gas depletion from coupled HNO₃ and water uptake by liquid particles. *Geophys. Res. Lett.*, **21**, 2479–2482.
- Chipperfield, M. P., D. Cariolle, P. Simon, R. Ramarosan, and D. J. Lary, 1993: A three-dimensional modeling study of trace species in the Arctic lower stratosphere during winter 1989–1990. *J. Geophys. Res.*, **98**, 7199–7218.
- Considine, D. B., A. R. Douglass, and C. H. Jackman, 1994: Effects of a PSC parameterization on ozone depletion due to stratospheric aircraft in a 2-D model. *J. Geophys. Res.*, **99**, 18,879–18,894.
- Considine, D. B., A. R. Douglass, and C. H. Jackman, 1995: Sensitivity of two-dimensional model predictions of ozone response to stratospheric aircraft: An update. *J. Geophys. Res.*, **100**, 3075–3090.
- Dobson, G. M. B., 1966: Annual variation of ozone in Antarctica. *Quart. J. Roy. Met. Soc.*, **92**, 546–550.
- Douglass, A. R., R. B. Rood, J. A. Kaye, R. S. Stolarski, D. J. Allen, and E. M. Larson, 1991: The influence of polar heterogeneous processes on reactive chlorine at middle latitudes: Three-dimensional model implications. *Geophys. Res. Lett.*, **18**, 25–28.
- Douglass, A. R., R. B. Rood, J. W. Waters, L. Froidevaux, W. Read, L. Elson, M. Geller, Y. Chi, M. Cerniglia, S. Steenrod, 1993: A 3-D simulation of the early winter distribution of reactive chlorine in the north polar vortex. *Geophys. Res. Lett.*, **20**, 1271–1274.
- Drdla, K., A. Tabazadeh, R. P. Turco, M. Z. Jacobson, J. E. Dye, C. Twohy, and D. Baumgardner, 1994: Analysis of the physical state of one Arctic polar stratospheric cloud based on observations. *Geophys. Res. Lett.*, **21**, 2475–2478.
- Eckman, R. S., W. L. Grose, R. E. Turner, W. T. Blackshear, J. M. Russell III, L. Froidevaux, J. W. Waters, J. B. Kumer, and A. E. Roche, 1995: Stratospheric trace constituents simulated by a three-dimensional general circulation model: comparison with UARS data. *J. Geophys. Res.*, **100**, 13,951–13,966.
- Farman, J. C., B. B. Bardiner, and J. D. Shanklin, 1985: Large losses of total ozone in Antarctica reveal seasonal ClO_x/NO_x interaction. *Nature*, **315**, 207–210.
- Fioletov, V.E. J.B. Kerr, D.I. Wardle, J. Davies, E.W. Hare, C.T. McElroy, and D.W. Tarasick, 1997: Long term decline over the Canadian arctic to early 1997 from ground based and balloon observations. *Geophys. Res. Lett.*, **24**, 2705–2708.
- Fleming, E. L., S. Chandra, C. H. Jackman, D. B. Considine, and A. R. Douglass, 1995: The middle atmospheric response to short- and long-term solar UV variations: Analysis of observations and 2-D model results. *J. Atmos. Terr. Phys.*, **57**, 333–365.
- Fraser, P., S. Penkett, M. Gunson, R. Weiss, and F. S. Rowland, 1994: Measurements, Chapter 1 in “NASA Report on Concentrations, Lifetimes, and Trends of CFC's, Halons, and Related Species,” edited by J. Kaye, S. Penkett, and F. Ormond, NASA Reference Publication 1339, Washington, D. C., 1.1–1.68.
- Gaines, E. E., D. L. Chenette, W. L. Imhof, C. H. Jackman, and J. D. Winningham, 1995: Relativistic electron fluxes in May 1992 and their effect on the middle atmosphere. *J. Geophys. Res.*, **100**, 1027–1033.
- Geller, M. A., Y. Chi, R. B. Rood, A. R. Douglass, J. A. Kaye, and D. J. Allen, 1993: Satellite observation and mapping of wintertime ozone variability in the lower stratosphere. *J. Atmos. and Terr. Phys.*, **55**, 1081–1088.
- Gille, J. C., and J. J. Barnett, 1992: The high resolution dynamics limb sounder (HIRDLs). An instrument for the study of global change, in “The Use of EOS for Studies of Atmospheric Physics,” J. C. Gille and G. Visconti, editors, 433–450.
- Grainger, R. G., A. Lambert, F. W. Taylor, J. J. Remedios, C. D. Rodgers, M. Corney, and B. J. Kerridge, 1993: Infrared absorption by volcanic stratospheric aerosols observed by ISAMS. *Geophys. Res. Lett.*, **20**, 1283–1286.
- Gunson, M. R., et al., Increase in levels of stratospheric chlorine and fluorine loading between 1985 and 1992, 1994: *Geophys. Res. Lett.*, **21**, 2223–2226.
- Hanson, D. R., A. R. Ravishankara, and S. Solomon, 1994: Heterogeneous reactions in sulfuric acid aerosols: A framework for model calculations. *J. Geophys. Res.*, **99**, 3615–3629.
- Hofmann, D. J., J. W. Harder, J. M. Rosen, J. V. Hereford, and J. R. Carpenter, 1989: Ozone profile measurements at McMurdo Station, Antarctica, during the spring of 1987. *J. Geophys. Res.*, **94**, 16,527–16,536.
- Hofmann, D. J., S. J. Oltmans, J. A. Lathrop, J. M. Harris, and H. Vomel, 1994: Record low ozone at the south pole in spring. *Geophys. Res. Lett.*, **21**, 421–424.
- Hollandswarth, S. M., R. D. McPeters, L. E. Flynn, W. Planet, A. J. Miller, and S. Chandra, 1995: Ozone trends deduced from combined Nimbus 7 SBUV and NOAA 11 SBUV/2 data. *Geophys. Res. Lett.*, **22**, 905–908.
- Holton, J. R., P. H. Haynes, M. E. McIntyre, A. R. Douglass, R. B. Rood, and L. Pfister, 1995: Stratosphere-troposphere exchange. *Reviews of Geophys.*, **33**, 403–439.
- Hood, L. L., and J. P. McCormack, 1992: “Components of interannual ozone change based on NIMBUS 7 TOMS data.” *Geophys. Res. Lett.*, **19**, 2309–2312.
- Huang, T. Y. W., and G. P. Brasseur, 1993: Effect of long-term solar variability in a two-dimensional interactive model of the middle atmosphere. *J. Geophys. Res.*, **98**, 20,413–20,427.
- IPCC, “Climate Change, 1994,” 1995: (J. Houghton, L. Filho, J. Bruce, H. Lee, B. Callander, E. Haites, N. Harris, and K. Maskell, Eds.) Cambridge University Press, Cambridge, U.K., 339 pp.
- IPO, Integrated Operational Requirements Document (IORD) I, March, 1996 IPO, Technical Requirements Document (TRD), Appendix D, NPOESS System EDR Requirements, June, 1998.

- Jackman, C. H., J. E. Nielsen, D. J. Allen, M. C. Cerniglia, R. D. McPeters, A. R. Douglass, and R. B. Rood, 1993: The effects of the October 1989 solar proton events on the stratosphere as computed using a three-dimensional model. *Geophys. Res. Lett.*, **20**, 459–462.
- Jackman, C. H., M. C. Cerniglia, J. E. Nielsen, D. J. Allen, J. M. Zawodny, R. D. McPeters, A. R. Douglass, J. E. Rosenfield, and R. B. Rood, 1995: Two-dimensional and three-dimensional model simulations, measurements, and interpretation of the influence of the October 1989 solar proton events on the middle atmosphere. *J. Geophys. Res.*, **100**, 11,641–11,660.
- Jensen, E. J., O. B. Toon, J. D. Spinhirne, and H. B. Selkirk, 1997: On the formation and persistence of subvisible cirrus clouds near the tropical tropopause, *J. Geophys. Res.*, in press.
- Kinnison, D. E., H. S. Johnston, and D. J. Wuebbles, 1994a: Model study of atmospheric transport using carbon 14 and strontium 90 as inert tracers. *J. Geophys. Res.*, **99**, 20,647–20,664.
- Kinnison, D. E., K. E. Grant, P. S. Connell, D. A. Rotman, and D. J. Wuebbles, 1994b: The chemical and radiative effects of the Mount Pinatubo eruption. *J. Geophys. Res.*, **99**, 25,705–25,731.
- Lefevre, F., G. P. Brasseur, I. Folkins, A. K. Smith, and P. Simon, 1994: Chemistry of the 1991–1992 stratospheric winter: three dimensional model simulations. *J. Geophys. Res.*, **99**, 8183–8197.
- Logan, J. A., 1994: Trends in the vertical distribution of ozone: An analysis of ozonesonde data. *J. Geophys. Res.*, **99**, 25,553–25,585.
- Mankin, W. G., and M. T. Coffey, 1984: Increased stratospheric hydrochloride in the El Chichon cloud. *Nature*, **226**, 170–174.
- Mankin, W. G., M. T. Coffey, and A. Goldman, Airborne observations of SO₂, HCl, and O₃ in the stratospheric plume of the Pinatubo volcano in July 1991. *J. Geophys. Res.*, **100**, 2953–2972.
- Manney, G.L., L. Froidevaux, M.L. Santee, R.W. Zurek, and J.W. Waters, 1997: MLS observations of the Arctic ozone loss in 1996–1997. *Geophys. Res. Lett.*, **24**, 2697–2700.
- Manney, G. L., L. Froidevaux, J. W. Waters, and R. W. Zurek, 1995: Evolution of microwave limb sounder ozone and the polar vortex during winter. *J. Geophys. Res.*, **100**, 2953–2972.
- Massie, S. T., P. L. Bailey, J. C. Gille, E. C. Lee, J. L. Mergenthaler, A. E. Roche, J. B. Kumer, E. F. Fishbein, J. W. Waters, and W. A. Lahoz, 1994: Spectral signatures of polar stratospheric clouds and sulfate aerosol. *J. Atmos. Sci.*, **51**, 3027–3044.
- McCormick, M. P., and J. C. Larsen, 1988: Antarctic measurements of ozone by SAGE II in the spring of 1985, 1986, and 1987. *Geophys. Res. Lett.*, **15**, 906–910.
- McCormick, M. P., L. W. Thomason, and C. R. Trepte, 1995: Atmospheric effects of the Mt. Pinatubo eruption. *Nature*, **373**, 399–404.
- McElroy, M. B., R. J. Salawitch, and S. C. Wofsy, 1986: Antarctic O₃: Chemical mechanisms for the spring decrease. *Geophys. Res. Lett.*, **13**, 1296–1297.
- Murphy, D., and G. B. Gary, 1995: Mesoscale temperature fluctuations and polar stratospheric clouds. *J. Atmos. Sci.*, **52**, 1753–1760.
- Nash, J., and F. Schmidlin, 1987: Final report of the WMO international radiosonde intercomparisons. WMO Report No. 30.
- National Plan for Stratospheric Monitoring 1988–1997, 1989: Dept. of Commerce/NOAA, FCM-P17-1989.
- Newman, P.A., J.F. Gleason, R.D. McPeters, and R.S. Stolarski, 1997: Anomalous low ozone over the Arctic. *Geophys. Res. Lett.*, **24**, 2689–2692.
- Oberbeck, V. R., J. M. Livingston, P. B. Russell, R. F. Pueschel, J. N. Rosen, M. T. Osborn, M. A. Kritz, K. G. Snetsinger, and G. V. Ferry, 1989: SAGE II aerosol validation: Selected altitude measurements, including particle micrometeorology. *J. Geophys. Res.*, **94**, 8367–8380.
- Osborn, M. T., J. M. Rosen, M. P. McCormick, P.-H. Wang, J. M. Livingston, and T. J. Swisler, 1989: SAGE II aerosol correlative observations: Profile measurements. *J. Geophys. Res.*, **94**, 8353–8366.
- Pitari, G., V. Rizi, L. Ricciardulli, and G. Visconti, 1993: High speed civil transport impact: Role of sulfate, nitric acid trihydrate and ice aerosols studied with a two-dimensional model including aerosol physics. *J. Geophys. Res.*, **98**, 23,141–23,164.
- Pollack, J. B., F. C. Witteborn, K. O'Brien, and B. Flynn, 1991: A determination of the infrared optical depth of the El Chichón volcanic cloud. *J. Geophys. Res.*, **97**, 3115–3122.
- Poole, L. R., and M. C. Pitts, 1994: Polar stratospheric cloud climatology based on Stratospheric Aerosol Measurement II observations from 1978–1989. *J. Geophys. Res.*, **99**, 13,083–13,089.
- Proffitt, M. H., J. A. Powell, A. F. Tuck, D. W. Fahey, K. K. Kelly, A. J. Drueger, M. R. Schoeberl, B. L. Gary, J. J. Margitan, K. R. Chan, M. Loewenstein, and J. R. Podolske, 1989: A chemical definition of the boundary of the Antarctic ozone hole. *J. Geophys. Res.*, **94**, 11,437–11,448.
- Randel, W. J., and J. B. Cobb, 1994: Coherent variations of monthly mean total ozone and lower stratospheric temperature. *J. Geophys. Res.*, **99**, 5433–5448.
- Rasch, P. J., B. A. Boville, and G. P. Brasseur, 1995: A three-dimensional general circulation model with coupled chemistry for the middle atmosphere. *J. Geophys. Res.*, **100**, 9041–9071.
- Reid, G. C., S. Solomon, and R. R. Garcia, 1991: Response of the middle atmosphere to the solar proton events of August–December 1989. *Geophys. Res. Lett.*, **18**, 1019–1022.
- Reinsel, G. C., G. C. Tiao, D. J. Wuebbles, J. B. Kerr, A. J. Miller, R. M. Nagatani, L. Bishop, and L. H. Ying, 1994: Seasonal trend analysis of published ground-based and TOMS total ozone data through 1991. *J. Geophys. Res.*, **99**, 5449–5464.
- Report of the International Ozone Trends Panel 1988. 1990: WMO Report 18.
- Rinsland, C. P., G. K. Yue, M. R. Gunson, R. Zander, and M. C. Abrams, 1994: Mid-infrared extinction by sulfate aerosols from the Mt. Pinatubo eruption. *J. Quant. Spectrosc. Radiat. Transfer*, **52**, 241–252.
- Rood, R. B., A. R. Douglass, J. A. Kaye, M. A. Geller, Y. Chi, D. J. Allen, E. M. Larson, E. R. Nash, and J. E. Nielsen, 1991: Three-dimensional simulations of wintertime ozone variability in the lower stratosphere. *J. Geophys. Res.*, **96**, 5055–5071.
- Rottman, G. J., T. N. Woods, and T. P. Sparr, 1993: Solar Stellar Irradiance Comparison Experiment 1: 1. Instrument design and operation. *J. Geophys. Res.*, **98**, 10,667–10,678.
- Russell, J. M., M. Luo, R. J. Cicerone, and L. E. Deaver, 1996: Satellite confirmation of the dominance of chlorofluorocarbons in the global stratospheric chlorine budget. *Nature*, **379**, 526–529.
- Santee, M.L., G.L. Manney, L. Froidevaux, R.W. Zurek, and J.W. Waters, 1997: MLS Observations of ClO and HNO₃ in the 1996–1997 Arctic polar vortex. *Geophys. Res. Lett.*, **24**, 2713–2716.
- Schäuffler, S. M., L. E. Heidt, W. H. Pollack, T. M. Gilpin, J. F. Vedder, S. Solomon, R. A. Lueb, and E. L. Atlas, 1993: Measurements of halogenated organic compounds near the tropical tropopause. *Geophys. Res. Lett.*, **20**, 2567–2570.
- Schoeberl, M. R., et al., 1993: The evolution of ClO and NO along air parcel trajectories. *Geophys. Res. Lett.*, **20**, 2511–2514.
- Solomon, S., 1990: Progress towards a quantitative understanding of the Antarctic ozone depletion. *Nature*, **347**, 347–354.
- Solomon, S., R. R. Garcia, F. S. Rowland, and D. J. Wuebbles, 1986: On the depletion of Antarctic ozone. *Nature*, **321**, 755–758.

- Solomon, S., R. W. Portmann, R. R. Garcia, L. W. Thomason, L. Poole, and M. P. McCormick, 1996: The role of aerosol variations in anthropogenic ozone depletion at northern midlatitudes. *J. Geophys. Res.*, **101**, 6713–6727.
- Sparling, L., et al., 1995: Trajectory modeling of emissions from lower stratospheric aircraft. *J. Geophys. Res.*, **100**, 1427–1438.
- Stolarski, R. S., A. J. Drueger, M. R. Schoeberl, R. D. McPeters, P. A. Newman, and J. C. Alpert, 1986: Nimbus 7 satellite measurements of the springtime Antarctic ozone decrease. *Nature*, **322**, 808–811.
- Stolarski, R. S., P. Bloomfield, R. D. McPeters, and J. R. Herman, 1991: Total ozone trends deduced from Nimbus 7 TOMS data. *Geophys. Res. Lett.*, **18**, 1015–1018.
- Tie, X. X., G. P. Brasseur, and C. Granier, 1994: Two-dimensional simulation of Pinatubo aerosol and its effect on stratospheric ozone. *J. Geophys. Res.*, **99**, 20,545–20,562.
- Toon, O. B., P. Hamill, R. P. Turco, and J. Pinto, 1986: Condensation of HNO_3 and HCl in the winter polar stratosphere. *Geophys. Res. Lett.*, **13**, 1284–1287.
- Toon, O. B., and M. Tolbert, 1995: Spectroscopic evidence against nitric acid trihydrate in polar stratospheric clouds. *Nature*, **375**, 218–221.
- Wallace, L., and W. Livingston, 1992: The effect of the Pinatubo cloud on hydrogen chloride and hydrogen fluoride. *Geophys. Res. Lett.*, **19**, 1209.
- Waters, J. W., L. Froidevaux, W. G. Read, G. L. Manney, L. S. Elson, D. A. Flower, R. F. Jarnot, and R. S. Harwood, 1993: Stratospheric ClO and ozone from the microwave limb sounder on the upper atmosphere research satellite. *Nature*, **362**, 597–602.
- Weisenstein, D. K., M. K. W. Ko, J. M. Rodriguez, and N. D. Sze, 1993: Effects on stratospheric ozone from high-speed civil transport: Sensitivity to stratospheric aerosol loading. *J. Geophys. Res.*, **98**, 23,133–23,140.
- Willson, R. C., and H. S. Hudson, 1991: “A solar cycle of measured and modeled total irradiance.” *Nature*, **351**, 42–44.
- World Meteorological Organization (WMO), 1992: Scientific assessment of ozone depletion: 1991, Global Ozone Res. and Monit. Proj., World Meteorol. Org., Rep. 25.
- World Meteorological Organization (WMO), 1995: Scientific assessment of ozone depletion: 1994, Global Ozone Res. and Monit. Proj., World Meteorol. Org., Rep. 37.
- Zander, R., M. R. Gunson, C. B. Farmer, C. P. Rinsland, F. W. Irion, and E. Mahieu, 1992: The 1985 chlorine and fluorine inventories in the stratosphere based upon ATMOS observations at 30 N latitude. *J. Atm. Chem.*, **15**, 171–186.

Chapter 7 Index

- 2-D models 317-318
 3-D models 318-319
 AASE II 321
 AEAP 322
 aerosols 315-316, 322, 325, 328, 330
 aircraft exhaust 320, 322
 AMLS 326-329
 ATMOS 321
 biological threat 311
 bromine 314-315, 324, 329
 calibration 327, 331
 carbon dioxide (CO₂) 311, 322
 carbon monoxide (CO) 332
 CFC 314, 321, 326
 CH₂Cl₂ 321
 CH₃Cl 314, 321
 CHCl₃ 321
 chlorine 312-327, 333
 CLAES 331
 climate change 311
 Cl_x 315, 322
 DAO 333
 Dobson units 312
 DU 312, 314, 319
 El Niño 315, 322
 energetic particles 316-317, 319
 ER-2 327
 foreign partners 333
 greenhouse forcing 311
 GSFC 324, 333
 H₂SO₄ 316, 320
 HALOE 318, 321, 323
 HCFC 321
 HIRDLS 326-332
 HIRS 323
 HO_x 314, 322, 325, 329
 HSCT 322
 IDS 331, 333
 interannual variability 315-316, 319
 IPCC 311
 IR 315
 ISAMS 331
 lightning 322
 man-made changes 320-322
 measurement requirements 323-333
 METEOR-3 329
 methane (CH₄) 314, 318, 322, 325, 329, 332
 MLS 313, 324-332
 MMIC 326-328
 modeling 317, 333
 MSU 323
 NAD 326-329
 NASA 324, 326, 328, 333
 NAT 320, 326-329
 natural changes 319-320
 NCAR 318
 Nimbus-7 311
 NOAA 323-324, 328
 NO_x 314, 319, 322, 325, 329
 NPOESS 324, 330
 OCS 316, 329
 OH 314, 321, 325-326, 329, 332
 OMI 326, 329-332
 ozone changes 312-315
 ozone chemistry 314-315
 ozone distribution 314, 317, 319-320
 ozone transport 315
 precipitation 319
 PSC 315-316, 318-322, 325, 327, 331
 QBO 315, 319, 322
 REP 317
 SAGE 313, 331
 SAGE III 313, 330-332
 SAM 316-317
 SBUV 313-314
 SOLSTICE 326, 330-331
 SPOT 333
 STP 312
 sulfate 319-320, 329
 sulfur 322
 sulfur dioxide (SO₂) 316, 319, 329-332
 sulfuric acid 316, 320
 TOMS 311-314, 326, 329-331
 TOVS 323-324, 331
 trace gases 317, 319, 328, 333
 UARS 313, 318-321, 323, 326-332
 UT 328
 UV 311, 327, 330-331
 UV-B 311, 330
 validation 327
 volcanoes 316, 322
 wind 312, 319, 323-324, 333
 WMO 311, 316-318, 320-321, 324
 WSR 316

Volcanoes and Climate Effects of Aerosols

LEAD AUTHORS

D. L. Hartmann and P. Mouginis-Mark

CONTRIBUTING AUTHORS

G. J. Bluth
J. A. Coakley, Jr.
J. Crisp
R. E. Dickinson
P. W. Francis
J. E. Hansen
P. V. Hobbs
B. L. Isacks
Y. J. Kaufman
M. D. King
W. I. Rose
S. Self
L. D. Travis

CHAPTER 8 CONTENTS

8.1	Importance of volcanoes, natural aerosols, and anthropogenic aerosols	341
8.2	Major scientific questions and hypotheses	342
8.2.1	Stratospheric volcanic aerosols and climate	342
8.2.1.1	Source gases for stratospheric aerosols	342
8.2.1.2	Explosiveness and plume history during individual eruptions	343
8.2.1.3	Frequency of eruptions, tectonic setting, rock/ash vs. SO ₂	343
8.2.1.4	Gas-to-particle conversion and removal mechanisms	343
8.2.1.5	Radiative properties and climatic effects of stratospheric aerosols	345
8.2.1.6	Needed satellite and in situ measurements	347
8.2.1.6.1	Global observations of stratospheric aerosol optical properties	347
8.2.1.6.2	Lidar measurements of aerosols	347
8.2.2	Volcanic aerosols and stratospheric ozone depletion	349
8.2.3	Climatic effects of tropospheric aerosols	349
8.2.3.1	Natural emission of tropospheric aerosols	349
8.2.3.2	Anthropogenic sources of aerosols	350
8.2.3.2.1	Sulfur emission and oxidation to sulfate particles	351
8.2.3.2.2	Biomass burning	351
8.2.3.3	Direct radiative effects of tropospheric aerosols	352
8.2.3.4	Indirect effects of aerosols on cloud abundance, lifetime, and optical properties	354
8.2.3.5	Science investigations using EOS data	355
8.2.3.6	Needed satellite and in situ measurements	355
8.2.3.6.1	Global observations of tropospheric aerosol optical properties	355
8.2.3.6.2	Surface monitoring of tropospheric aerosols	357
8.2.3.6.3	Intensive field campaigns	358
8.2.4	Volcanic hazards	358
8.2.4.1	Health hazards of tropospheric volcanic gases and aerosols	359
8.2.4.2	Lava flows and volcanic mud flows	361
8.2.4.3	Hazards to aircraft from eruption plumes	361
8.2.4.4	Needed satellite and in situ measurements	361
8.3	Required measurements and data sets	362
8.3.1	Stratospheric aerosols	362
8.3.2	Tropospheric aerosols	364
8.3.3	Volcanic aerosol precursor gases	364
8.3.4	Volcanic hazards	364
8.3.5	Importance of measurements collected by the missions of foreign partners	366
8.4	EOS contributions: Expected improvement in knowledge and national benefit	367
8.4.1	Monitoring of volcanic eruptions and aerosols and their effects on climate	367
8.4.2	Improved assessment of volcanic hazards on the ground and in the air	367
8.4.3	Improved knowledge of the global frequency and magnitude of volcanic eruptions	368
8.4.4	Global measurements of tropospheric aerosols	368
8.4.5	Assessment of the role of tropospheric aerosols in climate change	370
8.4.6	Inclusion of aerosol effects in model predictions of global climate change	371
8.4.7	Advertent climate modification by aerosols	372
	References	373
	Chapter 8 Index	378

8.1 Importance of volcanoes, natural aerosols, and anthropogenic aerosols

Volcanoes have a significant effect on the global environment. In the long term, they affect the gaseous composition of the atmosphere by emitting gases from the interior of the Earth and play a key role in the evolution of the Earth's atmosphere and climate. Variations in the output of volcanoes can cause variations of climate on a variety of time scales. It has been demonstrated that a sufficiently violent eruption can cause a measurable change in the Earth's climate with a time scale of a few years. The magnitude of the temperature change depends on the amount of sulfur that is injected into the stratosphere, among other factors. The sulfur gases are oxidized to sulfuric acid aerosols in the stratosphere, where they may reside for a year or more before being flushed out by sedimentation and the fluid motions of the stratosphere. Generally, a surface cooling is produced by these aerosols, because they reduce the amount of solar radiation reaching the surface more than they reduce the amount of escaping longwave emissions. It is conceivable that a modulation in the frequency of this type of eruption on time scales of decades or longer could cause a variation of the Earth's climate on the same time scale.

The periods of cooling associated with major eruptions must be accounted for in efforts to detect trends that might be associated with increasing greenhouse gases or other anthropogenic climate forcings. An important challenge to the research effort on global change, for the purpose of making policy decisions, will be the early detection and quantification of climate changes caused by human activities. It is essential to recognize and remove effects resulting from natural phenomena, of which volcanic aerosols are a significant example. We are still a long way from understanding fully the effects of volcanic eruptions on atmospheric composition, climate, and weather.

In addition to their effects on atmospheric composition and global climate, volcanic eruptions have effects in shaping the local landscape and can pose a serious hazard to life and property in their vicinity.

Volcanic emissions and resulting stratospheric aerosols can also have an important influence on stratospheric chemistry, both through chemical reactions that

take place on the surfaces of aerosols and through the temperature changes that aerosols can induce in the stratosphere. Stratospheric aerosols can result in heating of the stratosphere, which can have significant effects on stratospheric dynamics and transport.

Aerosols in the troposphere are also important for global climate. A wide variety of aerosol types exists, including sea salt and dust carried from the surface into the atmosphere by wind, and aerosols formed by chemical transformation from gaseous compounds to molecules that exist in solid or liquid form. In the upper troposphere, a significant fraction of the aerosol burden can come from advection or sedimentation from the stratosphere. The sources of aerosols are both natural and anthropogenic. Although the lifetime of aerosols in the troposphere is only a few weeks, the sources are strong enough to maintain a significant aerosol burden. The aerosols contributed by humans have been increasing, particularly those associated with sulfur dioxide (SO_2) released during the combustion of coal, petroleum, and biomass. It is currently estimated that the anthropogenic source of sulfuric acid aerosols in the troposphere is greater than the natural source. The primary effect of these aerosols is to cool the Earth by reflecting solar radiation, either directly, or by becoming incorporated into small cloud droplets or ice crystals. It is estimated that the direct effect of sulfate aerosols produced by humans on the Earth's energy balance is currently about -0.5 Wm^{-2} , compared to the forcing associated with the change in greenhouse gases during the industrial age of about $+2 \text{ Wm}^{-2}$. The indirect effect of human-produced aerosols on the properties of clouds may be of the same order, making tropospheric aerosols one of the major uncertainties in understanding climate change.

It is important to obtain accurate measurements of aerosols not only because of their importance for climate, but also to allow a higher degree of accuracy in remote sensing of surface properties such as sea surface temperature (SST), ocean color, and land surface properties. During major volcanic eruptions, satellite monitoring of stratospheric chemical and physical properties is also significantly affected by aerosols.

8.2 Major scientific questions and hypotheses

8.2.1 Stratospheric volcanic aerosols and climate

The year 1816, “the year without a summer,” is probably the best known putative example of a volcanically-induced climate cooling event. It was largely caused by the eruption of Tambora, Indonesia, in April 1815. Tambora erupted an estimated 50 cubic kilometers of magma and produced 100 megatons of sulfuric acid aerosols, in one of the largest known volcanic eruptions of the past few millennia. The aerosol veil caused cooling of up to 1°C regionally and probably more locally, with effects lasting until the end of 1816 and extending to both hemispheres. It snowed in New England in June, and abnormally low temperatures in Europe led to widespread famine and misery, although the possible connection to volcanic aerosols was not realized at the time.

Scientists first recognized and observed volcanic atmospheric dust veils after the eruption of Krakatau, Indonesia, in 1883, and it was then thought that fine-grained silicate dust was the cause of the atmospheric perturbations. However, since the discovery of the stratospheric sulfate aerosol layer in the 1960s, it has become evident that this layer in the atmosphere, which plays a large role in modulating the net incoming radiation, is strongly influenced by volcanogenic sulfide released from the magma.

Several recent eruptions have proven invaluable in improving our understanding of the connections among volcanism, aerosols, and climate change. Two eruptions of very sulfur-rich magma at El Chichón, Mexico, in 1982 and Mount Pinatubo, in Luzon, Philippines, in 1991 have been well documented in terms of the stratospheric aerosols produced, their spread and atmospheric residence time, and their climatic effects. El Chichón was a small-volume eruption of unusually sulfur-enriched magma that produced the first large aerosol veil to be tracked by instruments on satellites. Its impact on surface temperatures has, however, been difficult to assess. Pinatubo was the second-largest eruption in the twentieth century (the largest was Mt. Katmai in Alaska in 1912), and its aerosol veil enveloped the Earth for more than 18 months, causing spectacular sunrises and sunsets worldwide. There was more material in the aerosol layer than at any time since Krakatau erupted. General circulation models (GCMs) of temperature changes expected under this aerosol cloud predicted Northern Hemisphere surface cooling of as much as 0.5°C, and changes of this order are consistent with the meteorological data.

Recent studies have established a strong correlation between certain types of eruptions and climate change,

and it has been suggested that there may be a simple relationship between the sulfur yield of a volcanic eruption and decreases in surface temperature. It is known that enhanced levels of aerosols after volcanic eruptions coincide with periods of lowered incident solar radiation, lower surface and tropospheric temperatures, and stratospheric warming. The magnitude of the signal in the surface temperature record is difficult to detect against background variation, however, even for the largest historic eruptions. Recently, it has been suggested that for the Agung (1964) and El Chichón (1982) cases, subtracting the warming effects of El Niño from the temperature record makes the volcanic signal clearer. Simple models suggest that eruptions on the scale of large prehistoric events have the potential to alter climate to a much greater degree than has been observed following volcanic events in the historical record.

8.2.1.1 Source gases for stratospheric aerosols

Sulfur is released into the atmosphere during eruptions mainly as SO₂ gas, which is converted by photochemical oxidation to sulfuric acid (H₂SO₄) via OH. Sometimes H₂S can be the dominant sulfur-bearing gas species in an eruption cloud (Hobbs et al. 1981; Kotra et al. 1983). Sulfuric acid (70%) and water (30%) are the dominant components of the resulting aerosols. Aerosols form liquid spheres (~0.3 μm modal radius), with solid silicate (ash) cores dominant in the first month. Atmospheric residence time ranges from days to years, depending on particle size, injection history, and location of the aerosol in question.

Injection of other volatiles such as HCl and H₂O may alter atmospheric composition as well, but evidence for long-term residence of Cl compounds from volcanic HCl emission is lacking. Aerosol composition is further altered by heterogeneous reactions on sulfate aerosol surfaces.

SO₂ has been recognized as the major contributor to stratospheric aerosols. Based on magma chemistry, it is poorly known why other gases, and HCl in particular, are not injected into the stratosphere during violent volcanic eruptions. Some form of “scavenging mechanism” seems to exist wherein, perhaps, water vapor leaches out these other gases during plume ascent rather than allowing the gases to be injected into the stratosphere. The mechanism wherein separation of the ash from the gases within the plume takes place also needs to be understood. Detailed satellite observations of the plume are needed to help resolve this issue, as well as understand the dissipation of energy from the plume into the atmosphere.

8.2.1.2 *Explosiveness and plume history during individual eruptions*

Through study of historic eruptions and their atmospheric impacts, we have learned what types of eruptions can influence the Earth's climate. Climatic effects appear to ensue if the eruption cloud is powerful enough to inject material into the stratosphere, or if the eruption is of sufficient duration that a higher-than-normal level of tropospheric aerosols is maintained. The impact on climate also depends on the sulfur content of the magma: some volcanoes erupt sulfur-rich magmas, some magma with average amounts, and some magma with low sulfur content. The ultimate source of volcanic sulfur is yet to be determined: some may be primordial and some may be recycled in the Earth's lithosphere. If an eruption is large enough, even with a low magmatic sulfur content, sufficient magma is erupted to cause a significant release of sulfur gas, leading to the generation of aerosol particles.

8.2.1.3 *Frequency of eruptions, tectonic setting, rock/ash vs. SO₂*

Determining how large an impact an eruption can have on climate is a major issue. Volcanic eruptions are known to affect surface temperature, precipitation, and weather patterns, but what has not been studied in detail are either the short-term (1-3 years) effects of individual events, or the longer-term (10-50 years) changes that might be controlled by periods of enhanced volcanism. Although the greater the eruption, the lower the frequency of occurrence, eruptions have a frequency that varies according to type and magnitude of the event. We have an imperfect record of past eruptions and changes in temperature and weather. Future events will provide natural experiments in which we can study the impact of volcanic aerosols, an effort already begun.

Significant eruptions, and therefore aerosol clouds, occur every 10-20 years on average, with a major eruption perhaps every 100 years. Latitude and time of year of eruptions influence dispersal of volcanic aerosol clouds. Some magmas are richer in sulfate than others (e.g., El Chichón), but the duration of the eruption is also important for climate modification (e.g., 1783 Laki fissure eruption in Iceland).

8.2.1.4 *Gas-to-particle conversion and removal mechanisms*

The aerosol loading of the stratosphere is strongly driven by periodic volcanic eruptions that can produce a significant perturbation to the Earth-atmosphere system by injecting material into the stratosphere where, depending on the magnitude and altitude of the injection, it may per-

sist for several years. The material injected into the stratosphere may include ash, which typically does not remain for more than a few months, and gaseous components including water vapor and SO₂. Aerosols are produced when the SO₂ is chemically transformed into sulfuric acid (H₂SO₄), which rapidly condenses into aerosols since it has a very low saturation vapor pressure (McCormick et al. 1995). Additional sources of stratospheric aerosols include natural (e.g., biogenic Carbonyl Sulfide [COS]) and anthropogenic sources (e.g., SO₂ from industry and aviation).

The introduction of large amounts of sulfuric acid aerosol by a volcano into the stratosphere increases the planetary albedo, since these aerosol particles are efficient scatterers, but only weak absorbers, at solar wavelengths. For instance, following the eruption of Mt. Pinatubo, an analysis of data from the Earth Radiation Budget Experiment (ERBE) found that the albedo in July, August, and September 1991 increased to 0.250 from a 5-year mean of 0.236 (Minnis et al. 1993). To a first approximation, an increase in stratospheric opacity, such as that following the eruption of Mt. Pinatubo, should cool the Earth as the aerosol increases the albedo of the Earth-atmosphere system and therefore increases the amount of solar radiation scattered back into space. However, microphysical properties of the aerosol (in particular, aerosol size) determine whether the infrared absorptivity of stratospheric aerosols, which acts to warm the Earth, dominates the scattering of incoming solar radiation back into space (i.e., the albedo effect), which acts to cool the Earth (e.g., King et al. 1984). It has been shown (Lacis et al. 1992) that if the aerosol effective radius (i.e., the area-weighted mean radius of the aerosol size distribution) exceeds ~2 μm, the warming effect overrides the cooling effect. Following the Pinatubo eruption, measurements indicated an increase in the average particle radius from 0.3 μm prior to the eruption to about 1 μm after the eruption; thus cooling would be expected (Russell et al. 1993a, b; Thomason 1992; Grainger et al. 1995). The average size of volcanic aerosols varies with position and time after the eruption, but the dominant effect at the surface appears to be cooling.

Substantial heating in the stratosphere was observed immediately after the eruptions of El Chichón and Mt. Pinatubo (Labitzke et al. 1983; Labitzke and McCormick 1992). In the case of Mt. Pinatubo, this heating was sufficient to cause tropical stratospheric temperatures to increase by as much as three standard deviations above the 26-year mean at 30 hPa (~24 km). Analyses using the satellite-borne Microwave Sounding Unit (MSU) also indicate higher-than-average stratospheric temperatures in 1991 and 1992. By the end of

1993, however, stratospheric temperatures had decreased to the lowest values ever observed by MSU. This cooling may be related to the ozone loss observed in the stratosphere, since ozone is an effective absorber of solar radiation and is responsible for substantial heating in the stratosphere. The observed ozone loss was probably due in large part to heterogeneous chemical reactions on Pinatubo aerosols.

The negative radiative forcing associated with the eruption of Mt. Pinatubo exceeded the magnitude of the positive forcing associated with greenhouse gases during the second half of 1991 and much of 1992, and remained significant through 1993. In response to this forcing, the 1992 tropospheric temperature anomaly, adjusted for the effects of El Niño-Southern Oscillation (ENSO) variations, was -0.4°C , a decrease of more than 0.7°C from 1991 (Halpert et al. 1993). Data from MSU (Dutton and Christy 1992) yield a similar global decline in lower tropospheric temperatures of 0.5°C in mid-1992 with much of the decrease occurring in the Northern Hemisphere (0.7°C). In a globally averaged sense, the measured temperature anomaly is consistent with the value of -0.5°C estimated from a global climate model (Hansen et al. 1992). The departure is also comparable to the estimated impact of Tambora in 1815 (-0.4 to -0.7°C) and greater than that estimated for El Chichón in 1982 (-0.2°C) and Krakatau in 1883 (-0.3°C). It is surprising that the Pinatubo cooling exceeded that of Krakatau, since the latter is believed to have injected more SO_2 into the stratosphere. However, this anomaly may simply reflect uncertainties in the estimates of both stratospheric aerosol loading and global surface temperature, particularly for the earlier eruption. It should be noted that the small mean changes in global temperature are not evenly distributed, but consist of regions of both relative cooling and warming, the locations and magnitudes of which are dependent on season.

Injection of volcanic aerosol at high latitudes appears to be fairly well confined to the hemisphere of the injection, such as was observed following the eruption of Mt. St. Helens in May 1980. Volcanic injections at low latitudes and high altitudes exhibit relatively slow transport time scales of volcanic material out of the tropics to both hemispheres. Observations following the eruptions of El Chichón in 1982 and Nevada del Ruiz in 1985 revealed the presence of enhanced reservoirs of volcanic aerosol at low latitudes that persisted for several years (Yue et al. 1991). Poleward transport of aerosol into the winter hemisphere tends to be suppressed when easterly winds lie over the equator. During these conditions, strong horizontal wind shear lies in the subtropics, separating

the tropical easterlies and extratropical westerlies in the winter hemisphere. Large-scale potential vorticity gradients associated with these shears inhibit the horizontal mixing of air. When westerly winds lie over the equator, however, horizontal wind shear is weaker in the subtropics and meridional mixing occurs more readily. The reversal between easterly and westerly winds in the lower tropical stratosphere (the Quasi-Biennial Oscillation or QBO) dominates the circulation in the tropical stratosphere and has a period of approximately 28 months.

A similar signature of relatively slow tropical aerosol transport to high latitudes was evident after the eruption of Mt. Pinatubo. Easterly winds prevailed above 23 km in the lower tropical stratosphere for the first six months after the eruption. Above this height, airborne lidar (Winker and Osborn 1992) and satellite (Trepte and Hitchman 1992) observations of the volcanic plume found steep meridional gradients of aerosol near 20°N and 20°S . The tropical confinement of aerosol gives rise to a long-lived, zonal-banded pattern in stratospheric optical thickness following low-latitude eruptions (Trepte et al. 1994; Long and Stowe 1994; Grant et al. 1996). At lower altitudes, however, volcanic aerosol disperses more quickly poleward, and it was primarily this low-altitude transport that was responsible for the initial lidar observations of the Pinatubo aerosol in northern midlatitudes shortly after the eruption (e.g., Post et al. 1992).

Over the course of time, volcanic aerosol is transported from the stratosphere into the troposphere where a variety of mechanisms (mostly associated with clouds and precipitation) are effective in the deposition of the aerosol to the Earth's surface. Increasing the number of aerosol particles available to act as cloud condensation and ice nuclei tends to reduce the mean size of the resulting cloud particles. Since smaller particles are more efficient scatterers of visible radiation, this process increases the albedo of the cloud. It has been suggested that optically-thin (but radiatively important) cirrus (Sassen et al. 1995) and deep convection clouds may be subject to similar microphysical changes. Although it is not clear if any changes in the optical properties of cirrus following a volcanic eruption have been observed, Song et al. (1996) show an apparent effect of Pinatubo aerosols on high cloudiness of moderate or greater optical depths, as measured by the pattern of the outgoing longwave radiation (OLR) anomaly, that lasted for several years after the eruption. Gravitational sedimentation of the aerosol, subsidence in the winter hemisphere (particularly within the polar vortices), and episodic transport of stratospheric air into the troposphere through tropopause folds are responsible for the removal of aerosol from the stratosphere. Following the June 1991

eruption of Mt. Pinatubo, the total stratospheric aerosol mass decreased with an e-folding time of approximately one year.

The Mt. Pinatubo eruption is the best observed example of an explosive eruption with global effects. The large Pinatubo stratospheric SO₂ cloud began to spread rapidly and oxidize to form stratospheric sulfuric acid aerosols (Figure 8.1). About half of the SO₂ had been converted to sulfuric acid aerosols by four weeks after the eruption (Winker and Osborn 1992). The Microwave Limb Sounder (MLS) on the Upper Atmosphere Research Satellite (UARS) satellite detected minor amounts of unoxidized SO₂ for up to 170 days after the eruption. Accordingly, the average conversion time of SO₂ is about 33 days (Read et al. 1993). Multiwavelength stratospheric aerosol extinction measurements from the SAGE II and airborne and ground-based photometers revealed greatly

remained near the equator 4-5 months after the eruption (Figure 8.2, pg. 346). The typical size of volcanic aerosols observed several months following the eruption was in the range of 0.3 to 0.5 μm (Deshler et al. 1992a, 1993; Pueschel et al. 1992; Asano 1993; Asano et al. 1993), and aerosol size appeared to be a strong function of latitude and altitude (Grainger et al. 1995; Lambert et al. 1993). Numerical modeling has reproduced the observed microstructure and optical properties of the Pinatubo aerosols during the period of their formation and growth in the stratosphere (Zhao et al. 1995).

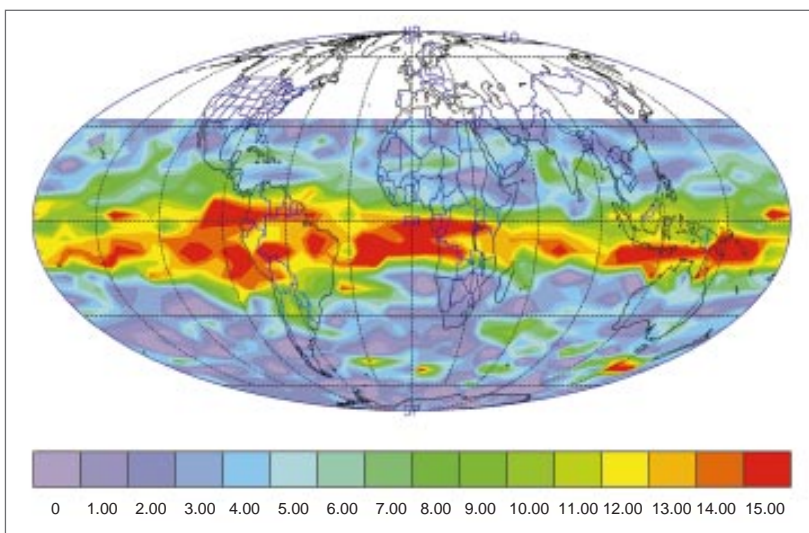
8.2.1.5 Radiative properties and climatic effects of stratospheric aerosols

Temporal variations of stratospheric aerosols alter both the solar radiative cooling of the Earth-atmosphere system and the thermal emission from the Earth to space.

Thus, determination of the climate forcing caused by stratospheric aerosols requires a knowledge of aerosol properties sufficient to define their influence on both solar and terrestrial spectra. Radiative transfer tools are available for accurately simulating the climate forcing by aerosols of known size and composition. Coakley and Grams (1976), Harshvardhan and Cess (1976), and Pollack et al. (1976) were among the first to realistically portray the effect of stratospheric aerosols on both solar and terrestrial radiation.

A comprehensive illustration of how radiative forcing by stratospheric aerosols depends upon aerosol properties was provided by Lacis et al. (1992). The principal parameter is the aerosol optical

FIGURE 8.1

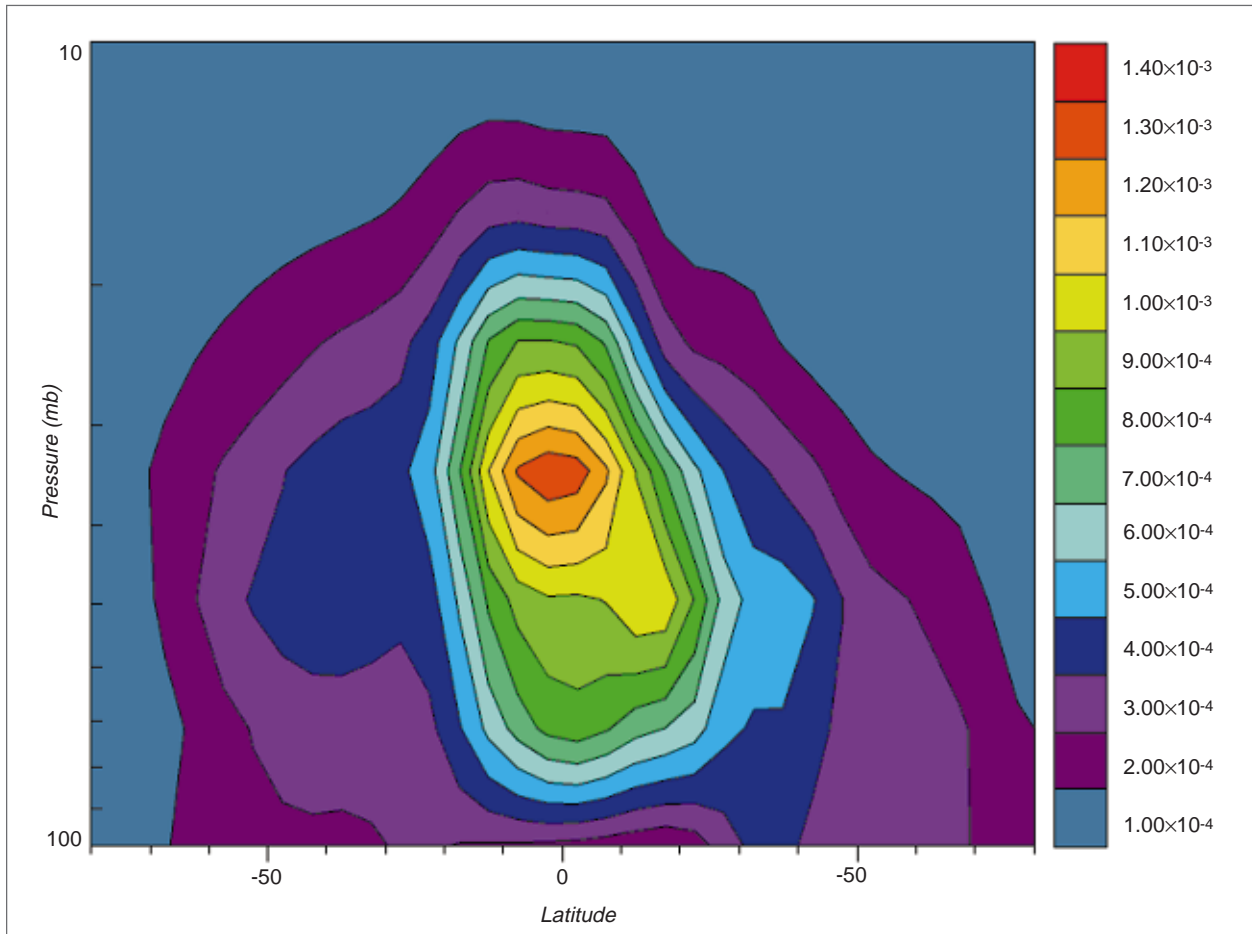


Map of the Mt. Pinatubo SO₂ cloud from MLS (Read et al. 1993).

increased extinction with an initial wavelength dependence indicating the presence of very small aerosols created by gas-to-particle conversion (Thomason 1992; Valero and Pilewskie 1992; Russell et al. 1993b; Dutton et al. 1994). These newly formed aerosols grew to larger sizes by condensation of sulfuric acid and water vapor and by the coagulation process (Russell et al. 1993a, b; Dutton et al. 1994), leading to optical-thickness spectra that peaked at midvisible (~0.5 μm) or longer wavelengths, starting about two months after the eruption. Over 90% of the particles collected from the volcanic clouds were composed of an H₂SO₄/H₂O solution (Deshler et al. 1992b). The highest concentration of aerosols re-

thickness, including its geographical distribution. The climate forcing also depends substantially on the effective radius of the particle size distribution. The radiative forcing is less sensitive to other characteristics of the size distribution, the aerosol composition, and the altitude of the aerosols. However, the radiative forcing, specifically the radiative flux change at the tropopause caused by the aerosols, does not completely define possible climate influence. Empirical studies (Kodera and Yamazaki 1994) and model analyses (Graf et al. 1993) suggest that changes in stratospheric temperature gradients can alter surface climate; thus, factors that influence stratospheric heating, such as aerosol composition, may also be important.

FIGURE 8.2



Zonal cross section of stratospheric zonal mean aerosol extinction for 8-11 November 1991 retrieved from atmospheric limb observations of the 12.1- μm aerosol emission of the Improved Stratospheric and Mesospheric Sounder on the Upper Atmosphere Research Satellite (Grainger et al. 1993).

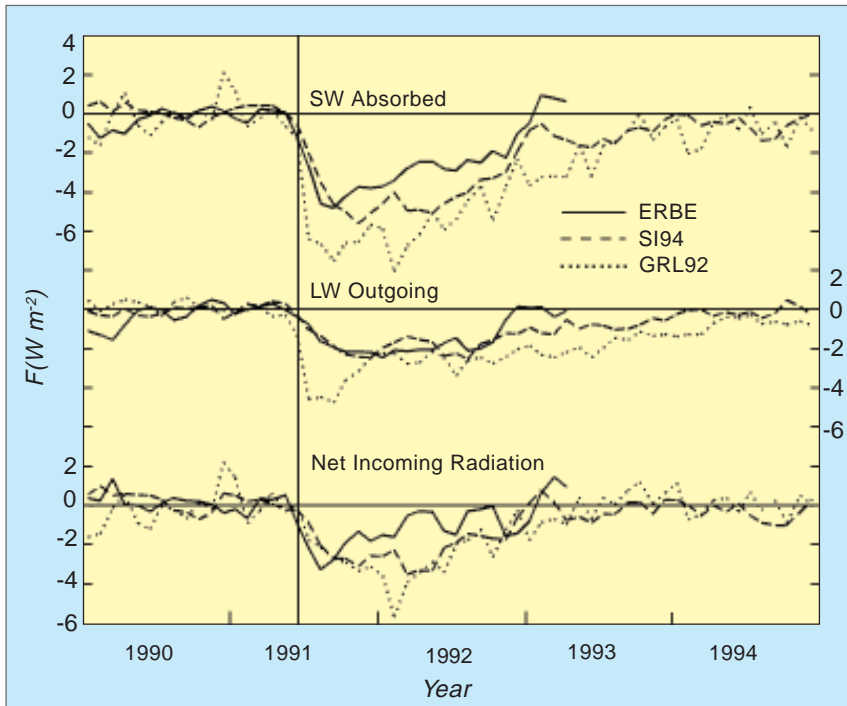
Aerosol heating can also affect the circulation of the stratosphere (Eluszkiewicz et al. 1996).

The aerosol radiative forcing resulting from the Mt. Pinatubo eruption is known much better as compared to previous large volcanic eruptions, principally because global satellite data were available for both solar spectra (especially the Stratospheric Aerosol and Gas Experiment [SAGE] II data; McCormick et al. 1995) and terrestrial spectra (especially Improved Stratospheric and Mesospheric Sounder [ISAMS] data; Grainger et al. 1993). About 20 to 30 Tg ($\text{Tg} = 10^{12} \text{ g}$) of new aerosol produced by the Pinatubo eruption was estimated by use of SAGE II (McCormick and Veiga 1992; McCormick et al. 1995), Cryogenic Limb Array Etalon Spectrometer (CLAES), and ISAMS data (Lambert et al. 1993). The mean mass, about 25 Tg of sulfate aerosol, requires that only 13 Tg of SO_2 are available to form it, if it is assumed that the aerosols are 75% H_2SO_4 and 25% H_2O (Hamill et al. 1977).

This estimate is somewhat smaller than those of SO_2 release. Infrared absorption by the Pinatubo aerosol also suggests that the composition is 59-to-77% H_2SO_4 , with the remainder being water (Grainger et al. 1993).

These satellite data have been used to infer aerosol optical thickness and effective radius of the Pinatubo aerosols as a function of time (Hansen et al. 1995), and in turn the aerosol properties have been used in the Goddard Institute for Space Studies (GISS) GCM to calculate the radiative flux anomalies at the top of the atmosphere for comparison with ERBE data (Figure 8.3). The observed flux anomaly is somewhat smaller than calculated in the model, but is probably consistent with measurement uncertainty. Both the observations and model imply a smaller forcing than was assumed in calculations immediately following the eruption (Hansen et al. 1992), which in large part accounts for the predicted cooling being somewhat greater than observed.

FIGURE 8.3



Radiation balance anomalies observed by ERBE for latitudes 40°S-40°N (Minnis *et al.* 1993), with the mean for the period 1985-1989 to remove the seasonal cycle and with the zero point defined by the mean anomaly for the 12 months preceding the month of the Mt. Pinatubo eruption. Model radiation balance anomalies are from the simulations of Hansen *et al.* (1992) and from current simulations with the SI94 climate model and the SI94 aerosols. (GRL92 refers to a model in which the radiation balance anomalies observed by ERBE are compared with the same quantities calculated in the climate simulations of Hansen *et al.* 1992.) (courtesy of James Hansen [Goddard Institute of Space Studies]).

When more fully analyzed, the Pinatubo eruption may improve our understanding of the sensitivity of climate to aerosols. However, because of the difficulty of separating a forced climate response from natural variability, definitive conclusions will probably require analysis of additional future volcanic eruptions. Thus, it is important to maintain over decades the measurement capabilities for stratospheric aerosols and other climate forcings.

8.2.1.6 Needed satellite and *in situ* measurements

8.2.1.6.1 Global observations of stratospheric aerosol optical properties

Spaceborne solar and lunar occultation measurements will be made during the EOS era using SAGE III, flying in a polar orbit (Meteor 3M-1), a mid-inclination orbit (Flight of Opportunity), and a low-inclination precessing orbit (International Space Station). These data will be used to derive vertical profiles of aerosol extinction coefficient and effective particle size, as well as a number of gaseous species, thereby extending the valuable solar occultation

measurements begun by the Stratospheric Aerosol Measurement (SAM) II, SAGE, and SAGE II satellite missions. The addition of lunar occultation on SAGE III will permit more occultations to be obtained than are possible with solar occultation alone, thereby increasing the sampling opportunities. Previous records of the global distribution and dispersion of stratospheric aerosol, obtained from the mid-inclination SAGE II on the Earth Radiation Budget Satellite (ERBS), have demonstrated the magnitude and spatial distribution of stratospheric aerosols as they dispersed globally following major volcanic eruptions. Figure 8.4 (pg. 348) shows a time series of stratospheric aerosol optical thickness preceding, immediately following, and 18 months after the eruption of Mt. Pinatubo.

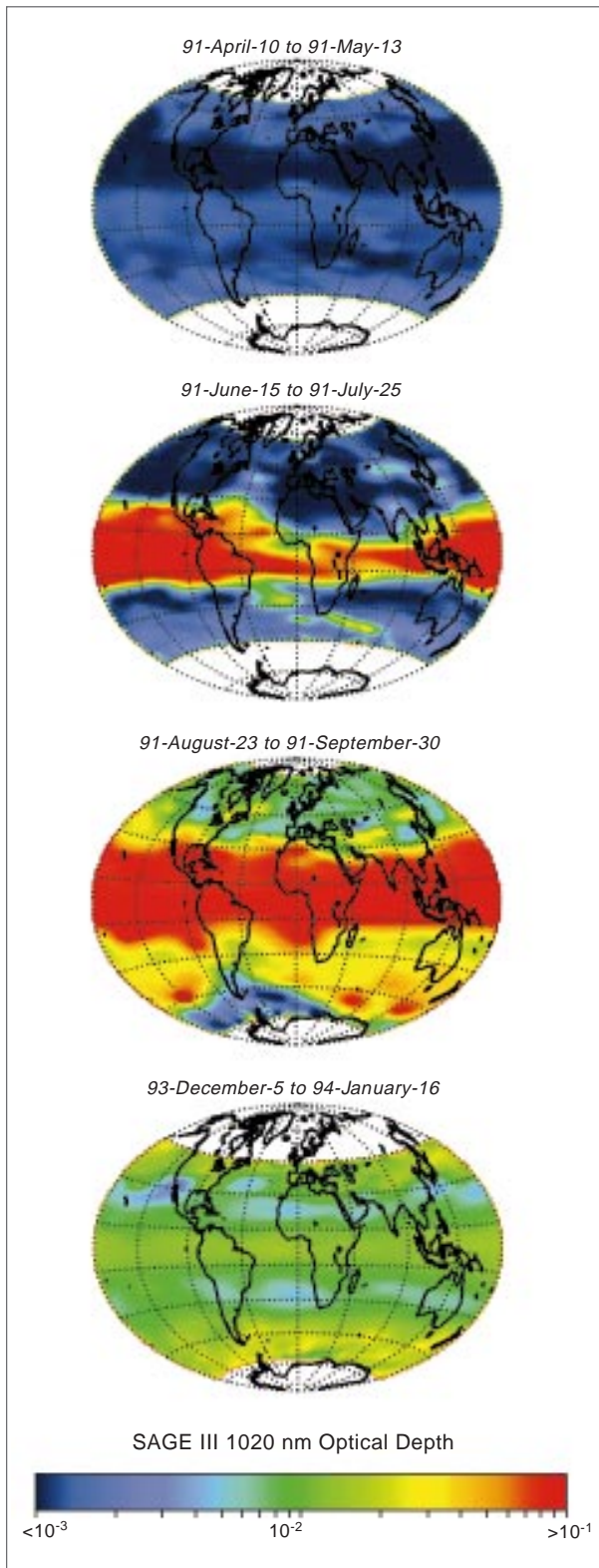
In addition to SAGE III, the High-Resolution Dynamics Limb Sounder (HIRDLS) on the Earth Observing System (EOS)

Chemistry-1 platform will be very sensitive to vertical profiles of stratospheric aerosol. HIRDLS has specifically-designed channels at 7.1, 8.3, 12.0, and 17.4 μm to sense the presence and optical properties of stratospheric aerosol through thermal emission using a limb-sounding technique. This will provide three-dimensional fields of the entire globe for altitudes above about 5-7 km under most atmospheric conditions, and the sensitivity will include particles smaller than 0.1 μm found in the midstratosphere. The vertical resolution will be 1 km, and by using an azimuth scanning capability with profiles measured every 10 seconds, a horizontal resolution of $5^\circ \times 5^\circ$ (averaging about 400 km \times 400 km) will be obtained, with a complete 3-D field twice per day. The UARS ISAMS and CLAES instruments, which both had poorer spatial resolutions, showed that the technique is highly effective for measuring the evolution of aerosol fields.

8.2.1.6.2 Lidar measurements of aerosols

Ground-based and airborne lidar measurements have made important contributions to our knowledge of stratospheric aerosol behavior in two main areas. The first of these con-

FIGURE 8.4



Aerosol optical depth measured by SAGE III before and after the eruption of Mt. Pinatubo on June 15, 1991 (P. McCormick).

cerns the long-term monitoring of the aerosol optical scattering characteristics from ground-based locations. At least two lidar stations now exist where measurements have been made continually from a single observing site for over twenty years (Osborn et al. 1995; Simonich and Clemesha 1995). These records show the injection of material by various volcanic eruptions, the earliest being that of Fuego in 1974, and the most recent and powerful being that of Pinatubo in 1991. The stratospheric effects of a number of other eruptions, many of them with much smaller impact, are clearly visible in these records. These data are the most extensive of a much larger number of data sets obtained from a global lidar network (McCormick 1993) that extends back to the mid 1960s. Taken together, these measurements form a valuable tool for examining the long-term global behavior of aerosols, particularly in terms of the magnitude and location of the volcanic sources and the dispersion and loss from the stratosphere of the injected material. Traditional wavelengths used for these systems have been in the visible or near infrared. The recent addition of CO₂ lidars operating near 10 μm has enabled the seasonal loss of stratospheric volcanic aerosols to the upper troposphere to be followed (Post 1986; Post et al. 1992), where they may be responsible for indirect radiative effects via aerosol modification of high-cloud characteristics. Lidar systems offer a high vertical resolution, allowing structures to be studied with vertical dimensions as small as a few meters. The use of multiple wavelengths provides information on particle size, allowing calculations to be made of mass loading and surface area. These quantities, or the multi-wavelength backscatter cross sections, may then be used as a basis for calculation of the radiative characteristics at other wavelengths.

The second main area in which lidars have been used to study stratospheric aerosols has been their use in airborne systems. The recent satellite-borne Lidar In-Space Technology Experiment (LITE) may be regarded as an extension of such systems. Airborne systems permit the study of the horizontal distribution of stratospheric aerosols, the extent of such studies being only limited by the cost and logistics of operating the platforms. These flight experiments have been unique in the detail they have shown of the horizontal and vertical structure of the stratospheric aerosol, providing insight into the dynamical processes responsible for producing and/or maintaining this structure. Such missions have normally been dedicated to the study of specific phenomena of interest (e.g., post-volcanic plumes [Winker and Osborn 1992] or polar stratospheric clouds [McCormick et al. 1993]). Airborne lidar measurements have also provided unique information on the transfer of material from the stratosphere to

the troposphere, showing the downward transfer of aerosol within tropopause fold structures (Browell et al. 1987). In addition to their direct application to the study of stratospheric aerosols, airborne lidars have an extensive history as validation instruments for SAM II, SAGE, and SAGE II aerosol measurements.

It is possible for an airborne lidar to map the aerosol distribution over a wide latitude range within a period of hours or days. This represents an order-of-magnitude improvement in time resolution over a satellite occultation instrument such as SAGE II or SAGE III, where the measurement location changes latitude relatively slowly with orbital drift and season, and less than 50 profiles can be obtained each day. An even more global and quasi-instantaneous picture can be obtained from a spaceborne lidar. In September 1994, LITE (McCormick 1995), operating over a 10-day period, provided a unique data set that included measurements on stratospheric aerosols, with 100° of latitude being covered in about 20 minutes.

Lidar measurements in support of EOS goals will be conducted with the Geoscience Laser Altimeter System (GLAS). The existing global ground-based network is strongly biased towards the Northern Hemisphere. More observing sites are required in both the tropics and the Southern Hemisphere. The lack of data within the equatorial reservoir zone is particularly noteworthy: no systematic stratospheric measurements have been made closer to the equator than 18° latitude. Improvements are also desirable in measurement techniques and data handling for low aerosol loadings. Lidar provides good and often unique data at times of strong volcanic activity. Technical improvements would allow lidar to contribute more readily to the important question of whether there is a long-term trend in this background concentration of stratospheric aerosol.

8.2.2 *Volcanic aerosols and stratospheric ozone depletion*

It has been realized recently that depletion of stratospheric ozone in temperate latitudes occurs after volcanic aerosol injections. Processes involving sulfate aerosols as sites for heterogeneous chemical reactions similar to those involving chlorine, which are thought to cause the ozone hole, are implicated. The role of stratospheric aerosols in ozone photochemistry is discussed in more detail in Chapter 8.

8.2.3 *Climatic effects of tropospheric aerosols*

Tropospheric aerosols affect the radiative forcing of climate through three primary mechanisms:

- 1) Direct forcing, in which radiation is scattered or absorbed by the aerosol itself. Scattering of shortwave radiation produces enhanced reflection of the Earth-atmosphere-ocean system (thereby increasing the planetary albedo), while longwave absorption enhances the atmospheric greenhouse effect. Absorption of solar and longwave radiation alters the atmospheric heating rate and may result in circulation changes;
- 2) indirect forcing, in which enhanced concentrations of aerosol particles result in enhanced concentration of cloud drops, albeit smaller in size, thereby increasing the albedo of clouds in the Earth's atmosphere; and
- 3) indirect effects of aerosols on heterogeneous atmospheric chemistry .

The first two of these mechanisms will be discussed below, following a discussion of sources of tropospheric aerosol in the Earth's atmosphere.

8.2.3.1 *Natural emission of tropospheric aerosols*

Volcanoes can be major local contributors to tropospheric aerosols, particular as a consequence of basaltic activity of long duration (months to years). Benjamin Franklin is usually credited with first making the association between a volcanic eruption and climate or weather. While he was U.S. Ambassador to France in 1783, he theorized (in an article published in 1784) that the awful haze or dry fog, presumably sulfuric acid aerosols, that hung over Paris in the latter part of 1783 was caused by an eruption in Iceland. In fact, one of the world's greatest historic lava-producing eruptions was happening at Laki, Iceland, from June 1783 to February 1784. In this event, most of the aerosols generated may have been limited to the troposphere; this is a good example of an eruption of long duration maintaining tropospheric aerosols. Under this haze, as with other aerosol veils, the sun's rays were dimmed, and anomalously cold weather occurred, including bitter cold in August and the coldest winter on record in New England.

Biological processes are an important source of aerosols. Particulates of biological origin are derived from living organisms, such as protein-containing cells, microorganisms, and fragments of living things (Jaenicke 1993). This includes a wide range of biogenic particles, such as small viruses, bacteria, algae, pollen grains, plant debris like leaf litter, and terpenes, consisting of unsaturated hydrocarbons, C₁₀H₁₆, found in essential oils and oleoresins of plants, such as conifers. Other natural sources include fires, dust from deserts, and conversion from sul-

fur-bearing biogenic emissions such as dimethyl sulfide (DMS) and sea salt. Biogenic aerosols with radii greater than 2 μm derive from plants that release pollen, spores, and terpenes into the atmosphere. Biological aerosol smaller than 2 μm in radius originate to some extent from the mechanism of bubble-bursting on the ocean surface (Blanchard and Syzdek 1972), but they are mostly produced by industrial (sewage plants), agricultural (fertilizing, etc.), or municipal activities. Hence, biological particles are derived both from natural sources and human activities, and can, under certain circumstances, have hygroscopic properties that affect the water- and ice-nucleating capacity of the atmosphere.

8.2.3.2 Anthropogenic sources of aerosols

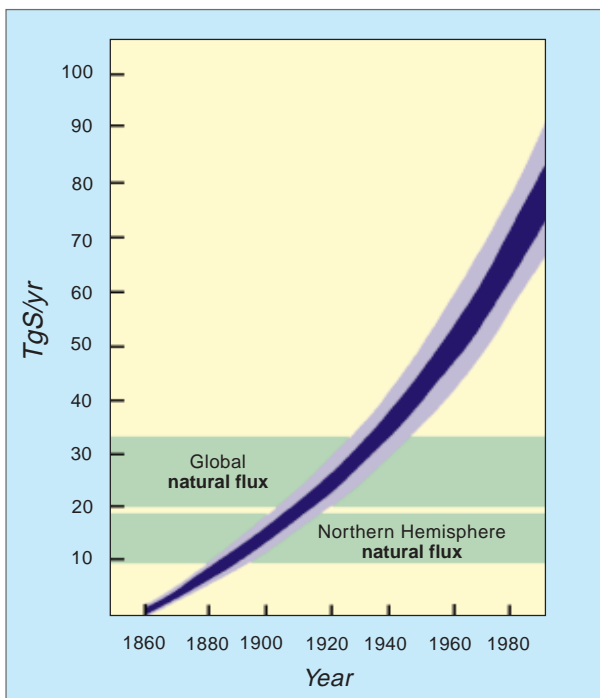
Except for increases in methane that may produce increased stratospheric water vapor, direct anthropogenic influences on stratospheric aerosols are thought to be small, although the injection of aerosols by subsonic aircraft flying in the lower stratosphere may be significant. Most of the sulfate produced by humans is converted to aerosol form in the troposphere and precipitated before it reaches the stratosphere. Stratosphere-troposphere exchange is not completely understood and the chemistry is complex, so this issue should be studied further.

The sources of aerosols associated with human activities are very important in the troposphere. Anthropogenic aerosol particles can be emitted directly (primary aerosol), or formed later in the air from oxidation of the emitted trace gases (secondary aerosol). The primary aerosols include industrial dust and soot, aircraft exhaust in the upper troposphere, automobile exhaust, particulates emitted through biomass burning, and organic particles produced in the process of biomass burning from hot unburned gases emitted from the fire and condensed immediately in the cooler air (IPCC 1995). Soil and desert dust also can be considered pseudo-anthropogenic (Prospero and Nees 1976) because of the human impact on land cover and desertification (Tucker et al. 1991). Tegen and Fung (1995) estimated the dust contribution from disturbed soils ("pseudo-anthropogenic") to be $50 \pm 20\%$ of total dust sources. Secondary aerosols include aerosol particles formed in the air from oxidation of anthropogenic SO_2 , NO_x , or volatile organic carbon (VOC). The oxidation can take place in the air or in clouds. These trace gases are also emitted from coal and oil burning in industrial or urban activities or automobile or aircraft exhaust emissions. VOC is emitted from evaporating organic compounds such as gasoline and industrial organic materials.

The effects of aerosol particles on radiative forcing (e.g., by reflecting sunlight to space), on the radiances measured from satellite sensors, on cloud formation, and on heterogeneous chemistry depend in part on their size distribution. The smaller the particles, the larger the number of particles formed for the same aerosol mass. Optically, the most effective particles are 0.2-0.8 μm in diameter. For smaller or larger particles, the particles scatter less visible radiation per unit mass. The particle size and properties are controlled by the production process. There are three main types of such processes: mechanical grinding producing mainly micrometer-size particles, gas-to-particle conversion (both oxidation and condensation) producing submicrometer particles, and production of black carbon (soot) as the unburned carbon remnant in combustion processes. Soot is emitted as very small particles ($<0.1 \mu\text{m}$), serving as condensation centers to other particles (organic particles from biomass burning), or forming chains and collapsing into round submicrometer aggregates in the presence of high humidity.

Based on the latest report of the Intergovernmental Panel on Climate Change (Intergovernmental Panel on Climate Change [IPCC] 1995), if we exclude the anthropogenic impact on soil and desert dust, the contribution of anthropogenic sources to micrometer-size particles is very small (5% of total mass). The contribution to submicrometer particles is large (~75%): sulfates - 140 Tg/yr (with a range between 120 and 180), organic particles from biomass burning - 80 Tg/yr (between 50 and 140), and VOC - 10 Tg/yr (between 5 and 25); this is out of a total budget of submicrometer particles from anthropogenic and natural sources of 390 Tg/yr ($\text{Tg} = 10^{12} \text{g}$). Soil dust also contributes to the population of submicrometer aerosols. Tegen and Fung (1995) estimate that disturbed soils contribute 50-150 Tg/yr of submicrometer particles. These numbers indicate that human activity controls the atmospheric concentration of submicrometer particles, and with that it probably influences the microphysical properties of clouds everywhere except at locations remote from human influence. The volume size distribution of most of these submicrometer aerosol types is in a size range with a large scattering cross section per unit volume. For sulfates, the volume distribution is between 0.1 and 0.4 μm in diameter (Hoppel et al. 1990; Hegg et al. 1993, 1995; Kaufman and Holben 1995) and for smoke between 0.2 and 0.4 μm (Andreae et al. 1988, 1994; Artaxo et al. 1994; Kaufman and Holben 1995). It follows from this discussion that sulfates and biomass burning are the two most significant anthropogenic sources of aerosol that can affect climate. For the same reason, these are the two types of aerosol that are

FIGURE 8.5



Time history of global emission of SO_2 (in Tg/yr) and estimates of the global and Northern Hemisphere natural flux (Charlson et al. 1992). Anthropogenic sulphur is emitted mainly (90%) in the Northern Hemisphere, and emissions greatly exceed the natural emissions. Width of shading represents the uncertainty.

the easiest to observe from space, due to their high scattering and backscattering efficiency. There is a remaining uncertainty in the anthropogenic component of soil dust, and in the role of VOC in controlling the number of cloud condensation nuclei (CCN). Though the rate of emission of VOCs is only one-eighth that of sulfates, due to their smaller size (less than $0.1 \mu\text{m}$) they may contribute as many CCN as sulfates (Rivera-Carpio et al. 1995) or even dominate the CCN concentration (Novakov and Penner 1993). The effect of aerosol on CCN and cloud microphysics is non-linear (Leitch et al. 1986); therefore, a large concentration of VOCs can have a substantial effect on clouds but also decrease the influence of sulfates on clouds as well. The subject of aerosol-cloud interactions has been reviewed by Hobbs (1993).

8.2.3.2.1 Sulfur emission and oxidation to sulfate particles

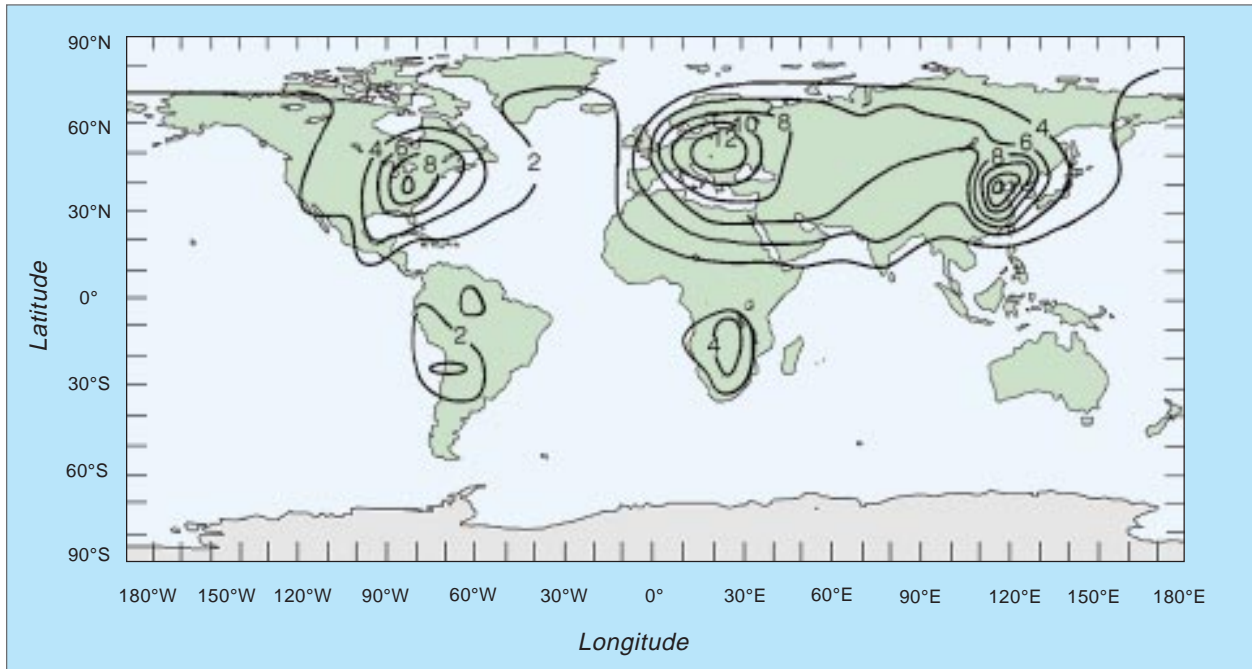
Most sulfur emission (in the form of SO_2) originates from the burning of fossil fuel (coal and oil) in the Northern Hemisphere. Muller (1992) estimated the strength and geographical distribution of the sources and the total source strength. Charlson et al. (1992) compared the total

anthropogenic sulfur budget in the last century, based on Muller's estimate, to the natural emissions (Figure 8.5). Volcanoes can make large short-term, localized contributions to the global inventory of SO_2 (Spiro et al. 1992). About half of the sulfur is deposited directly on the ground and half is oxidized in the atmosphere to form aerosol particles. Langner and Rodhe (1991) used a GCM with sulfur chemistry to simulate the transport and oxidation of the emitted anthropogenic SO_2 into aerosol particles, showing contour lines of concentrations of the particles. Figure 8.6 (pg. 352) reproduces their results. The model includes the two paths of oxidation into sulfate particles. Gas phase oxidation controls the population of particles smaller than $0.1 \mu\text{m}$, and oxidation in non-precipitating clouds controls the concentration of larger particles (~ 0.2 to $0.4\text{-}\mu\text{m}$ diameter, Hoppel et al. 1990). Langner et al. (1993) calculated with their GCM model that 88% of the anthropogenic sulfate is generated in clouds, while 12% is generated in the gas phase. The balance between these two processes and the value of maximum supersaturation reached in clouds is critical to the determination of the effect of sulfate on climate. While conversion of sulfate into larger particles in cloud processes increases their direct radiative forcing (Lelieveld and Heintzenberg 1992), it decreases the concentration of potential CCN by generating larger and fewer particles for the same sulfate mass concentration. This balance depends not only on the value of the maximum supersaturation reached in clouds, a measure that is highly unknown, but also on the variability in this value between non-precipitating clouds (Kaufman and Tanré 1994).

8.2.3.2.2 Biomass burning

Biomass burning is widespread, especially in the tropics, where $\sim 80\%$ of biomass burning takes place. It serves to clear land for shifting cultivation, to convert forest to agricultural and pasture land, and to burn dry vegetation to fertilize the soil. Biomass burning is also used for cooking and charcoal production mainly in the developing countries. Interest in biomass burning started when it was discovered to be a main missing source of greenhouse trace gases in the 1970s (Crutzen et al. 1979). It was later recognized as an important source of aerosol particles (Radke et al. 1991; IPCC 1995) that can affect clouds and the hydrologic cycle in the tropics (Crutzen and Andreae 1990) and solar radiation and climate (Penner et al. 1992). The type of aerosol produced in the burning depends on the fire temperature and oxygen supply. Hot flaming fires, typical of grassland fires in Africa and South America, produce a relatively small amount of organic particles, but a large amount of black carbon (Cachier et al. 1989;

FIGURE 8.6



Calculated distribution of the vertically-integrated amount of sulphate aerosol due to anthropogenic emissions only (Langner and Rodhe 1991: *slow oxidation case*). Values are annual averages expressed as mg sulphate per square meter and the maxima are associated with main industrialized regions. No comparable results are available for aerosol from biomass combustion.

Ward et al. 1992). Deforestation and other fires with a long smoldering phase produce little black carbon and a large amount of organic particles (Ward and Hardy 1991). In the last century the rate of biomass burning has increased substantially. Deforestation was almost nonexistent in the last century and now consumes 1300 Tg of carbon in biomass per year (Andreae 1995). Domestic use of biomass as fuel, and biomass burning associated with agriculture, probably increased proportional to the population expansion. Shifting agriculture consumes about 1500 ± 500 Tg of carbon per year, and grass fires an additional 1200 ± 800 Tg (Crutzen and Andreae 1990). These sources can emit a similar amount of organic particles as deforestation, and dominate the emission of black carbon. Detailed geographical estimates of biomass burning are given by Hao et al. (1990). But, in contrast to sulfate aerosols, evaluation of the global emission and distribution of smoke aerosols is still not available. The total estimate of biomass burning aerosol flux of 80 Tg/yr (IPCC 1995) corresponds roughly to 2% of the burned carbon or 1% of the burned biomass (Ward et al. 1992). The recently completed field phase of the Smoke Cloud and Radiation-Brazil (SCAR-B) study

should yield much new information on the properties of smoke particles from tropical biomass burning and their effects on the atmosphere.

8.2.3.3 Direct radiative effects of tropospheric aerosols

The direct effect of aerosols on the radiative forcing of climate is far more complex for tropospheric aerosols than for stratospheric aerosols, due to the wider range of chemical compositions, time and spatial distributions, range of particle sizes and shapes, interactions with water vapor and clouds, and overall global variability that is dependent on both natural sources of aerosols and human activities. In principle, the direct radiative forcing (both shortwave and longwave) by tropospheric aerosols can be computed if the optical properties of the aerosols are known, especially the spectral optical thickness, single-scattering albedo, and phase function, all of which depend on the size distribution and refractive index of the aerosols. Many of these optical and microphysical properties depend on the individual chemical species comprising the aerosols (e.g., sulfates, nitrates, silicates, sea salt, soot, organics, etc.).

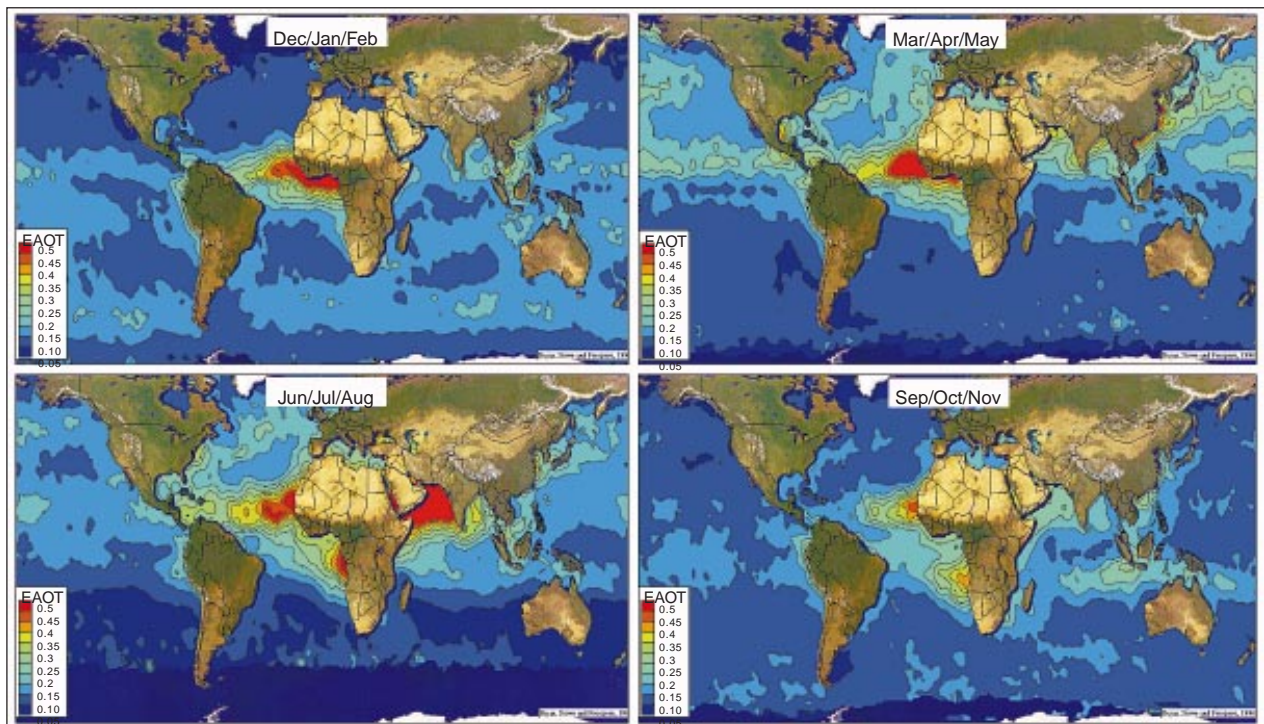
Unfortunately, reliable laboratory measurements of refractive indices of atmospheric aerosols are not available for most of the chemical species composing the atmospheric aerosol. Furthermore, since reliable particle size distributions are also incomplete, it is not currently possible to calculate with high accuracy the radiative forcing by tropospheric aerosols. This has led the scientific community to advocate the simultaneous acquisition of satellite-based radiance measurements, ground-based measurements of atmospheric transmission and sky radiance, and in situ measurements of aerosol optical and microphysical properties from aircraft. In these so-called “closure” experiments, it should be possible to verify that optical thicknesses and other radiative parameters retrieved from available satellite measurements, when inserted into a radiative transfer model, yield accurate estimates of the radiative forcing of tropospheric aerosols. The first comprehensive closure experiment was carried out in the Tropospheric Aerosol Radiative Forcing Observational Experiment (TARFOX) on the United States East Coast in the summer of 1996 (Stowe et al. 1995).

Since changes in column-integrated radiances are weakly dependent on aerosol properties, making reliable

retrieval of these properties difficult, improvements in measurement capability from current satellite systems are highly desirable to further advance our understanding of the role of tropospheric aerosols on climate. Advances from current systems are planned for the EOS missions through the use of improved radiometric accuracy and calibration (the Moderate Resolution Imaging Spectroradiometer [MODIS], the Multi-angle Imaging Spectro-Radiometer [MISR]), multi-wavelength capability over a wider spectral range (MODIS, MISR, OMI), multi-angle looks at the same scene (MISR, the Earth Observing Scanning Polarimeter [EOSP]), and multispectral polarimetric techniques to enable refractive index and characteristic aerosol types to be identified (EOSP). A necessary component of improving the determination of tropospheric aerosol properties from space is a ground-based sunphotometer and sky radiance network.

To assess the radiative forcing of industrial aerosols, it is necessary to establish the preindustrial global background aerosol with the same degree of reliability that the preindustrial greenhouse gas levels are known. Based on aerosol measurements in remote locations (e.g., Cape Grim, Tasmania, and Mauna Loa Observatory, U.S.), the global mean preindustrial aerosol optical thickness

FIGURE B.7



Aerosol abundance over the oceans estimated from satellites (Husar, Stowe, and Prospero 1996).

may have been in the range $0.02 \leq \tau_a \leq 0.05$. Andreae (1995) estimated that the global average natural aerosol background is $\tau_a = 0.07$.

The single-scattering albedo of desert dust is largely unknown, and this aerosol type is a dominant feature of global aerosol measurements over the ocean as obtained from space (Figure 8.7). For radiative transfer purposes, the precise form of the aerosol size distribution is not important, but rather the optical thickness and effective radius (Lacis and Mishchenko 1995). Typically, in models that calculate aerosol forcing of climate, aerosol types and sizes are described by a finite number of discrete categories, with optical thickness and vertical distribution as free parameters. Consistency is needed between those aerosol parameters used in radiative transfer models and those in field measurements, where a continuum of particle sizes and composition mixtures is encountered. Closure experiments will further enhance our confidence in this transformation.

8.2.3.4 *Indirect effects of aerosols on cloud abundance, lifetime, and optical properties*

The indirect effect of aerosols refers to their effects on cloud properties: droplet/ice particle number concentrations and sizes, water/ice amounts, cloud lifetime, and cloud boundaries. Through their influence on these properties, aerosols have an indirect effect on the Earth's radiative energy balance through the way that clouds affect the Earth's energy budget. The indirect effect is often referred to as the Twomey effect. Twomey (1977) first outlined the potential role of aerosols on cloud droplets and cloud radiative properties.

The subset of tropospheric aerosols that act as the nuclei for cloud droplet formation is known as cloud condensation nuclei (CCN). These nuclei serve as seeds around which water condenses to form droplets and ice crystals. Increased numbers of CCN are correlated with increased numbers of cloud hydrometeors (Warner and Twomey 1967; Martin et al. 1994). Often, however, the new droplets compete for the water that is available for condensation so that while increased CCN lead to increased numbers of hydrometeors, the size of the hydrometeors is smaller (Twomey 1977; Radke et al. 1989; King et al. 1993; Garrett and Hobbs 1995). Because scattering is proportional to the surface area of the scattering targets, a given mass of water scatters more light if it is distributed among smaller particles. Consequently, polluted clouds are expected to have higher reflectivities than their non-polluted counterparts. Satellite and aircraft observations have confirmed this increase in reflectivity (Coakley et al. 1987; Radke et al. 1989;

King et al. 1995). This increase is expected despite the absorption of sunlight by the aerosol, although if the optical thickness of the cloud and the absorption of sunlight by the aerosol are sufficient, the effect of the absorption can lead to a decrease in cloud reflectivity despite the increase in droplet number (Twomey 1977). This decrease has also been confirmed through satellite observations of the effects of biomass burning on cloud radiative properties (Kaufman and Nakajima 1993).

Through their influence on droplet and ice particle numbers and sizes, aerosols may influence bulk cloud properties, such as cloud amount, lifetime, cloud liquid/ice water amounts, and the locations of cloud boundaries. Clouds with large numbers of small droplets appear to show smaller occurrences of drizzle than do their counterparts having relatively few but large droplets. Consequently, clouds affected by increased aerosol burdens are expected to retain cloud water while unaffected clouds are expected to lose their water. Affected clouds have been predicted to last longer in the atmosphere than their unaffected counterparts (Albrecht 1989). The added lifetime could give rise to larger cloud cover fractions when averaged over time (Parungo et al. 1994; but see Norris and Leovy 1995). Results from the recently completed Monterey Area Ship Track Experiment show that these expectations are not always realized.

If one is to believe some of the simpler models for cloud properties, such as mixed-layer models for marine stratus, then hydrometeor size, through its influence on radiative heating, affects the thermodynamic environment of the cloud thereby influencing the location of the cloud boundaries (Pincus and Baker 1994). Such changes, however, are expected to be small, making them difficult to detect.

Because the evolution of aerosol precursors to CCN and ultimately to cloud droplets is fraught with uncertainty, assessments of the indirect effect are also fraught with uncertainty. The range of possibilities seems limitless (Kaufman et al. 1991) but may well be of the same order of magnitude as that due to the direct effect (Charlson et al. 1992). One obstacle to reducing the uncertainty is lack of knowledge linking precursor gases to the existing levels of CCN. What fraction of the precursor gases gives rise to new particles and new hydrometeors and what fraction is absorbed by existing particles and hydrometeors? For example, a major fraction of the SO_2 emitted into the atmosphere appears to be taken up by existing cloud droplets rather than giving rise to new particles (Langner et al. 1992).

The relationship between the number of particles and the number of cloud droplets appears to saturate at

high aerosol concentrations (Leaitch et al. 1992; Martin et al. 1994). Clouds can have such a large population of small droplets that adding new particles to the cloud has little if any effect on the droplet size distribution. Nevertheless, substantial changes have been observed, even for continental clouds with their large number concentrations and small droplet sizes (Braham 1974). Also, the effect of a transformation of droplet size on cloud radiative properties becomes saturated when the number of droplets is large and thus cloud reflectivities approach their upper limits (Charlson et al. 1992; Platnick and Twomey 1994).

8.2.3.5 *Science investigations using EOS data*

EOS aerosol data products will be used to study variations in the anthropogenic aerosol, its interactions in the atmosphere, and its radiative forcing of climate. Some of the research is planned by EOS investigators; other research will be done outside of EOS using EOS data. EOS data will be used to monitor the change in the aerosol global loading. Using global transport models that include atmospheric heterogeneous chemistry (e.g., Benkovitz et al. 1994), it should be possible to investigate to what degree changes in aerosol concentrations are due to changes in the source strength and redistribution of the location of the sources (e.g., reduction of emission in some areas and an increase in others) or due to changes in the rate of atmospheric processes that affect aerosol properties and sinks. Comparison between simultaneously-derived EOS aerosol concentration and properties with cloud abundance and properties (King et al. 1992) will be used to study the effect of aerosol on cloud droplet size, cloud reflectance, and maybe even cloud cover (Twomey 1977; Twomey et al. 1984; Coakley et al. 1987; Radke et al. 1989; Kaufman and Nakajima 1993; King et al. 1993). The aerosol distribution and properties will also be used to correct satellite observations of the land and ocean surface for aerosol effects (atmospheric correction).

8.2.3.6 *Needed satellite and in situ measurements*

Learning how aerosols affect the global climate requires: 1) The space-based monitoring of indices related to aerosol properties; 2) surface-based monitoring of indices related to aerosol properties; and 3) intensive field campaigns. The surface-based monitoring program should be designed to enhance the capabilities of the space-based program. Because the inference of aerosol properties from space is an ill-posed problem, a surface-based monitoring program is crucial to the success of the space-based program. The surface-based program will not only track the performance of space-based monitoring, it could provide additional information concerning the aerosol

properties for a number of major aerosol systems (maritime, urban, windblown dust, volcanic, biomass burning, etc.) that enhance the interpretation of the spaceborne observations. Field campaigns, in turn, are designed to refine knowledge gained from both the surface and space-based monitoring programs. The emphasis of the field campaigns will be to learn how aerosol properties are linked to sources and sinks, and how these properties are transformed by atmospheric processes. The links between aerosol properties and aerosol sources and sinks are essential to assessing the influence of aerosols on the climate system.

8.2.3.6.1 Global observations of tropospheric aerosol optical properties

The direct effect of aerosols can be observed from space through their effects on the scattering and absorption of sunlight. Since most aerosols have sizes in the 0.1-1.0 μm range, their effect on escaping longwave radiation is relatively small compared with their effect on sunlight. Aerosol properties are inferred primarily from reflectivities measured from cloud-free regions (Hansen and Travis 1974; Kaufman et al. 1990; King et al. 1992; Diner et al. 1988; Martonchik and Diner 1992; Tanré et al. 1995; Torres et al. 1998). Such strategies will be used to extract aerosol properties from MODIS, MISR, and OMI. The properties will thus be clearly limited to cloud-free conditions. While such conditions obviously bias the ensemble of observations, the ensemble is likely to remain stable over long periods and thus provide a useful index for monitoring change (Rao et al. 1989; Kaufman and Nakajima 1993).

The amount of sunlight reflected from the Earth system is a function of aerosol burden and aerosol properties such as particle size and single-scattering albedo. Short-term variations in reflected sunlight at visible wavelengths within cloud-free regions are linked to short-term variations in the column aerosol burden. Reflected sunlight in the near infrared ($>1 \mu\text{m}$) is expected to provide an index of particle size (small vs. large, with $r \sim 0.7 \mu\text{m}$ being the approximate size partition [Durkee et al. 1986]). This index helps characterize the aerosol and may ultimately help identify the source of the aerosol: urban, maritime, or windblown dust. Contrasts in reflected light over backgrounds with varying albedos, such as contrasts between small lakes and their surroundings, forests, and nearby grasslands, etc., are expected to provide an index for the single-scattering albedo (Kaufman 1978). Like particle size, such inferences will lead to better characterization of the aerosol and help with the identification of sources. Finally, since aerosols have sizes that are com-

parable to the wavelengths of incident sunlight, their presence changes the color of the Earth. Narrowband estimates of albedo changes due to aerosols will probably be biased. Broadband observations are needed to provide unbiased estimates of the effect of the aerosol on the Earth's albedo.

Because most of the light reflected from the cloud-free Earth is reflected by the surface, inferring aerosol properties from space poses substantial signal-to-noise problems, particularly when the aerosol concentrations are low, as they are far from sources, such as urban environments, deserts, etc. Nevertheless, over oceans, monitoring of aerosol burdens comparable to those expected from the natural background (optical thickness, t_a [$0.5 \mu\text{m}$] ~ 0.05) seems feasible (Rao et al. 1989). Similar capabilities may be achievable over dark, continental targets such as lakes and forests (King et al. 1992; Holben et al. 1992; Martonchik and Diner 1992). This will be a new challenge for EOS, with no previous experience on a global basis to determine the possible degree of success.

More reliable detection of aerosols over land is possible using near-ultraviolet wavelengths (380-400 nm) where the non-snow covered terrestrial surfaces become very dark (Eck et al. 1987; Herman & Celarier 1997). The large molecular (Rayleigh) scattering at these wavelengths has both advantages and disadvantages over the visible techniques. While it reduces the dependence of backscattered radiances on surface reflectivity and aerosol phase function, it makes them more sensitive to aerosol absorption, except when aerosols are close to the surface. Therefore, the technique is most useful for estimation of aerosol optical thickness near their source regions over land. It works particularly well in arid and semi-arid areas, where the visible techniques become unreliable.

Another UV technique developed recently (Krotov et al. 1997; Torres et al. 1998) using TOMS data is sensitive only to highly UV absorbing aerosols (volcanic ash, smoke, and mineral dust) and is insensitive to other aerosol types as well as clouds. The technique has the advantage that it works equally well over both land and water, and is the only known (passive) technique that can detect such aerosols over very bright scenes, including snow and underlying clouds. However, the technique suffers from strong sensitivity to aerosol height- the lower the height the less sensitive the technique. Its primary advantage is to help in the identification of aerosols detected by more conventional techniques.

Several EOS instruments will provide information about tropospheric aerosols. This includes three primary instruments designed for aerosol research (MODIS, MISR and EOSP). In addition, the OMI instrument on EOS/

CHEM, which has UV channels, would provide aerosol information similar to TOMS, and the GLAS lidar on ICESat will provide aerosol backscattering profiles.

MODIS, which will fly on both the EOS AM-1 and PM-1 platforms, will make reflected spectral measurements in the solar and infrared regions to obtain aerosol optical thickness. Over ocean it will also provide aerosol size distribution, namely the ratio of the concentration of micrometer to submicrometer particles, and the specific size of the dominant aerosol mode. Over land the information will be initially limited to the determination of whether the dominant mode is of micrometer or submicrometer size (King et al. 1992; Tanre et al. 1995). However, combination of MODIS with TOMS and OMI has the potential of improving the size information over land, as well as helping in the identification of aerosol types over both land and oceans.

MISR, which will fly on EOS AM-1, will make multi-angle measurements at four visible and near-infrared bands (Diner et al. 1998, 1991). The angular and spectral measurements will be used to derive the aerosol optical thickness and loading over land and ocean. With the help of an aerosol climatology to remove some of the indeterminacy of the aerosol properties from space observations, the MISR aerosol retrieval should be able to distinguish among many common particle "types" that represent constraints on a combination of particle shape, size distribution, and composition.

Combining spectral measurements in the solar spectrum with polarization measurements, to be obtained with EOSP, provides additional information on aerosol properties. EOSP may fly on an EOS AM-2 platform, along with advanced versions of MODIS and MISR. The addition of polarization measurements is expected to refine the EOS ability to measure the size distribution of the climatically-important small particles, and to help in establishing the aerosol refractive index, a parameter that is both important for the inversion of satellite-measured radiances to aerosol properties, and for illuminating the chemical composition and atmospheric influences on aerosol particles.

Again, the direct effect of aerosols can be extracted only for cloud-free conditions. Further, they are often seen as a small residual viewed against the noisy cloud-free background offered by the Earth's surface. In order to assure that global-scale aerosol systems are being fairly represented in the combination of space and surface-based monitoring, occasional surveys with spaceborne lidars, as recently undertaken by LITE, should be performed (McCormick et al. 1993). LITE frequently found aerosol systems, like smoke above extensive marine stratocumu-

lus layers to the west of South America, that may well be missed by conventional passive techniques being planned for aerosol monitoring. GLAS, to be launched in 2001 on the Ice, Clouds, and land Elevation Satellite-1 (ICESat-1), will provide a similar global capability of monitoring the vertical profile of aerosol layers in the troposphere and lower stratosphere. This will be especially important in polar regions, where multilayer cloud and aerosol systems are common and for which passive imaging systems are less capable.

The ability to differentiate tropospheric aerosols from stratospheric volcanic aerosol layers is clearly desirable. Techniques that rely on the intensity of reflected light to gain aerosol properties, such as those that will be employed with MODIS and MISR observations, cannot separate light reflected from the troposphere from that reflected from the stratosphere. Limb observations, such as those employed with SAGE III, are essential to accounting for the light reflected from volcanic haze layers (McCormick and Wang 1987). While observations of the polarization of reflected light might be used to infer indices of the vertical distribution of aerosol properties, it is doubtful that such indices can compete with the integrity of the solar occultation provided by the limb observations. Once accounted for, residual contributions to reflected light for cloud-free regions can then be used to infer the properties of tropospheric aerosols. So, limb viewing instruments such as SAGE III are crucial components to an aerosol monitoring program.

Once global distributions of aerosols are derived on a daily basis, they can be used with global models (Benkovitz et al. 1994; Langner and Rodhe 1991) to derive aerosol fluxes, calculate aerosol nonaqueous mass, determine their sources and sinks, and compute their radiative forcing effect on clouds and the hydrological cycle, and the effect of aerosols in atmospheric chemical processes.

The effect of aerosols on clouds is best manifested through changes in hydrometeor size, which in turn is best detected through changes in reflected sunlight at near-infrared wavelengths (King et al. 1992). Water and ice absorb in the near infrared. To a first approximation, the absorption cross sections of water droplets and ice particles are proportional to the particle volume, while the scattering cross sections are proportional to the particle area. The ratio of scattering to absorption thus becomes a sensitive function of particle size in the near infrared. The ratio of scattering to absorption is, in turn, linked to cloud reflectivity.

While upper-level clouds have often been characterized as having ice crystals with sizes ranging from

10-100 μm , evidence from multispectral emission in the infrared (Prabhakara et al. 1988; Lin and Coakley 1993) and from in situ observations (Strom 1993) suggests the presence of smaller particles for upper-level clouds. Such particles should also manifest their presence through their effect on reflected sunlight in the near infrared.

Links between cloud hydrometeor sizes and bulk properties of clouds such as cloud lifetime, cloud top altitude, cloud thickness, and liquid water content, could greatly alter the ways in which aerosols affect the Earth's radiation budget. Such links are anticipated, but evidence for these links will come only from careful long-term monitoring of cloud systems. The cloud properties that must be monitored are hydrometeor size, amounts of water and ice, the vertical extent of the cloud, and the fractional cloud cover of the cloud systems. Since all of these properties affect the way in which clouds affect the Earth's energy budget, these properties are expected to be monitored in any case (King et al. 1992). The monitoring, however, should be so extensive as to allow a study of large-scale cloud systems that are transected by aerosol systems so that one portion of the cloud system has a high probability of being affected by aerosols and a second portion has a low probability of being affected. Cloud systems that span an urban plume and surrounding areas that lie outside of the plume would be an example. In such cases, the affected and unaffected portions of the cloud system can be examined together. They would be expected to be very similar except for the effects of the aerosol. With extensive monitoring, ensembles for particular types of cloud systems can be built and studied for the effects of the perturbing aerosols.

8.2.3.6.2 Surface monitoring of tropospheric aerosols

Surface-based monitoring should be designed to improve space-based capabilities, since satellite measurements alone cannot detect all aerosol properties. Some aerosol properties must be pre-assumed, based on previous measurements, and/or measured in parallel with space observations (Wang and Gordon 1995). Because they will be used to track the performance of the spaceborne monitoring capability, the surface-based observations must be reliable. Sites for the surface-based observations should be distributed in order to characterize some of the well-known aerosol systems: urban haze, desert dust, smoke from biomass burning, etc. The observations should include measurements of radiation along with surface measurements of the physical and chemical properties of the aerosol. The coupling between radiation and physical and chemical properties of aerosols will lead to better estimates of the effect of aerosols on the Earth's radiative

energy budget. Furthermore, the inclusion of observing capabilities for the physical and chemical properties will help link aerosol properties to their sources and sinks (Charlson et al. 1992).

EOS, together with other international Earth science organizations, is planning a network of ground-based automatic instruments that will remotely sense aerosol properties from the surface (Holben et al. 1995). The ability to observe both the sun through the aerosol layer as well as aerosol scattering relative to the dark background of space (sky radiation), makes these ground-based remote-sensing measurements very powerful (Nakajima et al. 1989; Kaufman et al. 1994). Therefore, the EOS strategy is to complement the global distribution of aerosol properties derived from Earth-orbiting satellites on a daily or twice daily basis with ground-based measurements at ~100 stations worldwide. These observations should provide measurements of the diurnal cycle of aerosol concentration and optical properties, as well as supply statistics on some of the missing optical properties needed to analyze the spaceborne data. Other aerosol properties will be derived from chemical measurements and sampling by scientists worldwide.

In addition to the surface sunphotometer/sky radiance network, the surface sites should also include calibrated broadband radiometers. Simultaneous observations of multispectral radiances at the Earth's surface and from space for cloud-free conditions will enhance the ability to detect the absorption of sunlight that is otherwise difficult to infer from either surface or space-based observations alone.

8.2.3.6.3 Intensive field campaigns

To complement the surface and space-based observations of tropospheric aerosols, it is necessary to conduct periodic airborne intensive field campaigns. The roles of these campaigns include: 1) Intercalibration of spectral, angular, and polarimetric sensors on aircraft with their spaceborne counterparts; 2) in situ measurement of the optical and microphysical properties of the atmospheric aerosol, especially, aerosol size distribution and, where possible, the single-scattering albedo; and 3) providing an opportunity to confirm a closure of radiative transfer models of the transmission, reflection, and absorption of the Earth-atmosphere system with nearly simultaneous surface and spaceborne observations of sky radiance, aerosol properties, and radiative flux. These aperiodic campaigns should be carefully coordinated with the international scientific community, and should focus on particularly important aerosol climatological regimes (e.g., sulfate aerosol from the east coast of the U.S. and China, biomass burning aerosol in the tropics, Sahelian dust out-

breaks from Africa), as well as aerosols especially difficult to detect (Arctic haze, continental haze layers).

8.2.4 Volcanic hazards

Volcanoes represent significant hazards to people and property on the ground and in the air. Because each eruption is unique, it is challenging to develop a set of methodologies that can successfully identify and document the physical processes associated with all types of volcanic eruptions. For example, subtle differences in the percentage of water vapor vs. ash in an eruption plume, perhaps by interaction between the lava and surface water, can produce very different plumes that may not always be detected by thermal imagers. Ground deformation associated with swelling or subsidence of a volcano may not be accurately determined via radar interferometry due to decorrelation of the surface between observations, or due to atmospheric effects associated with the water vapor content of the atmosphere. Methodologies for the remote detection of the eruption of new lava flows, or the monitoring of the thermal output of on-going eruptions are still under development. Hyperspectral measurements at mid- and thermal-infrared wavelengths are needed to redress this situation.

Studies of volcanic hazards can be divided into three main categories. Hazard prevention refers to the analysis of dormant volcanoes, which are considered to be potentially active but show no signs of eruption in the near future. Hazard preparedness refers to restless volcanoes that currently have mild activity in the form of ground deformation, gas emissions, or elevated ground temperatures. Hazard relief is needed for active volcanoes, which may currently be erupting lava flows or undergoing explosive eruptions that generate eruption plumes, pyroclastic flows, or mudflows. Hazardous volcanoes are often particularly challenging to study because they may be located in areas where local logistics, weather, and personal safety limit access. A wide range of hazards also exists. Long-lasting emissions of tropospheric gases (HCl, SO₂, and HF) have a major impact on the health of people, livestock, and agriculture downwind of a volcano. Lava flows and, more particularly, volcanically-generated mudflows (lahars) have proven to be fatal to thousands of people in this century. A new hazard, associated with the use of aircraft flight paths over volcanically-active areas such as Indonesia and the Alaskan peninsula, places tens of thousands of jet aircraft at risk every year due to the potential for unexpected encounters with an eruption plume. Other volcanic hazards exist, including the potential that flank failure will generate tidal waves (tsunamis) in shallow marine environments (e.g., St. Augustine, Alaska).

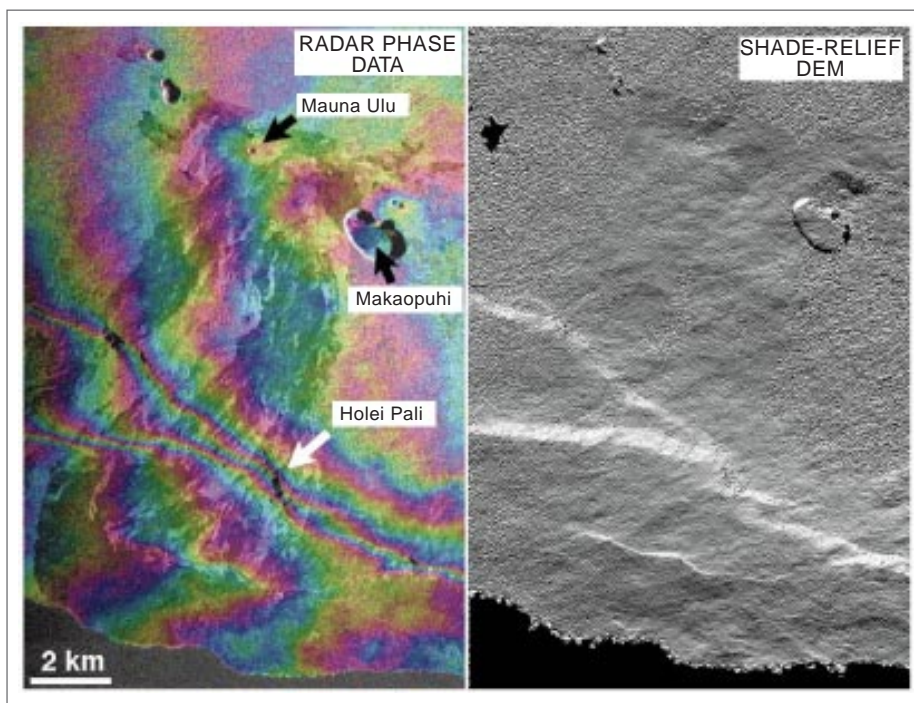
The major challenge to satellite-based observations of volcanic hazards is the development of techniques that can be used in a predictive manner to detect an evolving volcanic crisis, and to provide timely information to the relevant authorities on the ground.

8.2.4.1 Health hazards of tropospheric volcanic gases and aerosols

Basaltic volcanoes such as Kilauea, Hawaii, can be in near-continuous eruption for years (in Kilauea's case, more than 12 years). While the daily eruptions of volcanic gases (including H_2O , CO_2 , SO_2 , H_2 , CO , HCl , HF , and H_2S) are quite low, with average emissions in the range of 1000-2000 tons/day, the protracted nature of the eruptions can place local populations at serious health risk. In a more-extreme case, the 1783 eruption of the Laki Fissure in Iceland erupted ~ 125 Tg of SO_2 in five months (equivalent to five Mt. Pinatubo eruptions), and caused numerous weather anomalies in Europe including dry fogs and high optical thicknesses. This eruption is also believed to have caused a drop in the global mean surface temperature of ~ 1 -to- 3°C (Sigurdsson 1990).

H_2O and H_2 can be dismissed as significant health factors, either because of their low inherent toxicity, low concentration in volcanic emissions, or both. SO_2 , H_2S , and their reaction products present the greatest potential for adverse health effects, which are further magnified by their ultimate conversion in the atmosphere to a secondary acid aerosol, producing irritants with demonstrated adverse effects on the human respiratory system. HCl and HF emissions from volcanic vents, while very low relative to SO_2 , also contribute to the acidic nature of the atmosphere downwind of the volcano. Both are strong irritants capable of causing lung injury.

FIGURE 8.8

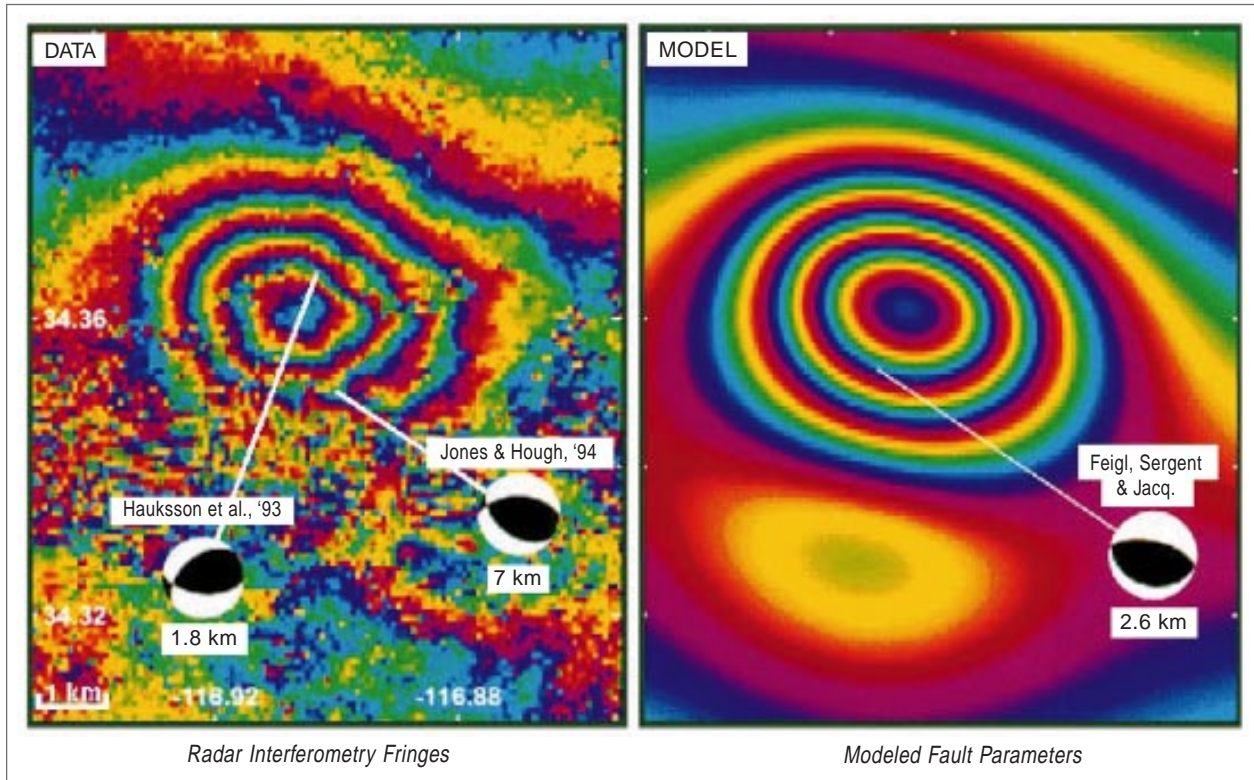


Radar interferometry will be used extensively to construct digital elevation models of volcanoes, using data from foreign-partner radars such as ENVISAT ASAR and RADARSAT. Space Shuttle Radar (SIR-C) data collected in October 1994 are used here first to construct a radar phase map (left) of the Mauna Ulu area of the Kilauea volcano in Hawaii. These phase data can then be unwrapped to generate a digital topographic map, which then can be used to produce the shaded relief map (right). Almost 1 km of relief is shown in this image, with the bright escarpment representing ~ 350 meters of elevation change (*unpublished data*; courtesy of Harold Garbeil and Peter Mougini-Mark [University of Hawaii]).

Sulfate concentrations in rain water due to ongoing eruptions also have a significant impact on the downwind population. Where lava flows enter the ocean, a further health hazard is generated by the production of steam clouds. In extreme cases, rain water has been found to have a pH in the range 2.4 to 2.8, and has been correlated with health problems in local populations that rely on rain for drinking water. Direct analysis of this steam plume indicates that it is an acid brine with a salinity ~ 2.3 times that of sea water and a pH ranging from 1.5 to 2.5!

CO_2 hazards from volcanoes should also not be forgotten. In Cameroon, the release of carbon dioxide gas from an overturned volcanic water lake resulted in hundreds of fatalities in 1986. Many deaths in the historical record are attributed to asphyxiation by volcanic gases, mostly by CO_2 and H_2S (Simkin and Siebert 1994). CO can also reach toxic levels as it did in Niragongo in 1972 (Faivre-Pierret and Le Guern 1983). The risk posed by such hazards can be assessed by means of modeling the ground flow of such gas discharges, provided that there is a high-quality digital elevation model (DEM) available.

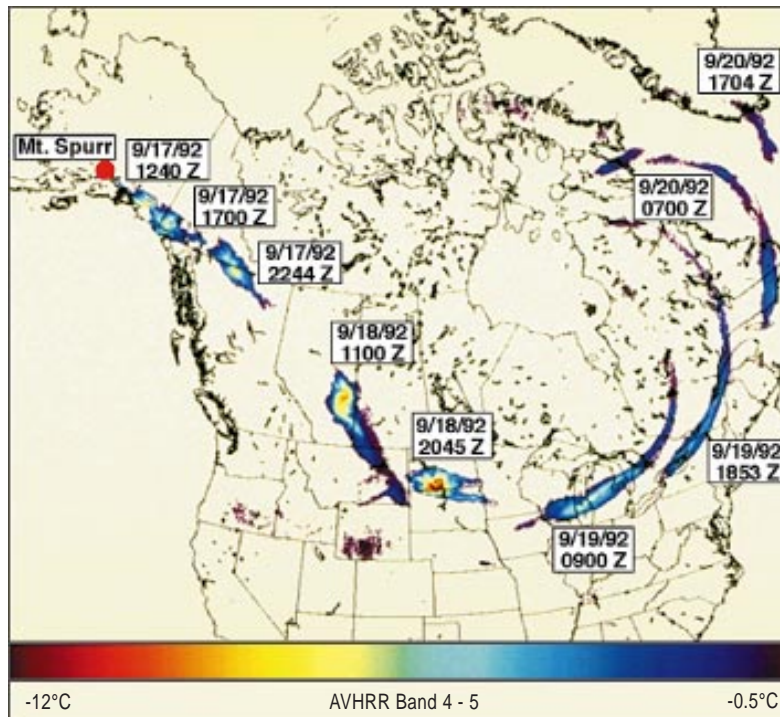
FIGURE 8.9



Fringes produced by a small ($M=5.1$) aftershock, as seen in an interferogram constructed from European Remote-Sensing Satellite-1 (ERS-1) radar images acquired on April 24, 1992 and June 18, 1993 (left: *Massonet et al., 1994*), and modeled using fault parameters estimated from the interferogram (right: *Feigl et al. 1994*). The interferometric signature is the sum of the main Landers shock (straight fringes in NE quadrant) and the aftershock (concentric circles near center). One fringe represents 28 mm of range change.

Weather satellite data are already used in an operational mode by the FAA, U.S. Geological Survey, and the Australian aviation community. These data are used to detect and track volcanic eruption clouds, which represent a great danger to air traffic along many of the world's busiest air routes. Due to the presence of silicate material in the cloud, the spectral properties of volcanic clouds and weather clouds are very different in the thermal infrared, allowing simple automatic detection algorithms to be developed in a comparable way to more-detailed analyses from MODIS. Here we see four days of coverage for the cloud from the September 17, 1992 eruption of Mt. Spurr in Alaska. This cloud was responsible for closing Chicago's O'Hare Airport for several hours, causing major problems for air traffic from Alaska to New England (*unpublished data; courtesy of Bill Rose [Michigan Technological University]*).

FIGURE 8.10



8.2.4.2 Lava flows and volcanic mud flows

Imaging radar aids the analysis of volcanoes due to its cloud-penetrating and all-weather capabilities. Radar interferometry has the potential to address all three categories of hazards through the collection of DEMs and the monitoring of centimeter-scale changes in topography (Figure 8.8). To date, Topographic Synthetic Aperture Radar (TOPSAR) DEMs have been used to assess the distribution of slopes on volcanoes (e.g., Mouginis-Mark and Garbeil 1993) and the thickness and width of lava flows as a function of distance from the vent (Evans et al. 1992). TOPSAR data could also permit hazard maps to be developed using numerical models for the emplacement of lava flows (Wadge et al. 1994) or pyroclastic flows (Malin and Sheridan 1982). Deformation studies of volcanoes are also possible using orbital radars. Analysis of the Landers earthquake (Figure 8.9) shows that changes on volcanoes undergoing tumescence (e.g., the summit of Mauna Loa, Hawaii) or erosions following eruptions (e.g., the lahars channels of Mt. Pinatubo, Philippines) can both be monitored.

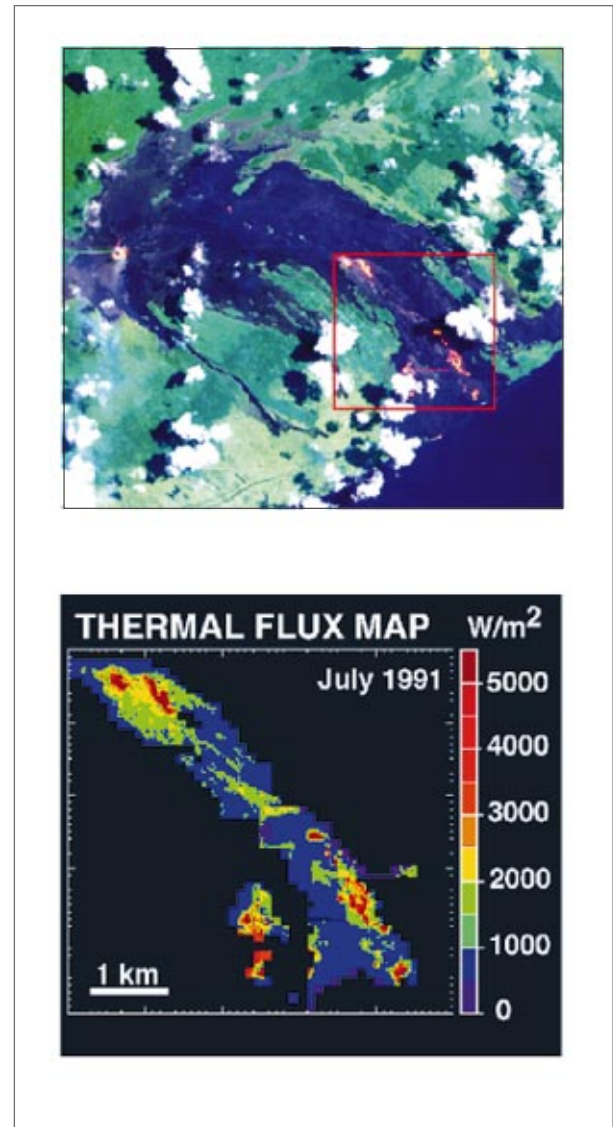
8.2.4.3 Hazards to aircraft from eruption plumes

Aircraft-ash encounters are another area of great concern. There have been several near-fatal accidents, the most spectacular being the 747 jumbo jet crippled by ash from Redoubt while entering Anchorage air space on 15 December 1989 (Brantley 1990). The Federal Aviation Administration (FAA) volcanic-ash-avoidance procedure is designed to avert future disasters from ash being ingested into aircraft engines (Casadevall 1994). Nevertheless, there is a critical need for increased surveillance of volcanoes in the context of aircraft safety, particularly over remote volcanoes along established commercial air routes (e.g., the North Pacific) (Figure 8.10).

8.2.4.4 Needed satellite and in situ measurements

The eruptions of the El Chichón (Robock and Matson 1983), Colo (Malingreau and Kaswanda 1985), Galunggung (Prata 1989), Augustine (Holasek and Rose 1991), and Redoubt (Kienle et al. 1990) volcanoes demonstrate the potential application of satellite images for detecting eruption plumes. A key factor in making future satellite observations useful for hazard assessment is the rapid identification of new eruptions under a variety of observational conditions such as time of day, viewing geometry, and solar azimuth angle. To be of value to, for instance, airlines and government agencies, a reliable technique has to be found for the automatic detection and analysis of eruption plumes using weather satellite images.

FIGURE 8.11



ASTER data will be routinely used to study the temperatures of active lava flows. Simulations of these data can be derived from Landsat Thematic Mapper data (top). Illustrated is the July 1991 eruption of the Kilauea volcano in Hawaii. While knowledge of the temperatures is important, a far more valuable data product is a map of the total thermal flux of the lava flow, since this provides information on the degree of vigor of activity and the relative age of day-old lava flows. The bottom panel shows a thermal flux map for the area shown in the red box in the top panel (Flynn et al. 1994).

To this end, the EOS Interdisciplinary Science (IDS) Global Assessment of Active Volcanism, Volcanic Hazards, and Volcanic Inputs to the Atmosphere investigation (Peter Mouginiis-Mark, PI) is working in close cooperation with the MODIS science team to develop a thermal anomaly trigger to identify active volcanic eruptions and lava flows (Figure 8.11). Once a volcanic eruption is identified, ASTER will be targeted to observe these volcanoes using the high-spatial-resolution thermal-infrared radiometer.

Numerous issues remain regarding the type of radar observations that are needed to enable radar interferometry experiments to be successful in the detection and mapping of volcanic hazards. The temporal frequency of the repeat-pass, the errors due to ionospheric perturbations and atmospheric water vapor, and the surface characteristics of volcanoes are all believed to be important, but none of these issues have been rigorously investigated. We can draw on the experience with the ERS-1 and the Shuttle Imaging Radar-C (SIR-C)/X-band Synthetic Aperture Radar (X-SAR) missions to make some recommendations for the use of future radars. However, it is clear that a combination of orbital radar observations and Global Positioning System (GPS) measurements in the field are both required for geodynamics and topographic analyses for two reasons. First, as was demonstrated with the analysis of the Landers earthquake data (Zebker et al. 1994), the radar-derived deformation map provides only line-of-sight changes with poor tem-

poral resolution. GPS data from well-documented sites are needed to provide the 3-axis ground movement and to provide a continuous record of ground deformation against which the radar data can be compared. Second, the neutral atmosphere will have a significant effect on the radar interferometry because the moisture in the atmosphere can induce a time delay equivalent to ground movement up to ~30 cm, which is far in excess of the ground movement that is typically expected from a dormant volcano (except during catastrophic eruptions). New techniques have been developed that use the time-delay information contained within the GPS signal to determine the water vapor content of the atmosphere (Bevis et al. 1994, unpublished data). If such measurements were to be obtained concurrent with imaging radar data for an interferometry experiment, it would be possible to remove this uncertainty in the resultant radar deformation map. For the detection and evaluation of volcanic hazards in the air due to eruption plumes, additional work is needed to determine why some plumes can be detected using the temperature-difference method pioneered using the Advanced Very High-Resolution Radiometer (AVHRR) data. This technique will incorporate MODIS Thermal Infrared (TIR) data to more accurately determine the silicate abundance within the plume, and the height, temperature, and topography of the plume. MISR, GLAS, HIRDLS, and Along-Track Scanning Radiometer (ATSR) (on ERS-2) data will also be used to assess the height and topography of the plume.

8.3 Required measurements and data sets

8.3.1 Stratospheric aerosols

For climate monitoring and prediction purposes, we need to be able to measure the aerosol loading between 40 km and the tropopause (Table 8.1). Column optical depth should be measured with a horizontal spatial resolution of 400 km and an accuracy of 0.001, which is about the natural background level. Higher spatial resolution would be useful for understanding the transport characteristics of the stratospheric aerosol, but this does not appear feasible with the limb-sounding measurement techniques necessary to acquire the required accuracy. The vertical distribution should be measured with a vertical resolution of 1 km.

Because of the limited mass of the stratosphere, stratospheric aerosol optical depths are generally small but can be measured accurately with high vertical resolution with limb-sounding instruments. SAGE III obtains high accuracy and precision in aerosol extinction measurements by solar or lunar occultation through the limb of the atmosphere. The longwave emission techniques used by HIRDLS offer greater spatial coverage and more-frequent sampling, but with somewhat reduced absolute accuracy. HIRDLS also offers some advantages in the spectroscopy of aerosols and detection of aerosols with radii less than 0.1 μm . Very high vertical resolution of about 1 km is possible with these techniques. Because of

TABLE B.1

PARAMETER NAME	UNITS	ACCURACY ABS::REL	TEMPORAL RESOLUTION	HORIZONTAL RESOL::COVER	VERTICAL RESOL::COVER	COMMENTS
SAGE III Aerosol Extinction Profiles (7 wavelengths)	1/km	5% :: 5%	1 profile/ (2 min), 30/day	<2 × <1 deg :: Global	1 km :: 0-40 km	
HIRDLS Aerosol Extinction Coefficient	1/km	5-10% :: 1-10%	2 global maps /day [d, n]	400 × 400 km :: Global	1 km :: 5-60 km (given accuracies for 7-30 km)	

Stratospheric aerosols

TABLE B.2

PARAMETER NAME	UNITS	ACCURACY ABS::REL	TEMPORAL RESOLUTION	HORIZONTAL RESOL::COVER	VERTICAL RESOL::COVER	COMMENTS
MODIS Aerosol Optical Depth, Spectral	dimensionless	0.05 (Ocean) 0.1(Land) :: 0.05 (Ocean) 0.1(Land)	1/day	50 × 50 km; 5 × 5 km :: Land; Ocean	N/A :: Atmos	
MODIS Aerosol Size-distribution (Radius-Dispersion)	μm, dimensionless	30-50% :: 30-50%	1/day	5 × 5 km :: Ocean	N/A :: Atmos	
MISR Optical Depth, Aerosol, Tropospheric	dimensionless	Larger of 0.05, 10% ::	1/(2-9 day) [d]	17.6 km :: Global	Column :: Atmos	
MISR Particle Size Distribution Parameters	various	N/A ::	1/mission (possible 1/yr update)	N/A :: N/A	N/A :: N/A	SCF generated
GLAS Aerosol Vertical Structure (Profile)	/m	20% ::	1/(2-16 day)	2-100 km :: Global	150 m :: Atmos	
GLAS Thin Cloud/ Aerosol Optical Depth	dimensionless	20% ::	1/(2-16 day)	2-100 km :: Global	N/A :: Atmos	
EOSP Aerosol Optical Thickness	dimensionless	0.05 :: 10%	1/day [d]	40 km :: Global	Column :: Atmos	
EOSP Aerosol Particle Size	μm	25% :: 25%	1/day [d]	100 km :: Global	N/A :: Aerosol_layer	Research product
EOSP Aerosol Refractive Index	dimensionless	0.03 :: 0.03	1/day [d]	100 km :: Global	N/A :: Aerosol_layer	Research product
EOSP Aerosol Profile	dimensionless	N/A ::	1/day [d]	100 km :: Global	:: Atmos	Research product
OMI Aerosol Optical Depth at 386 nm	dimensionless	0.05 :: 0.02 (for PBL aerosols) TBD (for others)	1/day [d]	13 × 24 km :: Global	N/A :: Atmos	Research product
OMI Aerosol Index	dimensionless	N/A ::	1/day [d]	13 × 24 km :: Global	N/A :: 1 km and up	For automated detection of volcanic ash, smoke & dust

Tropospheric aerosols

TABLE B.3

PARAMETER NAME	UNITS	ACCURACY ABS::REL	TEMPORAL RESOLUTION	HORIZONTAL RESOL::COVER	VERTICAL RESOL::COVER	COMMENTS
OMI SO ₂	mol/cm ²	2E16 :: 1E16 (except PBL) 4E16 :: 2E16 (in PBL)	1/day [d]	13 × 24 km :: Global	50 mb :: 1 km and up	Automated detection
MLS SO ₂ Concentration	mixing ratio	5-10% :: 3 ppbv	2 per day day & night	400 km :: Global	1-3 km 15-40 km	

Sulfur dioxide concentration

the long pathlength through the limb, the threshold for detection is quite low.

8.3.2 Tropospheric aerosols

To provide an adequate data set for detecting trends in climate forcing caused by tropospheric aerosols we require a measurement accuracy for optical depth of 0.01 (Table 8.2). In addition to optical depth, information on aerosol size and vertical distribution would be very valuable. The primary mechanism for observing aerosols from space is through the solar radiation that they scatter back to space. This backscattered radiation is weak and is best observed under cloud-free, sunlit conditions over a relatively dark surface. For these reasons, a scanning instrument with good spatial resolution is desirable for acquiring clear scenes. Spectral, angular, and polarization properties of the backscattered sunlight can provide information on the amount and character of the aerosol. In addition, in UV the interaction between the strong molecular scattering and strongly UV-absorbing aerosols (volcanic ash, smoke, and mineral dust) can help in separating these aerosols from other aerosol types. With the visible channels on MODIS it will be possible to determine aerosol optical depth with an accuracy of 0.05 over oceans, and also to determine two parameters of the size distribution such as mean radius and radius dispersion with accuracies of 30 to 50%. With MISR, visible radiance will be observed at 4 frequencies and at 9 angles, so that both spectral and angular information can be used to determine aerosol optical depth and properties at a location. Neither of these instruments, however, will give very useful data on the vertical distribution of the aerosols. GLAS is an active laser that will provide very good information on the altitude of the aerosols, but only along a line traced on the Earth's surface by the nadir-staring instrument, since it does not scan across track. GLAS is also able to determine the optical thickness of thin clouds or aerosols. EOSP will utilize polarization information as well as spectral and angular information. It is hoped that this will allow the measurement accuracy requirement of 0.01 in optical depth to be achieved. Polarization data will also allow more information about the other physical properties of the aerosol to be estimated. Finally, the OMI instrument will help in the detection of aerosols in conditions where the other techniques become unreliable, namely over arid and semi-arid areas. In addition, it will detect highly UV absorbing aerosols over snow and underlying clouds.

8.3.3 Volcanic aerosol precursor gases

An important precursor gas to stratospheric volcanic aerosols is SO₂. The global distribution of this gas in the

stratosphere will be measured by MLS. The Ozone Measuring Instrument (OMI) will measure the column amount of SO₂ using reflected UV radiation (Table 8.3).

MLS will also map the concentration of HCl, which will help answer the question of whether HCl can be injected into the stratosphere by volcanoes. The Tropospheric Emission Spectrometer (TES) will be capable of measuring SO₂ and other aerosol precursor gases such as H₂S and COS over regional areas in the troposphere, and specific volcanoes have been planned as targets to be monitored for creation of these gases.

8.3.4 Volcanic hazards

For deformation monitoring and change detection of volcanoes, we will need repeat-pass orbital radar interferometry data from foreign partner platforms (e.g., ENVISAT's ASAR). Surface determination at the sub-centimeter scale must be studied at high spatial resolution (~25 m/pixel) over areas measuring ~30 × 30 km in size. L-band data (from the Advanced Land Observation Satellite [ALOS]) as well as C-band data (from the Canadian Synthetic Aperture Radar Satellite II [Radarsat II] and the European Space Agency's Environmental Satellite [ENVISAT]) would be preferable to single-wavelength coverage due to the ease of phase unwrapping of the longer wavelength data sets in areas of high topography, such as the landscapes frequently encountered in volcanic areas.

Ground deformation on the order of 1-6 cm/year is expected at ~50 sites around the world each measuring ~30 × 30 km in size, so that Synthetic Aperture Radar (SAR) data need to be collected with well-constrained orbit baselines (within ~50 cm for C-band and ~300 m for L-band). Due to atmospheric effects on the SAR phase data, redundancy of observations is required so that atmospheric water vapor effects can be removed. In order to achieve this, SAR data should be collected over each site about once per month for each radar system.

Radars can also be used to derive DEMs of volcanoes for use with numerical models that predict the flow paths of lahars and pyroclastic flows (see Figure 8.8). Advanced Synthetic Aperture Radar (ASAR), Radarsat II, and ALOS data will all permit elevation models to be derived of the hazardous volcanoes (~50 worldwide). These DEMs can be augmented by stereo coverage from ASTER, which will provide the higher-spatial-resolution (15 m) coverage that is more effective in areas of high relief (i.e., complementary to radar-derived DEMs, which are more accurate in low-relief areas).

Thermal anomalies associated with new lava flows will be detected by MODIS, and will be studied at higher spatial resolution by the Advanced Spaceborne Thermal Emission and Reflection Radiometer (ASTER) and the

Enhanced Thematic Mapper Plus (ETM+). The MODIS data stream will be searched continuously as part of the Level 1 data processing, providing worldwide alerts at least once per day from AM-1 and PM-1. The 1-km pixels of the TIR MODIS bands provide a good compromise between spatial resolution and data volume, since six MODIS channels have to be intercompared in order to eliminate false alarms (sun glint, snow, forest fires, etc.). Thermal IR MODIS data are required at night to resolve the area/temperature of the anomalies. Shortwave infrared (SWIR) and TIR ASTER data at 30 and 90 m, respectively, are required to map at high resolution the distribution of new flows, and to identify small thermal anomalies associated with lava domes and pyroclastic flows.

The primary health hazard associated with volcanic eruptions is the long-duration (months to years) emission of tropospheric SO₂ that produces a combination of sulfate aerosols and sulfuric acid. These aerosols can be detected with MISR bidirectional observations, as well as Advanced Along-Track Scanning Radiometer (AATSR) observations from ENVISAT. Due to the localized nature of these plumes, tropospheric aerosol maps

with a spatial resolution of 240 m are required for localized areas measuring a few hundred to 1000 km downwind.

The hazards presented by eruption clouds produced by explosive eruptions are numerous, but the most pressing concerns are the height of the plume and the dispersal pattern away from the vent. Explosive eruptions can be detected using MODIS radiance values in the thermal IR; silicate particles in the plume enable an eruption plume to be distinguished from weather clouds. MODIS visible data can provide daytime estimates of plume-top topography and, by virtue of the shadows cast by plumes (which may be 15- to 40-km high), the height of the plume can be estimated. Stereo images collected by MISR and AATSR can also provide height estimates that need to be accurate to ~200 m if air traffic is to avoid encounters with the plume. Volcanic SO₂ and ash plumes from more than 100 volcanic eruptions have been detected by TOMS since 1978 using an automated detection technique (Krueger et al. 1995; Bluth et al 1997; Seftor et al. 1997; Krotov et al. 1997). These data show that the two plumes are not always colocated and must be tracked separately. The OMI instrument will improve SO₂ detection sensi-

TABLE B.4

PARAMETER NAME	UNITS	ACCURACY ABS::REL	TEMPORAL RESOLUTION	HORIZONTAL RESOL::COVER	VERTICAL RESOL::COVER	COMMENTS
ASTER DEM	m	<50 m :: <30 m	1/eruption	15 m :: Regional	30 m :: Surface	New DEM model needed after each eruption
ASTER Thermal Anomalies	K	5 K :: 2 K	1/6 days	90 m :: Land	N/A :: Surface	Target eruptions and 50 prime sites only
ASTER Surface Radiance	% reflectance	TBD :: TBD	once, then after each eruption	15 m :: Land 30 m :: Land 90 m :: Land	N/A :: Surface	Target eruptions and 50 prime sites only
MODIS Thermal Anomalies	K	5 K :: 2 K	2/day day & night	1 km :: Land	N/A :: Surface	Continuous real-time monitoring
MISR Plume Level Reference Altitude	km	0.1 km :: 0.2 km	every available orbit during eruption	240 m :: Regional	0.1-0.2 km :: Troposphere	Collect data during eruption within plume dispersal
OMI SO ₂ Column	mol/cm ²	2E16 :: 1E16	1/day [d]	13 × 24 km :: Global	N/A :: Atmos	Automated detection
Radars Ground Deformation	cm	1 cm :: 0.3 cm	1/month	25 km :: Land	1 cm :: Land	Interferometric data from foreign SARs
Radars Surface Topography	m	10 m :: 2 m	once per eruption	25 km :: Land	2 m :: Land	Interferometric data from foreign SARs

Volcanic hazards.

tivity by an order of magnitude, allowing the detection and tracking of nearly all volcanic eruptions. It will also provide an image of ash clouds, that can be seen even in the presence of underlying weather clouds. OMI will also make a quick automated estimate of the height of these clouds to within 50 mb, which may be refined by manually examining high spatial resolution images from other instruments (MODIS, MISR, AATSR).

In summary, EOS (and foreign) data sets relevant to volcanic hazards are included in Table 8.4.

8.3.5 Importance of measurements collected by the missions of foreign partners

Of major importance to the analysis of volcanic hazards in the EOS era are the measurements to be made by foreign partner imaging radars. ERS-1, ERS-2, Radarsat, the Japanese Earth Remote-Sensing Satellite-1 (JERS-1), ENVISAT ASAR, ALOS, and Radarsat II will all provide crucial data that are unavailable from EOS due to the lack of a NASA radar. In addition to providing all-weather, day/night imaging capabilities, these foreign radars provide the opportunity to collect topographic and ground deformation information on active volcanoes.

These foreign radars provide complementary information to each other, by virtue of their different wavelengths (C-band or L-band), incidence angles (23-60°), and operating modes (spatial resolutions). Differences in the orbit altitude also mean that the frequencies of repeat orbits, which are needed in order to coherently intercompare the radar phase data, vary from 24 to 44 days. Operating in the Scanning Synthetic Aperture Radar (SCANSAR) mode, Radarsat also enables images with different spatial resolutions (25-100 m/pixel) and swath widths (100-500 km) to be obtained, thereby enabling a given target to be imaged more often than from fixed-incidence-angle radars, albeit with different geometries that preclude interferometric measurements.

Another important aspect of the foreign partner platforms is the enhancement of the temporal coverage of transient phenomena such as eruption plumes. Given

that the primary energetic phase of an explosive eruption as it injects material into the stratosphere is measured in hours, it is quite likely that neither AM-1 nor PM-1 will observe the event during its "formative stage." Given the different imagers on board ENVISAT and ALOS, visible and near-infrared data from these foreign partner spacecraft may indicate an eruption earlier than EOS. Every data source that is available should be used to reassemble the temporal history of an eruption, particularly the larger Pinatubo-style events that have regional-to-hemispheric effects on the atmosphere.

International satellite sensors enabling remote sensing of tropospheric aerosols include the Medium-Resolution Imaging Spectrometer (MERIS), Global Imager (GLI), Ocean Color and Temperature Scanner (OCTS), Polarization and Directionality of Earth's Reflectances (POLDER), and GOME (Global Ozone Monitoring Experiment). In addition to augmenting the sampling strategy of EOS sensors (MODIS, MISR, and EOSP), these sensors offer enhanced capabilities in specific areas. GLI, to be launched on ADEOS II, contains 36 spectral bands (comparable to MODIS), with more bands (6 vs. 2) at 250-m resolution, but fewer bands in the longwave region past 12 μm . MERIS is primarily an ocean color sensor, with tilt capability, and POLDER has polarization imaging capability that enables observations of the same Earth target from 12 directions during a single satellite pass. These sensors provide additional complementary information to the tropospheric aerosol properties derived from EOS sensors.

For stratospheric aerosols, in addition to HIRDLS and SAGE III, complementary information will be provided by the Improved Limb Atmospheric Spectrometer (ILAS) on ADEOS II and Sciamachy and GOMOS on ENVISAT. In most of the foreign partner instruments mentioned above, EOS investigators are actively engaged as members of the science teams of these sensor systems. This provides not only additional linkages to the algorithm development progress, but also cooperation in coordinated calibration/validation programs.

8.4 EOS contributions: Expected improvement in knowledge and national benefit

8.4.1 *Monitoring of volcanic eruptions and aerosols and their effects on climate*

Observations acquired by EOS instruments will provide continuous global monitoring of volcanic eruptions. For the first time, we will be able to monitor the entire process of injection and dispersal, and the chemical/physical evolution of volcanic materials in the atmosphere. MODIS, MISR, OMI, ASTER, ETM+, and EOS-era radar instruments will be used to characterize the number, location, style, and duration of eruptions. Large eruptions will be studied with several EOS instruments, and some will be targeted for high-resolution observations by ASTER, ETM+, and MISR. Plume top altitude and topography obtained from MODIS, HIRDLS, and MISR will allow us to test physical models of plume rise and dispersal.

During the EOS era, we will be able to make a complete inventory of the gases, ash, and other aerosols that reach the stratosphere versus the troposphere. Measurements of SO₂ column abundance will continue to be produced for large eruptions using data from TOMS. This will be supplemented by measurements using TES, MLS, OMI, and ASTER, which can detect lower abundances of SO₂ than TOMS, and which also provide vertical distribution information in the stratosphere (MLS) and troposphere (TES). MLS on EOS will have the advantage of daily coverage at high latitudes in both hemispheres, a significant improvement over MLS on UARS which only looks in one direction at a time. In addition to SO₂, a major new advance will be our ability to measure several other volcanic gas species from satellites, including H₂S (Atmospheric Infrared Sounder [AIRS], Tropospheric Emission Spectrometer [TES]), HF (TES, MLS), HCl (TES, MLS), and CO and COS (TES). Measurements of these other gas species are important for both hazard mitigation and analysis of climate effects.

Several EOS instruments will monitor stratospheric and tropospheric aerosols, each resulting in different types of aerosol data products at different spatial and vertical resolutions (SAGE III, EOSP, MISR, MODIS, OMI, GLAS, HIRDLS). Rather than having to rely so heavily on lidar measurements collected from isolated ground stations as we did for Mt. Pinatubo and El Chichón, EOS will provide us with a complete global picture of aerosol distribution and properties. Improved measurements of stratospheric aerosol abundance and spatial distribution will provide a better understanding of their role in heterogeneous chemical reactions that destroy ozone, and the impact of volcanic aerosols on high-altitude clouds.

When large eruptions occur during the EOS era, we will be able to directly determine how the chemistry, temperature, and dynamics of the atmosphere are affected. The comprehensive nature of EOS will allow us to separate volcanic signals in the climate record from those produced by El Niño-Southern Oscillation, monsoons, and human activities. The 15 years of continuous measurements by MODIS, the Clouds and the Earth's Radiant Energy System (CERES), and SAGE III will provide an important record of the effect of volcanic aerosols on the Earth's radiation budget (CERES), and on global vertical profiles of atmospheric temperature and composition (MODIS and SAGE III). Other instruments (AIRS/Advanced Microwave Sounding Unit [AMSU]/Humidity Sounder Brazil [HSB], MLS, TES, and HIRDLS) will provide more-detailed information over a 6-12-year time period concerning changes in atmospheric temperature and composition that may result from volcanic eruptions. The EOS IDS Four-Dimensional Atmospheric-Ocean-Land Data Assimilation System (Richard Rood, PI) investigation will provide an internally consistent data set of atmospheric parameters for assessing climate effects of large eruptions and will provide wind information needed to analyze the dispersal of volcanic clouds.

8.4.2 *Improved assessment of volcanic hazards on the ground and in the air*

The range of volcanic hazards that can be studied by EOS is very large. The hazards include the long-term changes in the inflation rate of the volcano (an indication of impending eruptions), the likely paths of lava flows, lahars and pyroclastic flows, the radiative flux of active lava flows, the ratio of gases from primary melts (indicators of new magma reaching the near-surface), and the possibility of aircraft encountering an eruption.

In qualitative terms, EOS will provide the most complete near-real-time inventory of global eruptions thus far. Many (~30-50%) lava-producing eruptions may currently go unreported, and some may have great impact on local populations. MODIS data will enable this eruption inventory to be timely (same day) and near global in coverage.

Topographic mapping and deformation studies will rely to a considerable degree on foreign radars (e.g., ENVISAT ASAR). Only via radar interferometry can centimeter-scale deformation be detected from orbit. This deformation may be detected several weeks to months in advance of an eruption, enabling local authorities to be warned and, if required, evacuation plans to be developed.

Digital elevation models derived from stereo ASTER data will also aid in the prediction of lava flow and lahar flow paths.

MODIS, MISR, and OMI data will enable large eruption plumes to be studied in unprecedented detail compared to existing AVHRR analyses. Since each eruption is unique in terms of magma chemistry, vent geometry, volume erupted, and atmospheric conditions, a direct comparison between EOS investigations and earlier studies is not possible. However, improvements in spectral resolution of MODIS compared to AVHRR will enable more-subtle variations of silicate materials in the plume to be studied, thereby providing warning to nearby aircraft that the plume is dangerous if ingested by the engines. MISR data will also enable, via parallax measurements, the plume height to be determined to within a few hundred meters, thereby better defining the hazardous region that aircraft should avoid (see Figure 8.10).

Health hazards are a poorly studied aspect of the effects of volcanoes. Long-duration (months to years) eruptions can increase respiratory problems by more than an order of magnitude, and affect tens of thousands of people. MISR and EOSP data will be particularly good at detecting such low-level plumes via multi-zenith-angle studies of the scattering properties of the atmosphere.

8.4.3 Improved knowledge of the global frequency and magnitude of volcanic eruptions

Global coverage provided by MODIS will give the first comprehensive worldwide inventory of volcanic eruptions. Use of near-real-time processing of a segment of the MODIS data stream will enable the inventory to be made available to the world's volcanologists in only a few hours after data acquisition, thereby enabling field observations of certain eruptions that were previously unreported from the ground.

Major advances in the knowledge of the thermal properties of lava flows, volcanic domes, lava lakes, and summit water lakes will also be derived. In this instance, ASTER will provide the most important data set, due to the greater spatial resolution. However, the high dynamic range of the mid-IR (3.9 μm) MODIS data will permit the solution of both temperature and area for many hot volcanic targets. In many cases, the total energy released from an eruption has to be estimated from post-eruption assessments of the volume of material erupted (Figure 8.11). MODIS, ETM+, and ASTER will facilitate quantitative measurements of radiative flux from lava flows, enabling the magnitude of different eruptions to be intercompared.

Explosive eruptions will also be quantified by EOS for the first time. The height of eruption plumes will be

measured by MISR, MODIS, and GLAS, and the amount of SO_2 erupted will be measured by TOMS and OMI. TOMS data provide the longest continuous record (1978-1994) of stratospheric SO_2 emissions from volcanoes. These data are crucial for assessing the impact of volcanoes on the stratosphere. Additional observations by Earth Probe (EP) TOMS, Meteor-3 TOMS, and OMI on EOS Chemistry-1 will extend this time series. More detailed observations of gas chemistry from an explosive eruption will also be obtained from MLS and TES.

8.4.4 Global measurements of tropospheric aerosols

The early development of EOS has been contemporaneous with a growing realization of the importance of acquiring the capability to adequately monitor the characteristics of tropospheric aerosols globally. In the past, the difficulty of satellite remote sensing of tropospheric aerosols, along with the perception that improvement in characterizing cloud radiative forcing had a much higher priority, has resulted in only a very limited effort to monitor aerosols. Indeed, the only operational aerosol data product at present is the total column optical thickness retrieved using the AVHRR instrument on the NOAA polar-orbiting environmental satellites (cf. Rao et al. 1988). That retrieval employs the traditional approach of relying on the enhanced reflectance of scattered sunlight relative to a low albedo surface (viz., the cloud-free ocean away from sun glint). The present NOAA aerosol retrieval uses only AVHRR channel-1 (0.58-0.68 μm) radiances because of the variable effects of water vapor on channel-2 (0.725-1.10 μm) radiances (cf. Rao et al. 1989; Durkee et al. 1991). With information restricted to radiance at just one wavelength, the retrieval algorithm must employ a single, standard model for the aerosol and is thus subject to potentially substantial uncertainties associated with the wide range of aerosol types and properties.

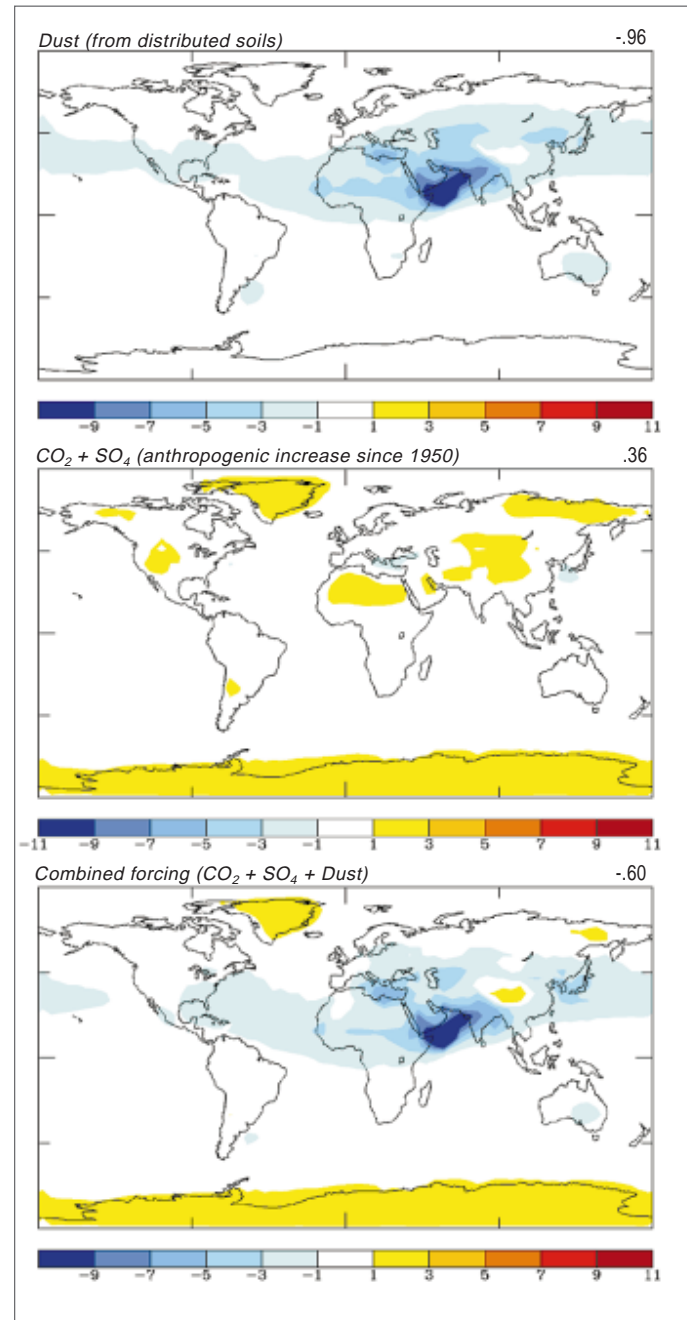
As discussed in previous sections, tropospheric aerosols must be monitored on a global basis and not just over the oceans where retrieval is somewhat easier. Furthermore, we require aerosol properties beyond just column optical thickness in order to adequately characterize their direct radiative forcing, their effect on clouds and the hydrological cycle, their sources and sinks, and their participation in atmospheric chemical processes. Because of the variability of aerosol loading for specific aerosol types and the difficult problem of distinguishing the contribution of the surface to the satellite observations, a credible program for global monitoring of tropospheric aerosols must necessarily emphasize taking advantage of as much of the information content of the scattered and reflected sunlight as possible, namely, multi-spectral and multi-angle radiance and polarization

measurements. In this regard, the EOS program offers significant advances because of its measurement capabilities that are attributable in part to serious consideration of aerosol objectives in both instrument conceptual designs and payload selection processes.

The three EOS instruments fundamental to tropospheric aerosols measurement objectives are MODIS, MISR, and EOSP. MODIS, to be flown on both the EOS AM-1 and PM-1 platforms, is a scanning spectroradiometer operating much like AVHRR but with significantly greater multi-spectral coverage, higher spatial resolution, and greatly enhanced on-board calibration capability. With 36 spectral bands covering the visible, near-infrared, and SWIR, MODIS measurements will provide aerosol optical-thickness retrievals for a broad range of wavelengths, from which we can infer information on aerosol size distribution. While aerosol retrievals with MODIS will be most straightforward and detailed over the ocean, there is the expectation that meaningful results over land can be realized by taking advantage of information on surface properties inherent in some of the spectral bands, particularly in the SWIR, and by using aerosol "climatology" or ancillary measurements to constrain aerosol models used in the retrieval algorithm. In addition, combination of MODIS with TOMS and OMI has the potential of improving MODIS retrievals over land, as well as extending the wavelength range to 340 nm for better detection of submicron particles. MODIS thermal and SWIR bands will also be useful in cloud screening (i.e., avoiding attempted aerosol retrievals for pixels that are "contaminated" with a very small cloud fraction or thin cirrus clouds).

A significant additional source of information is available from the multi-angle coverage in the plane containing the spacecraft ground track obtained from the nine cameras of the MISR instrument, which uses charge-coupled device (CCD) arrays to acquire cross-track spatial coverage in four spectral bands in the visible. MISR will be flown on the EOS AM platform series. Without resorting to any assumptions about spatial homogeneity of aerosol characteristics, the MISR views of the same location at nine zenith angles during the short time period of the spacecraft overflight can provide direct information on the aerosol angular scattering, or phase function, which is diagnostic of aerosol size dis-

FIGURE 8.12

Surface forcing (Wm^{-2}) (Tegen et al. 1996).

tribution and particle shape. Over relatively brighter, heterogeneous land surfaces, the MISR retrieval algorithm will employ an innovative technique (Martonchik and Diner 1992) based upon analysis of the spatial frequency power spectrum of the radiances over a scene with the assumption that the aerosol typically will produce no contribution to the power at any frequencies other than the very lowest. This technique offers the prospect of satel-

lite aerosol retrievals for the most difficult of scenes, but its narrower swath width requires 16 days to achieve full global coverage.

On the second of the EOS AM platforms, advanced versions of MODIS and MISR will be joined by EOSP, which measures the linear polarization as well as the radiance at 12 spectral bands in the visible, near-infrared, and SWIR. The advantage of polarimetry is both the very high measurement accuracy possible because linear polarization is a ratio of orthogonal intensities, and the fact that polarization is very sensitive to particle microphysics (Hansen and Travis 1974). Previous experience with polarimetry on planetary missions has demonstrated aerosol-retrieval capabilities in situations where radiance-only measurements are subject to model uniqueness problems. For example, the analysis of Cloud Photopolarimeter measurements from the Pioneer Venus Orbiter permitted the retrieval of small-particle ($0.25 \mu\text{m}$ radius) haze of optical thickness on the order of 0.02 extending above the main cloud of $1\text{-}\mu\text{m}$ particles with concurrent retrieval of refractive indices. Although retrievals of terrestrial tropospheric aerosols over land must deal with potentially variable and uncertain contributions from the surface reflectivity and polarization signatures, evidence that the polarized component of sunlight scattered from vegetation comes almost entirely from light that is specularly reflected at the leaf surfaces (Vanderbilt et al. 1985), together with the broad EOSP spectral coverage, suggests that the surface contributions can be appropriately treated.

Perhaps as important as the significant advance in EOS instrument capabilities with respect to tropospheric aerosol measurements, is the underlying EOS philosophy that emphasizes instrument calibration and retrieved product validation. Because of the inherent difficulties of satellite aerosol retrievals even with greatly improved capabilities, it is recognized that appropriate validation should include comparison of coincident measurements with ground-based sunphotometer and/or shadow-band radiometers. Remote sensing of aerosol properties with such upward-looking instruments has been demonstrated to be a very reliable technique and will be key to establishing the quality of the satellite-derived aerosol products (Kaufman et al. 1994). Moreover, the envisioned networks of ground-based instruments (e.g., Aerosol Robotic Network [AERONET]; Holben et al. 1996) will provide important information on diurnal variations of the concentration and properties of aerosols at the selected sites. It is also expected that the EOS validations will include a number of coordinated campaigns that employ in situ sampling of aerosols, both at the ground and from aircraft, to be compared with the satellite and ground-based instru-

ment remote sensing of aerosol characteristics. EOS support of such activities as a major part of the validation objectives is fundamental to the realization of appropriate global monitoring of tropospheric aerosols.

8.4.5 Assessment of the role of tropospheric aerosols in climate change

One of the greatest uncertainties in climate forcing is that due to tropospheric aerosols (e.g., Charlson et al. 1992; Charlson and Wigley 1994; IPCC 1995). Aerosols cause a direct climate forcing by reflecting sunlight to space and absorbing solar and terrestrial radiation in the atmospheric column, and an indirect climate forcing by altering cloud properties. Existence of the latter effect is supported by satellite observations of increased cloud brightness in ship wakes (Coakley et al. 1987), satellite observations of land-ocean and hemispheric contrasts of cloud droplet sizes (Han et al. 1994, 1996), and in situ data concerning the influence of aerosol condensation nuclei on clouds (Radke et al. 1989; King et al. 1993, 1995). Sulfate aerosols originating in fossil-fuel burning may produce a global climate forcing of the order -1 Wm^{-2} (Charlson et al. 1991; Houghton et al. 1996), and aerosols from biomass burning could conceivably produce a comparable forcing (Penner et al. 1992). Wind-blown dust, influenced by anthropogenic activities, has long been suspected of being an important forcing on some regional climates (Tanré et al. 1984; Joseph 1984; Coakley and Cess 1985; Tegen and Fung 1994). Tegen et al. (1996) estimate surface forcing caused by dust from disturbed soils is currently on the order of -1 Wm^{-2} , which is comparable in magnitude to the current effect of CO_2 and sulfate aerosols (Figure 8.12). It has also been suggested (Jensen and Toon 1992; Sassen 1992) that volcanic aerosols sedimenting into the upper troposphere may alter cirrus cloud microphysics, thus producing a possibly significant climate forcing, which could either be positive or negative. Unfortunately, no global data exist that are adequate to define quantitatively any of these aerosol climate forcings.

Aerosols can be seen against the dark ocean surface by the imaging instruments on present operational meteorological satellites (Rao et al. 1988; Jankowiak and Tanré 1992). For example, these images clearly show Sahara/Sahelian dust spreading westward from Africa, summertime sulfate aerosols moving eastward from the United States, and aerosols from seasonal biomass burning in the tropics. Similar data over both land and oceans can be seen in the TOMS images (Herman et al. 1998). However, the nature and accuracy of these data are inadequate to define the climate forcing, and, indeed, the

observed optical thicknesses may be in part due to thin cirrus clouds. The climate forcing issue requires aerosol data of much higher precision, including information on aerosol altitude and aerosol physical properties such as size and refractive index. Cloud properties, including optical thickness, particle size, and phase, must be monitored simultaneously to very high precision, so that the temporal and spatial variations of aerosols and clouds can be used to help define the indirect aerosol climate forcing.

MISR and MODIS on the EOS AM-1 spacecraft will provide aerosol optical-thickness measurements substantially better than aerosol information available from current instruments. Furthermore, MODIS will provide substantial improvements on current abilities to derive cloud optical and microphysical properties (see Chapter 3). The estimated accuracy of optical-thickness retrievals, 0.03 to 0.05, will contribute to aerosol process studies in regions of moderate to heavy aerosol loading. The higher accuracies needed for determination of aerosol climate forcing, about 0.01 (Hansen et al. 1995), and microphysical aerosol properties (refractive index, particle shape, and particle size) will be provided by EOSP, scheduled for the EOS AM-2 spacecraft. EOSP has also been proposed for flight on a microsat (Hansen et al. 1995) along with a Michelson interferometer that would be capable of measuring small changes in cloud optical and microphysical properties. A satellite-borne lidar would be an ideal complement to these latter instruments, providing a precise determination of vertical layering of aerosols and clouds. To this end, GLAS on the ICESat-1 spacecraft will provide valuable information on the vertical and spatial extent of significant stratospheric and tropospheric aerosol layers.

8.4.6 Inclusion of aerosol effects in model predictions of global climate change

Aerosol effects can be included in global climate model calculations, provided the aerosol amount, distribution, and optical properties are known. This knowledge is only available after the fact in the case of volcanic eruptions, but study of de facto volcanic aerosol injections can be valuable as a check on our understanding of the climate response to a radiative forcing. Calculations with simplified climate models have suggested that the largest volcanoes of the past century could have caused a global cooling of up to 0.5°C (Schneider and Mass 1975; Hunt 1977; Hansen et al. 1978; Robock 1983; MacCracken and Luther 1984). The mean observed global temperature response after the five largest eruptions is a cooling of about 0.25°C (Hansen et al. 1995), but the aerosol data and observed temperatures are not sufficiently precise to allow

determination of whether a significant discrepancy exists between the models and the observed climate change.

The 1991 eruption of Mt. Pinatubo provides the best chance to date for testing climate models against observed volcanoes. Climate simulations carried out immediately after the eruption with a GCM (Hansen et al. 1992) predicted a global cooling of about 0.5°C. Observations found a cooling of about 0.5°C over land and globally in the lower troposphere, but a smaller surface response over the ocean yielded a global surface cooling of only about 0.3°C (Hansen et al. 1995). At least part of the difference between model and observations can be accounted for by inaccuracy of the aerosol size distribution assumed in the Hansen et al. (1992) calculations, which yielded a maximum forcing just over 4 Wm⁻². More-precise aerosol data (Lambert et al. 1993; McCormick et al. 1995) now available yield a global forcing of about 3.5 Wm⁻² (Hansen et al. 1995); this smaller forcing is also more consistent with ERBE measurements of global radiative flux anomalies at the top of the atmosphere (Minnis et al. 1993). Comprehensive analyses of the Pinatubo case with the most realistic atmosphere-ocean models have yet to be made.

Modeling of tropospheric aerosols presents a greater challenge because of the large number of heterogeneously-distributed aerosols and the evidence that aerosols can alter cloud properties. The predominant anthropogenic aerosol is probably sulfate originating from the burning of fossil fuels. The regional distribution of these aerosols can be estimated from aerosol-formation models (Langner and Rodhe 1991) and used to calculate an approximate anthropogenic sulfate climate forcing (Kiehl and Briegleb 1993). There is a qualitative consistency among the regions of heavy aerosol amounts (eastern United States, Europe, and China), calculated aerosol coolings (Taylor and Penner 1994), and the observed temperature change of the past century (Karl et al. 1995).

The difficult task of realistically including aerosol effects in projections of future climate change requires quantitative knowledge of all the significant changing aerosols, including aerosols from biomass burning, dust from arid regions, biogenic aerosols, and industrial soot. Moreover, it is necessary to understand the aerosol effects on cloud properties. The challenge for EOS is to provide the data necessary to allow understanding and prediction of aerosol changes, as an essential aspect of assessing the causes of climate variability and climate change.

8.4.7 Advertent climate modification by aerosols

The human response to global change can take one of three generic forms: modify the human actions that are causing global change in order to mitigate the magnitude of the future changes, adapt to the changes that are caused, or introduce a new human action that will compensate for the causative action. The last option may be called the geo-engineering approach. For reducing the effect of greenhouse gases on climate warming, two approaches have been suggested (Committee on Science, Engineering, and Public Policy [COSEPUP] 1992): introducing aerosols into the stratosphere to act as a direct reflector of solar radiation, and introducing aerosols into the troposphere to increase the reflectivity of clouds. These two actions have the advantage of being reversible, since once the introduction of aerosol ceases, the aerosol burden will return to natural levels within a few weeks in the troposphere and within a year or so in the stratosphere. The Earth system is too poorly understood at present to enable all the consequences of such approaches to be predicted. However, EOS studies of aerosols and clouds will help improve understanding of the climate system to the point where the consequences of these actions to contravene the greenhouse warming may be predicted with reasonable confidence. In addition, EOS instruments will provide the technology necessary to monitor the levels of any such introduced aerosols and their effects on the climate system.

References

- Albrecht, B. A., 1989: Aerosols, cloud microphysics, and fractional cloudiness. *Science*, **245**, 1227–1230.
- Andreae, M. O., 1995: Climate effects of changing atmospheric aerosol levels. *World Survey of Climatology XVI: Future Climates of the World*, A. Henderson-Sellers, Ed., Elsevier.
- Andreae, M. O., E. V. Browell, M. Garstang, G. L. Gregory, R. C. Harris, G. F. Hill, D. J. Jacob, M. C. Pereira, G. W. Sachse, A. W. Setzer, P. L. Silva Dias, R. W. Tablot, A. L. Torres, and S. C. Wofsy, 1988: Biomass burning emissions and associated haze layers over Amazonia. *J. Geophys. Res.*, **93**, 1509–1527.
- Andreae, M. O., B. E. Anderson, D. R. Blake, J. D. Bradshaw, J. E. Collins, G. L. Gregory, G. W. Sachse, and M. C. Shipman, 1994: Influence of plumes from biomass burning on atmospheric chemistry over the equatorial and tropical South Atlantic during CITE 3. *J. Geophys. Res.*, **99**, 12,793–12,808.
- Artaxo, P., F. Gerab, M. A. Yamasoe, and J. V. Martins, 1994: Fine mode aerosol composition at three long-term atmospheric monitoring sites in the Amazon Basin. *J. Geophys. Res.*, **99**, 22,857–22,868.
- Asano, S., 1993: Estimation of the size distribution of Pinatubo volcanic dust from Bishop's ring simulations. *Geophys. Res. Lett.*, **20**, 447–450.
- Asano, S., A. Vchiyama, and M. Shiobara, 1993: Spectral optical thickness and size distribution of the Pinatubo volcanic aerosols as estimated by ground-based sunphotometry. *J. Meteor. Soc. Japan*, **71**, 165–173.
- Benkovitz, C. M., R. C. Easter, S. Nemesure, R. Wagener, and S. E. Schwartz, 1994: Sulfate over the North Atlantic and adjacent continental regions: Evaluation of October and November 1986 using a three-dimensional model driven by observation-derived meteorology. *J. Geophys. Res.*, **99**, 20,725–20,756.
- Bevis, M., S. Businger, S. Chiswell, T. A. Herring, R. A. Anthes, C. Rocken, and R. H. Ware, 1994: GPS meteorology: mapping zenith wet delays onto precipitable water. *J. Appl. Meteor.*, **33**, 379–386.
- Blanchard, D. C., and L. D. Syzdek, 1972: Concentration of bacteria in jet drops from bursting bubbles. *J. Geophys. Res.*, **77**, 5087–5099.
- Bluth, G. J. S., W.I. Rose, I.E. Sprod, and A.J. Krueger, 1997: Stratospheric loading from explosive volcanic eruptions. *J. Geophys. Res.*, **105**, 671–683.
- Braham, R. R., Jr., 1974: Cloud physics of urban weather modification—a preliminary report. *Bull. Amer. Meteor. Soc.*, **55**, 100–106.
- Brantley, S. R., 1990: The Eruption of Redoubt Volcano, Alaska, December 14, 1989–August 31, 1990. *U. S. Geological Survey Circular*, **1061**, 33 pp.
- Browell, E. V., E. F. Danielsen, S. Ismail, G. L. Gregory, and S. M. Beck, 1987: Tropopause fold structure determined from airborne lidar and in situ measurements. *J. Geophys. Res.*, **92**, 2112–2120.
- Cachier, H., M. P. Bremond, and P. Buat-Menard, 1989: Carbonaceous aerosol from different tropical biomass burning sources. *Nature*, **340**, 371–373.
- Casadevall, T. J., 1994: Volcanic ash and aviation safety. Proc. 1st Int. Symp. on Volcanic Ash and Aviation Safety, *U. S. Geological Surv. Bull.*, **2047**, 450 pp.
- Charlson, R. J., and T. M. L. Wigley, 1994: Sulfate aerosol and climatic change. *Sci. Amer.*, **270**, 48–57.
- Charlson, R. J., J. Langner, H. Rodhe, C. B. Leovy, and S. G. Warren, 1991: Perturbation of the Northern Hemisphere radiative balance by backscattering from anthropogenic sulfate aerosols. *Tellus*, **43**(AB), 152–163.
- Charlson, R. J., S. E. Schwartz, J. M. Hales, R. D. Cess, J. A. Coakley, Jr., J. E. Hansen, and D. J. Hofmann, 1992: Climate forcing by anthropogenic aerosols. *Science*, **255**, 423–430.
- Coakley, J. A., and G. Grams, 1976: Relative influence of visible and infrared optical properties of a stratospheric aerosol layer on the global climate. *J. Appl. Meteor.*, **15**, 679–691.
- Coakley, J. A., and R. D. Cess, 1985: Response of the NCAR community climate model to the radiative forcing of naturally occurring tropospheric aerosol. *J. Atmos. Sci.*, **42**, 1677–1692.
- Coakley, J. A., Jr., R. L. Bernstein, and P. A. Durkee, 1987: Effect of ship-stack effluents on cloud reflectivity. *Science*, **237**, 1020–1022.
- COSEPUP, 1992: Policy implications of greenhouse warming, mitigation, adaptation, and the science base. Panel on Policy Implications of Greenhouse Warming, Committee on Science, Engineering, and Public Policy, National Academy of Sciences, National Academy Press, 918 pp.
- Crutzen, P. J., and M. O. Andreae, 1990: Biomass burning in the tropics: Impact on atmospheric chemistry and biogeochemical cycles. *Science*, **250**, 1669–1678.
- Crutzen, P. J., L. E. Heidt, J. P. Krasnec, W. H. Pollock, and W. Seiler, 1979: Biomass burning as a source of atmospheric gases. *Nature*, **282**, 253–256.
- Deshler, T., D. J. Hofmann, B. J. Johnson, and W. R. Rozier, 1992a: Balloonborne measurements of the Pinatubo aerosol size distribution and volatility at Laramie, Wyoming during the summer of 1991. *Geophys. Res. Lett.*, **19**, 199–202.
- Deshler, T., A. Adriani, G. P. Gobbi, D. J. Hofmann, G. Di-Donfrancesco, and B. J. Johnson, 1992b: Volcanic aerosol and ozone depletion within the Antarctic polar vortex during the austral spring of 1991. *Geophys. Res. Lett.*, **19**, 1819–1822.
- Deshler, T., B. J. Johnson, and W. R. Rozier, 1993: Balloon measurements of Pinatubo aerosol during 1991 and 1992 at 41°N: vertical profiles, size distribution, and volatility. *Geophys. Res. Lett.*, **20**, 1435–1438.
- Diner, D. J., C. J. Bruegge, J. V. Martonchik, T. P. Ackerman, R. Davies, S. A. W. Gerstl, H. R. Gordon, P. J. Sellers, J. Clark, J. A. Daniels, E. D. Danielson, V. G. Duval, K. P. Klaasen, G. W. Lilienthal, D. I. Nakamoto, R. J. Pagano, and T. H. Reilly, 1988: MISR: A Multiangle Imaging Spectro-Radiometer for Geophysical and Climatological Research from EOS. *IEEE Trans. Geosci. and Remote Sens.*, **27**, 200–214.
- Diner, D. J., C. J. Bruegge, J. V. Martonchik, G. W. Bothwell, E. D. Danielson, E. L. Floyd, V. G. Ford, L. E. Hovland, K. L. Jones, and M. L. White, 1991: A Multi-angle Imaging Spectro-Radiometer for terrestrial remote sensing from the Earth Observing System. *Int. J. Imaging Systems and Technol.*, **3**, 92–107.
- Durkee, P. A., D. R. Jensen, E. E. Hindman, and T. H. Vonder Haar, 1986: The relationship between marine aerosol particles and satellite-detected radiance. *J. Geophys. Res.*, **91**, 4063–4072.
- Durkee, P. A., F. Pfeil, E. Frost, and R. Shema, 1991: Global analysis of aerosol particle characteristics. *Atmos. Environ.*, **25A**, 2457–2471.
- Dutton, E. G., and J. R. Christy, 1992: Solar radiation forcing at selected locations and evidence for global lower tropospheric cooling following the eruptions of El Chichón and Pinatubo. *Geophys. Res. Lett.*, **19**, 2313–2316.
- Dutton, E. G., P. Reddy, S. Ryan, and J. J. DeLuise, 1994: Features and effects of aerosol optical depth observed at Mauna Loa, Hawaii: 1982–1992. *J. Geophys. Res.*, **99**, 8295–8306.

- Eck, T.F., P.K. Bhartia, P.H. Hwang, and L.L. Stowe, 1987: Reflectivity of the earth's surface and clouds in ultraviolet from satellite observations. *J. Geophys. Res.*, **92**, 4287-4296.
- Eluszkiewicz, J., D. Crisp, R. Zurek, L. Elson, E. Fishbein, L. Froidevaux, J. Waters, R. G. Grainger, A. Lambert, R. Harwood, and G. Peckham, 1996: Residual circulation in the stratosphere and lower mesosphere as diagnosed from Microwave Limb Sounder data. *J. Atmos. Sci.*, **53**, 217-240.
- Evans, D. L., T. G. Farr, H. A. Zebker, J. van Zyl, and P. J. Mougini-Mark, 1992: Radar interferometric studies of the Earth's topography. *Eos Trans. AGU*, **73**, 553, 557-558.
- Faivre-Perret, R., and F. Le Guern, 1983: Health risks linked with inhalation of volcanic gases and aerosols. *Forecasting Volcanic Events*. H. Tazieff and J. C. Sabroux, Ed., Elsevier, NY, 69-81.
- Feigl, K. L., A. Sergent, and D. Jacq, 1994: Estimation of an earthquake focal mechanism from a satellite radar interferogram: application to the December 4, 1992 Landers aftershock. *Geophys. Res. Lett.*, **22**, 1037-1040.
- Flynn, L. P., P. J. Mougini-Mark, and K. A. Horton, 1994: Distribution of thermal areas on an active lava flow field: Landsat observations of Kilauea, Hawaii, July 1991. *Bull. Volcanology*, **56**, 284-296.
- Garrett, T. J., and P. V. Hobbs, 1995: Long-range transport of continental aerosols over the Atlantic Ocean and their effects on cloud structure. *J. Atmos. Sci.*, **52**, 1977-1984.
- Graf, H. F., I. Kirchner, A. Robock, and I. Schult, 1993: Pinatubo eruption winter climate effects: model versus observations. *Clim. Dyn.*, **9**, 81-93.
- Grainger, R. G., A. Lambert, F. W. Taylor, J. J. Remedios, C. D. Rodgers, M. Corney, and B. J. Kerridge, 1993: Infrared absorption by volcanic stratospheric aerosols observed by ISAMS. *Geophys. Res. Lett.*, **20**, 1283-1286.
- Grainger, R. G., A. Lambert, C. D. Rodgers, F. W. Taylor, and T. Deshler, 1995: Stratospheric aerosol effective radius, surface area, and volume estimated from infrared measurements. *J. Geophys. Res.*, **100**, 16,507-16,519.
- Grant, W. B., E. V. Browell, C. S. Long, L. L. Stowe, R. G. Grainger, and A. Lambert, 1996: Use of aerosols resulting from volcanic eruptions to study the tropical stratospheric reservoir, its boundary, and transport to northern latitudes. *J. Geophys. Res.*, **101**, 3,973-3,988.
- Halpert, M. S., C. F. Ropelewski, T. R. Karl, J. K. Angell, L. L. Stowe, R. R. Heim, Jr., A. J. Miller, and D. R. Rodenhuis, 1993: 1992 brings return to moderate global temperatures. *EOS Trans. AGU*, **74**, 433-439.
- Hamill, P., O. B. Toon, and C. S. Kiang, 1977: Microphysical processes affecting stratospheric aerosol particles. *J. Atmos. Sci.*, **34**, 1104-1119.
- Han, Q. Y., W. B. Rossow, and A. A. Lacis, 1994: Near-global survey of effective cloud droplet radii in liquid water clouds using ISCCP data. *J. Climate*, **7**, 465-497.
- Han, Q. Y., W. B. Rossow, J. Chou, and R. M. Welch, 1996: Indirect effect of aerosols on climate change. Submitted, *J. Geophys. Res.*
- Hansen, J. E., and L. D. Travis, 1974: Light scattering in planetary atmospheres. *Space Science Rev.*, **16**, 527-610.
- Hansen, J. E., W. C. Wang, and A. A. Lacis, 1978: Mount Agung eruption provides test of a global climate perturbation. *Science*, **199**, 1065-1068.
- Hansen, J., A. Lacis, R. Ruedy, and M. Sato, 1992: Potential climate impact of Mount Pinatubo eruption. *Geophys. Res. Lett.*, **19**, 215-218.
- Hansen, J., and 29 co-authors, 1995: A Pinatubo climate modeling investigation. NATO Advanced Science Institutes Series, Springer-Verlag.
- Hansen, J., W. Rossow, B. Carlson, A. Lacis, L. Travis, A. Del Genio, I. Fung, B. Cairns, M. Mishchenko, and M. Sato, 1995: Low-cost long-term monitoring of global climate forcings and feedbacks. *Clim. Change* (in press).
- Hao, W. M., M. H. Liu, and P. Crutzen, 1990: Estimates of annual and regional releases of CO₂ and other trace gases to the atmosphere from fires in the tropics, based on the FAO statistics for the period 1975-1980. *Fire in the Tropical Biota*, J. G. Goldammer, Ed., Springer-Verlag, Berlin, 440-462.
- Harshvardhan, and R. D. Cess, 1976: Stratospheric aerosols: effect upon atmospheric temperature and global climate. *Tellus*, **28**, 1-10.
- Hegg, D.A., P.V. Hobbs, R.J. Ferek, and A.P. Waggner, 1995: Measurements relevant to radiation forcing by aerosols on the east coast of the United States. *J. Appl. Meteor.*, **34**, 2306-2315.
- Hegg, D. A., R. J. Ferek, and P. V. Hobbs, 1993: Aerosol size distribution in the cloudy atmospheric boundary layer of the north Atlantic Ocean. *J. Geophys. Res.*, **98**, 8841-8846.
- Herman, J.R., and E. Celarier, 1997: Earth's surface reflectivity climatology at 340-380 nm from TOMS data. *J. Geophys. Res.*, **102**, 28,003-28,012.
- Herman, J.R., P. K. Bhartia, O. Torres, C. Hsu, C. Seftor, and E. Celarier, 1997: Global distribution of UV-absorbing aerosols from the Nimbus 7/TOMS data. *J. Geophys. Res.*, **102**, 16,911-16,922.
- Hobbs, P. V., 1993: Aerosol-cloud interactions. In *Aerosol-Cloud-Climate Interactions*, (P.V. Hobbs, Ed.), Academic Press.
- Hobbs, P. V., L. F. Radke, M. W. Elgroth, and D. A. Hegg, 1981: Airborne studies of the emissions from the volcanic eruptions of Mount St. Helens. *Science*, **211**, 816-818.
- Holben, B. N., E. Vermote, Y. J. Kaufman, D. Tanré, and V. Kalb, 1992: Aerosols retrieval over land from AVHRR data—Application for atmospheric correction. *IEEE Trans. Geosci. Remote Sens.*, **30**, 212-222.
- Holben, B. N., T. F. Eck, I. Slutsker, A. Setzer, A. Pereira, E. Vermote, J. A. Reagan, Y. J. Kaufman, and D. Tanré, 1995: Sunphotometer network measurement of aerosol properties in the Brazilian Amazon. Submitted to *Remote Sens. Environ.*
- Holben, B. N., T. F. Eck, I. Slutsker, D. Tanré, J. P. Buis, A. Setzer, E. Vermote, J. A. Reagan, Y. J. Kaufman, T. Nakajima, F. Lavenue, and I. Jankowiak, 1996: Automatic sun and sky radiometer system for network aerosol monitoring. *Remote Sens. Environ.*, in press.
- Holasek, R. E., and W. I. Rose, 1991: Anatomy of 1986 Augustine volcano eruptions as recorded by digital AVHRR weather satellite data. *Bull. Volcanology*, **53**, 420-435.
- Hoppel, W. A., J. W. Fitzgerald, G. M. Ferick, and R. E. Larson, 1990: Aerosol size distribution and optical properties found in the marine boundary layer over the Atlantic Ocean. *J. Geophys. Res.*, **95**, 3659-3686.
- Houghton, J. T., L. G. Meira Filho, B. A. Callander, N. Harris, A. Kattenberg, and K. Maskell, 1996: *Climate Change 1995: The Science of Climate Change*, 572, Intergovernmental Panel on Climate Change, Cambridge.
- Hunt, B. G., 1977: A simulation of the possible consequences of a volcanic eruption on the general circulation of the atmosphere. *Mon. Wea. Rev.*, **105**, 247-260.
- IPCC, 1995: *Climate Change 1994: Radiative Forcing of Climate Change and an Evaluation of the IPCC 92 Emission Scenarios*, J. T. Houghton, L. G. Miera Filho, J. Bruce, H. Lee, B. A. Callander, E. Haites, N. Harris, and K. Maskell, Eds., Intergovernmental Panel on Climate Change, Cambridge University Press, 339 pp.
- Jaenicke, R., 1993: Tropospheric aerosols. In *Aerosol-Cloud-Climate Interactions*, (P. V. Hobbs, Ed.), Academic Press.

- Jankowiak, I., and D. Tanré, 1992: Satellite climatology of Saharan dust outbreaks: Method and preliminary results. *J. Climate*, **5**, 646–656.
- Jensen, J. E., and O. B. Toon, 1992: The potential effects of volcanic aerosols on cirrus cloud microphysics. *Geophys. Res. Lett.*, **19**, 1759–1762.
- Joseph, J. H., 1984: The sensitivity of a numerical model of the global atmosphere to the presence of desert aerosol. *Aerosols and their Climatic Effects*. H. E. Gerber and A. Deepak, Eds., Deepak Publ., 215–226.
- Karl, T. R., R. W. Knight, G. Kukla, and J. Gavin, 1995: Evidence for radiative effects of anthropogenic sulfate aerosols in the observed climate record. *Aerosol Forcing of Climate*. R. J. Charlson and J. Heintzenberg, Eds., John Wiley & Sons, 363–382.
- Kaufman, Y. J., 1978: Influence of the atmosphere on the contrast of Landsat images. *Space Res.*, XVIII, Oxford, 65–69.
- Kaufman, Y. J., and T. Nakajima, 1993: Effect of Amazon smoke on cloud microphysics and albedo. *J. Appl. Meteor.*, **32**, 729–744.
- Kaufman, Y. J., and D. Tanré, 1994: Effect of variations in supersaturation on the formation of cloud condensation nuclei. *Nature*, **369**, 45–48.
- Kaufman, Y. J., and B. N. Holben, 1995: Hemispherical backscattering by biomass burning and sulfate particles derived from sky measurements. Submitted to *J. Geophys. Res.*
- Kaufman, Y. J., R. S. Fraser, and R. A. Ferrare, 1990: Satellite remote sensing of large scale air pollution—method. *J. Geophys. Res.*, **95**, 9895–9909.
- Kaufman, Y. J., R. S. Fraser, and R. L. Mahoney, 1991: Fossil fuel and biomass burning effect on climate—heating or cooling? *J. Climate*, **4**, 578–588.
- Kaufman, Y. J., A. Gitelson, A. Karnieli, E. Ganor, R. S. Fraser, T. Nakajima, S. Mattoo, and B. N. Holben, 1994: Size distribution and phase function of aerosol particles retrieved from sky brightness measurements. *J. Geophys. Res.*, **99**, 10,341–10,356.
- Kiehl, J. T., and B. P. Briegleb, 1993: The relative roles of sulfate aerosols and greenhouse gases in climate forcing. *Science*, **260**, 311–314.
- Kienle, J., K. G. Dean, H. Garbeil, and W. I. Rose, 1990: Satellite surveillance of volcanic ash plumes, application to aircraft safety. *Eos, Trans. Amer. Geophys. Union*, **71**, 266.
- King, M. D., Harshvardhan, and A. Arking, 1984: A model of the radiative properties of the El Chichón stratospheric aerosol layer. *J. Climate Appl. Meteor.*, **23**, 1121–1137.
- King, M. D., L. F. Radke, and P. V. Hobbs, 1993: Optical properties of marine stratocumulus clouds modified by ships. *J. Geophys. Res.*, **98**, 2729–2739.
- King, M. D., Y. J. Kaufman, P. Menzel, and D. Tanré, 1992: Determination of cloud, aerosol, and water vapor properties from the Moderate Resolution Imaging Spectrometer (MODIS). *IEEE Trans. Geosci. Remote Sens.*, **30**, 2–27.
- King, M. D., S. C. Tsay, and S. Platnick, 1995: In situ observations of the indirect effects of aerosol on clouds. *Aerosol Forcing of Climate*, R. J. Charlson and J. Heintzenberg, Eds., John Wiley and Sons, 227–248.
- Kodera, K., and K. Yamazaki, 1994: A possible influence of recent polar stratospheric coolings on the troposphere in the Northern Hemisphere winter. *Geophys. Res. Lett.*, **21**, 809–812.
- Kotra, J. P., D. L. Finnegan, W. H. Zoller, M. A. Hunt, and J. L. Moyers, 1983: El Chichón: Composition of plume gases and particles. *Science*, **222**, 1018–1021.
- Krotkov, N.A., A.J. Krueger, and P.K. Bhartia, 1997: Ultraviolet optical model of volcanic clouds for remote sensing of ash and sulfur dioxide. *J. Geophys. Res.*, **102**, 21,891–21,904.
- Krueger, A.J., L.S. Walter, P.K. Bhartia, C. C. Schnetzler, N.A. Krotkov, I. Sprod, and G.J.S. Bluth, 1995: Volcanic sulfur dioxide measurements from the Total Ozone Mapping Spectrometer (TOMS) instruments. *J. Geophys. Res.*, **100**, 14,057–14,076.
- Labitzke, K., and M. P. McCormick, 1992: Stratospheric temperature increases due to Pinatubo aerosols. *Geophys. Res. Lett.*, **19**, 207–210.
- Labitzke, K., B. Naujokat, and M. P. McCormick, 1983: Temperature effects on the stratosphere of the April 4, 1992 eruption of El Chichón, Mexico. *Geophys. Res. Lett.*, **10**, 24–26.
- Lacis, A. A., and M. Mishchenko, 1995: Climate forcing, climate sensitivity, and climate response: A radiative forcing modeling perspective on atmospheric aerosols. *Aerosol Forcing of Climate*, R. J. Charlson and J. Heintzenberg, Eds., John Wiley and Sons, 11–42.
- Lacis, A. A., J. E. Hansen, and M. Sato, 1992: Climate forcing by stratospheric aerosols. *Geophys. Res. Lett.*, **19**, 1607–1610.
- Lambert, A., R. G. Grainger, J. J. Remedios, C. D. Rodgers, M. Corney, and F. W. Taylor, 1993: Measurements of the evolution of the Mt. Pinatubo aerosol cloud by ISAMS. *Geophys. Res. Lett.*, **20**, 1287–1290.
- Lambert, A., R. G. Grainger, C. D. Rodgers, F. W. Taylor, J. L. Mergenthaler, J. B. Kumer, and S. T. Massie, 1996: Global evolution of the Mount Pinatubo volcanic aerosols observed by the infrared limb-sounding instruments CLAES and ISAMS on UARS. *J. Geophys. Res.*, in press.
- Langner, J., and H. Rodhe, 1991: A global three-dimensional model of the tropospheric sulfur cycle. *J. Atmos. Chem.*, **13**, 225–263.
- Langner, J., H. Rodhe, P. J. Crutzen, and P. Zimmermann, 1993: Anthropogenic influence on the distribution of tropospheric sulphate aerosol. *Nature*, **359**, 712–715.
- Leaitch, W. R., J. W. Strapp, G. A. Isaac, and J. G. Hudson, 1986: Cloud droplet nucleation and cloud scavenging of aerosol sulphate in polluted atmospheres. *Tellus*, **38B**, 328–344.
- Leaitch, W. R., G. A. Isaac, J. W. Strapp, C. M. Banic, and H. A. Wiebe, 1992: The relationship between cloud droplet number concentrations and anthropogenic pollution observations and climatic implications. *J. Geophys. Res.*, **97**, 2463–2474.
- Lelieveld, J., and J. Heintzenberg, 1992: Sulfate cooling effect on climate through in-cloud oxidation of anthropogenic SO₂. *Science*, **258**, 117–120.
- Lin, X., and J. A. Coakley, Jr., 1993: Retrieval of properties for semi-transparent clouds from multispectral infrared imagery data. *J. Geophys. Res.*, **98**, 18,501–18,514.
- Long, C. S., and L. L. Stowe, 1994: Using the NOAA/AVHRR to study stratospheric aerosol optical thickness following the Mt. Pinatubo eruption. *Geophys. Res. Lett.*, **21**, 2215–2218.
- MacCracken, M. C., and F. M. Luther, 1984: Preliminary estimate of the radiative and climatic effects of the El Chichón eruption. *Geofisica Internacional*, **23**, 385–401.
- Malin, M. C., and M. F. Sheridan, 1982: Computer-assisted mapping of pyroclastic surges. *Science*, **217**, 637–640.
- Malingreau, J., and P. Kaswanda, 1985: Monitoring volcanic eruptions in Indonesia using weather satellite data: The Colo eruption of July 28, 1983. *J. Volcano. Geo. Res.*, **27**, 179–194.
- Martin, G. M., D. W. Johnson, and A. Spice, 1994: The measurement and parameterization of effective radius of droplets in warm stratocumulus clouds. *J. Atmos. Sci.*, **51**, 1823–1842.
- Martonchik, J. V., and D. J. Diner, 1992: Retrieval of aerosol and land surface optical properties from multi-angle satellite imagery. *IEEE Trans. Geosci. Remote Sens.*, **30**, 223–230.

- Massonnet, D., K. Feigl, M. Rossi, and F. Adragna, 1994: Radar interferometric mapping of deformation in the year after the Landers earthquake. *Nature*, **369**, 227–230.
- McCormick, M. P., 1993: Third International Lidar Researchers Directory, Atmospheric Sciences Division, NASA Langley Research Center, Hampton, Virginia.
- McCormick, M. P., 1995: LITE—An overview. 1995 Spring Meeting of the Amer. Geophys. Union, *EOS supplement*, April 25, 67.
- McCormick, M. P., and P. H. Wang, 1987: Satellite measurements of stratospheric aerosols. *Transport Processes in the Middle Atmosphere*, G. Visconti and R. Garcia, Eds., D. Reidel Publishing, 103–120.
- McCormick, M. P., and R. E. Veiga, 1992: SAGE II measurements of early Pinatubo aerosols. *Geophys. Res. Lett.*, **19**, 155–158.
- McCormick, M. P., D. M. Winker, E. V. Browell, J. A. Coakley, C. S. Gardner, R. M. Hoff, G. S. Kent, S. H. Melfi, R. T. Menzies, C. M. R. Platt, D. A. Randall, and J. A. Reagan, 1993: Scientific investigations planned for the lidar in-space technology experiment (LITE). *Bull. Amer. Meteor. Soc.*, **74**, 205–214.
- McCormick, M. P., L. W. Thomason, and C. R. Trepte, 1995: Atmospheric effects of the Mt. Pinatubo eruption. *Nature*, **373**, 399–404.
- Minnis, P., E. F. Harrison, L. L. Stowe, G. G. Gibson, F. M. Denn, D. R. Doelling, and W. L. Smith, 1993: Radiative climate forcing by the Mt. Pinatubo eruption. *Science*, **259**, 1411–1415.
- Mouginis-Mark, P. J., and H. Garbeil, 1993: Digital topography of volcanoes from radar interferometry: An example of Mt. Vesuvius, Italy. *Bull. Volcano.*, **55**, 566–570.
- Muller, J. F., 1992: Geographical distribution and seasonal variation of surface emissions and deposition velocities of atmospheric trace gases. *J. Geophys. Res.*, **97**, 3787–3804.
- Nakajima, T., M. Tanaka, M. Yamano, M. Shiobara, K. Arai, and Y. Nakanishi, 1989: Aerosol optical characteristics in the yellow sand events observed in May, 1982 at Nagasaki-Part 2 Models. *J. Meteor. Soc. Japan*, **67**, 279–291.
- Norris, J. R., and C. B. Leovy, 1995: Comments on “Trends in global marine cloudiness and anthropogenic sulfur.” *J. Climate*, **8**, 2109–2110.
- Novakov, T., and J. E. Penner, 1993: Large contribution of organic aerosols to CCN concentration. *Nature*, **365**, 823–826.
- Osborn, M. T., R. J. DeCoursey, C. R. Trepte, D. M. Winker, and D. C. Woods, 1995: Evolution of the Pinatubo volcanic cloud over Hampton, Virginia. *Geophys. Res. Lett.*, **22**, 1101–1104.
- Parungo, F., J. F. Boatman, H. Sievering, S. W. Wilkinson, and B. B. Hicks, 1994: Trends in global mean cloudiness and anthropogenic sulfur. *J. Climate*, **7**, 434–440.
- Penner, J. E., R. E. Dickinson, and C. A. O’Neill, 1992: Effects of aerosol from biomass burning on the global radiation budget. *Science*, **256**, 1432–1434.
- Pincus, R., and M. Baker, 1994: Effect of precipitation on the albedo susceptibility of marine boundary layer clouds. *Nature*, **372**, 250–252.
- Platnick, S., and S. Twomey, 1994: Determining the susceptibility of cloud albedo to changes in droplet concentration with the Advanced Very High Resolution Radiometer. *J. Appl. Meteor.*, **33**, 334–347.
- Pollack, J. B., O. B. Toon, C. Sagan, A. Summers, B. Baldwin, and W. Van Camp, 1976: Volcanic explosions and climatic change: A theoretical assessment. *J. Geophys. Res.*, **81**, 1071–1083.
- Post, M. J., 1986: Atmospheric purging of El Chichón debris. *J. Geophys. Res.*, **91**, 5222–5228.
- Post, M. J., C. J. Grund, A. O. Langford, and M. H. Proffitt, 1992: Observations of Pinatubo ejecta over Boulder, Colorado by lidars of three different wavelengths. *Geophys. Res. Lett.*, **19**, 195–198.
- Prabhakara, C., R. S. Fraser, G. Dalu, M-L. C. Wu, and R. J. Curran, 1988: Thin cirrus clouds: Seasonal distribution over oceans deduced from Nimbus-4 IRIS. *J. Climate Appl. Meteor.*, **27**, 279–299.
- Prata, A. J., 1989: Infrared radiative transfer calculations for volcanic ash clouds. *Geophys. Res. Lett.*, **16**, 1293–1296.
- Prospero, J. M., and R. T. Nees, 1976: Dust concentration in the atmosphere of the equatorial North Atlantic: Possible relationship of Saharan drought. *Science*, **196**, 1196–1198.
- Pueschel, R. F., D. F. Blake, K. G. Snetsinger, A. D. A. Hansen, S. Verma, and K. Kato, 1992: Black carbon (soot) aerosol in the lower stratosphere and upper troposphere. *Geophys. Res. Lett.*, **19**, 1659–1662.
- Radke, L. F., D. A. Hegg, P. V. Hobbs, J. D. Nance, J. H. Lyons, K. K. Laursen, P. J. Reagan, and D. E. Ward, 1991: Particulate and trace gas emission from large biomass fires in North America. *Global Biomass Burning: Atmospheric, Climatic, and Biospheric Implications*, J. S. Levine, Ed., MIT Press, 209–224.
- Radke, L. F., J. A. Coakley, Jr., and M. D. King, 1989: Direct and remote sensing observations of the effects of ships on clouds. *Science*, **246**, 1146–1149.
- Rao, C. R. N., L. L. Stowe, and E. P. McClain, 1989: Remote sensing of aerosols over the ocean using AVHRR data: Theory, practice and application. *Int. J. Remote Sens.*, **10**, 743–749.
- Rao, C. R. N., L. L. Stowe, E. P. McClain, J. Sapper, and M. P. McCormick, 1988: Development and application of aerosol remote sensing with AVHRR data from the NOAA satellites. *Aerosols and Climate*, P. V. Hobbs and M. P. McCormick, Eds., A. Deepak Publishing, 69–80.
- Read, W. G., L. Froidevaux, and J. W. Waters, 1993: Microwave limb sounder measurement of stratospheric SO₂ from the Mt. Pinatubo volcano. *Geophys. Res. Lett.*, **20**, 1299–1302.
- Rivera-Carpio, C. A., C. E. Corrigan, T. Novakov, J. E. Penner, C. F. Rogers, and J. C. Chow, 1995: Derivation of contributions of sulfate and carbonaceous aerosol to CCN from mass distributions. Submitted to *J. Geophys. Res.*
- Robock, A., 1983: The dust cloud of the century. *Nature*, **301**, 373–374.
- Robock, A., and M. Matson, 1983: Circumglobal transport of the El Chichón volcanic dust cloud. *Science*, **221**, 195–197.
- Russell, P. B., J. M. Livingston, R. F. Pueschel, J. A. Reagan, E. V. Browell, G. C. Toon, P. A. Newman, M. R. Schoeberl, L. R. Lait, L. Pfister, Q. Gao, and B. M. Herman, 1993a: Post-Pinatubo optical depth spectra vs. latitude and vortex structure: airborne tracking sunphotometer measurements in AASE II. *Geophys. Res. Lett.*, **20**, 2571–2574.
- Russell, P. B., J. M. Livingston, E. G. Dutton, R. F. Pueschel, J. A. Reagan, T. E. DeFoor, M. A. Box, D. Allen, P. Pilewskie, B. M. Herman, S. A. Kinne, and D. J. Hoffman, 1993b: Pinatubo and pre-Pinatubo optical depth spectra: Mauna Loa measurements, comparisons, inferred particle size distributions, radiative effects, and relationship to lidar data. *J. Geophys. Res.*, **98**, 22,969–22,985.
- Sassen, K., 1992: Evidence for liquid-phase cirrus cloud formation from volcanic aerosols: Climatic implications. *Science*, **257**, 516–519.
- Sassen, K., D. O’C. Starr, G. G. Mace, M. R. Poellot, S. H. Melfi, W. L. Eberhard, J. D. Spinhirne, E. W. Eloranta, D. E. Hagen, and J. Hallet, 1995: The 5-6 December 1991 FIRE IFO II jet stream cirrus case study: The influence of volcanic aerosols. *J. Atmos. Sci.*, **52**, 97–123.
- Schneider, S. H., and C. Mass, 1975: Volcanic dust, sunspots, and temperature trends. *Science*, **190**, 741–746.

- Seftor, C. J., N. C. Hsu, J. R. Herman, P. K. Bhartia, O. Torres, W. I. Rose, D. J. Schneider, and N. Krotkov, 1997: Detection of volcanic ash clouds from Nimbus7/Total Ozone Mapping Spectrometer. *J. Geophys. Res.*, **102**, 16,749–16,759.
- Sigurdsson, H., 1990: Assessment of the atmospheric impact of volcanic eruptions. *Global Catastrophes in Earth History*, V. L. Sharpton and P. D. Ward, Eds., Geo. Soc. Amer. paper 247, 99–110.
- Simkin, T., and L. Siebert, 1994: *Volcanoes of the World*, 2nd ed., Geoscience Press, Tucson, 349 pp.
- Simonich, D. M., and B. R. Clemesha, 1995: Comparison between El Chichón and Pinatubo aerosol clouds. IUGG XXI General Assembly, Boulder, Colorado, July 2–14, 1995, Abstracts Week B, p. B250.
- Song, N. D., O' C. Starr, D. J. Wuebbles, K. Kunkel, A. Williams, V. Bowersox, and S. Larson, 1996: Effects of volcanic aerosols on global cloudiness. Submitted to *Science*.
- Spiro, P. A., D. J. Jacob, and J. A. Logan, 1992: Global inventory of sulfur emissions with $1^\circ \times 1^\circ$ resolution. *J. Geophys. Res.*, **97**, 6023–6036.
- Stowe, L. L., P. V. Hobbs, and P. Russell, 1995: Plans for the implementation of the tropospheric aerosol radiative forcing observational experiment. Paper MB52A-12, p. 308 Abstracts for Week B, XXI Assembly IUGG, Boulder Colorado.
- Stowe, L. L., I. M. Ignatov, and R. R. Singh, 1996: Development, validation, and potential enhancements to the second-generation operational aerosol product at NOAA/NESDIS. *J. Geophys. Res.* (in press).
- Strom, J., 1993: *Numerical and airborne experimental studies of aerosol and cloud properties in the troposphere*. Ph.D. thesis, Dept. of Meteorology, Stockholm University.
- Tanré, D., J. F. Geleyn, and J. Slingo, 1984: First results of the introduction of an advanced aerosol-radiation interaction in the ECMWF low resolution global model. *Aerosols and their Climatic Effects*. H. E. Gerber and A. Deepak, Eds., Deepak Publ., 133–177.
- Tanré, D., M. Herman, and Y. J. Kaufman, 1995: Remote sensing of aerosol properties over oceans using the EOS-MODIS reflected spectral radiance: Theoretical approach information on the aerosol size distribution, contained in the reflected spectral radiance of EOS-MODIS. Submitted to *J. Geophys. Res.*
- Taylor, K. E., and J. E. Penner, 1994: Anthropogenic aerosols and climate change. *Nature*, **369**, 734–736.
- Tegen, I., and I. Fung, 1994: Modeling of mineral dust in the atmosphere: Sources, transport, and optical thickness. *J. Geophys. Res.*, **99**, 22,897–22,914.
- Tegen, I., and I. Fung, 1995: Contribution to the atmospheric mineral aerosol load from land surface modification. *J. Geophys. Res.*, **100**, 18,707–18,726.
- Tegen, I., A. A. Lacis, and I. Fung, 1996: The influence of mineral aerosols from disturbed soils on climate forcing. *Nature*, **380**, 419–422.
- Thomason, L. W., 1992: Observations of a new SAGE II aerosol extinction mode following the eruption of Mt. Pinatubo. *Geophys. Res. Lett.*, **19**, 2179–2182.
- Torres, O., P. K. Bhartia, J. R. Herman, Z. Ahmad, and J. Gleason, 1998: Derivation of aerosol properties from satellite measurements of backscattered ultraviolet radiation: Theoretical basis. *J. Geophys. Res.*, **103**, 17,099–17,110.
- Trepte, C. R., and M. H. Hitchman, 1992: The stratospheric tropical circulation deduced from satellite aerosol data. *Nature*, **355**, 626–628.
- Trepte, C. R., L. W. Thomason, and G. S. Kent, 1994: Banded structures in stratospheric aerosol distributions. *Geophys. Res. Lett.*, **21**, 2397–2400.
- Tucker, C. J., H. E. Oregne, and W. W. Newcomb, 1991: Expansion and contraction of the Sahara desert from 1980 to 1990. *Science*, **253**, 299–301.
- Twomey, S. A., 1977: The influence of pollution on the shortwave albedo of clouds. *J. Atmos. Sci.*, **34**, 1149–1152.
- Twomey, S. A., M. Piepgrass, and T. L. Wolfe, 1984: Assessment of the impacts of pollution on the global albedo. *Tellus*, **36B**, 356–366.
- Valero, F. P. J., and P. Pilewskie, 1992: Latitudinal survey of spectral optical depths of the Pinatubo volcanic cloud-derived particle sizes, columnar mass loadings, and effects on planetary albedo. *Geophys. Res. Lett.*, **19**, 163–166.
- Vanderbilt, V. C., L. Grant, L. L. Biehl, and B. F. Robinson, 1985: Specular, diffuse, and polarized light scattered by two wheat canopies. *Appl. Optics*, **24**, 2408–2418.
- Wadge, G., P. A. V. Young, and I. J. McKendrick, 1994: Mapping lava flow hazards using computer simulation. *J. Geophys. Res.*, **99**, 489–504.
- Wang, M., and H. R. Gordon, 1995: Estimation of aerosol columnar size distribution and optical thickness from the angular distribution of radiance exiting the atmosphere: Simulation. *Appl. Opt.*, **33**, 7088–7098.
- Ward, D. E., and C. C. Hardy, 1991: Smoke emissions from wildland fires. *Environment. Intl.*, **17**, 117–134.
- Ward, D. E., R. Susott, J. Kauffman, R. Babbitt, B. N. Holben, Y. J. Kaufman, A. Setzer, R. Rasmussen, D. Cumming, and B. Dias, 1992: Emissions and burning characteristics of biomass fires for cerrado and tropical forest regions of Brazil-BASE-B experiment. *J. Geophys. Res.*, **97**, 14,601–14,619.
- Warner, J., and S. Twomey, 1967: The production of cloud nuclei by cane fires and the effect on cloud droplet concentration. *J. Atmos. Sci.*, **24**, 704–706.
- Winker, D. M., and M. T. Osborn, 1992: Airborne lidar observations of the Pinatubo volcanic plume. *Geophys. Res. Lett.*, **19**, 167–170.
- Yue, G. K., M. P. McCormick, and E. W. Chiou, 1991: Stratospheric aerosol optical depth observed by the Stratospheric Aerosol and Gas Experiment II: Decay of the El Chichón and Ruiz volcanic perturbations. *J. Geophys. Res.*, **96**, 5209–5219.
- Zebker, H. A., P. A. Rosen, R. M. Goldstein, A. Gabriel, and C. L. Werner, 1994: On the derivation of coseismic displacement fields using differential radar interferometry: the Landers earthquake. *J. Geophys. Res.*, **99**, 19,617–19,634.
- Zhao, J., R. P. Turco, and O. B. Toon, 1995: A model simulation of Pinatubo volcanic aerosols in the stratosphere. *J. Geophys. Res.*, **100**, 7315–7328.

Chapter 8 Index

- AATSR 365-366
 ADEOS 366
 AERONET 370
 aerosol abundance 353-354
 aerosol indirect effects of 355-358, 362-366
 aerosol measurements 368-371
 aerosol radiative effects 352-355
 aerosol radiative properties 345-347
 aerosol sources 349-354
 aerosol, climate effects of 349-358, 370-372
 aerosol, climate modification by 372
 agriculture 352, 358
 Agung 342
 aircraft exhaust 350
 aircraft hazards 361-362
 AIRS/AMSU/HSB 367
 ALOS 364-366
 ASTER 361, 364-368
 ATSR 362
 AVHRR 360, 362, 368-369
 biomass burning 341, 350-358, 370-371
 calibration 353, 366, 369-370
 carbon dioxide (CO₂) 348, 359, 369-370
 carbon monoxide (CO) 332, 359, 367
 CCD 369
 CCN 351, 354
 CERES 367
 CHEM-1 368
 chlorine 349
 CLAES 346, 347
 convection 344
 COS 343, 364, 367
 COSEPUP 372
 DEM 359, 361, 365, 365
 DMS 350
 El Chichón 342-344
 El Niño 342, 344, 367
 ENSO 344
 ENVISAT 359, 364-367
 EOS AM 356, 369-371
 EOSP 353, 356, 363-364, 366-371
 EP 368
 ERBE 343, 346
 ERS 360, 366
 ETM+ 367-368
 FAA 360-361
 field campaigns 358
 Franklin, Benjamin 349
 gas-to-particle conversion 343-345
 GISS 346
 GLAS 349, 356, 358, 362-371
 GLI 366
 GOMOS 366
 GPS 362
 H₂SO₄ 342-343, 345-346
 HCl 342, 358-359, 364, 367
 health hazards, volcanic 359-361
 HIRDLS 347, 362-363, 366-367
 HSB 367
 humidity 350, 367
 ICESat 356, 371
 IDS 362, 367
 ILAS 366
 IPCC 350-352, 370
 IR 365, 368
 ISAMS 346-347
 JERS 366
 Krakatau 342, 344
 lidar 344, 347-349, 356, 367, 371
 MERIS 366
 METEOR-3 347, 368
 MISR 353-357, 362-371
 MLS 345, 363-364, 367
 modeling 345, 371
 MODIS 353, 356, 362-370
 Mt. Katmai 342
 Mt. Pinatubo 343-348, 361, 366-367, 371
 Mt. Saint Helens 344
 MSU 343-344
 NASA 366
 Nevada del Ruiz 344
 NOAA 368
 NO_x 350
 ocean circulation 341, 366
 OCTS 366
 OLR 344
 OMI 350, 355-356, 363-365
 POLDER 366
 precipitation 343-344
 QBO 344
 RADARSAT 359, 364, 366
 SAGE 350
 SAGE II 347
 SAGE III 347, 363, 367
 salinity 359
 SAM 349
 SAR 362, 364
 SCANSAR 366
 SCF 363
 sulfate 41-352, 359, 365, 370-371
 sulfur 341-343, 351
 sulfur dioxide (SO₂) 41-346, 350-354, 358-359, 365, 367-368
 sulfuric acid 342-343, 345-346
 SW 347
 SWIR 365, 369-370
 Tambora 342, 344
 TARFOX 353
 TIR 362, 365
 TOMS 356, 365, 367-369
 topography 361-367
 TOPSAR 361
 trace gases 350-351
 validation 349, 366, 370
 VOC 350-351
 volcanic detection 360-362, 368
 volcanic hazards 358-362, 367
 volcanic measurements, international 368
 volcanoes 341-372
 water vapor 342-345, 350, 352, 358, 362, 364, 368
 wind 341, 344, 367, 370
 year without a summer 342

Acronyms

ACRONYMS

2D	Two Dimensional	ATSR	Along Track Scanning Radiometer
3D	Three Dimensional	AVHRR	Advanced Very High-Resolution Radiometer
4DDA	4-Dimensional Data Assimilation	AVIRIS	Airborne Visible-Infrared Imaging Spectrometer
A		AWS	Automatic Weather Stations
A/SA	arid/semi-arid	B	
AABW	Antarctic Bottom Water	BAHC	Biospheric Aspects of the Hydrological Cycle
AASE II	Airborne Arctic Stratospheric Expedition II	BATS	Biosphere-Atmosphere Transfer Model
AATSR	Advanced Along Track Scanning Radiometer	BIOME	Biogeochemical Information Ordering Management Environment
ACRIM I	Active Cavity Radiometer Irradiance Monitor I	BOREAS	Boreal Ecosystems Atmosphere Study
ACSYS	Arctic Climate System Study	BRDF	bidirectional reflectance distribution function
ADEOS	Advanced Earth Observing System	BSRN	Baseline Surface Radiation Network
AEAP	Atmospheric Effects of Aviation Program	BUV	Backscatter Ultraviolet
AERONET	Aerosol Robotic Network	C	
AESOPS	Antarctic Environment Southern Ocean Process Study	CALM	Circumpolar Active Layer Monitoring
AGCM	atmospheric general circulation models	CART	Cloud and Radiation Testbed
AHM	(model)	CASES	Cooperative Atmosphere-Surface Exchange Study
AIRS	Atmospheric Infrared Sounder	CCD	Charge-Coupled Device
AIRSAR	Airborne Synthetic Aperture Radar	CCN	Cloud Condensation Nuclei
ALOS	Advanced Land Observation Satellite	CDIAC	Carbon Dioxide Information and Analysis Center
ALT	Altimeter	CDOM	Colored Dissolved Organic Matter
AMI	Active Microwave Instrument	CEM	cumulus ensemble model
AMIP	Atmospheric Model Intercomparison Project	CERES	Clouds and the Earth's Radiant Energy System
AMLS	Array MLS	CESBIO	Centre d'Études Spatiales de la Biosphère
AMSR	Advanced Microwave Scanning Radiometer	CFC	Chlorofluorcarbon
AMSR-E	Advanced Microwave Scanning Radiometer (EOS Version)	CH₂Cl₂	Dichloromethane
AMSU	Advanced Microwave Sounding Unit	CH₃Cl	Methyl chloride
APAR	Absorbed Photosynthetically-Active Radiation	CHCl₃	Chloroform
ARM	Atmospheric Radiation Measurement	CHEM-1	Chemistry Mission-1
ASAR	Advanced Synthetic Aperture Radar	CLAES	Cryogenic Limb Array Etalon
ASF	Alaska SAR Facility	CLASS	Canadian Land Surface Scheme
ASTER	Advanced Spaceborne Thermal Emission and Reflection Radiometer	CLIVAR	CLimate VARIability and prediction
ATBD	Algorithm Theoretical Basis Document	CIO_x	oxides of chlorine family
ATLAS	Atmospheric Laboratory for Applications and Science	CMDL	Climate Monitoring and Diagnostics Laboratory
ATMOS	Atmospheric Trace Molecule Spectroscopy		

COARE	Coupled Ocean-Atmosphere Response
COS	Carbonyl Sulfide
COSEPUP	Committee on Science, Engineering, and Public Policy
COV	Coefficient of Variation
CPR	Cloud Profiling Radar
CR	Correlation Radiometry
CRYSYS	Use of the Cryospheric System to Monitor Global Change in Canada (EOS IDS)
CTM	Chemistry and Transport Model
CZCS	Coastal Zone Color Scanner

D

DAAC	Distributed Active Archive Center
DAO	Data Assimilation Office
DAS	Data Assimilation System
DDL	Direct Downlink
DECAFE	Dynamique et Chimie de l' Atmosphere en Foret Equatoriale
DEM	Digital Elevation Model
DFA	Dual-Frequency radar Altimeter
DIC	Dissolved Inorganic Carbon
DMS	Dimethyl Sulfide
DMSP	Defense Meteorological Satellite Program
DOC	Dissolved Organic Carbon
DoD	Department of Defense
DoE	Department of Energy
DOM	Dissolved Organic Matter
DORIS	Doppler Orbitography and Radiopositioning Integrated by Satellite
DT	Delta T (Temperature)
DU	Dobson Unit

E

ECHIVAL	European International Project on Climate and Hydrological Interactions between Vegetation, Atmosphere, and Land Surfaces
ECLIPS	Experimental Cloud Lidar Pilot Study
ECMWF	European Centre for Medium-Range Weather Forecasts
EDC	EROS Data Center
EFEDA	ECHIVAL Field Experiment in Desertification-Threatened Areas
EGIG	Expédition Glaciologique Internationale au Groenland

ENSO	El Niño-Southern Oscillation
ENVISAT	Environmental Satellite, ESA
EOS	Earth Observing System
EOS PM	EOS afternoon-crossing satellite
EOSDIS	EOS Data and Information System
EOSP	Earth Observing Scanning Polarimeter
EP	Earth Probe
ER-2	NASA Research Aircraft
ERB	Earth Radiation Budget
ERBE	Earth Radiation Budget Experiment
ERBS	Earth Radiation Budget Satellite
EROS	Earth Resources Observation System
ERS	European Remote-Sensing Satellite
ERS-1	European Remote-Sensing Satellite-1
ESA	European Space Agency
ESCC	Electrically Self-Calibrating Cavity
ESMR	Electronically Scanning Microwave Radiometer
ESSC	Earth System Sciences Committee
ET	Evapotranspiration
ETM	Enhanced Thematic Mapper
ETM+	Enhanced Thematic Mapper Plus
EURECA	European Retrievable Carrier

F

FAA	Federal Aviation Administration
FAO	Food and Agriculture Organization
FAPAR	Fraction Absorbed Photosynthetically Active Radiation
FIFE	First ISLSCP Field Experiment
FIRE	First ISCCP Regional Experiment
FLUXNET	Flux Network
FPAR	Fraction of Photosynthetically-Active Radiation
FSSP	Forward Scattering Spectrometer Probe
FTS	Fourier Transform Spectrometer

G

GAIM	Global Analysis, Interpretation, and Modeling
GAP	Gap Analysis Project
GCIP	GEWEX Continental-Scale International Project

GCM	General Circulation Model (also Global Climate Model)
GCOS	Global Climate Observing System
GCTE	Global Change in Terrestrial Ecosystems
GEBA	Global Energy Balance Archive
GENESIS	Global Environmental and Ecological Simulation of Interactive Systems
GEOS	Goddard Earth Observing System
GERB	Geostationary Earth Radiation Budget
GEWEX	Global Energy and Water Cycle Experiment
GFDL	Geophysical Fluid Dynamics Laboratory
GFO	Geosat Follow-On
GGD	Global Geocryology Database
GHCN	Global Historical Climatology Network
GIS	Geographic Information System
GISP	Greenland Ice Sheet Program
GISS	Goddard Institute for Space Studies
GLAS	Geoscience Laser Altimeter System
GLCTS	Global Landcover Test Site Initiative
GLI	Global Imager
GLIMS	Global Land Ice Monitoring from Space
GLOBE	Global Learning and Observations to Benefit the Earth
GLOBEC	Global Ocean Ecosystem Dynamics
GMS	Geostationary Meteorological Satellite
GNP	Gross National Product
GOALS	Global Ocean-Atmosphere-Land System
GOES	Geostationary Operational Environmental Satellite
GOMOS	Global Ozone Monitoring By Occultation of Stars
GPCP	Global Precipitation Climatology Project
GPP	Gross Primary Productivity
GPS	Global Positioning System
GRDC	Global Runoff Data Center
GSFC	Goddard Space Flight Center
Gt	Gigaton
GTOS	Global Terrestrial Observing System
GVaP	GEWEX Water Vapor Project

H

HALOE	Halogen Occultation Experiment
HAPEX	Hydrological-Atmospheric Pilot Experiment
HCFC	Hydrochlorofluorocarbon
HH	Horizontal, Horizontal Polarization
HIRDLS	High-Resolution Dynamics Limb Sounder

HIRS	High-Resolution Infrared Radiation Sounder
HNLC	High Nutrient, Low Chlorophyll
HO_x	odd hydrogen family
HRDI	High-Resolution Doppler Imager
HSB	Humidity Sounder, Brazil
HSCT	High-Speed Civil Transport

IABP	International Arctic Buoy Program
ICESat	Ice, Clouds, and Land Elevation Satellite
ICRCCM	Intercomparison of Radiative Codes for Climate Models
ICSU	International Council of Scientific Unions
IDS	Interdisciplinary Science Investigation (EOS)
IFC	Intensive Field Campaign
IFO	intensive field observation
IFOV	Instantaneous Field of View
IGAC	International Global Atmospheric Chemistry
IGBP	International Geosphere-Biosphere Programme
IGPPDI	Global Primary Production Data Initiative
IHP	International Hydrological Program
ILAS	Improved Limb Atmospheric Spectrometer
IMAS	Integrated Multispectral Atmospheric Sounder
IOC	Intergovernmental Oceanographic Commission
IOP	Intensive Observing Period
IPCC	Intergovernmental Panel on Climate Change
IR	infrared
ISAMS	Improved Stratospheric and Mesospheric Sounder
ISCCP	International Satellite Cloud Climatology Project
ISLSCP	International Satellite Land Surface Climatology Project
IT	Instrument Team
ITCZ	Inter-Tropical Convergence Zone
IWP	ice water path

J

JERS	Japanese Earth Remote-Sensing Satellite
JERS-OPS	Japanese Earth Remote-sensing Satellite-OPS
JGOFS	Joint Global Ocean Flux Study

JPLAIRSAR JPL Airborne Synthetic Aperture Radar
JPO Joint Planning Office

K

KINEROS Kinematic wave overland flow, channel routing and Erosion model

L

LAI Leaf-Area Index
Landsat Land Remote-Sensing Satellite
LBA Large Scale Biosphere-Atmosphere Experiment in Amazonia
LERTS Laboratoire d'Etudes et de Recherches en Teledetection Spatiale
LHH L-band HH
LIS Lightning Imaging Sensor
LITE Lidar In-space Technology Experiment
LOICZ Land Ocean Interactions in the Coastal Zone
LS Lower Stratosphere
LSM Land-Surface Model
LSP Land-Surface Parameterizations
LTER Long-Term Ecological Research
LW longwave
LWP liquid water path

M

MAAT Mean Annual Air Temperatures
MAPS Measurement of Air Pollution from Satellites
MCS mesoscale convective systems
MERIS Medium-Resolution Imaging Spectrometer
METEOR-3 Russian Operational Weather Satellite
METOP Meteorological Operational Satellite
MHS Microwave Humidity Sounder
MIMR Multifrequency Imaging Microwave Radiometer
MISR Multi-angle Imaging Spectroradiometer
MIT Massachusetts Institute of Technology
MLS Microwave Limb Sounder
MM mesoscale model
MMIC Microwave Monolithic Integrated Circuit
MMS Modular Modeling System

MODIS Moderate-Resolution Imaging Spectroradiometer
MODLAND MODLIS Land
MOPITT Measurements of Pollution in the Troposphere
MOU Memorandum of Understanding
MSG Meteosat Second Generation
MSU Microwave Sounding Unit
MT Megaton
MVI MODIS Vegetation Index

N

NAD Nitric Acid Dihydrate
NADW North Atlantic Deep Water
NASA National Aeronautics and Space Administration
NASDA National Space Development Agency
NAT Nitric Acid Trihydrate
NBIOME Northern Biosphere Observation and Modeling Experiment
NCAR National Center for Atmospheric Research
NCDC National Climatic Data Center
NCEP National Centers for Environmental Prediction
NDVI Normalized Difference Vegetation Index
NESDIS National Environmental Satellite, Data, and Information Service
NEXRAD Next Generation Weather Radar
NH Northern Hemisphere
NIR Near Infrared
NMC National Meteorological Center
NMHC Non-Methane Hydrocarbons
NOAA National Oceanic and Atmospheric Administration
NOPEX Northern Hemisphere Climate-Processes Land-Surface Experiment
NO_x odd nitrogen family
NPOESS National Polar-orbiting Operational Environmental Satellite System
NPP Net Primary Production
NRC National Research Council
NSCAT NASA Scatterometer
NSF National Science Foundation
NSIDC National Snow and Ice Data Center
NWP Numerical Weather Prediction

O

OCS	Carbonyl Sulfide
OCTS	Ocean Color and Temperature Scanner
OH	Hydroxyl
OLR	Outgoing Longwave Radiation
OMI	Ozone Measuring Instrument
ONR	Office of Naval Research
ORNL	Oak Ridge National Laboratory
OSU	Oregon State University
OTTER	Oregon Transect Terrestrial Ecosystem Research

P

PAR	Photosynthetically-Active Radiation
PARCA	Program for Arctic Regional Climate Assessment
PEM	Production Efficiency Model
PI	Principal Investigator
PIK	Potsdam Institute for Climate Impact Research
PILPS	Project for Intercomparison of Land-Surface Parameterization (LSP) Schemes
PNZ	Phytoplankton-nutrient-zooplankton
POLDER	Polarization and Directionality of the Earth's Reflectance
POLES	Polar Exchange at the Sea Surface (IDS)
ppm	parts per million
PR	Precipitation Radar
PSC	Polar Stratospheric Cloud
PSU	Pennsylvania State University
PW	precipitable water

Q

QBO	Quasi-Biennial Oscillation
------------	----------------------------

R

Radarsat	Radar Satellite, Canada
RAMS	Regional Atmospheric Modeling System
RC	radiative-convective
REP	Relativistic Electron Precipitation
RGPS	Radarsat Geophysical Processor System

S

S.D.	Standard Deviation
SAFARI	South African Fire—Atmospheric Research Initiative
SAGE	Stratospheric Aerosol and Gas Experiment
SALSA	Semi-Arid Land-Surface-Atmosphere
SAM	Stratospheric Aerosol Measurement
SAR	Synthetic Aperture Radar
SAVI	Soil-Adjusted Vegetation Index
SBUV	Solar Backscatter Ultraviolet
SCA	Snow-Covered Area
SCANSAR	Scanning Synthetic Aperture Radar
SCAR-B	Smoke Cloud and Radiation-Brazil
SCARAB	Scanner for Radiation Budget
SCF	Science Computing Facility
SCICEX	Submarine Arctic Science Cruise (Program)
SCOPE	Scientific Committee on Problems of the Environment
SeaWiFS	Sea-viewing Wide Field-of-view Sensor
SEB	Surface Energy Balance
SEDAC	Socioeconomic Data and Applications Center
SGP	Southern Great Plains
SHEBA	Surface Heat Budget of the Arctic Ocean
SiB	Simple Biosphere Model
SIMIP	Sea Ice Model Intercomparison Project
SIR-C	Shuttle Imaging Radar-C
SLR	Satellite Laser Ranging
SMM	Solar Maximum Mission
SMM/I	Special Sensor Microwave/Imager
SMMR	Scanning Multispectral Microwave Radiometer
SOHO	Solar Heliospheric Observatory
SOLAS	Surface Ocean Lower Atmosphere Study
SOLSTICE	Solar Stellar Irradiance Comparison Experiment
SPCZ	South Pacific Convergence Zone
SPE	Solar Particle Event
SPOT	Systeme pour l'Observation de la Terre
SRB	Surface Radiation Budget
SRBEX	Susquehanna River Basin Experiment
SSALT	Solid State radar Altimeter
SSM/I	Special Sensor Microwave/Imager
SST	Sea-Surface Temperature
SSU	Stratospheric Sounding Unit
STP	Standard Temperature and Pressure
STS	Space Transport System

SVAT	Soil-Vegetation-Atmosphere Transfer Model
SVI	Spectral Vegetation Indices
SW	shortwave
SWE	Snow Water Equivalent
SWIR	Shortwave Infrared

T

T-S	temperature-salinity
TARFOX	Tropospheric Aerosol Radiative Forcing Observational Experiment
TEM	Terrestrial Ecosystem Model
TES	Tropospheric Emission Spectrometer
THM	Terrestrial Hydrology Model
TIR	Thermal Infrared
TM	Thematic Mapper
TMI	TRMM Microwave Imager
TMR	TOPEX Microwave Radiometer
TOA	top of the atmosphere
TOGA	Tropical Ocean Global Atmosphere
TOMS	Total Ozone Mapping Spectrometer
TOP	Terrestrial Observation Panel
TOPEX/ Poseidon	Ocean Topography Experiment
TOPORAD	(model)
TOPSAR	Topographic Synthetic Aperture Radar
TOVS	TIROS Operational Vertical Sounder
TRACE-A	Transport and Chemistry near the Equator over the Atlantic
TRAGNET	United States Trace Gas Network
TRMM	Tropical Rainfall Measuring Mission
TSI	total solar irradiance

U

UARS	Upper Atmosphere Research Satellite
UKMO	United Kingdom Meteorological Office
UMCP	University of Maryland, College Park
UNEP	United Nations Environment Program
UNESCO	United Nations Educational, Scientific, and Cultural Organization
USAF	United States Air Force
USDA	United States Department of Agriculture
USGCRP	U.S. Global Change Research Program
USGS	United States Geological Survey

UT	Upper Troposphere
UV	Ultraviolet
UV-B	Ultraviolet-B

V

VEMAP	Vegetation/Ecosystem Modeling and Analysis Project
VHRR	Very High Resolution Radiometer
VI	Vegetation Index
VIC	Variable Infiltration Capacity
VIRGO	Variability of solar Irradiance and Gravity Oscillations
VIRS	Visible Infrared Scanner
VIS	Visible
VNIR	Visible and Near Infrared
VOC	Volatile Organic Carbon

W

WCRP	World Climate Research Program
WDC-A	World Data Center-A
WFPS	Water-Filled Pore Space
WMO	World Meteorological Organization
WOCE	World Ocean Circulation Experiment
WSR	Weather Surveillance Radar

X

X-SAR	X-Band Synthetic Aperture Radar
--------------	---------------------------------

Index

INDEX

- 2-D models 18, 317-318, **43**
 3-D models 18, 318-319, **43**
 4-D assimilation 32, 207, **30-31**
 4DDA (also see data assimilation)
 204, 207, 216, 367
 24 key variables 10, **9**
- A**
- A/SA 216, 238
 AABW 123
 AASE II 321
 AATSR 67, 69, 365-366
 absorption, scattering, and emission,
 aerosol 50
 absorption, scattering, and emission,
 cloud 51-52
 absorption, scattering, and emission,
 Earth's surface 52-55
 absorption, scattering, and emission,
 gas 49-50
 ACRIM 8, 11, 22, 43-47, 66-67, 69,
 91, 103, **9, 12, 19**
 ACSYS 20, 274, 297
 ADEOS 14, 24-27, 69, 87, 89, 139,
 366, **19, 21**
 AEAP 322
 AERONET 370
 aerosols 19, 27, 29, 31, 208, 315-316,
 322, 325, 328, 330, **8, 13, 19, 42-44, 46, 49**
 aerosol abundance 353-354
 aerosol indirect effects of 355-358,
 362-366, **47-48**
 aerosol measurements (see also
 instrument names) 368-371
 aerosol radiative effects 352-355
 aerosol radiative properties 345-347
 aerosol sources 349-354
 aerosol, climate effects of 349-358,
 370-372
 aerosol, climate modification by 372
 AESOPS 150
 AGCMs (see GCMs)
- agriculture 26, 30, 34-35, 179, 203,
 206, 210, 213, 220, 230, 234,
 238, 352, 358
 Agung 48, 342
 aircraft exhaust 26, 320, 322, 350, **43**
 aircraft hazards 361-362, **8**
 AIRS/AMSU/HSB 12-13, 21, 26-29,
 31-32, 35, 50, 52, 55, 59, 62, 67-
 71, 78-82, 94-99, 102, 105, 140-
 141, 142, 210, 212, 217, 292,
 367, **14, 16-18, 20-21, 39, 41**
 AIRSAR 176, 285
 ALOS 236, 364-366
 AMIP 55, 80, 86, 271, 282, 289
 AMLS 326-329, **44**
 AMSR 55, 62, 75-76, 79, 87-88, 95,
 97, 101, 104-105, 139-141, 152,
 206, 212
 AMSR-E 14-15, 18, 28-29, 35, 52, 62,
 67, 72, 75-76, 79, 87-88, 96-100,
 139, 151, 283, 289, 292-293,
 298, **18-19, 21, 24, 35, 37, 39-41**
 anthropogenic aerosols (see aerosol
 sources)
 APAR 228, 234, 242
 ARM 20, 50, 55, 72, 90, 91, 94, 102,
 215, 217-218, 245, **22**
 assimilation data sets (see 4DDA)
 ASTER 13, 17-19, 22, 29-31, 52-55,
 66, 69, 72, 94, 96, 210, 213-214,
 217, 234, 275, 285, 288, 290,
 294-296, 298, 361, 364-368, **17, 20, 34-35, 40-41, 49**
 ATBD 176
 ATLAS 44, 47
 ATMOS 321
 atmospheric chemistry (see also
 greenhouse gases, CHEM-1) 15-
 16, **7-8, 28-29, 31, 48**
 atmospheric circulation (see also
 QuikSCAT, SeaWinds) 14, 87-
 89, 96
 atmospheric forcings 204
 atmospheric temperature 21, **21-22**,
 49, 96-97, 101
 ATSR 73, 362
- AVHRR 28, 52, 66-67, 75, 87, 90, 94,
 171, 206, 208, 221-229, 233,
 239-240, 249, 284-288, 291,
 294-298, 360, 362, 368-369, **13, 20, 34, 40-41**
 AVIRIS 213, 289
 AWS 298
- B**
- BAHC 213, 246, 249-250
 BATS 201, 213
 biodiversity 26, 33-34, 136, 249
 biogenic aerosols (see aerosol sources)
 biogeochemistry 136-138, 149, 156,
28, 32-33
 biogeochemistry, river 222-223
 biogeochemistry, terrestrial 231-232
 biological threat 311
 biomass burning 11, 15-16, 19, 29, 31,
 34, 50, 176, 181, 184, 341, 350-
 358, 370-371, **8, 13, 27-31, 46**
 BIOME2 175, 232, 252, **32**
 bio-optical measurements 1453
 biospheric responses-dynamics 208-
 209, 232
 BOREAS 20, 237, 239, 241-244, 297
 boundary layer fog 64
 boundary layer cloud 64
 BRDF 92, 207, 233-234, 243, 246
 bromine 9, 314-315, 324, 329, **42-43**
 BSRN 20, 55, 70-71, 91, 102, **22**
- C**
- calibration 7-8, 21-25, 46-48, 66-69,
 70-74, 82, 86, 90-94, 99, 102,
 104, 129, 151, 205-206, 221,
 226, 233-234, 237-239, 273,
 292, 327, 331, 353, 366, 369-
 370, **7, 18, 21**
 calibration strategy 23-25
 CALM 285
 Carbon America 247

- carbon cycle 16, 101, 117, 130, 132, 135, 150, 154, 156, 168, 170-177, 181-188, 228-229, 231-232, 238, 241, 243, 246-249, 252, **24, 29-30**
- carbon dioxide (CO₂) 7, 9, 11, 14-16, 18, 20, 23, 25, 28, 30-33, 48-49, 56, 59, 61, 65-66, 80, 84, 88, 91, 117, 130-136, 142-148, 153-156, 167-173, 176, 181, 184-190, 201-209, 219-238, 240-251, 270-271, 274, 279, 286, 297, 311, 322, 348, 359, 369-370, **25-29**
- carbon monoxide (CO) 14-16, 22, 26, 31-35, 132, 154, 167-168, 178-183, 187-190, 332, 359, 367, **12, 19, 27-31, 38**
- CART 102, 237-239, 245
- CART-ARM 239, 245
- CASES 239, 245
- CCD 233, 246, 369
- CCN 351, 354
- CDIAC 174
- CDOM (see DOM)
- CEMs 63-64, **16**
- CERES 11, 13, 19, 21, 25, 28-29, 31-32, 50-55, 62, 66-67, 69-71, 79, 92-94, 102, 104, 207, 210, 217, 295, 297, 367, **13-16, 19-20, 40-41, 49**
- CESBIO 251
- CFC 314, 321, 326, **44**
- CH₂Cl₂ 321
- CH₃Cl 182, 314, 321
- CHCl₃ 321
- CHEM-1 (see also ozone, see also specific sensor names) 16, 347, 368
- chemistry, stratospheric (see CHEM-1)
- chemistry, tropospheric 22
- chlorine 9, 18, 25-27, 312-327, 333, 349, **42-43**
- chlorophyll *a* (see phytoplankton)
- CLAES 331, 346, 347
- CLASS 275
- climate change 311, **28, 32, 36, 40-42**
- climate change, long term 30-33
- CLIVAR 20, 101-102, 149, **18-22**
- Cl_x 315, 322
- cloud modeling 59-63
- cloud observations 57-58
- cloud property measurements 72, 94, 104
- clouds 12, 21, 25, **8, 10-16, 19-25, 35, 42-43, 48**
- clouds, aerosol effects on (see aerosol indirect effects)
- clouds, marine 57
- CMDL 247, 250
- CO₂ 7, 9, 11, 14-16, 18, 20, 23, 25, 28, 30-33, 48-49, 56, 59, 61, 65-66, 79, 84, 87, 90-91, 117, 130-135, 141-148, 154-156, 167-173, 176, 181, 184-190, 201-209, 219-238, 240-251, 270-271, 274, 279, 286, 297, 311, 322, 348, 359, 369-370, **25-29**
- CO₂ fluxes 132, 143, 156
- COARE 63-64, 83, 101, 140, 149
- coastal zone 35
- coccolithophorid 145-146
- continuity 23-25
- convection 12-13, 43-45, 56-58, 62-65, 77-83, 87, 104-106, 121-123, 149, 151, 169, 173, 179, 251, 279, 344, **14-18, 25, 28, 38**
- convection and clouds in climate models 56, 80, 82
- coral reefs 136, 148-149
- COS 190, 343, 364, 367
- COSEPUP 372
- COV 266
- CPR 52, 91
- CR 183
- cryosphere 17-18, 237, 240, 263-267, 271, 278-279, 281, 284, 286, 298-299, **8, 36-38**
- cryosphere albedo 264
- cryosphere-EOS instruments-measurements 264-266, 287-298
- cryosphere-EOS interdisciplinary investigations 298
- cryosphere-freshwater 279
- cryosphere modeling 264, 271-278, 280-281
- cryosphere-related programs-ACSYS, BOREAS, PARCA, SCICEX, SHEBA 297
- cryosphere-sea-level rise 263
- cryosphere-thermal diffusivity 264
- cryosphere volume 264-266
- cryospheric climate linkage 264, 278-279
- cryospheric variability 266, 281-287
- CRYSYS 240, 268, 290, 298
- cyanobacteria 144-146
- CZCS 145-146, 154
- ## D
- DAAC 68-69, 299, **15, 35**
- DAO 19, 206, 210, 218, 228, 236, 333
- DAS 79, 215
- data assimilation 55-57, 79, 81, 89, 97, **17, 45**
- DECAFE 181
- DEC-CEN 20
- DEM 218, 273, 289, 359, 361, 365, 365
- DFA 99, 141, 143
- DIC 146
- diurnal sampling 21, 23, **10**
- DMS 145, 154, 350
- DMSP 25, 75, 88, 139, 291
- Dobson units 312
- DOC (see DOM)
- DoD 90, 139-140
- DoE 20, 102, 236, 239, 245, **22**
- DOM 136, 143-146, 153
- DORIS 142
- droughts 221, 230, **7, 33**
- DT 177
- DU 312, 314, 319
- ## E
- Earth's energy balance, cloud effects on 56-57
- ECHIVAL (see EFEDA)
- ECLIPS 20, 102, **22**
- ECMWF 56, 81, 89, 204, 210
- ecosystem 20, 26, 30, 33-34, 128, 132-137, 144, 146, 154-155, 168, 178, 187, 202-204, 214, 218, 225, 228-231, 235-238, 243-244, 247-251, 267, 270, 283, 297-298, **29**

- EDC 54, 69, 72, 234-235
 EFEDA 244
 EIGIG 270
 El Chichón 342-344
 El Niño 15, 23-24, 28, 33, 52, 79, 83, 100, 119, 121, 124, 129, 173, 201, 212, 231, 247, 315, 322, 342, 344, 367, **25**
 energetic particles (see also SPEs, REPs) 316-317, 319, **42-43**
 ENSO 15, 52, 79, 85-87, 103, 128, 132, 134, 136-137, 145, 148-150, 154-155, 173, 212, 221, 344, **25**
 ENVISAT 66, 69, 73, 129, 139-140, 359, 364-367
 EOS instrument products (see also named instruments) 205-206, 208
 EOS AM 12, 22, 25, 49, 52-54, 66-70, 92, 101-102, 179, 204, 208, 217, 223, 233, 240, 356, 369-371, **16, 19, 27**
 EOS PM 14, 55, 66, 75, 82, 88, 92, 101, 139, 212, 214, **18-19**
 EOSDIS 48, 86, 214, 218, 233, 236, 251, 299
 EOSP 11, 13, 19, 29, 31-32, 50, 52, 59, 62, 67, 72, 75-79, 94-97, 102, 104-105, 208, 353, 356, 363-364, 366-371, **13-14, 17, 20, 49**
 EP 368
 ER-2 327
 ERB 8, 43-48, 54, 67-68, **12, 14-15**
 ERBE 11-12, 21, 44, 49, 51-56, 59, 66-70, 89, 281, 343, 346, **13-16**
 ERBS 44, 46-47
 EROS 234
 ERS 27-28, 30, 120, 129, 131, 140, 171, 176-177, 215, 236, 241, 285, 288, 291, 294-297, 360, 366
 ESA 23, 27, 46, 66, 72, 87, 139-140
 ESSC 43
 ESMR 87
 ESSC 7, 7
 ETM+ (see Landsat-7) 17-19, 22, 234-235, 294-295, 367-368, **34, 49**
 EURECA 44
 evapotranspiration (ET) 188, 209-214, 222-225, 233-234, 239, 244, 246, 251, **33**
 extreme hydrologic events-severe storms, floods, droughts 218-222
F
 FAA 360-361
 FAO 216-217
 FAPAR 172, 181
 field campaigns (see also specific names) 20, 358, **7, 10, 22**
 FIFE 205-206, 209-210, 214, 228, 237-239, 243
 FIRE 20, 64, 70-76, 94, 100-101, **22**
 fires 22, 206, **29, 34-35, 39-40, 49**
 floodplains 177, 220-222
 fluxes, radiative 48, 50, 52, 54, 65-66, 71-72, 91, 93, 97, 102, 104-105, **12-17, 19-20, 22-25**
 fluxes, surface 48-49, 52, 54, 65, 67-70, 79, 83, 93, 104
 fluxes, TOA 51, 59, 66-72, 92-93, 104
 fluxes, within atmosphere 71-73
 FLUXNET and EUROFLUX 241, 246-247
 foreign partners 333
 FPAR 206, 210, 214, 223, 225-226, 246
 Franklin, Benjamin 349
 freshwater cycle 279
 freshwater forcing 121-123, **25, 27, 37-38**
 freshwater resources 35
 frozen ground (permafrost) 269, 275, 295-296, **35-38, 40-41**
 FSSP 75
 FTS 184
G
 GAIM 249-252
 GAP 249
 gas-to-particle conversion 343-345
 GCIP 20, 54-55, 91, 214, 239, 245
 GCMs 48, 54, 58, 60-62, 65, 90, 102, 201, 203, 205-210, 219, 221, **12, 15, 32-33, 37-38**
 GCOS/GTOS TOP 237-238, 281
 GCTE 246, 249-252
 GEBA 70, 217, 268
 GENESIS 57, 261, 268, 270, 277
 GEOS 55-57, 79, 81
 GERB 92
 GEWEX 11, 20, 48, 54, 81, 90, 101, 214-217, 245, 251, 275, **10, 13, 22, 38**
 GFDL 175, 232, 251
 GFO 129, 140
 GGD 285
 GHCN 86
 GIS 238-239, 248
 GISP 270
 GISS 217, 280, 346
 glaciers (see ice sheets)
 GLAS (see also lidar) 12-13, 18-20, 24-25, 32-35, 66-69, 72, 74, 78-79, 52, 66-69, 71-72, 74, 79, 94-96, 101, 295, 349, 356, 358, 362-371, **14, 17, 20, 35, 41, 49**
 GLCTS 241, 249
 GLI 67, 69, 148, 153, 366, **24**
 GLIMS 278
 GLOBE 216
 GLOBEC 20, 132, 135-136, 150, 155
 GMS 87
 GNP 117
 GOALS 20, 101, 149
 GOES 80, 82, 87, 90, 212, 217, 239, 290
 GOMOS 366
 GPCP 84-86, 89, 213
 GPS 141, 236, 362
 GRDC 213
 greenhouse forcing 311, **42**
 Gross Primary Production (GPP) 173
 GSFC 19, 68-69, 92, 213, 215, 217, 297, 324, 333, **45**
 GVAP 81

H

H₂SO₄ 316, 320, 342-343, 345-346, **46-47**
 HALOE 318, 321, 323
 HAPEX-Sahel 206, 238, 243
 HCFC 321
 HCl 342, 358-359, 364, 367, **44**
 health hazards, volcanic 359-361
 heterogeneity 209-210
 HH 176
 HIRDLS 13, 18-19, 26-27, 29, 31-32, 35, 49, 78, 82, 94, 187, 208, 210, 326-332, 347, 362-363, 366-367, **18-21, 29, 44-45, 49**
 HIRS 21, 67-68, 78, 82, 323, **14-15**
 HNLC 134-135
 HO_x 314, 322, 325, 329
 horizontal energy transport 123
 HRDI 324
 HSB 12-14, 21, 31-32, 35, 55, 59, 67-71, 78-79, 82, 87, 98-99, 105, 210, 212, 217, 292, 367, **14, 17-18, 21, 39, 41**
 HSCT 322
 human dimensions 7, 8, 26, 34-35, 7
 human health 33, 35, 169, 179
 human impacts (see also ocean economics) 154-155
 humidity 8, 12, 21, 43, 43, 52, 55, 59, 77-82, 88, 92-96, 98-99, 103, 105-106, 118, 121, 138, 140, 151, 188, 204, 206-207, 217-218, 228, 236, 247-248, 292, 350, 367, **11, 17, 21, 30, 39**
 hydrology 16-17, 54-55, 156, 169, 174, 176, 181, 201, 252, **8, 28-33**

I

IABP 297
 ice mass balance 274, 277, 283, 291-293
 ice sheets 15, 17-18, 32, 34, 128-129, 263-264, 266, 269-270, 275-278, 285-287, 296-298
 ICESat 278, 286, 292, 295-296, 298, 356, 371, **35, 39-40**
 ICRCCM 50
 ICSU 237, 250

IDS (see also IDS field sites) 1-2, 15, 48, 52, 55, 59, 62-64, 79-80, 170, 185, 201-257, 331, 333, 362, 367, **24, 35**
 IDS field sites 238
 IFOV 215
 IGAC 246
 IGBP 7, 20, 136, 150, 213, 216, 235, 237, 241, 246, **10**
 IGPPDI 251
 IHP 237
 ILAS 366
 infiltration and deep percolation 16, 216, **33**
 interannual variability 11, 15-18, 20, 28-29, 43, 48, 52, 81, 89, 96, 101, 119, 124, 149-150, 152, 163, 173, 201, 208, 223, 227, 231, 241, 249, 265-268, 293, 298, 315-316, 319, **7, 11, 13, 19, 23, 28, 33, 36, 43**
 IOC 237
 IPCC 50, 84, 136, 170, 263, 267, 271, 274, 276-277, 281-282, 311, 350-352, 370, **14-15, 22**
 IR 66, 81, 86-87, 95, 99, 104, 207, 234, 294, 315, 365, 368, **18**
 ISAMS 331, 346-347
 ISCCP 49, 51-57, 59, 62, 64, 67-74, 100, **14-15, 22**
 ISLSCP 54, 205, 217, 243
 IT 238-239
 ITCZ 83-87, 212
 IWP 76

J

Jason-1 15, 22, 24, 31, 34, 129, 140, 142, 152, **24**
 JERS 171, 176, 215, 288, 294, 366
 JGOFS 20, 132, 135, 137, 147-149, 150, 153, **10**
 JPO 237

K

KINEROS 213
 Krakatau 342, 344

L

LAI 16-17, 33, 172, 181, 188-206, 214, 223-233, 238, 241-244, 248, **30-31**
 lake ice 17, 263, 268-269, 274-275, 284, 293-295, **35-38, 40-41**
 land-climate interaction 201-210, **32**
 land cover (see land vegetation)
 land cover/land-use change 168, 170-172, 181, **28-33**
 land ecosystems 16-17, 30, 33-34, **8, 28, 32**
 land hydrology 16, 201-233, **32-33**
 land processes 103, **23, 32**
 land-surface water balance 218, **33**
 land-vegetation 223-232, 241-243, **32**
 Landsat-7 23, 224-225, 234-235, 295, **34**
 LBA 239, 244-245
 LERTS 251
 LHH 176-177
 lidar 52, 67, 69, 71-74, 82, 89, 94, 96, 99, 102, 178, 208, 246, 344, 347-349, 356, 367, 371, **17, 20, 22, 49**
 lightning 12, 23, 97, 219, 322, **15, 21**
 LIS 12, 62, 97, 208, **15-21**
 LITE (see lidar)
 LOICZ 132
 LS 328
 LSMs 203-206, 208-210, 239, **32-33**
 LSPs 201, 210, 221, **32**
 LTER 236-237, 248
 LW 48-59, 66-72, 92, 93, **14-15**
 LWP 62, 66, 69, 75-76, 97, 105, **14**

M

man-made changes 320-322
 MAPS 179-182
 MAPSS 224, 232, 252
 marine biosphere (see also biogeochemistry) 130-138, 142-148, **26**

- MAAT 269
MCS 64, 76-78
measurement requirements 323-333
measurement strategy (see also simultaneity) 21-25, 70, 284, **7**, **10** overlap strategy, calibration strategy, validation strategy, continuity methane (CH₄) 174-176, 181-182
- MERIS 67, 69, 148, 153, 366, **24**
- METEOR-3 26-27, 329, 347, 368
- methane (CH₄) 18, 22, 26-27, 29, 31-32, 35, 49, 167-168, 181-182, 190, 222, 247-248, 314, 318, 322, 325, 329, 332, **42**
- METOP 66, 69, 75, 87, 98, 100, 139
- MHS 21
- MIMR 88, 97-100, 104-105, 139-141, 206-207, **14**, **21**
- MISR 11-13, 17-19, 26-35, 50-54, 66-67, 69-74, 79, 92-97, 102, 104-105, 172, 206, 208, 210, 217, 224-227, 233-234, 288, 294, 353-357, 362-371, **13-14**, **17**, **20**, **34**, **49**
- MIT 213
- MLS 13, 18-19, 25-27, 29, 31, 35, 49, 77-78, 82, 97-99, 105, 313, 324-332, 345, 363-364, 367, **18**, **21**, **44-45**, **48-49**
- MMIC 326-328, **43**
- MMS 12, 63-65, 213
- modeling 12, 20, 24, 31, 48-49, 52-54, 59-64, 72, 77-80, 83-84, 89-90, 93, 99, 101-102, 105, 121, 125-126, 129-130, 136, 149-50, 154-156, 172, 185-190, 213-217, 224-228, 232-252, 270, 273-278, 282, 289, 296-299, 317, 333, 345, 371, **8**, **10**, **13**, **15**, **22-24**, **27-28**, **33**, **35**, **38**, **44**, **49**
- MODIS 12, 15-19, 21-23, 25, 28-31, 50-55, 62, 66-76, 79, 92-105, 132-139, 141-148, 152-153, 168, 171-172, 184, 208, 210, 213-214, 217, 220, 223-229, 231-233, 272, 284, 288, 291-295, 298, 353, 356, 362-370, **14**, **17**, **19-20**, **24**, **27**, **29**, **33-35**, **37**, **39-41**, **49**
- MODLAND 248
- MODLERS 248
- momentum exchange 119-121, **25**
- MOPITT 16, 22, 26, 31, 35, 49, 167, 179, 181-183, 187, 232, **29**
- MOU 237
- Mt. Katmai 342
- Mt. Pinatubo 343-348, 361, 366-367, 371, **12**, **47-48**
- Mt. Saint Helens 344
- MSG 92
- MSU 323, 343-344
- MVI 228, 233
- N** —————
- NAD 326-329
- NADW 123
- NASA 7, 15, 19, 43, 54, 66, 89-90, 139-140, 215-217, 236, 299, 324, 326, 328, 333, 366, **44**
- NASDA 23, 69, 88, 139-140
- NAT 320, 326-329
- National Snow and Ice Data Center 299
- natural changes 319-320, **42-43**
- natural variability 28-31, **40**
- NBIOME 240
- NCAR 63, 251, 271, 318
- NCDC 86
- NCEP 81
- NDVI (see vegetation indices) 172-173, 214, 223, 233, **34**
- near-surface meteorology 217-218, **33**
- NESDIS 282, 288
- Nevada del Ruiz 344
- NEXRAD 86, 212, 239
- NH 280, 283
- Nimbus-7 311
- NIR 223, 226, 294
- nitric oxide (NO) 16, 177-178, **28-29**
- nitrous oxide (N₂O) 9, 15-16, 29, 168, 170, 177-178, **28-29**
- NMC 81, 89, 91, 210
- NMHCs 178-179, 188, **31**
- NOAA 21, 23, 26-27, 67-68, 78, 81, 86-87, 90, 102, 206, 212, 217, 227, 236, 241, 247, 250, 281-283, 288, 323-324, 328, 368, **14**, **15**, **40**
- NOPEX 245-246
- NO_x 167-168, 177-179, 314, 319, 322, 325, 329, 350
- NPOESS 324, 330
- NPP 16-17, 33, 170, 173, 223, 227-229, 241-242, 249-251, **30**, **33**
- NRC 7, 219
- NSCAT 28, 120, 139, 152
- NSF 236, 241, 245, 285, 297-298
- NSIDC 299
- NWP 54, 81, 274, 287-290
- O** —————
- ocean-atmosphere surface coupling 118-123, **25**
- ocean carbon (see marine biosphere; see also CO₂ fluxes) 169-170, 173-174, **28-29**
- ocean circulation (see also Jason-1) 14-15, 24, 118-119, 123-130, 134-140, 140-141, 147-156, **8**, **13**, **24-26**
- ocean color 15, 23, 28, 34, 131, 133, 143-148, 153-156, 167, 174, 188, 341, 366, **23-24**, **30**
- ocean economics (see also human impacts) 117
- ocean food stocks 132
- ocean surface topography 22
- ocean tides (see also sea level) 128-130, 142, 154
- oceanic processes 99-101
- OCS 316, 329
- OCTS 153, 366, **24**
- OH 182-183, 314, 321, 325-326, 329, 332, **44-47**
- OLR 49, 53-56, 93, 279-281, 344, **39**
- OMI 19, 25, 326, 329-332, 350, 355-356, 363-365, **49**
- ONR 297

- ORNL 251
 OSU 137, 175, 232, 251-252
 OTTER 228, 243-244
 overlap strategy 21-22, **10**
 ozone (see tropospheric ozone, see ozone precursors) 18-19, 25-28, **8, 28-29, 42-44, 47**
 ozone changes (see also man-made change, natural changes) 312-315
 ozone chemistry 314-315
 ozone distribution (see also natural changes, man-made changes) 314, 317, 319-320
 ozone precursors 178-181, 183
 ozone transport 315
- P**
- PAR 142, 144, 204, 214, 226, 228, 233, 247, 265, 267, **36**
 PARCA 297
 Pathfinder data 54
 PEM 228
 PIK-NPP 232, 250-252
 PILPS 251
 phytoplankton 118, 132-137, 143-148, 153-155, **27**
 PNZ 137
 POLDER 66, 69, 73-76, 208, 366
 POLES 299
 policy-relevant questions 9
 PR 14, 87, 207, 212, **18, 21**
 precipitation 13-14, 43-106, 138, 140-141, 151-155, 211-213, 233, 236-243, 247-249, 263, 266, 268, 270-273, 280-283, 319, 343-344, **8, 11, 14, 16, 18-19, 21, 23, 25-26, 32-33, 35**
 precision orbit determination (see sea level)
 productivity 117-156, **8, 24, 26-27, 29, 32, 36**
 PSC 315-316, 318-322, 325, 327, 331, **43, 44**
 PSU 63, 213, 217
- Q**
- QBO 315, 319, 322, 344
 QuikSCAT 14, 24, 89, 139, **19, 21**
- R**
- RADARSAT 176, 215, 241, 278, 282-283, 285, 288, 291-296, 359, 364, 366, **39**
 radiation 216-217, **8, 11-16, 18-23, 25, 27, 29-30, 33-39, 42-43, 47-49**
 radiation fluxes 11-12
 radiation in climate models 55
 RAMS 63-64
 RC 48
 reactive nitrogen (see also nitric oxide and nitrous oxide) 178
 REP 317
 RGPS 283
 river ice 268-269, **35-36**
 runoff 213, **25, 33, 37-40**
- S**
- SAFARI 181
 SAGE 313, 331, 350, **44-45, 49**
 SAGE II 347, **14**
 SAGE III 19, 26-27, 31, 78-79, 82, 94-99, 105, 208, 210, 313, 330-332, 347, 363, 367, **18, 20-21, 44-45, 49**
 salinity 83, 123, 125-126, 129, 138, 140, 143, 151-155, 359
 SALSIA 216, 238
 SAM 316-317, 347, 349
 SAR 176-177, 213, 221, 236, 241, 264, 273, 275, 278, 282-298, 362, 364, **37, 40-41**
 satellite measurements 87-89, 91, 99, 128, 137-140, 150, **14, 19, 22, 45**
 SAVI 226
 SBUV 313-314
 SCA 266-267, 272, 282-290
 SCANSAR 366
 SCARAB 67-68, **14-15**
 SCF 363
 SCICEX 297
 SCOPE 250
 sea ice 25, 267-268, 273-274, 283-284, 291-293, **25, 35-40**
 sea level (see also Jason-1) 24, 31, 117-156, **25-26, 35, 37**
 SeaWiFs 15, 28, 135, 145, 153, **8, 24, 38**
 SeaWinds 14-15, 24, 28, 31, 88, 99, 100, 139, 141, 151-152, **19, 21, 24**
 SEB 138-139, 150, 152, 264, 271, 279-280, 284, 291, 298
 SEDAC 174
 SHEBA 20, 297
 SiB 53, 201, 203, 239
 SIMIP 274
 SLR 130, 142
 SMM 23, 43-47
 SMMR 75, 81, 87, 177, 215, **40**
 snow cover 17-18, 25-35, 83, 177, 207, 211, 240, 263-267, 271-273, 281-283, 287, **13, 35-40**
 snow-water equivalence 267, 272-273, 281-290, 295, 297, **37, 40**
 SOHO 44-47
 soil moisture (see also wetlands) 169, 176-177, 215-216, **28-33**
 soils data 216, 235-236
 SOLAS 150
 SOLSTICE 22, 31, 144, 326, 330-331, **44**
 SPCZ 85
 SPOT 148, 171, 294, 333
 SRB (see Earth's surface absorption) 11-12, 54, 67-68, 204 **13-15**
 SRBEX 239
 SSM/I 25, 67-68, 75-76, 81, 87-88, 139-140, 177, 215, 239-240, 282, 288, 294-296, **14-15, 40-41**
 SST 15, 23-25, 28, 32, 58, 60-61, 65, 80, 86-89, 100, 103, 219-221, 241, **18, 24, 30**
 SST measurements 121, 126, 132, 138-139

stem and soil carbon 229-230
 steric change (see sea level)
 STP 184, 312
 sulfate (see SO₂) 11, 19, 26, 29, 31, 50, 319-320, 329, 341-352, 359, 365, 370-371, **13, 47**
 sulfur (see also SO₂) 19, 26, 50, 174, 322, 341-343, 351, **46-49**
 sulfur dioxide (SO₂) 19, 26-29, 316, 319, 329-332, 341-346, 350-354, 358-359, 365, 367-368, **46-48**
 sulfuric acid 316, 320, 342-343, 345-346, **46-47**
 surface energy balance (SEB) (see also Earth's surface absorption) 270, 279, 280, 291, **38** clouds effect on 56-57
 surface flux 70, 72, 102, 118, 125, 142, 151-153
 surface flux measurements 137-138
 surface forcing 102, 126, 129, 132, 142
 surface insolation 49
 surface observations 58, 74, 86, 99, 101, 149, 152, 177, 215, **29**
 SVAT 54
 SVI 228
 SW 48-59, 66-71, 92-93, 267, 279-280, 347, **14-15**
 SWE 212-213, 240, 290
 SWIR 234, 295-296, 365, 369-370
 Synthetic Aperture Radar (SAR) 176

T

T-S 125-126
 Tambora 342, 344, **47**
 TARFOX 353
 TEM 175, 225, 229, 232, 240, 251
 temperature profiles 81, 97, 99, **21, 45**
 TES 49-50, 96, 183, 187, **29, 49**
 thermal fluxes 121, **25**
 thermohaline circulation 121-126, **25**
 THM 213
 tides (see sea level, see also ocean tides)

TIR 215, 234, 294, 296, 362, 365
 TM 221, 234-235, 241, 249, 284-290, 295-296, **40-41**
 TMI 14, 67-68, 75, 87-88, 207, 212, **14-15, 18**
 TOA 11-12, 21, 25, 217, **12, 14, 16-17, 20**
 TOGA 63-64, 83, 101, 140, 149, 152
 TOMS 19, 25-27, 311-314, 326, 329-331, 356, 365, 367-369, **49**
 TOPEX/Poseidon 22-23, 28, 129-131, 140, 142, 152
 topography 22, 64, 124, 129, 140-144, 149, 202, 212, 221-222, 229, 234-236, 243, 271-273, 277-278, 286-289, 295-296, 361-367, **48-49**
 TOPSAR 236, 361
 TOVS 21, 78-81, 298, 323-324, 331
 tower sites 246
 trace-gas exchange (see marine biosphere)
 trace gases 11, 20, 27, 31, 48-49, 156, 167-168, 170, 172, 178, 182-190, 317, 319, 328, 333, 350-351, **29, 31**
 TRAGNET 246-247
 TRMM 12, 14, 23, 65-70, 75, 87, 92, 94, 97, 99, 101, 104-105, 140, 212, **15-16, 18, 20-21, 26**
 tropospheric ozone (O₃) 168-169, 178-181, **28**
 TSI 8, 11, 22, 29, 31, 43-47, 103, **12**

U

UARS 313, 318-321, 323, 326-332, **12, 14, 44**
 UKMO 175, 232, 251
 UMCP 251
 UNEP 237
 UNESCO 237
 USAF 289
 USDA 238-239
 USGCRP 7-9, 20, 26, 26, 55, 102, **7-8, 10, 22**
 USGS 54, 213, 250
 UT 328

UV 311, 327, 330-331, **42-43**
 UV-B 311, 330

V

validation 12-13, 18, 24, 29, 49, 54-55, 59-60, 64-75, 81-82, 86, 90-94, 99, 101-104, 146, 152, 155, 174, 201, 204-208, 213-216, 229, 234-252, 272, 274-275, 281-282, 287, 289-291, 297, 299, 327, 349, 366, 370, **8, 15-17, 22**
 validation strategy 24
 variability, trend detection 105
 VCL 19-20
 vegetation indices 16-17, 202, 207-208, 223, 226-227, **33-34**
 vegetation phenology 203, 223, 227, 234, 242, **33**
 vegetation structure 241-243
 VEMAP 174-175, 214, 218, 229, 232, 236, 239, 240, 251-252
 vertical circulation 135
 VHRR 281
 VI (see vegetation indices)
 VIC 213
 VIRGO 44, 46-47
 VIRS 52, 66-76, 87, 92, 94, 207, 212, **14-15, 17-18, 20**
 VIS 14, 87, 104, 223, 226, 294, **18**
 VNIR 234, 295-296
 VOC 350-351
 volcanic detection 360-362, 368
 volcanic eruptions (see specific event names)
 volcanic hazards 358-362, 367, **8, 46-48**
 volcanic measurements, international 368
 volcanoes 18-20, 22, 26, 29, 31, 206, 316, 322, 341-372, **8, 46, 48**

W

water-leaving radiance 144
 water transparency 147-148

- water vapor 8, 11-16, 19-22, 25, 29,
32, 36, 43-106, 342-345, 350,
352, 358, 362, 364, 368, **8, 11,**
13-14, 17-23, 33
- WCRP 20, 51, 70-74, 90, 101-103,
204, 213, 237, 241, 245, 251,
274, 281, 288, **22, 39-40**
- WDC-A 293, 297, 299
- wetlands (see also soil moisture) 176-
177, **28, 38**
- WFPS 178
- wind 13-15, 19-24, 29, 34, 48, 55, 79,
88-89, 99-105, 117-156, 167,
173, 174, 181, 187-188, 206-207,
217, 219-220, 248, 269, 272, 312,
319, 323-324, 333, 341, 344, 367,
370, **19-24, 30, 38, 44-46**
- wind fields 121, 142-143, **45**
- wind stress 181, **23-25, 30**
- WMO 237, 311, 316-318, 320-321,
324
- WOCE 30, 101, 131, 149, 152-153
- WSR 86, 212, 245, 316

Y

- year without a summer 342



National Aeronautics and
Space Administration

January 1999

NP-1998-12-069-GSFC